Max-Planck-Institut
für
Radioastronomie

Proceedings of the first ENIGMA-meeting

in Lochmühle, Mayschoss

May 11-14, 2003

organized by the
Max-Planck-Institut für
Radioastronomie
Bonn

European
Network for the
Investigation of
Galactic nuclei through
Multifrequency
Analysis

Contributions to the 1^{st} team meeting, of the ENIGMA* network held in Mayschoss, Germany, May 2003

The meeting was organized by the

MPIfR group of Dr. Anton Zensus, managing director

*ENIGMA is a Research Training Network funded within the FP5 program of the EC

1^{st} Team meeting -
Local Organisation: Arno Witzel
Scientific Organisation: Silke Britzen
Editors of Proceedings:
Marcus Hauser, Uwe Bach, and Silke Britzen
Network Coordinator: Stefan Wagner

Contents

ENIGMA program

ENIGMA meeting

Hotel Lochmühle, Mayschoß, 10.05.-14.05.2003

- Saturday, 10.5.2003
  - Arrival of the participants

- Sunday, 11.5.2003
  - Arrival of the participants
  - 15:00 Welcome (A. Zensus, A. Witzel)
  - Welcome ENIGMA (S. Wagner)
  - Program and General Remarks (SOC & LOC)
  - 15:45 – 16:00 coffee
  - 16:00 – 18:15 The science programs of the 8 teams (Introduction)
  - 18:30 Dinner
  - 20:00 Concert (Anna Zetel)

Concert of Anna Zetel

Winner of the I. Chopin-Contest Cologne 1994 and of the
III. International Chopin-Contest Göttingen 1995

L. v. Beethoven (1770-1827)	*Prestissimo, f-moll op. 2 Nr. 1* *Adagio cantabile As-Dur op. 13* *Presto alla tedesca G-Dur op. 79*
J. Haydn (1732-1809)	*Vivace molto e-moll hob. XVI: 34*
W.A. Mozart (1756-1791)	*Allegro maestoso a-moll KV 310* *Allegro moderato C-Dur KV 330* *Rondo D-Dur KV 485*
F. Chopin (1810-1849)	*Presto non tanto h-moll op. 58*
Pause	
A. v. Henselt (1814-1889)	*Vier Konzert-Etüden* *Es-Dur, b-moll, Fis-Dur, Ges-Dur*
F. Chopin (1810-1849)	*Fünf Etüden aus op. 10 cis-moll,* *Ges-Dur, es-moll, C-Dur, F-Dur*

- Monday, 12.05.2003
  - 9:00 – 11:05 Session I: Towards automated, fast, and accurate photometry
    - Chair and Introduction: N. Smith
    - 9:20 M. Xilouris: The 2.3m telescope ARISTARCHOS
    - 9:40 N. Smith: High-precision, high time resolved photometry of AGN
    - 10:10 L. Hanlon: Small robotic observatories
    - 10:30 L. Takalo: Status of the KVA-telescope on La Palma
    - 10:50 J. Heidt: Complementary IDV observations from the T1T
  - 11:05 – 11:30 coffee
  - 11:30 - 13:00 Session II: Separating intrinsic and extrinsic Intraday Variability
    - Chair and Introduction: C. Raiteri
    - 11:50 A. Witzel: IDV observations with the 100m radiotelescope
    - 12:15 L. Fuhrmann: Investigations of IDV blazar cores
    - 12:30 G. Cimo: Statistical Study of Intraday Variable Sources
    - 12:45 V. Impellizzeri: Short-time polarisation variability in 0716+714
  - 13:00– 14:00 Lunch

- Monday, 12.05.2003
  - 14:00 – 15:10 Session II: Separating intrinsic and extrinsic Intraday Variability
    - Chair: C. Raiteri
    - 14:00 U. Bach: Kinematical study of the Blazar 0716+714
    - 14:15 T. Beckert: Quenched Scintillation of intraday-variable Quasars
    - 14:35 C. Raiteri: Preliminary results of the 2001 radio-optical WEBT campaign on BL Lacertae
    - 14:55 E. Valtaoja: „Southern IDV“
  - 15:10– 15:40 coffee
  - 15:40 – 17:40 Session III: Variations of Source Structure and Flux
    - Chair and Introduction: A. Witzel
    - 16:00 M. Tornikoski: Long Term Radio Variability: Statistics and Predictions
    - 16:20 K. Nilsson: Current monitoring program at TUORLA
    - 16:40 E. Middelberg: Where has all the polarization gone?
    - 16:55 S. Friedrichs: Measuring the polarization in 0954+658
    - 17:10 D. Gabuzda: New views of the polarization structure of compact AGN fom multi-wavelength data

- Monday, 12.05.2003
  - 17:40 – 19:15 Session IV: Radiation processes at high energies
    - Chair and Introduction: L. Takalo
    - 18:00 A. Lähteenmäki: Millimetre Observations as a Tool for Studying Gamma-Ray Emission in Blazars
    - 18:20 I. Papadakis: The complex X-ray variability behaviour of Mkn421 as seen by XMM
    - 18:40 A. Sillanpää: Status of MAGIC telescope
    - 18:50 A. Sillanpää: INTEGRAL Blazars
  - 19:00 Dinner
  - After Dinner: Team Leaders
    - Recruitment
    - Administration
    - Reports
    - Finances

- Tuesday, 13.05.2003
  - 9:00 - 10:20 Session V: Particle acceleration in MHD outflows
    - Chair and Introduction: K. Tsinganos
    - 9:20 N. Vlahakis: Formation and kinematic properties of relativistic MHD jets
    - 9:40 K. Tsinganos: On the acceleration, formation and shocks in MHD jets
    - 10:00 A. Mastichiadis: Particle acceleration and radiation in blazar jets
  - 10:20 - 12:55 Session VI: The power of jets
    - Chair and Introduction: G. Ghisellini
    - 10:40 S. Britzen: The kinematics of AGN
  - 11:00 – 11:30 coffee
    - 11:30 T.P. Krichbaum: mm-VLBI observations of AGN
    - 11:55 A. Brunthaler: Evolution of the Seyfert I galaxy IIIZw2
    - 12:10 I. Agudo: VLBI observations and numerical modeling of the inner jets in AGNs
    - 12:40 T. Arshakian: Statistical Analysis of bright radio sources at 15 GHz
  - 12:55 – 14:00 Lunch

- Tuesday, 13.05.2003
  - 14:00 – 15:15 Session VI: The power of jets
    - Chair: G. Ghisellini
    - 14:00 B. Sbarufatti: The host galaxies of BL Lac objects
    - 14:15 C. Raiteri: A helical jet model to explain the Mkn 501 SED variations
    - 14:35 E. Körding: Radio and X-ray emission from XRBs and AGN
    - 14:50 G. Krishna: Comments on S5 0716+714
    - 15:00 G. Ghisellini: Theory of blazars, modelling of spectra, etc.
  - 15:20-15:40 coffee
  - 15:45 Visit of the Effelsberg telescope
  - 19:00 Dinner
  - After Dinner: A. Marscher: Blazar variability: multiwaveband correlations

- Wednesday, 14.05.2003
  - 9:00 – 10:30 Team Leaders
    - Winter school
    - Future meetings
    - Etc.
  - 10:30 – 11:00 coffee
  - 11:00 Joined observing programs
  - 12:30 Joined research programs
  - 13:00 Lunch

Chapter 1

Introduction (S. Wagner)

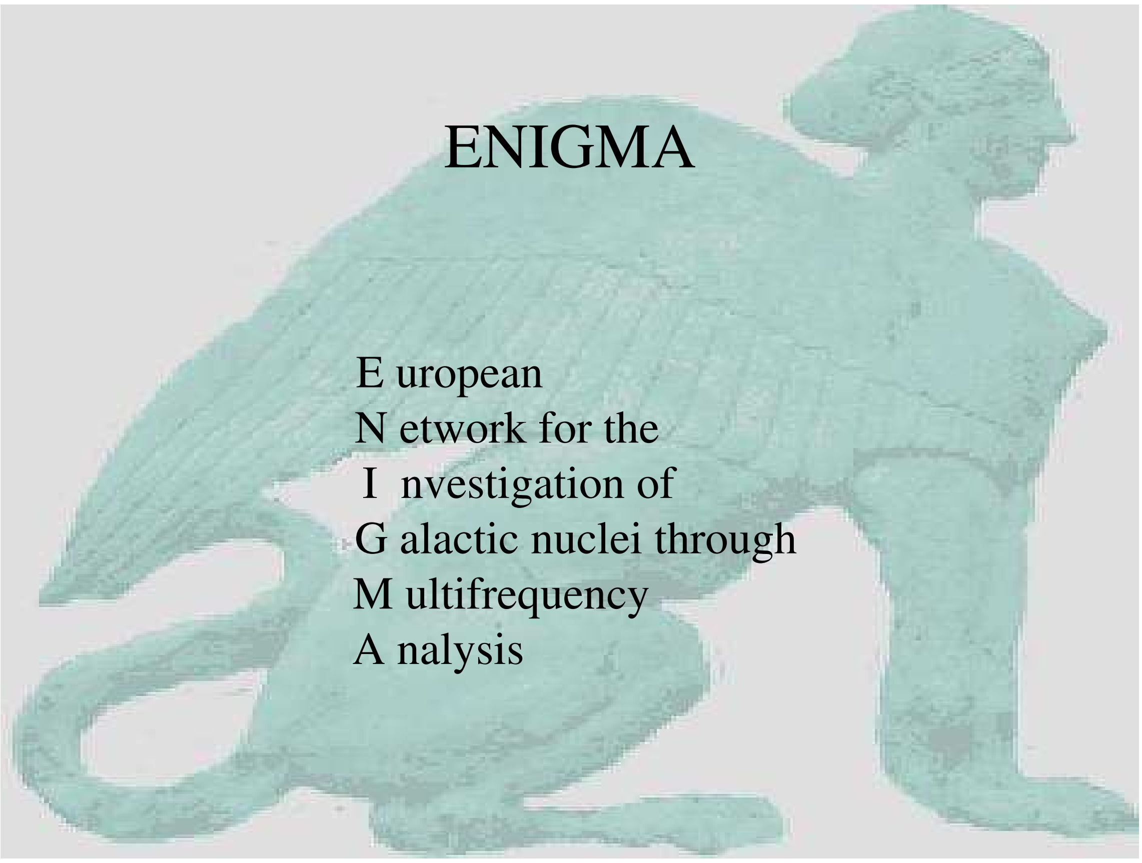

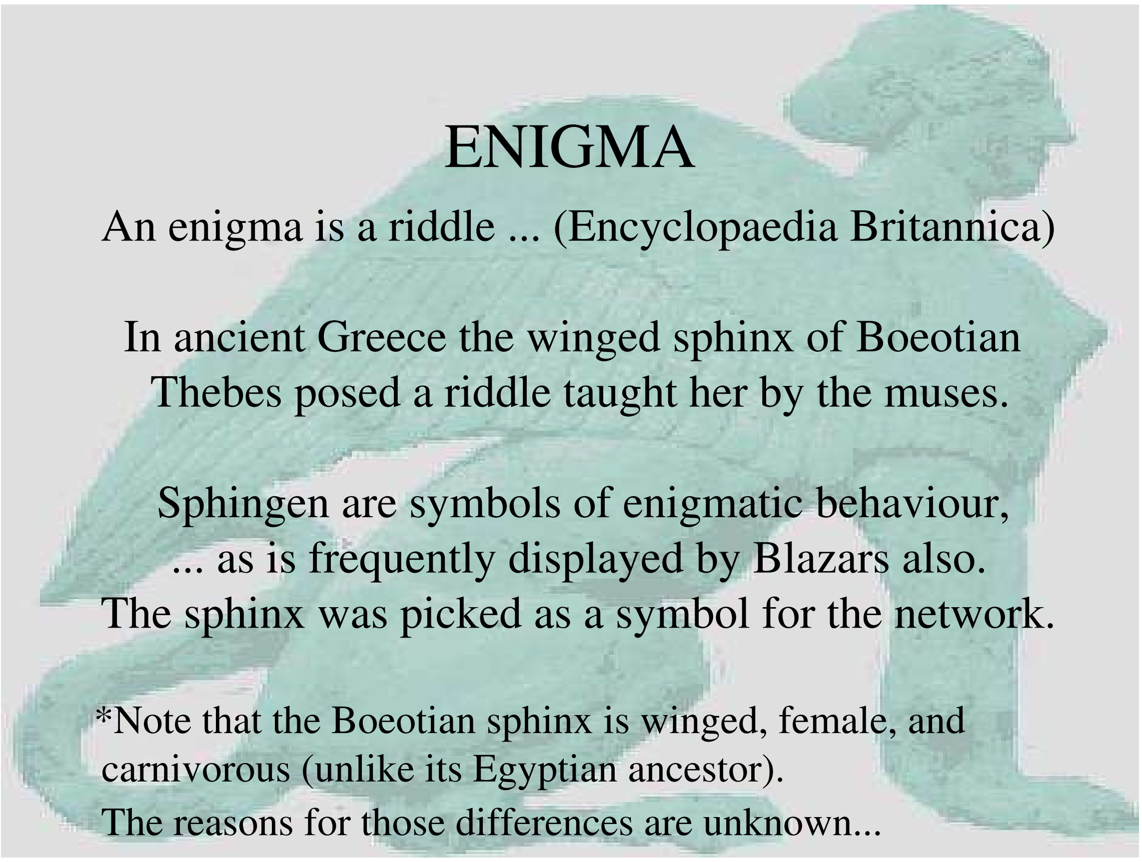
ENIGMA
An enigma is a riddle ... (Encyclopaedia Britannica)
In ancient Greece the winged sphinx of Boeotian Thebes posed a riddle taught her by the muses.
Sphingen are symbols of enigmatic behaviour,
... as is frequently displayed by Blazars also.
The sphinx was picked as a symbol for the network.
*Note that the Boeotian sphinx is winged, female, and carnivorous (unlike its Egyptian ancestor).
The reasons for those differences are unknown...

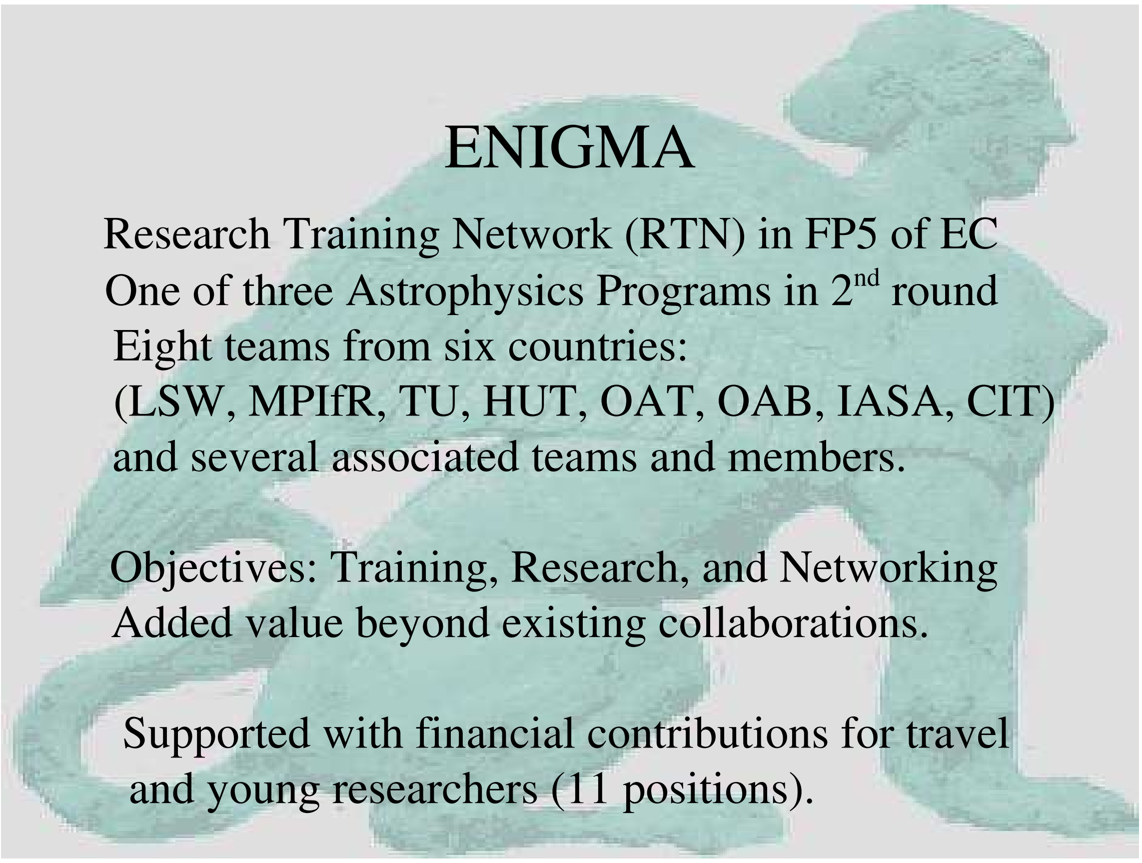
ENIGMA
Research Training Network (RTN) in FP5 of EC
One of three Astrophysics Programs in 2nd round
Eight teams from six countries:
(LSW, MPIfR, TU, HUT, OAT, OAB, IASA, CIT)
and several associated teams and members.
Objectives: Training, Research, and Networking
Added value beyond existing collaborations.
Supported with financial contributions for travel and young researchers (11 positions).

General information

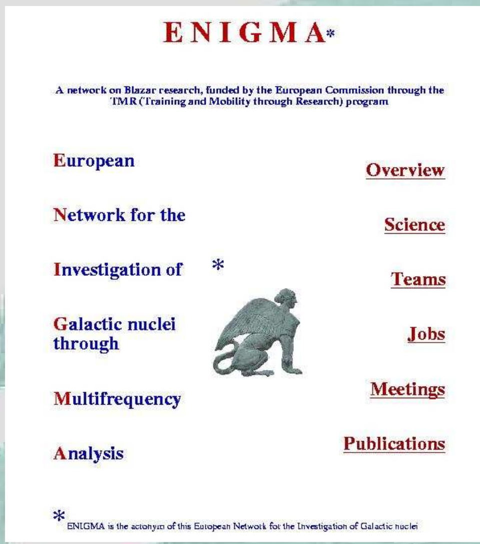

ENIGMA*

A network on Blazar research, funded by the European Commission through the TMR (Training and Mobility through Research) program

European

Network for the

Investigation of

Galactic nuclei through

Multifrequency

Analysis

Overview

Science

Teams

Jobs

Meetings

Publications

* ENIGMA is the acronym of this European Network for the Investigation of Galactic nuclei

- WWW
  http://www.lsw.uni-heidelberg.de/enigma.html
- Linked pages:
  enigmavac.html
  enigmasci.html
- Comments, corrections, and additions welcome.
- On-line editing at this meeting (see Peter Strub)

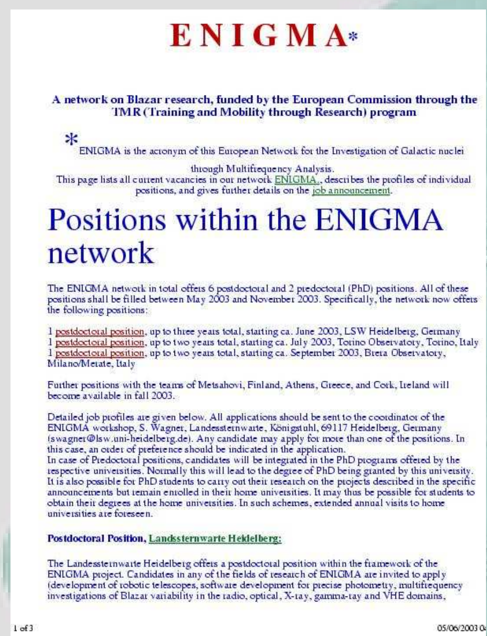

ENIGMA*

A network on Blazar research, funded by the European Commission through the TMR (Training and Mobility through Research) program

* ENIGMA is the acronym of this European Network for the Investigation of Galactic nuclei through Multifrequency Analysis.

This page lists all current vacancies in our network ENIGMA., describes the profiles of individual positions, and gives further details on the job announcement.

Positions within the ENIGMA network

The ENIGMA network in total offers 6 postdoctoral and 2 predoctoral (PhD) positions. All of these positions shall be filled between May 2003 and November 2003. Specifically, the network now offers the following positions:

1 postdoctoral position, up to three years total, starting ca. June 2003, LSW Heidelberg, Germany
1 postdoctoral position, up to two years total, starting ca. July 2003, Torino Observatory, Torino, Italy
1 postdoctoral position, up to two years total, starting ca. September 2003, Brera Observatory, Milano/Merate, Italy

Further positions with the teams of Metsahovi, Finland, Athens, Greece, and Cork, Ireland will become available in fall 2003.

Detailed job profiles are given below. All applications should be sent to the coordinator of the ENIGMA workshop, S. Wagner, Landessternwarte, Königstuhl, 69117 Heidelberg, Germany (swagner@lsw.uni-heidelberg.de). Any candidate may apply for more than one of the positions. In this case, an order of preference should be indicated in the application.
In case of Predoctoral positions, candidates will be integrated in the PhD programs offered by the respective universities. Normally this will lead to the degree of PhD being granted by this university. It is also possible for PhD students to carry out their research on the projects described in the specific announcements but remain enrolled in their home universities. It may thus be possible for students to obtain their degrees at the home universities. In such schemes, extended annual visits to home universities are foreseen.

Postdoctoral Position, Landssternwarte Heidelberg:

The Landessternwarte Heidelberg offers a postdoctoral position within the framework of the ENIGMA project. Candidates in any of the fields of research of ENIGMA are invited to apply (development of robotic telescopes, software development for precise photometry, multifrequency investigations of Blazar variability in the radio, optical, X-ray, gamma-ray and VHE domains,

1 of 3 05/06/2003 0

Homepage: ENIGMA - Mozilla

File Edit View Go Bookmarks Tools Window Help

http://www.lsw.uni-heidelberg.de/~swagner/enigmasci1.html#science Search

Home Bookmarks The Mozilla Or... SuSE - The Lin...

Science

The science activities of this network are addressed in six different research themes. They are closely connected to each other. While all of the empirical themes drive the requirements of the hardware/software theme, the empirical projects aim at maximizing efficiency by teaming up observational resources and coordinated campaigns. The two theoretical themes have many links among themselves and obvious connections to the three empirical subjects.

1) Towards automated, fast, and accurate photometry:

Currently most optical monitoring programs are run by observers specifying individual exposures, achieving accuracies of about 1% with sampling times of a few 100 to 10 000 sec. In order to improve quality and quantity of optical monitoring the network aims at determining a better understanding of the parameters that affect the quality of the photometry of point sources in differential photometry and implementing programs that allow measurements with accuracies close to the photon flux limit. In parallel it aims at an assessment of the technological requirements for robotic telescopes and practical implementation of a network of robotic telescopes that shall be operated by several teams of the network.
Convener: N. Smith, CIT, Ireland, Depute: S. Wagner, LSW, Germany

2) Separating intrinsic and extrinsic Intraday Variability:

Nearly 15 years ago rapid radio variability was discovered. Fast changes of flux density could be due to interstellar scattering, but would then be restricted to low radio frequencies. If they are intrinsic in nature, very high apparent brightness temperatures are required. Both explanations are linked, and it is important to separate intrinsic effects from interstellar scintillation to determine plasma properties and radiation mechanisms of intrinsic IDV and to make use of RISS induced variability as an ultra-high resolution interferometer. The network plans to follow several routes to separate intrinsic and extrinsic effects: We intend to carry out several pioneering experiments involving monitoring at cm, sub-mm, IR, and optical frequencies to separate the role of interstellar scintillation (which would be negligible in the sub-mm regime), followed by the implementation of observing strategies for optimized dedicated programs which will be possible using large-scale European facilities. A second attempt aims at determining brightness temperatures at optical and IR wavelengths from very fast optical fluctuations.
Convener: C. Raiteri, OAT, Italy, Depute: A. Witzel, MPIfR, Germany

3) Radiation processes at high energies:

Coordinated multi-frequency monitoring is an essential for the understanding of radiation mechanisms. The high-energy end of the synchrotron branch and the Compton-scattered emission are of special importance. The network shall develop efficient techniques for the long-term operation of a network of robotic stations. First steps include the establishment of an archive, and development of efficient statistical tools for detailed analysis of variability data. It will set up strategies for coordinated long-term monitoring programs, which will be used to carry out such long-term simultaneous observations in parallel with the European Missions AGILE and INTEGRAL and which will act as a trigger to the European TeV facilities HESS and MAGIC. Detailed studies shall be carried out for periods of about two weeks together with XMM, INTEGRAL, and ground-based Cerenkov telescopes about twice a year on sources of different overall properties. The results of short-term and long-term monitoring will be used to improve our understanding of radiation mechanisms and particle acceleration in different environments.

We plan to arrange and carry out coordinated multi-frequency campaigns, making use of the first-time availability of a complete wavelength coverage, including radio-, mm-, near-IR, optical, X-ray, and gamma-ray instrumentation.
Convener: L. Takalo, Tuorla, Finland, Depute: S. Wagner, LSW, Germany

4) Variations of Source Structure and Flux:

Imaging studies at high resolution are only possible in the radio domain. They exhibit structure on all linear scales that have been probed so far. Substructure on small scales is obviously associated with variability on time scales comparable to the travel time through the source. The details of this relation are linked to the kinematics of substructure in the jets, and hence with the MHD properties. They can best be explored in the overlapping region where the fastest changes in structural variations correspond to well-sampled long-term flux-density monitoring. This requires a dramatic increase in sampling rate and dynamic range of VLBI campaigns. We intend to carry out a pioneering experiment to determine optimum strategies for several campaigns. In parallel we plan to set up an international data-base for well-sampled sources in parallel with long-term studies.

We want to combine the existing data sets in the different institutions which have been acquired to study long term variations. Combinations of these data will provide a much denser coverage and enable us to study the low-frequency end of the important fast variations. We want to exploit the huge data-base assembled by several of the teams on the peculiar object OJ 287, which is the best case known for periodic variability. The origin of the periodicity is unknown but likely to hold important clues to quasar variability in general.
Convener: A. Witzel, MPIfR Bonn, Germany, Depute: M. Tornikoski, HUT, Finland

References: A. Zensus, 1997, Ann. Rev. Astron. Astrophys., 35, 607.

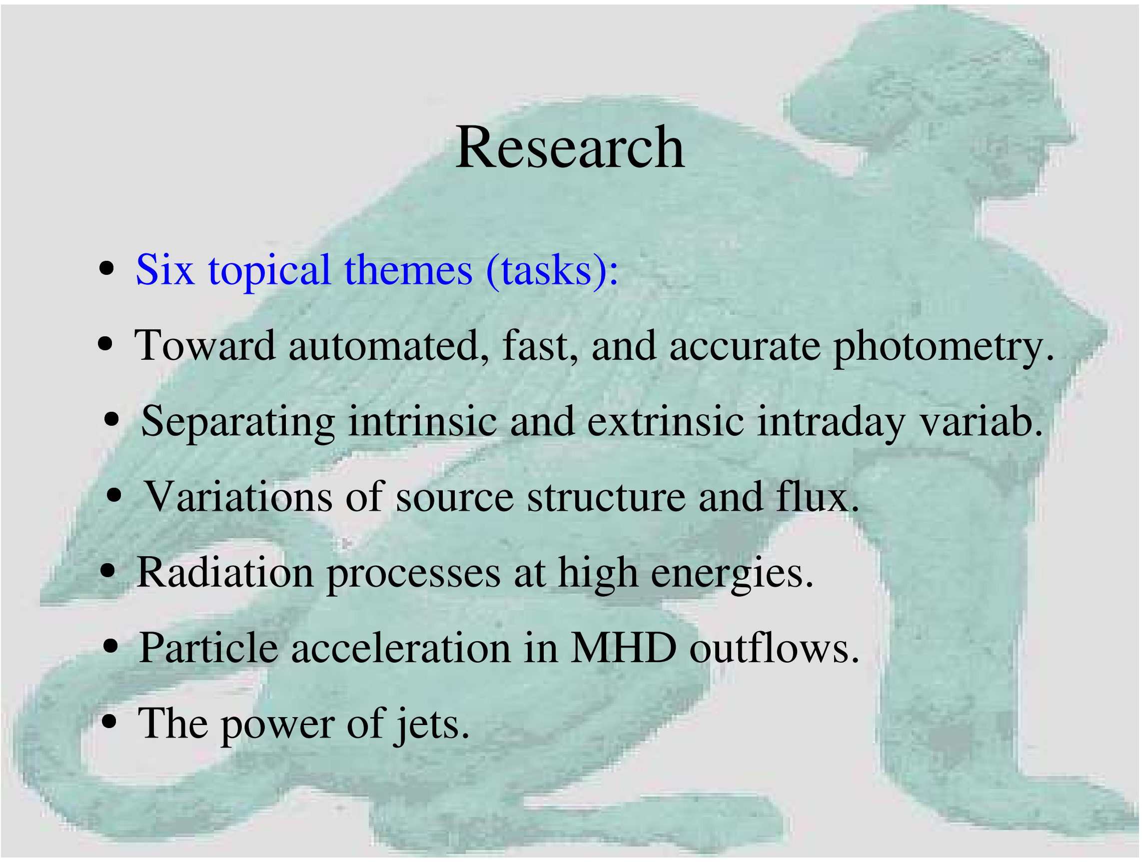
Research
• Six topical themes (tasks):
• Toward automated, fast, and accurate photometry.
• Separating intrinsic and extrinsic intraday variab.
• Variations of source structure and flux.
• Radiation processes at high energies.
• Particle acceleration in MHD outflows.
• The power of jets.

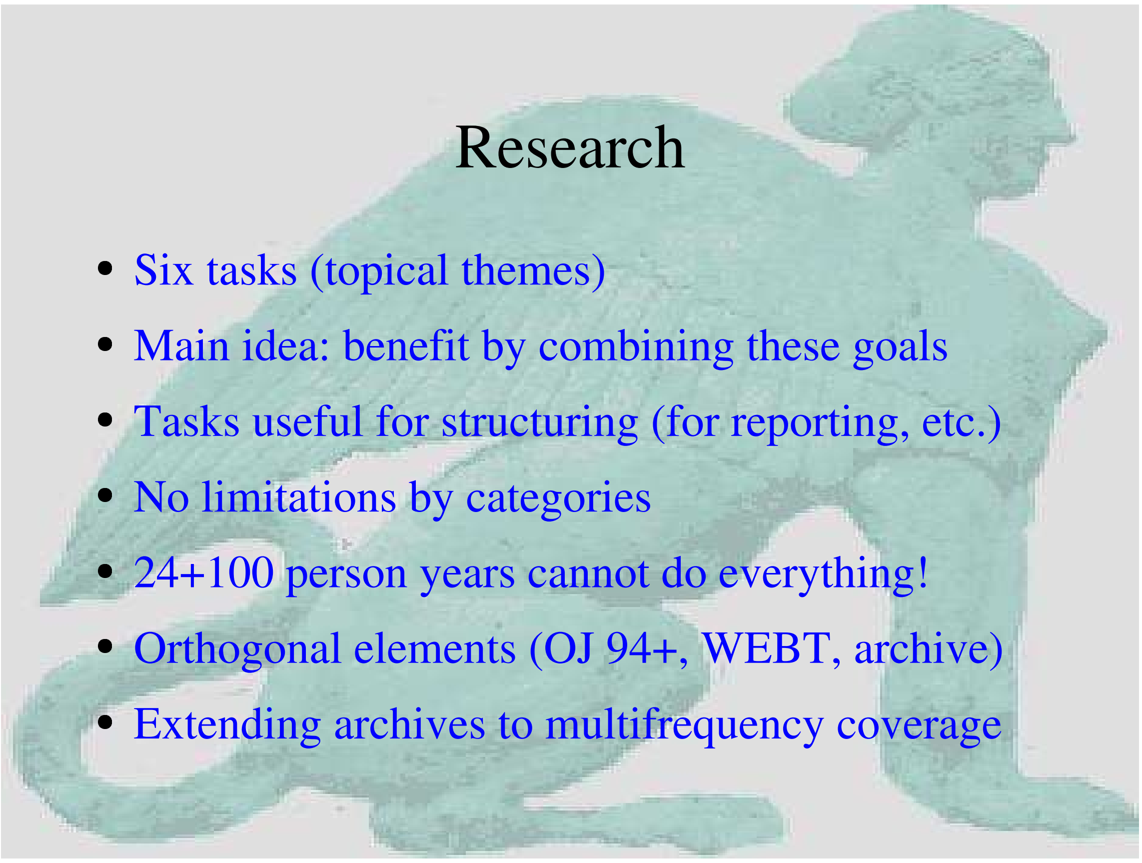
Research
• Six tasks (topical themes)
• Main idea: benefit by combining these goals
• Tasks useful for structuring (for reporting, etc.)
• No limitations by categories
• 24+100 person years cannot do everything!
• Orthogonal elements (OJ 94+, WEBT, archive)
• Extending archives to multifrequency coverage

Training

- EC targetting for ENIGMA students/postdocs.
- Other students/postdocs of teams shall profit also.
- Participation in local PhD and postgrad programs.
- Two specific ENIGMA training schools.
- Eight ENIGMA team meetings (3+4 days).
- Exchange programs/visits within network (tasks).
- Cooperative visits at network coordinator team.

Why do we do this?

- Research aims: Variability of AGN (Blazars).
- Multifrequency approach required.
- Single teams cannot cover all bands, epochs, ...
- Collaboration required.
- EC scheme for support (manpower, cooperation) and advice (admin.: EC, science: Alan Marscher)
- 50 researchers in 3.5 years can make an impact!

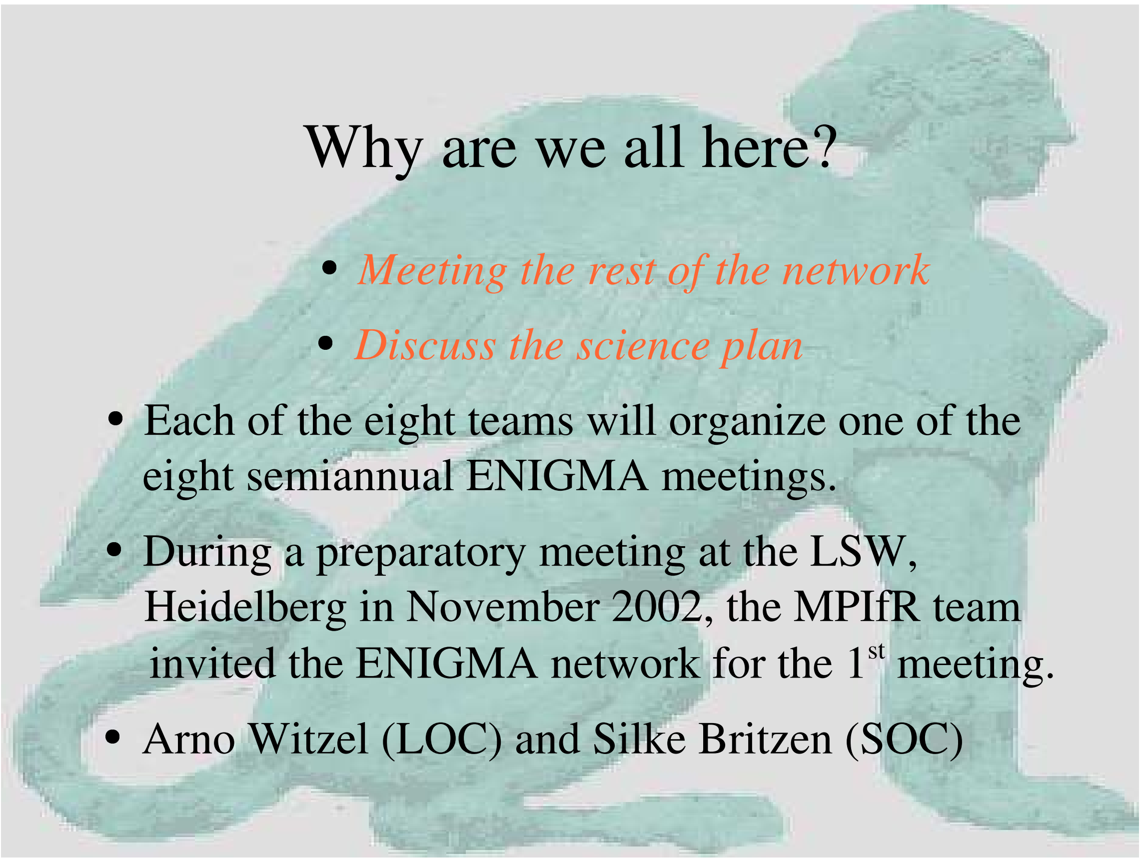
Why are we all here?
• Meeting the rest of the network
• Discuss the science plan
• Each of the eight teams will organize one of the eight semiannual ENIGMA meetings.
• During a preparatory meeting at the LSW, Heidelberg in November 2002, the MPIfR team invited the ENIGMA network for the 1st meeting.
• Arno Witzel (LOC) and Silke Britzen (SOC)

1.1 Task 1: Robotic Telescopes

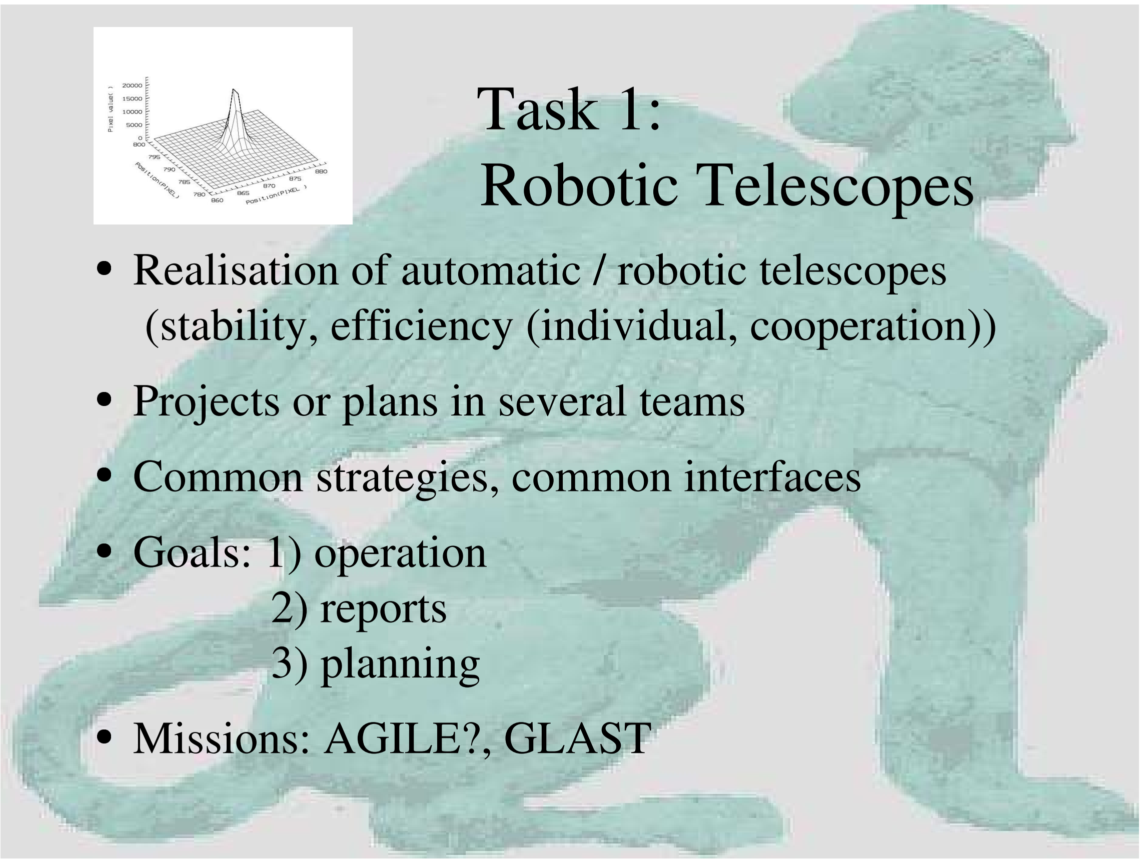

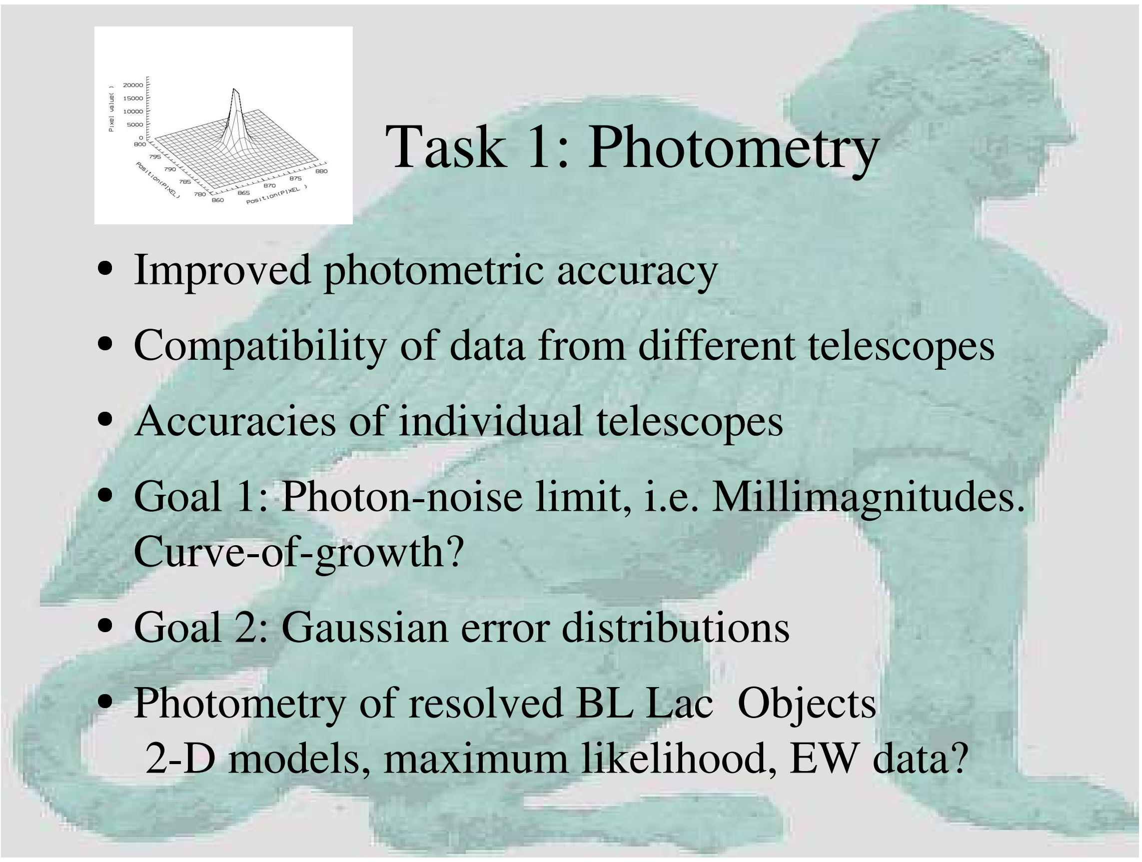
Task 1: Photometry
• Improved photometric accuracy
• Compatibility of data from different telescopes
• Accuracies of individual telescopes
• Goal 1: Photon-noise limit, i.e. Millimagnitudes. Curve-of-growth?
• Goal 2: Gaussian error distributions
• Photometry of resolved BL Lac Objects
2-D models, maximum likelihood, EW data?

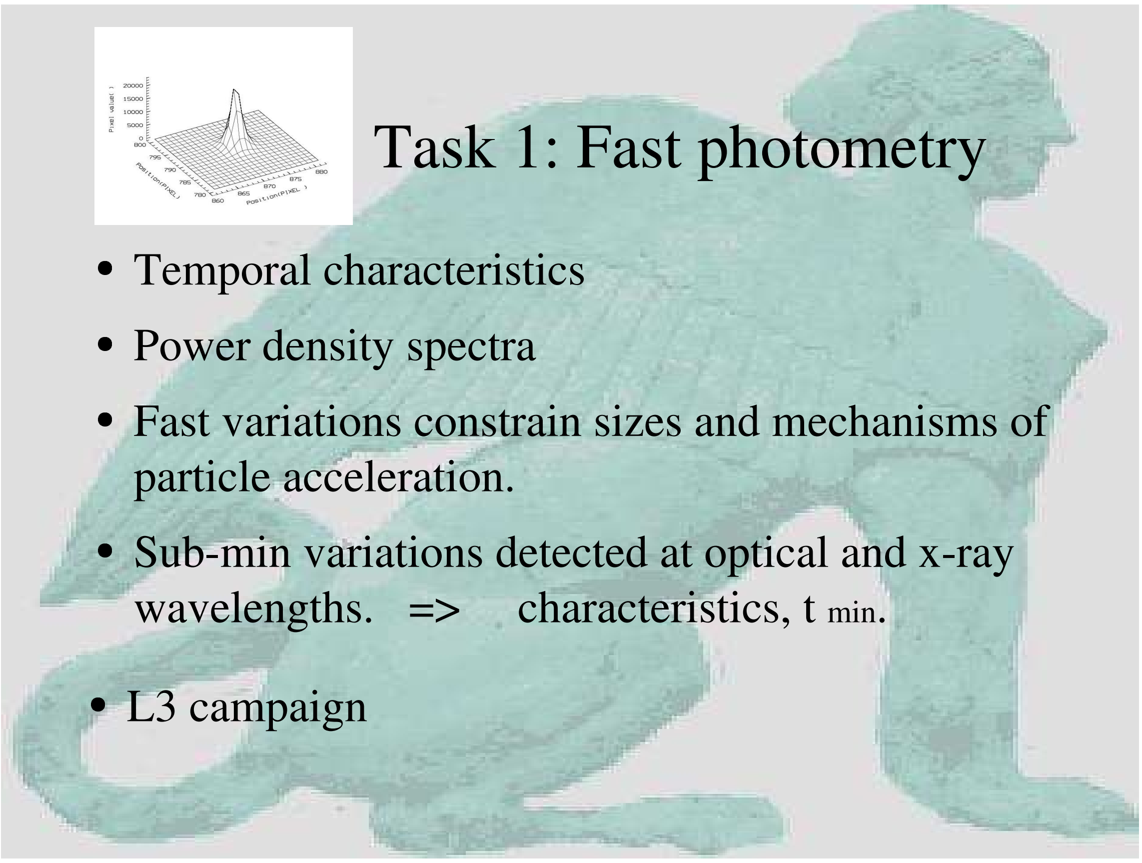
Task 1: Fast photometry
• Temporal characteristics
• Power density spectra
• Fast variations constrain sizes and mechanisms of particle acceleration.
• Sub-min variations detected at optical and x-ray wavelengths. => characteristics, t min.
• L3 campaign

1.2 Task 2: IDV

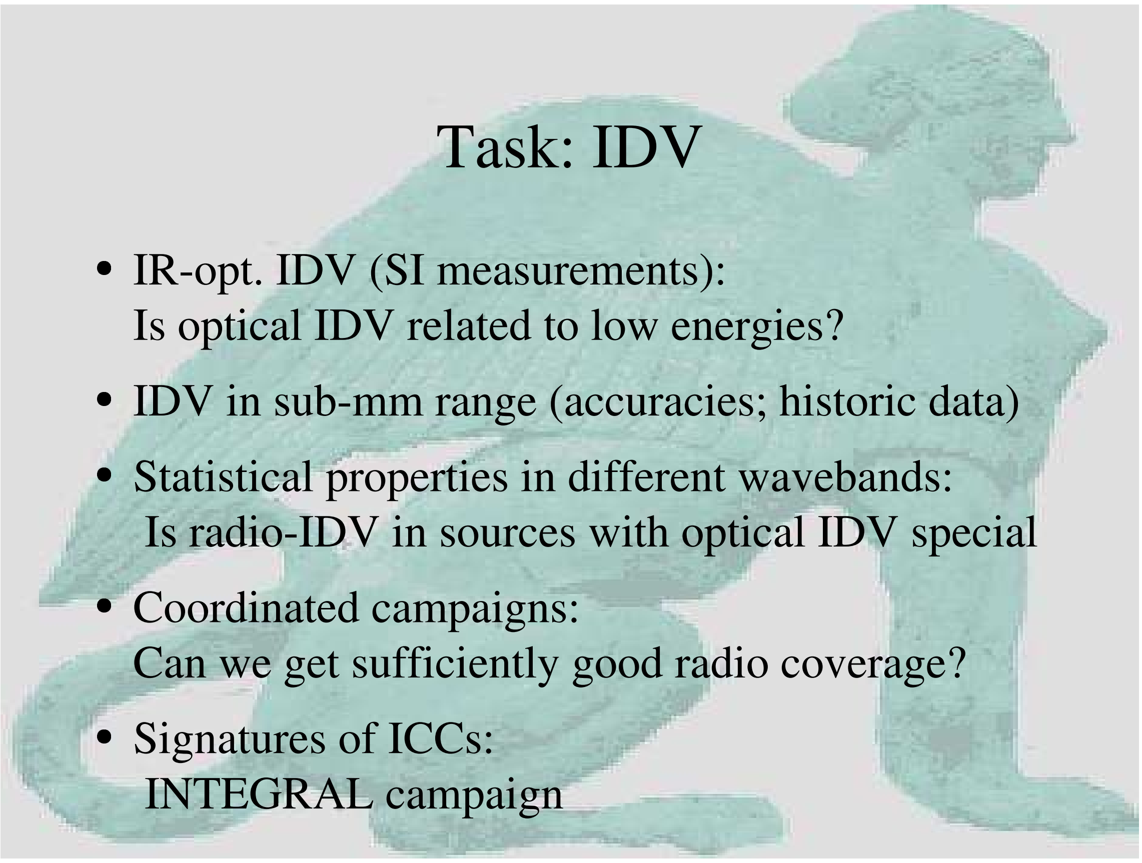
Task: IDV
• IR-opt. IDV (SI measurements):
Is optical IDV related to low energies?
• IDV in sub-mm range (accuracies; historic data)
• Statistical properties in different wavebands:
Is radio-IDV in sources with optical IDV special
• Coordinated campaigns:
Can we get sufficiently good radio coverage?
• Signatures of ICCs:
INTEGRAL campaign

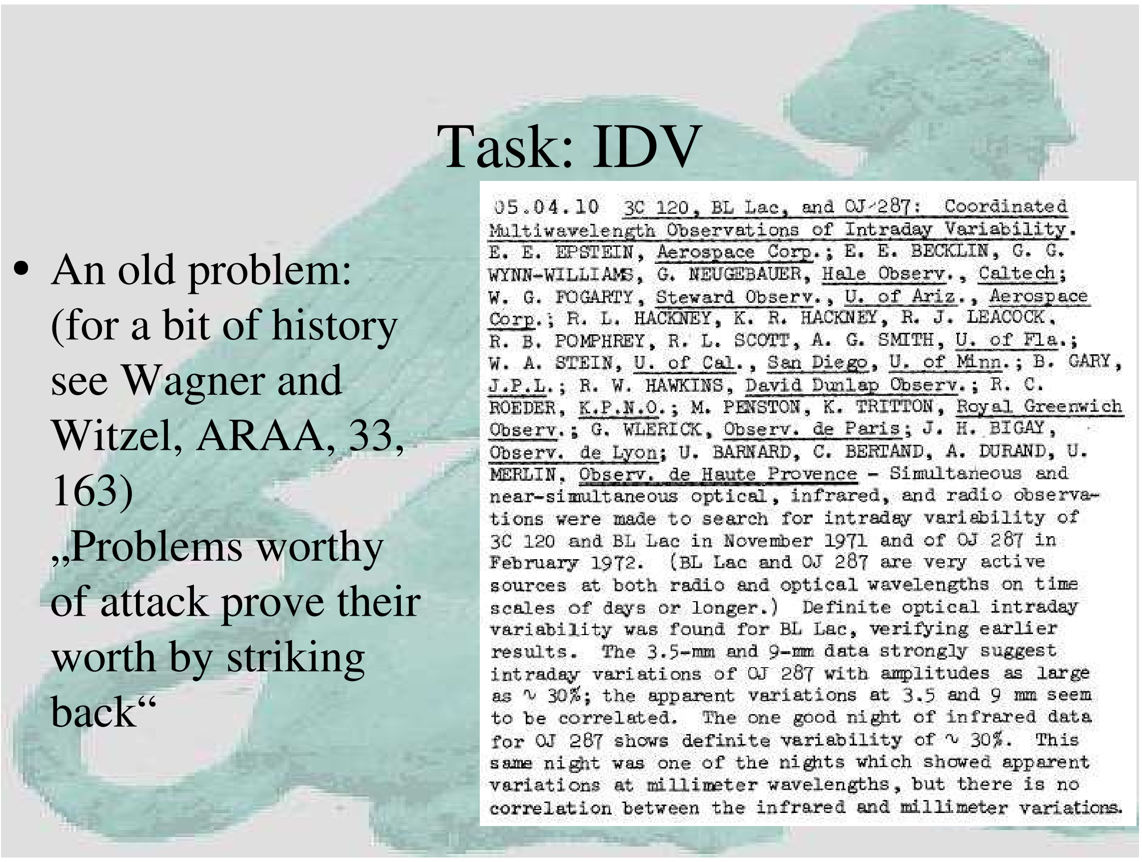

05.04.10 3C 120, BL Lac, and OJ 287: Coordinated Multiwavelength Observations of Intraday Variability. E. E. EPSTEIN, Aerospace Corp.; E. E. BECKLIN, G. G. WYNN-WILLIAMS, G. NEUGEBAUER, Hale Observ., Caltech; W. G. FOGARTY, Steward Observ., U. of Ariz., Aerospace Corp.; R. L. HACKNEY, K. R. HACKNEY, R. J. LEACOCK, R. B. POMPHREY, R. L. SCOTT, A. G. SMITH, U. of Fla.; W. A. STEIN, U. of Cal., San Diego, U. of Minn.; B. GARY, J.P.L.; R. W. HAWKINS, David Dunlap Observ.; R. C. ROEDER, K.P.N.O.; M. PENSTON, K. TRITTON, Royal Greenwich Observ.; G. WLERICK, Observ. de Paris; J. H. BIGAY, Observ. de Lyon; U. BARNARD, C. BERTAND, A. DURAND, U. MERLIN, Observ. de Haute Provence - Simultaneous and near-simultaneous optical, infrared, and radio observations were made to search for intraday variability of 3C 120 and BL Lac in November 1971 and of OJ 287 in February 1972. (BL Lac and OJ 287 are very active sources at both radio and optical wavelengths on time scales of days or longer.) Definite optical intraday variability was found for BL Lac, verifying earlier results. The 3.5-mm and 9-mm data strongly suggest intraday variations of OJ 287 with amplitudes as large as ∿ 30%; the apparent variations at 3.5 and 9 mm seem to be correlated. The one good night of infrared data for OJ 287 shows definite variability of ∿ 30%. This same night was one of the nights which showed apparent variations at millimeter wavelengths, but there is no correlation between the infrared and millimeter variations.

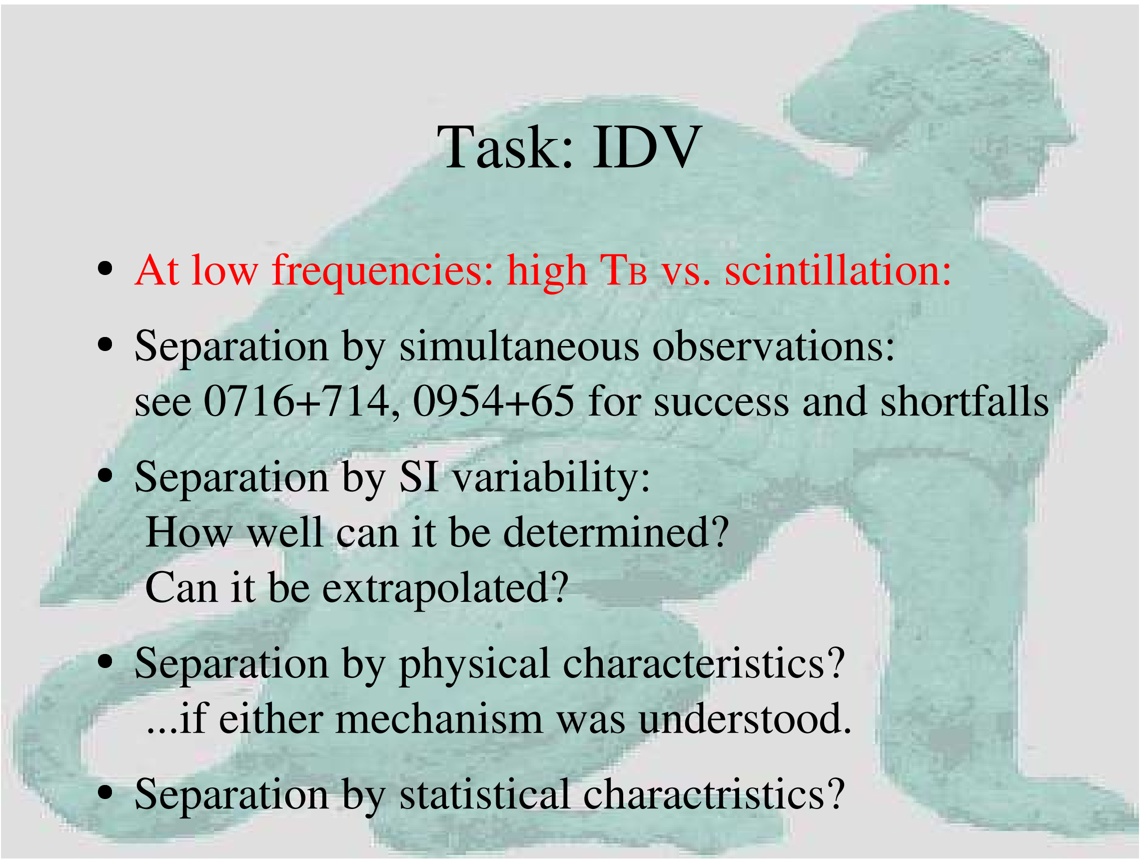

1.3 Task 3: High energy emission

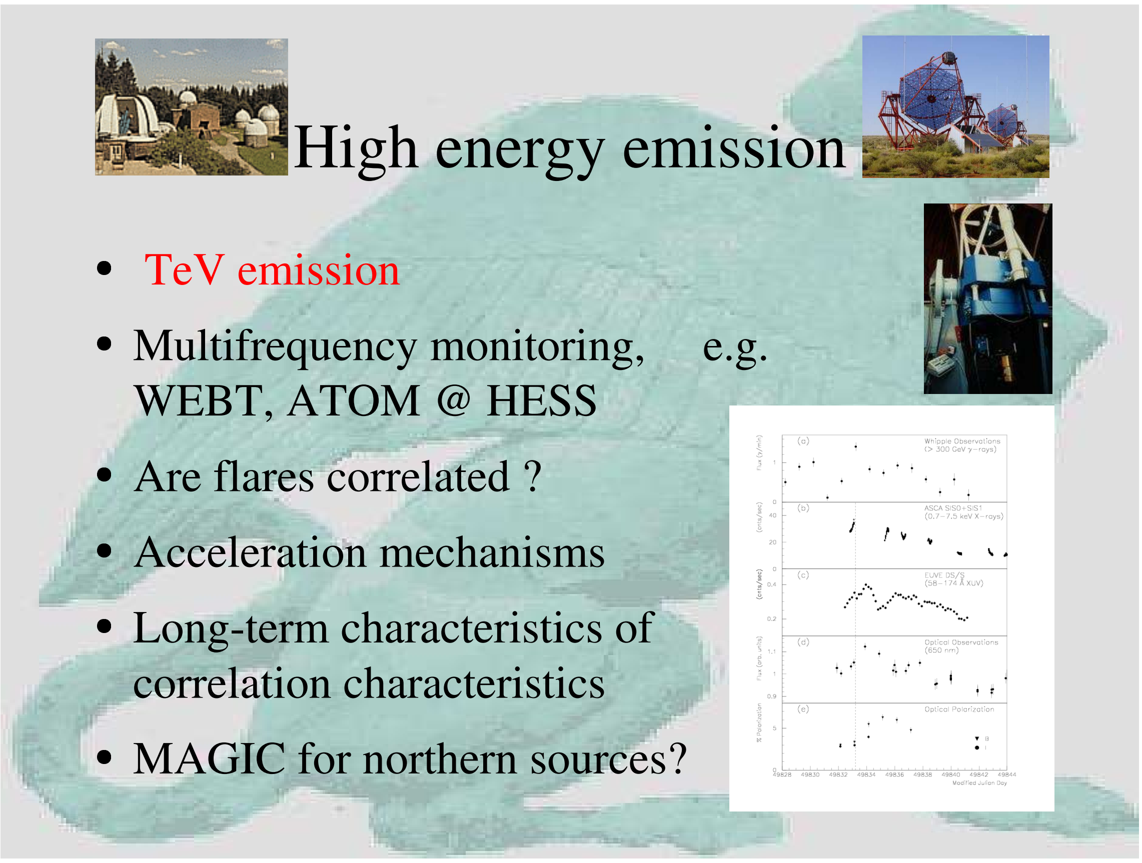

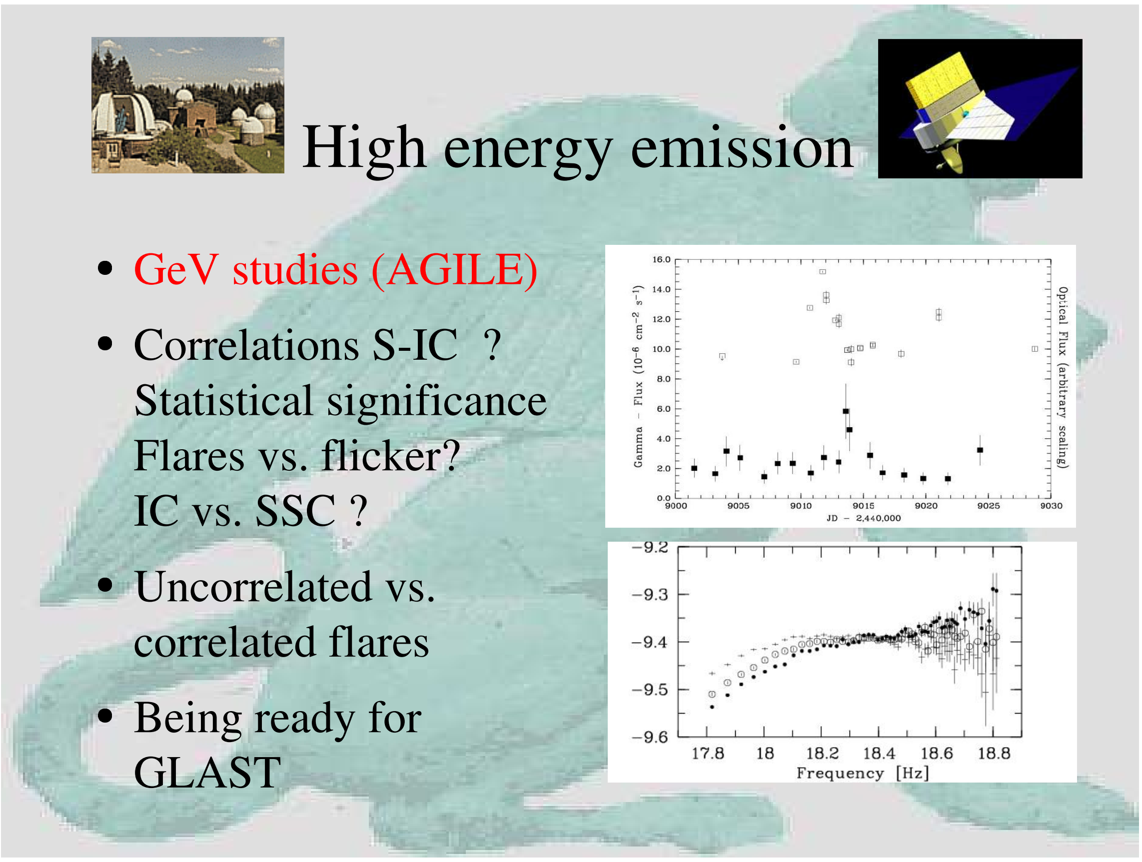
High energy emission
• GeV studies (AGILE)
• Correlations S-IC ?
Statistical significance
Flares vs. flicker?
IC vs. SSC ?
• Uncorrelated vs.
correlated flares
• Being ready for
GLAST
JD – 2,440,000
Optical Flux (arbitrary scaling)
Frequency [Hz]

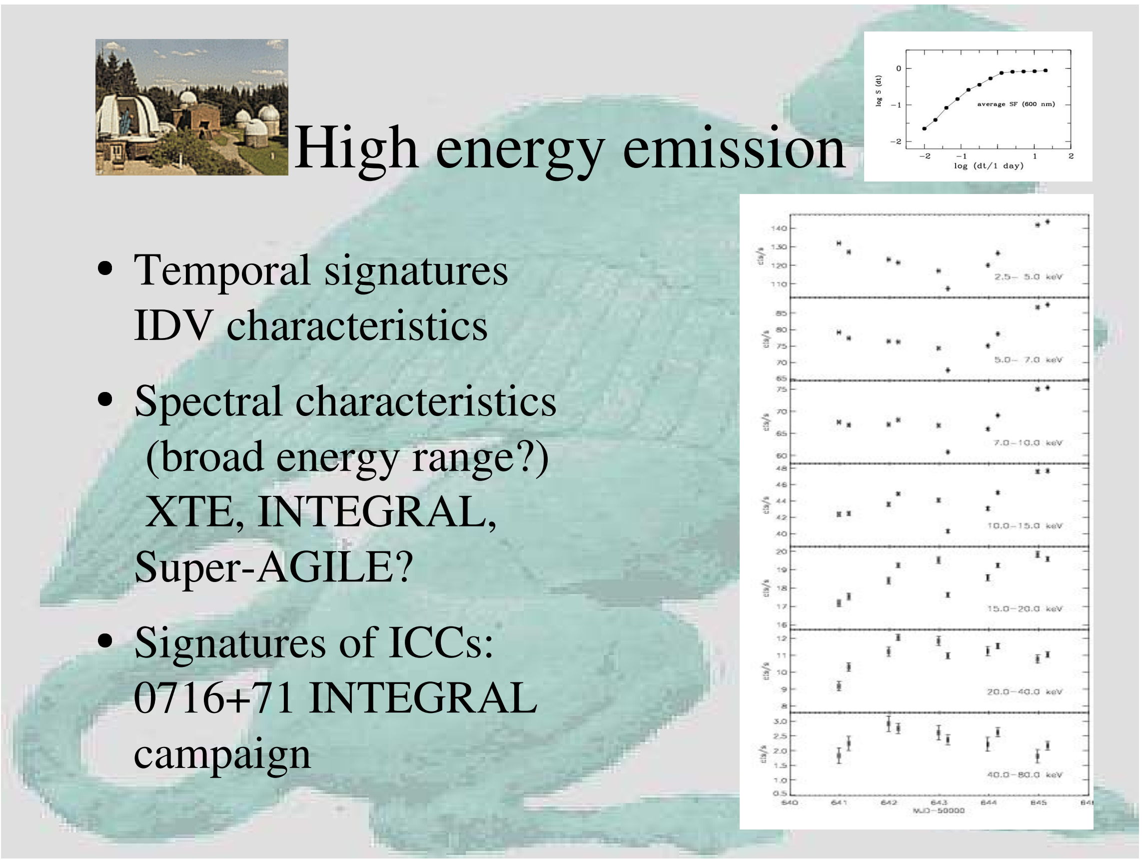
High energy emission
• Temporal signatures
IDV characteristics
• Spectral characteristics
(broad energy range?)
XTE, INTEGRAL,
Super-AGILE?
• Signatures of ICCs:
0716+71 INTEGRAL
campaign
average SF (600 nm)
log (dt/1 day)
MJD–50000

1.4 Team Heidelberg - S. Wagner

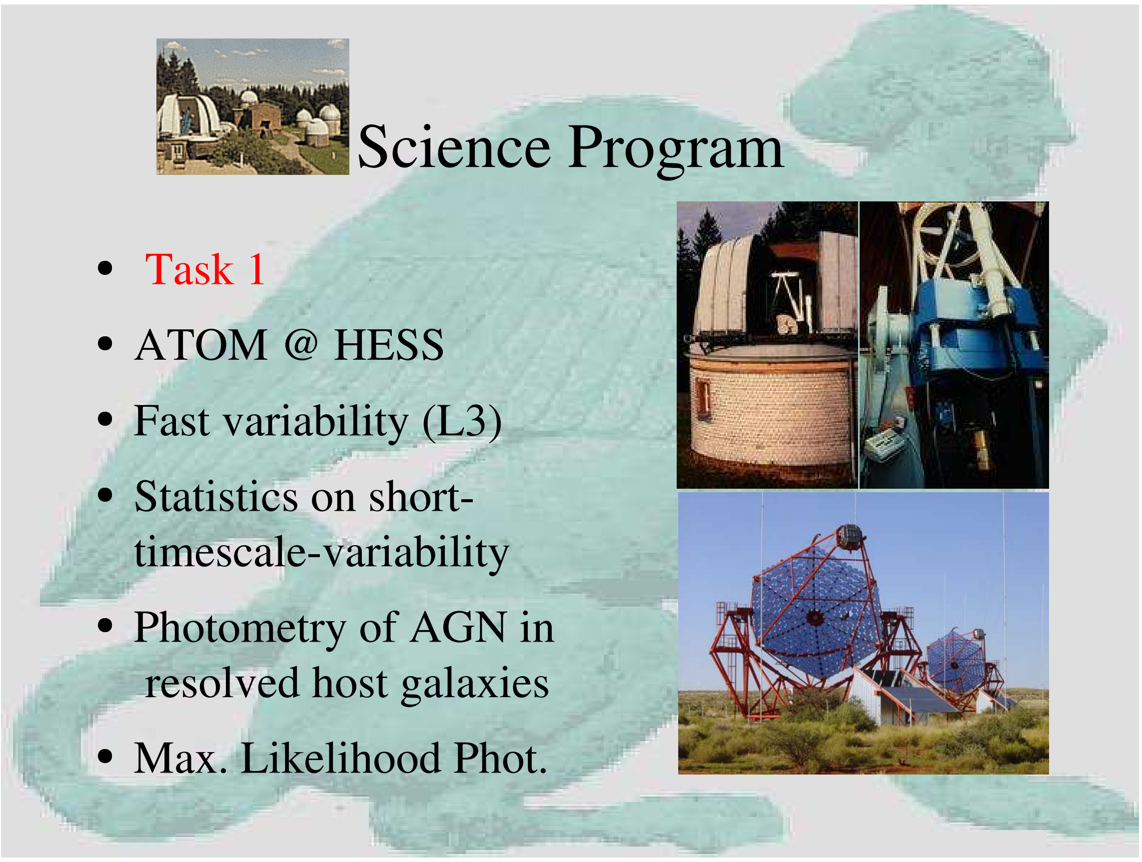
Science Program
• Task 1
• ATOM @ HESS
• Fast variability (L3)
• Statistics on short-timescale-variability
• Photometry of AGN in resolved host galaxies
• Max. Likelihood Phot.

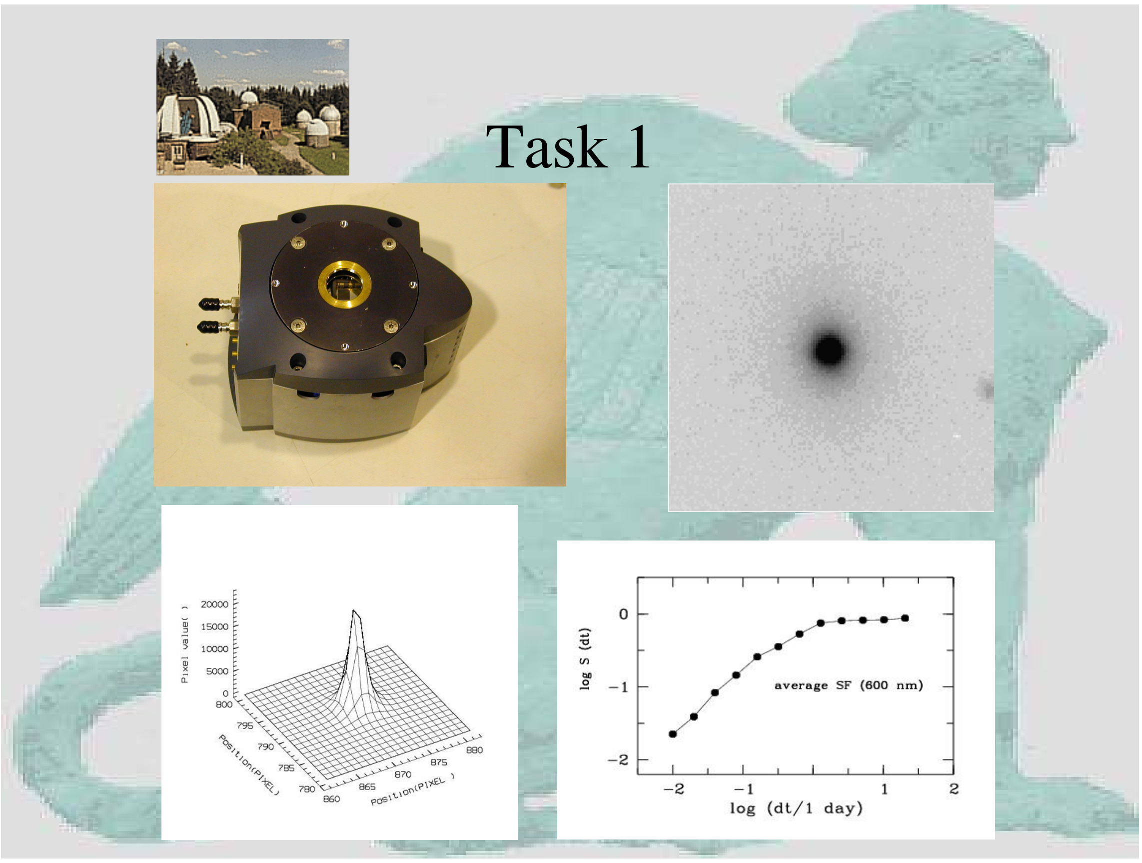
Task 1
Pixel value
Position(PIXEL)
log S (dt)
average SF (600 nm)
log (dt/1 day)

Task: IDV

- IR-opt. IDV (SI)
- IDV in sub-mm range
- Statistical properties in different wavebands.
- Coordinated campaigns???
- Signatures of ICCs
- SB, JH, DK, SW

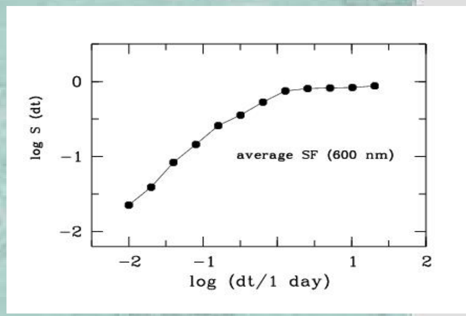

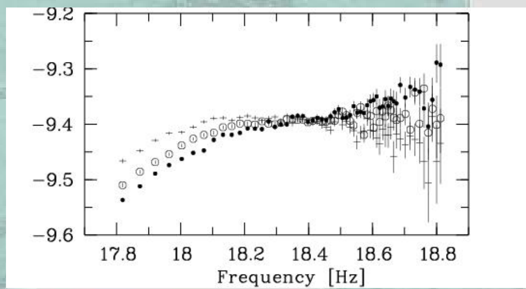

Task: Variations of structure and flux

- Special presentation (Silke Britzen)
- Very fast variations of source structure?
- Correlations indicative of variable boosting in curved jets?
- Core flares/jet flares?
- SB, SW

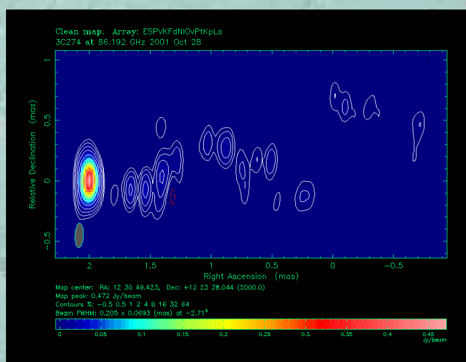

M87, T.P. Krichbaum, priv. comm.

Task: H.E. emission

- TeV studies (HESS)
- Synch-IC correlations in TeV sources
- ICC studies with INTEGRAL
- Un- vs. correlated flares (AGILE)
- SB, MH, GP, JH, SW

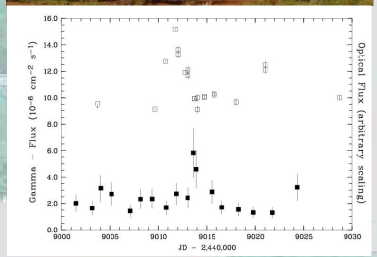

Task: Particle acceleration

- Acceleration time scales
  Comparison to shortest time-scales in blazars.
- Sizes of acceleration zones.
  Travel time vs. Acceleration time (scaling?)
- Do losses determine the maximum energy?
  Secular changes in individual objects?
- Alternatives to diffusive acceleration?
- DE, JK, PS, SW

The power of jets

- Separate presentation
- (Max Camenzind)
- Where do radiative losses (variability) dominate?
  Distances of flaring regions from the nucleus
- Variability in FR I and FRII sources
  amplitudes, time-scales, max. energies, rates as function of jet-power?
- MC (+), JK, PS, SW

Contacts:

- Automated, fast, ... photometry: Marcus Hauser
- IDV: Jochen Heidt
- Flux and structure: Silke Britzen
- Radiation processes @ H.E.: Gerd Pühlhofer
- Particle acceleration: John Kirk
- The power of Jets: Max Camenzind

some of this will change (ENIGMA personnel)

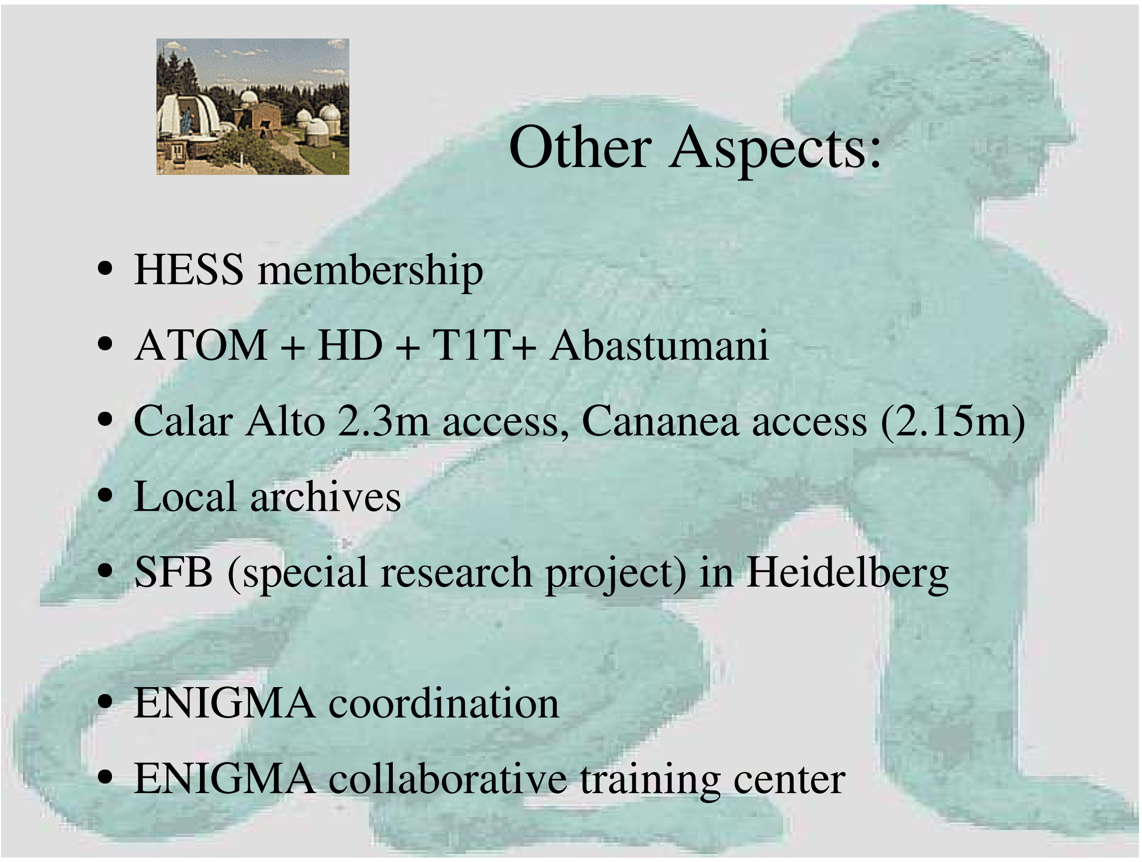
Other Aspects:
• HESS membership
• ATOM + HD + T1T+ Abastumani
• Calar Alto 2.3m access, Cananea access (2.15m)
• Local archives
• SFB (special research project) in Heidelberg
• ENIGMA coordination
• ENIGMA collaborative training center

1.5 Team Bonn - A. Witzel (oral)

1.6 Team Tuorla - L. Takalo

Tuorla AGN Science Program

Participants:
Scientists: Kari Nilsson, Markku Lainela, Tapio Pursimo (NOT), Aimo Sillanpää, Leo Takalo, Esko Valtaoja, Kaj Wiik

Students:
PhD: Elina Lindfors, Mikko Pasanen, Tuomas Savolainen, Joni Virtanen
MsC: Elina Nieppola, Pia-Maria Saloranta

Degrees obtained:
PhD: Kari Nilsson 1997
Harri Pietilä 1999
Tapio Pursimo 2000
Seppo Wiren 2000
Kaj Wiik 2002

MsC: Mari Hanski 2000
Tuomas Savolainen 2001
Joni Virtanen 2002
Tiina Schafeitel 2002
Elina Lindfors 2003
Mikko Pasanen 2003

Science:

1. **Monitoring programs**

Tuorla 1m telescope (BV)R ST1001E
Monitoring since 1980.
KVA: ST8 UBVRI. Apogee CCD with B,R,WL polarization. Automation in progress!

Multifrequency Campaigns:

Have taken part in several campaigns, involving satellites and TeV-telescopes.
MAGIC, INTEGRAL
Full member of MAGIC Collaboration since 2002.
Co-investigators in several INTEGRAL AGN programs.

2. **Host galaxies of BL Lac objects**

1Jy sources, RGB objects (100 sources).

3. **RAFI:**

Identifying RASS-FIRST sources.

4. **OJ 287:**

Last outburts 1994/95. Next outburts 2006/07!!!

5. **Modelling and Theory**

Started together with Bochum University team and with Marc Türler from INTEGRAL Science Center.

6. **Planck satellite**

1.7 Team Metsähovi - M. Tornikoski

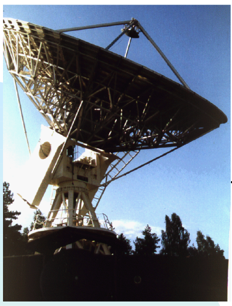

Metsähovi Radio Observatory

Metsähovi / HUT

- Operated by the Helsinki University of Technology.

- 13.7 m dish.
- 22, 37 (+ 90) GHz.
- No open time for other observers --> time consuming projects possible.
- Small AGN group, close collaboration with Tuorla scientists.

Merja Tornikoski
Metsähovi Radio Observatory

AGN Science: Team

Dr. Merja Tornikoski:
Radio/submillimetre variability
Southern sources
Multifrequency studies
Planck extragalactic foregrounds

Dr. Anne Lähteenmäki:
Radio to high-E connections
Planck extragalactic foregrounds

Ilona Torniainen:
Inverted-spectrum radio sources etc.

Mikko Parviainen:
Planck Quick Detection System

+ undergrad. students working part-time (observations and thesis projects)

+ Dr. Markku Lainela (Tuorla):
SEST observations, Southern sources

Merja Tornikoski
Metsähovi Radio Observatory

Science: Radio / high-E

- Activity in radio related to high-E?
- Emission mechanisms, constraints.
- Why are some radio-loud AGNs detected in gamma and some are not?
- Why are some gamma blazars not always detected in gamma?
- What are the unidentified extragalactic gamma-ray sources?

Merja Tornikoski
Metsähovi Radio Observatory

Science: Planck extragalactic foreground

- Inverted-spectrum radio sources
  - "Genuine GPS sources", other inverted-spectrum sources, extreme GPS sources, etc.
  - Contribution to high radio f (Planck foreground).
  - Unification models.
- Radio properties of BL Lacertae Objects
  - Radio-selected -- IBL -- X-ray selected.
  - Radio-quiet BLOs?
  - Variability, contribution to high radio f.

Merja Tornikoski
Metsähovi Radio Observatory

... Planck extragalactic foreground

- Models for the radio variability in AGNs
  - Timescales, amplitudes, superposed flare components, connection to VLBI components.
  - Shock models for radio variability.
  - "Predictions" or educated guesses about the variability state (e.g., for Planck).
  - Planck quick-time detection system (QDS) s/w and related tools + science (simulation s/w, source catalogs, models).

Merja Tornikoski
Metsähovi Radio Observatory

Science: Radio / Optical

- When are radio and optical emission correlated, when not?
  (different kinds of flares,
  different kinds of sources, ...)
- Can we predict a correlation [from previous observations]?
- Constraints on models.

Merja Tornikoski
Metsähovi Radio Observatory

Most of our activities are related to ENIGMA science themes:

- 4. Variations of Source Structure and Flux.
- 3. Radiation Processes at High Energies.
- 2. Separating Intrinsic and Extrinsic Intraday Variability.

Merja Tornikoski
Metsähovi Radio Observatory

1.8 Team Torino - C. Raiteri

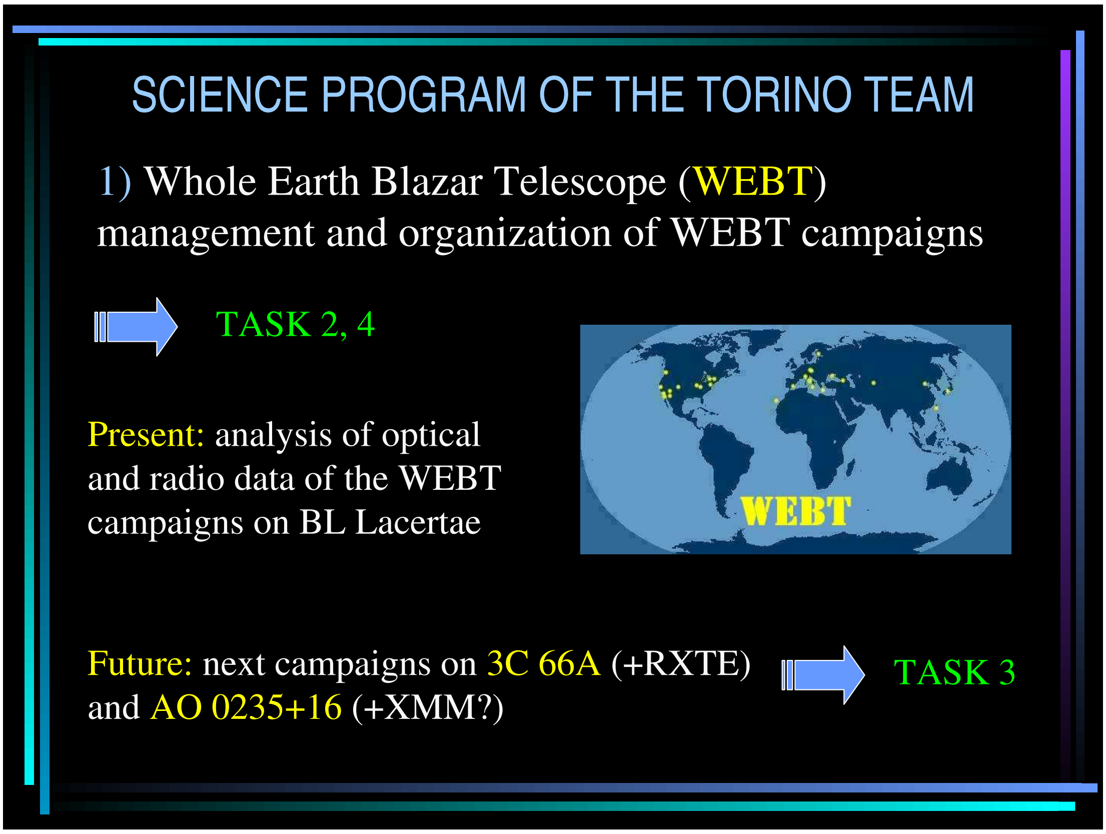

2) Optical photometric monitoring of blazars with the 1.05 m REOSC telescope of the Torino Observatory – soon (!?) robotic

TASK 1, 4

3) Near-IR observations of OJ 287, 3C 273, 3C 279, PKS 1510 at TIRGO

- Bad weather
- Technical problems
- Soon closed?

4) Optical Spectroscopy ?: proposals submitted to the ESO NTT and to the Telescopio Nazionale Galileo (TNG)

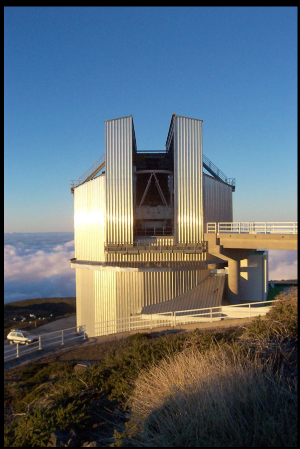

In particular: we asked for a spectroscopic monitoring of AO 0235+16 at TNG to see the relative variation of the continuum and the broad Mg II line strength

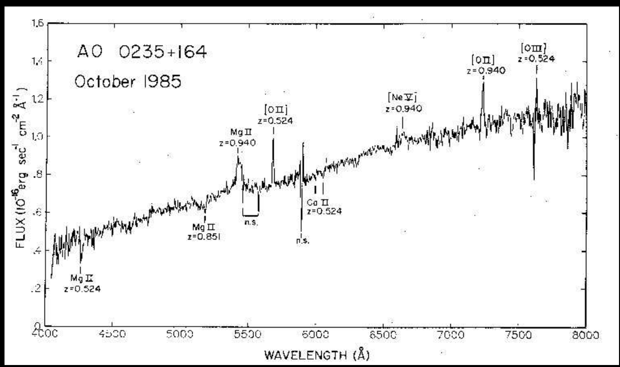

TASK 2, 4

5) Analysis of multifrequency data:

- Spectral behaviour
- Search for characteristic variability time scales/periodicities
- Correlations and time lags

GC 0109+224 ***(Ciprini et al. 2003, A&A 400, 487)***

AO 0235+16 ***(Raiteri et al. 2001, A&A 377, 396)***

S5 0716+71 ***(Villata et al. 2000, A&A 363, 108; Raiteri et al. 2003, astroph)***

ON 231 ***(Tosti et al. 2002, A&A 395, 11)***

BL Lacertae ***(Villata et al. 2002, A&A 390, 407; Villata et al. 2003, in preparation)***

AO 0235+16

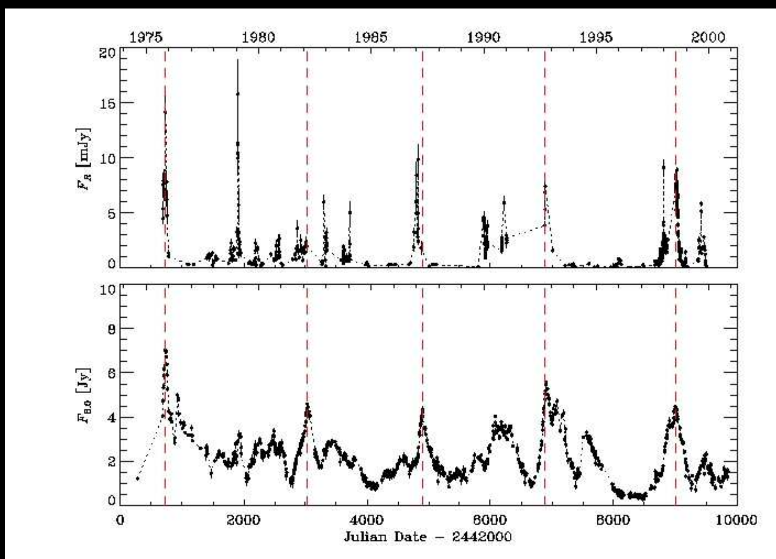

S5 0716+71

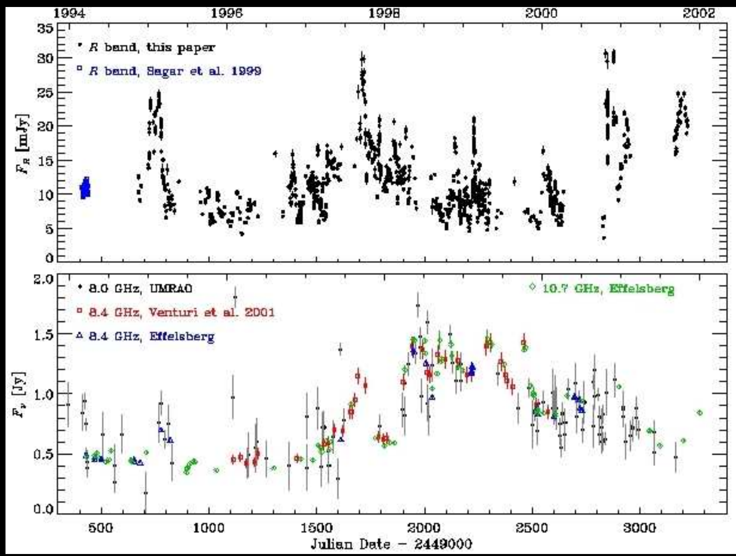

6) Modelling blazar emission variability: the rotating helical jet model

TASK 4

First proposed by Villata & Raiteri (1999; paper 1) to explain the dramatic changes of the Mkn 501 synchrotron component observed by BeppoSAX

Since then we are testing the model on both the low- and the high-energy components for several blazars (paper 2, still in preparation!)

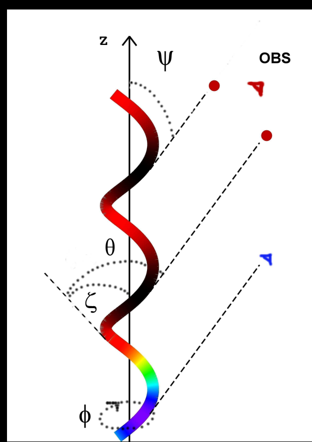

Ostorero 2003– PhD thesis – application to AO 0235+16 SED and light curves

1.9 Team Brera - G. Ghisellini

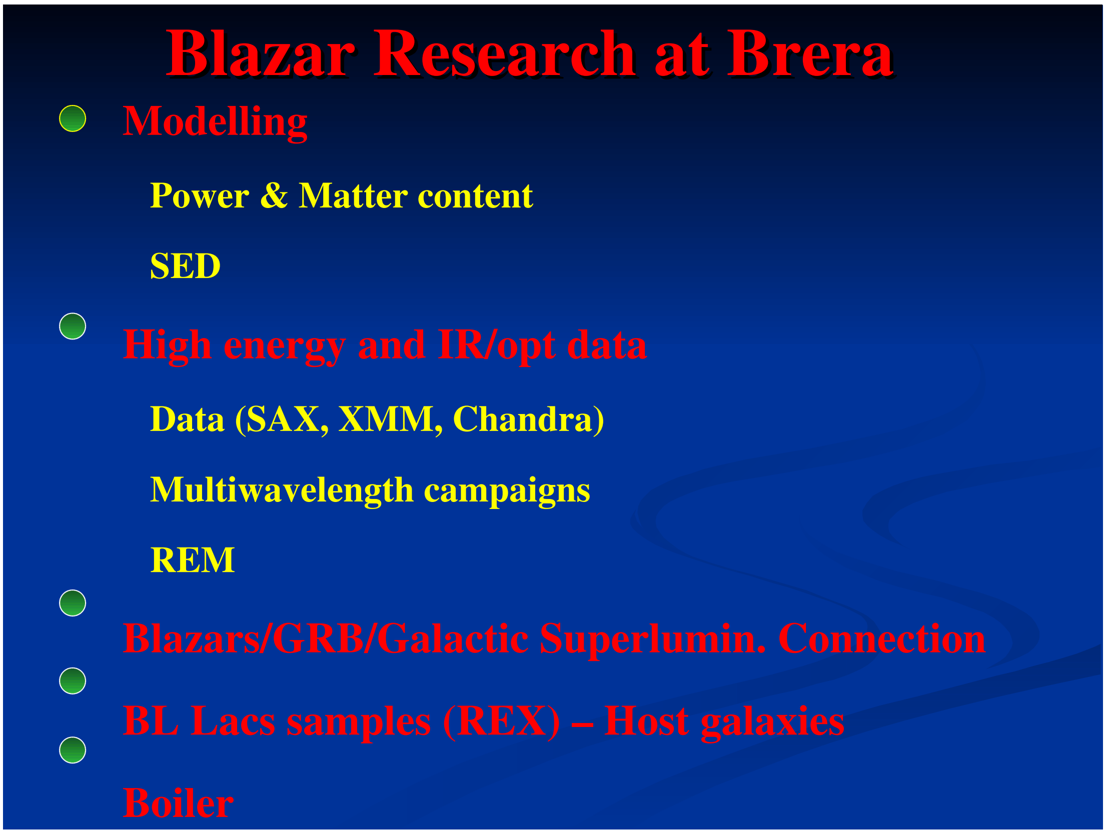

Blazars people at Brera

Laura Maraschi (Director)

Gabriele Ghisellini

Tommaso Maccacaro

Gianpiero Tagliaferri

Aldo Treves (Univ. of Como)

Anna Wolter

Fabrizio Tavecchio (Postdoc)

Boris Sbarufatti (PhD Student)

Marcello Ravasio (PhD Student)

Modelling

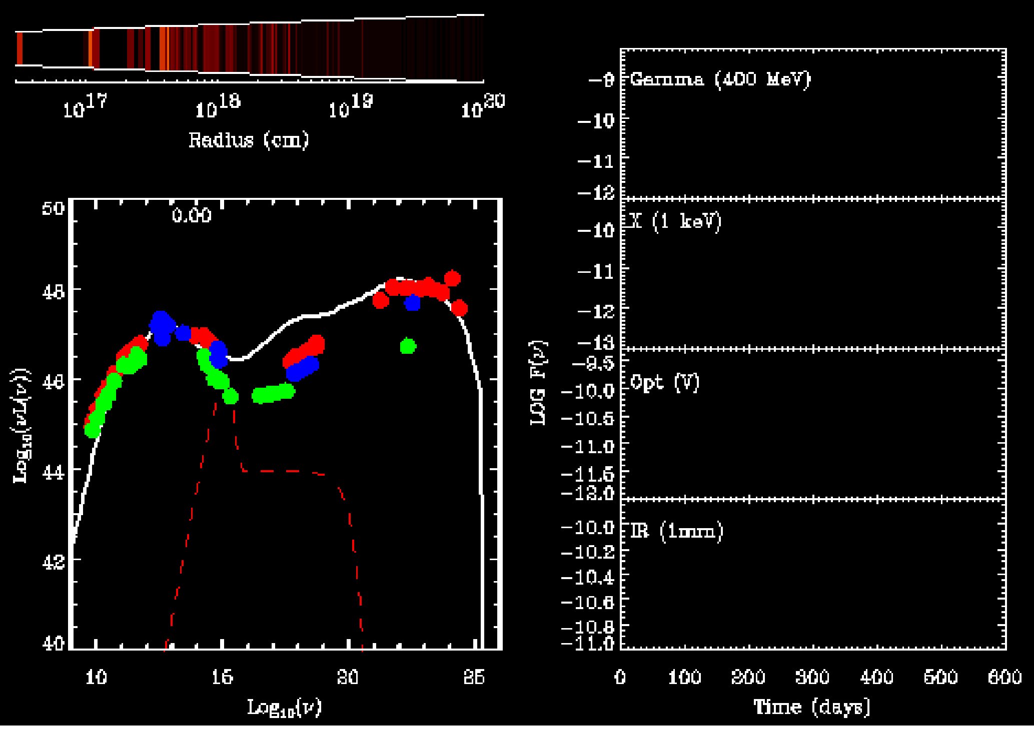

High energy

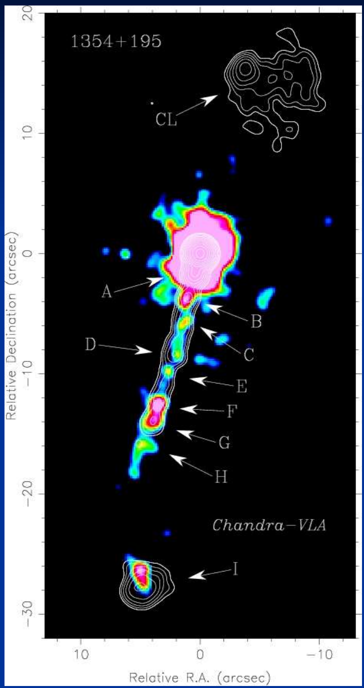

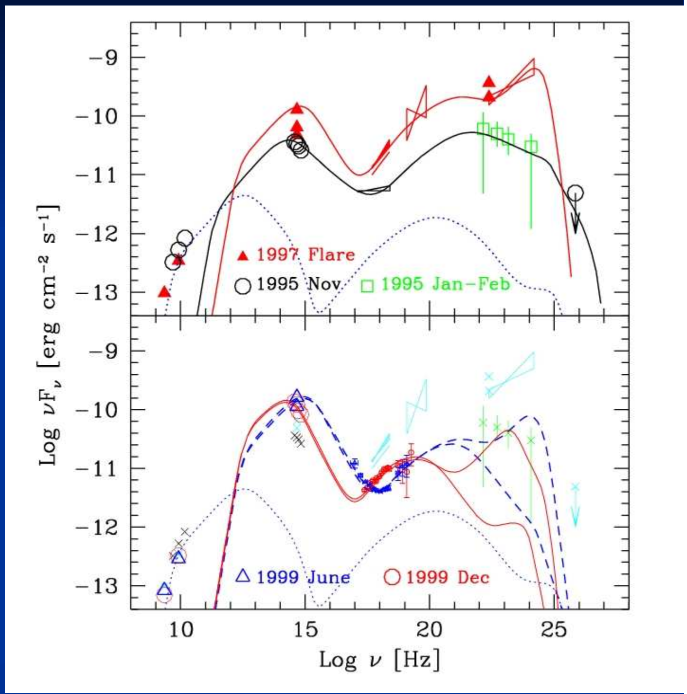

REM: Rapid Eye Mount

Infrared and optical telescope for follow-up of GRBs

Diameter: 60 cm

Fast slewing

Completely robotic

During idle time can observe blazars


REM
ISA - Integration and Site Assistance
Notre Dôme
Happy New Year in La Silla

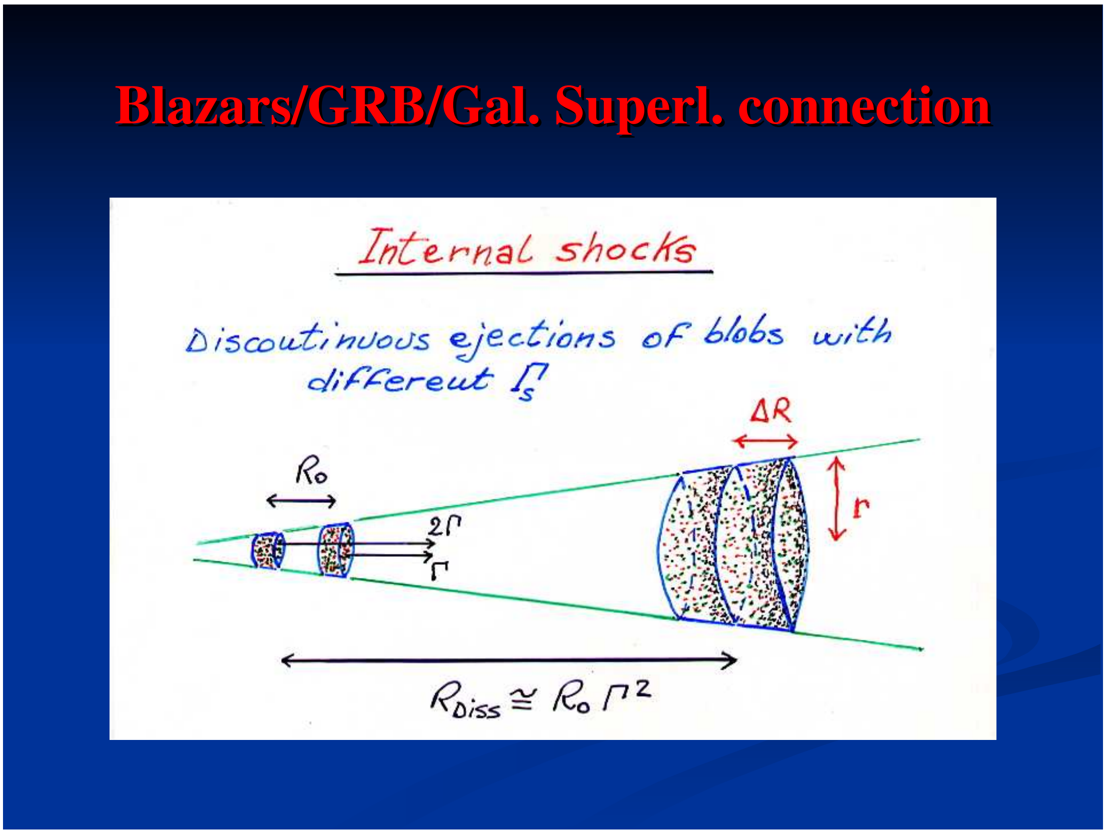
Blazars/GRB/Gal. Superl. connection
Internal shocks
Discoutinuous ejections of blobs with
differeut Γs
ΔR
R₀
2Γ
Γ
r
R_Diss ≅ R₀ Γ²

BL Lac Samples

REX: Radio Emitting X-ray sources

Serendipitous sources from Rosat pointed observations, wavelet algorithm

Cross correlation with radio catalogues

Optical identification of all candidates

Boiler

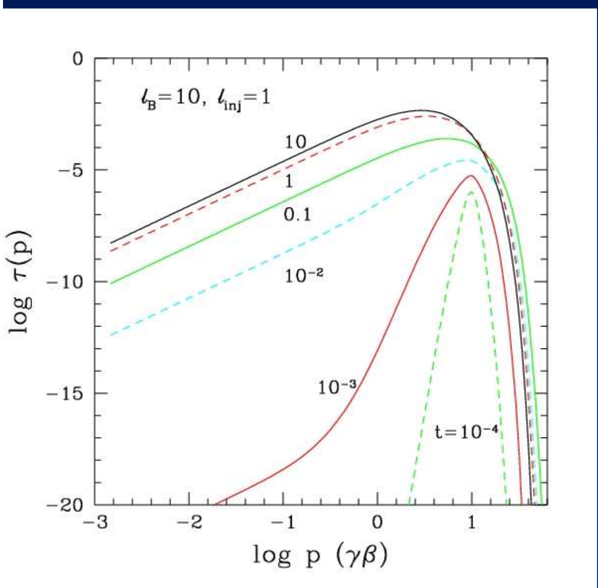

Thermalization of relativistic particles due to emission and absorption of synchrotron radiation

Useful for blazar jets at VLBI scales and beyond

Can it explain the lack of Faraday depolarization?

1.10 Team Athens - K. Tsinganos

ENIGMA RESEARCH AND TRAINING NETWORK
First Annual Meeting

10th -14th May 2003, Mayschoss, Germany

ATHENS/HERAKLION TEAM

INSTITUTE OF ACCELERATING SYSTEMS & APPLICATIONS

I A S A

P.O. Box 17214, GR–10024 ATHENS, GREECE

Team members:

K. Tsinganos, A. Mastichiadis, N. Vlahakis, E. Rokaki
(Section of Astrophysics & Astronomy, Dept. of Physics, Univ. of Athens)
E. Xilouris (National Observatory of Athens)
J. Papadakis (Univ. of Crete, Heraklion)

OBSERVATIONS (Joseph Papadakis, Emmanuel Xilouris, E. Rokaki et al.)

Experience in observing and data reduction with optical telescopes.

Experience in short and medium-term optical variability of AGN by using the 1.3 m telescope of the Skinakas (Crete) observatory to observe Blazars with the aim of studing the intra-night optical variations (study of flux and spectral variations) and also monitoring blazars on a daily basis for a period of a few weeks in order to study their medium-term variations (time scales of days/weeks). Plan to continue this work in the near future as well.

Analysis of HST archival data on AGN/comparison with sample of normal galaxies.

X-ray variability of blazars : flux & spectral variations of Blazars in X-rays, using satellite data, such as RXTE and recently XMM. Collaboration with the other teams, in initiating a detailed study of the X-ray variability in Blazars using archival data from satellites (J. P.)

Experience in the analysis of ISO & SCUBA observations (E. X.)

Experience in analysis of V,R,X ray observations and applications to the Disk-Jet system in superluminals quasars (E. Rokaki).

Involvement in the construction & operation of the 2.3 m Aristarchos telescope (E. X.).

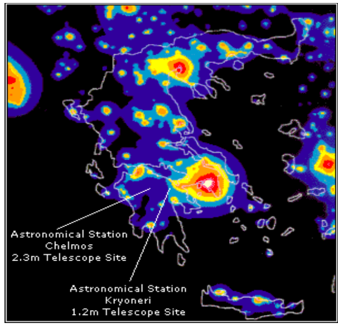

Location: Chelmos	
Geogr. Longitude	22°13' E
Geogr. Latitude	37°59' N
Elevation above sea level	2340 m
Distance to Athens (straight line)	130 km
Cloudiness statistics (yearly)	33 %
Temperature range (°C)	-15° +30°
Seeing (median)	0.7 "

THEORY (K. Tsinganos, A. Mastichiadis, N. Vlahakis et al.)

Experience in constructing steady analytical 3-D models of MHD winds and jets (relativistic & nonrelativistic).

Experience in constructing self-similar solutions, demonstration of the role of the critical surfaces, developing criteria for the collimation of MHD outflows, the asymptotics of collimated and cronical solutions, the structural stability of MHD outflows and the efficiency of magnetic acceleration.

Numerical simulations of time-dependent MHD winds/jets, demonstration of magnetic collimation & shock formation, acceleration of relativistic jets. Gamma ray bursts.

Time-dependent radiative transfer. Spectrum formation from synchrotron, synchro self-Compton and external Compton processes. Particle acceleration in shock waves and coupling with radiation. Application to blazars and gamma-ray bursts.

1.11 Team Cork - N. Smith (oral)

Chapter 2

Session I: Towards automated, fast an accurate photometry (N. Smith)

2.1 G. Tosti: The Long Term Perugia University Optical Blasar Monitoring

The Long Term Perugia University Optical Blazar Monitoring

http://wwwospg.pg.infn.it

A detailed study of the Blazar flux variations can provide a considerable amount of information on the physics and dynamics of the emitting region.
In particular, the knowledge of the possible variability modes of BL Lac objects in the optical band is very useful to understand the significance of the correlation with the variability observed in other spectral bands.

The Perugia program would contribute to the better understanding of the flux variations of a sample of bright BL Lac objects in the optical bands trough a systemantic daily (when possible) sapling of their light curves.

The automatic program started in 1994.

All observations during the last years were performed using a small size automatic telescope equipped with CCD camera and standard set of BVRI filters for multiband photometry.

The Perugia University 0.4m Automatic Imaging telescope

- Diameter of the primary mirror D= 40 cm
- Focal ratio f/5
- Newtonian optical configuration
- equatorial mount

- CCD Camera + Johnson-Cousins BVRI filters

Fully automatic Data Acquisition and Reduction.

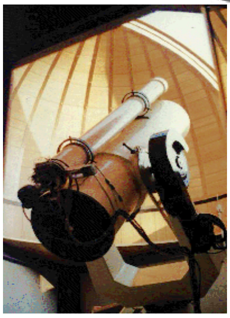

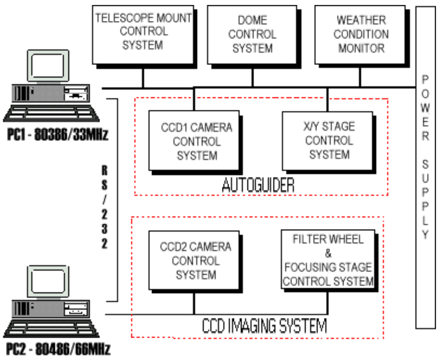

Report

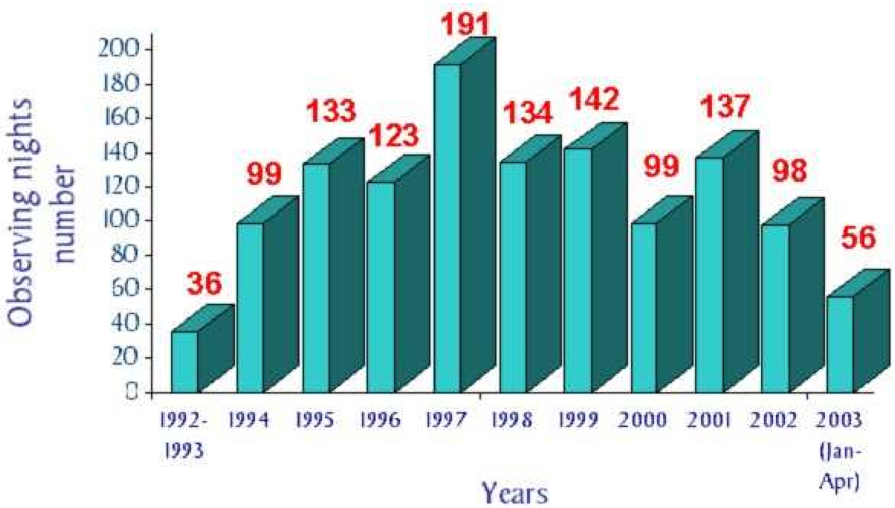

The best sampled Blazars

Common Name	AR	DEC	z	Type	Max[R]	Min[R]
S2 0109+22	01 12 05.8	+22 44 39		BL	14.82	16.21
3C 66A	02 22 39.6	+43 02 08	0.444	HPQ	13.79	14.94
AO 0235+164	02 38 38.8	+16 36 59	0.94	BL	14.98	16.94
4C 47.08	03 03 35.2	+47 16 16	0.475	BL	15.9	16.7
NGC 1275	03 19 48.1	+41 30 42	0.0176	UG	13.47	13.65
1H 0323+022	03 26 14.0	+02 25 15	0.147	BL	15.73	16.59
1H 0414+009	04 16 53.8	+01 04 57	0.287	BL	16.11	16.58
PKS 0422+00	04 24 46.8	+00 36 06	0.31	BL	14.06	15.46
S5 0716+71	07 21 53.4	+71 20 36	0.3	BL	13.71	14.81
PKS 0735+17	07 38 07.4	+17 42 19	0.424	OVV	15.42	16.57
1ES 0806+524	08 09 49.1	+52 18 59	0.138	BL	15.38	15.81
PKS 0829+046	08 31 48.9	+04 29 39	0.18	BL	14.74	15.56
OJ 287	08 54 48.9	+20 06 31	0.306	OVV	14.67	16.27
S4 0954+65	09 58 47.2	+65 33 55	0.368	BL	15.43	16.46
OM 280	11 50 19.2	+24 17 54	0.2	BL	15.6	16.49
TON 605	12 17 52.1	+30 07 01	0.13	OVV	14.22	14.63
W Com	12 21 31.7	+28 13 59	0.102	BL	13.65	15
3C 273	12 29 06.7	+02 03 09	0.1583	LPQ	12.71	12.88
3C 279	12 56 11.1	-05 47 22	0.5362	HPQ	14.46	15.95
OQ 530	14 19 46.6	+54 23 15	0.151	BL	15.15	15.86
PKS 1424+240	14 27 00.4	+23 48 00		BL	14.13	14.39
MS 1458.8+2249	15 01 01.9	+22 38 06	0.235	BL	15.54	16.16
3C 345	16 42 58.8	+39 48 37	0.5928	HPQ	16.02	16.79
MRK 501	16 53 52.2	+39 45 37	0.0337	BL	13.34	13.49
H 1722+119	17 25 04.4	+11 52 16	0.018	HPQ	14.31	14.83
I Zw 187	17 28 18.6	+50 13 10	0.0554	BL	15.54	15.9
3C 371	18 06 50.7	+69 49 28	0.051	OVV	14.23	14.49
1ES 1959+650	19 59 59.8	+65 08 55	0.047	BL	14.66	15.19
PKS 2032+107	20 35 22.3	+10 56 07	0.601	BL	15.01	15.33
BL Lac	22 02 43.3	+42 16 40	0.0686	BL	13.51	15.2
PKS 2254+074	22 57 17.3	+07 43 12	0.19	BL	15.98	16.63
1ES 2344+514	23 47 04.8	+51 42 18	0.044	BL	14.82	15.16

OJ 287

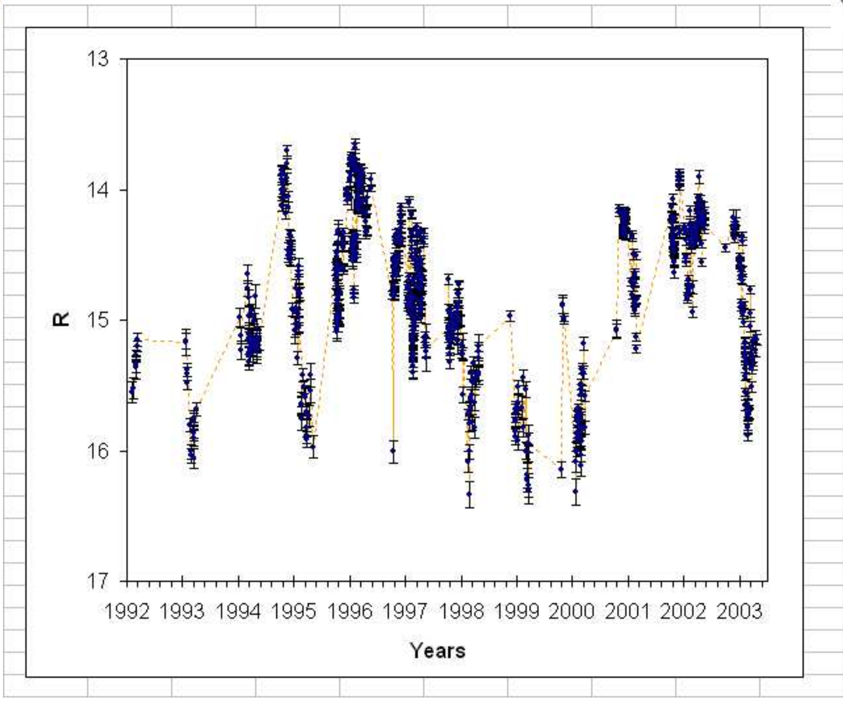

IRAIT & Mid-Infrared monitoring from Antarctica

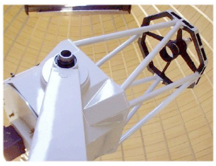

Italian Robotic Antarctic Infrared Telescope: 80cm automatic telescope for mid-infrared observation at the Italian-French base of Dome C (3280m asl on the Antarctica Plateau)

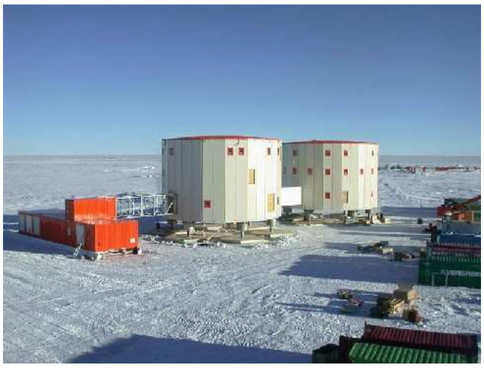

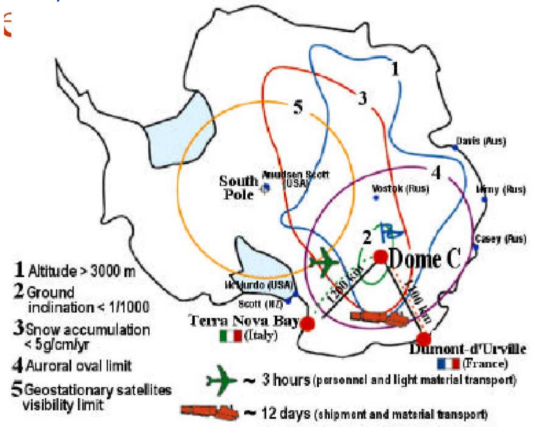

Extragalactic issues for IRAIT and moderate sized infrared Antarctic telescopes

- IRAIT and moderate size telescopes placed at Dome C could carry out a photometric monitoring of the mid-IR variability, and could provide a mid-IR support for the observing multiwavelength campaigns of southern blazars and other AGNs.
- Preliminary estimations of the flux limit for IRAIT: (Si:As 256x256 array, 2-25 micron, in background limited performances and S/N=3): 20-50 mJy at 10 microns, and 50-100 mJy at 20 microns. (---> about 40 known southern blazars and 50 known southern ultraluminous IR galaxies (ULIRGs) achievable).
- This Other important extragalactic programs: other AGN classes (Seyfert galaxies, radiogalaxies and radio-quiet quasars), study of bright nearby galaxies, search for galaxies in the Zone of Avoidance (Great Attractor), identification of the compact galaxies colors at moderate distances, diagnostic photometry of starburst galaxies and ULIRGs.

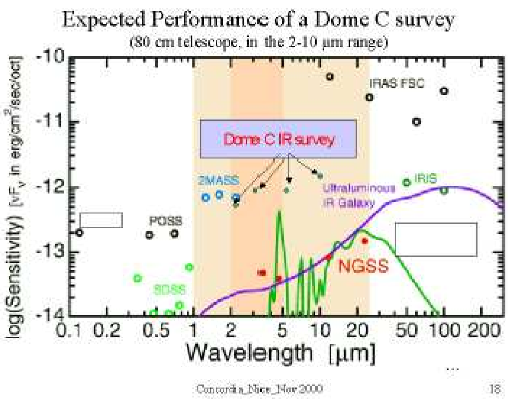

Correlation between the infrared peak emission and the gamma-ray peak emission (IRAIT-GLAST synergy).

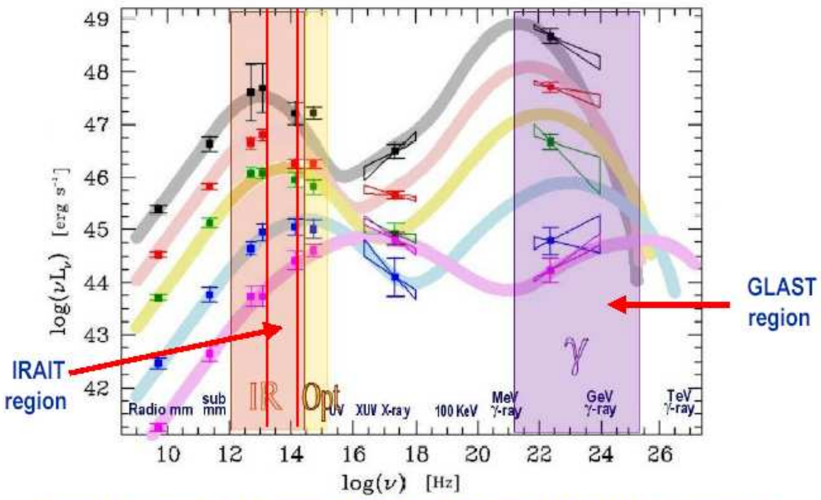

Possible correlation between infrared-optical synchrotron flux and gamma-ray, inverse Compton flux.

20

Student Work on Robotic Telescope IRAIT

- design and implementation of remote control system
- qualification tests of specific components/subsystems (motors,encoder,controller cables, connectors, etc.) necessary for the telescope adaptation to antarctic conditions
- Development of the robotic control system of the Mid-IR Camera
- overall integration and test (in Italy at Coloti Observatory)

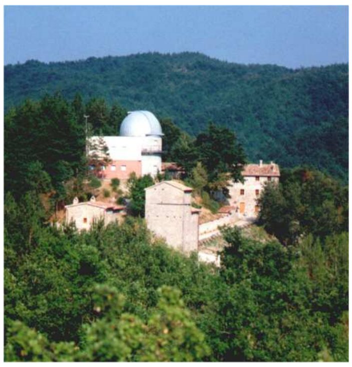

2.2 N. Smith: High Precision, High Time Resolved Photometry of AGN

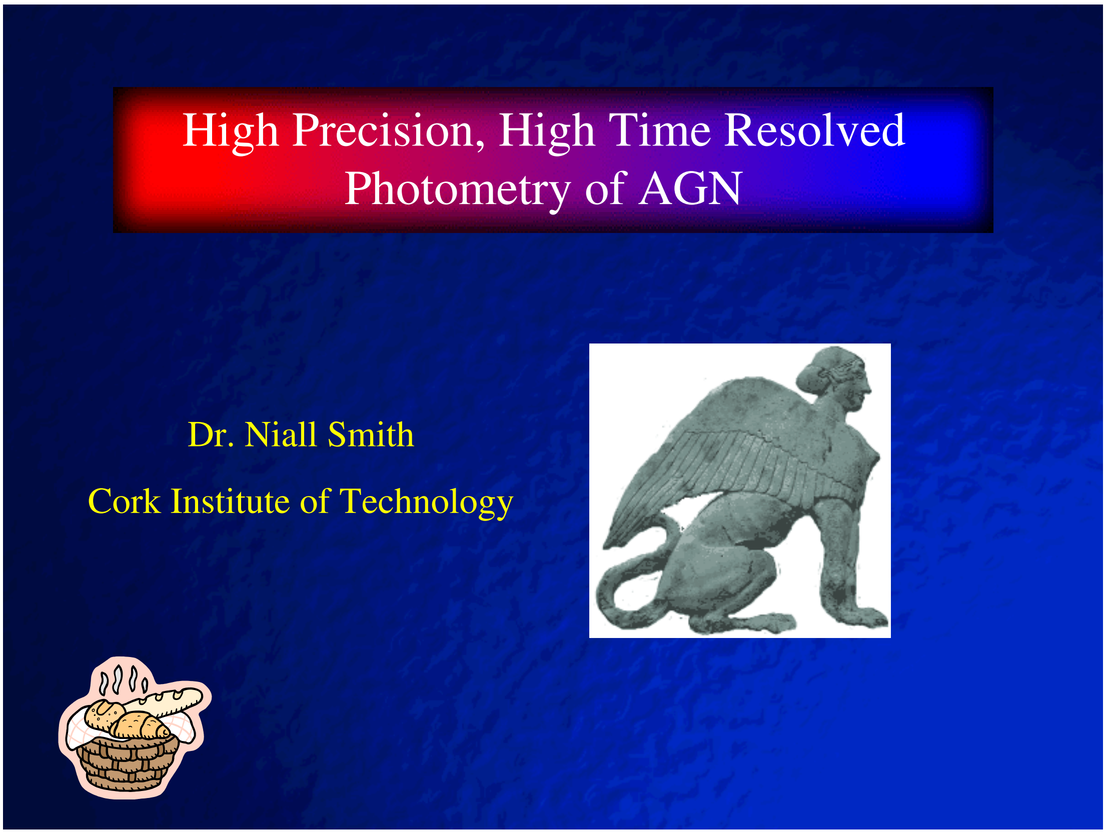

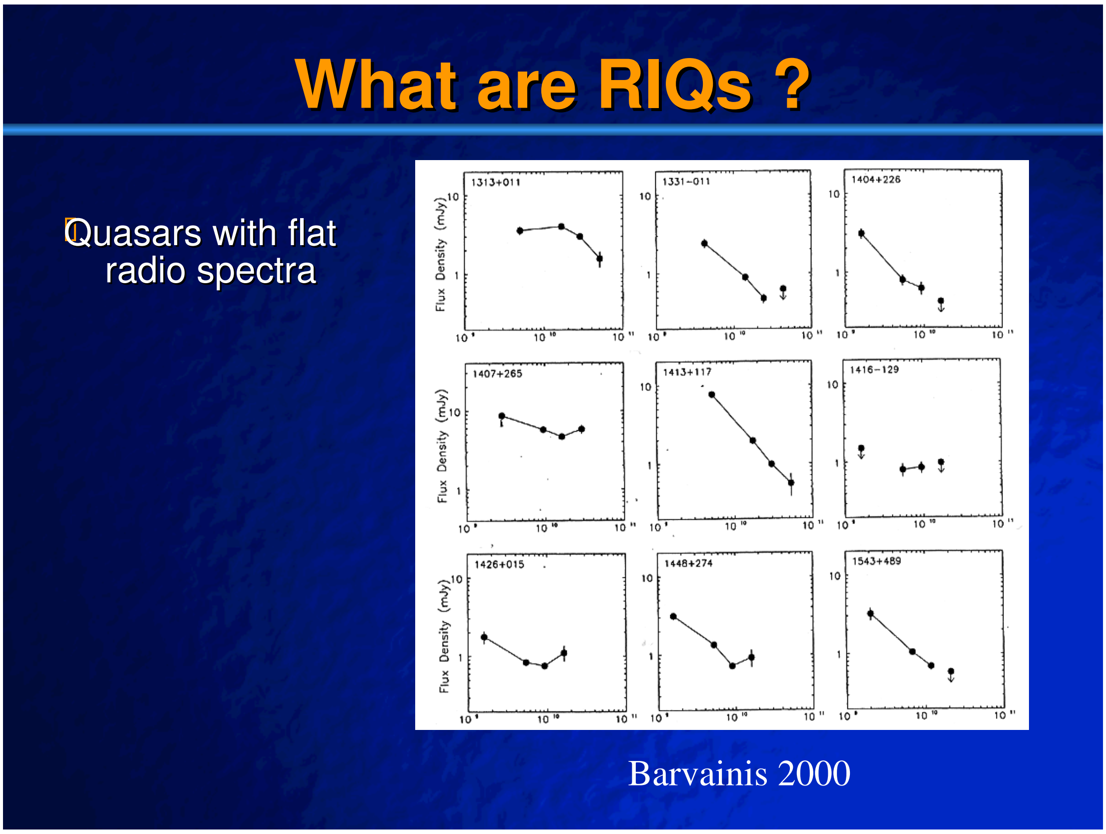
What are RIQs ?
Quasars with flat radio spectra
1313+011
1331−011
1404+226
1407+265
1413+117
1416−129
1426+015
1448+274
1543+489
Flux Density (mJy)
Barvainis 2000

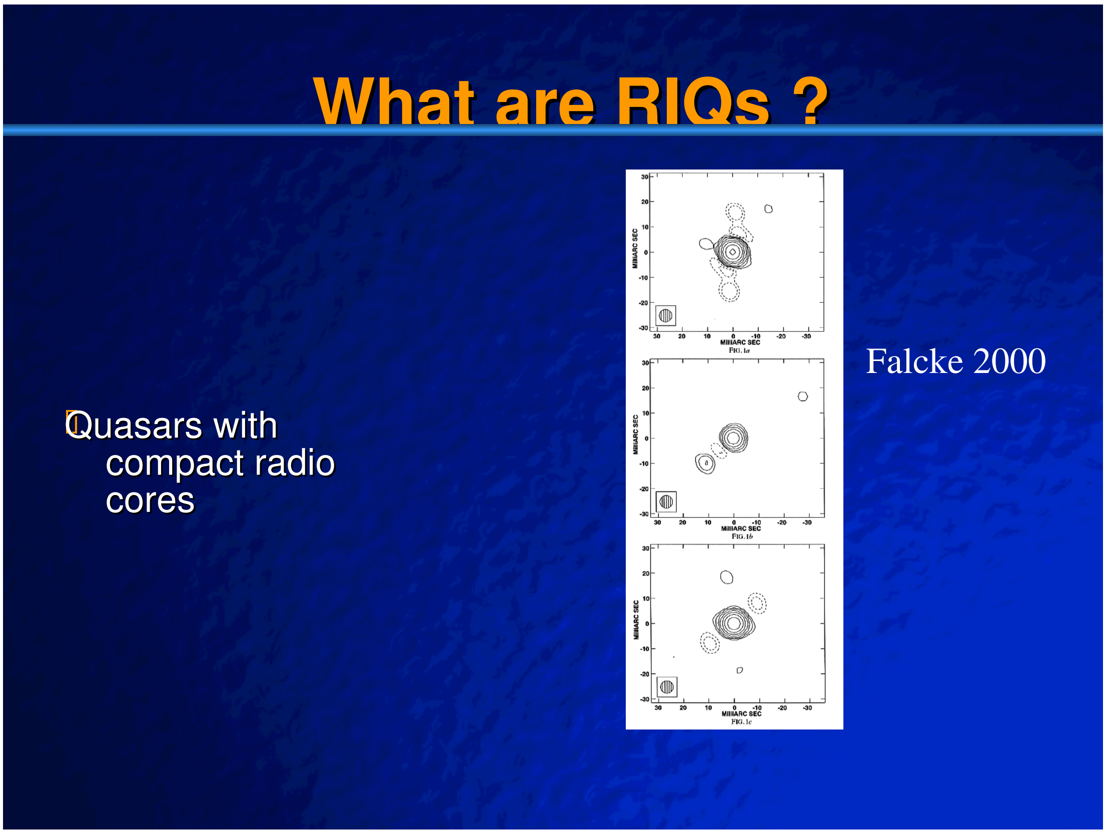
What are RIQs ?
Quasars with compact radio cores
Falcke 2000

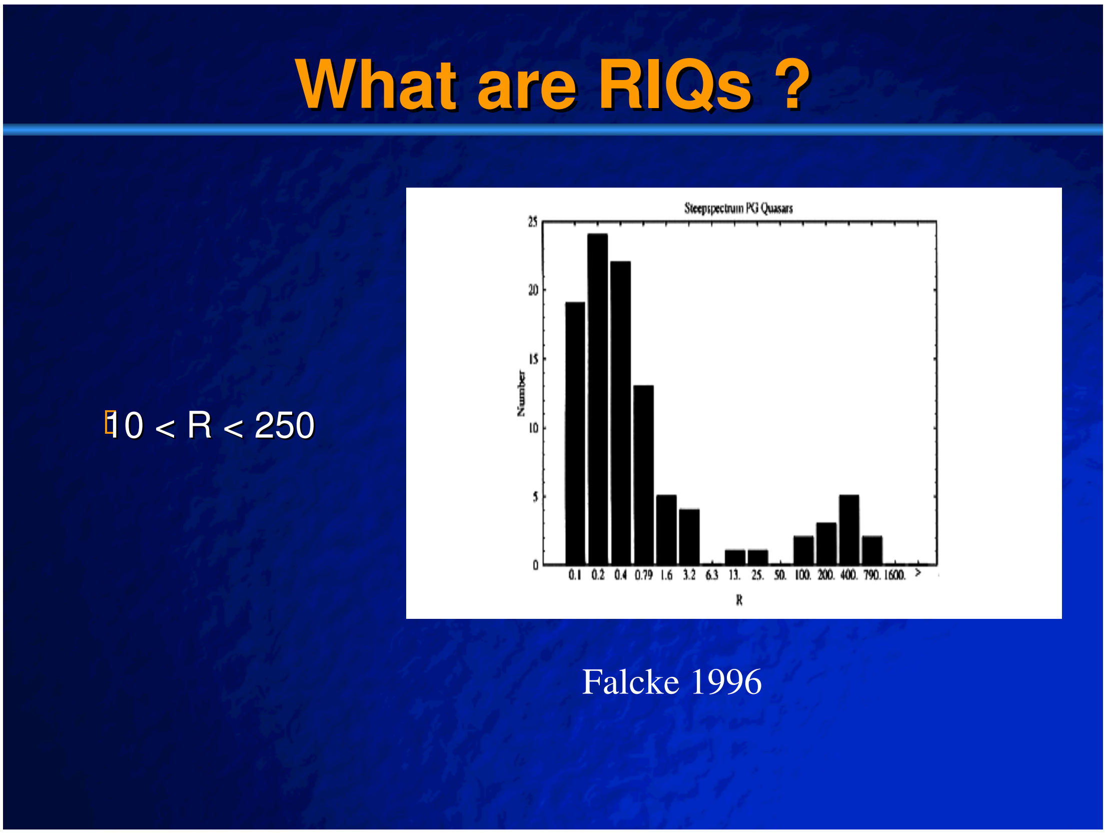
What are RIQs ?
10 < R < 250
Steepspectrum PG Quasars
Number
R
0.1 0.2 0.4 0.79 1.6 3.2 6.3 13. 25. 50. 100. 200. 400. 790. 1600. >
0 5 10 15 20 25
Falcke 1996

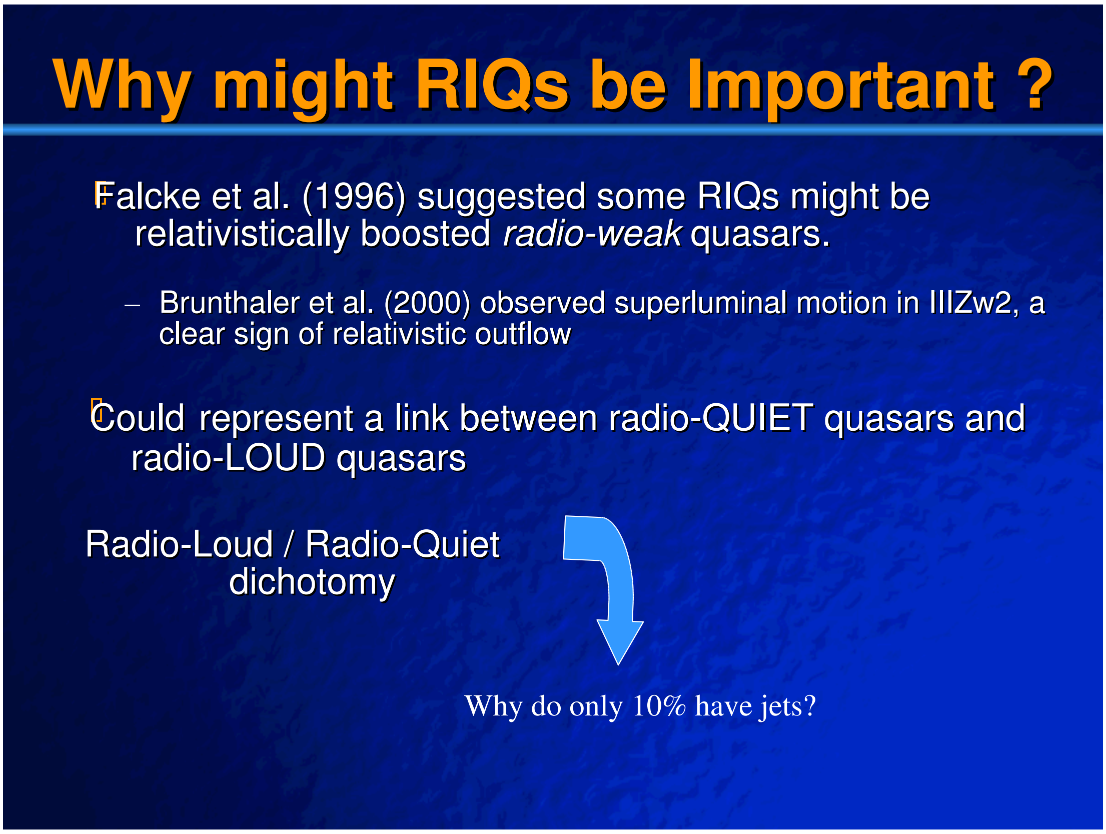
Why might RIQs be Important ?
Falcke et al. (1996) suggested some RIQs might be relativistically boosted *radio-weak* quasars.
– Brunthaler et al. (2000) observed superluminal motion in IIIZw2, a clear sign of relativistic outflow
Could represent a link between radio-QUIET quasars and radio-LOUD quasars
Radio-Loud / Radio-Quiet dichotomy
Why do only 10% have jets?

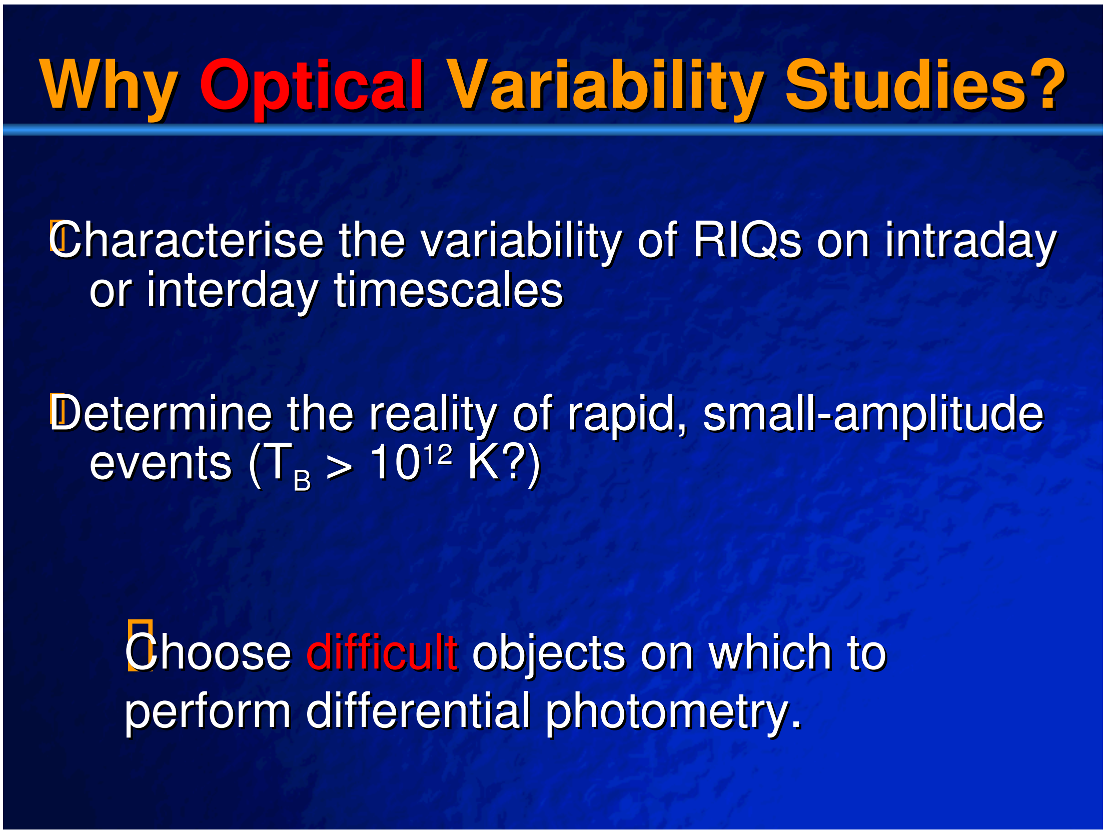
Why Optical Variability Studies?
Characterise the variability of RIQs on intraday or interday timescales
Determine the reality of rapid, small-amplitude events ($T_B > 10^{12}$ K?)
Choose difficult objects on which to perform differential photometry.

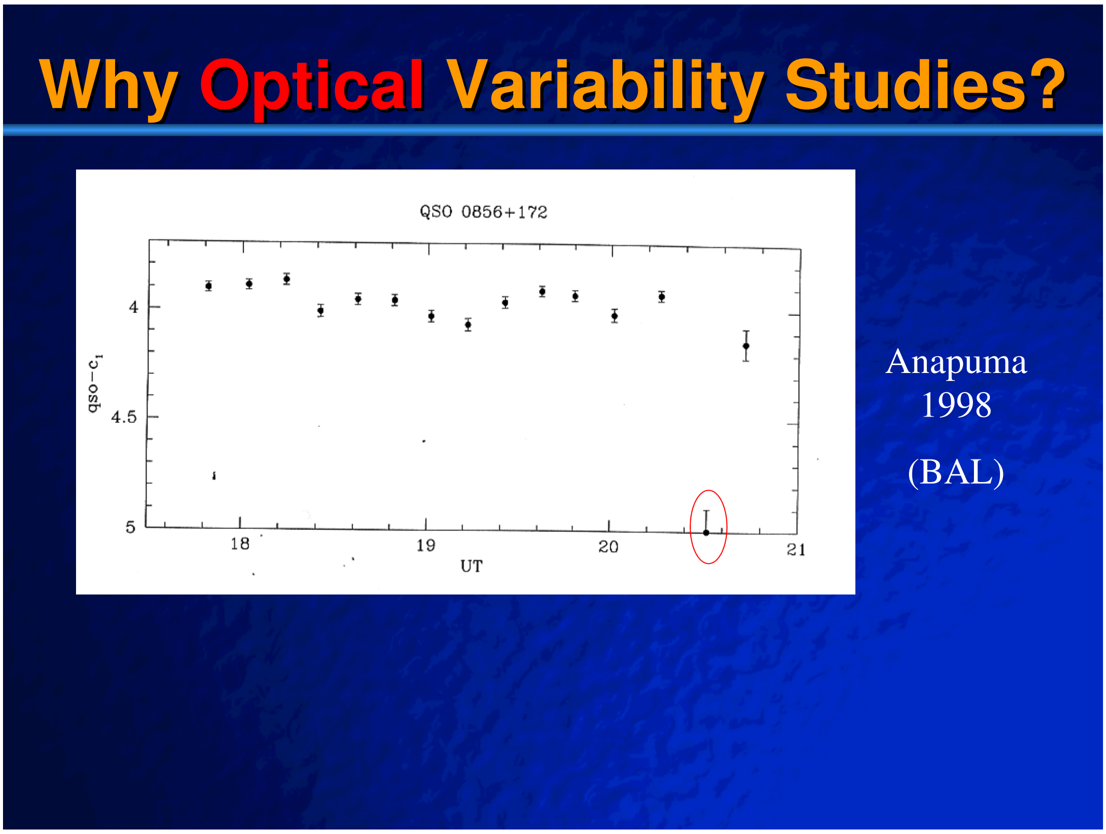
Why Optical Variability Studies?
QSO 0856+172
qso−c1
4
4.5
5
18
19
20
21
UT
Anapuma
1998
(BAL)

The Sample

Object	Log L_{disk}	R
0003+15	46.4	178
0007+106	45.4	158
0044+03	46.5	24.2
1821+64	45.9	24
2209+184	44.9	91.8
2308+09	46.1	139

Data Acquisition

- Master flatfields in B and V
  - 40 V flats with 20k counts each
  - 38 B flats with 20k counts each
- Maximum counts <45k in all sources under clearest conditions
- Images re-centered night-to-night
- Observations repeated at same airmasses

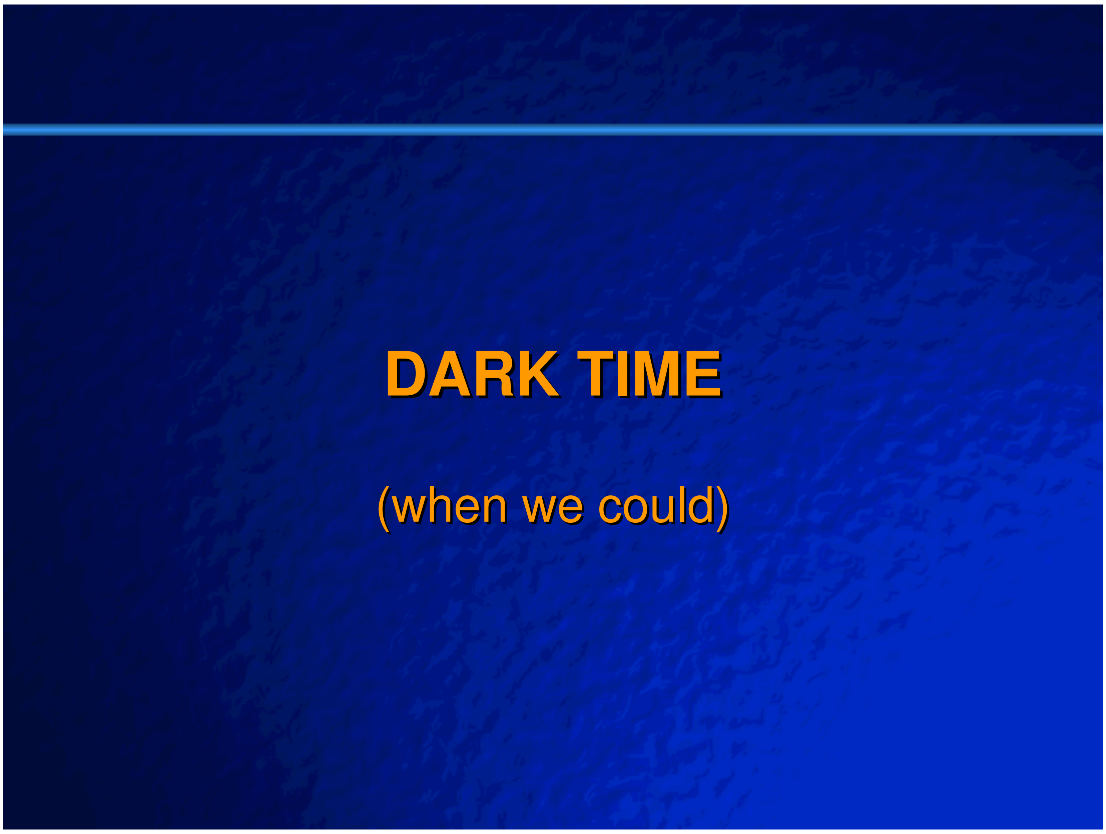
DARK TIME
(when we could)

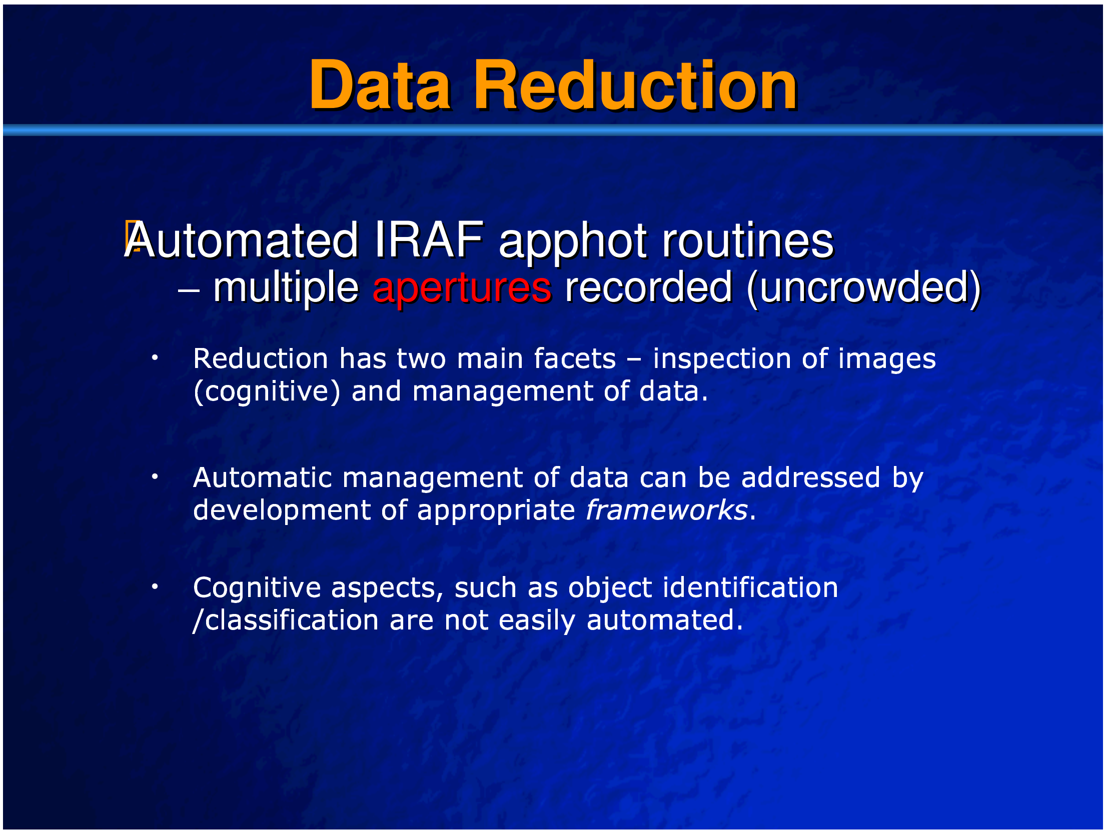
Data Reduction
Automated IRAF apphot routines
– multiple apertures recorded (uncrowded)
• Reduction has two main facets – inspection of images (cognitive) and management of data.
• Automatic management of data can be addressed by development of appropriate *frameworks*.
• Cognitive aspects, such as object identification /classification are not easily automated.

Rejection of Cosmic Rays

- In our application we trained a simulated artificial neural network to classify detected objects in an image as either stars or noise artifacts (cosmic rays).
- A training set consisting of 1000 image sections classified by human experts was used.

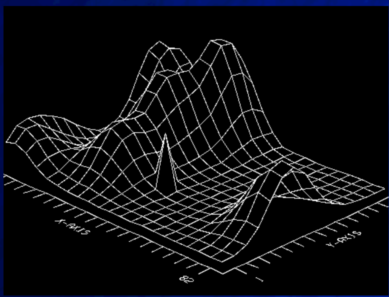

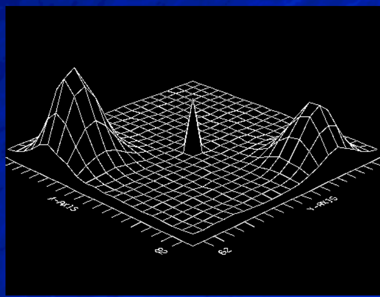

Neural Networks Work

- Experimental results show that the neural network was very successful at this classification task.

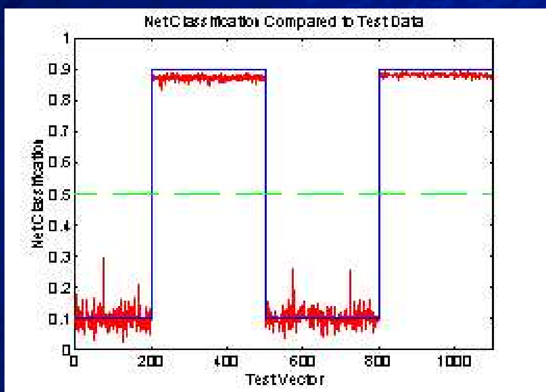

Generation of Lightcurves

- Output is piped to IDL program “qvar”
  - –performs differential photometry using a master reference star (composed of 4-8 stars typically)
  - –provides statistical tests of variability
  - –allows different background determination methods to be used
  - –tracks variations in fwhm, position, apparent magnitude, airmass
  - –allows rejection of variable stars or data points affected by cosmic rays

Data Reduction

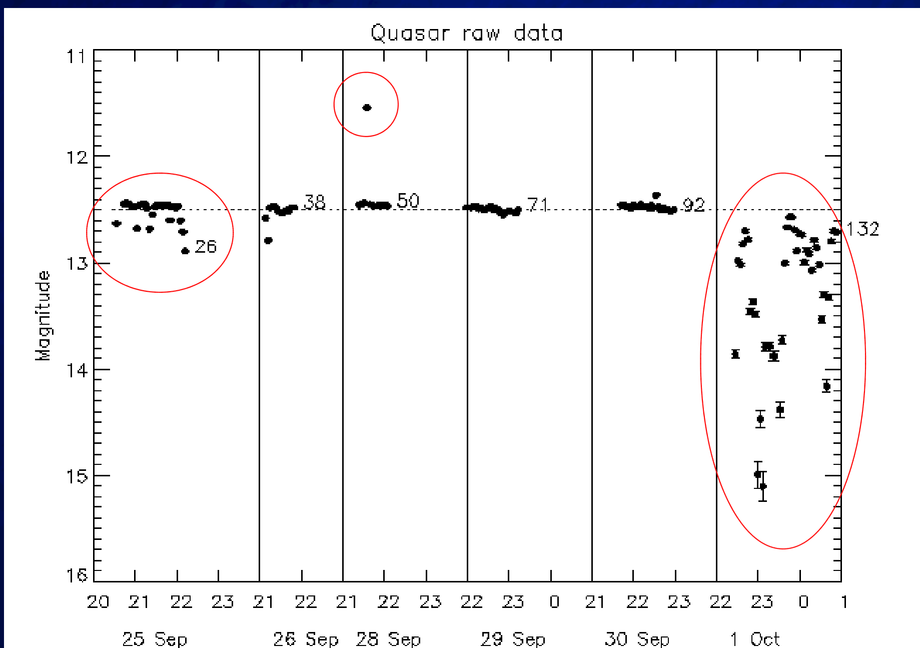

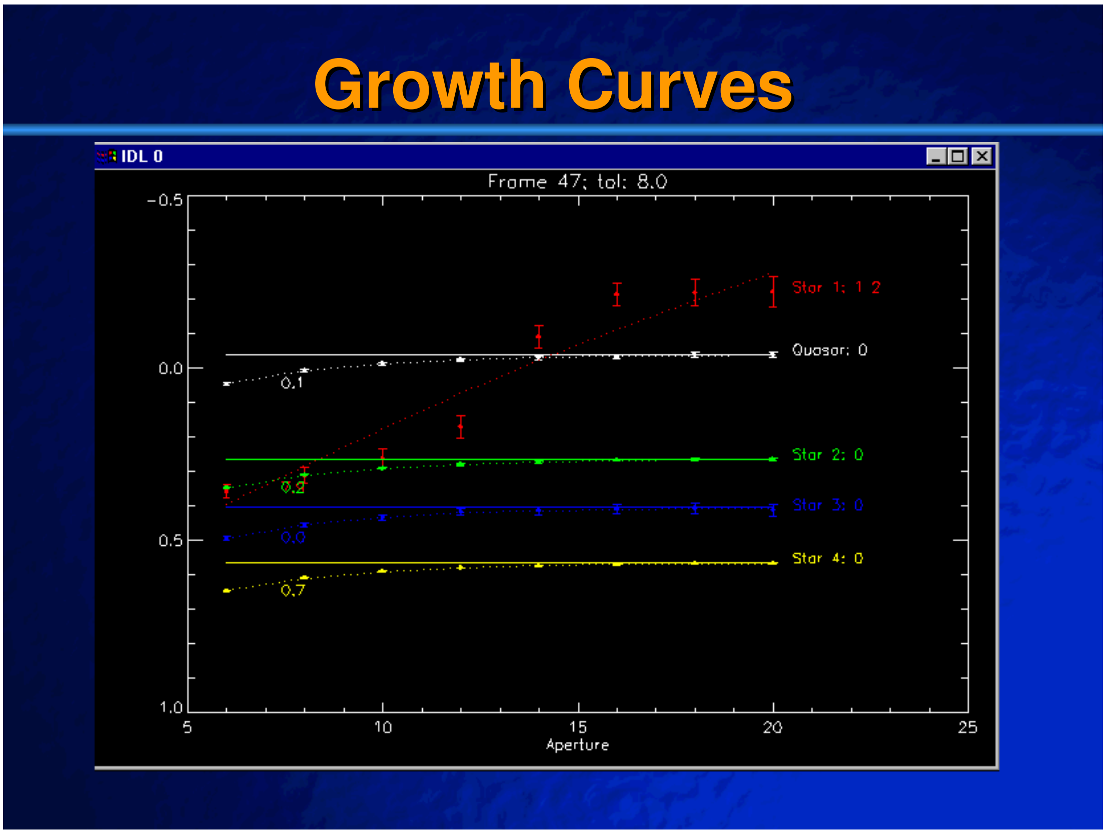
Growth Curves
IDL 0
Frame 47; tol: 8.0
Star 1: 1 2
Quasar: 0
Star 2: 0
Star 3: 0
Star 4: 0
0.1
0.2
0.0
0.7
Aperture

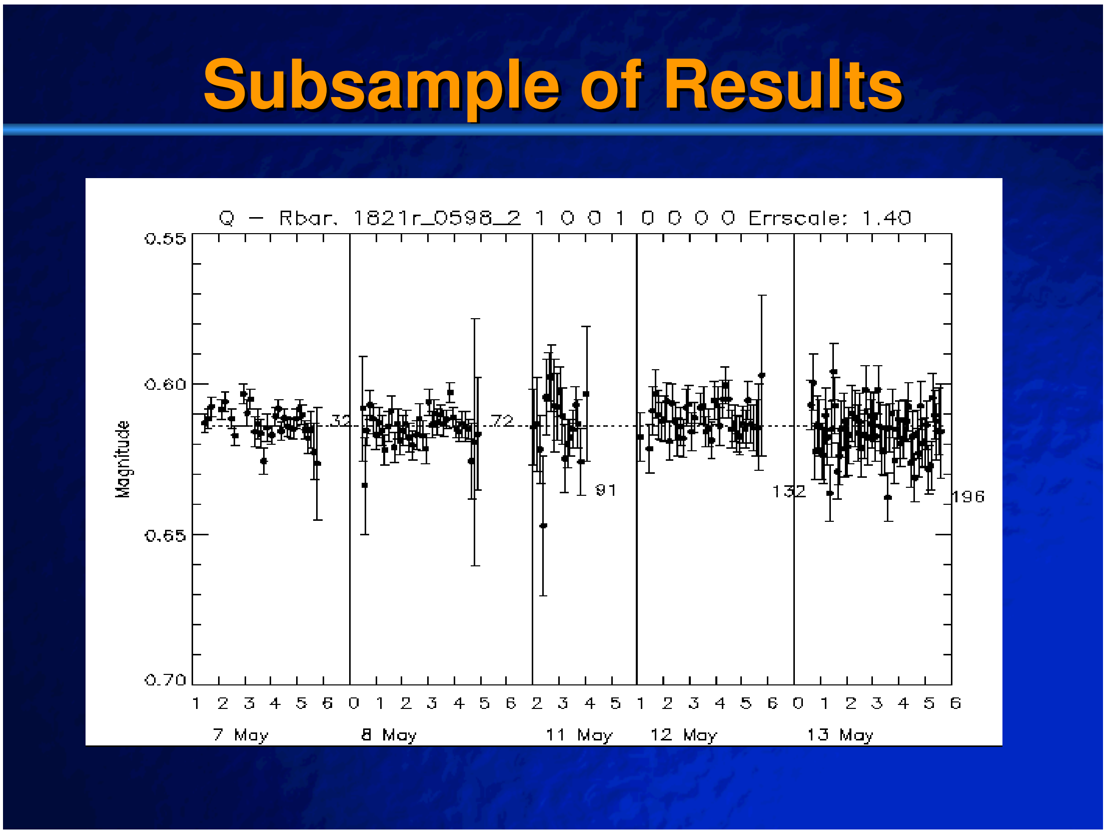
Subsample of Results
Q – Rbar. 1821r_0598_2 1 0 0 1 0 0 0 0 Errscale: 1.40
Magnitude
7 May
8 May
11 May
12 May
13 May

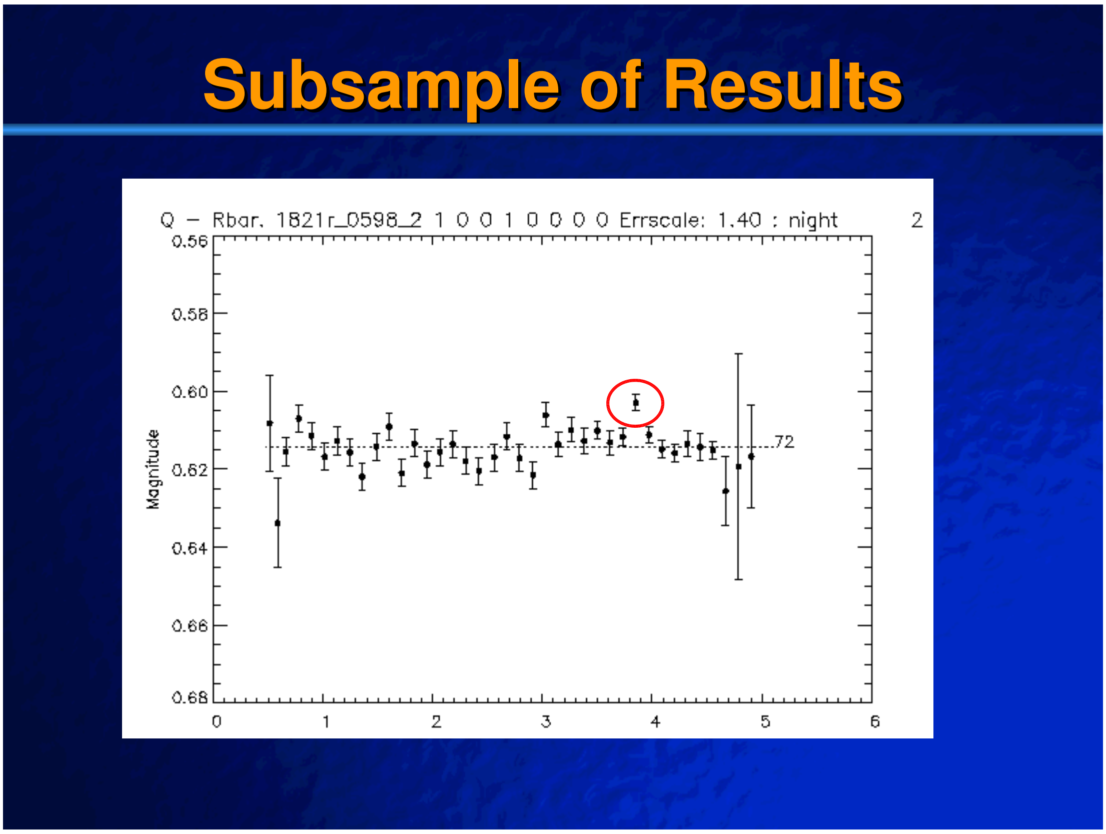
Subsample of Results
Q – Rbar. 1821r_0598_2 1 0 0 1 0 0 0 0 Errscale: 1.40 : night 2
Magnitude
0.56
0.58
0.60
0.62
0.64
0.66
0.68
0 1 2 3 4 5 6
.72

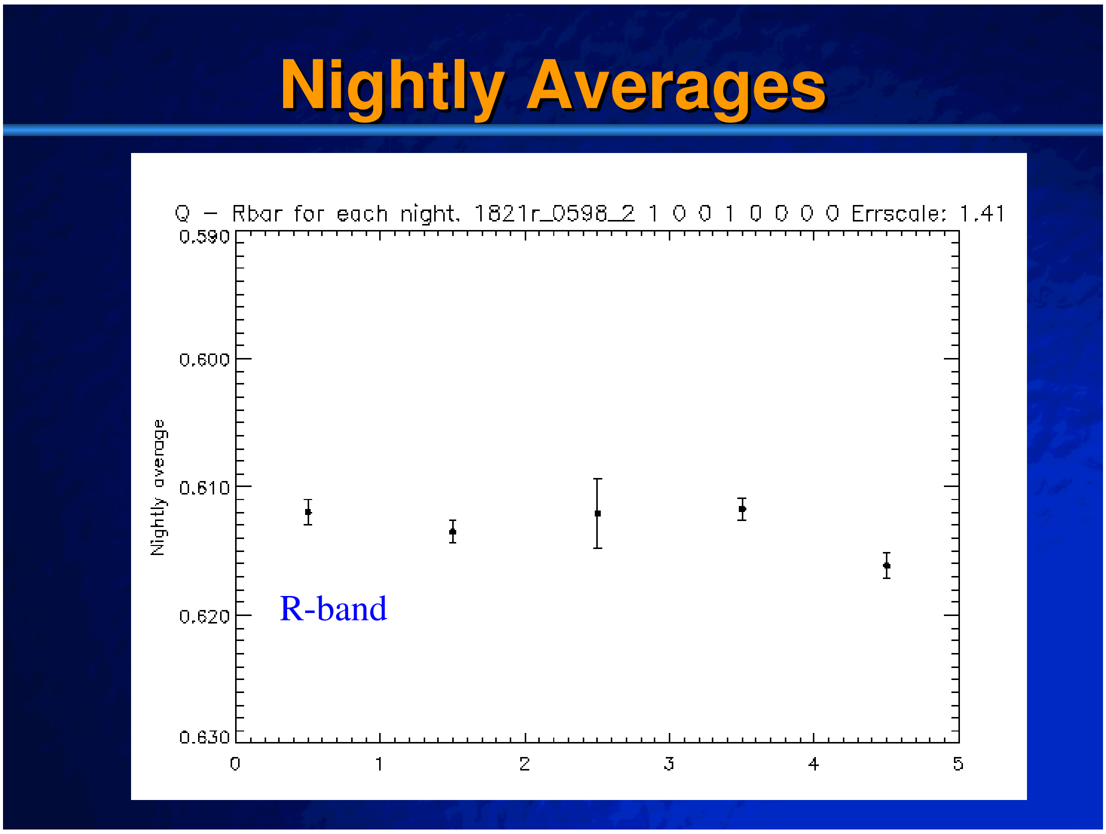
Nightly Averages
Q – Rbar for each night. 1821r_0598_2 1 0 0 1 0 0 0 0 Errscale: 1.41
Nightly average
0.590
0.600
0.610
0.620
0.630
0 1 2 3 4 5
R-band

Nightly Averages

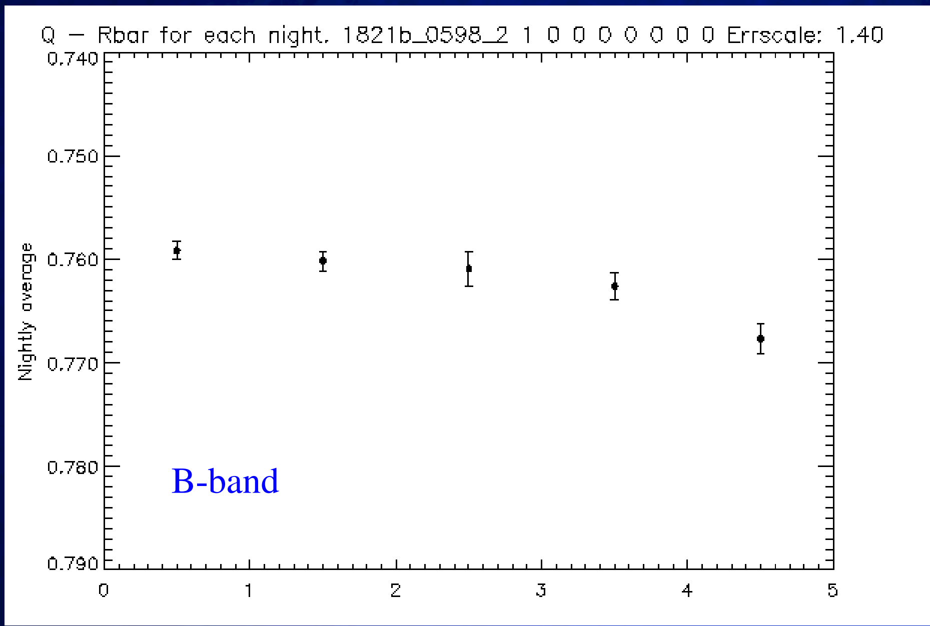

What do we find in RIQs?

- Short-timescale variabilty seems to be of very low amplitude
  – hint of variability in a couple of sources
- B-band variability may be more pronounced
- No ultra-rapid variability from single data points, or small groups of data points
- Ensemble of reference stars and many data points provide robust results
  – try combinations of reference stars, apertures, etc.

Future RIQ Prospects

- Understand how to reach photon limit with CCDs and differential photometry (0.0005^m)
  - focussing
  - undersampling/oversampling
  - airmass
  - tracking/seeing
  - field of view
- Small telescopes very important
  - regular intensive monitoring
  - large number of sources with $m_V < 19$
- Careful selection of fields
- EVN data

Not all fields are photometrically equal

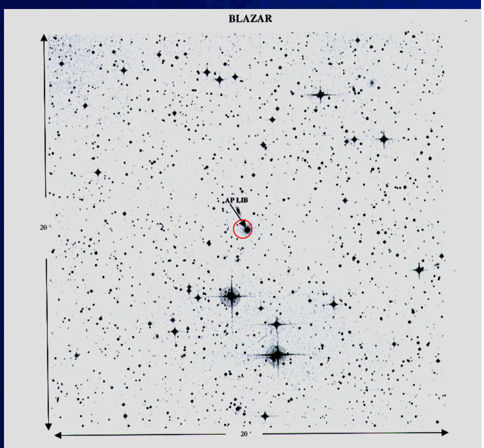

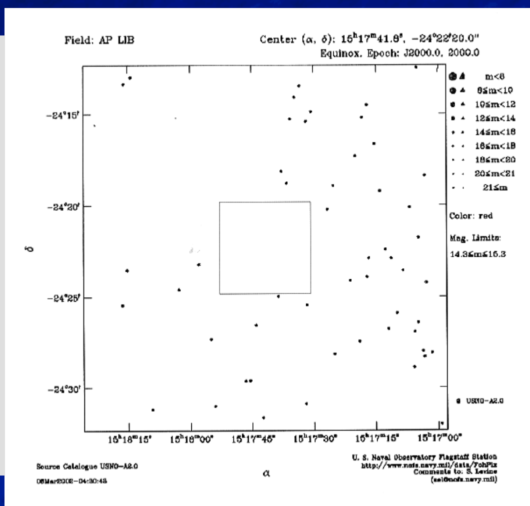

AP Lib

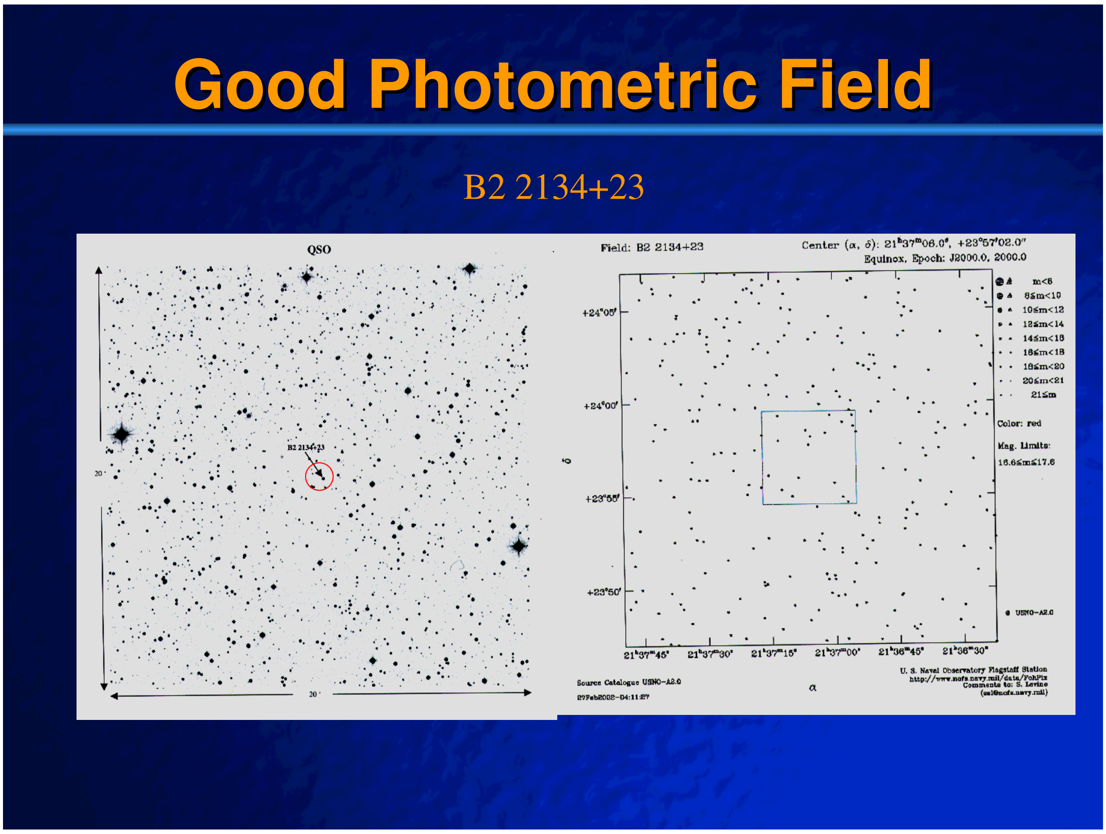
Good Photometric Field
B2 2134+23
QSO
B2 2134+23
Field: B2 2134+23
Equinox, Epoch: J2000.0, 2000.0
+24°05'
+24°00'
+23°55'
+23°50'
Color: red
Mag. Limits:
USNO-A2.0
Source Catalogue USNO-A2.0
U. S. Naval Observatory Flagstaff Station

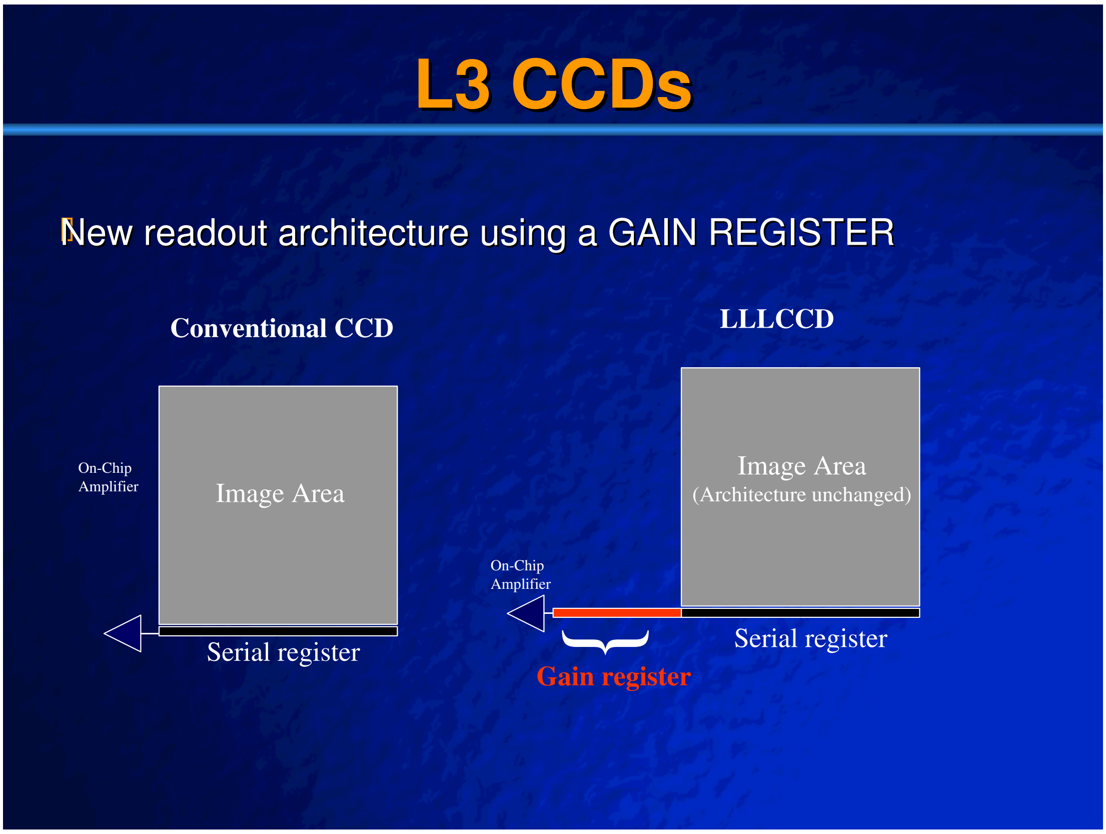
L3 CCDs
New readout architecture using a GAIN REGISTER
Conventional CCD
LLLCCD
On-Chip Amplifier
Image Area
Serial register
On-Chip Amplifier
Image Area
(Architecture unchanged)
Serial register
Gain register

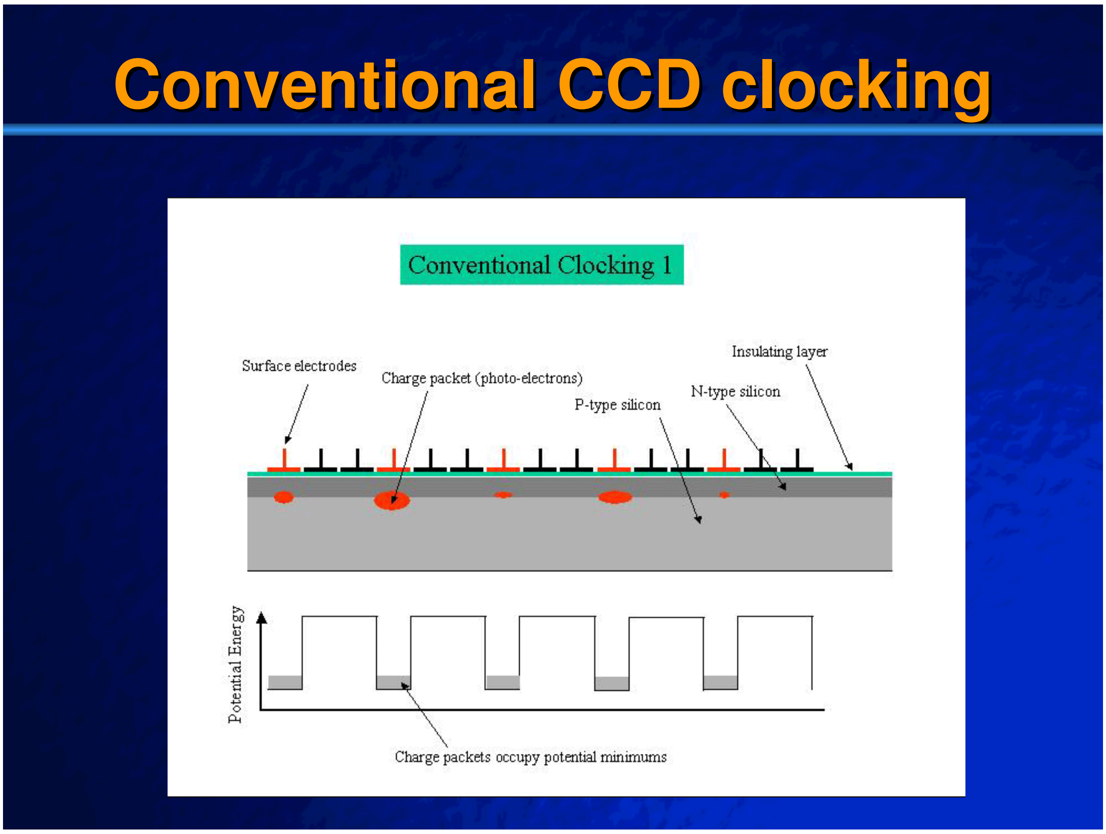
Conventional CCD clocking
Conventional Clocking 1
Surface electrodes
Charge packet (photo-electrons)
Insulating layer
N-type silicon
P-type silicon
Potential Energy
Charge packets occupy potential minimums

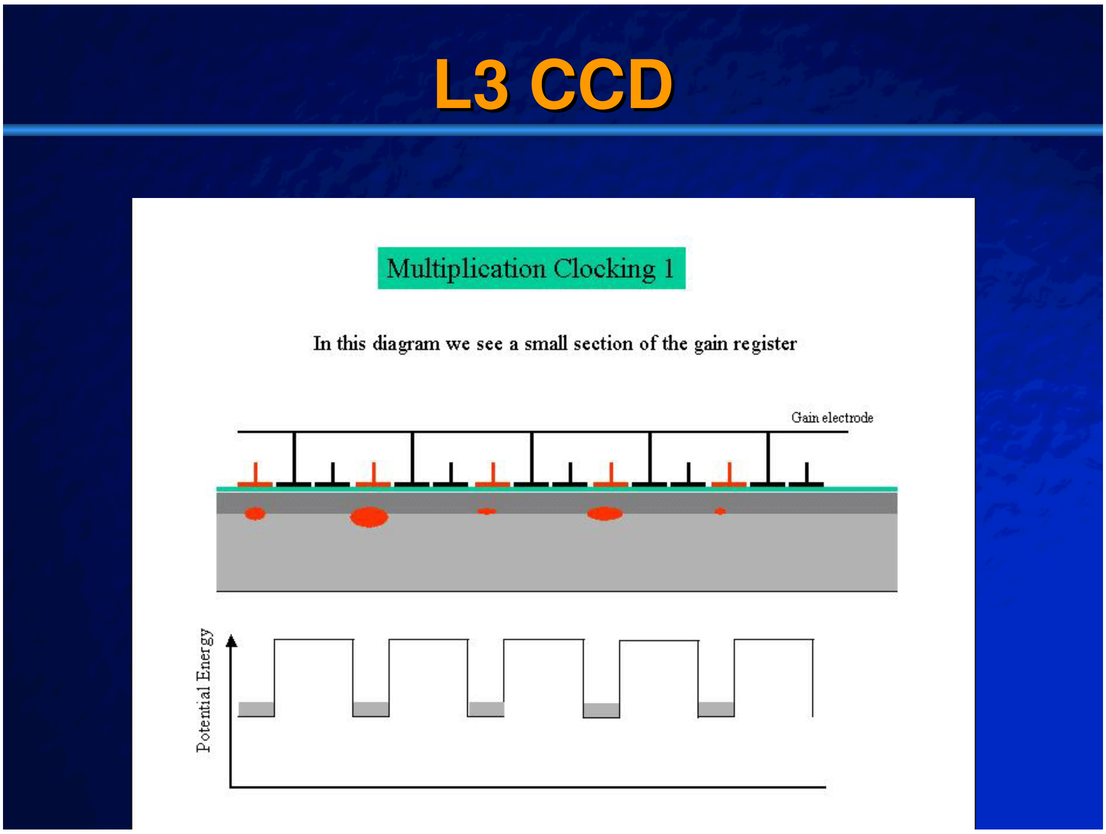
L3 CCD
Multiplication Clocking 1
In this diagram we see a small section of the gain register
Gain electrode
Potential Energy

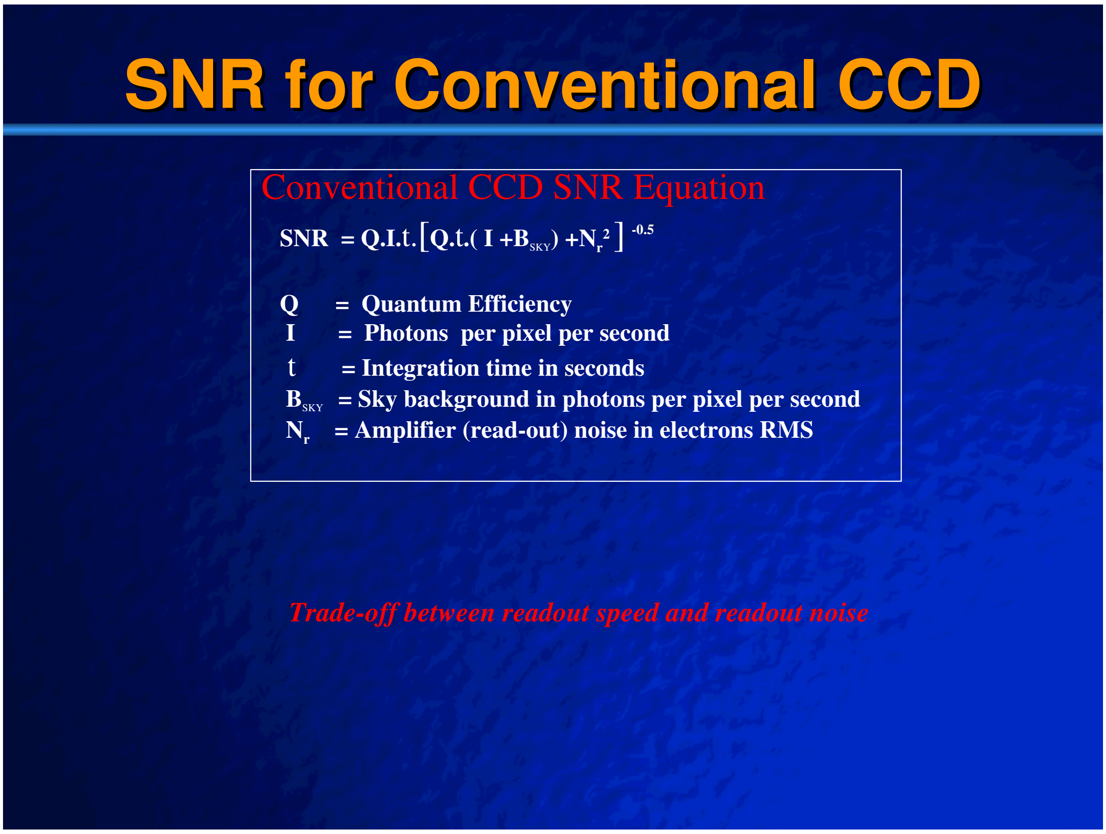
SNR for Conventional CCD
Conventional CCD SNR Equation
$SNR = Q.I.t.\left[Q.t.(I + B_{SKY}) + N_r^2\right]^{-0.5}$
Q = Quantum Efficiency
I = Photons per pixel per second
t = Integration time in seconds
B_{SKY} = Sky background in photons per pixel per second
N_r = Amplifier (read-out) noise in electrons RMS
Trade-off between readout speed and readout noise

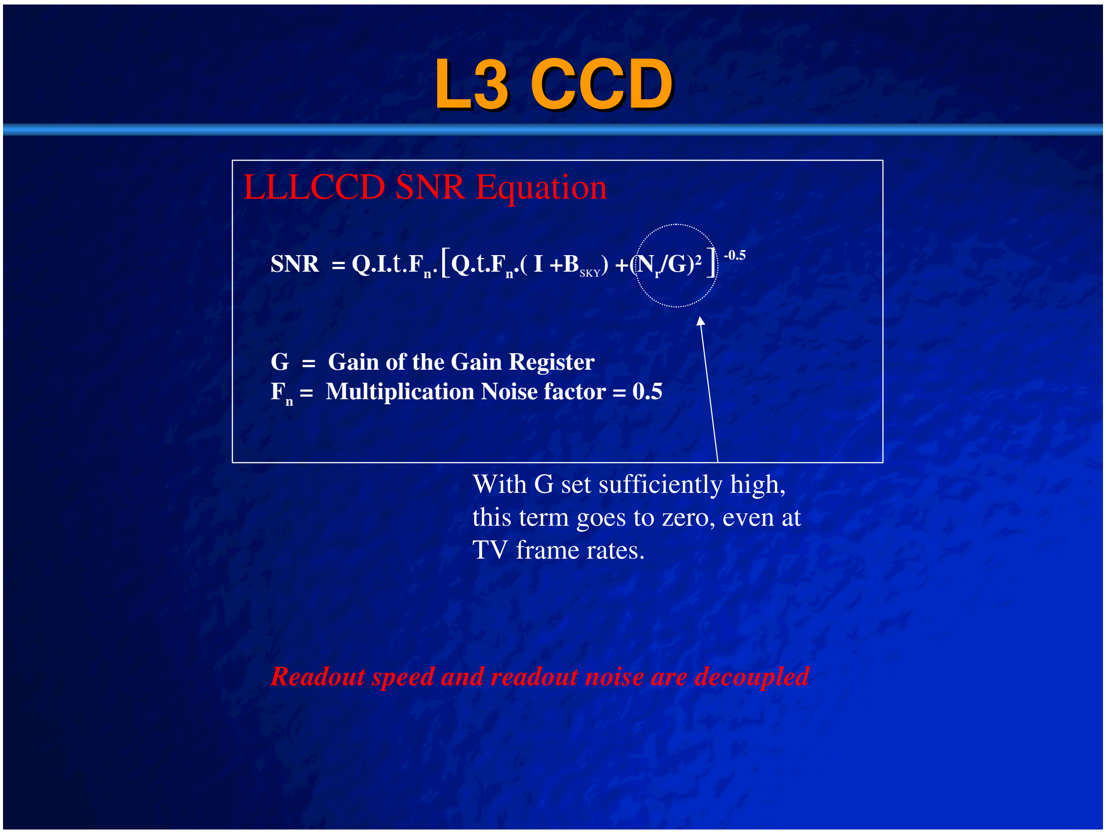
L3 CCD
LLLCCD SNR Equation
$SNR = Q.I.t.F_n.\left[Q.t.F_n.(I + B_{SKY}) + (N_r/G)^2\right]^{-0.5}$
G = Gain of the Gain Register
F_n = Multiplication Noise factor = 0.5
With G set sufficiently high, this term goes to zero, even at TV frame rates.
Readout speed and readout noise are decoupled

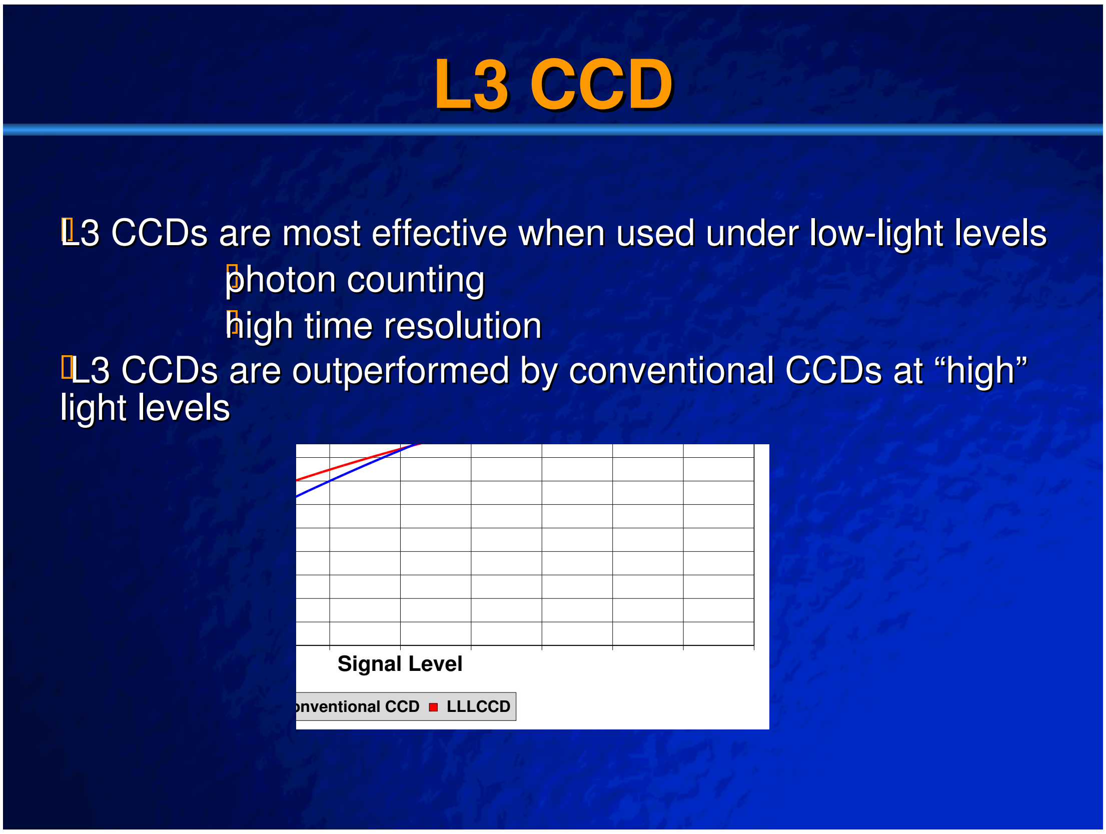
L3 CCD
L3 CCDs are most effective when used under low-light levels
photon counting
high time resolution
L3 CCDs are outperformed by conventional CCDs at “high” light levels
Signal Level
nventional CCD
LLLCCD

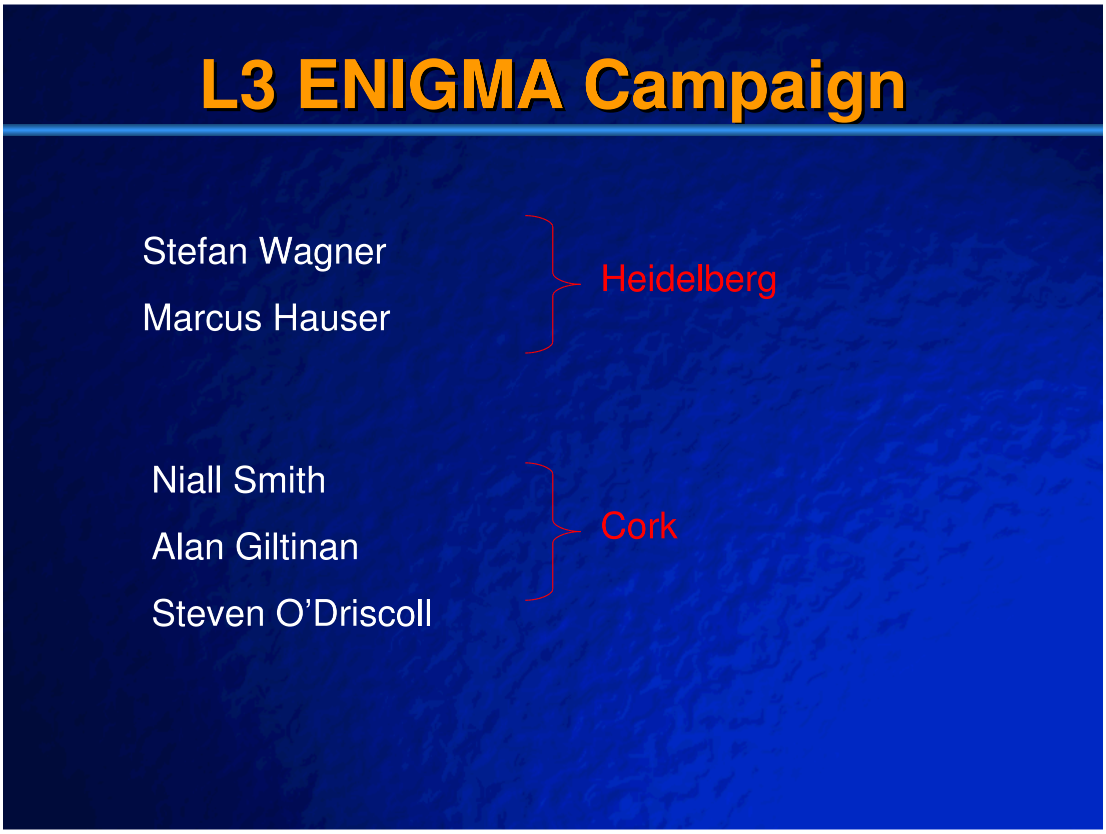
L3 ENIGMA Campaign
Stefan Wagner
Marcus Hauser
Heidelberg
Niall Smith
Alan Giltinan
Steven O’Driscoll
Cork

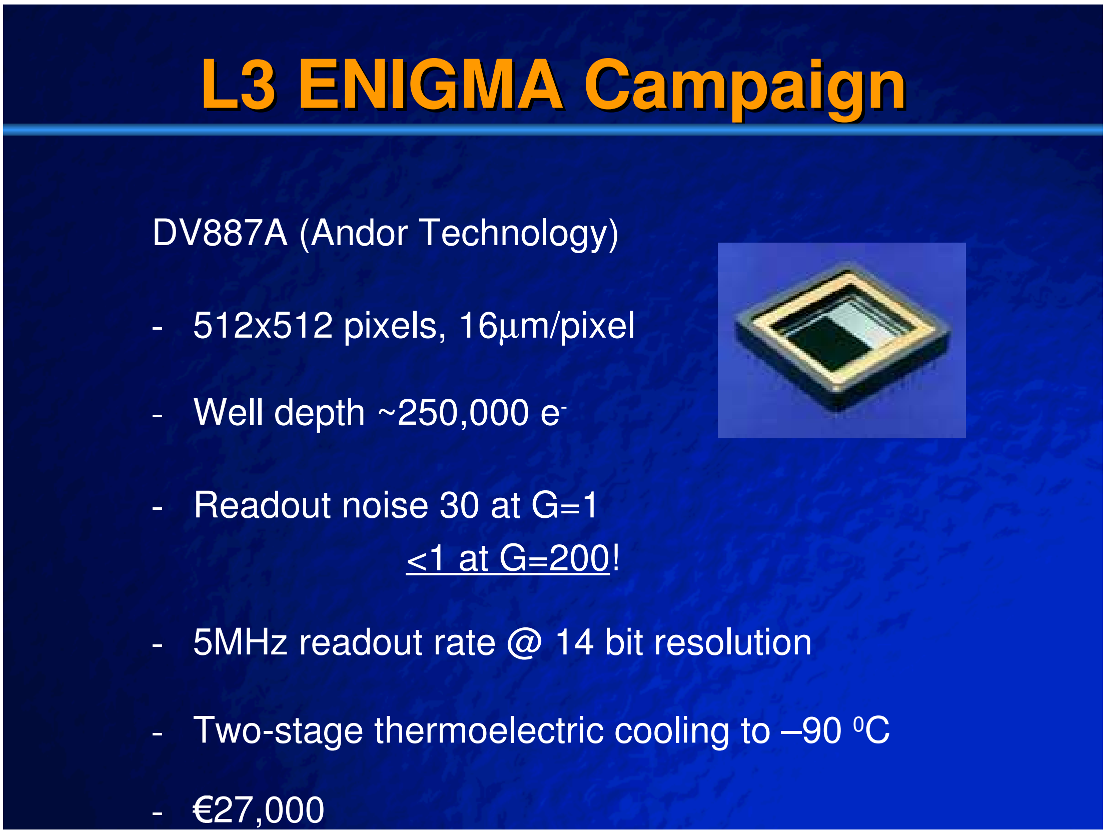
L3 ENIGMA Campaign
DV887A (Andor Technology)
- 512x512 pixels, 16µm/pixel
- Well depth ~250,000 e-
- Readout noise 30 at G=1
<1 at G=200!
- 5MHz readout rate @ 14 bit resolution
- Two-stage thermoelectric cooling to –90 ⁰C
- €27,000

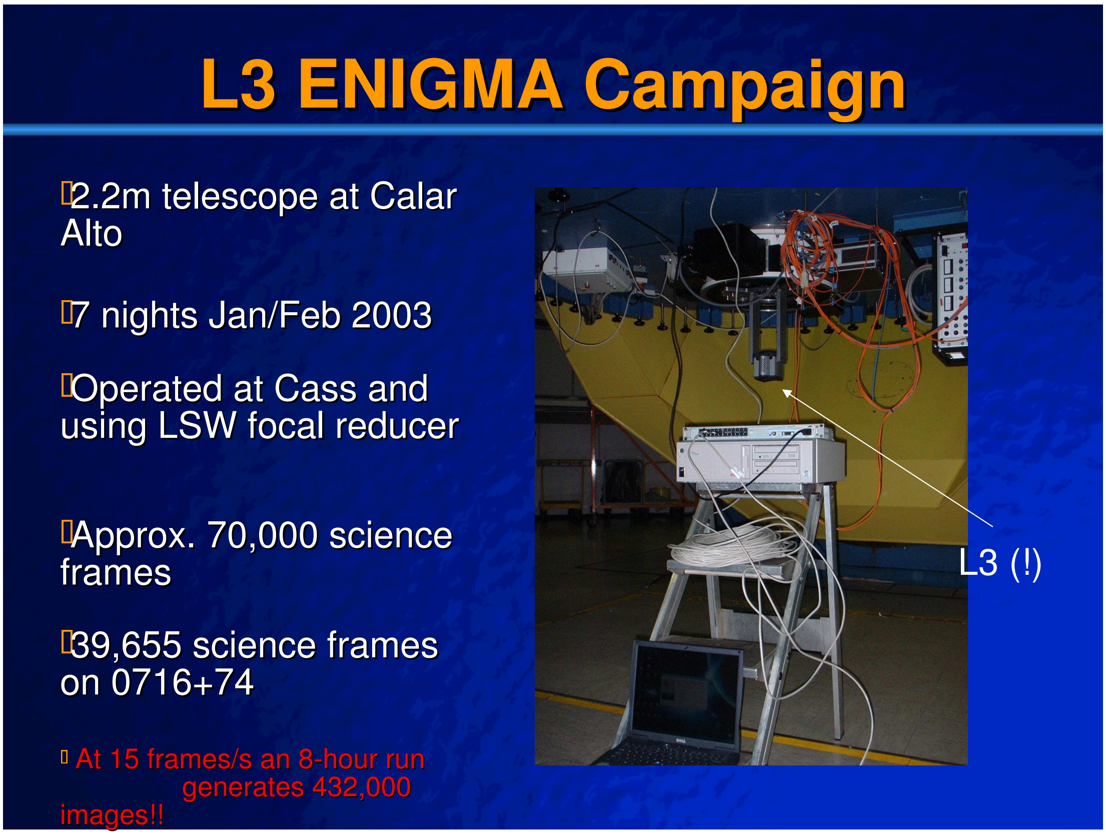
L3 ENIGMA Campaign
2.2m telescope at Calar Alto
7 nights Jan/Feb 2003
Operated at Cass and using LSW focal reducer
Approx. 70,000 science frames
39,655 science frames on 0716+74
At 15 frames/s an 8-hour run generates 432,000 images!!
L3 (!)

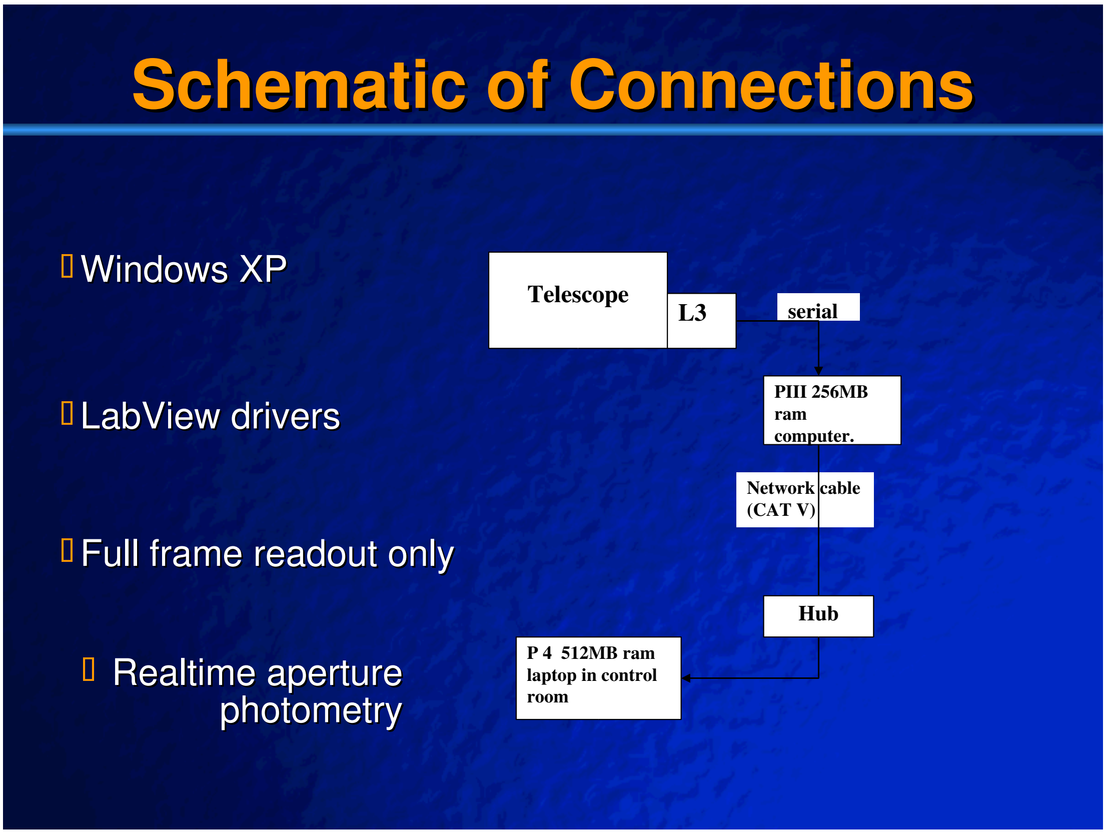
Schematic of Connections
Windows XP
LabView drivers
Full frame readout only
Realtime aperture photometry
Telescope
L3
serial
PIII 256MB ram computer.
Network cable (CAT V)
Hub
P 4 512MB ram laptop in control room


Markarian 421

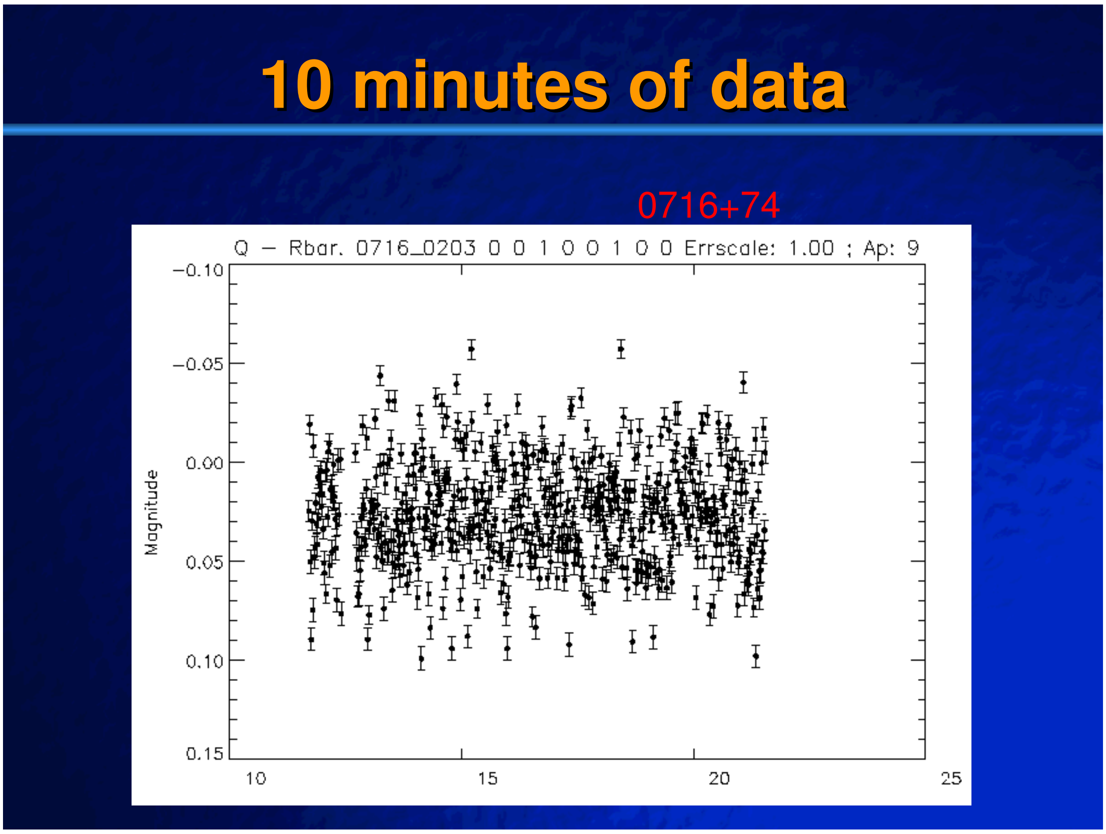
10 minutes of data
0716+74
Q — Rbar. 0716_0203 0 0 1 0 0 1 0 0 Errscale: 1.00 ; Ap: 9
Magnitude
−0.10
−0.05
0.00
0.05
0.10
0.15
10
15
20
25

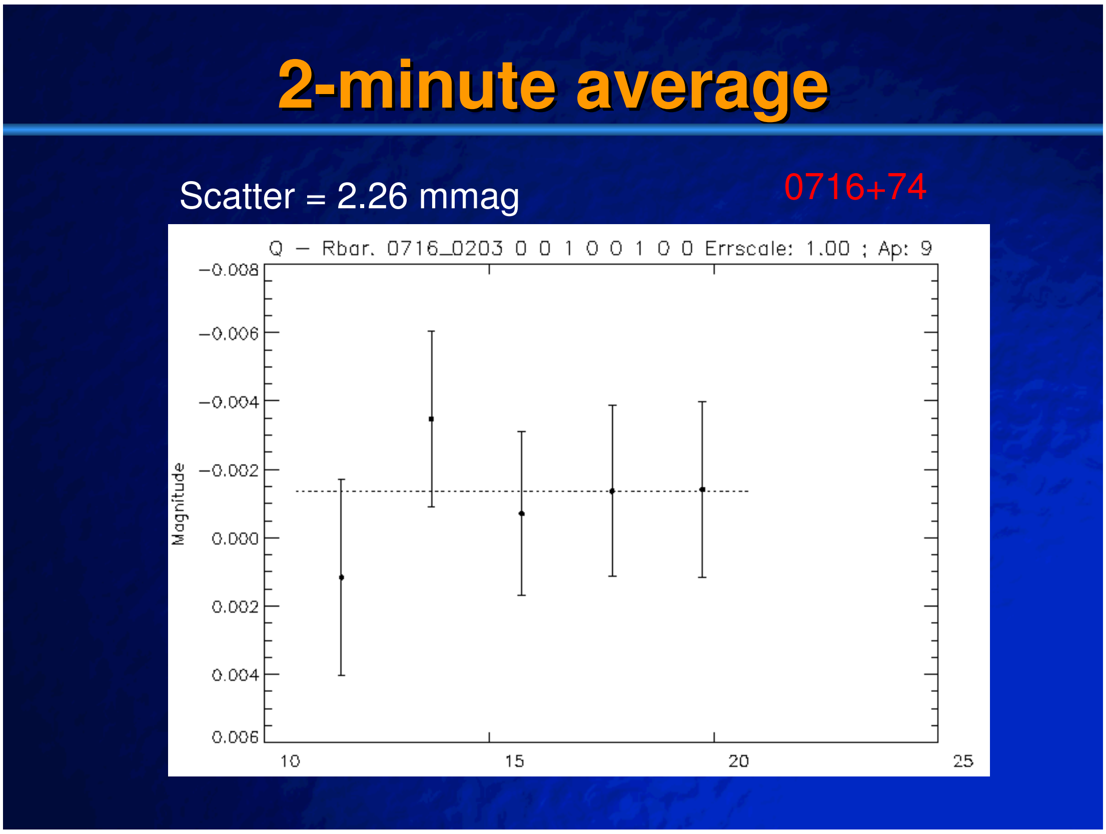
2-minute average
Scatter = 2.26 mmag
0716+74
Q — Rbar. 0716_0203 0 0 1 0 0 1 0 0 Errscale: 1.00 ; Ap: 9
Magnitude
−0.008
−0.006
−0.004
−0.002
0.000
0.002
0.004
0.006
10
15
20
25

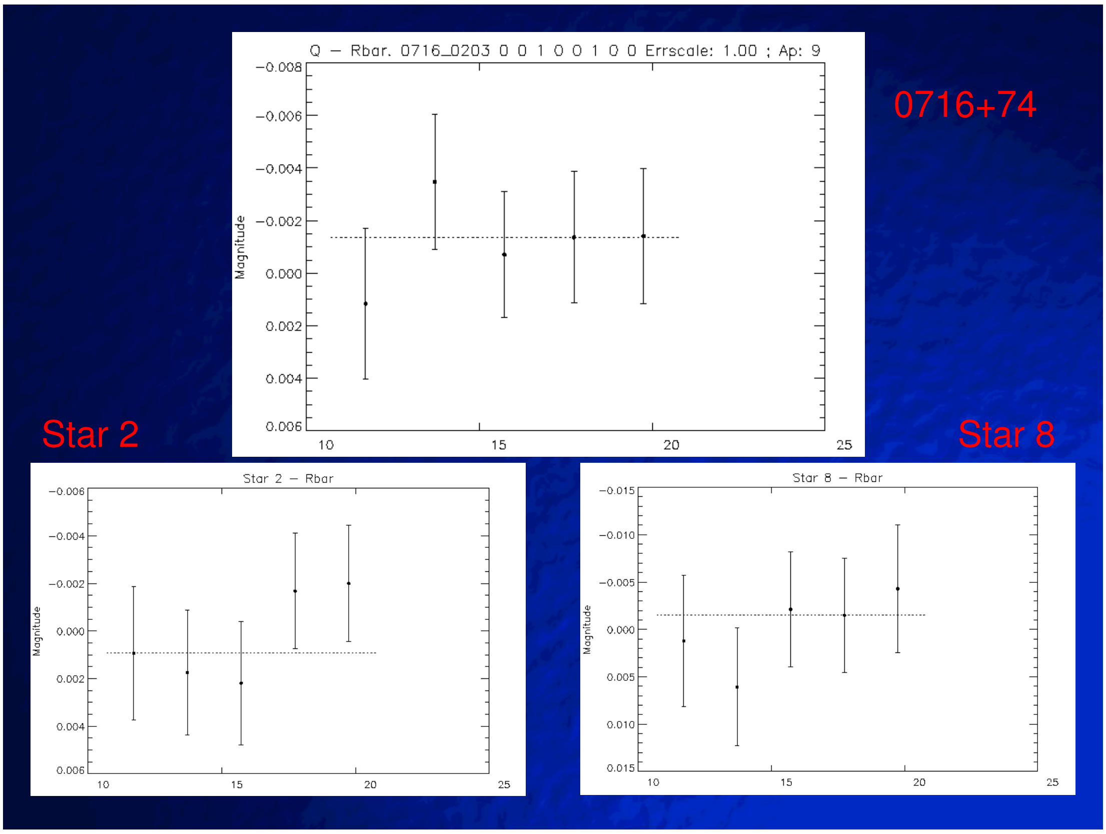
Q − Rbar. 0716_0203 0 0 1 0 0 1 0 0 Errscale: 1.00 ; Ap: 9
Magnitude
0716+74
Star 2
Star 8
Star 2 − Rbar
Star 8 − Rbar

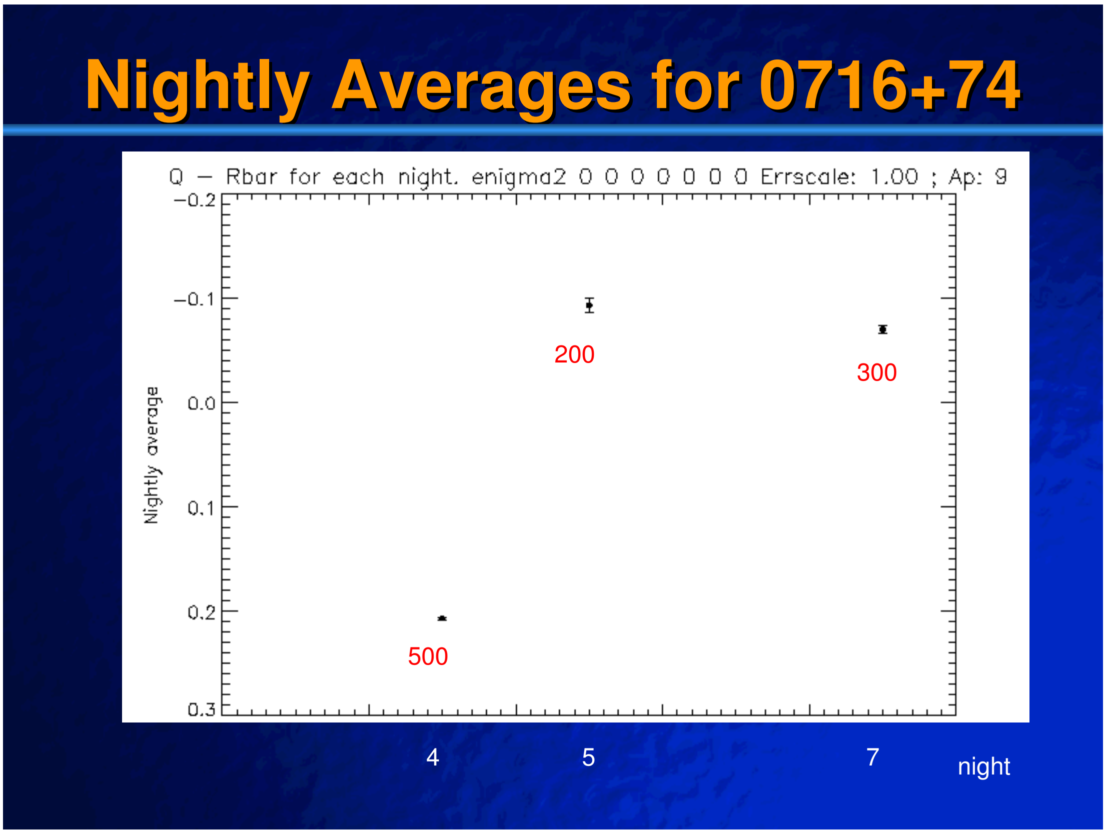
Nightly Averages for 0716+74
Q − Rbar for each night. enigma2 0 0 0 0 0 0 0 Errscale: 1.00 ; Ap: 9
Nightly average
200
300
500
4
5
7
night

Conclusions

- Preliminary results hint at stability of L3 and good prospects for use in high precision photometry
- Potential to generate enormous quantities of data very quickly
- Noiseless readout means data generation rates are aperture independent
- Caution – data reduction from observing run has only begun!

Robotic Telescope at Boyden

- Privately funded 16”-18” telescope
- Paramount mount
- Operational early 2004
- Associated 1.5m telescope

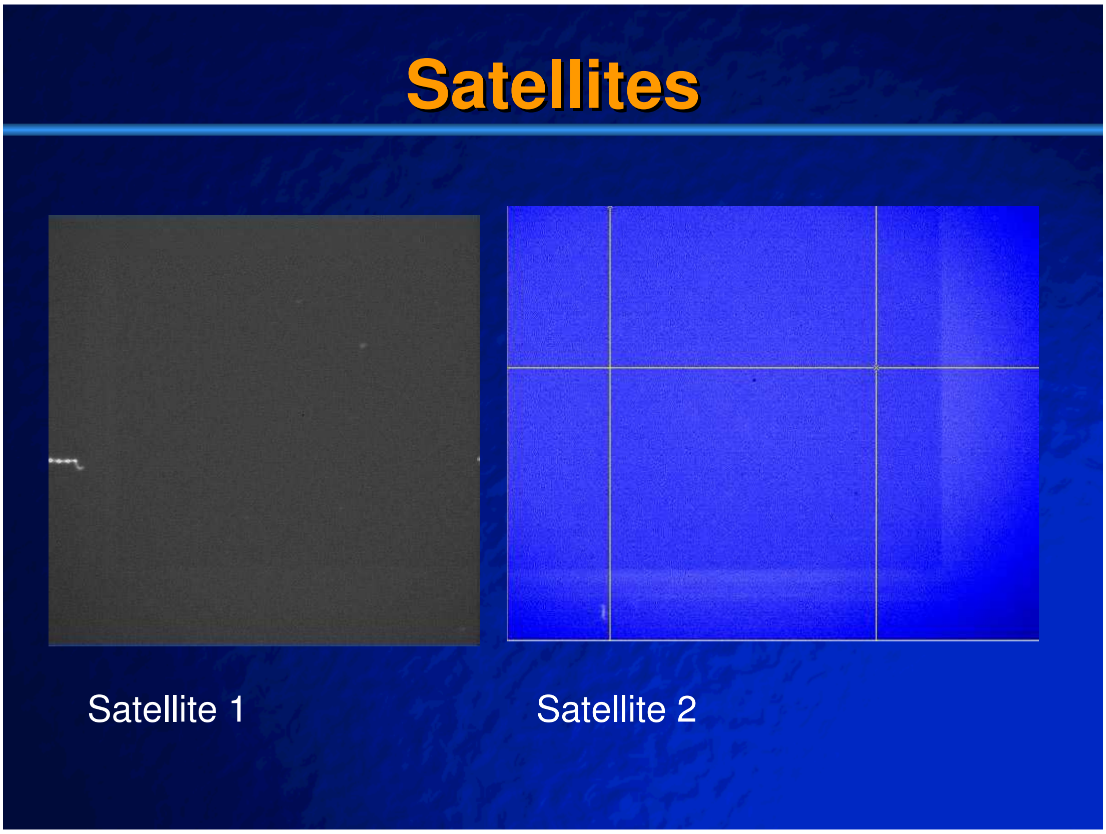
Satellites
Satellite 1
Satellite 2

2.3 L. Hanlon: Small robotic observatories

Small Robotic Observatories

Lorraine Hanlon
University College Dublin

Current Status

- 90 robotic observatories worldwide
  - Most operational
  - Some still in planning phase
- Comprehensive listing of sites: http://www.gcn.gsfc.nasa.gov

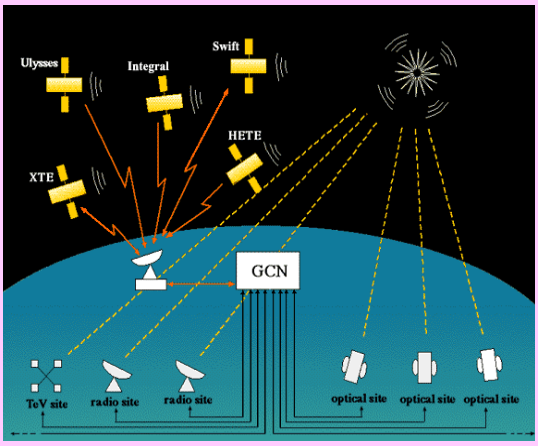

Why?

- Hardware relatively cheap - driven mainly by the amateur market
- Fully integrated instrumentation available off the shelf
- Communications technology relatively mature now
- Impressive range of science which can be done for modest capital outlay

Robotic telescopes excel at:

- Monitoring sources e.g.
  - AGN
  - Extrasolar planet host stars
  - Variable stars
- Rapid response e.g.
  - Targets of Opportunity e.g. blazar flares
  - Gamma-ray Bursts
  - Supernovae & Novae
- Supporting satellite observations

The Watcher Project

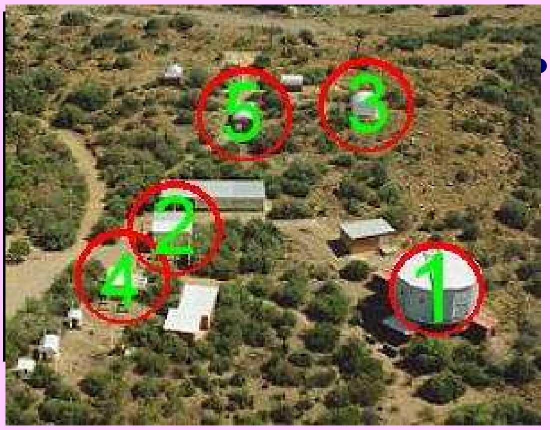

- Collaboration between UCD, CIT and the University of the Free State (UVS), Bloemfontein, South Africa at Boyden Observatory.

•Site has ~300 clear nights per year

•Typical seeing ~1-1.5″

Scientific Goals

- GRB flashes & afterglows
  - Southern hemisphere at African longitudes not currently covered
  - Launch of NASA's SWIFT in December 2003
    - 300 GRBs/year localised to better than few arcminutes
- Extrasolar planet discovery using transit method
- Blazar monitoring

System Design

Drivers:

- Components must be cheap, high quality and available off-the-shelf.
- System field of view should be well-matched to expected SWIFT GRB localisation capability (arcseconds to arcminutes) & to requirements for differential photometry.
- Any part of the accessible sky should be reachable within ~30 seconds.

System Description

- 40cm f/14 classical Cassegrain design from Optical Guidance Systems
- Fast slewing (20 s) equatorial mount from Wide-Sky Optics

System Description

- AP6 1Kx1K CCD from Apogee Instruments
  - thermoelectrically cooled (NB for autonomous observing)
  - 1.3MHz readout rate
  - 24 μm pixels & f-ratio of 14
  - ––> system FOV of ~ 12′x12′
- Filter wheel & weather station not yet selected.

Telescope Operation

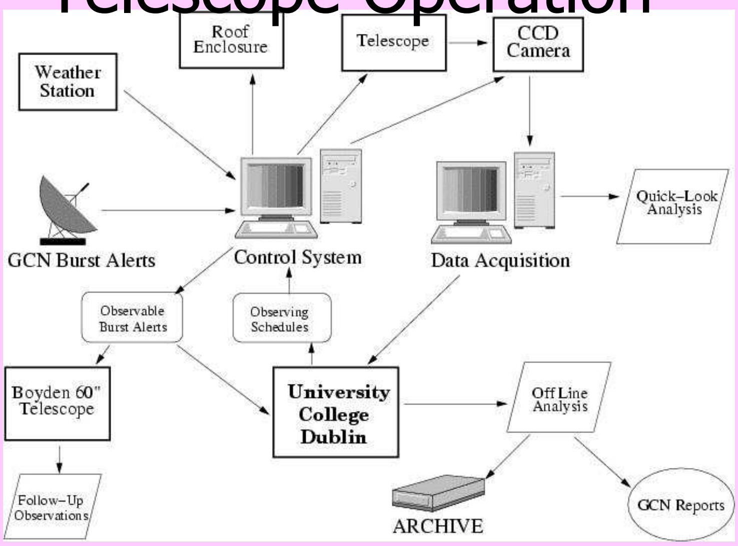

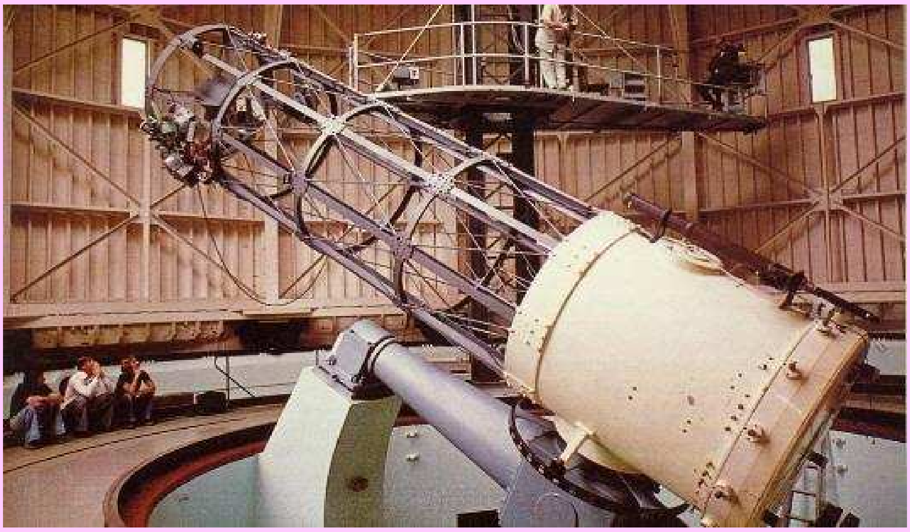

Telescope Enclosure

Watcher Capabilities

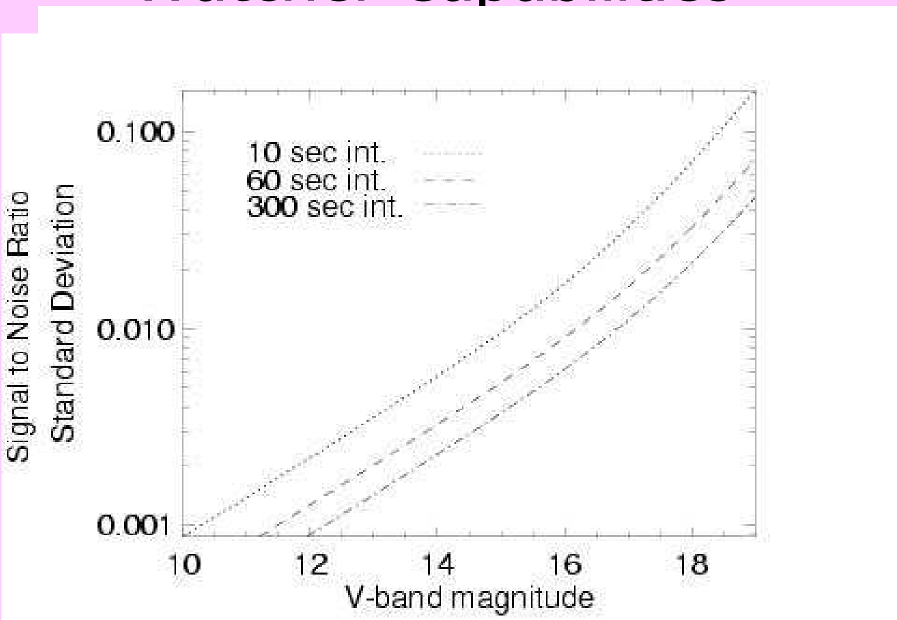

Watcher Science

- GRBs

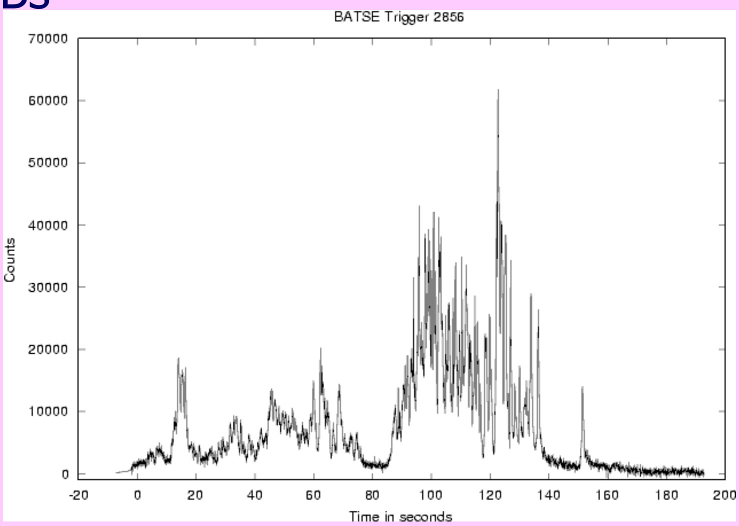

- Optical flashes during GRB events
  - Reverse shock
  - GRB990123 flash reached V_{mag} of 9, decayed to V_{mag} of 14 after ~ 20sec
  - How rare/common are they?
- Early afterglows

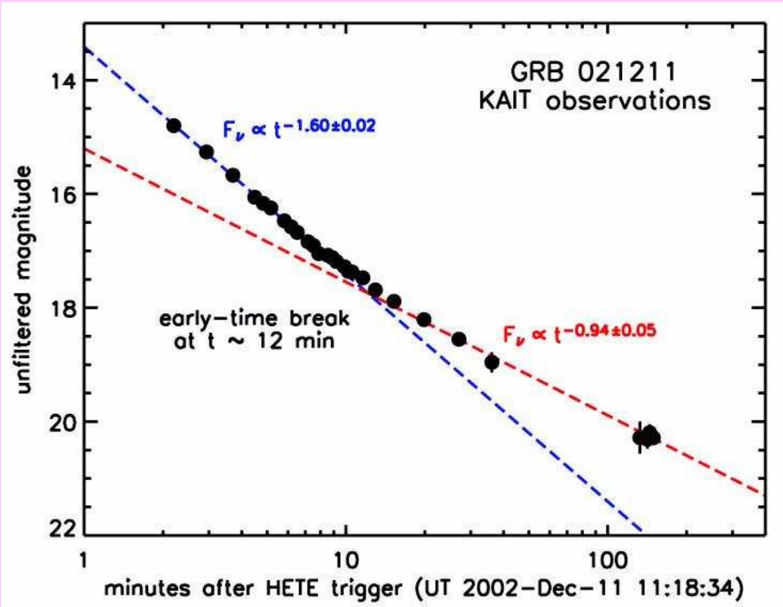

Extrasolar Planet Searches

- First ESP has been discovered using the transit method
- We plan to monitor lightcurves of ~ 10,000 stars to detect transit signatures
- Probably won't be sensitive to earth mass planets

Blazar Monitoring

- Routine monitoring of BL Lacs
- Coordinated observations with satellite and/or ground-based campaigns
- Anything you would like us to look at

Project Schedule

- CCD already acquired & being tested
- Telescope & mount to be delivered to UCD in summer 2003
- Fully tested and integrated system to be shipped to Boyden end 2003
- Watcher-1 commissioned and operational by Spring 2004

2.4 L. Takalo: Status of the KVA telescope on La Palma

Status of the KVA telescope

KVA is located on La Palma, close to the MAGIC site. It is a 60cm telescope, with a 35cm telescope attached to the same frame. Both telescopes are equiped with a CCD camera.

These telescopes can be used simultaneously!!!

The 60cm telescope is optimized now for polarimetric observations in B, R or white light. The limiting magnitude is around V=18 for polarimetric observations with the accuracy of 1% , in 30 minutes!!!
The 35cm telescope is optimized for UBVRI photometry!!!

These telescopes were used (both in photometric mode) in December 2002 and late February- early March for multifrequency campaign observations of MKN 421!!!!
CT1 and VERITAS were monitoring MKN 421 at TeV energies and RXTE in X-rays during these times.
During the last campaign we obtained 1700 CCD frames of MKN 421 during 8 nights!! The observers were Mikko Pasanen and Martin Merck. Data reduction and analysis is in progress.

We are also in the process of making the telescope automatic, with the help of the Perugia Observatory. There has been quite good progress in this. We can already use the telescope from Tuorla vai Internet.

2.5 J. Heidt: Complementary IDV observations from the T1T

Complementary IDV observations from the T1T

Jochen Heidt, Landessternwarte Heidelberg
in collab. with J. Ohlert, Institute of Technology Gießen

- **T1T:** Trebur 1m telescope (nowadays 1.2m telescope) located about 80km north of Heidelberg and some 30km southwest of Frankfurt
- Private foundation (M. Adrian), ”first light” in 1996
- Statutes: support of scientific astronomical observations

$\Longrightarrow$ perform complementray IDV observations within ENIGMA activities

CCD

• 1300×1340 pix backside-illuminated EEV-CCD from Princeton instruments

• 20μ-pix, thermoelectrically cooled (-40^oC), low dark current and RON, good cosmetics and high QE

Configuration

Direct imaging: f/9.3 $\Rightarrow$ 0.44”/pix $\Rightarrow$ 9.9’ $\times$ 9.6’

Focal reducer: f/5.1 $\Rightarrow$ 0.81”/pix $\Rightarrow$ 18.1’ $\times$ 17.5’

• Standard UBVRI Johnson-filter (ordered, promised within the next weeks)

• Telescope operated in tracking mode (no guiding). Tracking is very stable at least up to 10mins

ToBeDone - in the next few months

Measuring the sky brightness (light pollution may be a problem), check flatfielding etc..

$\Rightarrow$ Need to know the mag range we may cover and the accuracy we can get within the mag range + duty cycle possible

Training of people on site (amateurs) of how to observe and to reduce data

”Simulate” observing campaign by observations of a few sources during several subsequent nights

• Aim is to be ready for complementary IDV observations by late summer/early fall

What can the T1T do for ENIGMA?

$\star$ Dedicated observations during short periods (few days), e.g. during Integral pointings

$\star$ Dedicated observations lasting 2-3 weeks for multi-lambda campaigns

$\star$ IDV observations of specific targets (weeks to months) with high duty cycle

$\star$ Long-term monitoring of selected sources

Chapter 3

Session II: Sepataring intrinsic and extrinsic Intraday Variability (C. Raiteri)

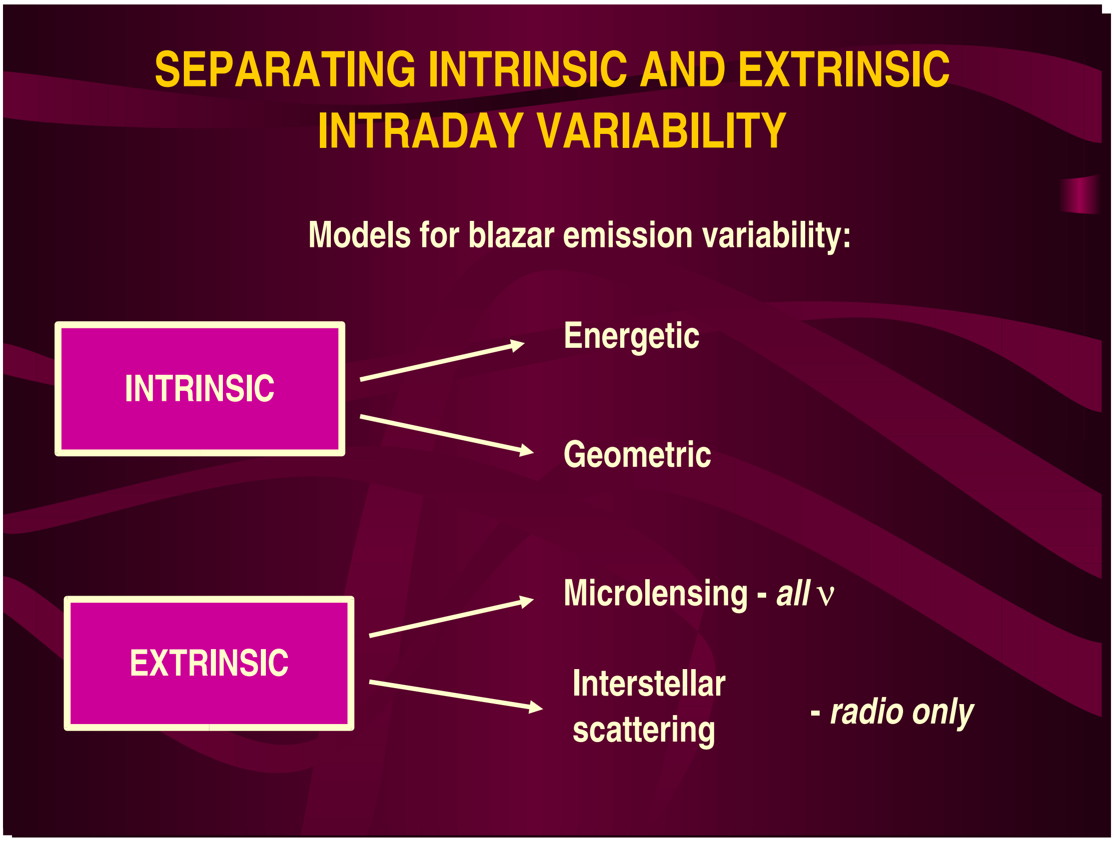

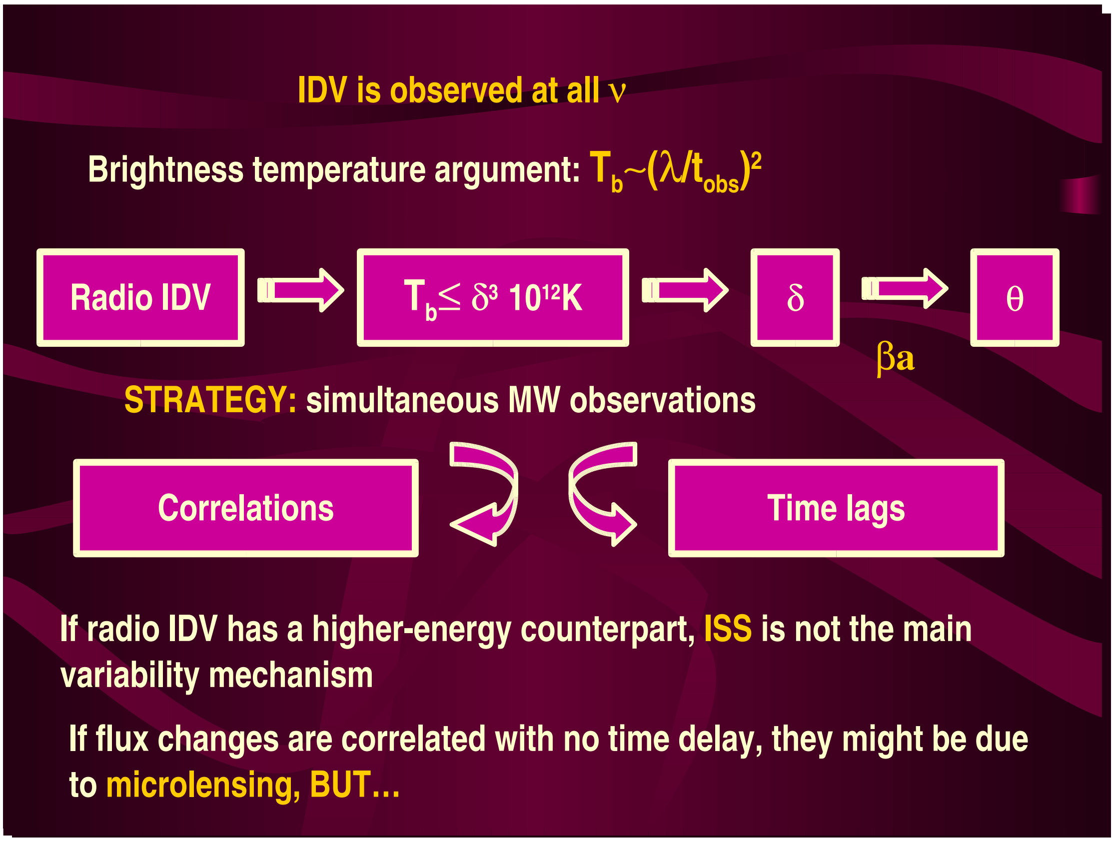
IDV is observed at all ν
Brightness temperature argument: $T_b \sim (\lambda / t_{obs})^2$
Radio IDV
$T_b \leq \delta^3\ 10^{12}$K
δ
θ
βa
STRATEGY: simultaneous MW observations
Correlations
Time lags
If radio IDV has a higher-energy counterpart, ISS is not the main variability mechanism
If flux changes are correlated with no time delay, they might be due to microlensing, BUT…

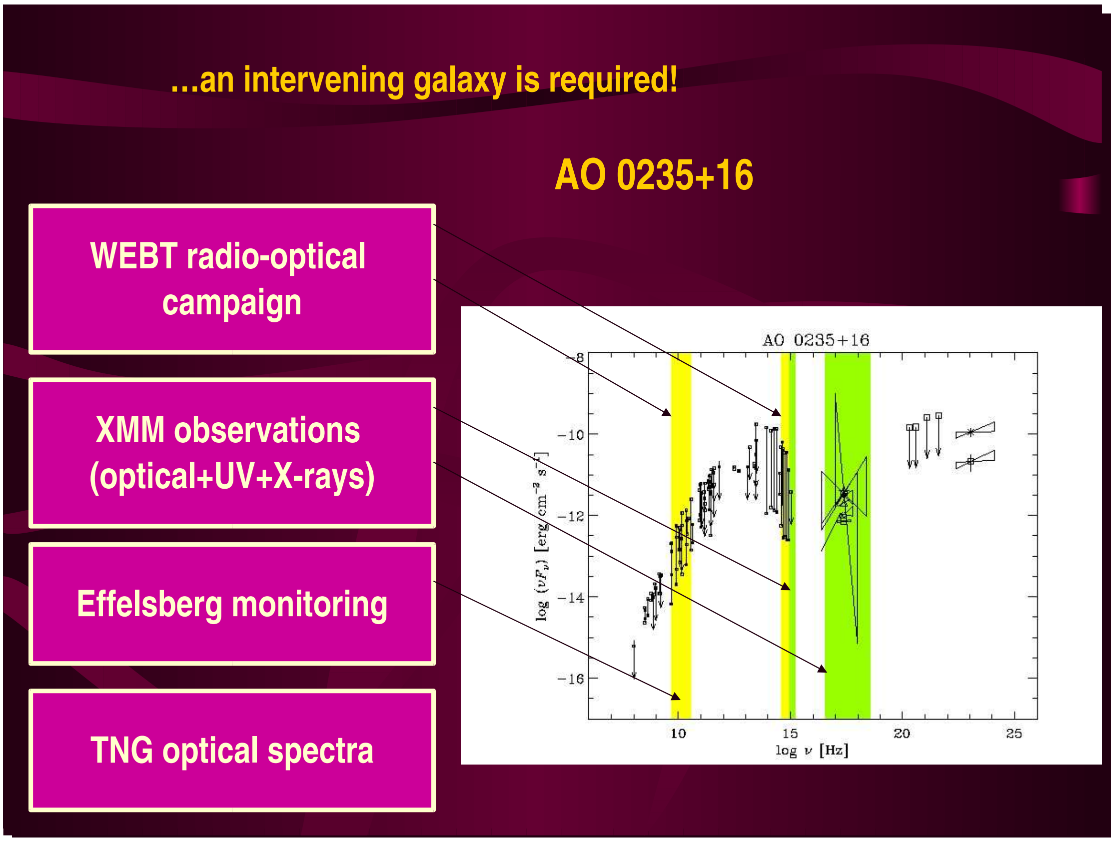
…an intervening galaxy is required!
AO 0235+16
WEBT radio-optical campaign
XMM observations (optical+UV+X-rays)
Effelsberg monitoring
TNG optical spectra
AO 0235+16
log (νF_ν) [erg/cm⁻² s⁻¹]
−8
−10
−12
−14
−16
10
15
20
25
log ν [Hz]

3.1 L. Fuhrmann: Investigations of IDV blazar cores

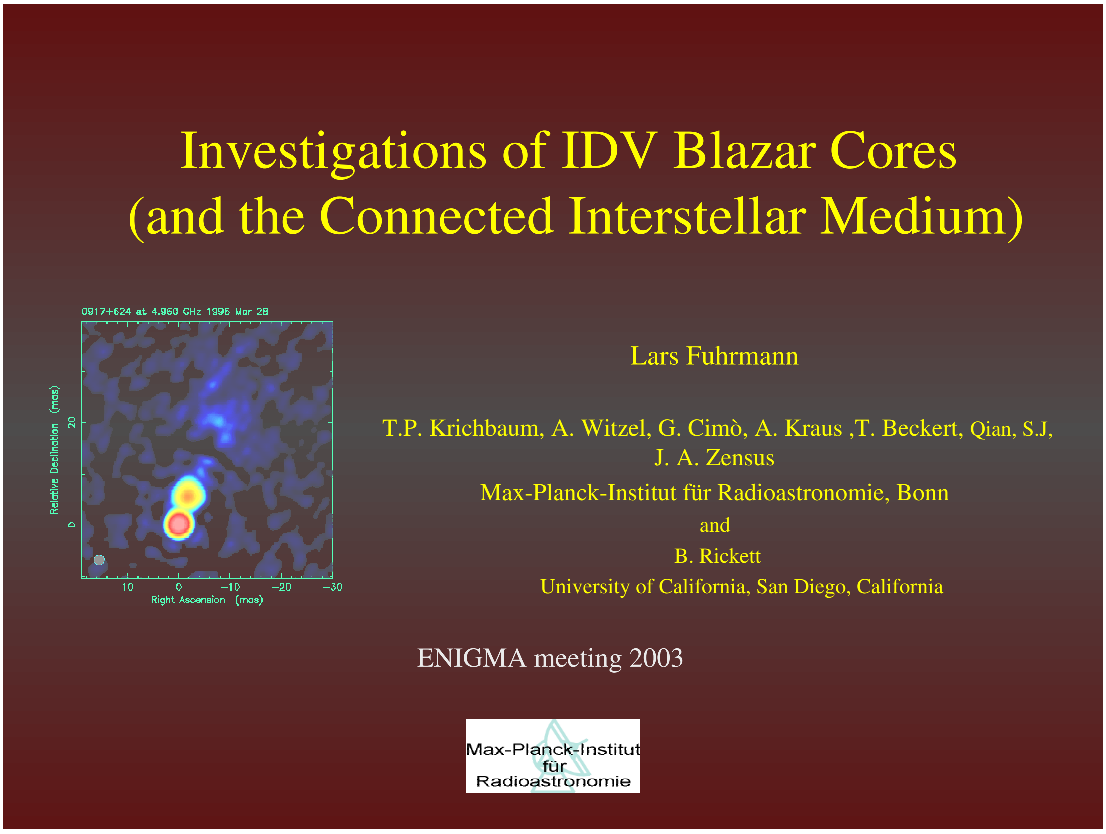

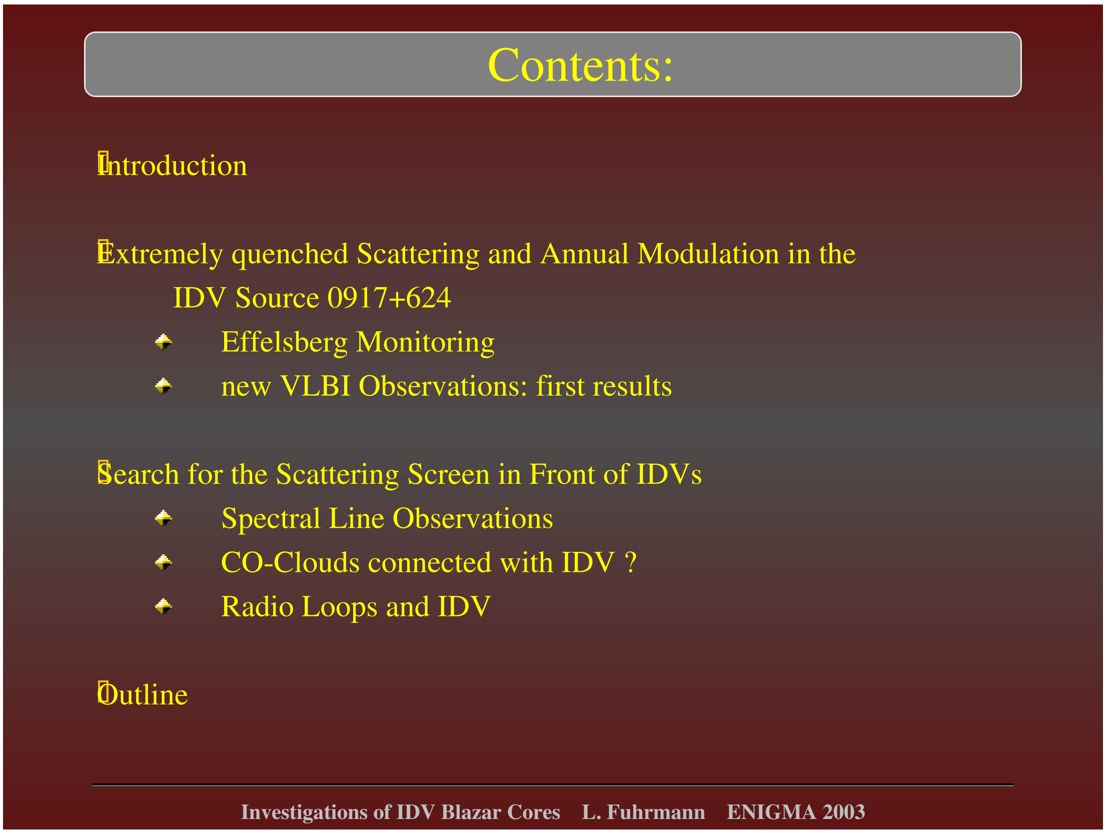
Contents:
Introduction
Extremely quenched Scattering and Annual Modulation in the IDV Source 0917+624
Effelsberg Monitoring
new VLBI Observations: first results
Search for the Scattering Screen in Front of IDVs
Spectral Line Observations
CO-Clouds connected with IDV ?
Radio Loops and IDV
Outline
Investigations of IDV Blazar Cores L. Fuhrmann ENIGMA 2003

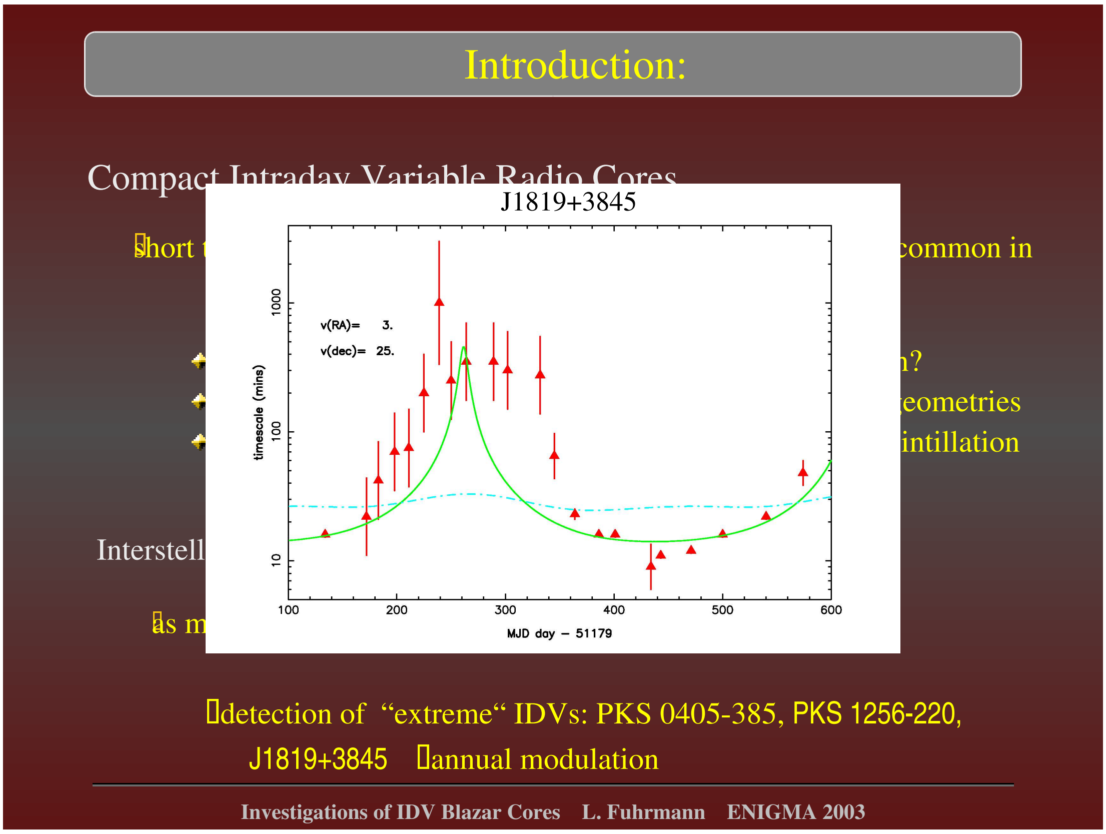
Introduction:
Compact Intraday Variable Radio Cores
Short t
common in
n?
eometries
intillation
Interstell
as m
J1819+3845
v(RA)= 3.
v(dec)= 25.
timescale (mins)
1000
100
10
100
200
300
400
500
600
MJD day − 51179
detection of “extreme“ IDVs: PKS 0405-385, PKS 1256-220, J1819+3845 annual modulation
Investigations of IDV Blazar Cores L. Fuhrmann ENIGMA 2003

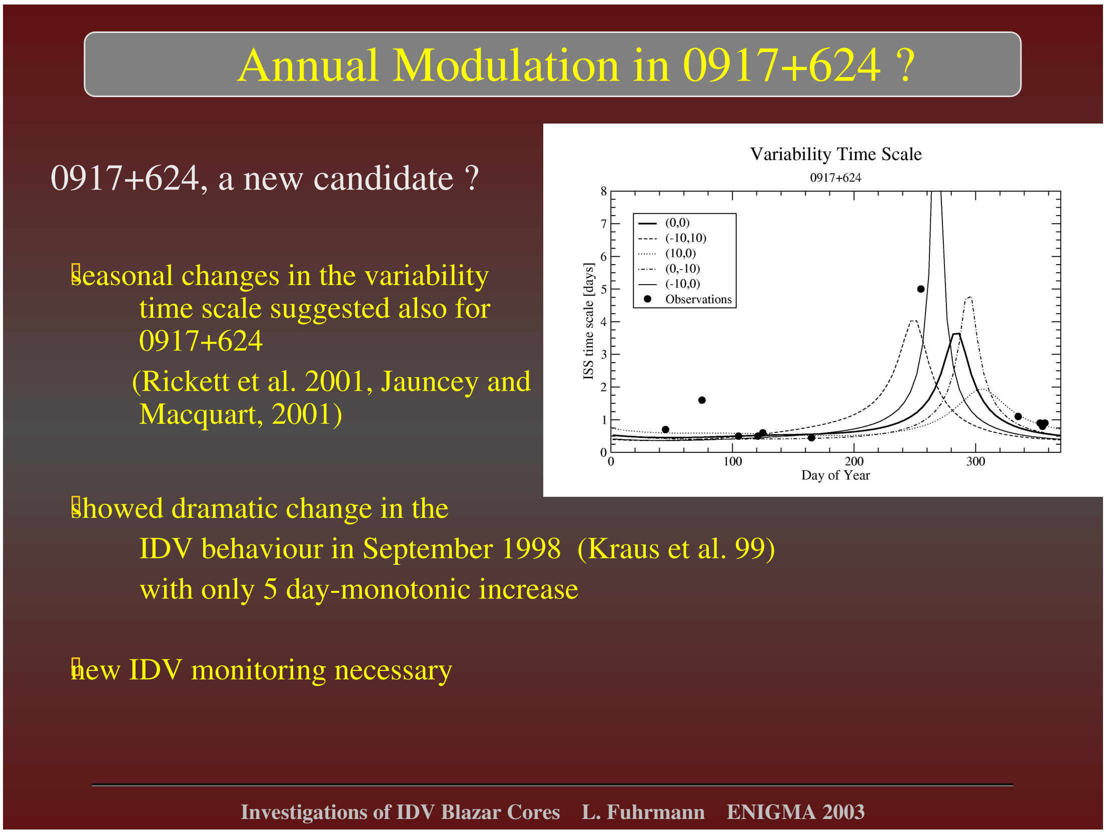
Annual Modulation in 0917+624 ?
0917+624, a new candidate ?
seasonal changes in the variability time scale suggested also for 0917+624
(Rickett et al. 2001, Jauncey and Macquart, 2001)
Variability Time Scale
0917+624
ISS time scale [days]
Day of Year
(0,0)
(-10,10)
(10,0)
(0,-10)
(-10,0)
Observations
showed dramatic change in the IDV behaviour in September 1998 (Kraus et al. 99) with only 5 day-monotonic increase
new IDV monitoring necessary
Investigations of IDV Blazar Cores L. Fuhrmann ENIGMA 2003

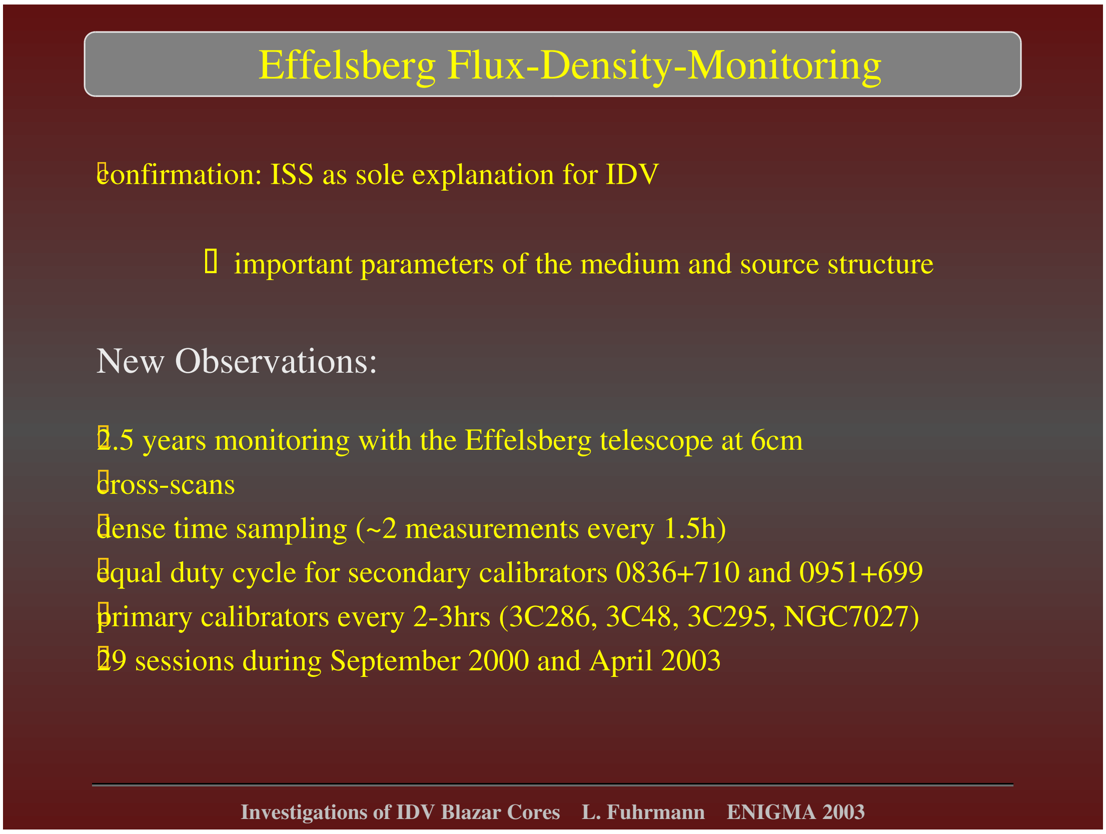
Effelsberg Flux-Density-Monitoring
confirmation: ISS as sole explanation for IDV
important parameters of the medium and source structure
New Observations:
2.5 years monitoring with the Effelsberg telescope at 6cm
cross-scans
dense time sampling (~2 measurements every 1.5h)
equal duty cycle for secondary calibrators 0836+710 and 0951+699
primary calibrators every 2-3hrs (3C286, 3C48, 3C295, NGC7027)
29 sessions during September 2000 and April 2003
Investigations of IDV Blazar Cores L. Fuhrmann ENIGMA 2003

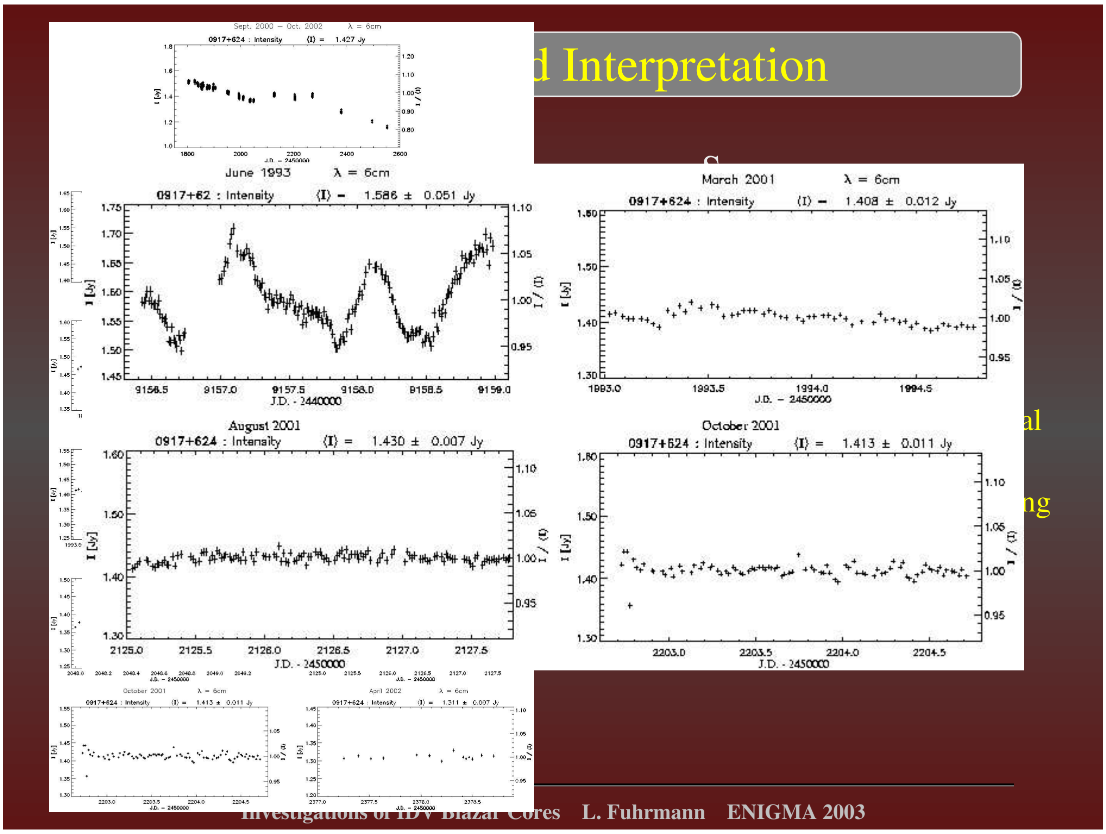

Results and Interpretation

annual modulations ? – problems:

- no restart of the rapid variability in 0917+624
- m appears to be variable
- other nearby sources don´t show seasonal ISS effects

possible scenarios:

1) ISM much more complex
   - change in scattering size

decrease of electron densities or increase of distance to the screen

moving clouds, layers or holes?

=> angular size smaller than a few degrees

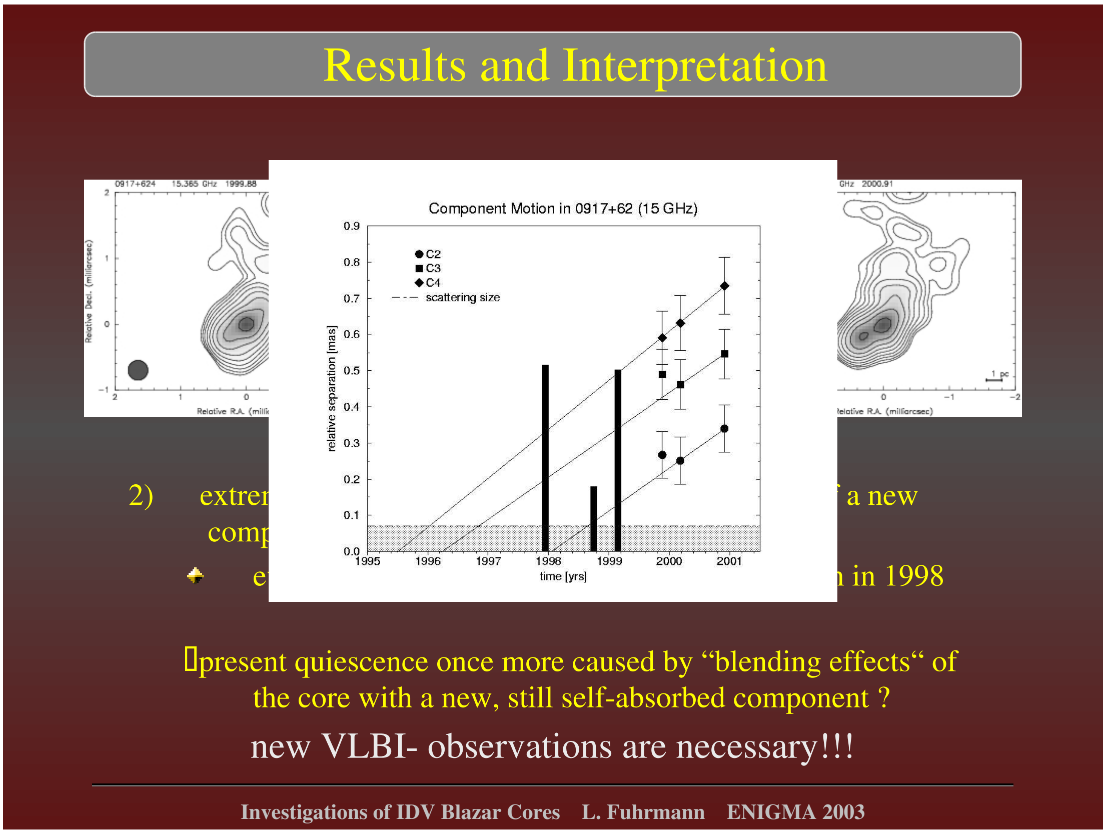
Results and Interpretation
Component Motion in 0917+62 (15 GHz)
C2
C3
C4
scattering size
relative separation [mas]
time [yrs]
2) extre
comp
a new
e
in 1998
present quiescence once more caused by "blending effects" of the core with a new, still self-absorbed component ?
new VLBI- observations are necessary!!!
Investigations of IDV Blazar Cores L. Fuhrmann ENIGMA 2003

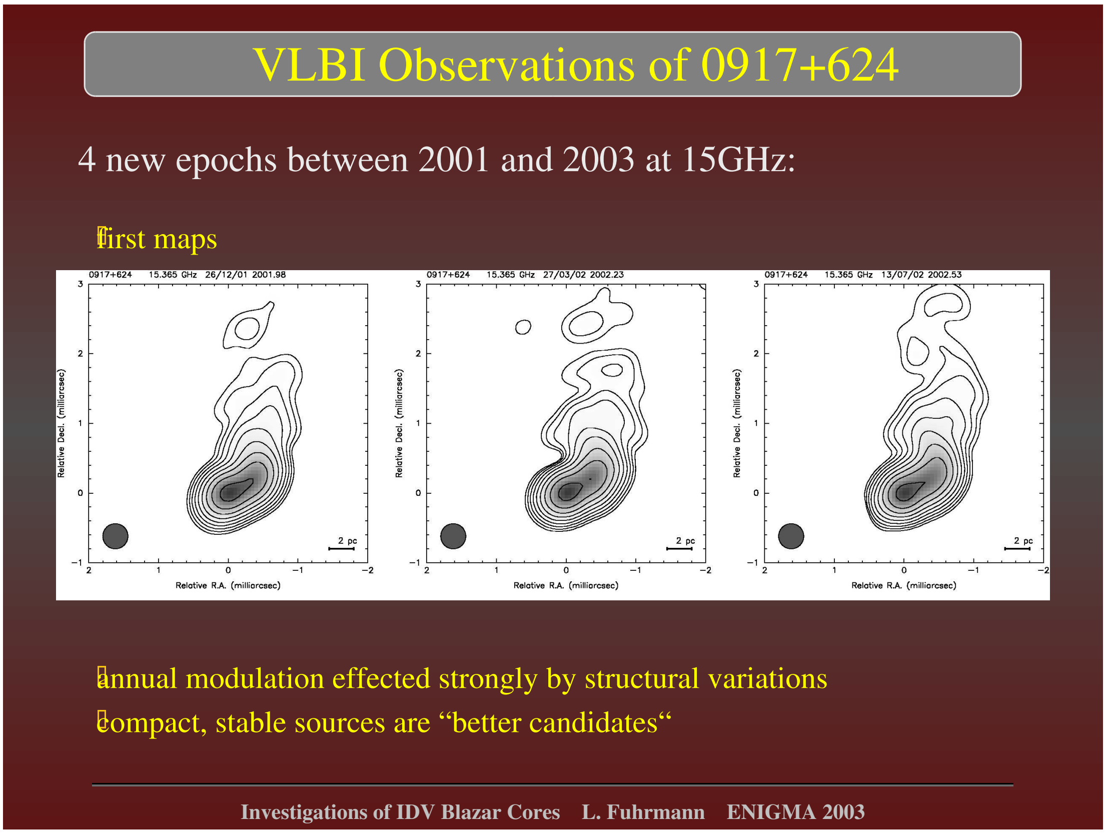
VLBI Observations of 0917+624
4 new epochs between 2001 and 2003 at 15GHz:
first maps
0917+624 15.365 GHz 26/12/01 2001.98
0917+624 15.365 GHz 27/03/02 2002.23
0917+624 15.365 GHz 13/07/02 2002.53
Relative Decl. (milliarcsec)
Relative R.A. (milliarcsec)
annual modulation effected strongly by structural variations
compact, stable sources are "better candidates"
Investigations of IDV Blazar Cores L. Fuhrmann ENIGMA 2003

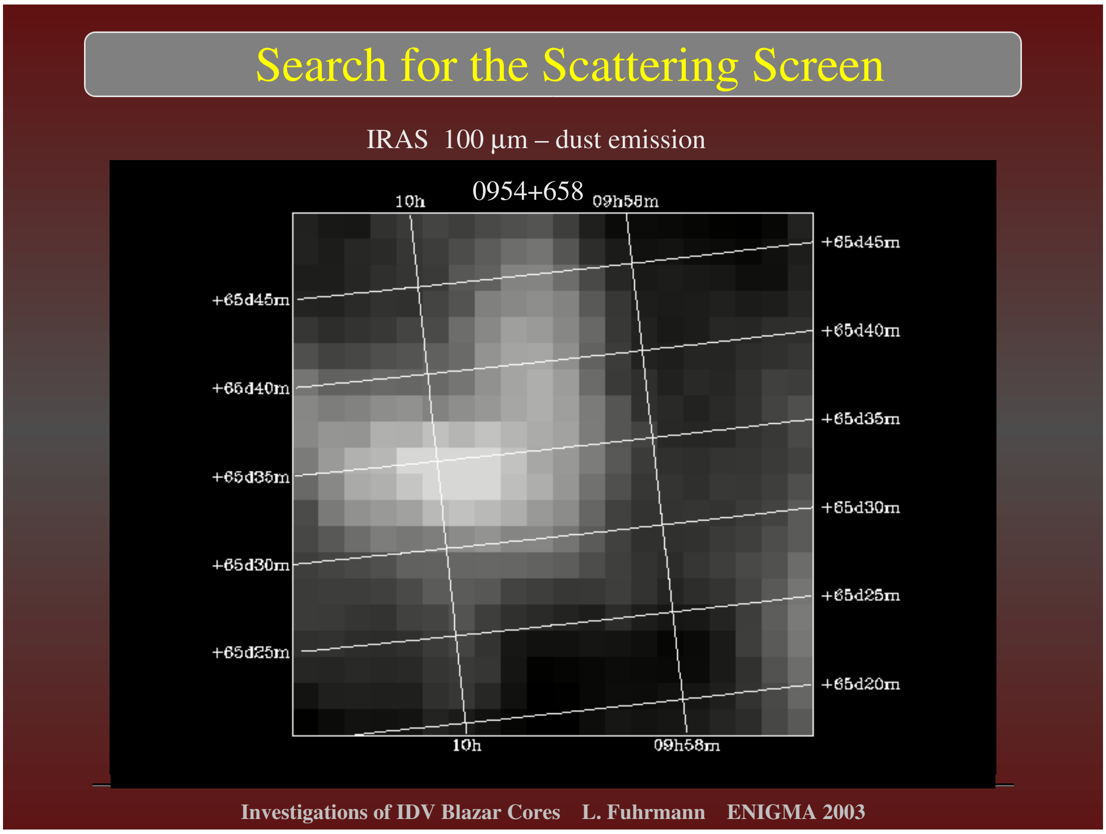
Search for the Scattering Screen
IRAS 100 µm – dust emission
0954+658
10h
09h58m
+65d45m
+65d40m
+65d35m
+65d30m
+65d25m
+65d20m
Investigations of IDV Blazar Cores L. Fuhrmann ENIGMA 2003

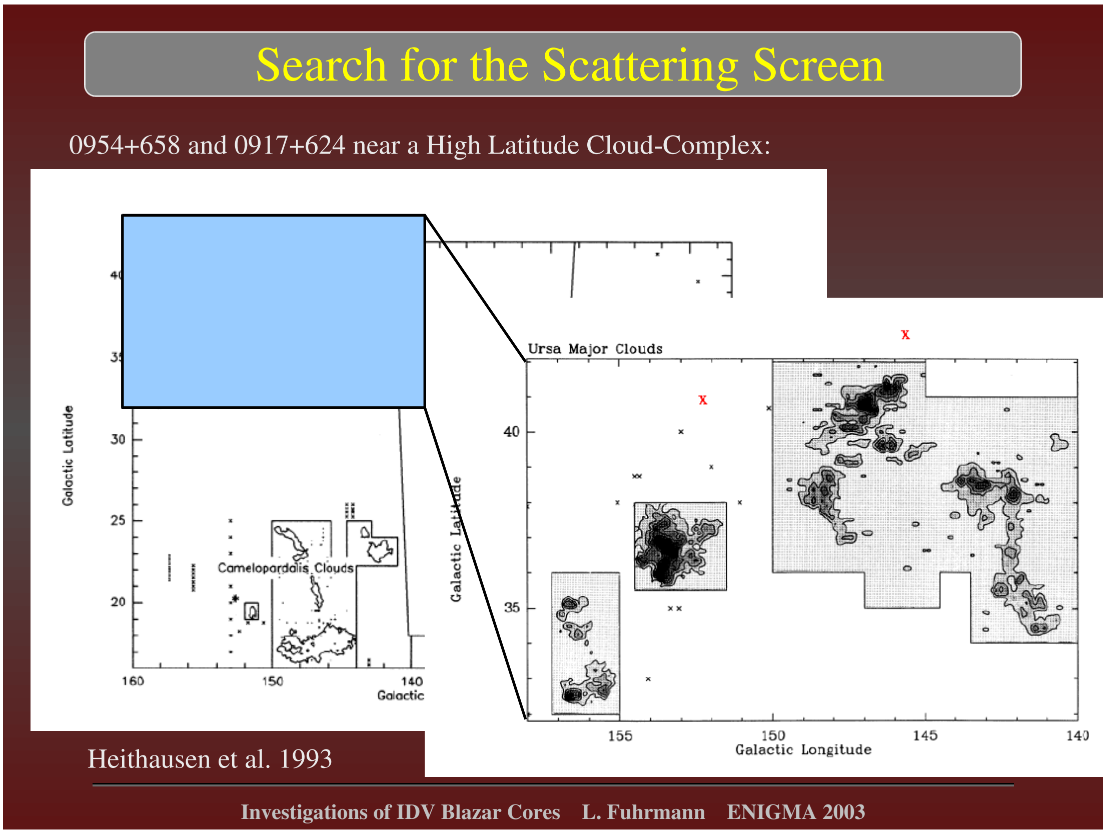
Search for the Scattering Screen
0954+658 and 0917+624 near a High Latitude Cloud-Complex:
Camelopardalis Clouds
Galactic Latitude
160
150
140
Galactic
Ursa Major Clouds
Galactic Longitude
155
150
145
140
40
35
Heithausen et al. 1993
Investigations of IDV Blazar Cores L. Fuhrmann ENIGMA 2003

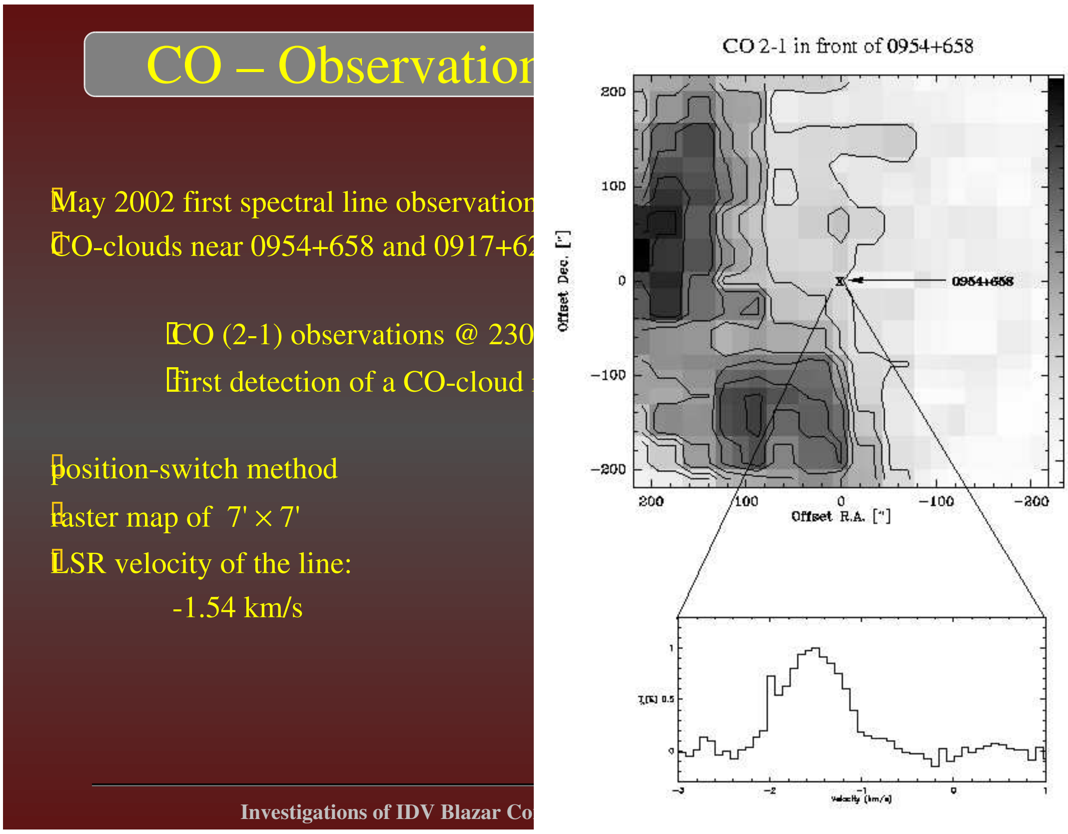
CO – Observation
May 2002 first spectral line observation
CO-clouds near 0954+658 and 0917+62
CO (2-1) observations @ 230
first detection of a CO-cloud
position-switch method
raster map of 7' × 7'
LSR velocity of the line:
-1.54 km/s
Investigations of IDV Blazar Co
CO 2-1 in front of 0954+658
Offset Dec. ["]
Offset R.A. ["]
0954+658

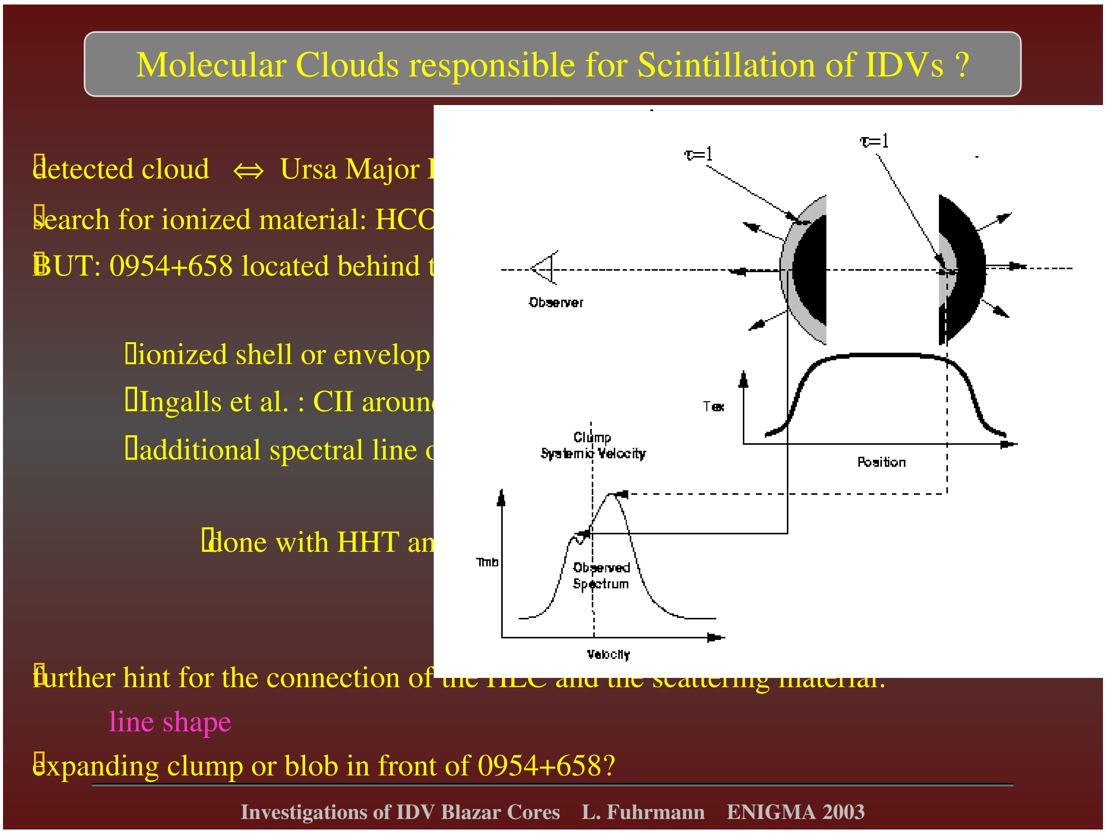
Molecular Clouds responsible for Scintillation of IDVs ?
detected cloud ⇔ Ursa Major
search for ionized material: HCO
BUT: 0954+658 located behind
ionized shell or envelop
Ingalls et al. : CII aroun
additional spectral line
done with HHT an
further hint for the connection of the HLC and the scattering material:
line shape
expanding clump or blob in front of 0954+658?
Investigations of IDV Blazar Cores L. Fuhrmann ENIGMA 2003
τ=1
τ=1
Observer
Tex
Position
Clump
Systemic Velocity
Tmb
Observed
Spectrum
Velocity

CO-Clouds as Origin of Scattering Material for IDVs?

Follow-up Observations with Pico Veleta:

- Search for ^{12}CO (1-0) in small sample of IDV-positions
  - 3 new detections (0153+744, 0454+844, 0602+67)

Large Scale ISM-Structures and IDV

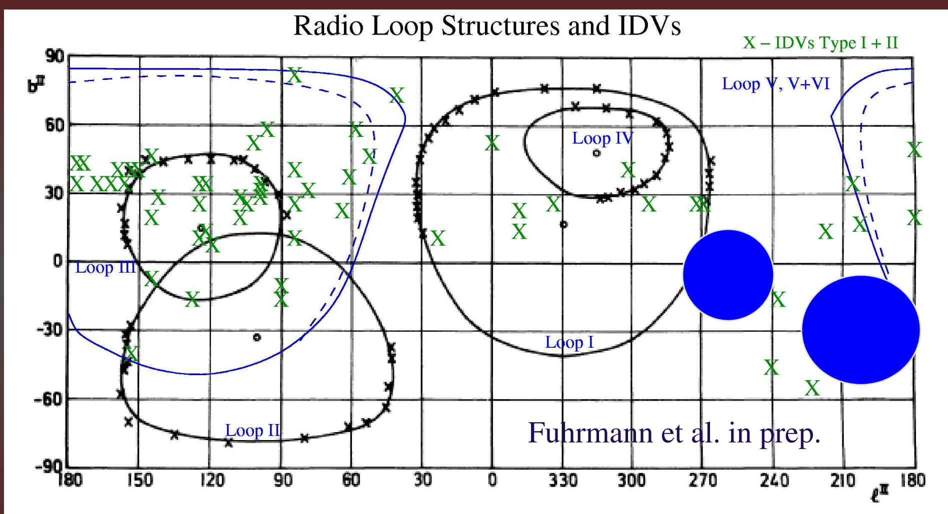

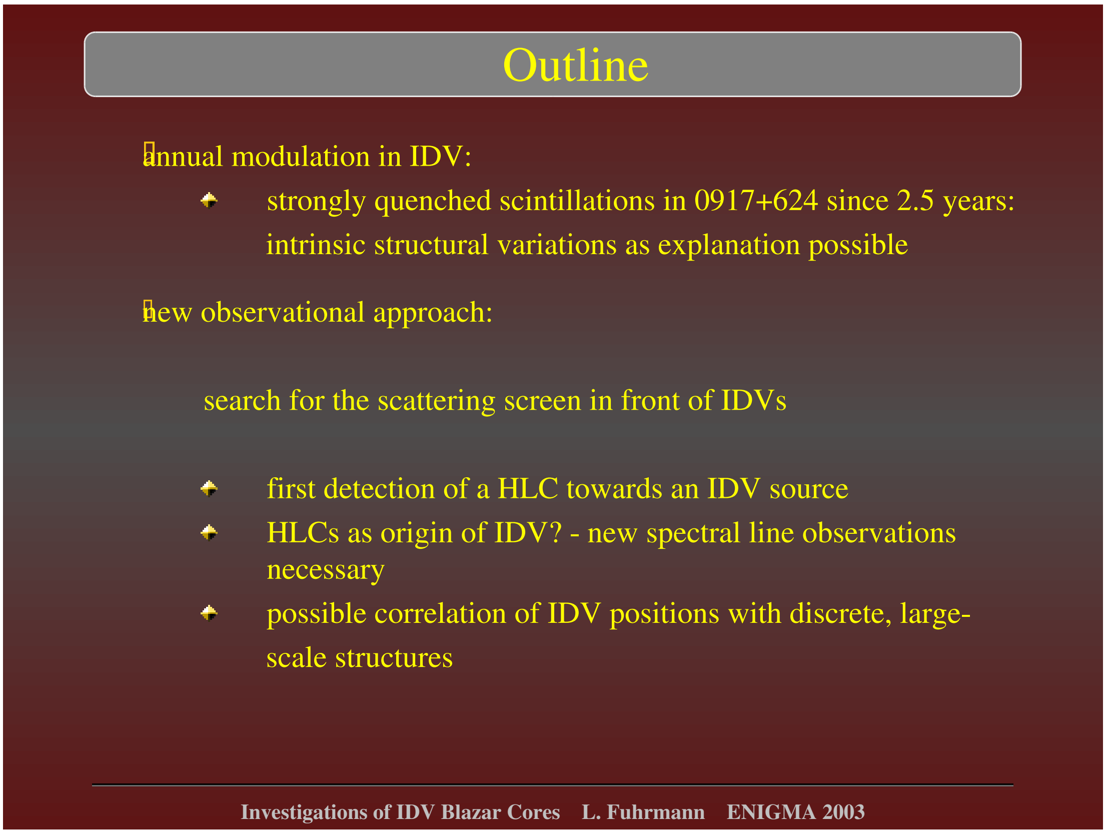
Outline
annual modulation in IDV:
strongly quenched scintillations in 0917+624 since 2.5 years: intrinsic structural variations as explanation possible
new observational approach:
search for the scattering screen in front of IDVs
first detection of a HLC towards an IDV source
HLCs as origin of IDV? - new spectral line observations necessary
possible correlation of IDV positions with discrete, large-scale structures
Investigations of IDV Blazar Cores L. Fuhrmann ENIGMA 2003

3.2 G. Cimò: Statistical Study of Intraday Variable Sources

Statistical Study of Intraday Variable Sources

Giuseppe Cimò
L. Fuhrmann
T. P. Krichbaum
T. Beckert
A. Kraus
A. Witzel
J. A. Zensus

Max-Planck-Institut
für
Radioastronomie

The IDV Phenomenon

- IDV in total ($\sim 20 - 30\,\%$) and polarized ($\sim$ factor 3 or more) flux density
- quasi-periodicity
- (anti-) correlation between variations in total and polarized flux density
- present in $\sim 30\,\%$ of all flat spectrum radio sources (Quirrenbach et al. 1992)
- broad-band correlations (Wagner et al. 1993)

If the variations are source-intrinsic:

- very small source sizes ($\leq c\Delta t$)
- extremely high $T_B = 10^{18} - 10^{21}$ K
- violation of the inverse Compton limit (10^{12} K)

Source-Intrinsic Scenarios:

Shock-in-jet models

$$T_B^{\text{obs}} = T_B^{\text{intrinsic}} \cdot D^{3-\alpha}$$

The relativistic effects as the superluminal motions observed in the VLBI cores ($v_{app} \approx 40c$, *Marscher et al. 2000*), can explain only moderate values of D, but much higher values ($D = 100 - 1000$) would be needed to bring the brightness temperature down to 10^{12} K.

Special geometry effects can be taken into account (Qian et al. 1991). The apparent brightness temperature can be reduced using only moderate Doppler and Lorentz factors: $T_b \propto \Gamma^2 D^3$ and the required factors are similar (even slightly greater) to those involved from superluminal motions.

Refractive InterStellar Scintillation:

The turbulence in the interstellar medium causes a change in the phase of the incoming radio waves: the paths of the waves are distorted producing spatial variations in the received flux density. The phenomenon of *scintillation* then occurs since the turbulent medium is in motion with respect to the observer.

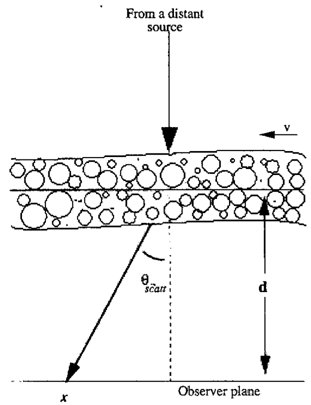

Two spatial scales define the scintillation:

$$r_F = \sqrt{\frac{\lambda \cdot \mathrm{d}}{2\pi}} \quad \textit{Fresnel scale}$$

$$r_d = \frac{\lambda}{2\pi\,\theta_{scatt}} \quad \textit{diffractive scale}$$

In case of *refractive* interstellar scintillation,

$$\theta_{scatt} = \sqrt{\frac{\lambda}{2\pi \mathrm{d}}}$$

defines the scattering strength:

strong scattering: $\theta_{source} \lesssim \theta_{scatt}$. Strong effects become less prominent if the source size is comparable to the scattering size.

weak scattering: $\theta_{source} \gtrsim \theta_{scatt}$. We are in the regime of *quenched scattering*. The variations involved become smaller and they disappear for $\theta_{source} > \theta_{weak} = r_F/\mathrm{d}$.

IDV source sizes are smaller than scattering size in our galaxy and scintillation effects must be present.

Scintillation depends on wavelength (see Narayan 1992, Rickett et al. 1995).

$$m \propto \lambda^2$$

where m is the modulation index of the variability.

The relative velocity between the orbital motion of the Earth and the scattering screen is modulated by the composition of the Earth's velocity vector and the velocity vector of the screen: it results in a seasonal change of the time scale, so-called, *annual modulation*

$$\vec{v} = \vec{v}_{\oplus} + \vec{v}_{\odot} + \vec{v}_s$$

The transverse velocity consists of three components: the Earth's orbital motion $\vec{v}_{\oplus}$, the motion of the sun towards the solar Apex $\vec{v}_{\odot}$ and the motion of the scattering screen $\vec{v}_s$ with respect to the Local Standard of Rest.

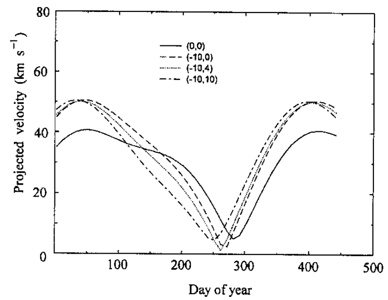

(Qian et al. 2001)

Summary about the IDV phenomenon

- Very small source structures involved ➡ μas
- Still controversial, after more than 15 years
  - Sole EXTRINSIC
  - Mixture of both INTRINSIC & EXTRINSIC

➡ EXTRINSIC: IDV related to the ISM characteristics
NO High Frequency IDV (scintillation vanishes)
Annual modulation

➡ MIXTURE: IDV related to the ISM &
source-intrinsic characteristics

Statistical analysis of a complete sample of flat-spectrum radio sources

Observations

Data consist in a complete sample of high declination ($\delta > 50°$) flat-spectrum ($\alpha < 0.5$, we use: $S \propto \nu^{-\alpha}$) radio sources extracted from the 1 Jy catalog (Kühr et al 1981).

- This catalogue consists of 518 objects and, at 5 GHz, is complete with a flux density limit of 1 Jy.
- high declination ($\delta > 50$) sources: 60
- flat-spectrum radio source ($\alpha < 0.5$): 32

The sample contains 18 quasars (QSO), 9 BL Lacs (BL), 3 galaxies (GAL) and 2 empty fields (EF). In galactic coordinates, these sources are distributed in the region defined by $10° \leq b \leq 60°$.

Date	Frequencies [GHz]						
05/1985		2.70*					
08/1985		2.70*					
12/1985		2.70*					
12/1989			4.75		10.55		
07/1990		2.70	4.75				
05/1991		2.70	4.75				
12/1991		2.70*	4.75*		10.55*		
04/1993			4.75				
06/1993			4.75				
09/1995		2.70	4.85				
12/1997a			4.85		10.45		
12/1997b		2.70	4.85		10.45		
09/1998			4.85		10.45		32*
02/1999			4.85				
03/2000		2.70	4.85		10.45		
05/1989	1.49		4.86	8.44		15.0	
01/1990	1.49*		4.86*	8.44*		15.0*	
10/1992	1.49*		4.86*	8.44*			

(Heeschen et al. 1987, Kraus et al. 2003, Quirrenbach et al. 2000)

Mathematical tools

Modulation index: $m[\%] = 100 \cdot \frac{\sigma_S}{<S>}$

Variability Amplitude: $Y[\%] = 3\sqrt{m^2 - m_0^2}$

Chi-square test: $\chi^2 = \sum_{i=1}^{N} \left(\frac{S_i - <S>}{\delta S_i} \right)^2$

Autocorrelation function: $\rho(\tau) =< (S(t) \cdot S(t-\tau)) >_t$

Structure Functions: $SF(\tau) =< (S(t) - S(t+\tau))^2 >_t$

The structure function provides typical time scales and periodicity of the variations in a light curve.

At $\tau \to 0$, the structure function yields to the noise level of the measurements. For large values of τ, the structure function is proportional to the variance of the variations, i.e. to the square of the modulation index: $SF(\tau \gg) = 2\sigma_S^2 \propto m^2$.

The different types of intraday variability are defined according to the shape of the structure function. Following Heeschen et al. 1987, we define three IDV classes: **Type II** = fast variable, **Type I** = long-term variable and **Type 0** non-variable sources.

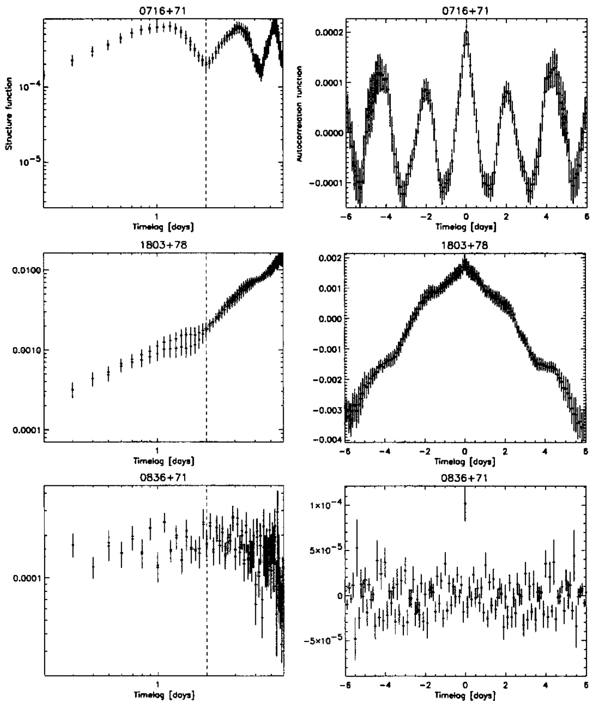

Some results...

Galactic latitude dependence of IDV

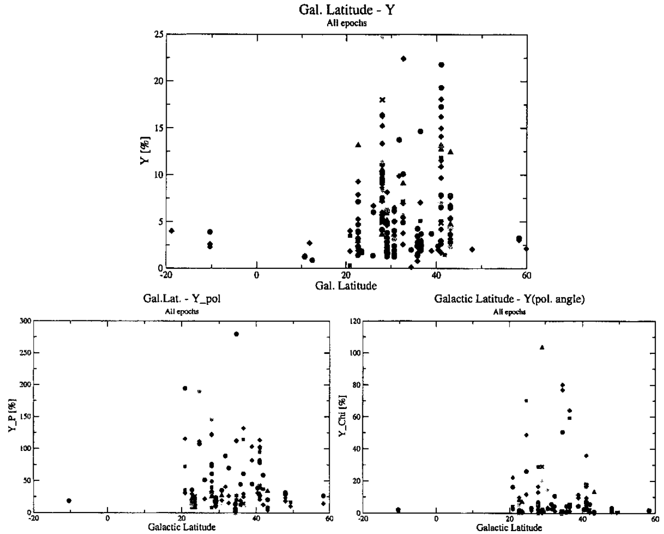

No evidence for correlations is found either in the total intensity or in the polarization variability.

$\Downarrow$

the scattering is not caused by the global matter distribution in the ISM, but could be due to clouds localized and homogeneously distributed in our surrounding.

Redshift dependence of IDV

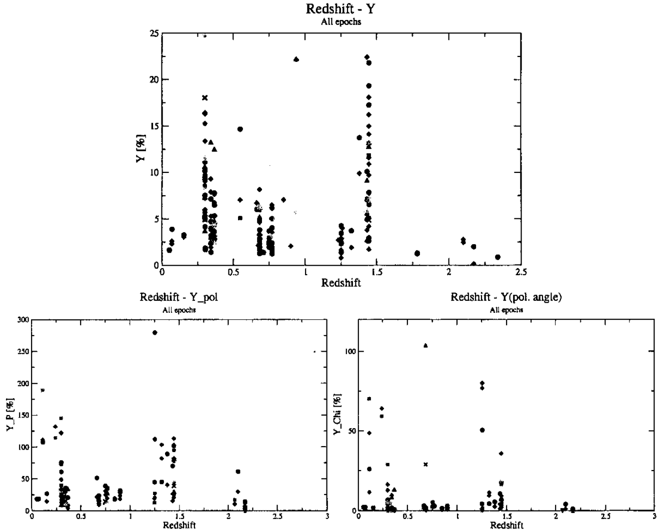

No evidence for z-dependence found either in the total intensity or in the polarization variability ($\Rightarrow$ local scattering screen).

Furthermore, the same variable sources show different IDV behaviors at different epochs $\Rightarrow$ Intrinsic structural changes could play an important role in IDV.

Spectral index dependence of IDV

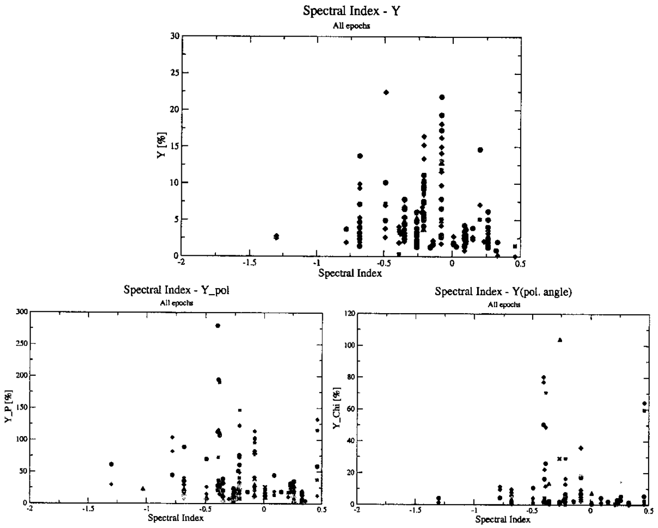

Highest variability in total intensity and polarization is associated with very flat-spectrum radio core (α from ~ -0.5 up to ~ 0).

Here, indication that even very inverted-spectrum sources show less variability.
The emission of a new component produces an increase in the spectral index: the spectrum becomes flatter or, in case of flat self-absorbed components, more inverted.

Analysis of the time scales

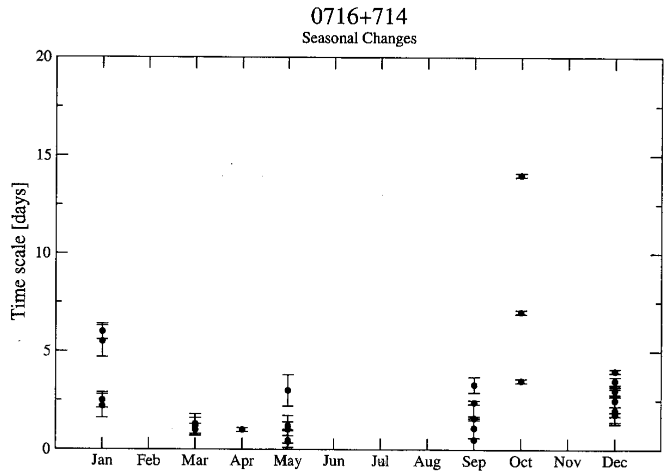

It is possible to test whether the observed rapid variability could be caused by an annual modulation, which is due to the orbital motion of the Earth.

The slow-down of the variability around October could be an indication of a seasonal modulation of the IDV.

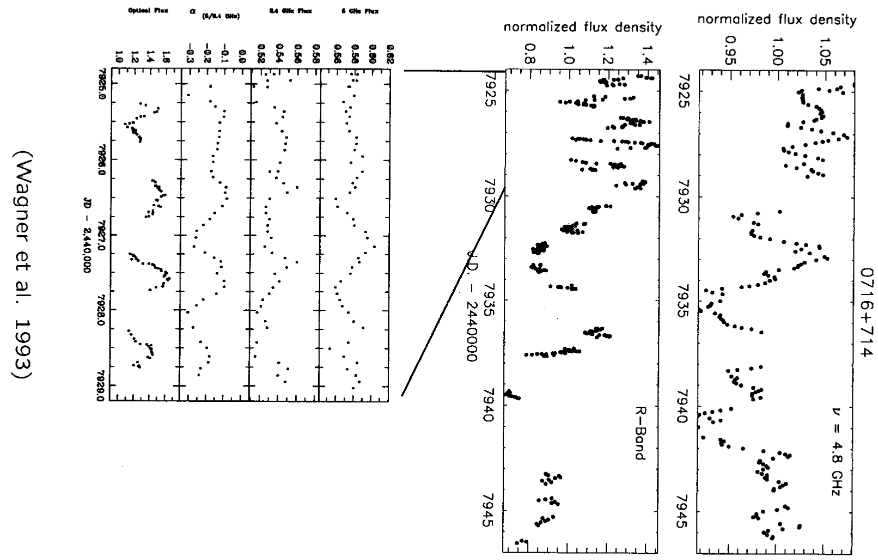

Summary of Multi-frequency IDV

- Different IDV behaviors at different epochs
- Larger variability towards higher frequencies
- Different mechanisms for the short-term variability in radio and optical bands
- Quenched scintillation qualitatively reproduces the observed IDV characteristics
- Multi-Frequency observations of Intraday variable sources can provide information about:
  - the apparent source sizes
  - the clouds in the ISM

IDV can be used as a tool to study the structures either in the source or in the interstellar medium.

High frequency IDV → the sole RISS is not sufficient: intrinsic?

3.3 V. Impellizzeri: Short-time polarisation variability in 0716+714

Short-Time Polarisation Variability in 0716+714

Violette Impellizzeri
L. Fuhrmann
T. P. Krichbaum
G. Cimò
U. Bach
A. Witzel
J.A. Zensus

Max-Planck-Institut
für
Radioastronomie

The Sample

Criteria for selection:

- averaged flux density $S_{5GHz} \geq 1Jy$.
- flat or inverted spectrum with $\alpha \leq 0.5$.
- declination $\delta \geq 60°$.
- IDV type II.

Name	ID	z
0716+714	BL Lac	> 0.3
0954+658	BL Lac	0.9
0917+624	QSO	1.446
0346+800	QSO	–
0615+820	QSO	0.03

Aim of the experiment

- IDV is a frequent phenomenon of compact radio sources.
- total flux density and polarised flux density can be correlated or anti-correlated.
- Polarisation angle χ swing.

$\Rightarrow$ Origin of these variations?

Search for:

1. Total and Polarised Intensity correlations.
2. Rapid polarisation angle changes in stationary and moving components.
3. IDV related structural variations on timescales of days to weeks.
4. Correlations with single dish telescope observations

Observations

• VLBA Obervations at 5 GHz with
• Simultaneous Flux Density Monitoring at Effelsberg.

Four Epochs:

- first two epochs separated by 24 hours.
- last two epochs, two weeks later, also 24 hours apart.

The observing epochs were 2000.921 and 2000.924(December 3 and 4) and again 2000.959 and 2000.962 (December 17 and 18) with a global of 10 VLBA antennas. Each observation lasted 8 hours.

Single Dish measurements were conducted simultaneously to the VLBA observations.

Each epoch calibrated and imaged separately using the VLBI Caltech Software Package DIFMAP and AIPS.

UV-Coverage

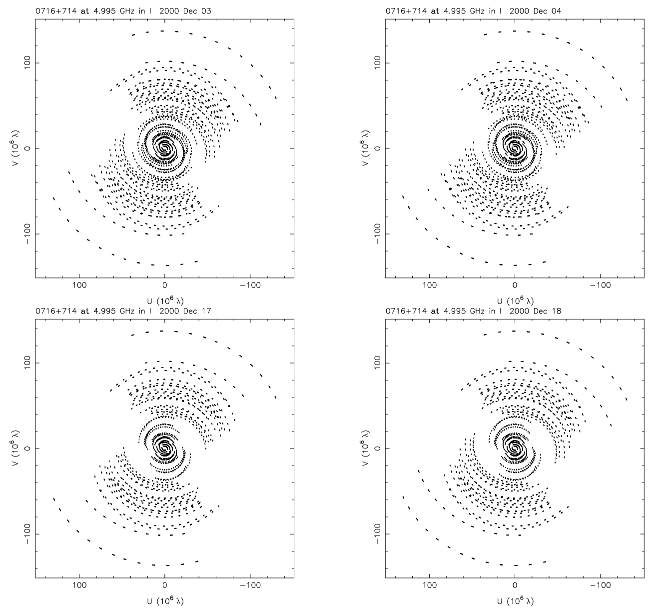

Figure 1: UV-coverage at four epochs. The top panels show the first two epochs 24 hours apart. The bottom panels show the coverage two weeks later, also 24 hours apart

Total Intensity Maps 0716+714

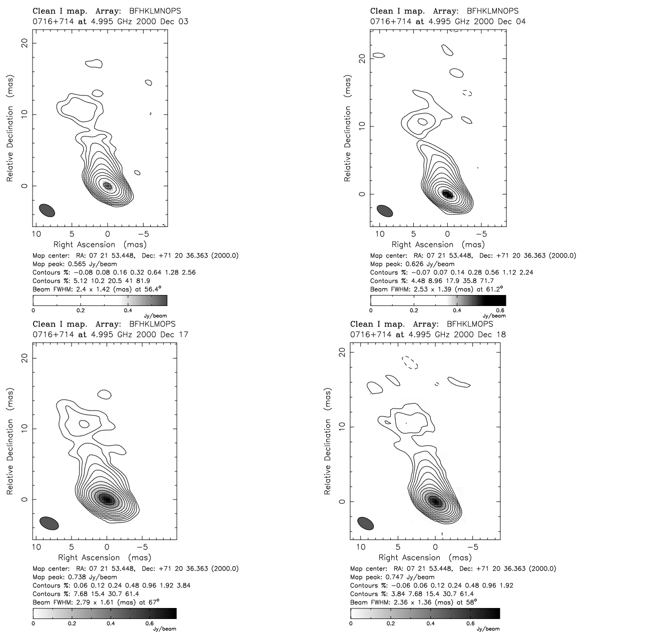

Figure 2: Total Intensity Flux Density maps. Four epochs are shown, the top ones 24 hours apart, the bottoms ones were observed two weeks later and are again 24 hours apart

Total Intensity & Polarisation Maps

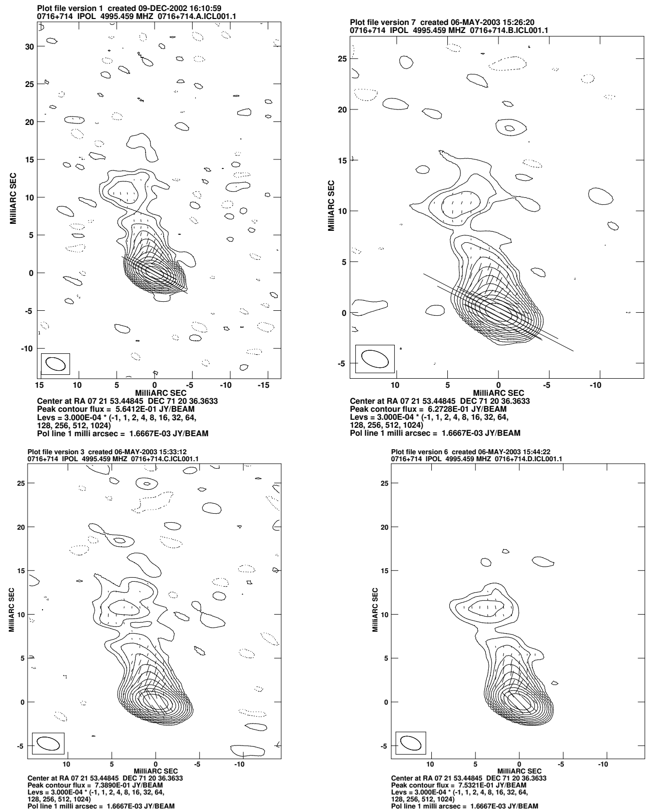

Figure 3: 0716+714

Total Intensity & Polarisation Maps

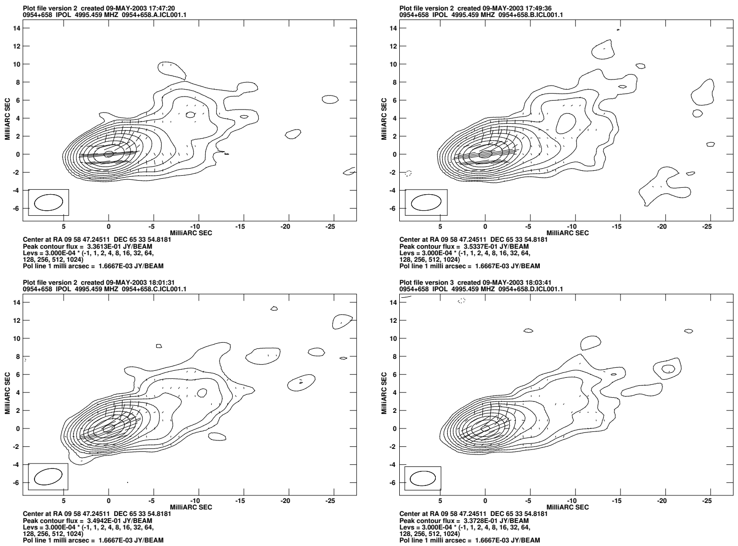

Figure 4: 0954+658

Polarisation Maps

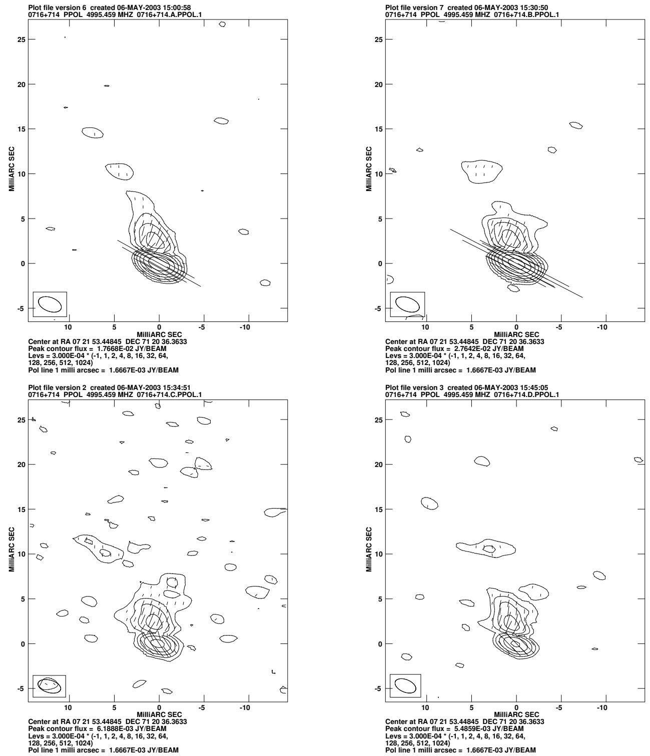

Figure 5: 0716+714 Total Polarised Flux Density maps with polarisation vectors

Core/Jet Emission Comparison

	A	B	C	D
$I_{core}[mJy]$	600	665	770	777
$I_{jet}[mJy]$	22	25	25	25
$P_{core}[mJy]$	17(2.8%)	25(3.8%)	6(0.8%)	6.2(0.8%)
$P_{jet}[mJy]$	6.2(28%)	5.5(22%)	3.7(15%)	5.3(21%)
$\chi_{core}[^\circ]$	55°	58°	32°	42°
$\chi_{jet}[^\circ]$	−29°	−27°	−27°	−25°
$\Delta(\chi_{c-j})[^\circ]$	84°	85°	59°	67°

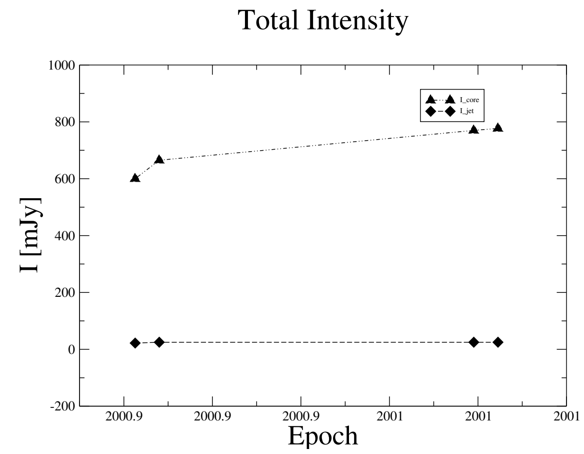

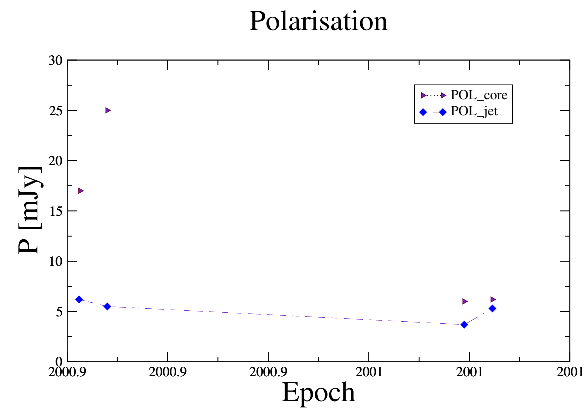

Total intensity and polarisation variations over the four epochs, in the core and jet

Effelsberg Observations

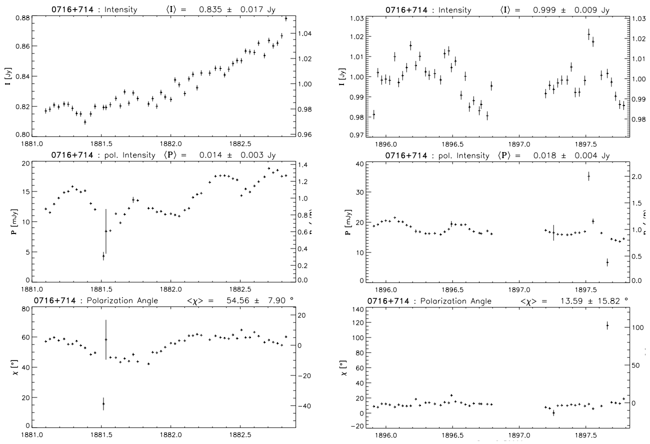

Left Panel show the first two epochs. Right panel the last two epochs, observed two weeks later.

Summary of Results

- Increase in Total Flux Density observed both at Effelsberg and with VLBA. On VLBA scale increase is found to be in the core of the source.
- Variations in Polarised Flux Density observed within the four epochs, also relatively to the core of the source.
- A change in Polarisation Angle χ also observed between second and third epoch.
- No variations have been observed in structure of source within the four epochs.

3.4 U. Bach: Kinematical study of 0716+714

Kinematical study of 0716+714

Uwe Bach

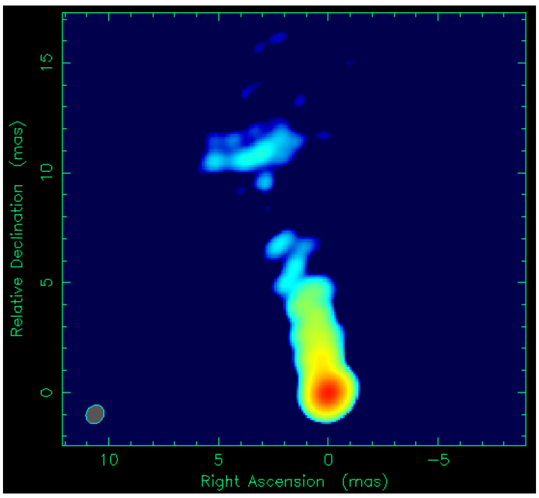

in collaboration with:
T.P. Krichbaum, S. Britzen, E. Ros, A. Witzel and J.A. Zensus

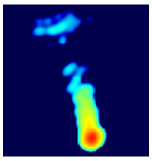

Facts about 0716+714

- S5 blazar and one of the most active BL Lac objects.
- Extremely variable on time scales from hours to months.
- Yet no known redshift. Optical imaging however suggests an redshift of z > 0.3.
- Intraday variable (IDV) in the radio bands.
- Very flat radio spectrum, extending up to at least 300 GHz.
- Correlated variability over wide ranges of the electromagnetic spectrum.
- VLBI studies covering more than 20 years show a core-dominated evolving jet extending to the north.
- VLBI jet is oriented at 90° with respect to the VLA jet.

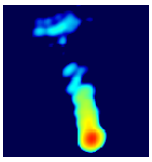

Observations

Our analysis is based on 26 epochs:

- 4 epochs from the CJF-Survey at 5 GHz between 1992 and 1999 (Britzen et al. 1999)
- 1 VSOP observation at 5 GHz (2000)
- 3 epochs from astrometric observations at 8.4 GHz (Ros et al. 2000) between 1994 and 1999
- 2 own observation at 8.4 GHz (1994 & 1995)
- 5 epochs at 15 GHz from the 2 cm-Survey from 1994 to 2001 (Kellermann et al. 1998).
- 7 epochs at 22 GHz from Jorstad et al. (2001) between 1995 and 1997
- 4 epochs at 22 GHz from own observations from 1992 to 1996.

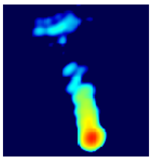

Maps at 5, 8.4 and 15 GHz

5 GHz

8.4 GHz

15 GHz

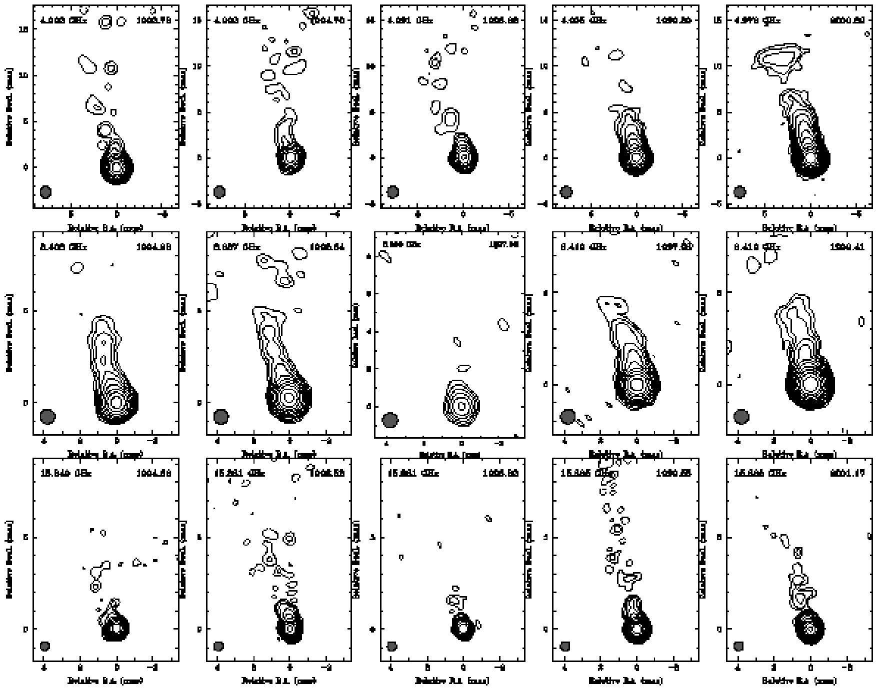

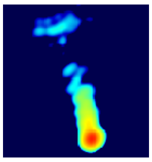

Maps at 22 GHz

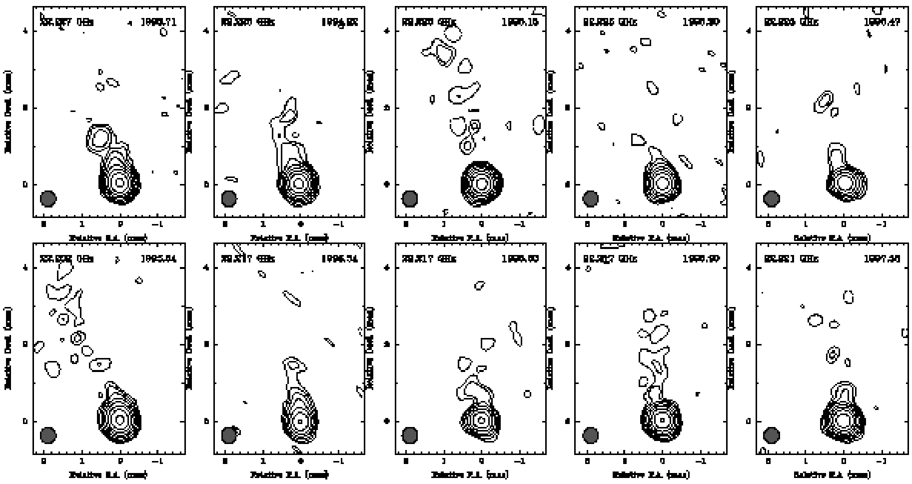

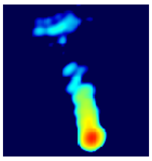

The Model

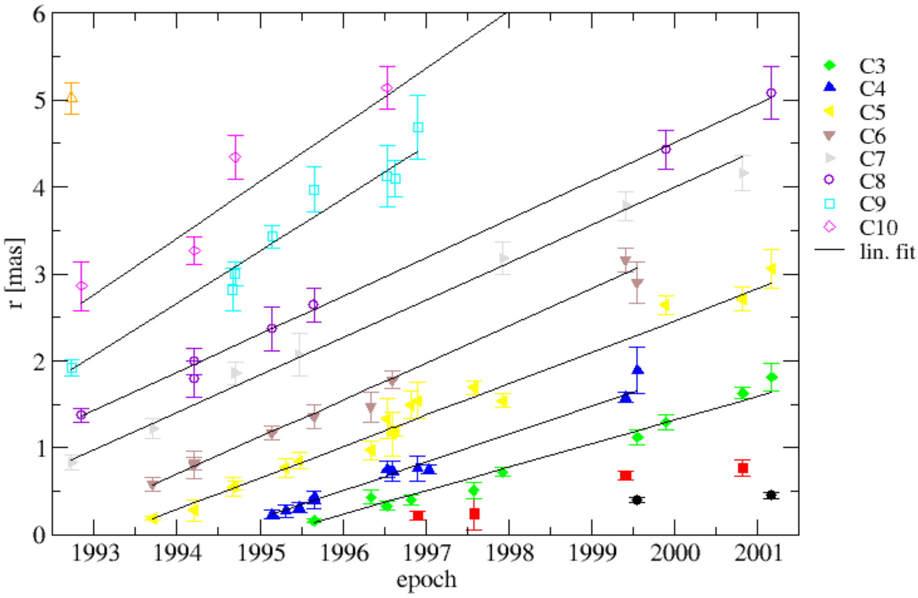

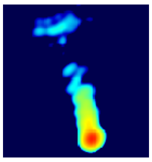

Component Summary

Comp	#	μ [mas/yr]	$\beta^{b}_{\rm app}$	Ejection date
C3	10	0.270 ±0.012	4.98 ±0.22	1995.12 ±0.11
C4	11	0.321 ±0.008	5.93 ±0.16	1994.42 ±0.08
C5	17	0.362 ±0.010	6.69 ±0.18	1993.20 ±0.13
C6	9	0.426 ±0.016	7.87 ±0.30	1992.37 ±0.20
C7	7	0.430 ±0.015	7.94 ±0.28	1990.72 ±0.25
C8	7	0.441 ±0.010	8.14 ±0.19	1989.76 ±0.19
C9[a]	8	0.600 ±0.037	11.08 ±0.68	1989.56 ±0.49
C10[a]	5	0.651 ±0.126	12.03 ±2.33	1988.76 ±1.68
C11[a]	4	0.857 ±0.124	15.82 ±2.29	1986.71 ±1.59

[a] Components are not well defined by the linear fits, due to the lack of data for these components.

[b] $z \geq 0.3$, $H_0 = 65\,{\rm km\,s^{-1}\,Mpc^{-1}}$ and $q_0 = 0.3$.

Kinematics and geometry

$$\beta_{\rm app} = \frac{\beta \sin\theta}{1-\beta\cos\theta}$$

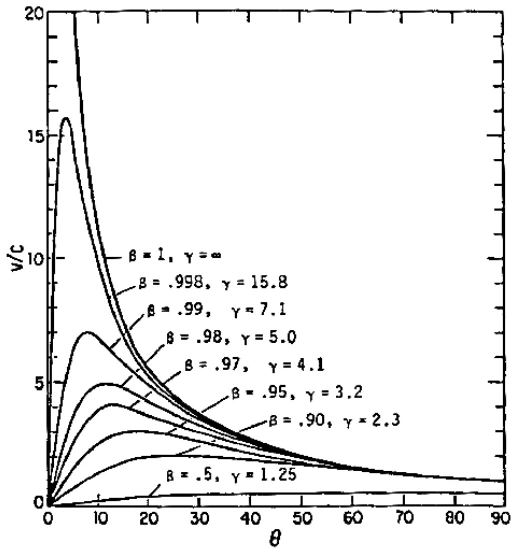

For $\beta \to 1$:

$$\theta_{\rm max} = 2\arctan(1/\beta_{\rm app}) \approx 14^\circ$$

For $\cot\theta = \beta_{\rm app}$:

$$\gamma_{\rm min} = \frac{1}{\sin\theta} = \sqrt{1+\beta_{\rm app}^2} \approx 8.2$$
$$\theta \approx 7^\circ$$

which corresponds to a Doppler-Factor of:

$$\delta = [\gamma - \sqrt{\gamma^2-1}\,\cos\theta)]^{-1} \approx 8$$

But for IDV $\delta \approx 30-50$:

$$\gamma \approx 16.1 - 25.6$$
$$\theta \approx 1.0^\circ - 0.4^\circ$$

Doppler Factor vs. apparent velocity

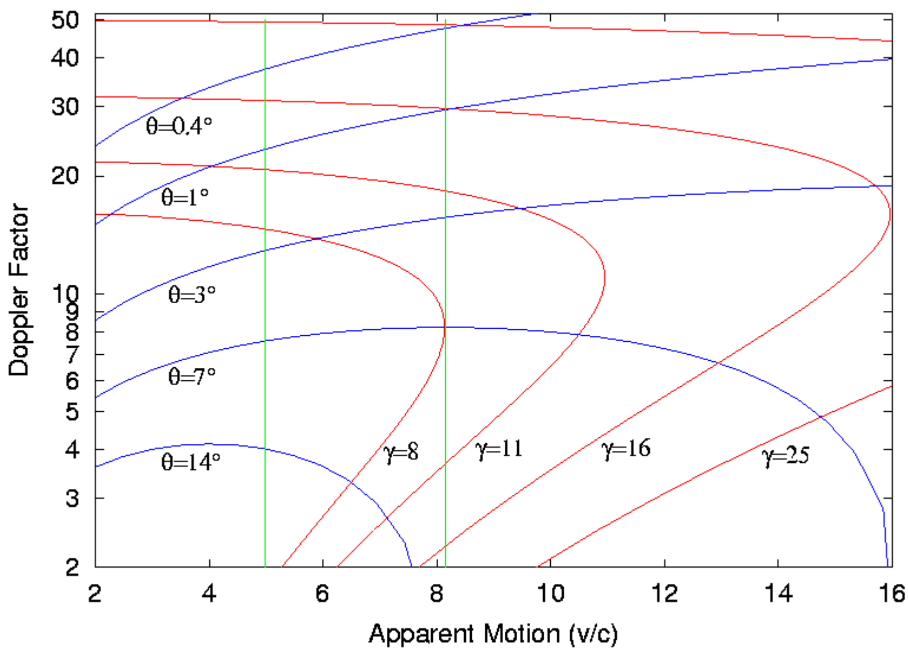

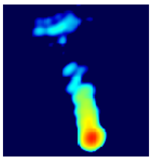

Summary

- Reanalysed 26 epochs of VLBI data at 5, 8.4, 15, 22 GHz
- Obtained:
  - a satisfactory model for the motion of the components, where the components move with an average speed of ~7 c
  - a lower limit for the Lorentz Factor of ~8
  - a maximum angle to the line of sight of ~14°
  - But more probable are $\gamma > 11$ and $\theta < 3°$, which correspond to a Doppler Factor > 16

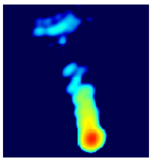

Radio light-curves

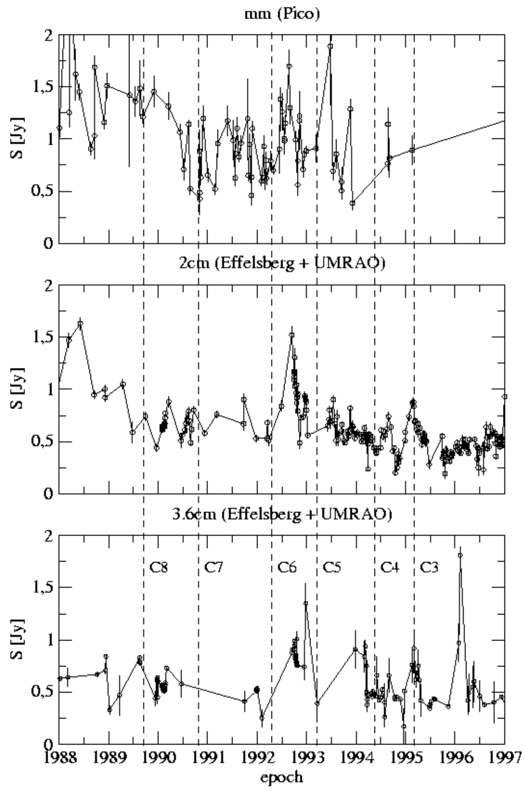

3.5 T. Beckert: Quenched Scintillation of IDV Quasars

Quenched Scintillation of Intraday Variable (IDV) Quasars

Thomas Beckert, MPIfR, Bonn

- The Scintillation Hypothese for IDV
- Power Spectrum, Structure Functions & Quenched Scintillation
- What we can learn about the source and the ISM
- Results & Conclusions

Introduction

- Variability of compact (flat- spectrum, core-dominated) Quasars & BL Lacs at GHz- frequencies (< 15 GHz)
- Typical time- scales: 0.6 - 3 days
- Modulation index: m = 1- 10% $$m = \frac{\sqrt{\langle S^2 - \langle S \rangle^2 \rangle}}{< S >}$$
- Brightness temperatures $10^{16 \dots 21}$ K (Source size from light travel time) $$T_B = \frac{F_\nu}{2 k_B A} \lambda^2$$
- Superluminal motion is common ($v \leq 10$ c $\rightarrow$ $\delta \leq 20$)

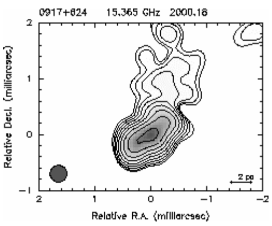

Introduction (cont.)

- 0954+65 shows short and long extreme scattering events (G. Cimo 2002)
- Annual modulation (possibly in 0917+62)
- Extreme IDV sources: J1819 +38 (Westerbork) and PKS 0405- 38 (Australia) with time- scales < 1h and m > 20%
- On longer time- scales > 7 days $\rightarrow$ Flickering

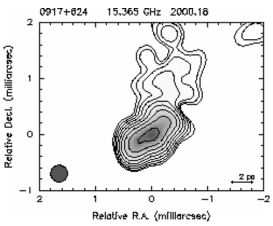

What is Interstellar Scintillation ?

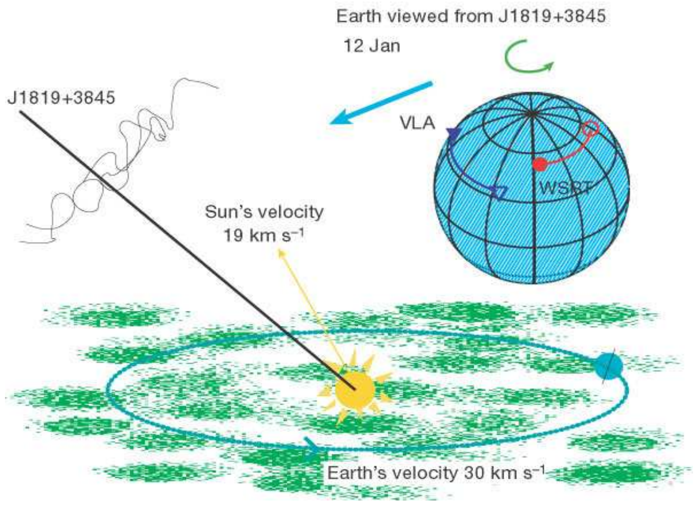

Dennett-Thorpe & De Bruyn, 2002, Nature 415, 57

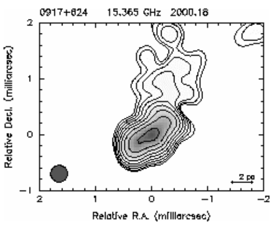

Interstellar Scintillation (Geometry)

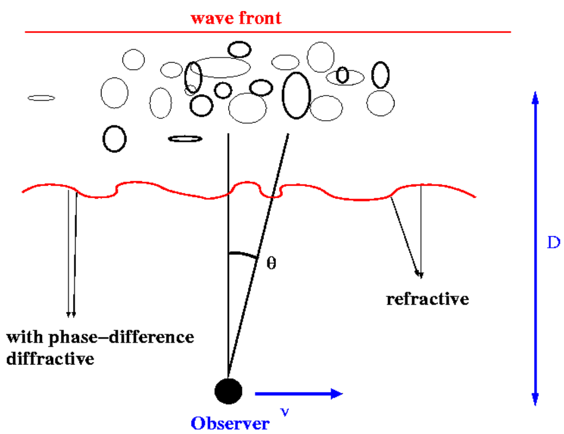

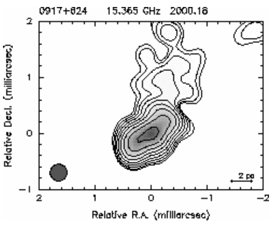

Interstellar Scintillation (Theory)

What we observe: Intensity $I(t) = \langle E(s)E^*(s)\rangle$

What we derive: Two-point intensity correlation

$$C(s, s_0) = \langle E(s)E^*(s)E(s_0)E^*(s_0)\rangle$$

which is a special case of the 4th-moment of the wave-field

$$Z(a, b, c, d) = \langle E(a)E^*(b)E(c)E^*(d)\rangle$$

$$C(s - s_0) \longleftarrow Z(a, a, c, c) + Z(a, b, b, a)$$

refractive and ← with $(a = b, c = d,\ a - c = s - s_0)$

diffractive part ← or $(a = d, b = c,\ a - b = s - s_0)$

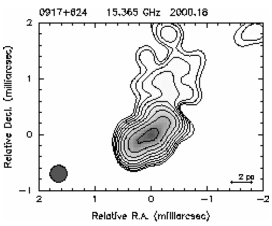

Interstellar Scintillation (Theory 2)

Autocorrelation of intensity variations
(e.g. Rumsey 1975, Coles et al. 1987) :

$$\rho(\vec{x}) = \int \mathrm{d}^2\vec{q}\ \exp[i\vec{q}\cdot\vec{x}]\ W(\vec{q}) \cdot |V(\vec{q})|^2$$

$$W(\vec{q}) = \int \mathrm{d}^2\vec{s}\ \exp[-i\vec{q}\cdot\vec{s}]C(\vec{s} - \vec{s}_0)$$

Density fluctuations (in the ISM) are described by power spectrum

$$\Phi(z, q) = C_N^2(z)q^{-\beta}$$

Wave number q; amplitude $\mathbf{C}_N^{\ 2}$ along line of sight coordinate z

Kolmogorov spectrum: $\beta = 11/3$

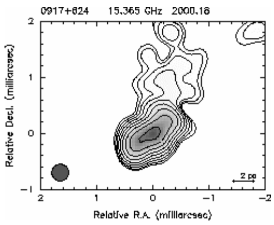

Comparison with Observations: Structure Functions of IDV

Definition: $SF(\tau) = \left\langle [I(t) - I(t+\tau)]^2 \right\rangle_t$

Relation to Autocorrelation

$SF(\tau) = 2\,[\rho(0) - \rho(\vec{x} = \vec{v}\tau)]$

Characteristics:

Correlation time-scale t_{IDV}

Plateau for $t > t_{IDV}$ at level $2m^2$

Slope ≤ 2 for $t > t_{IDV}$

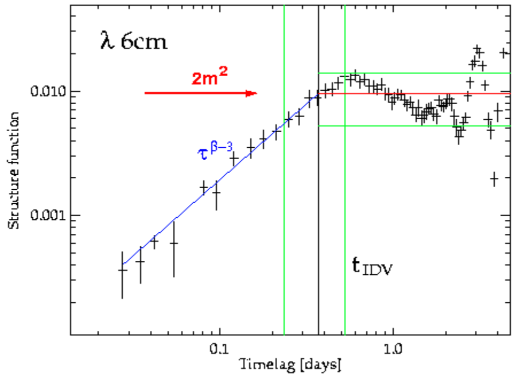

From *SF*-fitting : slope ~ 1.2 !!!

Structure Functions of IDV

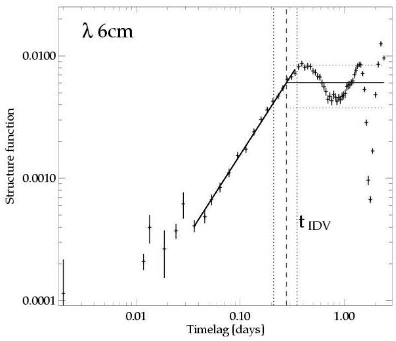

Other examples:

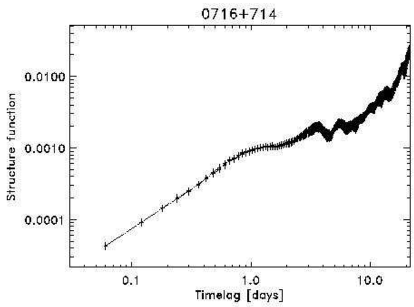

0917+624

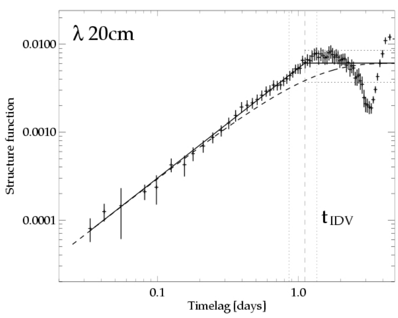

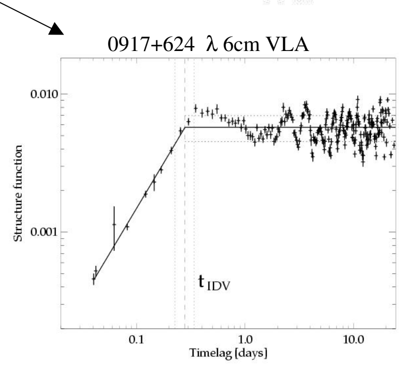

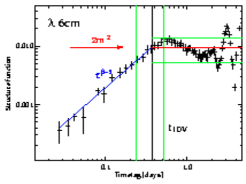

Scintillation Power Spectrum

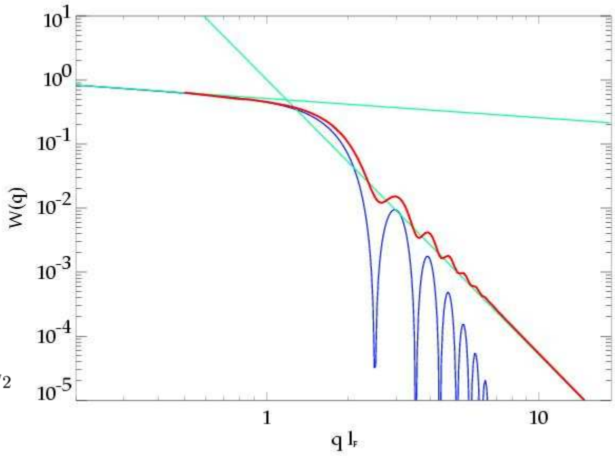

The Fresnel scale separates refractive and diffractive effects and gives the position of the break of *W(q)* in weak scattering

$$l_F = D\,\theta_F = \sqrt{\frac{D\lambda}{2\pi}}$$

$$\theta_F = \sqrt{\frac{\lambda}{2\pi D}} = 11\mu\text{as}\left[\frac{\nu}{5\text{GHz}}\cdot\frac{D}{100\text{pc}}\right]^{-1/2}$$

The transition weak to strong scattering for steep spectra (β > 4) has not been explored before (strong case: Goodman & Narayan 1985)

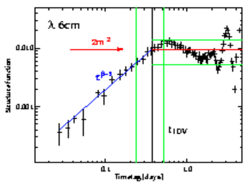

Scintillation Power Spectrum (II)

Moderately strong scattering:
Fourier-Transform W(q) for a point source
Distinction between refractive and diffractive scale

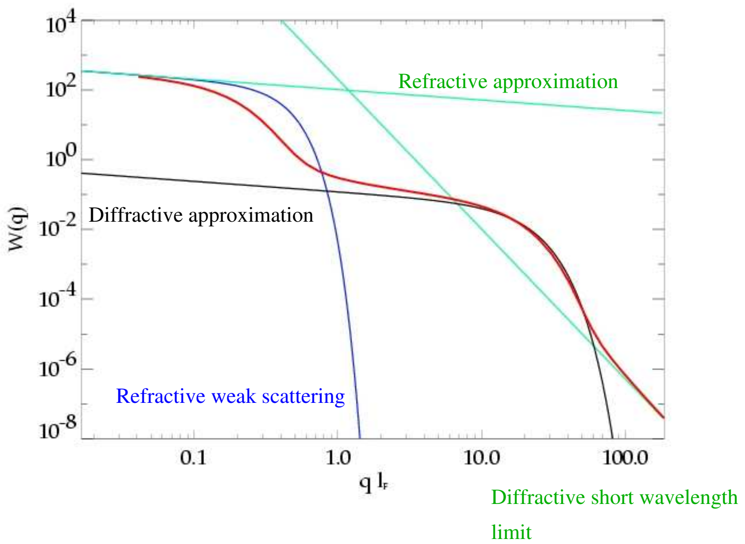

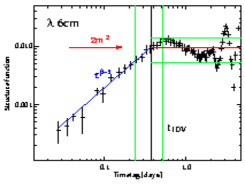

Scintillation Power & Visibility

Moderately strong scattering & Kolmogorov spectrum: $\beta = 11/3$:

Fourier-Transform W(q) for a point source

& Visibility for an extended source: $\theta = 3\,\theta_F$ (uniform disk)

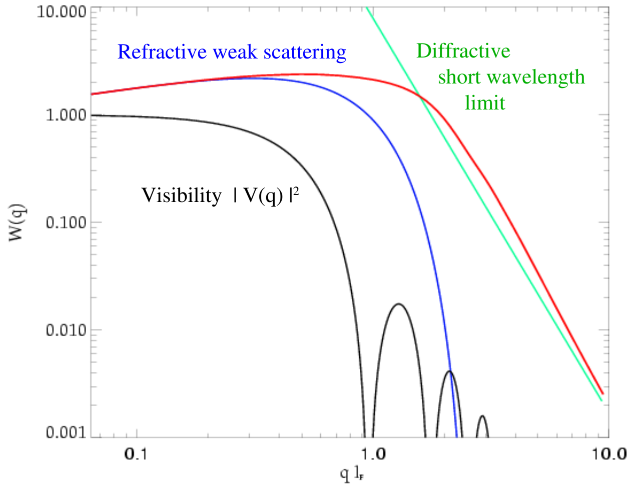

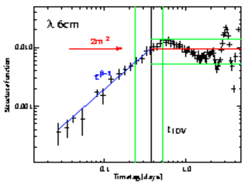

Quenched Scintillation

Incoherent synchrotron sources are much larger than the Fresnel scale:

$$\theta = 0.42\text{mas}\ \frac{(1+z)}{\delta}\left[\frac{\nu}{5\text{GHz}}\right]^{-1}\left[\frac{F_\nu}{\text{Jy}}\cdot\frac{10^{11}\ \text{K}}{T_b}\right]^{1/2}$$

1) Variations are quenched by the source size.

2) The time- scale is streched.

3) → Clouds in the local ISM (50 - 150 pc)
are potential sources for scattering
(e.g. the wall of the 'local bubble')

4) Standard assumption: Slab model for the ISM
and Gaussian brightness distribution for the source

5) Problem: The slope of the *SF* comes out wrong.

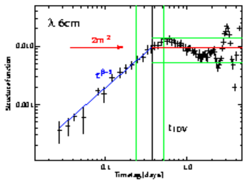

Non gaussian source models

Source with constant brightness distribution

=> Visibility is a Besselfunction $J_1(x)/x$

=> reasonable mod. Index m and SF- slope

$$\rho(0) = m^2 = 2\left(\frac{r_e}{D\theta^2}\right)^2 \lambda^4 (D\theta)^{\beta-2} SM \cdot F_1(\beta) \qquad (8)$$

$$SF(\tau) = 2\rho(0)\left(\frac{v\tau}{D\theta}\right)^{\beta-3} \frac{G_1(\beta)}{F_1(\beta)} \qquad (9)$$

F_1 function of order unity; SM scattering measure

Relation between size and time- scale: $$\theta = \frac{v}{D}\frac{t_{\mathrm{IDV}}}{2} \qquad (10)$$

Estimate for the distance to the slab: (v = 20 km/s; t_{IDV}=1day)

$$D = 137\mathrm{pc}\left[\frac{\nu}{5\mathrm{GHz}}\right]\left[\frac{T_b}{10^{11}\mathrm{K}}\right]\left[\frac{\delta}{10}\right]\left[\frac{F_\nu}{1\mathrm{Jy}}\right]^{-1/2} \qquad (11)$$

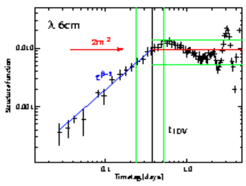

Unquenched Scintillation

The structure function is **steeper** from scintillation by a ISM slab for a point source compared with quenched scintillation.

$$\rho(0) = m^2 = 2\left(\frac{r_e}{D}\right)^2 (D\lambda)^{\beta/2+1} SM \cdot F_3(\beta)$$

$$SF(\tau) = 2\,(r_e\lambda)^2\,(v\tau)^{\beta-2}\ SM \cdot G_3(\beta)$$

$$t_{\mathrm{IDV}} = \frac{\sqrt{D\lambda}}{v} H_3(\beta)$$

1) The SF slope is $\beta - 2$ for time lags shorter than the correlation timescale for point sources : $q\, l_F > 1$ (weak scattering)

2) Even for quenched scintillation (when $\tau < t_{\mathrm{IDV,Point}}$) SF gets steeper

3) → Break in the observed SF expected, but not seen

4) This would determine the intrinsic size

Beyond Quenched Scintillation ?

Cimo et al. 2002, EVN-Symposium

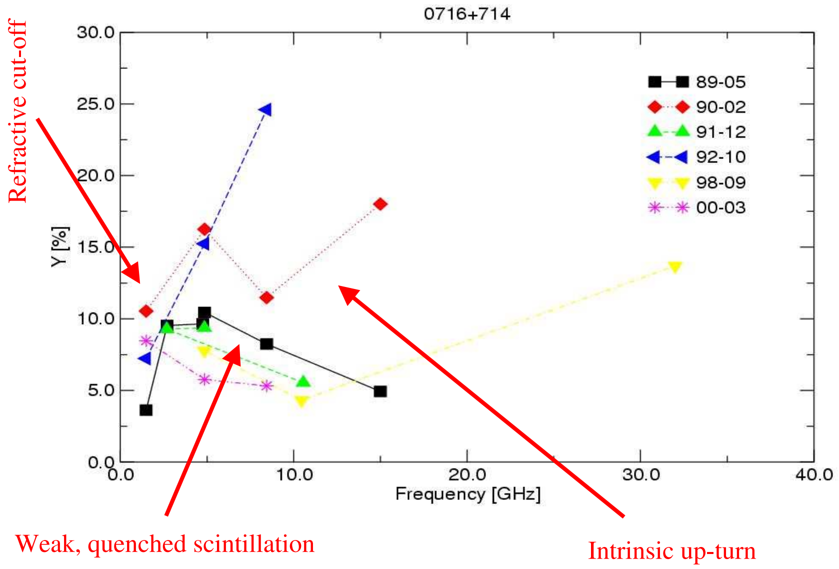

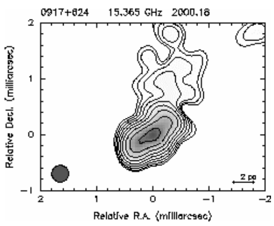

Results & Conclusions

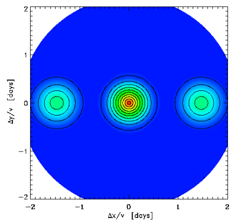

1) IDV can be understood as quenched scintillation
2) The source size should dominate over refractive/diffractive effects
3) A single screen model might not be sufficient
4) The screen in the ISM is either very close (D ~10 pc; source is large $\rightarrow \theta_{6cm} > 1.2$ mas ; $\beta \sim 4.2$) requires a huge scattering measure !!!
5) Or far away (D > 700 pc; $\beta \sim 3.2$; source is smaller than Fresnel scale $\rightarrow \theta_{6cm} < 4.2\ \mu$as -> $T_B \sim 7\ 10^{15}$ K $/\delta$) Does not solve the IDV problem !!!

3.6 C. Raiteri: The WEBT campaign on BL Lacertae

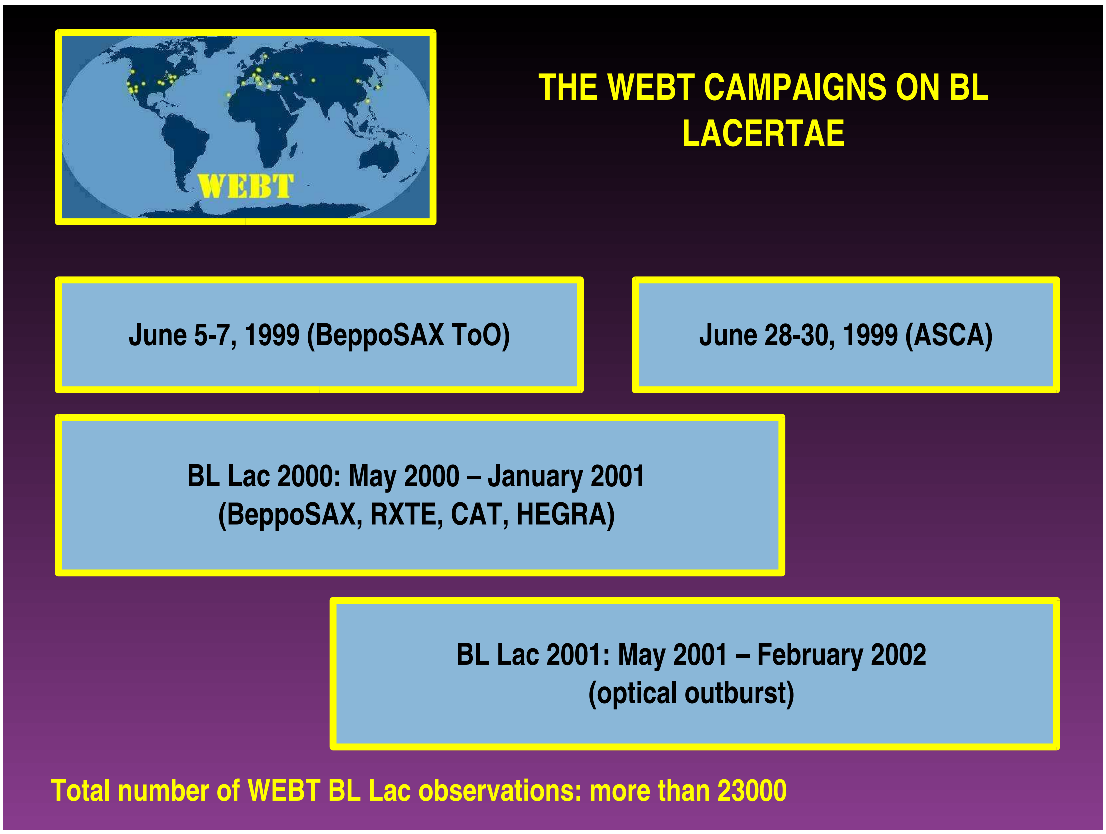

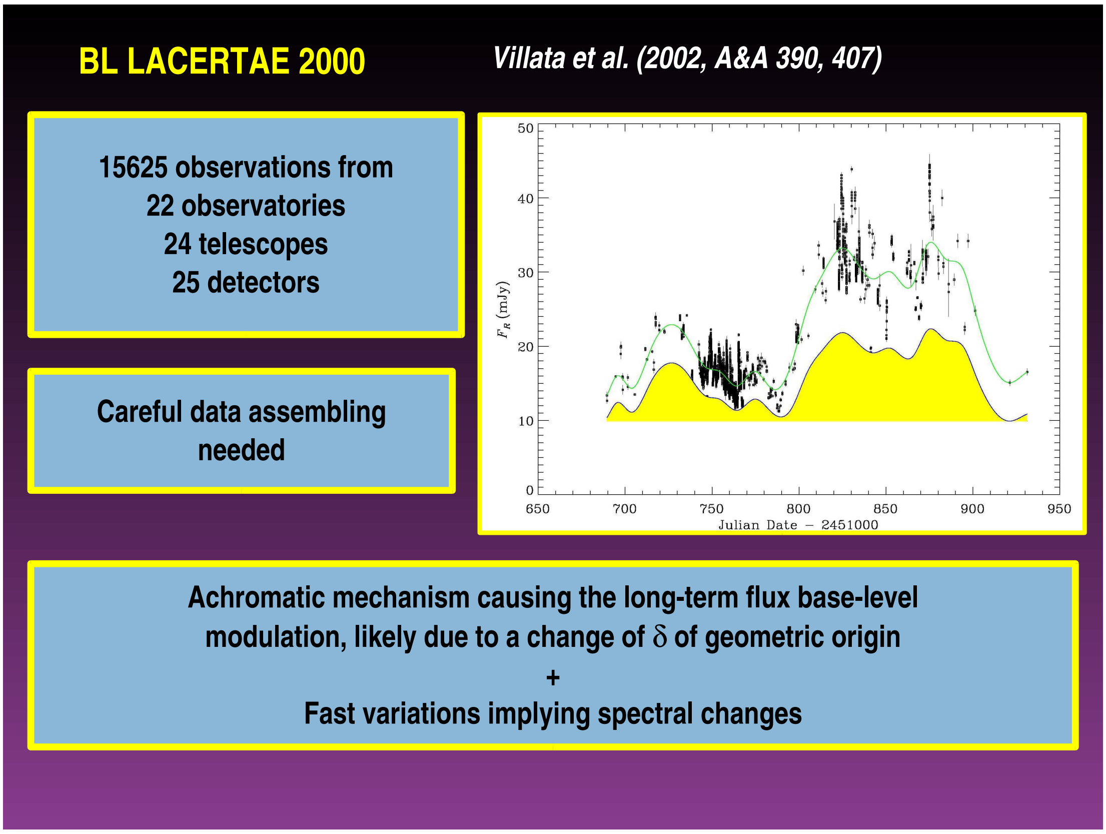
BL LACERTAE 2000
Villata et al. (2002, A&A 390, 407)
15625 observations from
22 observatories
24 telescopes
25 detectors
Careful data assembling
needed
F_R (mJy)
Julian Date − 2451000
Achromatic mechanism causing the long-term flux base-level
modulation, likely due to a change of δ of geometric origin
+
Fast variations implying spectral changes

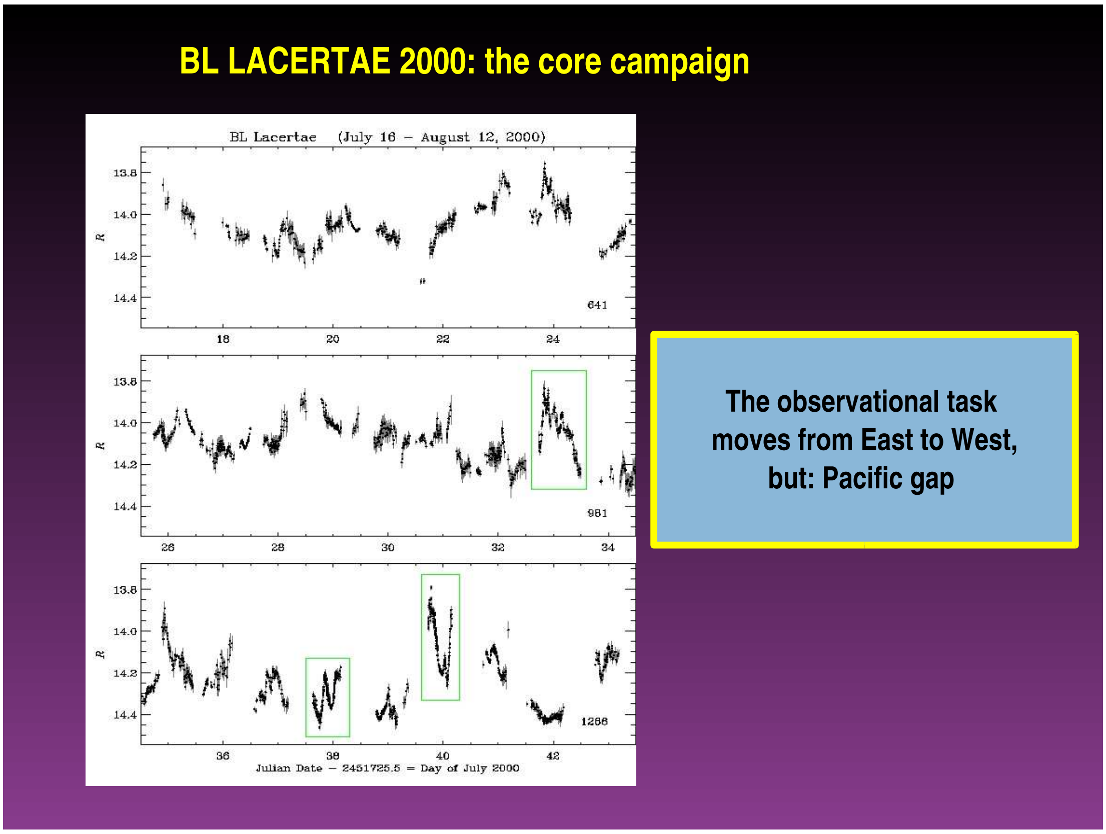
BL LACERTAE 2000: the core campaign
BL Lacertae (July 16 − August 12, 2000)
R
641
981
1268
Julian Date − 2451725.5 = Day of July 2000
The observational task
moves from East to West,
but: Pacific gap

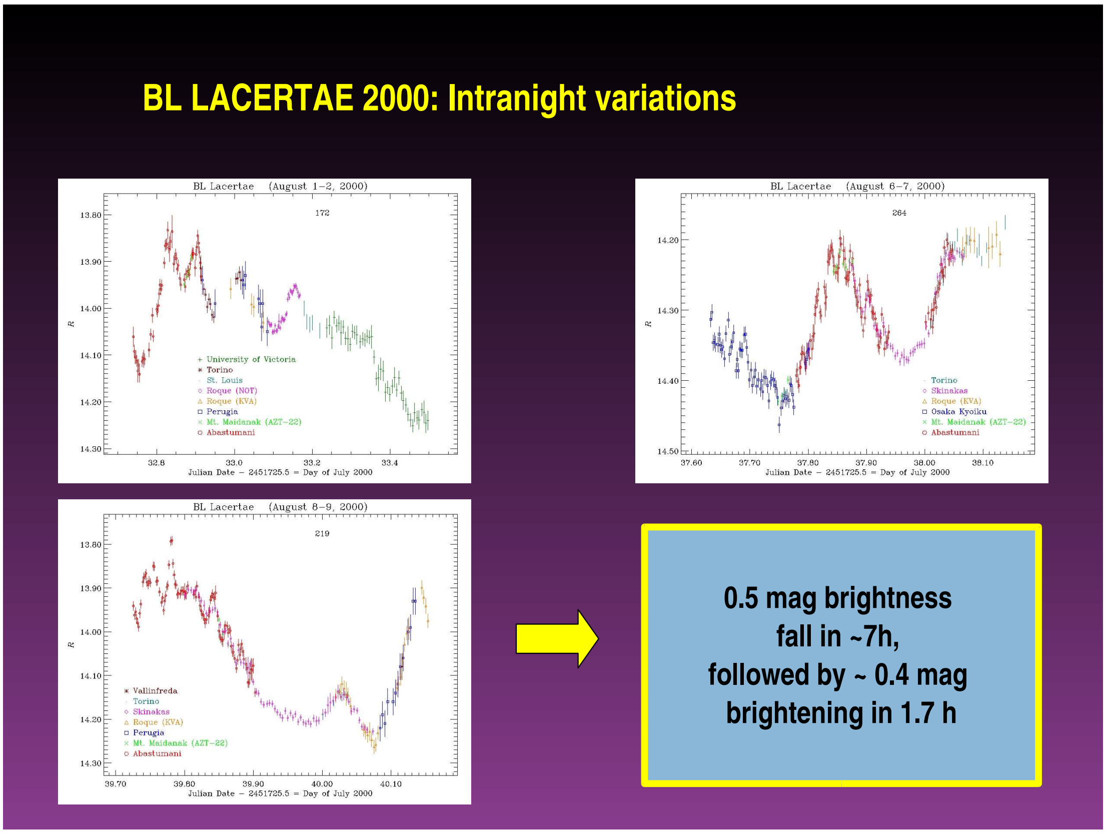
BL LACERTAE 2000: Intranight variations
BL Lacertae (August 1–2, 2000)
BL Lacertae (August 6–7, 2000)
BL Lacertae (August 8–9, 2000)
Julian Date – 2451725.5 = Day of July 2000
0.5 mag brightness
fall in ~7h,
followed by ~ 0.4 mag
brightening in 1.7 h

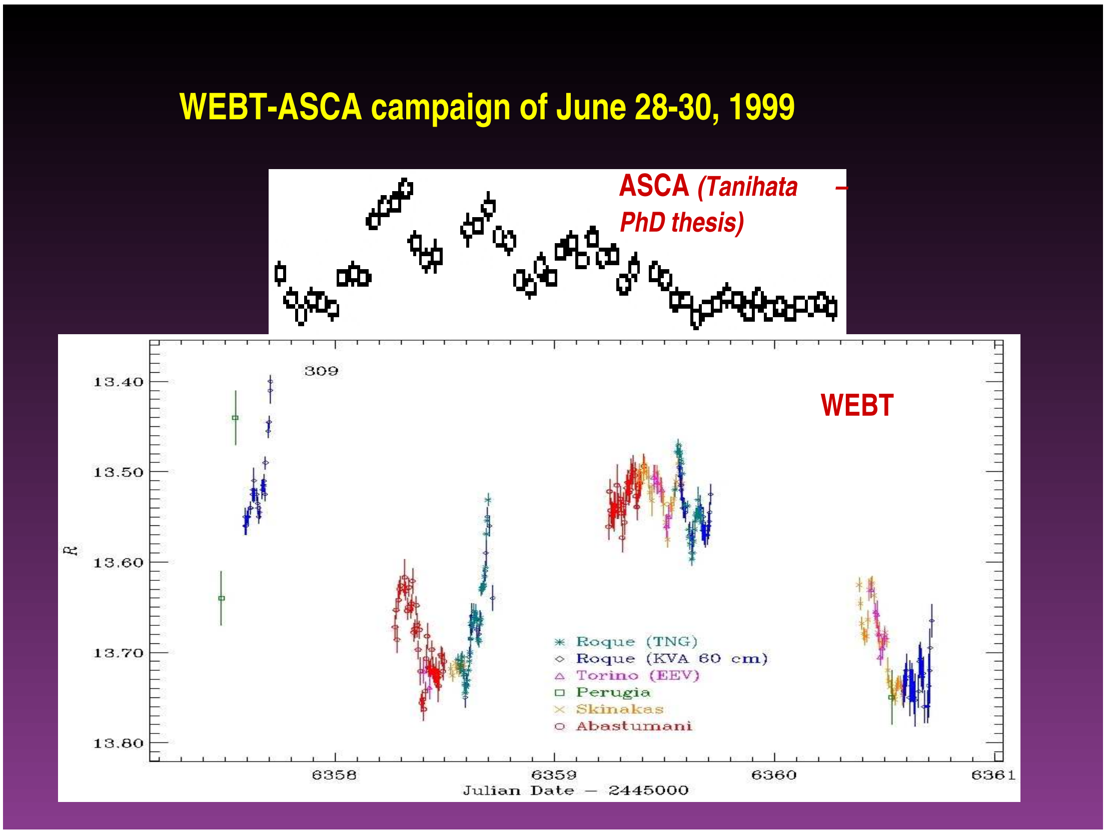
WEBT-ASCA campaign of June 28-30, 1999
ASCA (Tanihata
PhD thesis)
WEBT
309
R
13.40
13.50
13.60
13.70
13.80
6358
6359
6360
6361
Julian Date – 2445000
Roque (TNG)
Roque (KVA 60 cm)
Torino (EEV)
Perugia
Skinakas
Abastumani

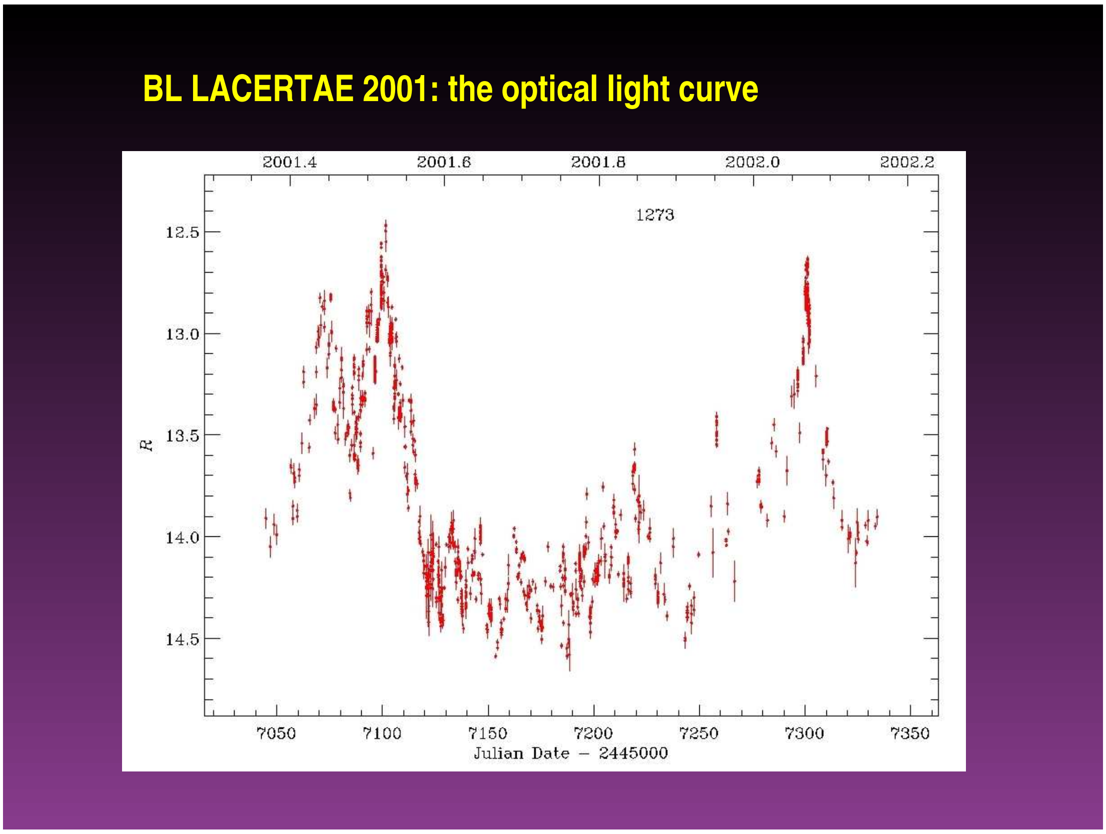
BL LACERTAE 2001: the optical light curve
2001.4
2001.6
2001.8
2002.0
2002.2
1273
R
12.5
13.0
13.5
14.0
14.5
7050
7100
7150
7200
7250
7300
7350
Julian Date − 2445000

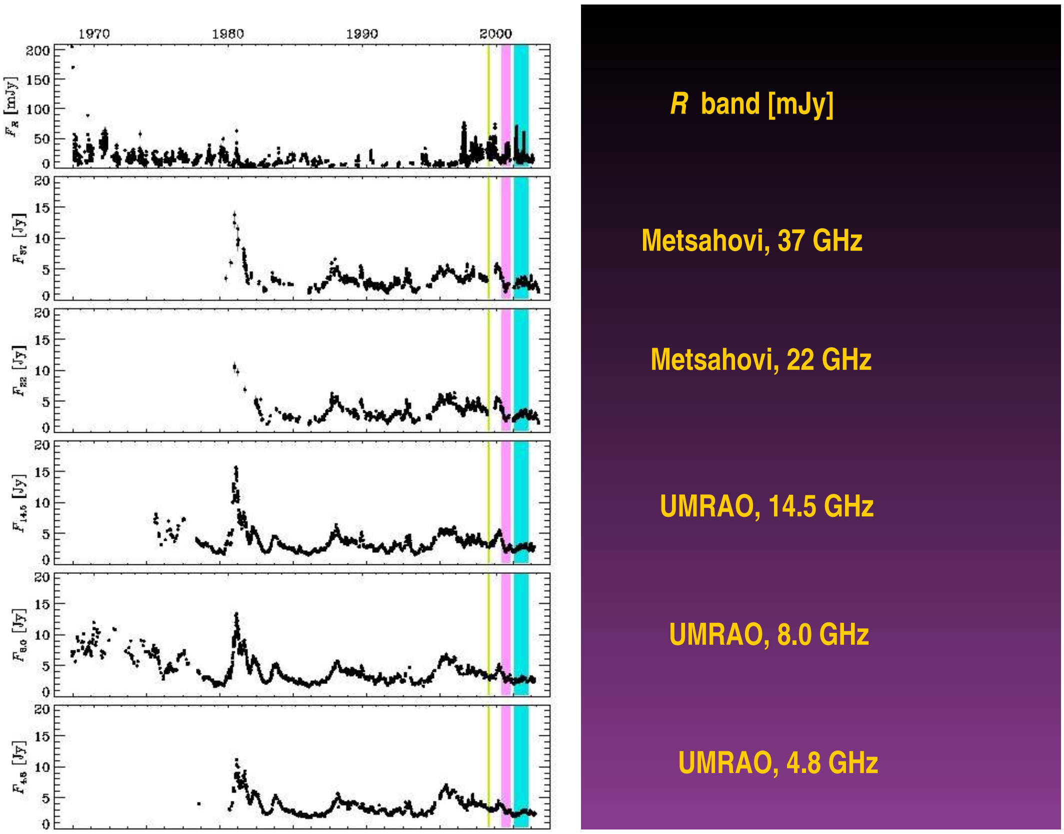
1970
1980
1990
2000
R band [mJy]
Metsahovi, 37 GHz
Metsahovi, 22 GHz
UMRAO, 14.5 GHz
UMRAO, 8.0 GHz
UMRAO, 4.8 GHz

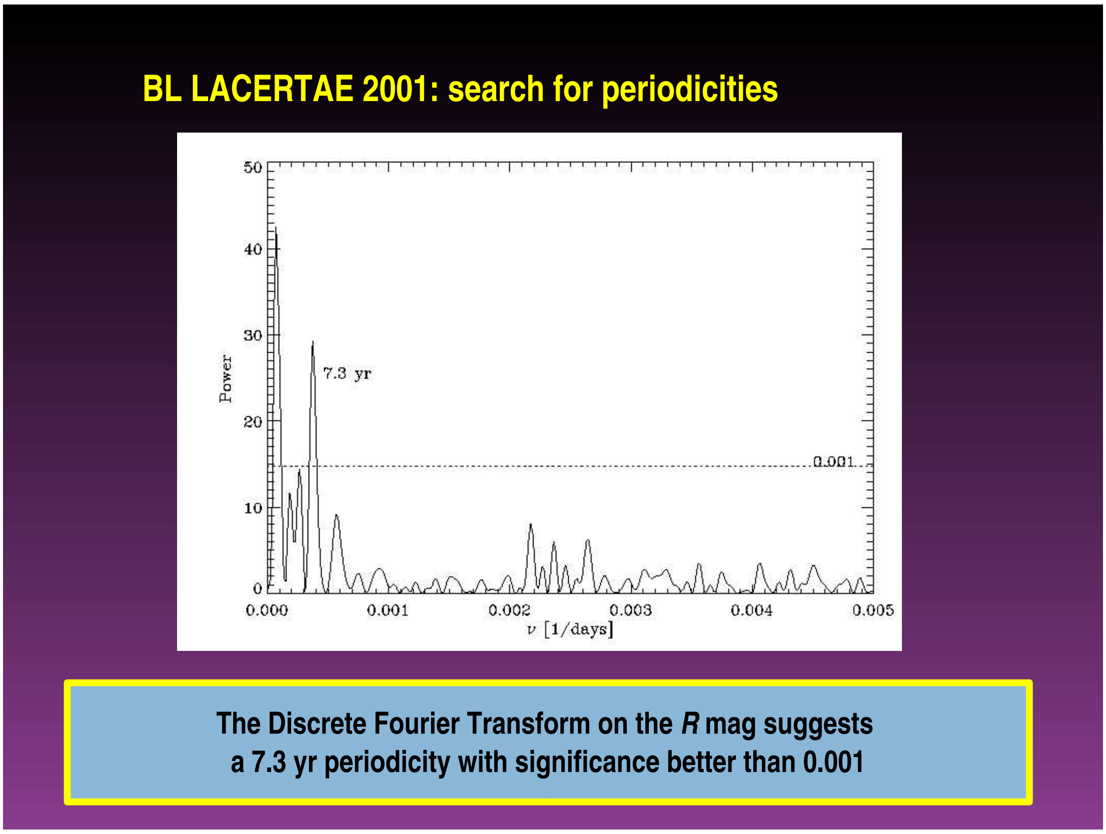
BL LACERTAE 2001: search for periodicities
Power
7.3 yr
0.001
ν [1/days]
The Discrete Fourier Transform on the R mag suggests
a 7.3 yr periodicity with significance better than 0.001

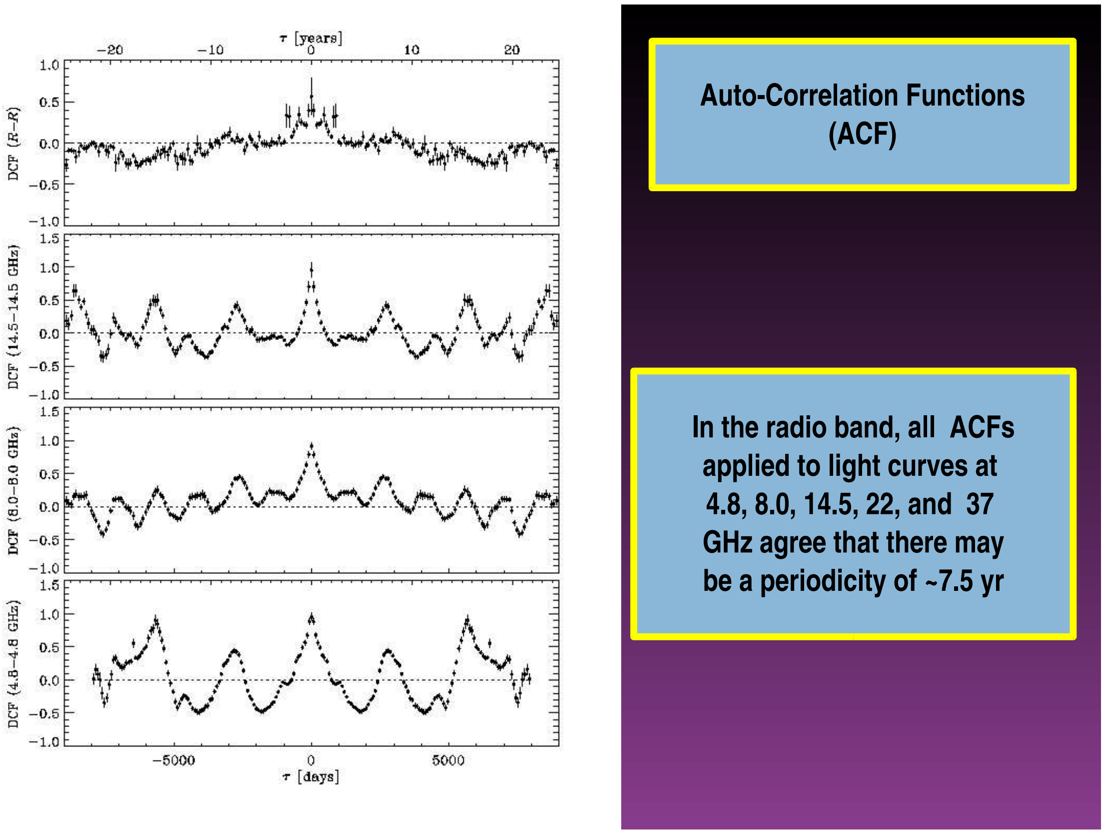
τ [years]
DCF (R−R)
DCF (14.5−14.5 GHz)
DCF (8.0−8.0 GHz)
DCF (4.8−4.8 GHz)
τ [days]
Auto-Correlation Functions
(ACF)
In the radio band, all ACFs
applied to light curves at
4.8, 8.0, 14.5, 22, and 37
GHz agree that there may
be a periodicity of ~7.5 yr

BL LACERTAE 2001: radio-radio correlations

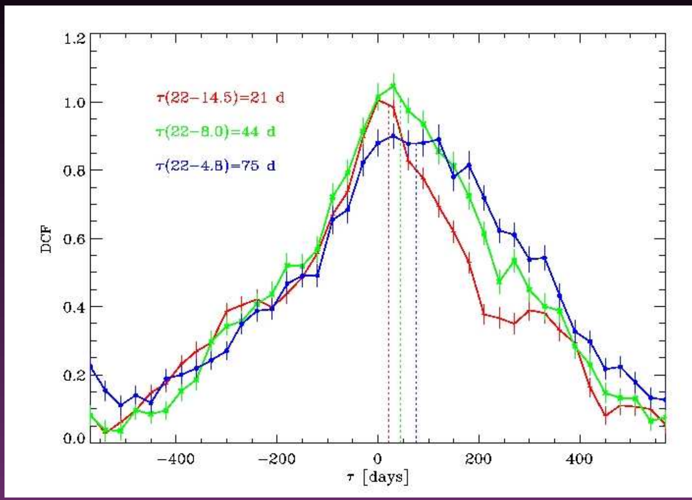

τ(14.5-8.0)+ τ(8.0-4.8) ~ τ(14.5-4.8)

28 d 37 d 67 d

BL LACERTAE 2001: optical-radio correlations

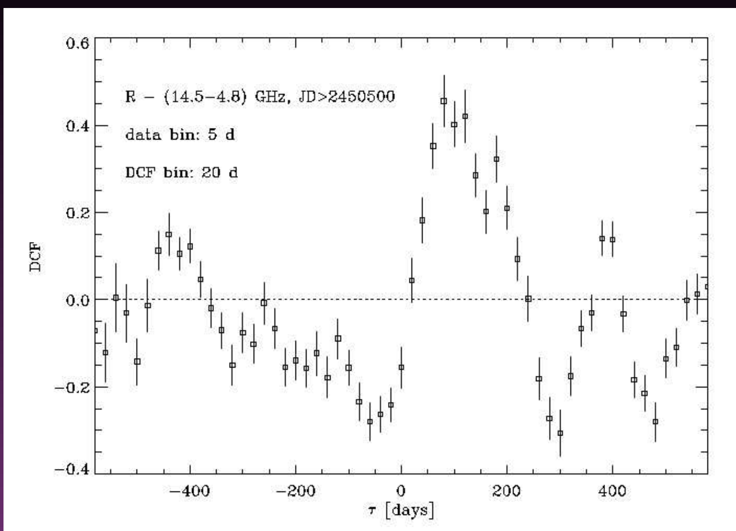

From 1997 on, a moderate correlation with delay of ~100 d is found after cleaning the radio light curve from the “radio-only” features

3.7 E. Valtaoja: Interstellar Scintillation and Radio IDV

There is now strong evidence to supporting Interstellar Scintillation as the principal cause of IDV at cm wavelengths. This comes from two types of observations:

Firstly, from the presence of a time delay in the IDV pattern arrival times at widely spaced telescopes. Here it is for PKS 1257-326 between the ATCA and the VLA.

Pattern Time Delay Observed between the ATCA and the VLA.

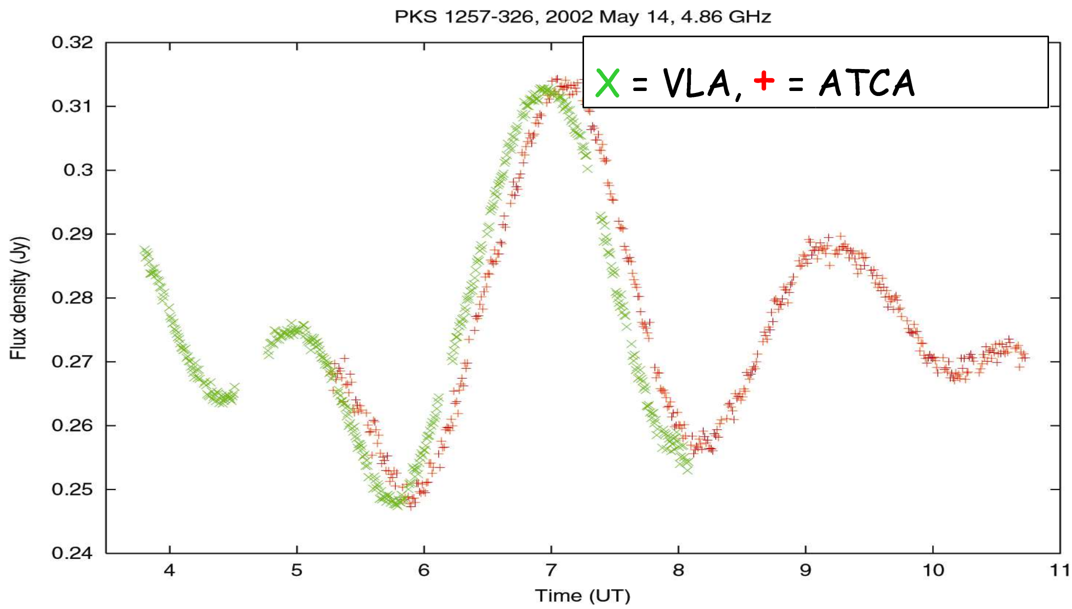

The presence of a time delay has only been used for the most rapid IDV sources PKS 0405-385, PKS 1257-326 and J1819+3845.

The second method to establish ISS has been through the discovery of an annual cycle in the characteristics of the IDV over the course of a year.

This has been found for a number of sources, and there is increasing evidence that this behavior is widespread. This is beautifully illustrated by

PKS 1257-326

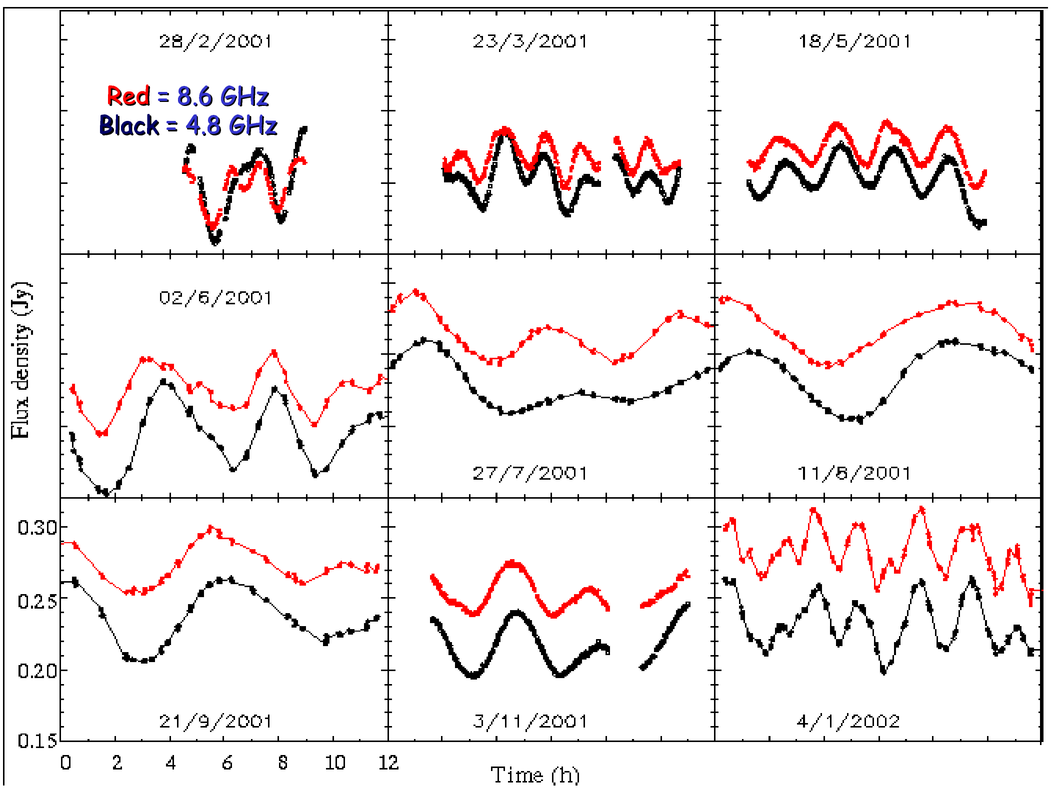

The presence of an annual cycle implies the source size is ~ the angular size of the first Fresnel zone. For reasonable screen distances that is microarcseconds.

In summary;
there is conclusive evidence
for Interstellar
Scintillation.

And Vincent Van Gogh
understood this very well

ISS is caused by scattering in the interstellar medium of the Galaxy, and is present for all sources. *As* illustrated by Katsushika Hokusai from the 53 Stages of the Tokaido:

"You can run
but you can't hide"

what next?

Make use of this
Interstellar Telescope
to survey the northern
sky at 5 GHz.

Micro-**A**rcsecond **S**cintillation-
Induced **V**ariability Survey

MASIV

Jim Lovell, Dave Jauncey,
Hayley Bignall, Lucyna
Kedziora-Chudczer,
J-P Macquart, Barney Rickett,

Tasso Tzioumis

The Need for a MASsIVe Survey

- So far surveys have been:
  - Small (~100 sources in total)
  - Limited to bright sources
- We need a statistically significant sample of scintillators (~100)
- 2/3 extreme scintillators were discovered serendipitously
  - How common are they?
- What is the population of scintillators amongst weaker sources?

$$\boxed{T_B \sim \frac{S}{2}}$$

- Correlations with z, b, VLBI T_B, α, X-ray, γ-ray etc
- Study AGN structure at μas resolution
- Study the structure of the ISM

VLA Observations

"These are the Australians who are doing that infamous experiment." – Ken Sowinski, Jan 2002

- First of four 72 hr epochs Jan 19-22 2002 during D $\rightarrow$ A reconfiguration
- Operating in 5 sub-arrays of 5 or 6 antennas each. Observations at 5 GHz, 60 sec on-source per scan. ~6 scans per source per day.
- 3C286 and 2355+498 used for primary flux density calibration.

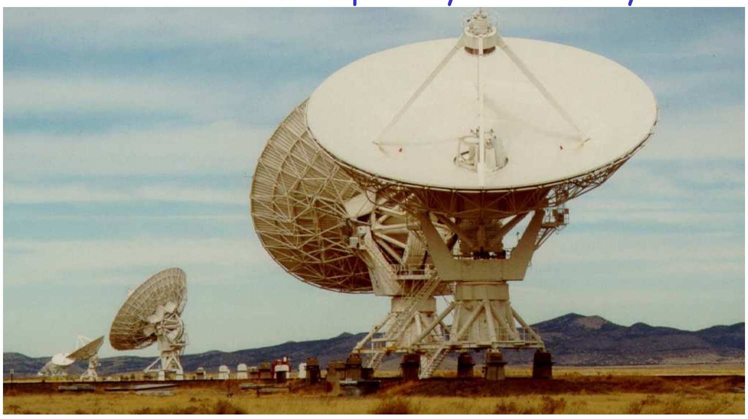

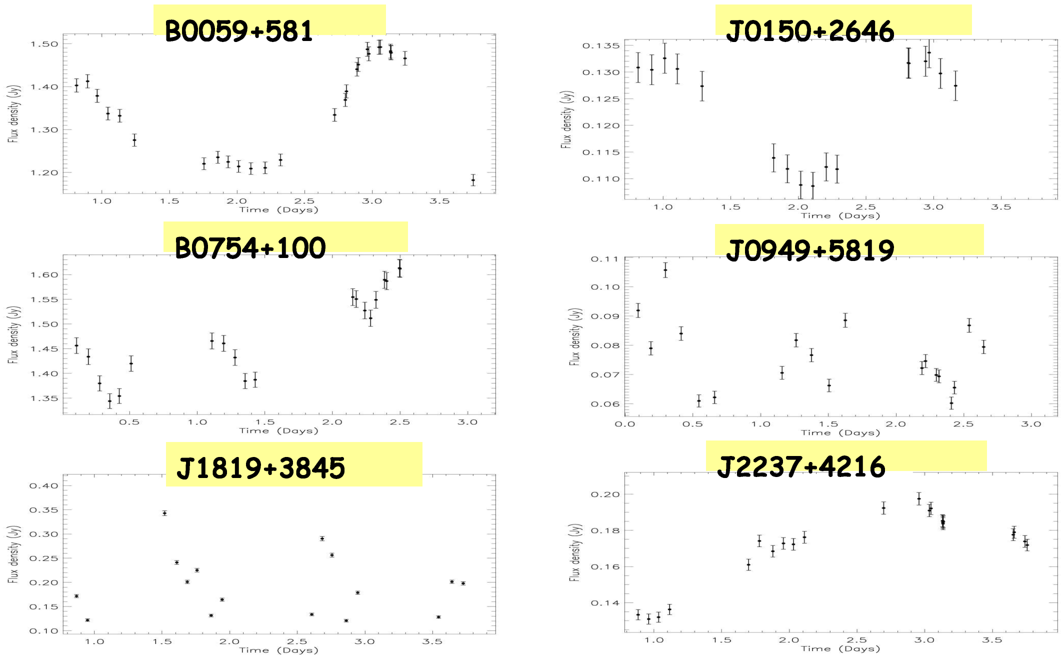

Figure 2.1: Example light curves of the variable sources detected in the first epoch of the MASIV Survey.

Preliminary Conclusions

(from MASIV I)

- Of the 710 sources observed a total of 95 (13%) are classified as variable.
- More, and more extreme (>4%) variables in the weaker population.
- Sources like PKS 1257-326 & J1819+3845 are rare.
- Wide ranging implications for
  - AGN physics: probing pc and sub-pc scales.
  - Inter-Stellar Medium
  - Cosmology: a standard "ruler" for θ vs z?
  - SKA
  - Geodesy & phase-referencing

The MASIV IDV Survey will yield 100 to 150 IDV sources over the northern sky. The investigation of the properties of such a sample will be important for Enigma.

- An example of the quality of flux density monitoring that is being done with the 30 m radio telescope at Ceduna, run remotely from the University of Tasmania.
- The source is PMN J1326-5256, the observations were taken over a week in April at 6.5 GHz.
- Strong IDV is clearly present.

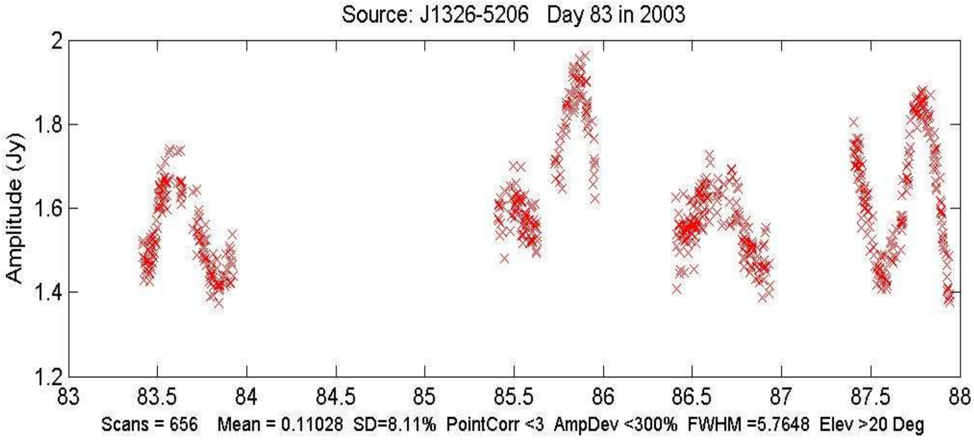
Source: J1326-5206 Day 83 in 2003
Amplitude (Jy)
2
1.8
1.6
1.4
1.2
83
83.5
84
84.5
85
85.5
86
86.5
87
87.5
88
Scans = 656 Mean = 0.11028 SD=8.11% PointCorr <3 AmpDev <300% FWHM =5.7648 Elev >20 Deg

Chapter 4

Session III: Variations of Source Structure and Flux (A. Witzel)

4.1 M. Tornikoski: Long Term Radio Variability: Statistics and Predictions

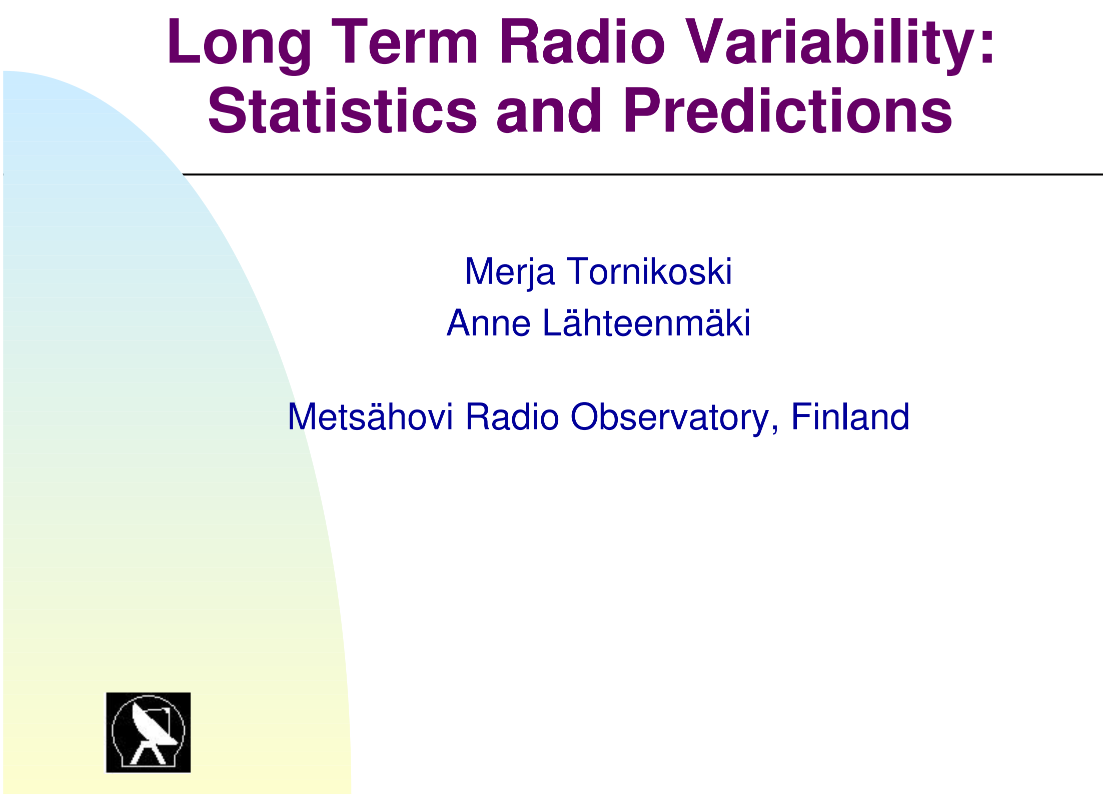

Variability

- Individual flares in individual sources
  Related to theoretical work:
  Models & Parameters.
  - e.g. Valtaoja 1999; Lähteenmäki & Valtaoja 1999; Türler et al. 2000
- Observational statistics:
  ”What are we likely to see?” and ”How often?”

Merja Tornikoski
Metsähovi Radio Observatory

Current activities

- Mostly Planck satellite -related studies
  - Quick Detection System: software, parameters.
  - Foreground map/catalogue.
  - Source activity ”predictions” / educated guesses.
- Also: studies on some individual sources + source samples.
  - CTA102, OA129, ...
  - Inverted-spectrum sources + others.

Merja Tornikoski
Metsähovi Radio Observatory

Data sets

- Metsähovi + SEST
  + data from the literature.
- Current focus on SEST database
  - Data paper + Variability statistics will be published in 2003.
  - 90 + 230 GHz, Oct 1987– ~ present.
  - 173 + 156 sources, 2887 + 1658 data points.

Merja Tornikoski
Metsähovi Radio Observatory

"Millimetre dilemma"

- Very limited availability of telescope time.

1. Focus on well-known, bright, variable sources.
2. Sources that are *assumed* to be faint are usually ignored / excluded.
3. Conclusions often based on few-epoch (or even one-epoch!) observations.

Merja Tornikoski
Metsähovi Radio Observatory

... well-known sources

- Not necessarily representative of their class.

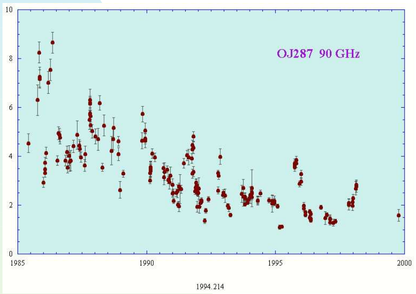

- Cluster analysis:
  Many of the "famous" sources are outliers.

Merja Tornikoski
Metsähovi Radio Observatory

... "faint" sources

- Source selection for mm-studies often based on (few-epoch) low-frequency catalog data.
- Many interesting sources or even source populations are excluded from mm-studies!

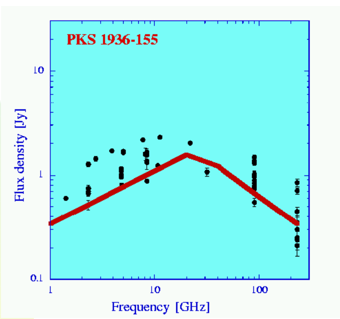

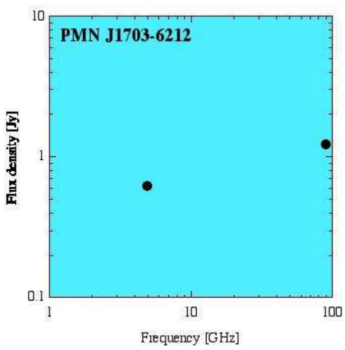

Merja Tornikoski
Metsähovi Radio Observatory

... few epochs

- At 90 GHz, a random observation is likely to see an AGN in a quiescent or intermediate state! (At 230 GHz,even more so!)

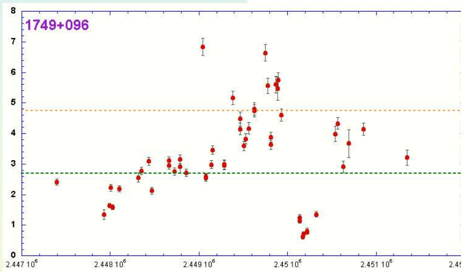

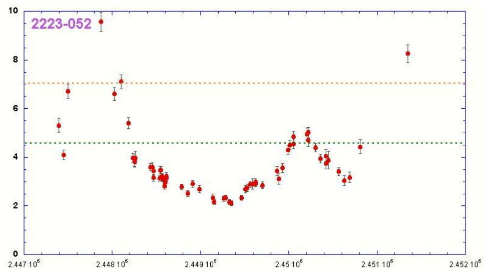

Merja Tornikoski
Metsähovi Radio Observatory

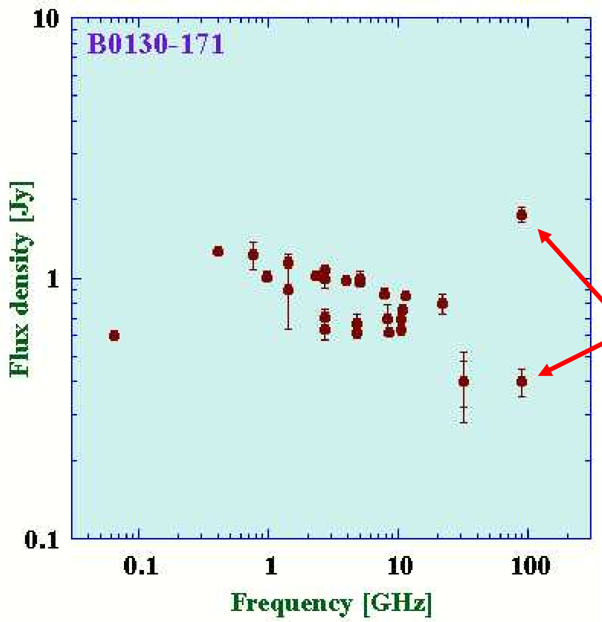

Sometimes
few-epoch observations
can reveal the true (?)
variability!
(Time btw the 2
90 GHz data points
= 14 years!)

Merja Tornikoski
Metsähovi Radio Observatory

Variability characteristics (90 GHz)

- Var vs. number of data points.
  - "More data points, more variable".
  - < 15 data points: no reliable info on true fluxes.
- "Activity timescales"
  - Every 3.6 yrs (for ca. 4 months).
- "Flare timescales"
  - What is a flare???
  - Enhanced flux where

$$S_{peak} - S_{base} > 1/3\ (S_{max} - S_{min})$$

  - Every 2.6 yrs.

Merja Tornikoski
Metsähovi Radio Observatory

Conclusions

- In order to determine flux minima & maxima, shape of the continuum spectrum etc.
  - Few-epoch observations are not enough!
  - Preferably long rather than very dense data sets.
- Lots of interesting (= bright at times) sources and even source populations have been excluded from mm-studies.

Merja Tornikoski
Metsähovi Radio Observatory

- Planck foreground work:
  - Larger set of sources, larger frequency range.
  - “Educated guesses” based on source behaviour and statistical data.
  - QDS parameters: Emphasis on “surprising” events and sources.
- ENIGMA:
  - Observational data & variability models.
  - Radio to submm collaboration.

Merja Tornikoski
Metsähovi Radio Observatory

4.2 K. Nilsson: Tuorla optical monitoring program

Tuorla optical monitoring program

K. Nilsson, L. O. Takalo, E. Lindfors, M. Pasanen
Tuorla Observatory, Finland

Tuorla Observatory

- 14 km E of Turku, Finland
- $\lambda = 22^\circ$ 27'
  $\phi = 60^\circ$ 24'
- altitude: 50 m
- observing season:
  Aug 15th - May 1st
- 50–100 clear nights per season
- FWHM 3"– 6"

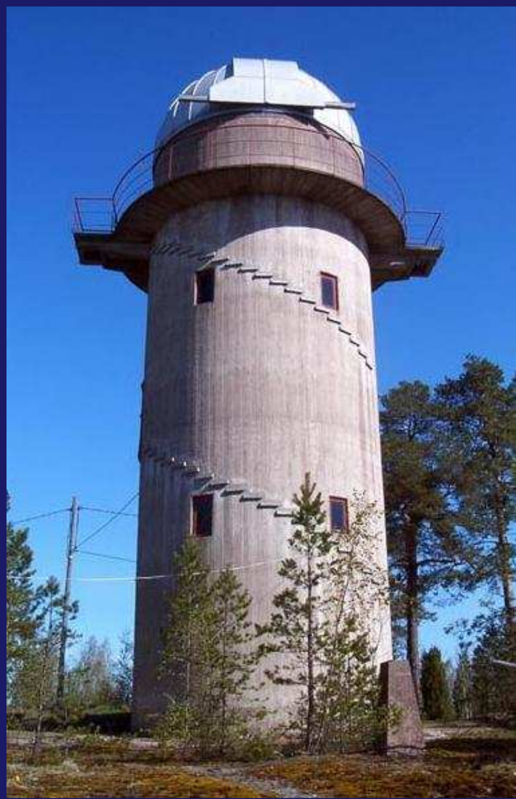

•First •Prev •Next •Last •Go Back •Full Screen •Close •Quit

The imaging system

- 1.03 m equatorial Dall-Kirkham telescope (f/8.5)
- telescope and control system built at Tuorla
- BVR-filters
- SBIG ST-1001E CCD (1024×1024 pix.)
  - pixel scale 1.2"/pix.
  - field size 10' × 10'

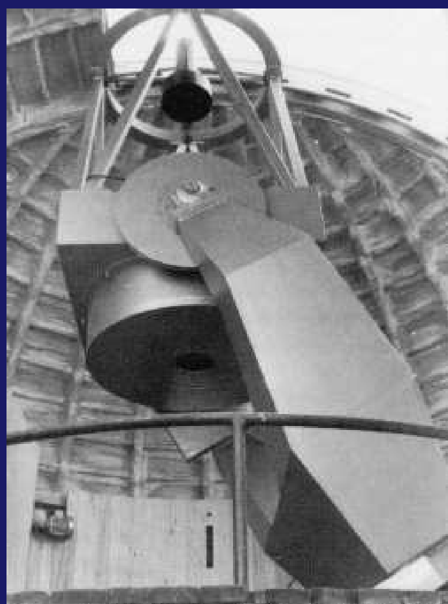

•First •Prev •Next •Last •Go Back •Full Screen •Close •Quit

The sample

- All Tev sources and Tev candidates from Costamante & Ghisellini (2002) with $\delta > +20^{\circ}$.

●First ●Prev ●Next ●Last ●Go Back ●Full Screen ●Close ●Quit

The sample

- All Tev sources and Tev candidates from Costamante & Ghisellini (2002) with $\delta > +20^{\circ}$.
- 24 objects :

1ES 0033+595	1ES 1011+496	RGB 1417+257
1ES 0120+340	1ES 1028+511	1ES 1426+428
RGB 0136+391	Mkn 421	1ES 1544+820
RGB 0214+517	RGB 1117+202	Mkn 501
3C 66A	Mkn 180	OT 546
1ES 0647+250	RGB 1136+676	1ES 1959+650
1ES 0806+524	ON 325	BL Lac
OJ 287	1ES 1218+304	1ES 2344+514

●First ●Prev ●Next ●Last ●Go Back ●Full Screen ●Close ●Quit

The 2002-2003 season

Goals:

- obtain $\approx$ 10 d interval monitoring data of all objects
- calibrate the system
- calibrate comparison stars for previously unobserved objects

●First ●Prev ●Next ●Last ●Go Back ●Full Screen ●Close ●Quit

The 2002-2003 season

Goals:

- obtain $\approx$ 10 d interval monitoring data of all objects
- calibrate the system
- calibrate comparison stars for previously unobserved objects

Results:

- data obtained during 43 nights
  - 1200 monitoring data points
  - BVR calibration data of comparison stars
  - filters calibrated

●First ●Prev ●Next ●Last ●Go Back ●Full Screen ●Close ●Quit

Example lightcurves

No variability (6/24 objects) :

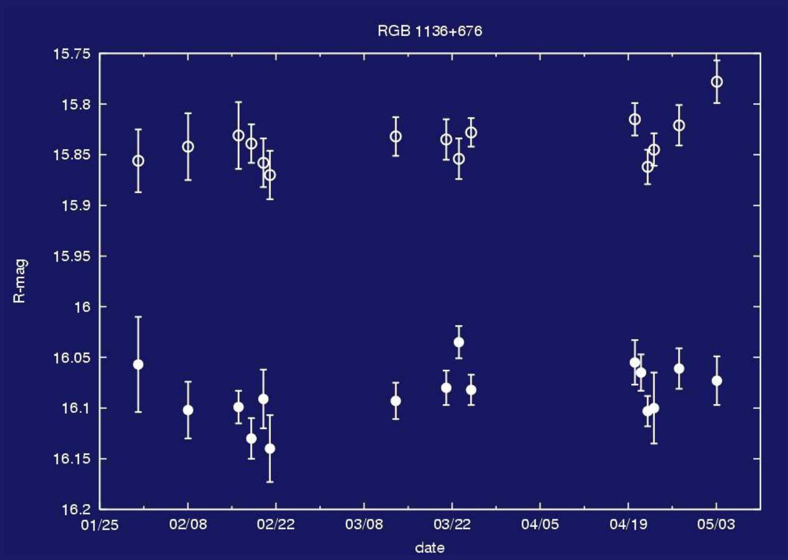

●First ●Prev ●Next ●Last ●Go Back ●Full Screen ●Close ●Quit

Example lightcurves

No variability (6/24 objects) :

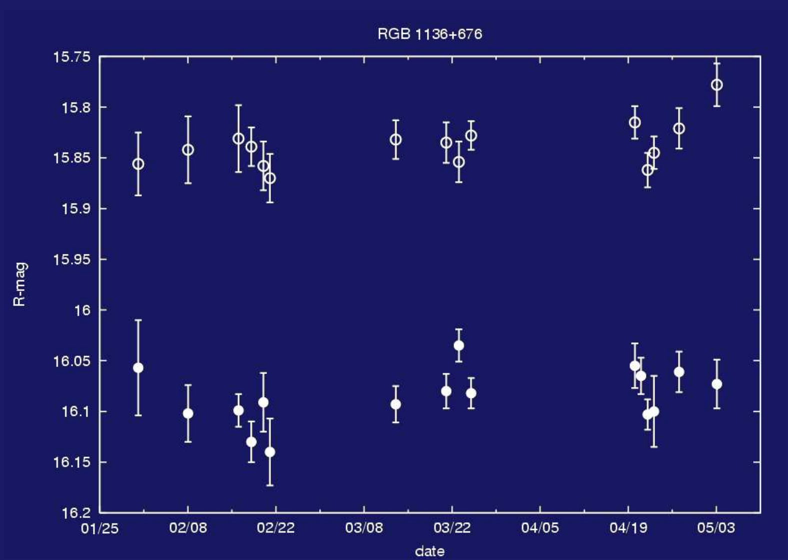

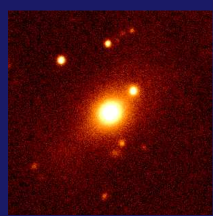

57"

●First ●Prev ●Next ●Last ●Go Back ●Full Screen ●Close ●Quit

Example lightcurves

No variability (6/24 objects) :

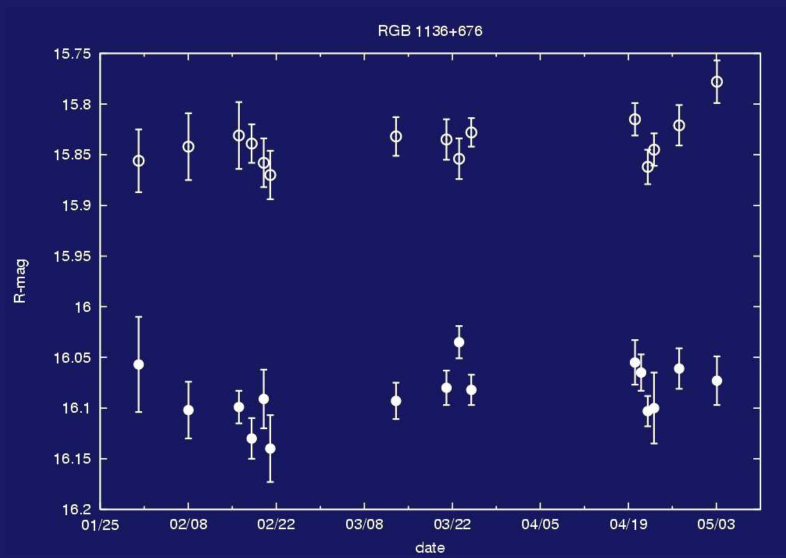

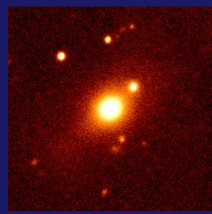

57''

14/12/98 NOT :

$$R_{core} = 18.2$$
$$R_{host} = 15.9$$

●First ●Prev ●Next ●Last ●Go Back ●Full Screen ●Close ●Quit

“Mildly variable” ($\triangle$m $<$ 0.3 mag) (12/24) :

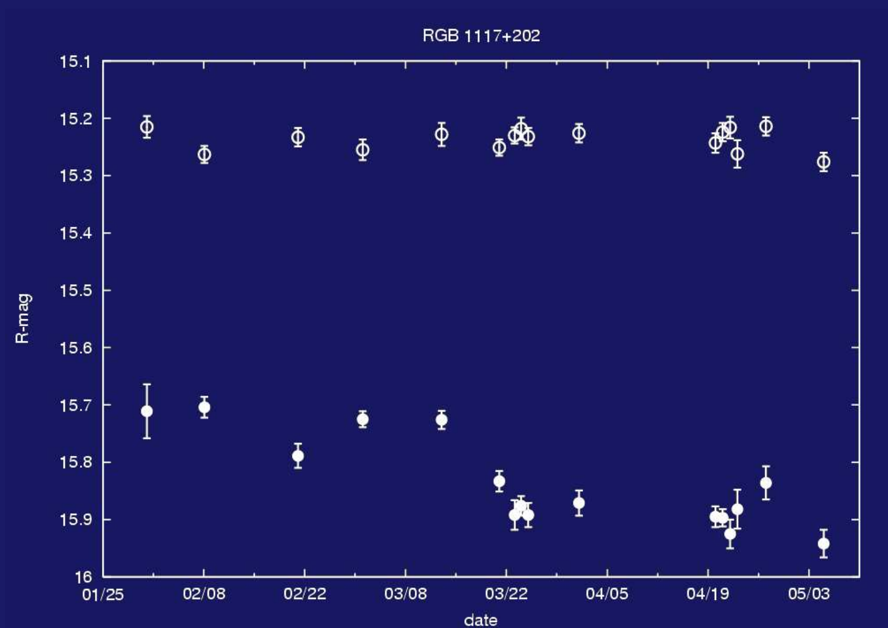

●First ●Prev ●Next ●Last ●Go Back ●Full Screen ●Close ●Quit

“Highly variable” (Δm > 0.3 mag) (6/24) :

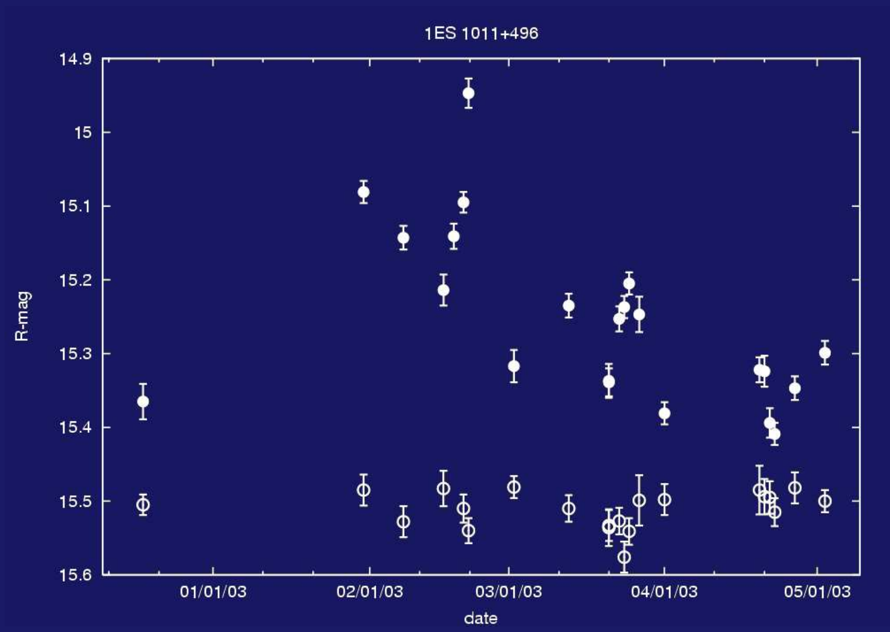

●First ●Prev ●Next ●Last ●Go Back ●Full Screen ●Close ●Quit

Highest variability : OJ 287 (Δm = 1.7 mag)

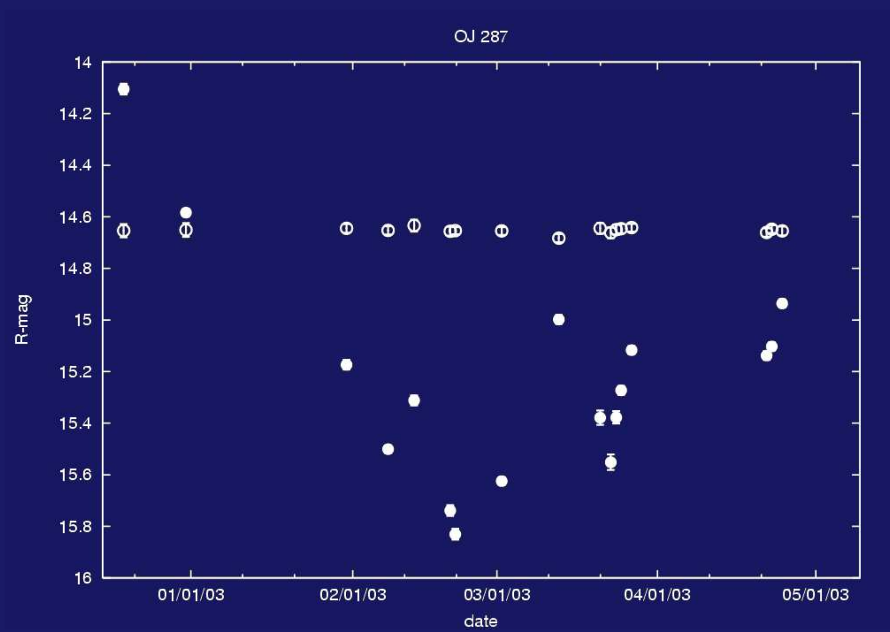

●First ●Prev ●Next ●Last ●Go Back ●Full Screen ●Close ●Quit

Conclusions

"What's there for ENIGMA?"

●First ●Prev ●Next ●Last ●Go Back ●Full Screen ●Close ●Quit

Conclusions

"What's there for ENIGMA?"

- A 1m class telescope with BVR filters for
  - long-term optical monitoring
  - monitoring campaigns
  - calibration of comparison stars

●First ●Prev ●Next ●Last ●Go Back ●Full Screen ●Close ●Quit

Conclusions

"What's there for ENIGMA?"

- A 1m class telescope with BVR filters for
  - long-term optical monitoring
  - monitoring campaigns
  - calibration of comparison stars
- Robotic operations are not foreseen in near future.

4.3 E. Middelberg: Where has all the polarisation gone?

Introduction

Synchrotron emission: High (> 50 %) degrees of polarization

Polarized emission + ionized gas + magnetic fields = Faraday rotation

$$\Theta = RM\,\lambda^2 \propto \int n_e\, B\, dl$$

Ionized plasma alone causes free-free absorption:

$$\tau \propto \int n_e^2\, dl$$

<u>Together, one can determine both n_e and B.</u>

Sample selection

Which objects have polarizat~~ion +~~ ionized plasma ?

$\longrightarrow$ Which objects have free-free absorption?

$\longrightarrow$ Which objects have spectral indices > 2.5 along the jet?

<u>Final sample:</u>

Source	Dist. / Mpc	Type	Spectral index
NGC 1052	19,4	LINER	> +3.0
NGC 4261	34,4	FR I	> +3.0
Centaurus A	4,2	FR I	+ 3.8
Hydra A	248	FR I	+ 0.8
Cygnus A	259	FR II	+ 1.0

Observations

Pilot observations carried out with VLBA @ 15 GHz / 13 GHz.

15 GHz:	- high resolution:	< 1 mas
	- good sensitivity:	rms ~ 0.2 mJy / beam
	- less depolarization:	$1/\nu^2$
	- less absorption:	$1/\nu^2$

Two polarization calibrators, residual D-terms < ~0.3 %

Primary calibration in AIPS, mapping in DIFMAP,
final polmaps in AIPS

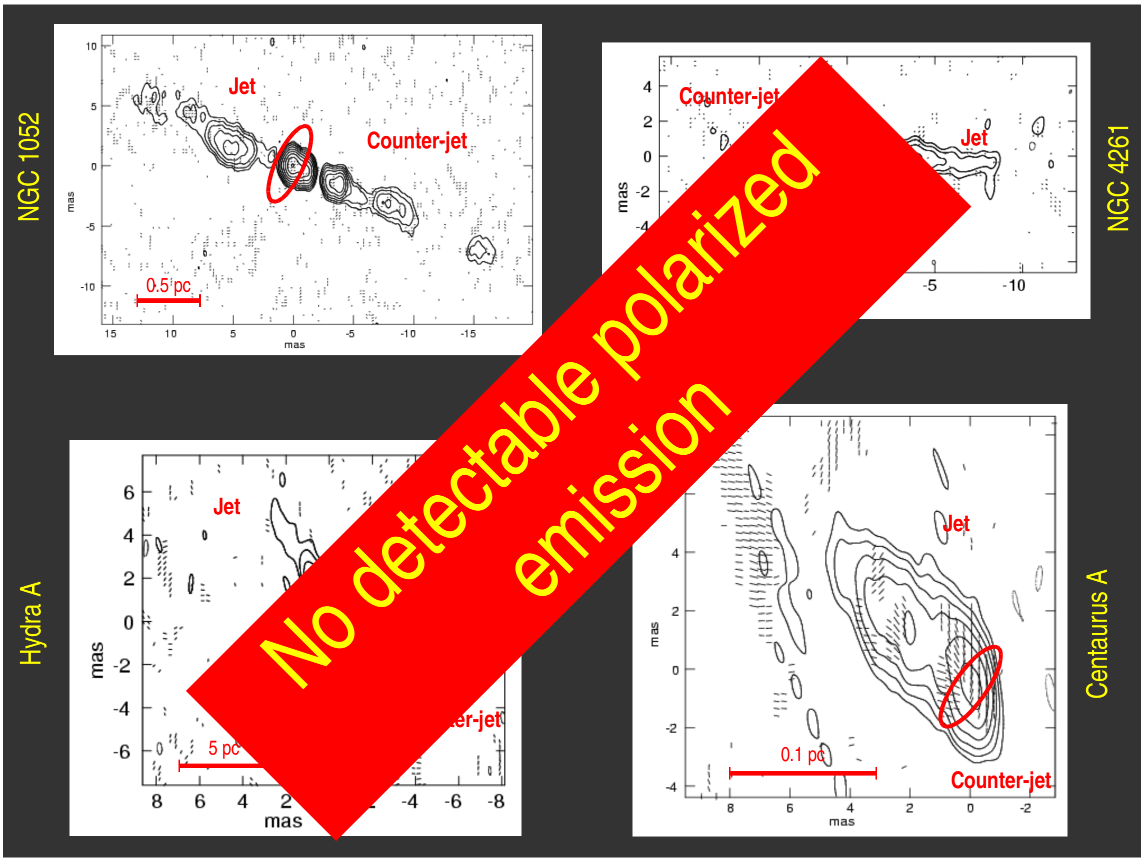

Results

Cygnus A

15 GHz

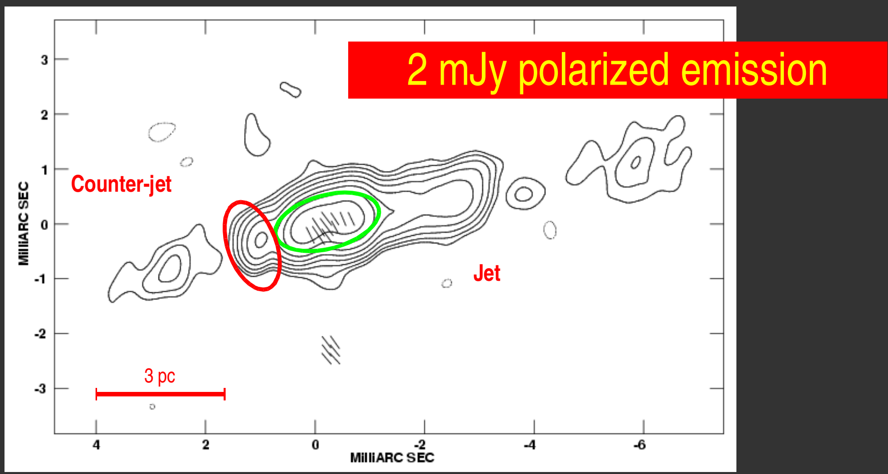

rms, I = 0.42 mJy / beam
rms, P = 0.12 mJy / beam
Peak = 315 mJy / beam

Results

Summary

Except for Cyg A, none of the sources is polarized,
neither in the absorbed gap nor in any jet parts.

This is contrary to quasars and BL Lacs.

Desired B field measurements not possible.

Discussion

Depolarization intrinsic or extrinsic?

Intrinsic causes

Tangled B fields cause beam depolarization

Possible to obtain limits on cell size

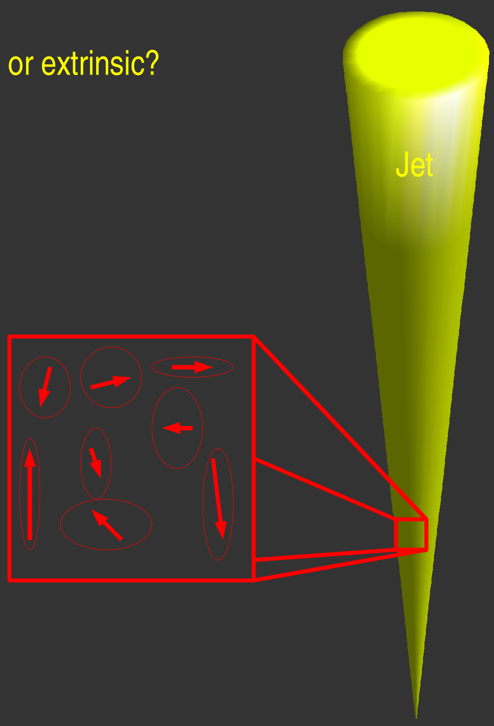

Discussion

Extrinsic - Bandwidth-depolarizationby high RM

$$p(\lambda) = p(\lambda_0)\exp(i\,RM\,(\lambda^2 - \lambda_0^2))$$

$$\langle p \rangle = \frac{p(\lambda_0)\exp(-i\,RM\,\lambda_0^2)}{\lambda_1 - \lambda_0} \int_{\lambda_1}^{\lambda_0} \exp(i\,RM\,(\lambda^2))\,d\lambda$$

In 15 GHz band, $\langle p \rangle / p(\lambda_0) = 0.5$ requires RM = 2.2 10^6 rad/m^2

Typical RMs of 10^4 rad/m^2 cause 0.00012% depolarization

Discussion

What conditions cause RM > 10^6 ?

$n_e = 10^4\ \mathrm{cm}^{-3}$, L = 1 pc, $B_{||} = 0.1$ mG $\longrightarrow$ ~ 10^6 rad/m^2

But: free-free absorption is $\tau_{ff} \approx 5\ 10^{-8} \left(\frac{T}{10^4\ K}\right)^{-3/2} \left(\frac{n_e}{c\ m^{-3}}\right)^{2} \left(\frac{\nu}{GHz}\right)^{-2} g \left(\frac{d}{pc}\right)$

$\longrightarrow$ $\tau \approx 1$ at 5 GHz
$\longrightarrow$ $\tau \approx 0.1$ at 15 GHz

Only way out: absorber needs to be extended or hot, or both!
$\longrightarrow$ hot gas phase filling inner few pc above torus?

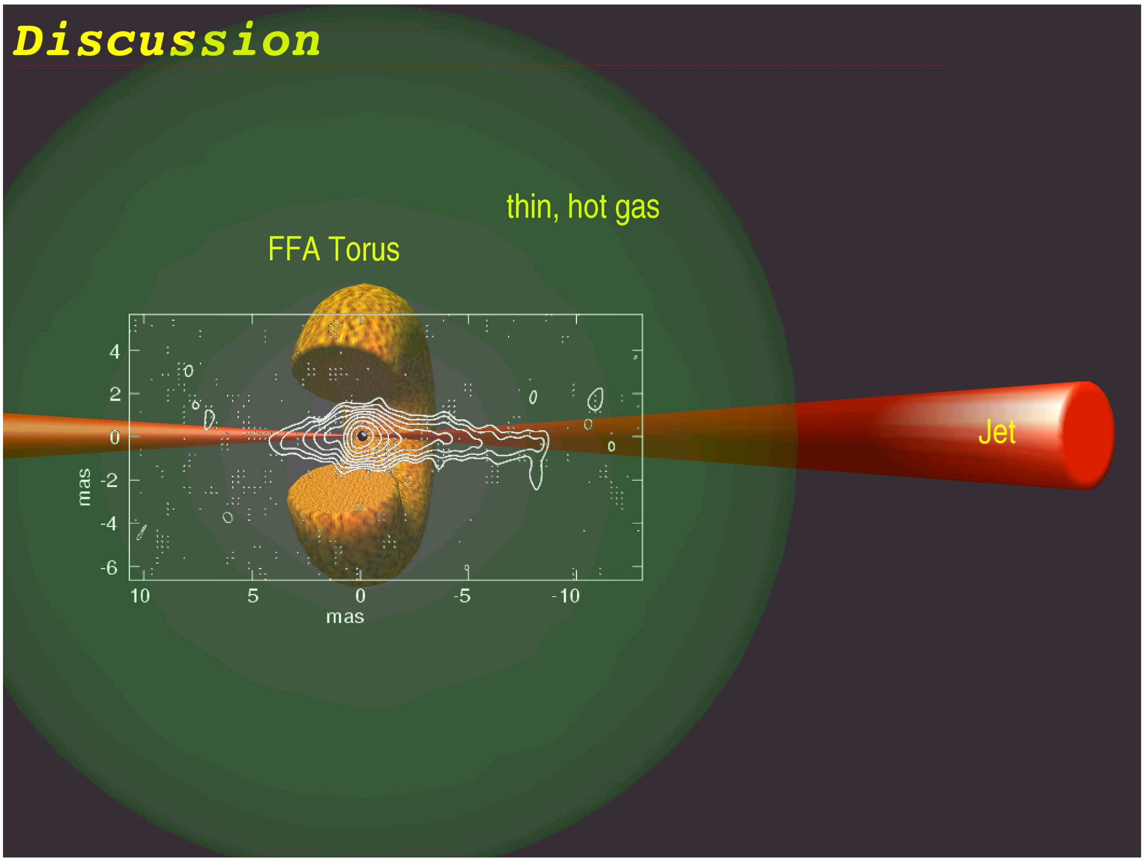

Discussion

Extrinsic - Depolarization by tangled magnetic fields

Initially polarized emission passes through Faraday screen with tangled magnetic fields.

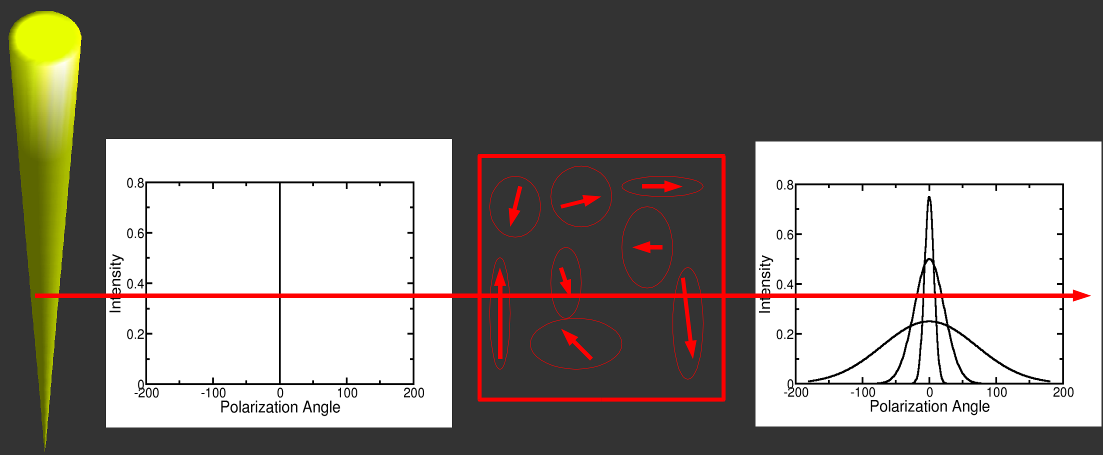

Conclusions

NGC 1052
Evidence for spherical absorber (Kameno et al. 2001).
High RMs possible! Depolarized?

NGC 4261
Jet is flat spectrum, not inverted. *Absorber unlikely. Depolarized?*

Centaurus A
Properties of inner jet uncertain. Jet bend 0.05 pc away from core?

Hydra A
Jets have steep spectra. *Absorber unlikely. Depolarized?*

Cygnus A
Polarized emission from jet. *Future RM measurements possible. Depolarized nevertheless?*


Now in radio astronomy:
Propose one and
GET ONE FREE!!!

4.4 S. Friedrichs: Polarisation Measurements of 0954+658 with VSOP

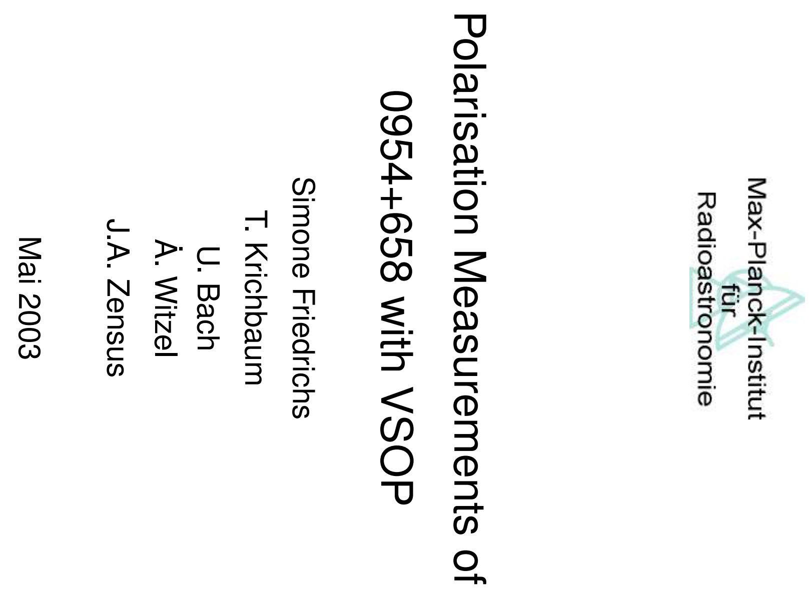

→ The source: BL Lac 0954+658

z = 0.368
well-studied short-time variable source

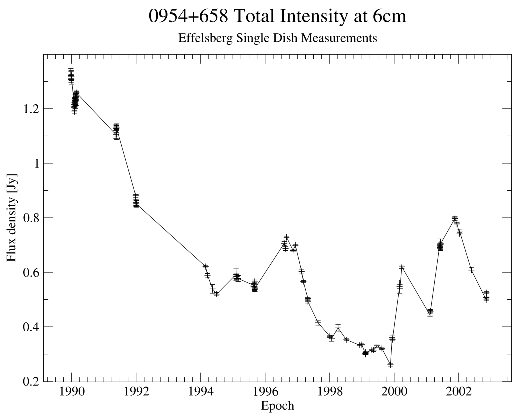

→ Aim of the experiment:

High-resolution imaging on structures of the inner jet
Changes in polarisation intensity and angle
Separation between polarisation in the core and the innermost jet
5 GHz VLBI + HALCA observations in October 2000
(first epoch VLBA + Y + HALCA)

→ Data reduction in AIPS (Astronomical Image Processing System of the NRAO)
and Difmap (part of Caltech VLBI Software Package)

→ Preliminary results:

Modelfits
Polarisation maps

What is so special about HALCA?

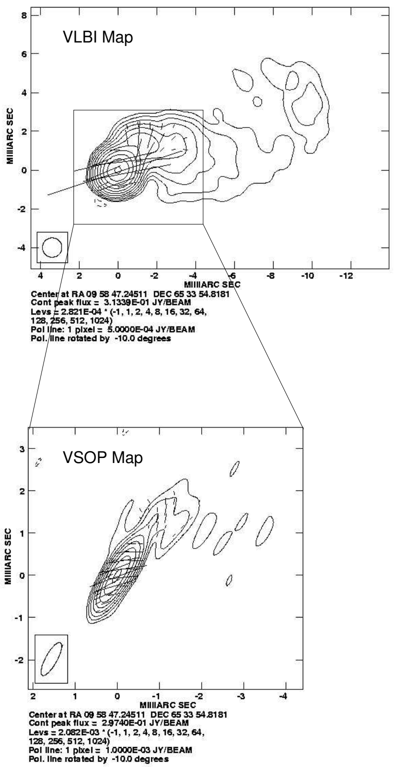

VSOP uv coverage 16 October 2000, 20 to 21 October 2000

(top left to bottom right)

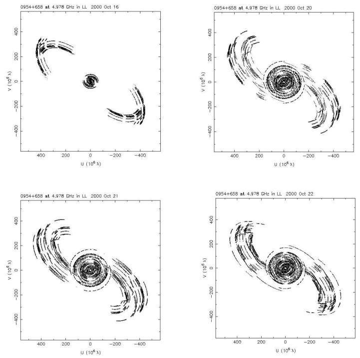

VLBI uv coverage 16 October 2000, 20 to 21 October 2000

(top left to bottom right)

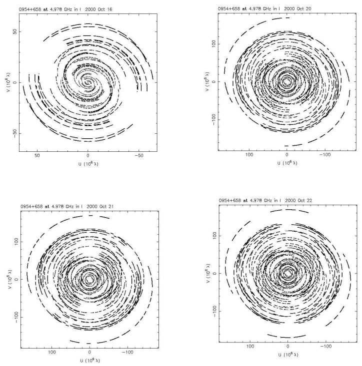

Modelfits of the epochs a) 20 October 2000, b) 21 October 2000

and c) 22 October 2000 for the VSOP Data

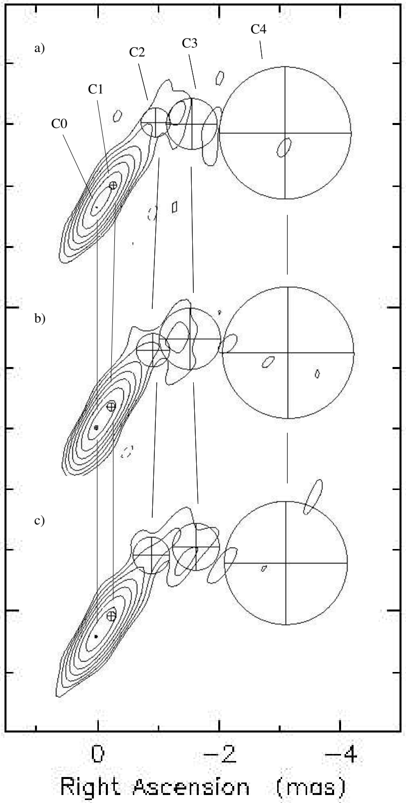

VSOP Modelfit Components

20 October 2000

COMP.	S [JY]	RADIUS	THETA
C0	0.226228	0.00000	0.00000
C1	0.133375	0.454011	-37.2044
C2	0.0150889	1.70682	-34.9404
C3	0.0142515	2.09157	-48.8986
C4	0.0272404	3.35352	-68.5754

21 October 2000

COMP.	S [JY]	RADIUS	THETA
C0	0.214362	0.00000	0.00000
C1	0.159429	0.423147	-35.8382
C2	0.0171262	1.58721	-36.3375
C3	0.0184052	2.13418	-46.6218
C4	0.0288946	3.41079	-68.7085

22 October 2000

COMP.	S [JY]	RADIUS	THETA
C0	0.218441	0.00000	0.00000
C1	0.149624	0.419775	-37.5588
C2	0.0196756	1.62340	-34.5017
C3	0.0144174	2.22184	-48.2611
C4	0.0264727	3.37378	-68.9336

Modelfits of the epochs of a) 20 October 2000, b) 21 October 2000 and c) 22 October 2000 for the VLBI Data

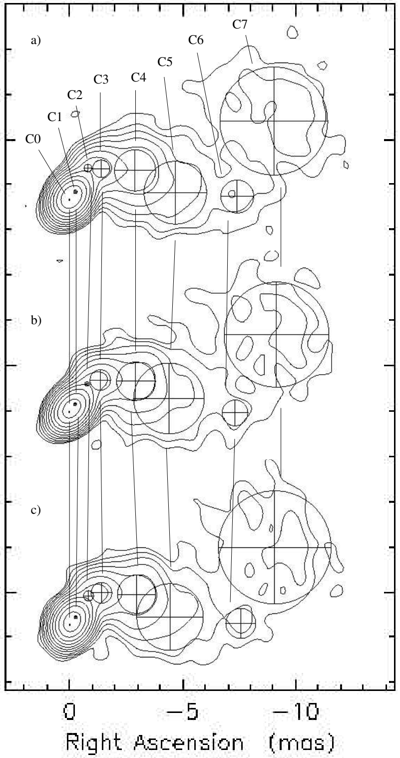

VLBI Modelfit Components

20 October 2000

COMP.	S [JY]	RADIUS	THETA
C0	0.221299	0.00000	0.0000
C1	0.133993	0.44212	-37.8019
C2	0.00989428	1.63125	-30.6035
C3	0.0199519	1.98117	-45.9009
C4	0.0235060	3.21660	-66.0959
C5	0.00761891	4.75066	-86.2524
C6	0.00142830	7.51047	-88.9329
C7	0.0122111	9.79024	-69.0261

21 October 2000

COMP.	S [JY]	RADIUS	THETA
C0	0.195387	0.00000	0.0000
C1	0.156849	0.42043	-38.2393
C2	0.00946904	1.47877	-32.8156
C3	0.0244932	1.98406	-44.4781
C4	0.0203259	3.26903	-65.3545
C5	0.0103960	4.49593	-82.4186
C6	0.00108659	7.40557	-90.3817
C7	0.0119687	9.87937	-69.6410

22 October 2000

COMP.	S [JY]	RADIUS	THETA
C0	0.202860	0.00000	0.0000
C1	0.147849	0.425639	-38.6831
C2	0.0115222	1.53974	-33.1685
C3	0.0220153	2.01065	-44.9300
C4	0.0203517	3.28316	-65.5772
C5	0.00929113	4.49917	-85.6362
C6	0.00106722	7.65047	-89.5558
C7	0.0129170	9.79688	-69.3781

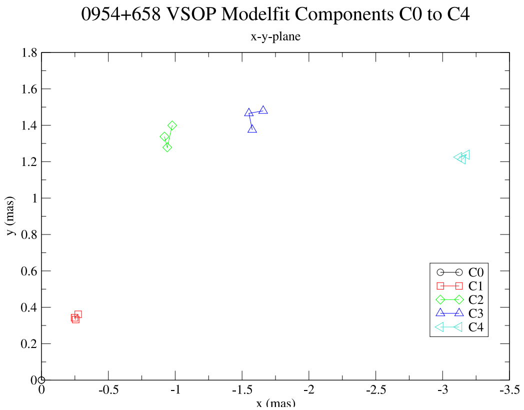

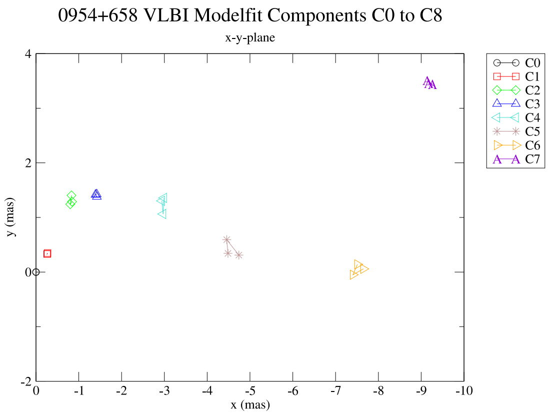

VSOP Total Intensity

EPOCH	S_{Core} [MJY]	S_{Jet} [MJY]	$\sum$ [MJY]
16 October	335.2	31.3	366.5
20 October	362.4	44.1	406.5
21 October	376.9	44.4	420.3
22 October	372.1	45.7	417.8

VLBI Total Intensity

EPOCH	S_{Core} [MJY]	S_{Jet} [MJY]	$\sum$ [MJY]
16 October	368.7	27.2	395.9
20 October	371.5	45.9	417.4
21 October	369.0	48.0	417.0
22 October	373.2	44.9	418.0

VSOP Polarisation Images of Epochs 20 - 22 October 2000

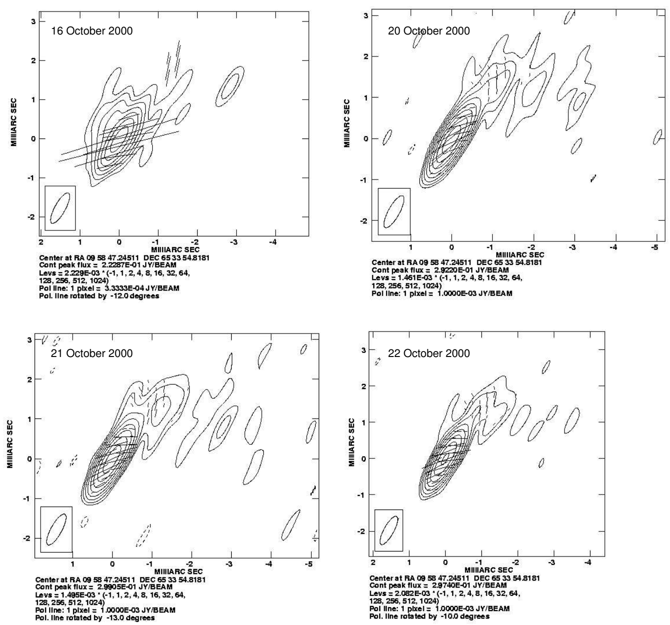

VLBI Polaristaion Images of Epochs 20 - 22 October 2000

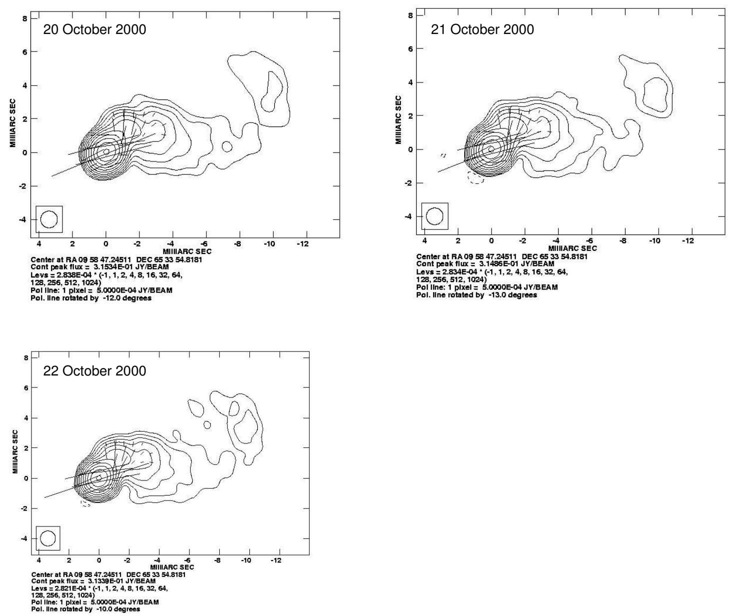

VSOP Polarisation Intensity

EPOCH	S_{Core} [MJY]	S_{Jet} [MJY]	m_{Core}[%]	m_{Jet}[%]
16 October	13.0	4.5	3.9	16.54
20 October	15.8	6.3	4.4	13.72
21 October	15.9	8.1	4.2	16.87
22 October	16.6	6.5	4.5	14.48

VLBI Polarisation Intensity

EPOCH	S_{Core} [MJY]	S_{Jet} [MJY]	m_{Core}[%]	m_{Jet}[%]
16 October	12.0	3.2	3.3	11.8
20 October	14.4	5.3	3.9	11.5
21 October	13.7	5.9	3.7	12.3
22 October	14.7	5.4	3.9	12.0

VSOP Polarisation Angles

EPOCH	χ_{Core}	χ_{iJet}
20 October	-75°	+89°
21 October	-75°	-89°
22 October	-70°	-87°

VLBI Polarisation Angles

EPOCH	χ_{Core}
20 October	-67°
21 October	-68°
22 October	-71°

Polarisation angles in the jet ?

$\rightarrow$ Still some things left to do

4.5 D. Gabuzda: New views of the polarization structure of compact AGN from multi-wavelength data

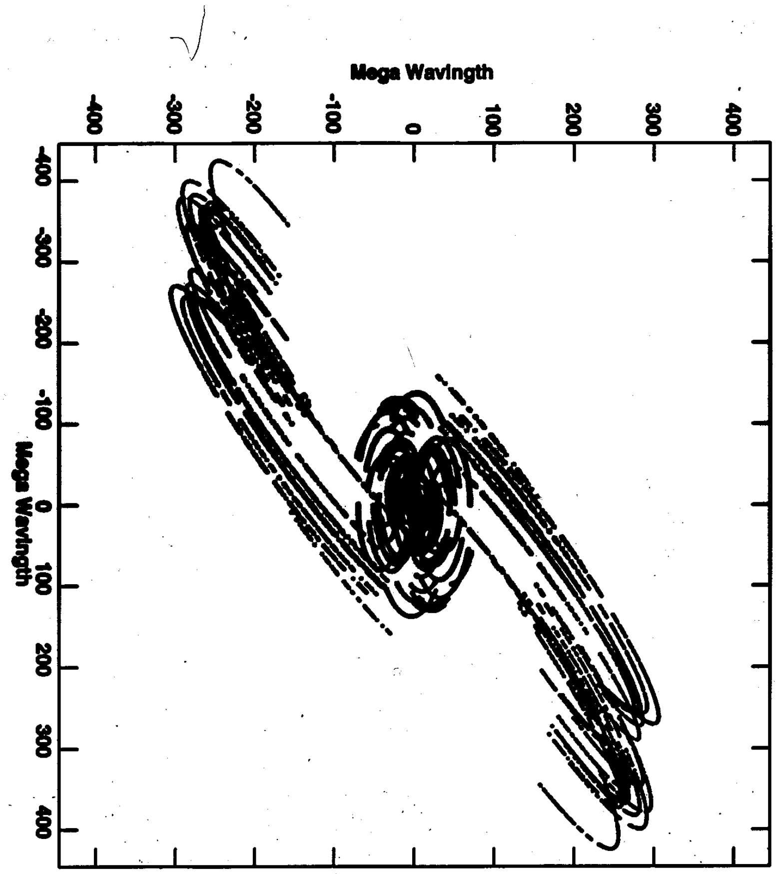

5 GHz
April 4, 1999

Gabuzda & Gómez, MNRAS 2001

OJ287 — ground array only

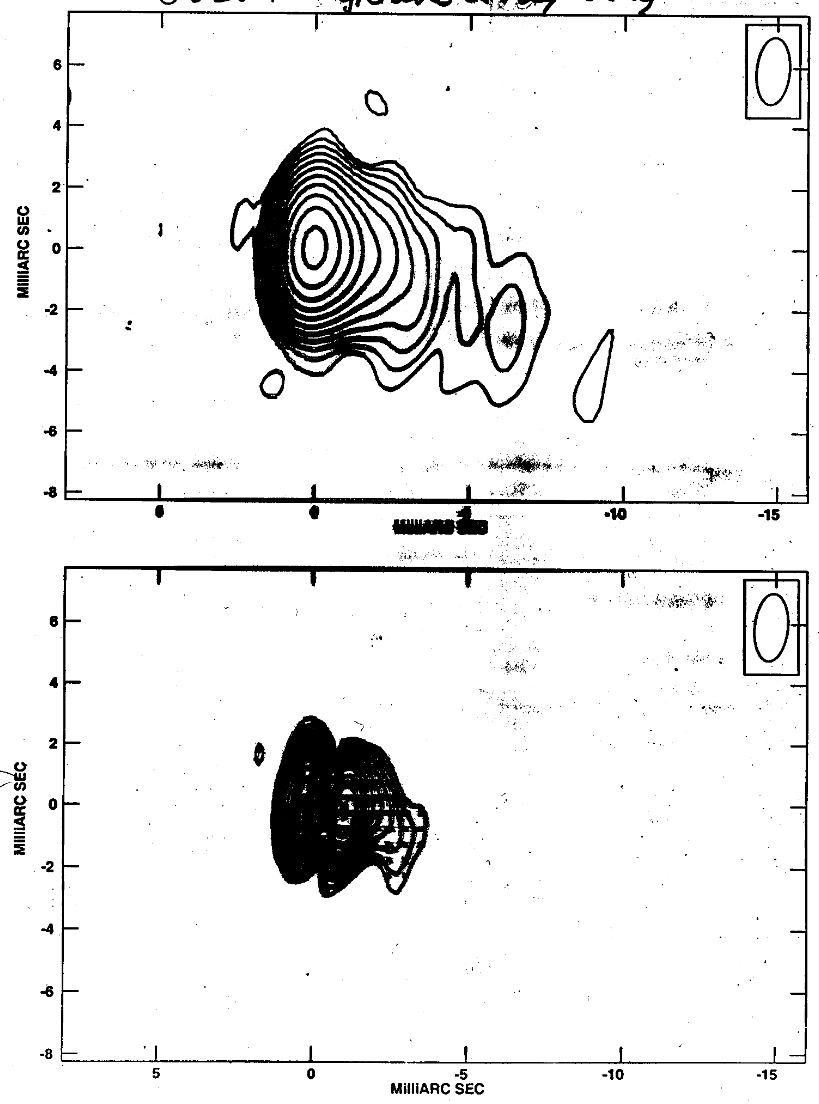

Gabuzda & Gómez MNRAS (2001)

VSOP 5 GHz April 4, 1999

VLBA 22 GHz March 19, 1999

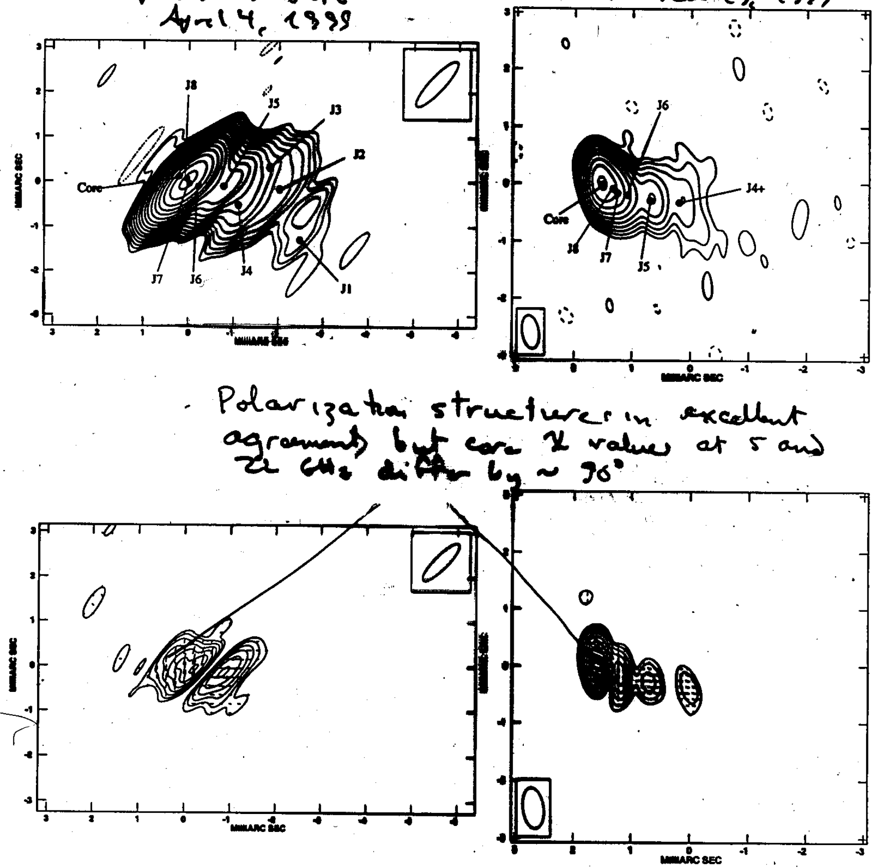

· Polarization structures in excellent agreement but core χ values at 5 and 22 GHz differ by ~ 90°

∴ Core is optically thick at 5 GHz ($\chi \parallel \vec{B}$), but ~~optically~~ thin, at 22 GHz ($\chi \perp \vec{B}$).

⟹ In either case, B is transverse to jet direction in the core

Core and Inner Jet of OJ287 at 6 and 1.3 cm

	I_6 (mJy)	$I_{1.3}$ (mJy)	α	χ_6 (deg)	$\chi_{1.3}$ (deg)	$\Delta\chi_{6\text{-}1.3}$ (deg)
C	300	1238	+0.92	− 2	71	73
J8	400	194	−0.47	−10	−6	4
J7	598	274	−0.51	—	—	—
J6	194	106	−0.39	−12	−24	12
J5	214	79	−0.65	−97	−97	0

Theoretically predicted 90° flip in χ in the transition from optically thin → thick directly detected!

5 GHz VSOP
Gabuzda & Gomez 2001 MNRAS

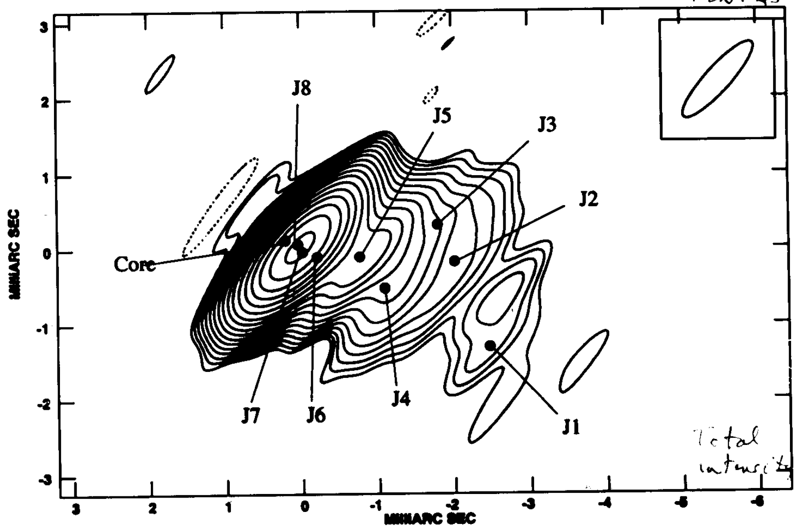

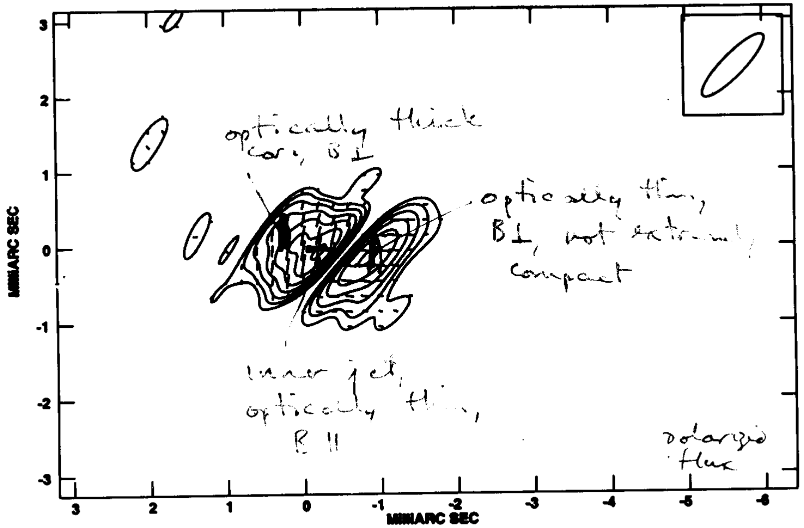

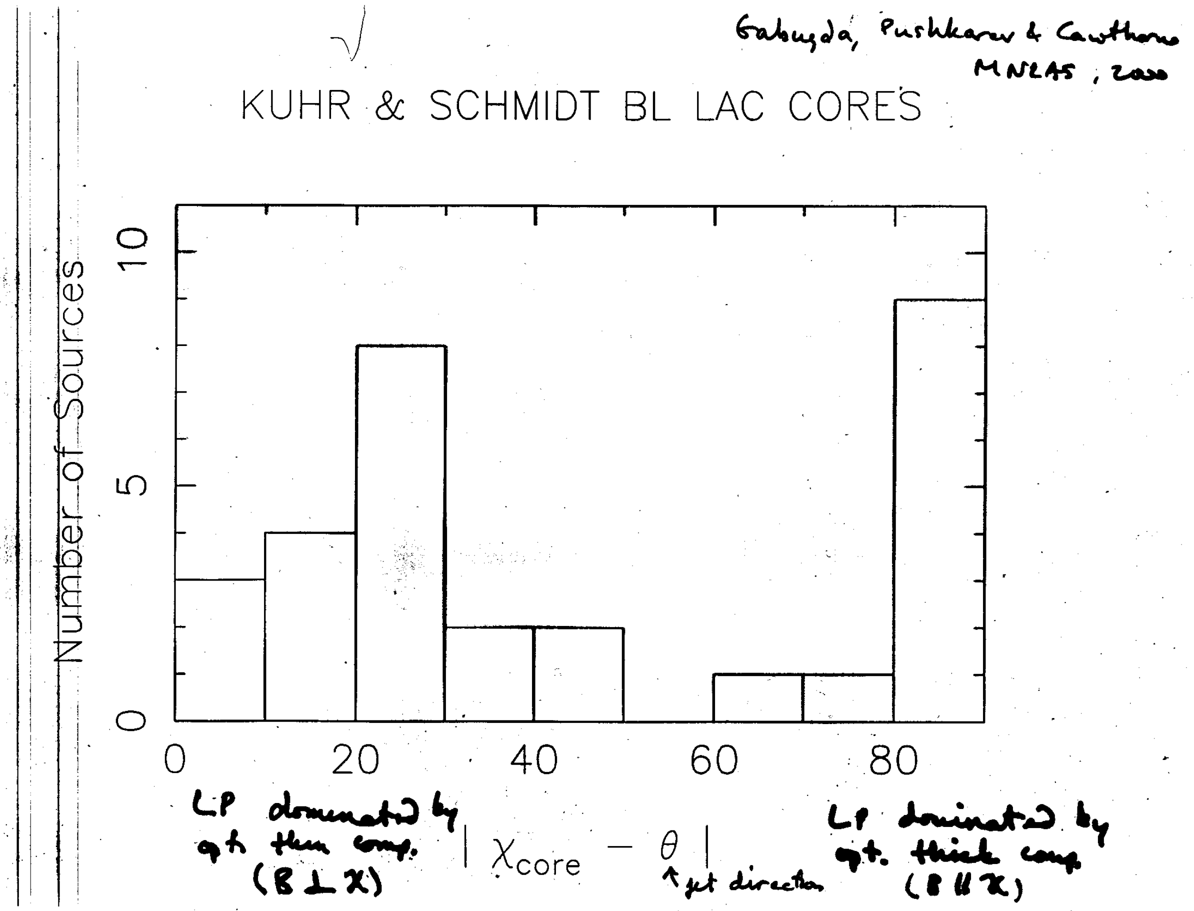
Gabuzda, Pushkarev & Cawthorne
MNRAS, 2000
KUHR & SCHMIDT BL LAC CORES
Number of Sources
$|\chi_{core} - \theta|$
LP dominated by opt. thin comp. (B ⊥ X)
LP dominated by opt. thick comp. (B ∥ X)
jet direction

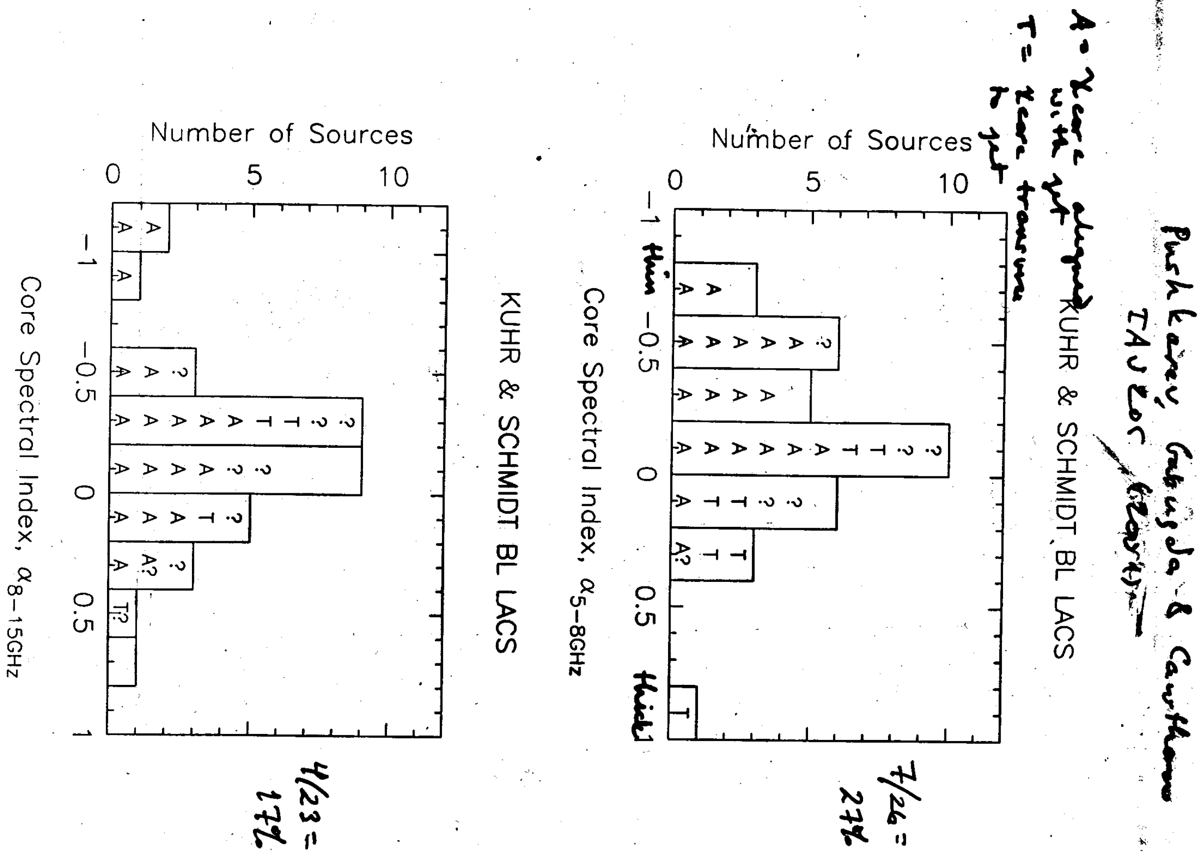
KUHR & SCHMIDT BL LACS
Number of Sources
Core Spectral Index, $\alpha_{8-15GHz}$
4/23 = 17%
KUHR & SCHMIDT BL LACS
Number of Sources
Core Spectral Index, α_{5-8GHz}
thin
thick
7/26 = 27%
Pushkarev, Gabuzda & Cawthorne

optical + 5 GHz VLBI polarization data

1996AJ....112.1877G

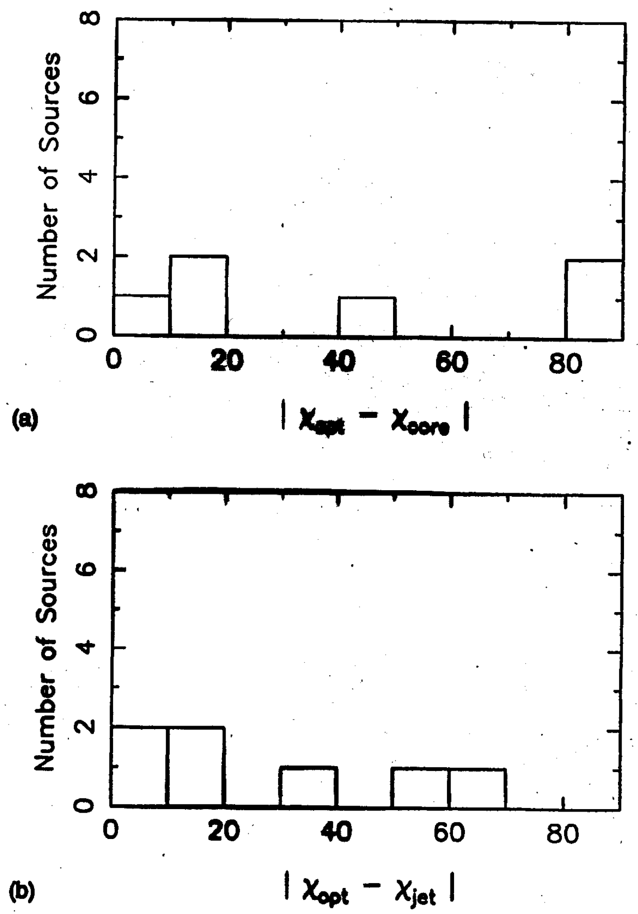

FIG. 6. **Histograms** of the differences between (a) χ_{opt} and χ_{core} and (b) χ_{opt} and χ_{jet}.

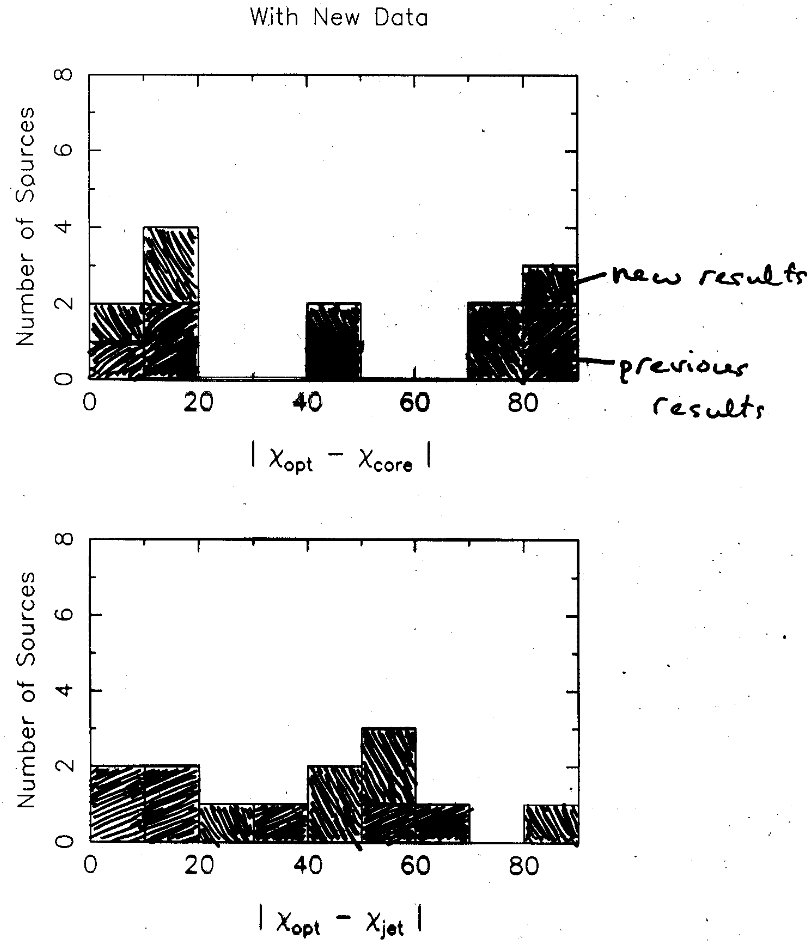

Binomial probability distribution for two outcomes A and B with unequal probabilities:

$$P_{chance} = (P_A)^{n_A} * (P_B)^{n_B} * \frac{n_{total}!}{n_A! n_B!}$$

Taking the two outcomes to be $\chi_{opt} - \chi_{VLBI}$ either near the edges or in the centre of the histogram of $\chi_{opt} - \chi_{VLBI}$ values:

$$P_{chance} = (P_{edge})^{n_{edge}} * (P_{centre})^{n_{centre}} * \frac{n_{total}!}{n_{edge}! n_{centre}!}$$

$$P_{chance} = \left(\frac{4}{9}\right)^{n_{edge}} * \left(\frac{5}{9}\right)^{n_{centre}} * \frac{n_{total}!}{n_{edge}! n_{centre}!}$$

Probabilities for optical+VLBI measurements up to 1993 (Gabuzda, Sitko & Smith 1996):

Optical vs. Core: $n_{total} = 6,\ n_{edge} = 5,\ n_{centre} = 1$
$P_{chance} = 6\%$

Optical vs. Jet: $n_{total} = 7,\ n_{edge} = 4,\ n_{centre} = 3$
$P_{chance} = 29\%$

Probabilities for optical+VLBI measurements up to 1996 (Gabuzda, Smith & Garnich, in prep.):

Optical vs. Core: $n_{total} = 13,\ n_{edge} = 11,\ n_{centre} = 2$
$P_{chance} = 0.3\%$

Optical vs. Jet: $n_{total} = 13,\ n_{edge} = 5,\ n_{centre} = 8$
$P_{chance} = 20\%$

- There is a clear tendency for χ_{opt} to be either $\parallel$ or $\perp$ 5GHz VLBI χ_{core}
- This makes sense if

$\chi_{opt} \parallel \chi_{core}$ when radio core polarization is dominated by optically thin regions

$\chi_{opt} \perp \chi_{core}$ " optically thick regions

- Simple Predictions:

→ If we compare simultaneous optical polarization data with higher frequency VLBI pol. data, more cores should have $\chi_{opt} \parallel \chi_{core}$.

→ If we make the comparison using multi-λ VLBI data, those cores with $\chi_{opt} \parallel \chi_{core}$ should be "optically thin" while those with $\chi_{opt} \perp \chi_{core}$ should be "optically thick"

New Quasi-simultaneous Optical + VLBP Observations (43+22+15 GHz)
Gabuzda, Rastorgueva & Smith

VLBI Epoch	Source	Optical Polarization (%)
7 Aug 2002	1418+546	6.54±0.42
	1538+149	Not observed
	1732+389	Not observed
	1749+096	9.65±0.45
	1823+568	9.41±0.55
	2131–021	2.39±0.94
	2200+420	Not observed
	2254+074	13.75±0.59
5 Mar 2003	0048–097	Not observed
	0138–097	Not observed
	0256+075	Not observed
	0735+178	2.69±0.10 (86.7°)
		2.16±0.10 (62.5°)
	0823+033	5.36±0.49
	OJ287	18.48±0.14 (180.1°)
		19.43±0.10 (154.8°)
	1147+245	7.60±0.18 (58.4°)
		7.90±0.19 (60.7°)
	1219+285	5.61±0.07 (107.6°)
		4.25±0.07 (90.4°)
	3C279	24.01±0.24 (54.9°)
		25.67±0.30 (54.5°)
	1334–127	10.41±0.16 (55.9°)
		12.67±0.19 (32.8°)
	1538+149	20.91±0.24 (145.8°)
		29.24±0.30 (151.4°)
	1732+389	17.16±0.44 (62.8°)
		15.04±0.34 (69.2°)

Total objects with successful optical+VLBP obs: 14/18 proposed.

One possible scenario:

- Intrinsic jet B field is characteristically ⊥ jet direction, beginning on small scales within the observed radio cores.
  - → χ_{opt} ∥ jet
  - → χ_{core} ∥ or ⊥ jet, depending on optical depth
- A number of sources (primarily BL Lac objects) are observed to have ⊥ B fields over extended regions of jet.
  - → Dominance of toroidal/helical B field component?

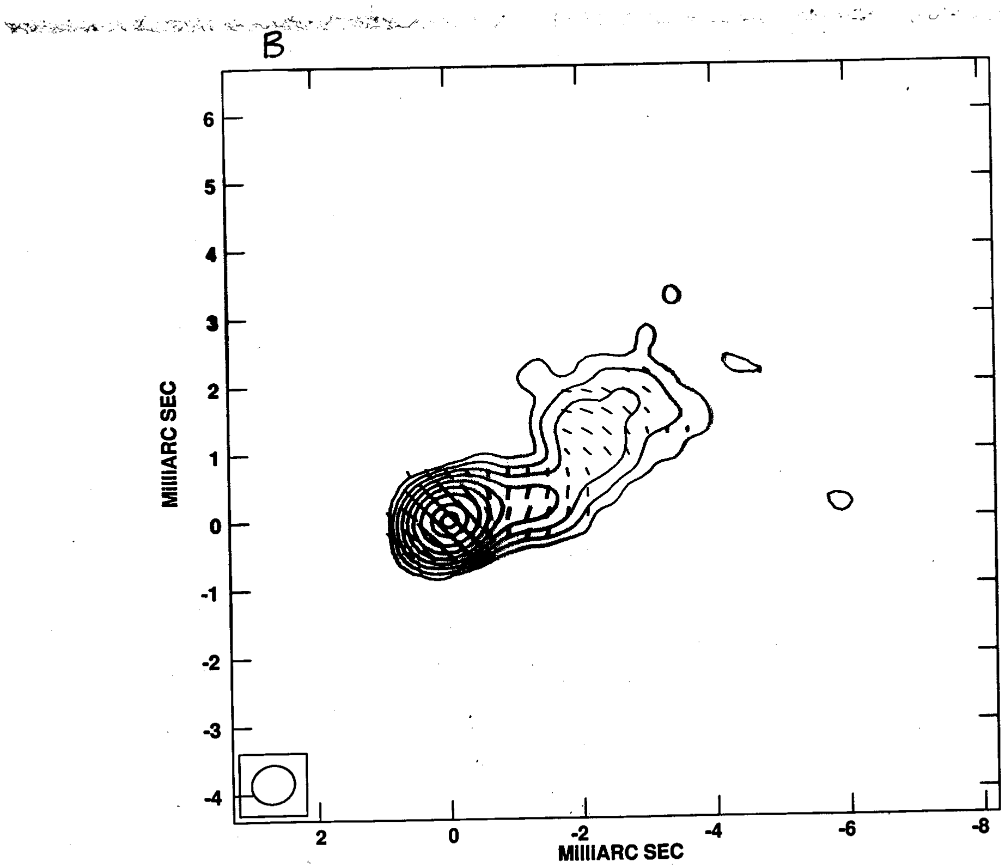

1749+701
15 GHz
Gabuzda
PASA, 2002

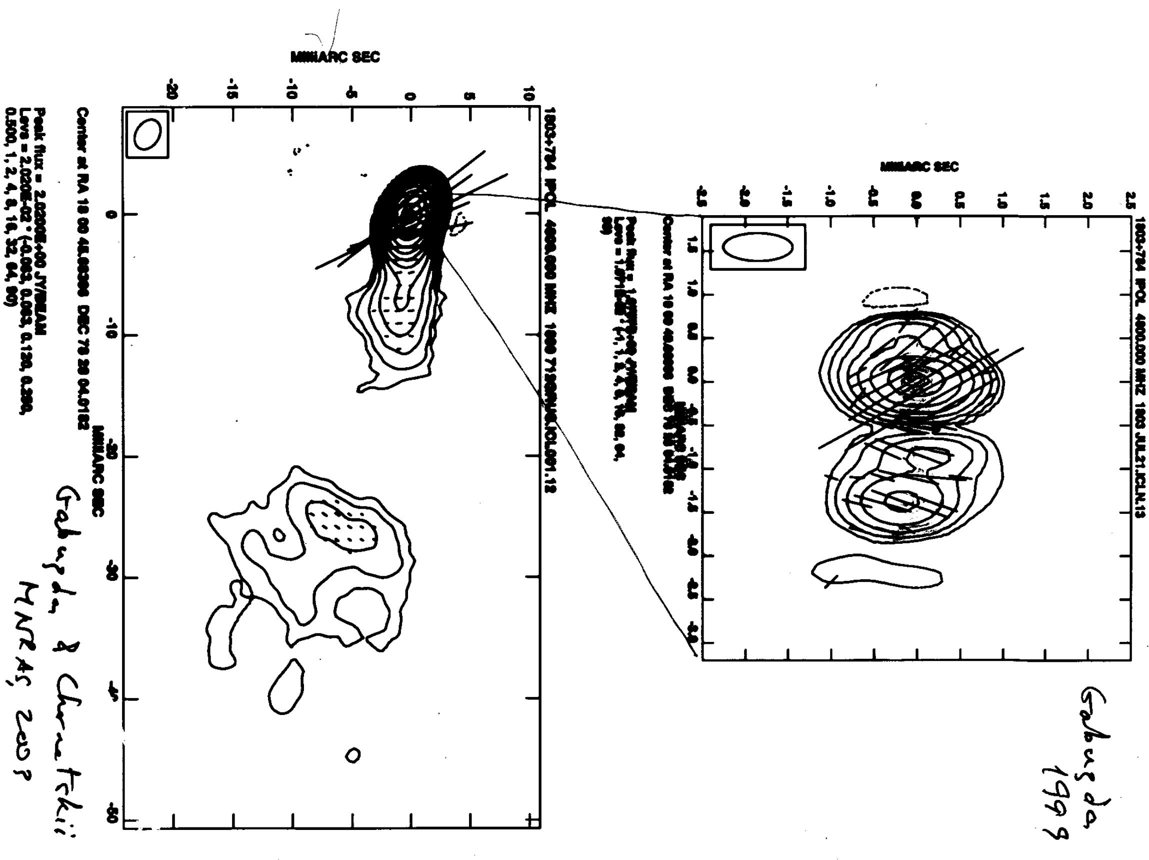

Gabuzda & Chernetskii
MNRAS, 2002

Gabuzda
1999

THEORY (K. Tsinganos, A. Mastichiadis, N. Vlahakis et al.)

- Experience in constructing steady analytical 3-D models of MHD winds and jets (relativistic & nonrelativistic)
- Experience in constructing self-similar solutions, demonstration of the role of the critical surfaces, developing criteria for the collimation of MHD outflows, the asymptotics of collimated and cronical solutions, the structural stability of MHD outflows and the efficiency of magnetic acceleration.
- Numerical simulations of time-dependent MHD winds/jets, demonstration of magnetic collimation & shock formation, acceleration of relativistic jets. Gamma ray bursts.
- Time-dependent radiative transfer. Spectrum formation from synchrotron, synchro self-Compton and external Compton processes. Particle acceleration in shock waves and coupling with radiation. Application to blazars and gamma-ray bursts.

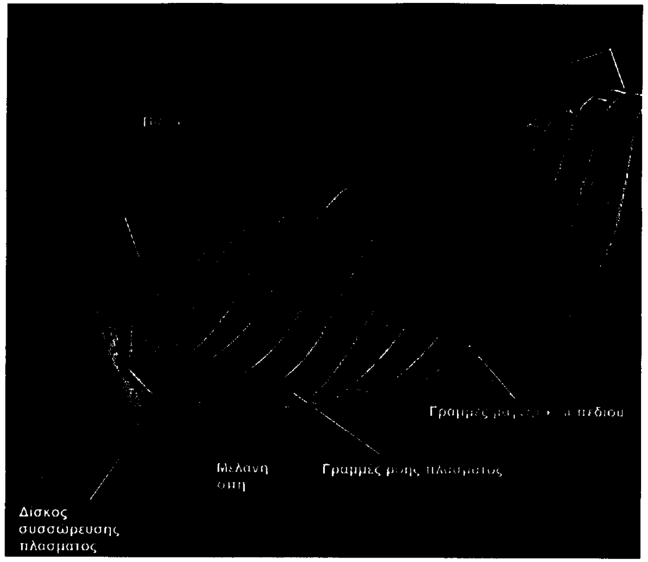

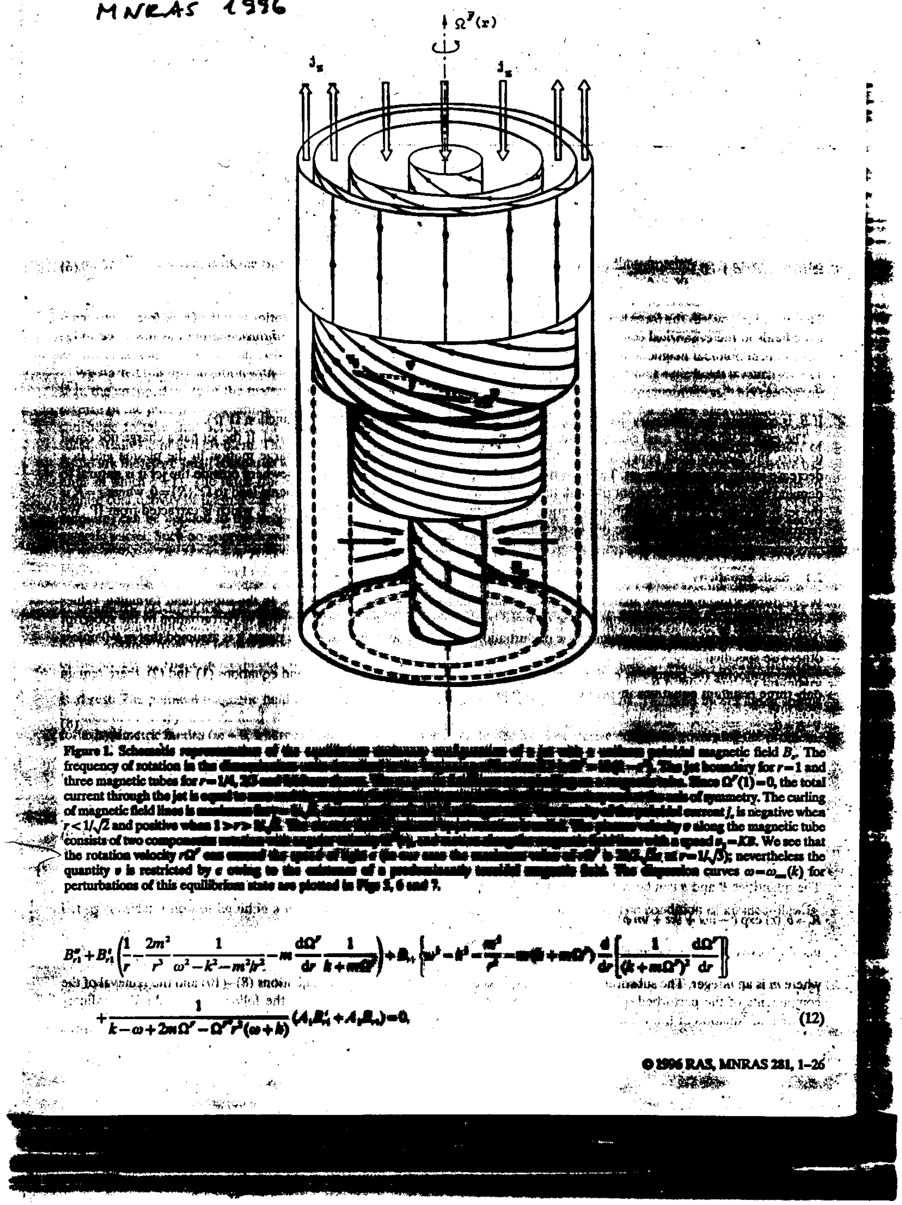

Figure 1. Schematic [illegible] magnetic field B_z. The frequency of rotation in the [illegible] jet boundary for $r=1$ and three magnetic tubes for $r=1/4$, [illegible] Since $\Omega'(1)=0$, the total current through the jet is [illegible] of symmetry. The curling of magnetic field lines is [illegible] current j_z is negative when $r<1/\sqrt{2}$ and positive when $1>r>$ [illegible] along the magnetic tube consists of two components [illegible] We see that the rotation velocity $r\Omega'$ can [illegible] at $r=1/\sqrt{3}$); nevertheless the quantity v is restricted by c owing to the existence of a [illegible] The dispersion curves $\omega=\omega_{m}(k)$ for perturbations of this equilibrium state are plotted in Figs 5, 6 and 7.

$$B''_{r1}+B'_{r1}\left(\frac{1}{r}-\frac{2m^2}{r^3}\frac{1}{\omega^2-k^2-m^2/r^2}-m\frac{d\Omega'}{dr}\frac{1}{k+m\Omega'}\right)+B_{r1}\left\{\omega^2-k^2-\frac{m^2}{r^2}-m(k+m\Omega')\frac{d}{dr}\left[\frac{1}{(k+m\Omega')^2}\frac{d\Omega'}{dr}\right]\right\}$$

$$+\frac{1}{k-\omega+2m\Omega'-\Omega'^2r^2(\omega+k)}(A_1B'_{r1}+A_2B_{r1})=0, \quad (12)$$

© 1996 RAS, MNRAS 281, 1–26

Gabuzda et al.
MNRAS 2001

- Possible observational test for presence of toroidal/helical jet B fields:

→ Faraday rotation gradients across the jets, due to variation in line of sight jet B field component

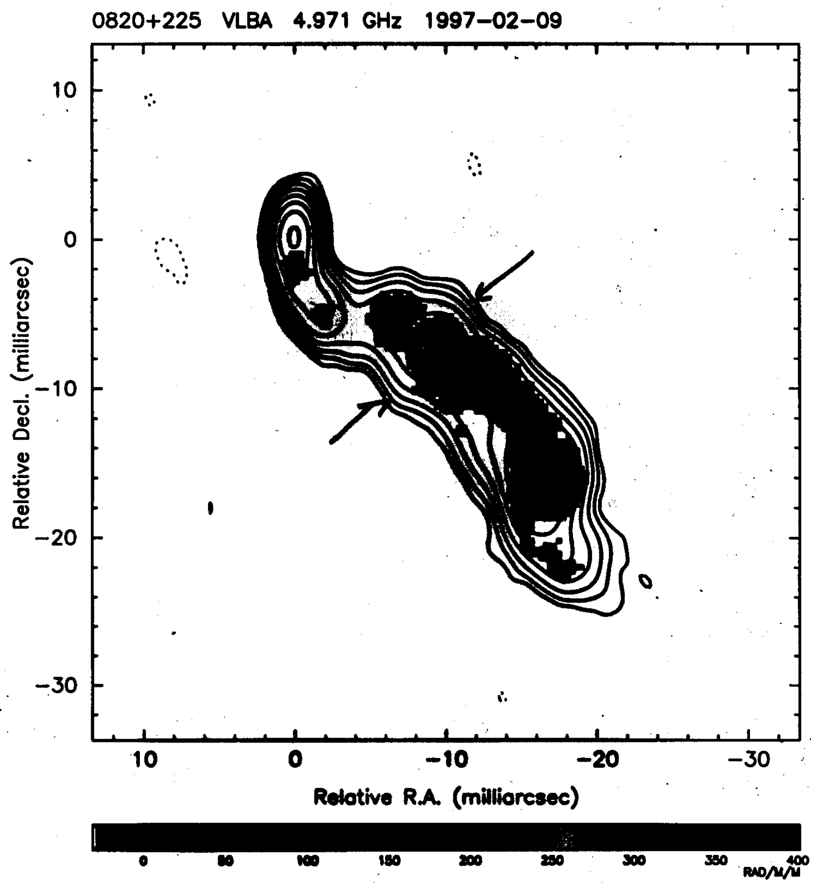

3C273

2002

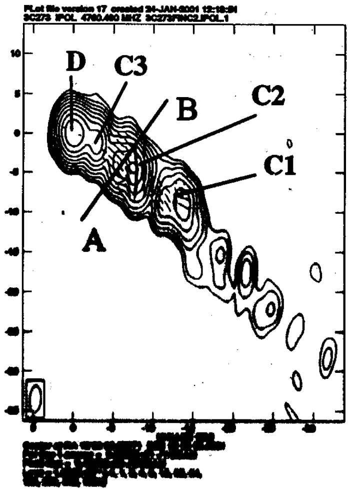

Fig. 3.

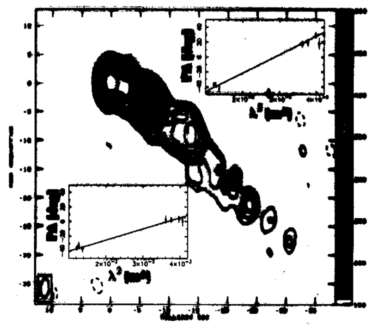

Fig. 8.

RM gradient across VLBI jet — interpreted as being due to helical field.

Gabuzda & Murray (2003)

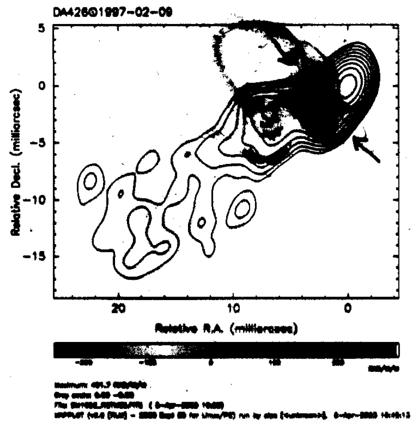

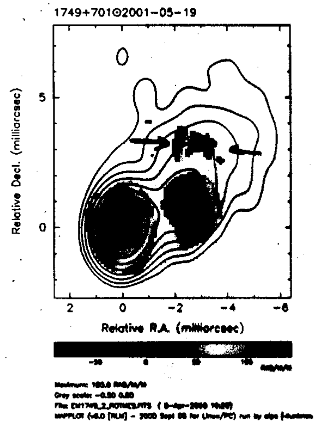

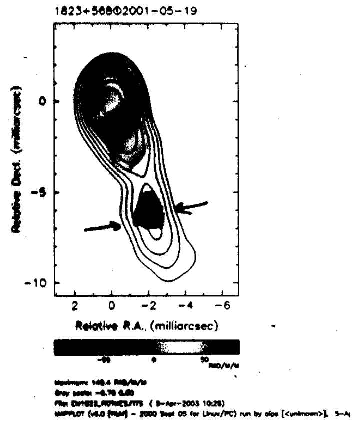

New VLBA observations targetted at searching for transverse Faraday rotation gradients just approved.

SUMMARY

- Roughly bimodal distribution of χ_{core} relative to direction of inner VLBI jet may be due to optical depths of VLBI cores (thin or thick)

- Bimodal distribution of $\chi_{opt} - \chi_{core}$ could be due to same effect:

  → $\chi_{opt} \parallel \chi_{core}$ radio core opt. thin

  → $\chi_{opt} \perp \chi_{core}$ radio core opt. thick

  → New simultaneous optical + multi-λ VLBI polarization data to test this idea to be reduced this summer by E. Rastorgueva

- One possible simple scenario (at least for BL Lac objects):

→ B field throughout most of jet is $\perp$ jet, beginning on scales within the observed radio cores

  → winding up of seed field by rotation of black hole + accretion disk

  → toroidal B field due to jet current

Chapter 5

Session IV: Radiation processes at high energies (L. Takalo)

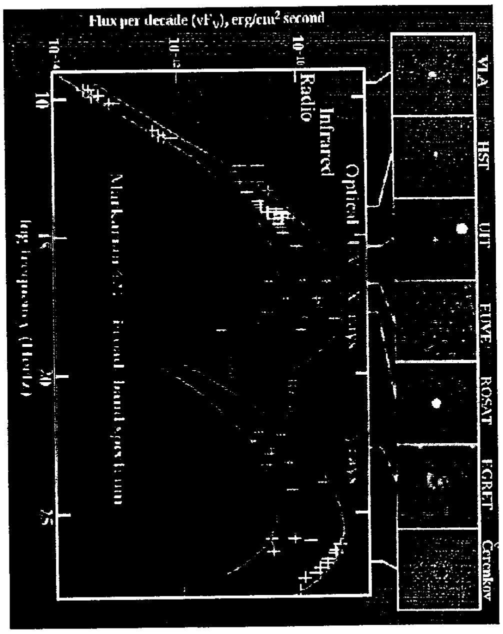

TASK 5

ARCHIVE
- objects
- Frequences

Campaigns
- long terms
- objects

- Intensive
- objects

Integaal 2004 ?
AGILE , GLAST

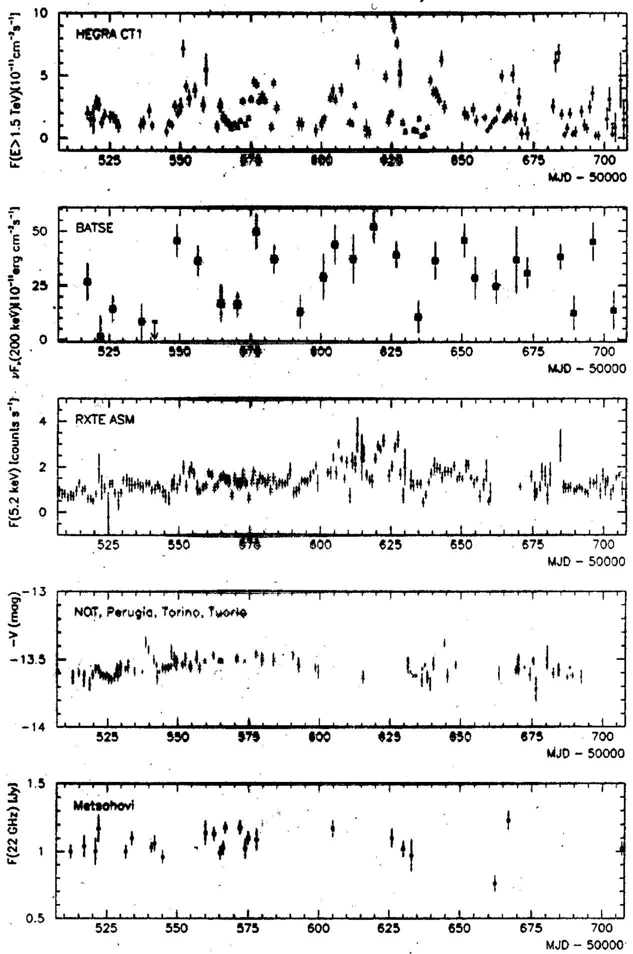

FIG. 1.—Light-curve data that were used in this paper to construct weekly spectral energy distributions. See § 2 for references.

5.1 A. Läheenmäki: Millimeter observations as a Tool for Studying Gamma-Ray Emission in Blazars

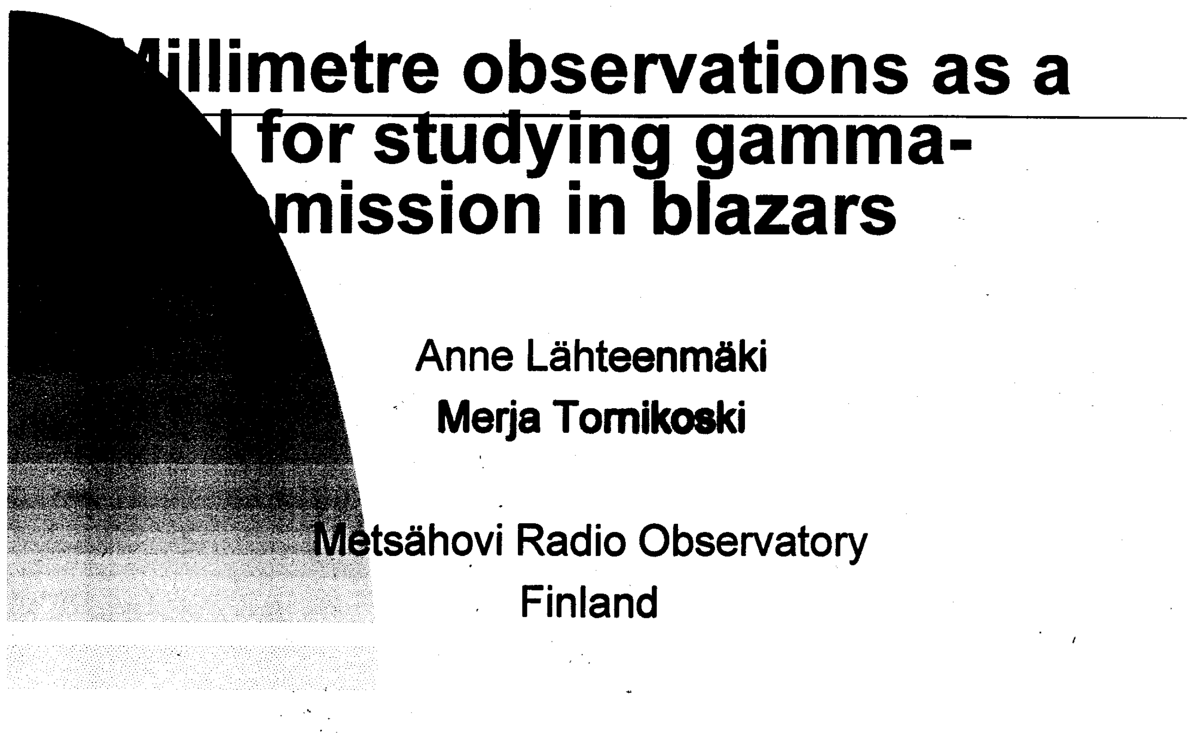

Testing of IC models for AGNs

- sähovi 22/37 GHz monitoring data & EGRET gamma-ray emission are correlated
- -quiet AGNs detected by EGRET —but dio-bright AGNs detected either
  - time variability, beaming effects ?
    - HPQs with rising high frequency radio flux
- SSC mechanism —in shocks far ~~downstream~~ of the accretion disk

Anne Lähteenmäki
Metsähovi Radio Observatory

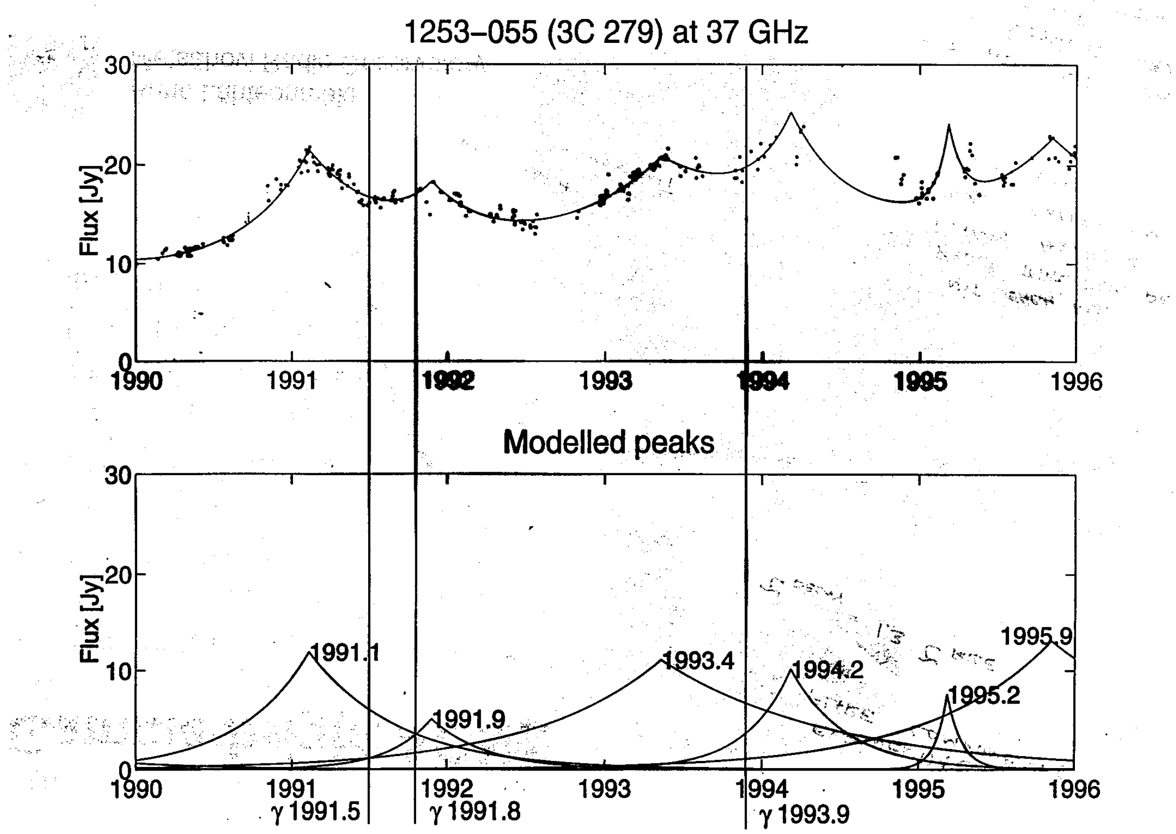

Average properties

rage observed gamma-ray flux is correlated:

ntz factor Γ (98.7 %)

ge radio flux S_{ave} (91.8 %)

probability depends on:

source type —preferably HPQs (>99%)

- blazars as a class are not strong gamma-ray emitters (HPQs yes, LPQs & BLOs no)

- $T_{b,var}$ (98.6%) and Γ (96.8%)
- maximum observed radio flux S_{max} (95.2 %)

Anne Lähteenmäki
Metsähovi Radio Observatory

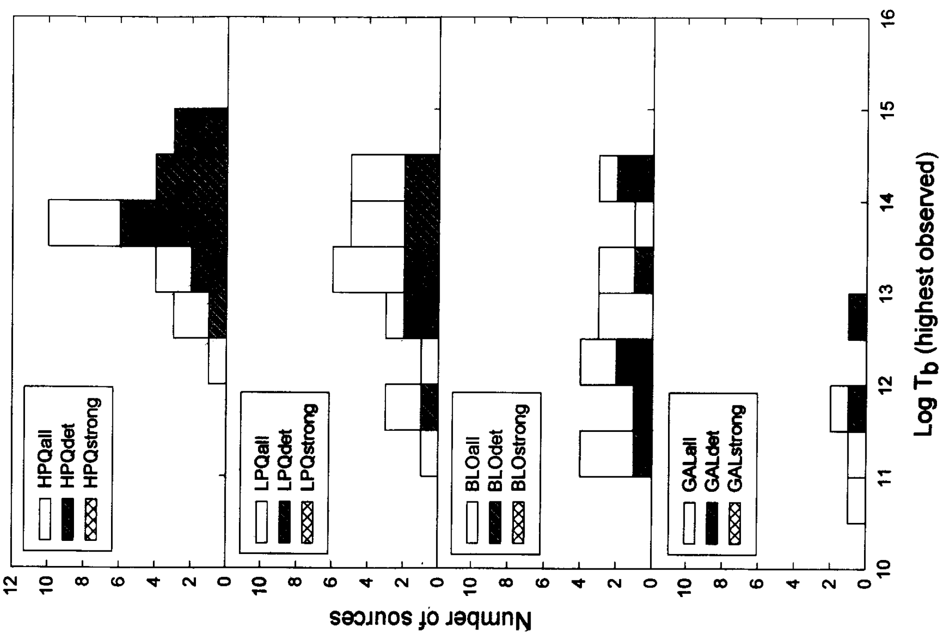

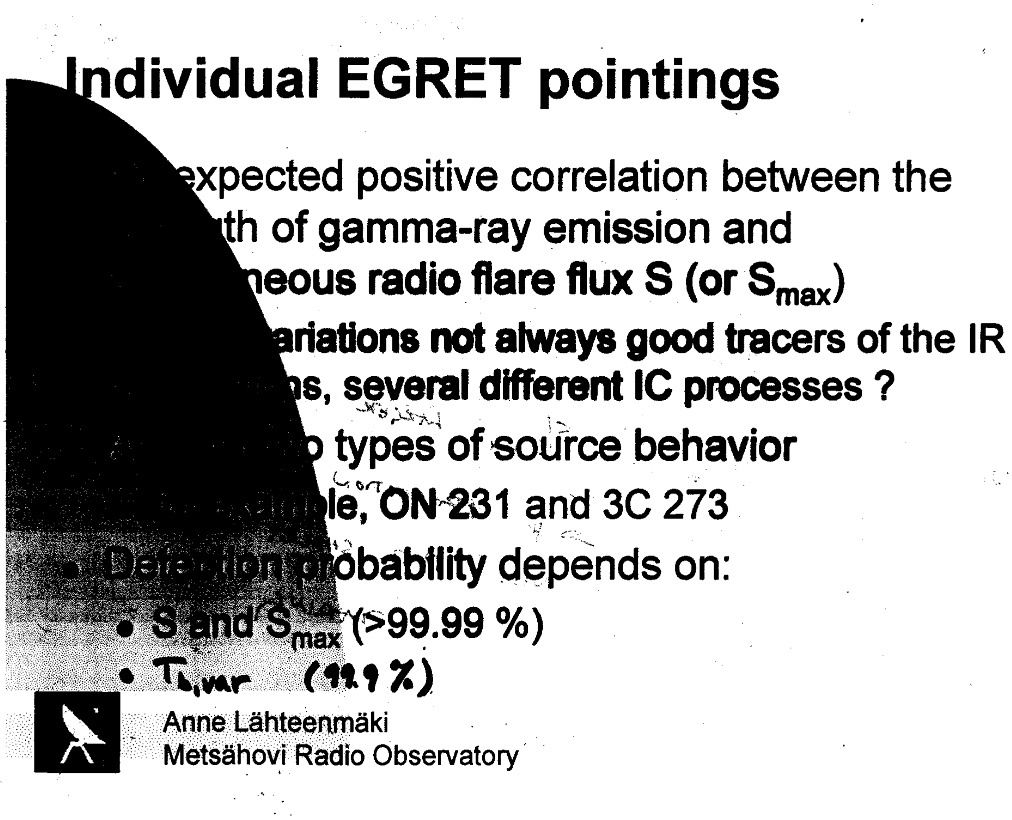
Individual EGRET pointings
xpected positive correlation between the
th of gamma-ray emission and
eous radio flare flux S (or S$_{max}$)
ariations not always good tracers of the IR
s, several different IC processes ?
types of source behavior
le, ON 231 and 3C 273
Detection probability depends on:
• S and S$_{max}$ (>99.99 %)
• T$_{b,var}$ (99.9 %)
Anne Lähteenmäki
Metsähovi Radio Observatory

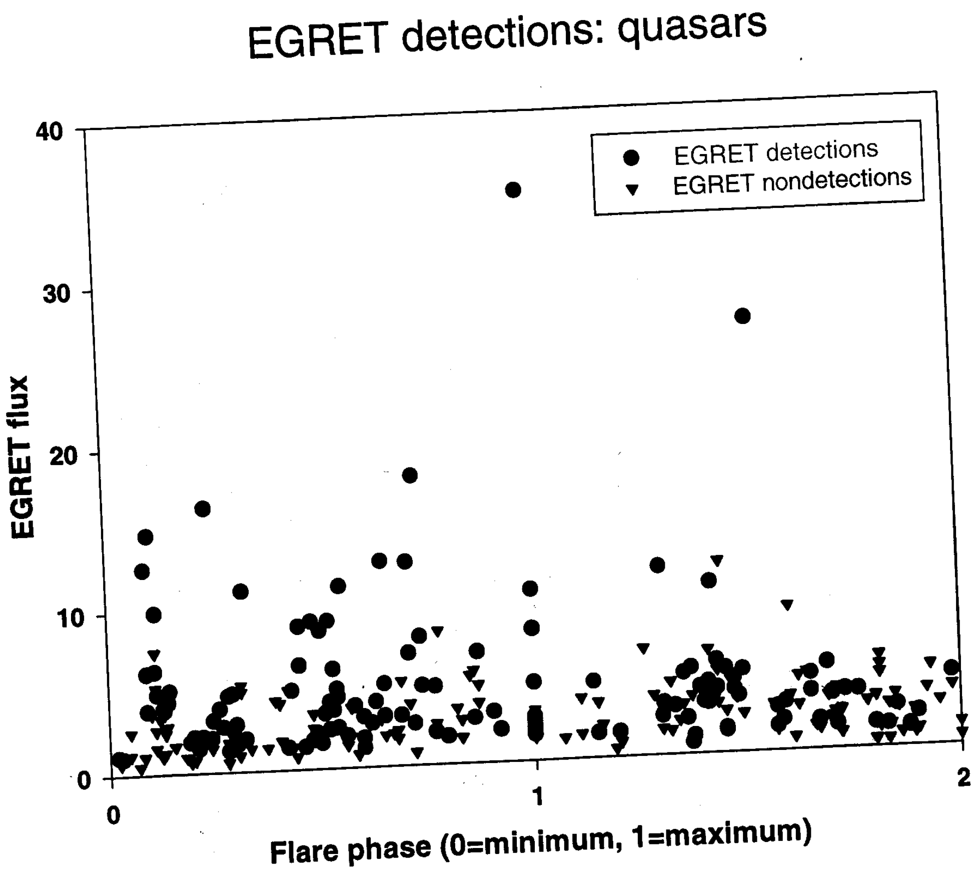
EGRET detections: quasars
EGRET detections
EGRET nondetections
EGRET flux
40
30
20
10
0
0
1
2
Flare phase (0=minimum, 1=maximum)

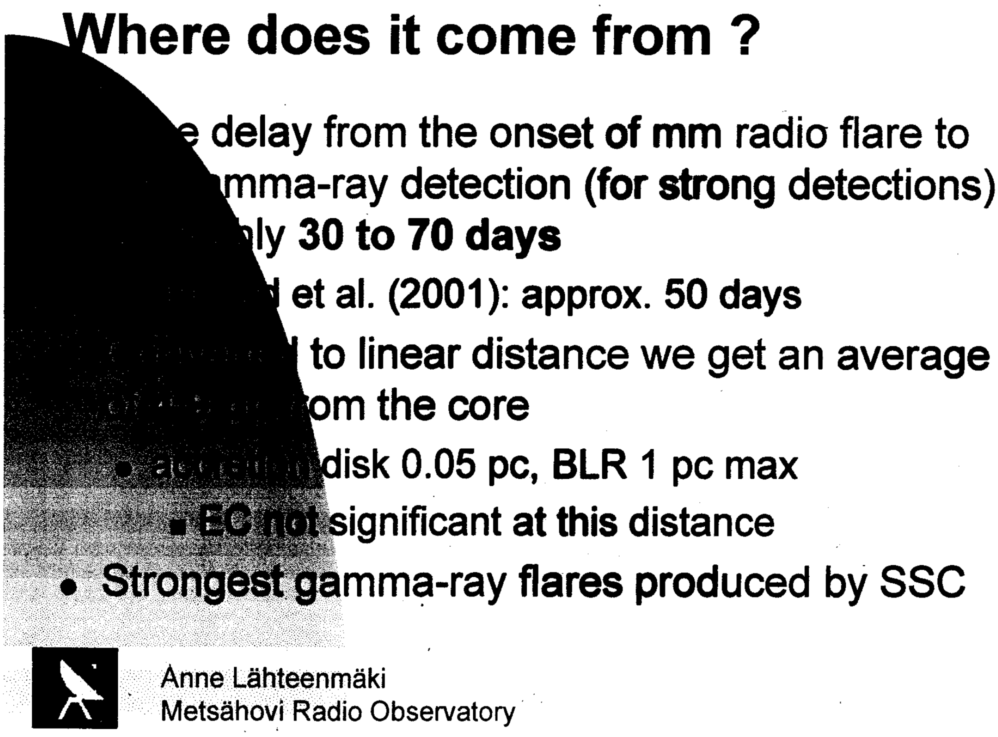
Where does it come from ?
e delay from the onset of mm radio flare to
mma-ray detection (for strong detections)
ly 30 to 70 days
et al. (2001): approx. 50 days
to linear distance we get an average
om the core
disk 0.05 pc, BLR 1 pc max
significant at this distance
Strongest gamma-ray flares produced by SSC
Anne Lähteenmäki
Metsähovi Radio Observatory

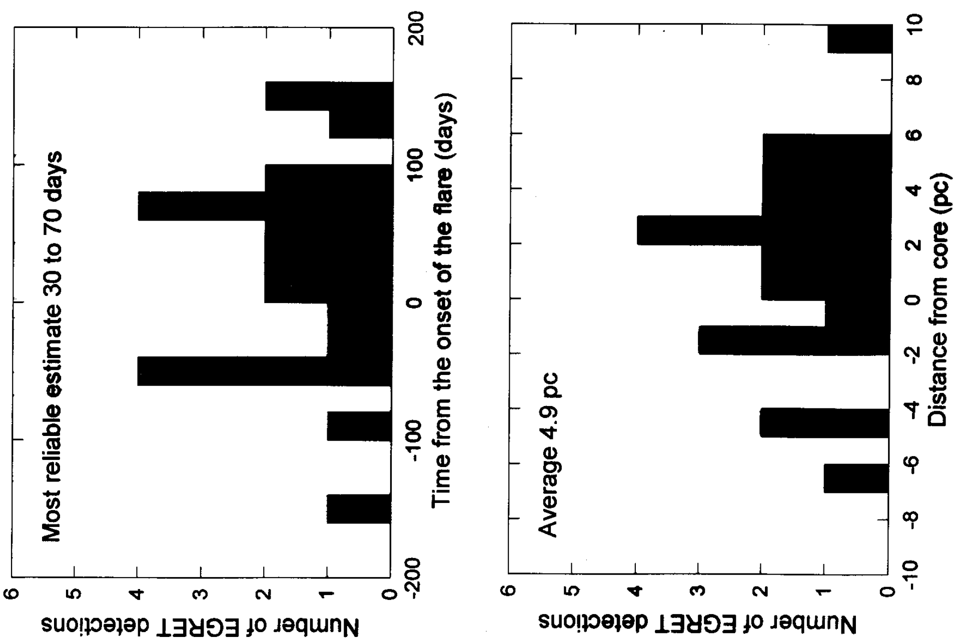
Most reliable estimate 30 to 70 days
Time from the onset of the flare (days)
Number of EGRET detections
Average 4.9 pc
Distance from core (pc)
Number of EGRET detections

Summary

- ...RET detection probability and the strength of ...a-ray emission depend on the ...eous radio state of the source
- ...uction of prominent gamma-ray flares is ... to shocks, about 5 pc from the AGN core ...)
- Mostly HPQs detected —BLOs are weak
  - SSC — EC ?
    - “baseline” weak gamma-ray emission etc ?

Anne Lähteenmäki
Metsähovi Radio Observatory

Why study gamma-ray sources ...radio wavelengths?

- ... 66 high-confidence AGN identifications ... practically all are bright and variable ...limeter-domain.
- ...creasing evidence that the activity ...r waves is linked to the gamma-ray activity.

Merja Tornikoski
Metsähovi Radio Observatory

The most probable AGN to be detected in gamma-rays is a source with...

An ongoing and still rising high-frequency radio flare.
An inverted/flat spectrum up to 100 GHz during the active state.

In order to be an EGRET-counterpart a source must be bright and variable in the mm-domain!

Merja Tornikoski
Metsähovi Radio Observatory

3EG lower-confidence identifications with Southern AGNs ("a" in 3EG)

	No!	Maybe?
[illegible]71	B0537–286	B0506–612
[illegible]77	B0539–057	B0521–365
[illegible]83	B1716–771	B1504–166
B1[illegible]–241	J1808–5011	
B1127–145		

Merja Tornikoski
Metsähovi Radio Observatory

Radio observations as a target-of-opportunity –tool for gamma

- ...bly ~100 GHz.
- ...g suitable gamma-ray source candidates:
  - Flat radio continuum spectrum up to ...0 GHz in the active state.
  - Bright in the active state.
- Triggering a ToO:
  - Beginning of the radio flare!

Merja Tornikoski
Metsähovi Radio Observatory

5.2 I. Papadakis: The complex X-ray variability behavior of Mkn421 as seen by XMM

The complex X-ray variability behaviour of Mkn 421
as seen by XMM-Newton

I. E. Papadakis
(Physics Department, University of Crete)

W. Brinkman, J.W.A den Herder, F Haberl
(MPE, SRON Utrecht, MPA)

INTRODUCTION

Blazars have long been known to exhibit rapid variability, high polarization, high luminosity and superluminal motion. These are thought to indicate that the readiation is produced in relativistic jets oriented close to the line-of-sight.

Spectral and flux variability observations can provide valuable information about the acceleration and cooling processes occuring in the inner jet. Although the true situation may be very complex, some limiting cases are easy to "predict". For example, if monoenergetic electrons are injected impulsively and evolve via radiative cooling, the electron spectrum will soften with time, so that softer photons will lag harder ones. Conversly, if the acceleration occurs on a time scale longer than the electron cooling time, the electron spectrum will harden with time and harder photons will lag softer ones.

Determining the value and direction of the lag would indicate which of the two regimes causes the spectral evolution, allowing a measure or upper limit of the cooling time to be derived.

The observational situation is currently in dispute. In the case of Mkn 421, Takahashi et al. (1996) found "soft" lags, in which the "soft" band (0.7-1.5 keV) lagged behind the hard (3-7 keV) in an ASCA observation of the source, Fossati et al. (2000) found the opposite, "hard" lags, in a Beppo Sax observation, and Takahashi et al. (2000) found both hard and soft lags in a very long ASCA observation.

Mkn 421 is the brightest BL Lac object at X-ray and UV wavelengths and it is the first extragalactic source discovered at TeV energies. It has been observed by all previous X-ray missions and always shows large amplitude, fast flux variations. XMM-Newton, with its excellent sensitivity in the 0.2 – 10 keV band, is ideal in order to resolve the intensity variations of the source on time scales as short as ~ 100 sec.

In this talk, I will present the results from a detailed variability analysis of archival XMM-Newton observations of MKN 421 that we have recently performed.

OBSERVATIONS

Mkn 421 was observed by XMM - Netwon 8 times during 5 orbits in the period between May 2000 - May 2002, as a calibration source.

EPIC-PN was in SW mode (5 times), LW mode (2 times) and Timing mode (once). Filter was thick in all cases but once. Exposure times were ~ 30-50 ksec.

We used PN data, XMMSAS version 5.3.3, response matrices released in April 2002, and disregarded central region pixels (to minimize the effects of pile up).

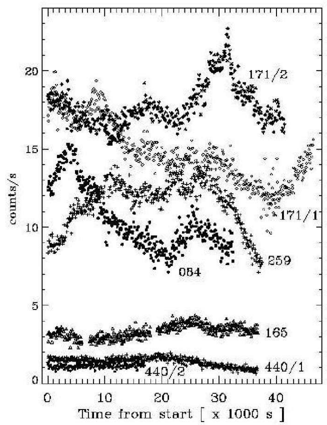

First, in order to study the observed variations, we used 80-sec binned, 0.2-0.8 keV (soft) and 2.4-10 keV (hard) band light curves, and simply divided them by their mean. We find that:

SBAND min_to_max variations < HBAND min_to_max variations
(~ 10% - 40/%) (~30% - 70%)

Then, we computed the "Hardness Ratio"
(HR=[0.2-0.8 keV]/[2.4-10 keV])
and plotted it as a function of the total band count rate (0.2-10keV) in order to study flux related spectral variations.

Based on the HR plots and well defined, large amplitude flux variations in the light curves, we divided the light curves into various sub-intervals/sub-parts.

We find that:

1) In almost all cases, as flux increases, the spectrum "flattens" (i.e. HR increases), while as flux decreases, the spectrum "softens" (i.e. HR decreases).

2) The spectrum hardens/softens at a rate which varies from observation to observation.

3) There is a strong indication that, as the flux increases, the spectral variability rate increases as well.

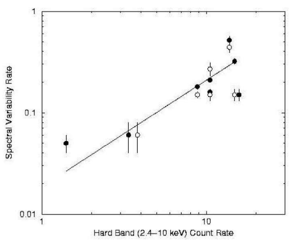

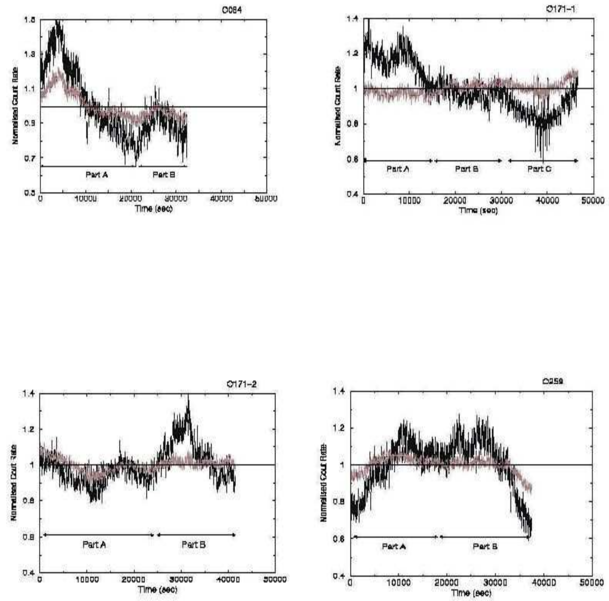

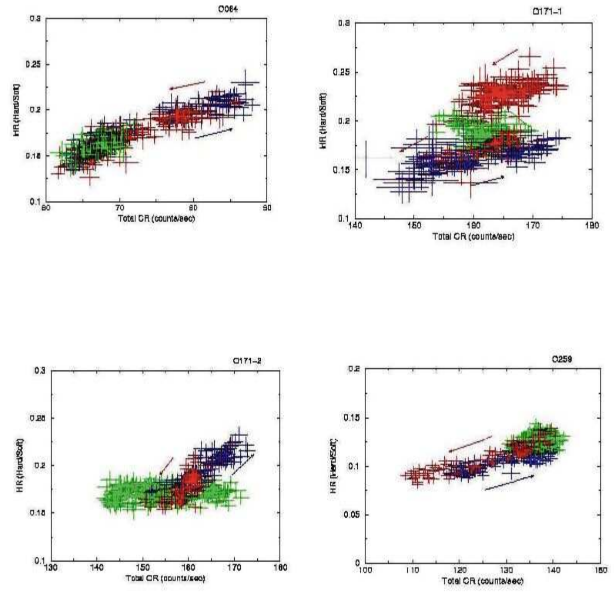

CROSS CORRELATION ANALYSIS

In order to investigate the cross-links between the soft and hard energy band variations, we computed the cross-correlation function between the soft and hard energy band light curves, using the full length light curves and the various sub parts that we have identified in each light curve.

The results are quite different in each case!

When we consider the results from the CCF analysis of the various sub-intervals of the light curves, we find that:

1) The variations in the two bands are well correlated in most cases.

2) We find that in many cases, the CCFs are asymmetric towards positive or negative lags.

3) In two cases we find significant positive lags (i.e. the soft band variations *lead* the hard band variations) and in 4 cases, we find significant negative lags (i.e. the hard band *leads* the soft band variations). The observed lags are very small, of the order of ~ 5 min.

4) In the cases where we do detect significant lags we also observe characteristic loop-like structures in the HR plots.

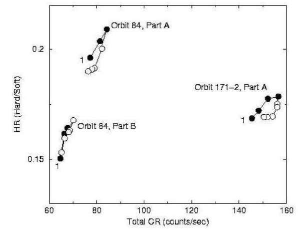

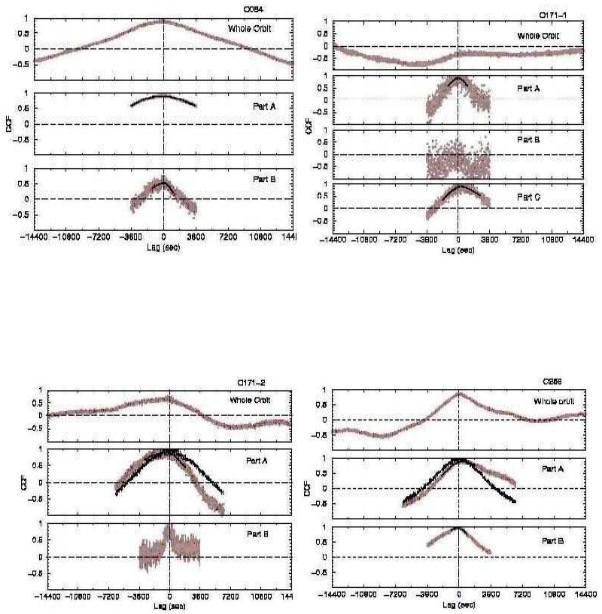

FUTURE WORK

Perform a detailed study of the energy spectrum of the source. Due to the current uncertainties associated with the EPIC PN response at lower energies, we could not study the energy spectrum of the source in detail. However, it is clear that:

The spectrum is very complex and cannot be fitted adequately by a broken power law or a continuously curved model.

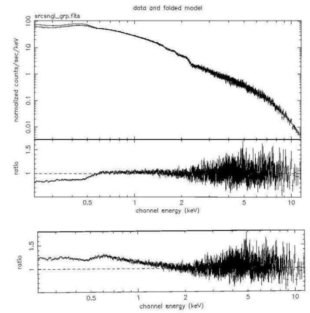

AND

Acquire more data! We have asked for a ~ 3.5 days, continuous observation with CHANDRA and XMM in order to resolve (??) the the observational situation with the interband lags in Mkn 421!

5.3 E. Körding: Radio/X-ray Correlation from XBRs to AGN

Radio/X-ray Correlation from XRBs to AGN

Max-Planck-Institut
für
Radioastronomie

Elmar Körding
with Heino Falcke

'Active Black Holes'

XRBs

- Mass: $5 - 20 M_{\odot}$
- Luminosities: $\approx 10^{38} \frac{erg}{sec}$
- Relativistic jets (low state)

AGN

- Mass: $10^{6} - 10^{10} M_{\odot}$
- Luminosities: $\approx 10^{46} \frac{erg}{sec}$
- Relativistic jets
- Flat Radio core

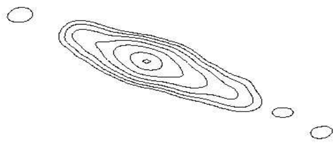

GRS1915 by Mirabel

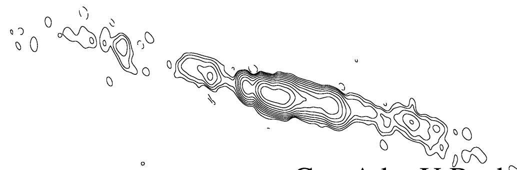

Cyg A by U.Bach

Similar Central Engine: Black Hole, Accretion Flow, Jet

Spectrum of XRB in the low/hard state

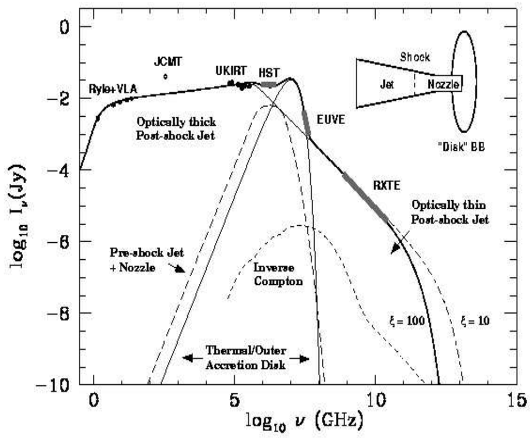

XTEJ1118+480

(Markoff, Falcke,Fender 2001)

Disk/Jet Models can be used to fit the spectrum

Coupled Disc Jet model:

- Disc:
  - Visible mainly in UV
  - Inner part: ADAF
  - Outer part: Standard thin disc
- Jet:
  - Synchrotron emission dominant for X-Rays and Radio

Jet dominated AGN

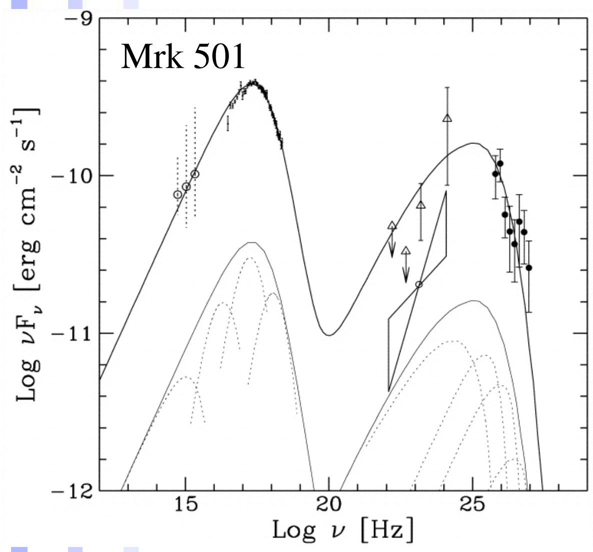

Maraschi et al. 99

- Sync. peak freq. varies
  - HBL/LBL
- To compare sources: Look at synchrotronpower law before cutoff!
- Objects:
  - BL Lac
  - FRI
  - Liner

Change of Accretion Rate

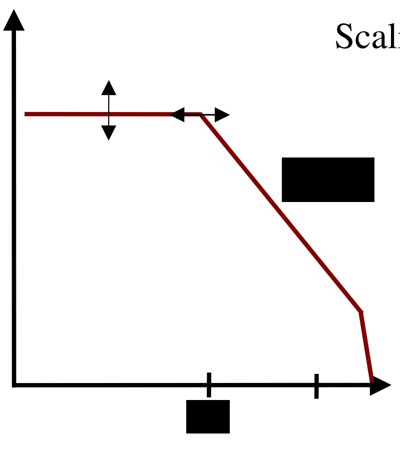

Scaling laws for jet predict (Falcke & Biermann 95):

[redacted]

and for the turnover frequency (SSA)

$$\nu_c \sim \dot{M}^{2/3}$$

For X-ray emission (if below cutoff)

$$S_{\mathrm{X-ray}} = S_{\mathrm{Radio}} \left(\frac{\nu_c}{\nu_X}\right)^{\alpha} \text{ with } \alpha \approx 0.6$$

$$S_{\mathrm{X-ray}} = S_{\mathrm{Radio}}^{m} \text{ Const}$$

with [redacted]

Radio - X-ray/Optical Correlation

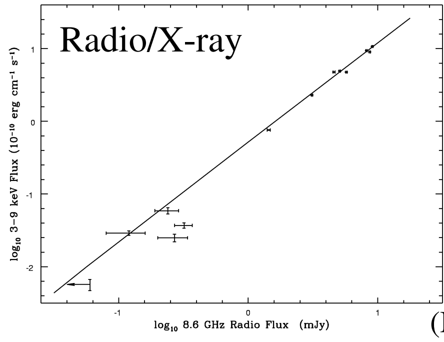

XRB in the low/hard state: GX339-4
Recently: Jet detected!
Different Epochs
The fit yields: 1.41

(Markoff, Nowak, et al 2002)

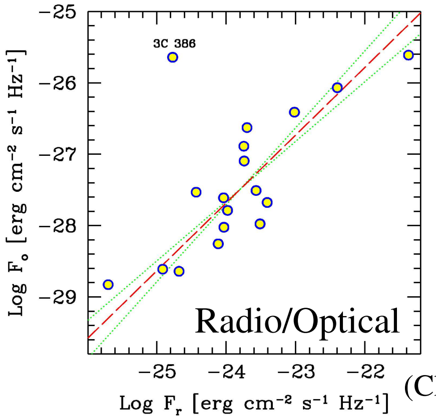

FRI Radio Galaxies
Radio-Optical Correlation
The fit is around 1, but correlation not so tight.

(Chiaberge 99)

Equivalent X-ray flux

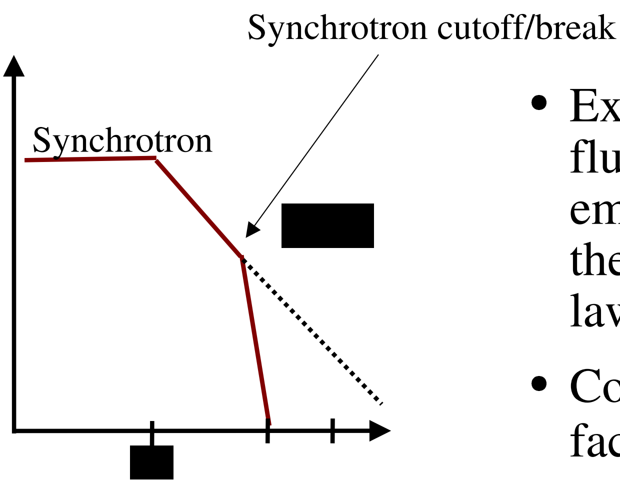

- Extrapolated X-ray flux, as if the X-ray emisson is created by the synchrotron power law.
- Correction for Doppler factor (only linear)

Observing frequencies: FRI,BL Lac : Optical
XRB, Liner : X-ray

Radio/X-ray correlation for AGN

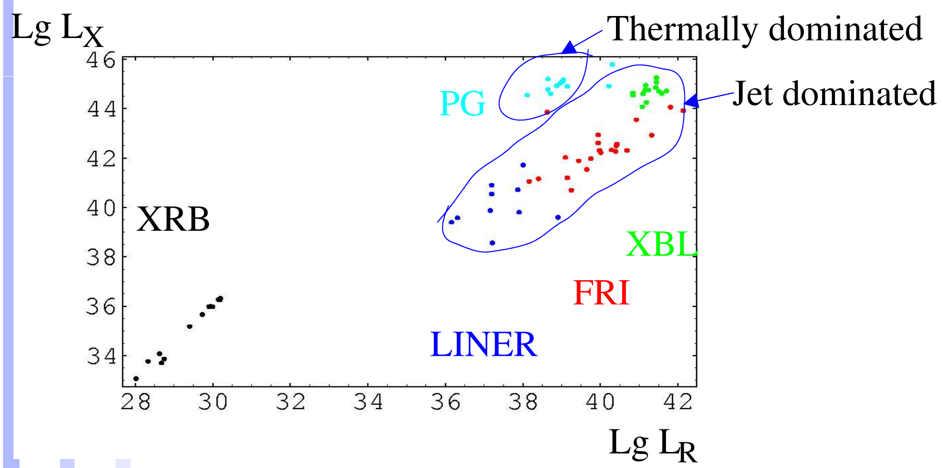

Black: GX339-4 (Corbel et al.)
Blue: Liner (Terashima & Wilson)
Red: FRI (Chiaberge et al.)
Green: BL Lac (Sambruna et al.)
Turquois: PG Quasars

- No continous correlation from XRB to AGN

Change of BH mass

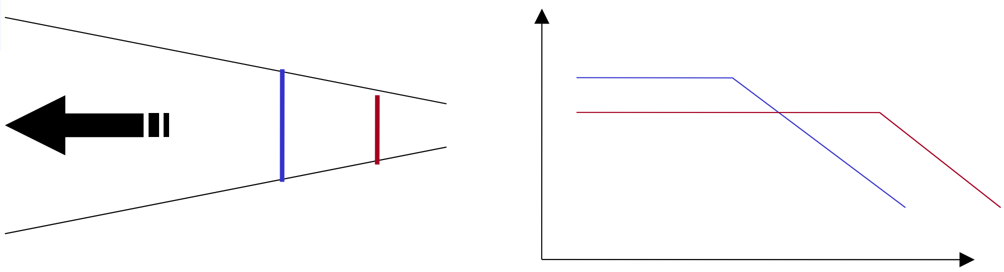

Assumption: Similar geometry for all black hole masses, particle acceleration always starts around 100 R_G

$$\nu_c \sim M^{-1} \Rightarrow S_{\mathrm{X-ray}} \sim S^{m}_{Radio} M^{-0.7}$$

Blazars: IR
XRBs: UV

Therefore:Scale X-ray Flux by M^0.7

Radio/Xray: XRB to AGN!

PRELIMINARY!

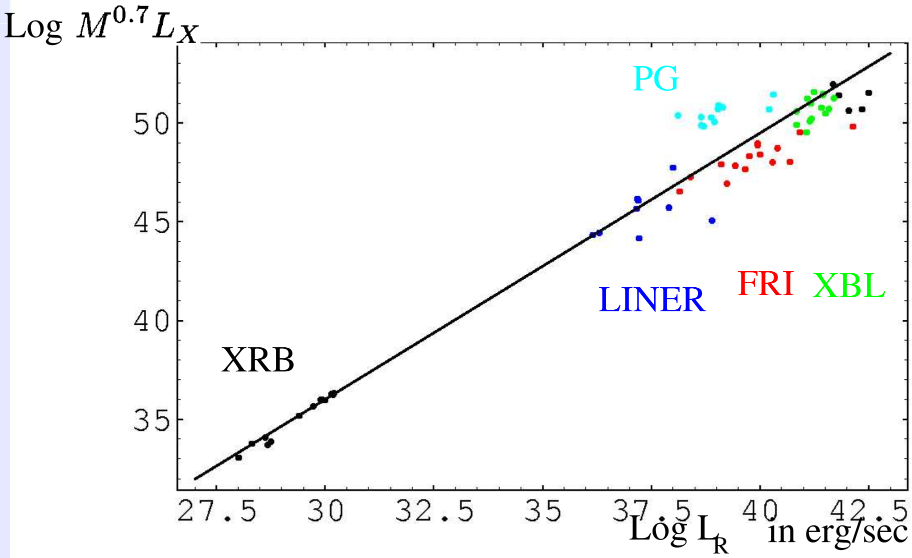

Correlation continues if mass-scaling is taken into account

Conclusions

- Non-thermally dominated AGN occupy a fundamental plane in a radio luminosity, equiv. X-ray lum. and mass parameter space.
- Radio/Equivalent X-ray correlation can be traced from XRBs to AGN
- Assumption that the acceleration region is at roughly 100 R_G seems to be reasonable
- Power-unification: XRB, LINER, FRI, BL Lacs can probably be unified if one takes jet power, mass and orientation into account.

5.4 A. Sillanpää: Status of MAGIC telescope

Status of MAGIC

MAGIC is the largest Cherenkov telescope and it operates in the energy range between 30 GeV–10TeV. This means that it will operate also in the “virginal” energy range 30 GeV–250 GeV.

If we just make a simple estimate using the observing area, energy range and sensitivity we expect to see altogether 923 sources in the sky!

first signals from stars seen 8.3.2003

part of the optics ready for real observations

camera is ready for real observations

we expect to make the first scientific observations in June 2003

5.5 A. Sillanpää: INTEGRAL Blazars

INTEGRAL BLAZARS

We are starting a new program with INTEGRAL:

- **Our main aim is to study all the blazars bright enough using all the main INTEGRAL instruments (OMC, IBIS, JEM-X) onboard INTEGRAL satellite when it is scanning the galactic equator ~every week (Core program). Every single integration is ~3000 seconds**
- **Only seven suitable blazars found with coordinates less than +- 13 degrees from the equator and optically brighter than 17^{m}**
- **The object list:**

BL Lac	**(Costamante&Ghisellini list)**
1ES 2344+514	**TeV-source**
8C 0149+710	
87GB 02109+5130	**(Cos&Ghi)**
4C 47.08	
1ES 0647+250	**(Cos&Ghi)**
PKS 0823-223	

- **Preliminary spectrum estimations show that 5 of these seven are visible with all the INTEGRAL instruments almost all the time and also the rest two objects part of the time**
- **All these seven objects are also in the MAGIC-object list and they are observed regularly**
- **We will get continuously overall spectrum info of seven blazars during the next 3-5 years (once per week from radio – TeV)**
- **Our program is getting also an “official” sub-topic status**

Chapter 6

Session V: Particle acceleration in MHD outflows (K. Tsinganos)

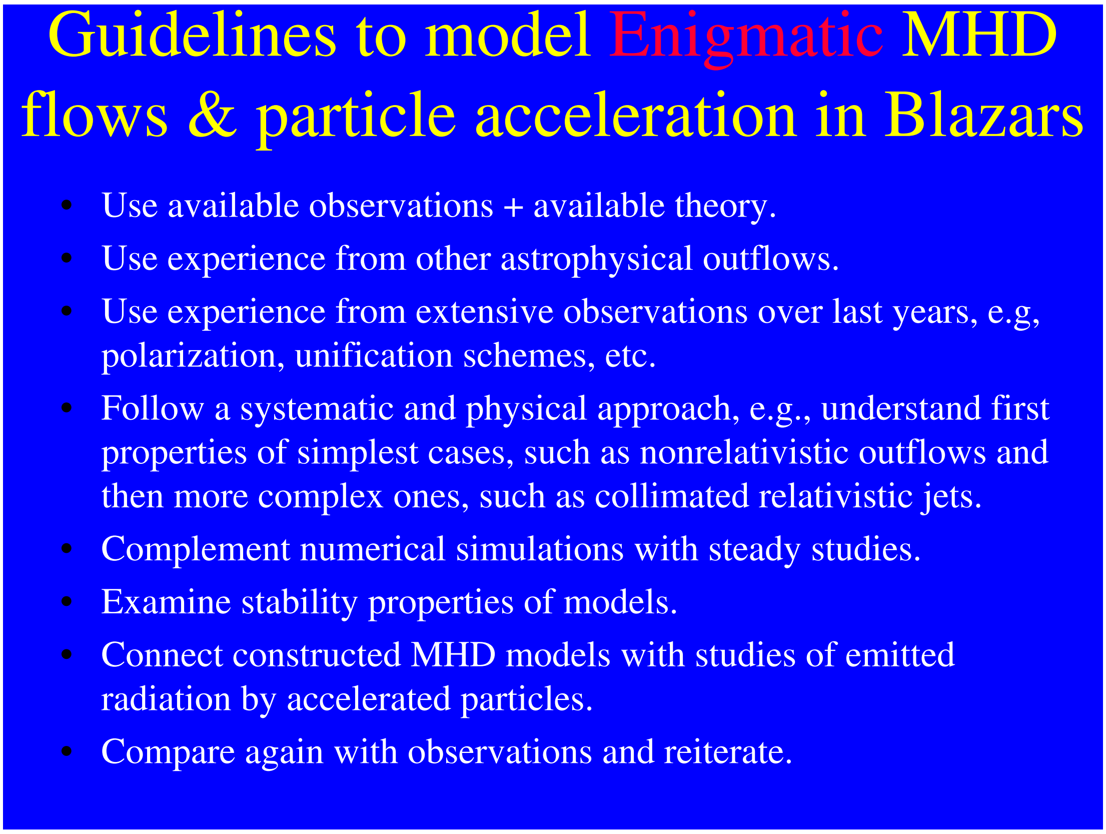

The following talks

- K.T: A flavor of MHD modelling of jets.
- Nek Vlahakis: Formation and kinematic properties of relativistic MHD jets.
- Apostolos Mastichiadis: Particle acceleration and radiation in Blazar jets.
- Gabriele Ghisellini...

Coffee Break

(a flavor of) MHD Modeling of Jets

Kanaris Tsinganos
Department of Physics, University of Athens and IASA, Greece

In collaboration with :
N. Vlahakis (Athens), C. Sauty (Meudon), E. Trussoni (Torino), S. Bogovalov (Moscow)

The Dichotomy of Winds and Jets

- Winds = no collimation
- Jets = tight collimation

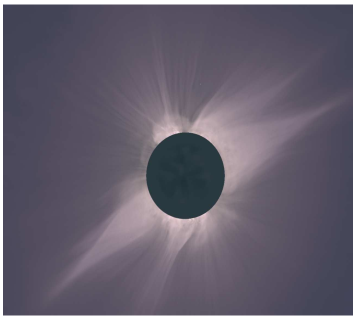

0. Solar Wind

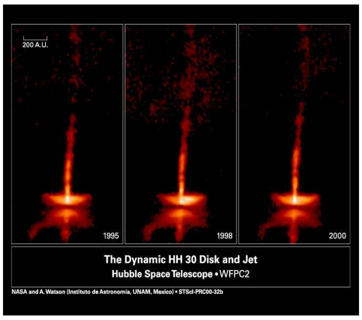

1. Star-birth

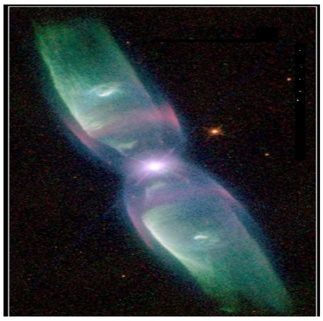

2. Star-death

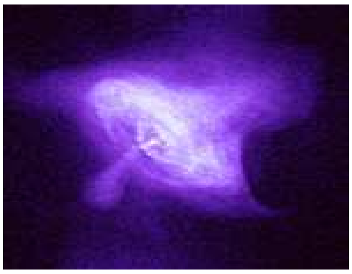

3. Pulsars

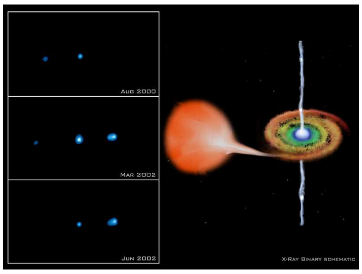

4. BHXR Transients

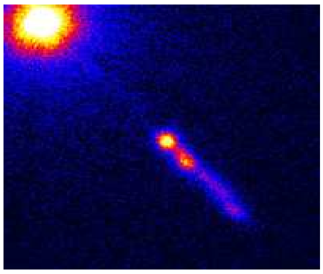

5. AGN

List of unsolved pbs for a theoretician

- Outflow source & acceleration: magnetocentrifugal acceleration
  (thermal or radiation pressure, waves) ?
- Outflow confinement: thermal pressure, or,
  magnetic hoop stress ?
- Outflow stability: hydrodynamic, or,
  hydromagnetic stability ?
- Outflow speed: nonrelativistic, or,
  relativistic ?
- Radiation: particle acceleration, shocks, etc, ?
- Outflow composition: electron-proton, or,
  electron-positron plasma ?

Jet source :

- Accretion disk
- Central object
- Accretion disk-central object interface

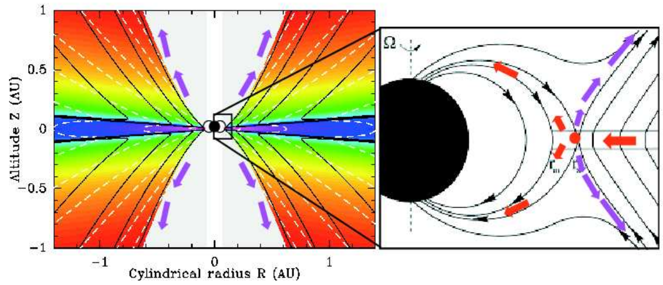

Disk-Winds, X-winds, Star-Winds (Shu, Ferreira, Sauty, et al)

Plasma acceleration :

- Pressure gradient driving (thermal, radiation, waves, etc)
- Magnetocentrifugal driving

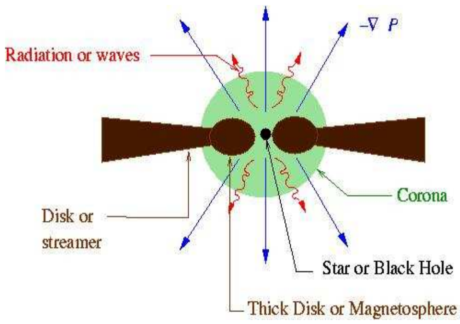

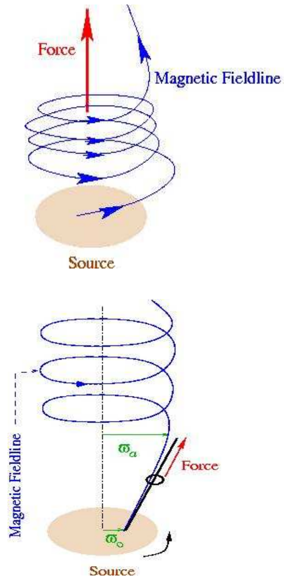

Plasma collimation :

- pressure gradient confinement (thermal, radiation, waves, etc)

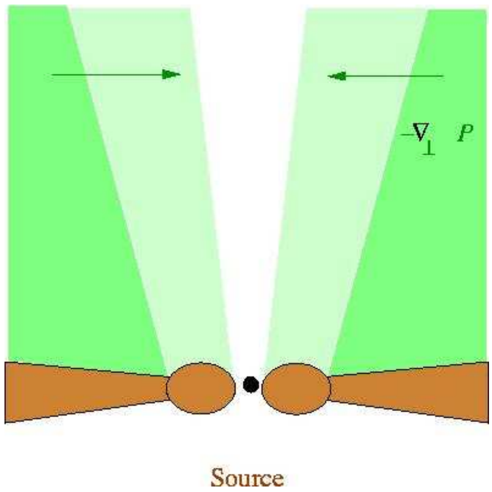

- magnetic confinement (magnetic hoop stress)

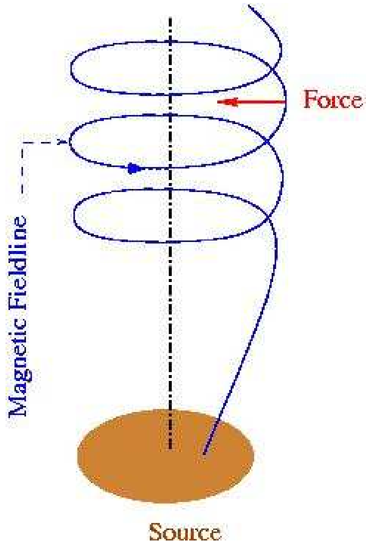

MHD modelling of cosmical outflows

- *I. Steady models*

Advantages:

- analytical treatment
- parametric study
- physical picture
- cheap method

Difficulties:

- Nonlinearity (MHD set !)
- 2-dimensionality (PDEs !)
- Causality (unknown critical surfaces !)

- *II. Time-dependent models*

Advantages:

- temporal evolution
- nonideal MHD effects

Difficulties:

- 3D MHD code (magnetic flux conservation !)
- large grid space (large lengths of jets !)
- correct boundary conds (boundary effects !)
- expensive method !

I. Time-independent (steady) studies: some general conclusions

(available analytical methods, problem of causality, a criterion for the formation of cylindrically collimated jets vs. conically expanding winds, classification of observed outflows from AGN in terms of efficiency of the magnetic rotator, distribution of electric current, etc.)

I. STEADY and AXISYMMETRIC MHD MODELS

Moving from 3D to 2D (the Poloidal Plane)

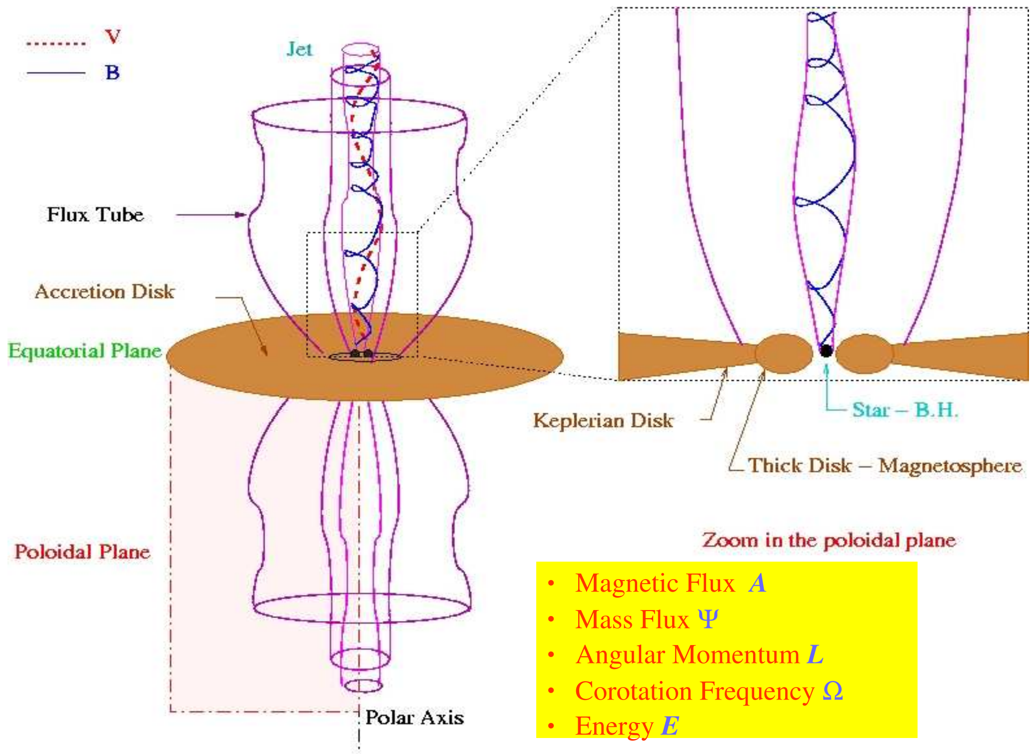

Two wide classes of exact MHD wind-type solutions:
MHD Mach numbers depend only on meridional angle, or, radius

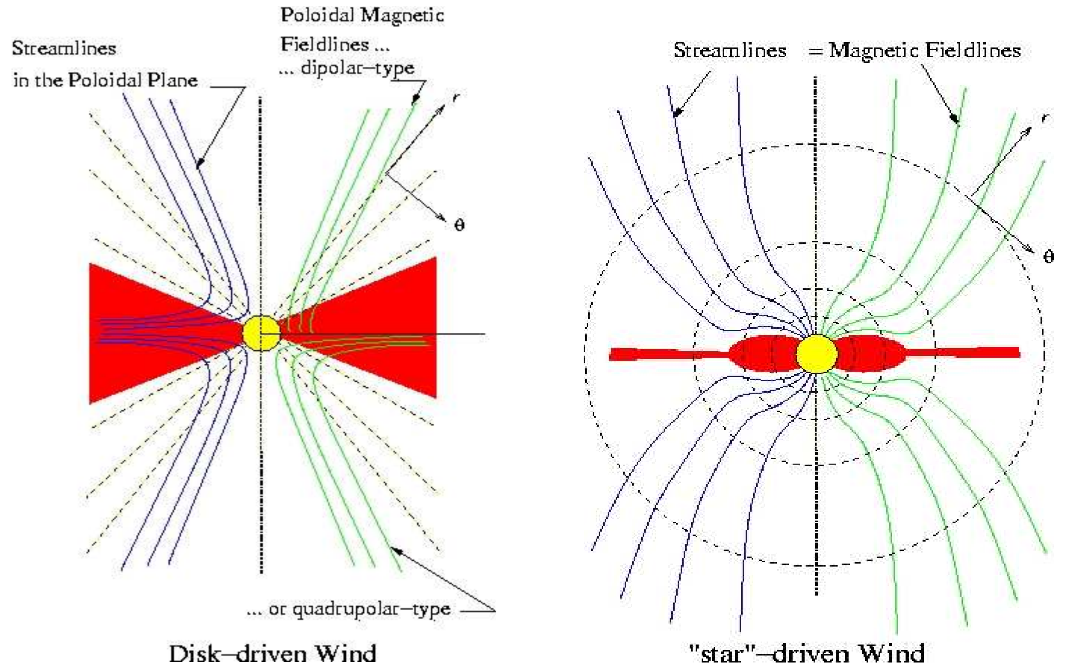

Prototype is Blandford & Payne (1982) model

Prototype is Sauty & Tsinganos (1994) model

The problem of causality:

The set of steady MHD equations are of mixed elliptic/hyperbolic character.
In hyperbolic regimes exist separatrices separating causally areas which cannot communicate with each other via an MHD signal. [They are the analog of the limiting cycles in Van der Pol's nonlinear differential equation, or, the event horizon in relativity.]

The MHD critical points appear on these separatrices which do not coincide in general with the fast/slow MHD surfaces. To construct a correct solution we need to know the limiting characteristics, but this requires an a priori knowledge of the solution we seek for !

Critical Surfaces in 1D

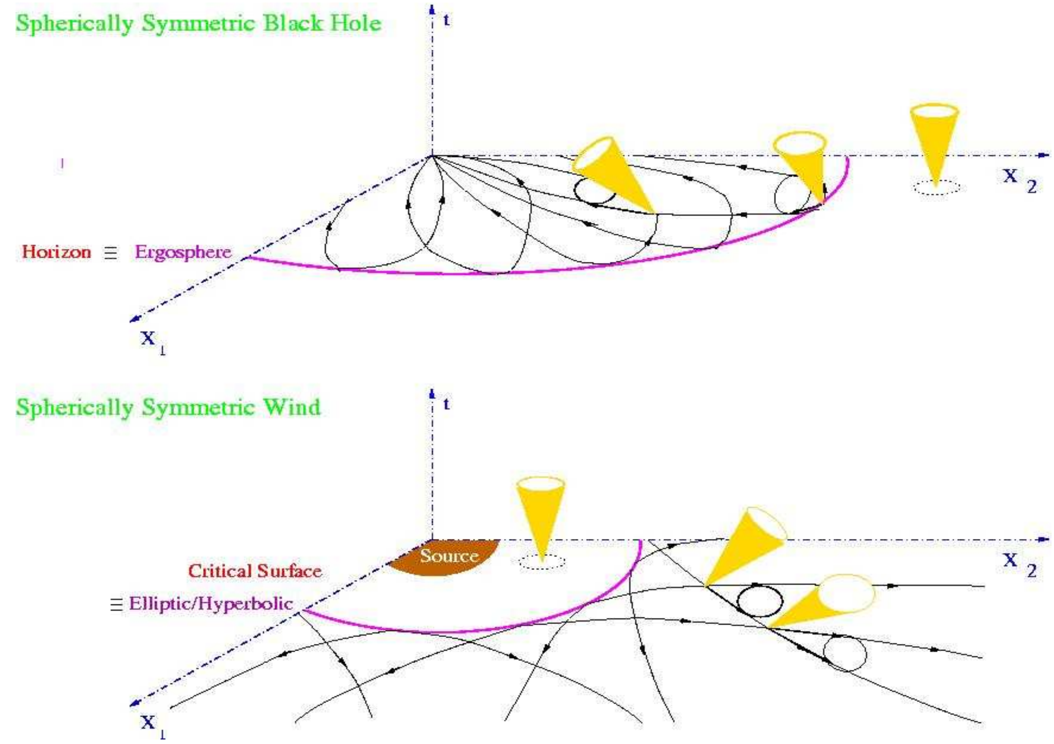

Critical Surfaces in 2D

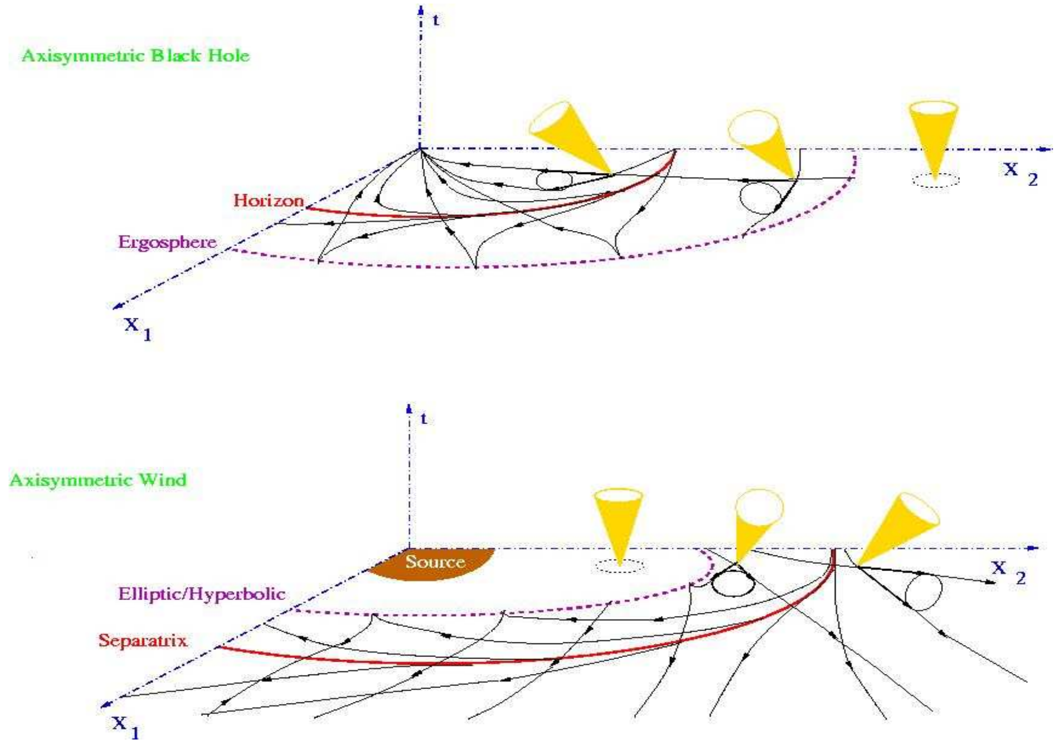

Example solutions of meridionally selfsimilar MHD outflows

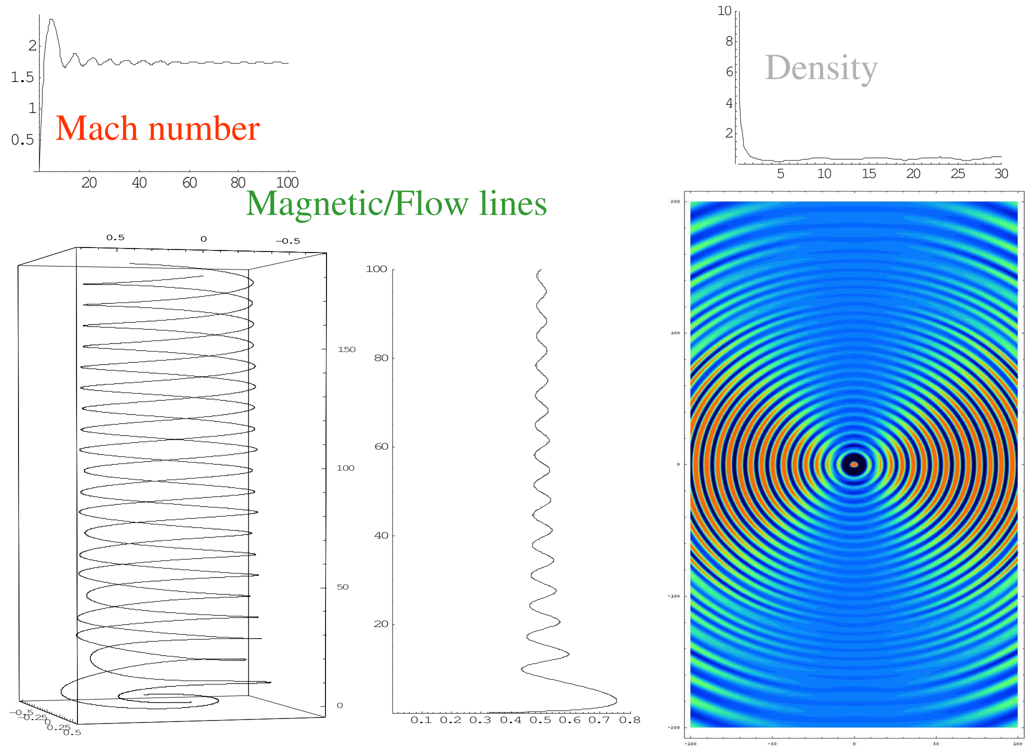

Balance of various MHD forces along and across the jet from base to infinity

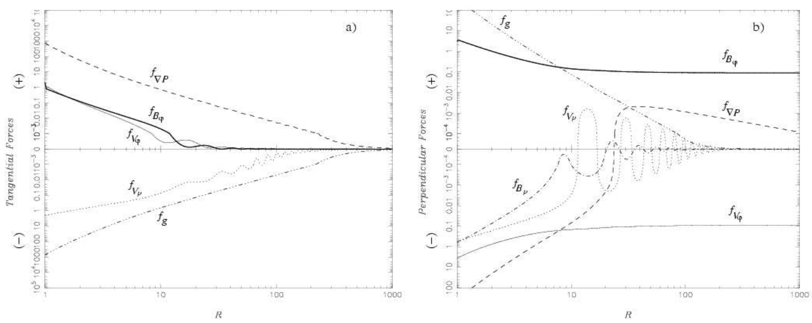

Families of solutions

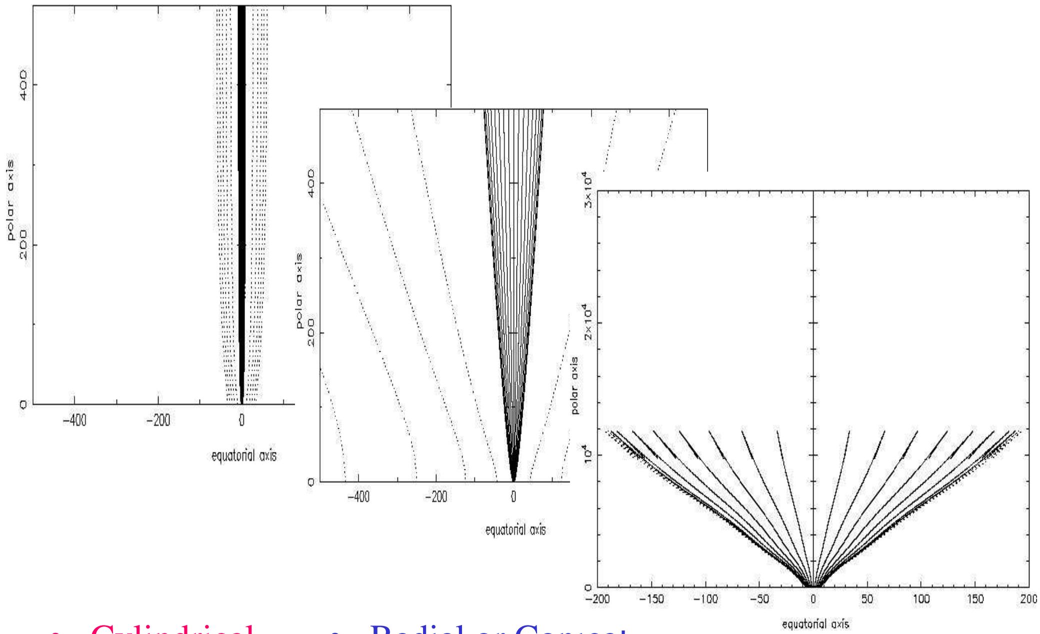

- Cylindrical (jets)
- Radial or Conical (Winds)
- Terminated (no steady solns)

An energetic criterion for cylindrical collimation:

$$\varepsilon' = \frac{\Delta(\ E)}{L\,\Omega}$$

$\Delta f = f$(non polar streamline) - f(polar axis)

- $\varepsilon' < 0$ --> No collimation
- $\varepsilon' > 0$ --> Collimation

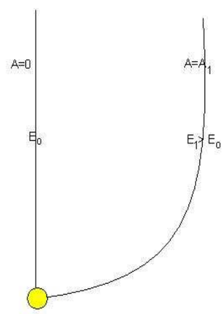

$\varepsilon' = \mu + \varepsilon$

Efficiency of Pressure Confinement

$$\mu \sim \frac{\Delta P}{P} =$$

Efficiency of the Magnetic Rotator

$$\varepsilon = \frac{L\,\Omega - E_{R,o} + \Delta E_G^{¿}}{L\,\Omega} \quad \text{where} \quad \Delta E_G^{¿} = -\frac{\mathbf{GM}}{r_0}\left(\frac{-\Delta T}{T_0}\right)$$

- $\varepsilon > 0$ --> Efficient Magnetic Rotator (EMR)

$\varepsilon < 0$ --> Inefficient Magnetic Rotator (IMR)

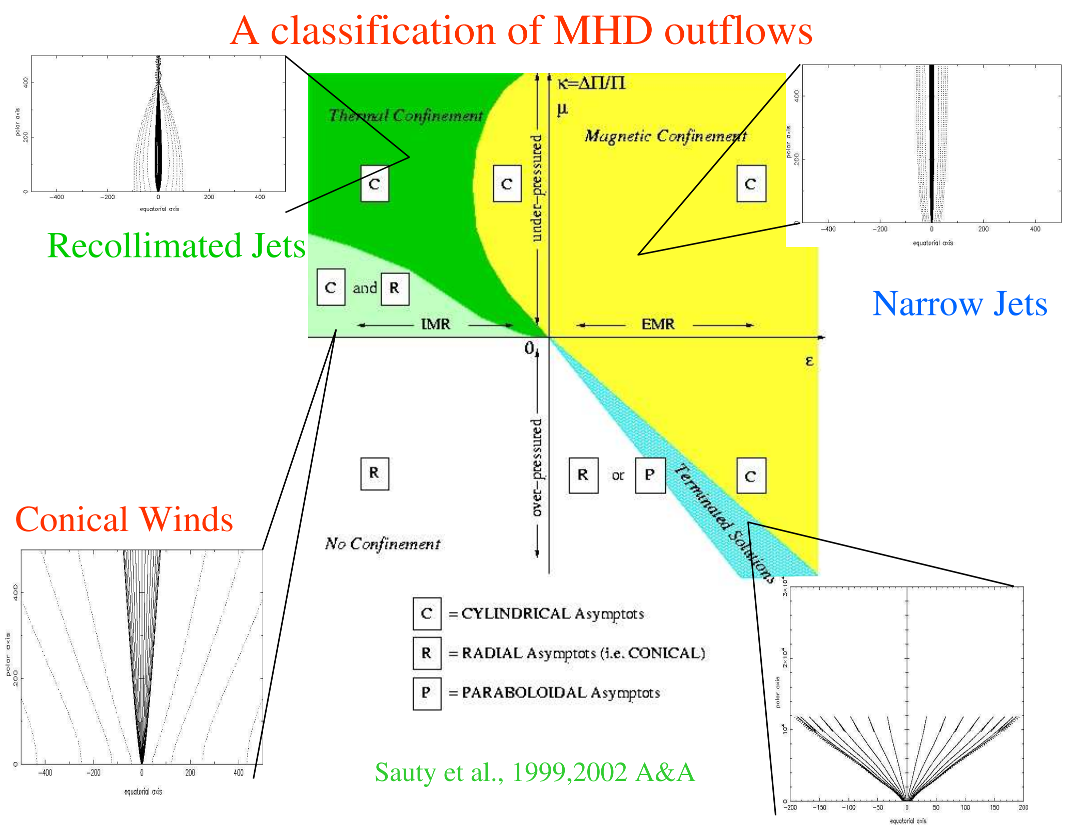

A classification of MHD outflows
Recollimated Jets
Thermal Confinement
Magnetic Confinement
Narrow Jets
C
and
R
IMR
EMR
κ=ΔΠ/Π
μ
under–pressured
over–pressured
ε
0
or
P
Terminated Solutions
No Confinement
Conical Winds
C = CYLINDRICAL Asymptots
R = RADIAL Asymptots (i.e. CONICAL)
P = PARABOLOIDAL Asymptots
Sauty et al., 1999,2002 A&A

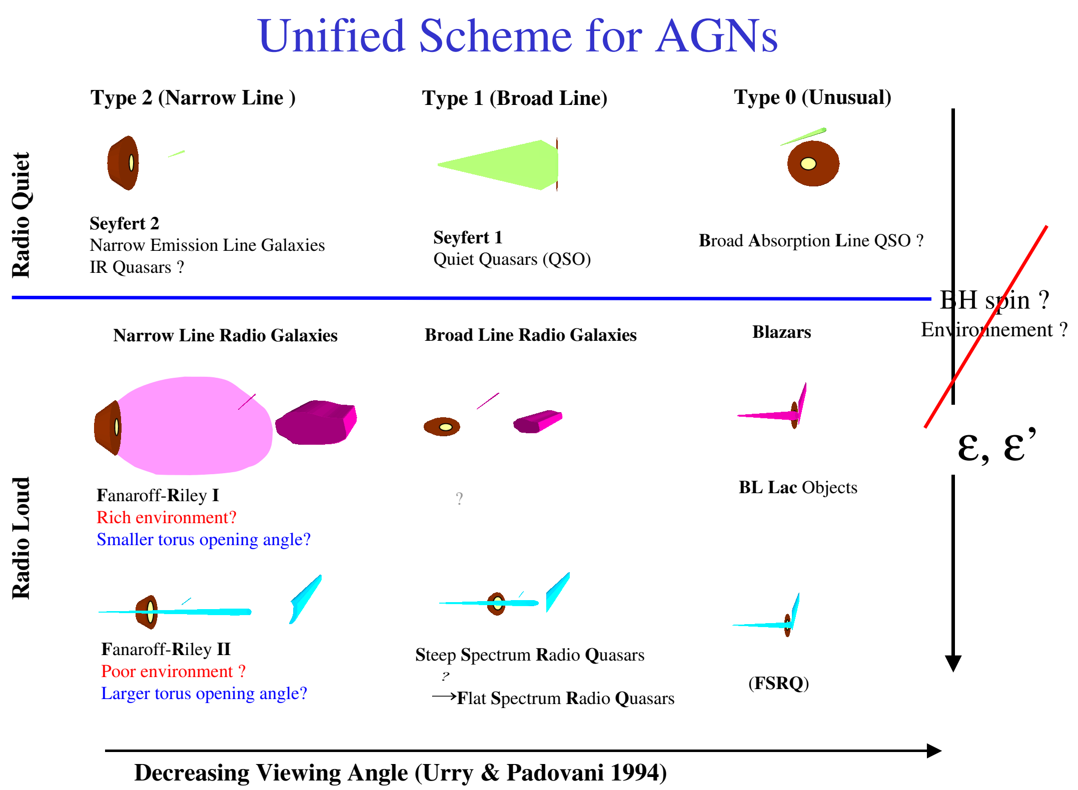

Unified Scheme for AGNs
Type 2 (Narrow Line)
Type 1 (Broad Line)
Type 0 (Unusual)
Radio Quiet
Seyfert 2
Narrow Emission Line Galaxies
IR Quasars ?
Seyfert 1
Quiet Quasars (QSO)
Broad Absorption Line QSO ?
BH spin ?
Environnement ?
Narrow Line Radio Galaxies
Broad Line Radio Galaxies
Blazars
Radio Loud
Fanaroff-Riley I
Rich environment?
Smaller torus opening angle?
?
BL Lac Objects
ε, ε'
Fanaroff-Riley II
Poor environment ?
Larger torus opening angle?
Steep Spectrum Radio Quasars
?
→Flat Spectrum Radio Quasars
(FSRQ)
Decreasing Viewing Angle (Urry & Padovani 1994)

Galactic Jets

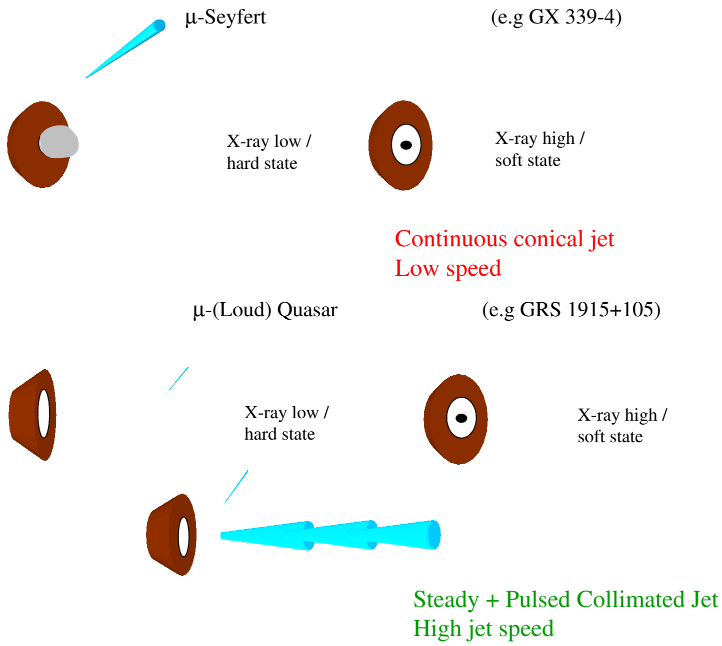

II. Time-dependent studies:

a movie showing the formation of a tightly collimated jet once a radial outflow along a radial (monopole) magnetic field, starts rotating.

But difficulty to collimate a relativistic outflow..

Weak collimation of Wind from a *Slow* Magnetic Rotator (the Sun) vs.
Strong collimation of Wind from a *Fast* Magnetic Rotator (a YSO)

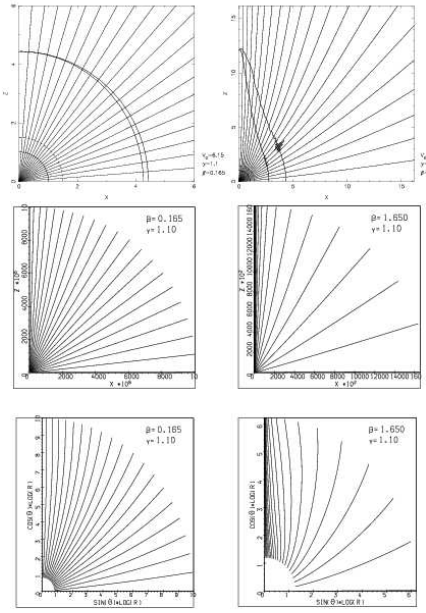

Very weak direct collimation of relativistic plasma

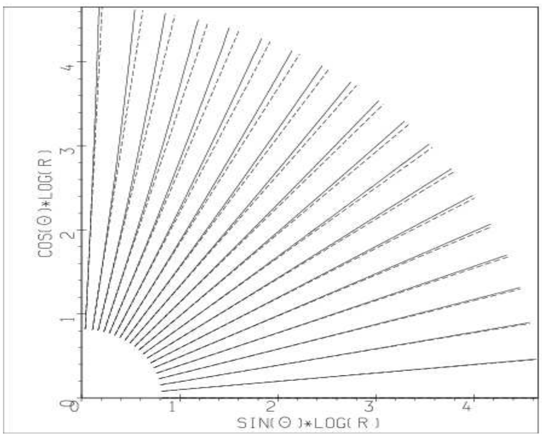

A two-compenent model for jets from a system of a central source+disk

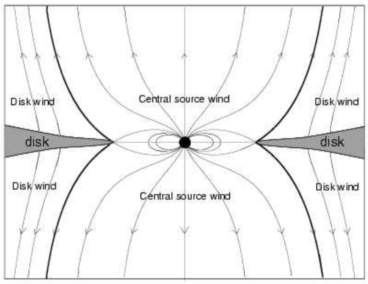

Recent numerical simulations and analytical models of magnetically collimated plasma outflows from a uniformly rotating central gravitating object and/or a Keplerian accretion disk have shown that relatively low mass and magnetic fluxes reside in the produced jet. Observations however indicate that in some cases, as in jets of YSO's, the collimated outflow carries higher fluxes than these simulations predict. A solution to this problem is proposed by the above model where jets with high mass flux originate in a central source which produces a noncollimated outflow provided that this source is surrounded by a rapidly rotating accretion disk. The relatively faster rotating disk produces a collimated wind which then forces all the enclosed outflow from the central source to be collimated too. This conclusion is confirmed by self-consistent numerical solutions of the full set of the MHD equations.

Shock formation in a 2-component outflow by a rotating disk-wind

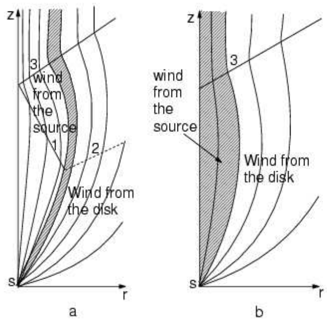

In panel (a) a sketch of the shock waves and singular surfaces which are expected to be formed in the general case of a two-component outflow is presented. The oblique shock front marked by '1' is formed at the collision of the two parts of the collimated and still uncollimated flows. An outgoing weak discontimuity from the one end of this shock is marked by '2'. The shock front marked by '3' is formed at the self reflection of the collimated flow at the axis of rotation. Under special conditions this collision shock may not be formed. In this case, the structure a shock as the one shown in panel (b) is expected

Collaboration ?

- MHD model polarization in Blazars
- MHD model particle acceleration & radiation
- MHD model jet confinement (thermal vs. B)
- MHD model efficiency of E-transformation
- etc….

Available positions

- 1 ENIGMA post-doc available Nov. 2003

and

- two, one-year each, post-doc positions,

or,

two, one year each, pre-doc positions

available now.

6.1 N. Vlahakis: Formation and kinematic properties of relativistic MHD jets

Formation and Kinematic Properties of Relativistic MHD Jets

Nektarios Vlahakis

Outline

- ideal MHD in general
- semianalytical modeling
  - r-self similarity
    - AGN outflows
    - GRB outflows
  - z-self similarity
    - Crab-like pulsar winds
- summary – meet the observations

Ideal Magneto-Hydro-Dynamics

- How the jet is collimated and accelerated? Need to examine outflows taking into account
  - matter: velocity $\mathbf{V}$, rest density ρ_0, pressure P, specific enthalpy ξc^2
  - electromagnetic field: $\mathbf{E}\,,\mathbf{B}$
- ideal MHD equations:
  - Maxwell: $\nabla\cdot\mathbf{B}=0=\nabla\times\mathbf{E}+\dfrac{\partial\mathbf{B}}{c\partial t}\,,\ \nabla\times\mathbf{B}=\dfrac{\partial\mathbf{E}}{c\partial t}+\dfrac{4\pi}{c}\mathbf{J}\,,\ \nabla\cdot\mathbf{E}=\dfrac{4\pi}{c}J^0$
  - Ohm: $\mathbf{E}+\dfrac{\mathbf{V}}{c}\times\mathbf{B}=0$
  - mass conservation: $\dfrac{\partial(\gamma\rho_0)}{\partial t}+\nabla\cdot(\gamma\rho_0\mathbf{V})=0$
  - specific entropy conservation: $\left(\dfrac{\partial}{\partial t}+\mathbf{V}\cdot\nabla\right)\left(\dfrac{P}{\rho_0^\Gamma}\right)=0$
  - momentum: $\gamma\rho_0\left(\dfrac{\partial}{\partial t}+\mathbf{V}\cdot\nabla\right)(\xi\gamma\mathbf{V})=-\nabla P+\dfrac{J^0\mathbf{E}+\mathbf{J}\times\mathbf{B}}{c}$

Integration

- assume
  - axisymmetry $(\partial/\partial\phi = 0\,,\ E_\phi = 0)$
  - steady state $(\partial/\partial t = 0)$
- introduce the magnetic flux function A
  ($A = const$ is a poloidal field-streamline)
- the full set of ideal MHD equations can be partially integrated to yield five fieldline constants:
  ① the mass-to-magnetic flux ratio (continuity equation)
  ② the field angular velocity (Faraday + Ohm)
  ③ the specific angular momentum ($\hat{\phi}$ component of momentum equation)
  ④ the total energy-to-mass flux ratio (momentum equation along $\mathbf{V}$)
  ⑤ the adiabat (entropy equation)
- two integrals remain to be performed, involving the Bernoulli and transfield force-balance
- boundary conditions?

r self-similarity

If the boundary conditions on the conical disk surface $\theta = \theta_i$ are power laws:

$B_r = -\mathcal{C}_1 r^{F-2}\,,\ B_\phi = -\mathcal{C}_2 r^{F-2}\,,$
$V_r/c = \mathcal{C}_3\,,\ V_\theta/c = -\mathcal{C}_4\,,\ V_\phi/c = \mathcal{C}_5\,,$
$\rho_0 = \mathcal{C}_6 r^{2(F-2)}\,,\ P = \mathcal{C}_7 r^{2(F-2)}\,,$

then the variables $r\,,\theta$ are separable and the system reduces to ODEs.
The solution should cross the Alfvén and the modified fast singular points.
[Blandford & Payne – (nonrelativistic)
Li, Chiueh, & Begelman (1992) and Contopoulos (1994) – (cold)
Vlahakis & Königl (2003, astro-ph/0303482,0303483) – (including thermal/radiation effects)]

F (the only parameter of the model) controls the current distribution:
$I \propto \varpi B_\phi \propto r^{F-1}$

- $F > 1$: current-carrying jet (near the rotation axis)
- $F < 1$: return-current (possibly at large ϖ)

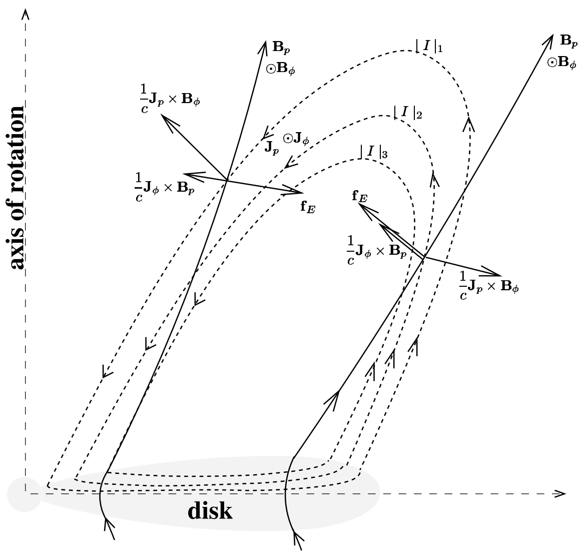

AGN outflows (Vlahakis & Königl in preparation) (modeling the sub-pc-scale jet in NGC 6251)

VLBI measurements show sub-pc scale acceleration of the radio-jet in NGC 6251, from $V(r = 0.53\text{pc}) = 0.13c$ to $V(r = 1\text{pc}) = 0.42c$ [Sudou, H., et al. 2000, PASJ, 52, 989]

Adopting the best fit model of Melia et al. 2002, ApJ, 567, 811 (consistent with the limits set by Jones et al. 1986, ApJ, 305, 684) and assuming $n \propto r^{-2}$ we find

- temperature: $T = 10^{12}\left[\frac{r(pc)}{0.026}\right]^{-4/3}$ °K
- sound speed: $\frac{C_s}{c} = 0.5573\left[\frac{r(pc)}{0.026}\right]^{-2/3}$
- specific enthalpy: $\xi = 1 + 0.466\left[\frac{r(pc)}{0.026}\right]^{-4/3}$

Thus, for 0.53pc$< r < 1$pc the flow is supersonic and the quantity $\xi\gamma - 1$ changes from 0.01562 at $r = 0.53$pc to 0.106 at $r = 1$pc.
As for hydrodynamic flows $\xi\gamma - 1 = const.$, the conclusion is that the flow is not hydrodynamically accelerated. We propose the magnetic acceleration as a plausible explanation of the observations.

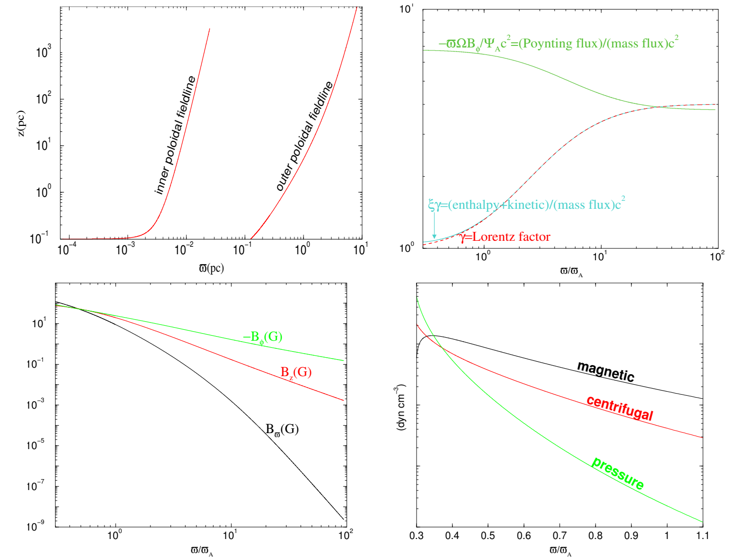

GRB outflows (including time dependence, $e^{\pm}$, radiation)

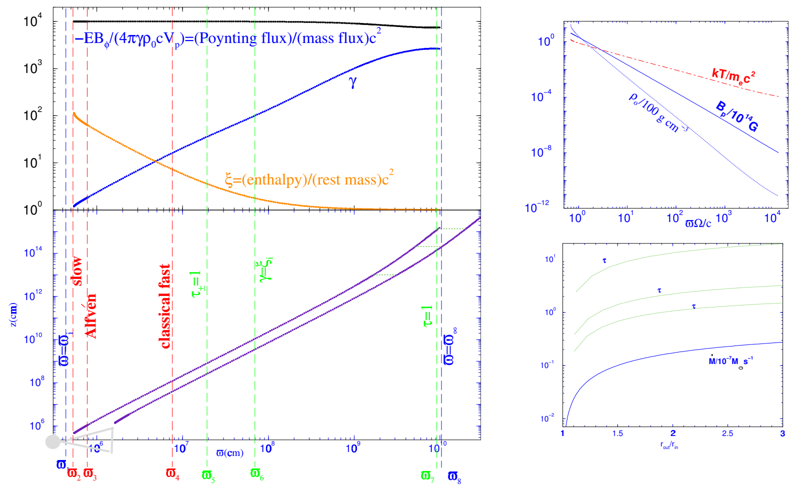

- $\varpi_1 < \varpi < \varpi_6$: Thermal acceleration - force free magnetic field ($\gamma \propto \varpi$, $\rho_0 \propto \varpi^{-3}$, $T \propto \varpi^{-1}$, $\varpi B_\phi = const$, parabolic shape of fieldlines: $z \propto \varpi^2$)
- $\varpi_6 < \varpi < \varpi_8$: Magnetic acceleration ($\gamma \propto \varpi$, $\rho_0 \propto \varpi^{-3}$)
- $\varpi = \varpi_8$: cylindrical regime - equipartition $\gamma_\infty \approx (-EB_\phi/4\pi\gamma\rho_0 V_p)_\infty$

Collimation – Acceleration

- The flow is centrifugally accelerated for $V_\phi \gtrsim V_p \Rightarrow V_p \lesssim \frac{c}{\sqrt{2}}$.
- Thermal acceleration is important for $\gamma \lesssim \xi_i$.
- For $\gamma \gtrsim \xi_i$, $\xi \approx 1$ and the magnetic acceleration takes over.
- How efficient is the magnetic acceleration? ($\sigma_\infty = ?$)
  - For $F > 1$ the flow reaches asymptotically a rough equipartition between kinetic and Poynting fluxes ($\sigma_\infty \approx 1$). The Lorentz force is capable of collimating the flow reaching cylindrical asymptotics (the collimation is possible for $\gamma \lesssim$ a few $\times 10$, following $\gamma^2 \varpi \sim \mathcal{R}$).
  - For $F < 1$, the acceleration is more efficient. The collimation is not so strong and the flow eventually approaches conical asymptotics.
- Is the 100% acceleration efficiency possible ($\sigma_\infty = 0$)?
  Super-Alfvénic asymptotic solutions show that it is!

Crab-like pulsar winds

Integrate transfield force-balance equation under the z self-similar ansatz $z = \mathcal{F}_1(A)\mathcal{F}_2(\varpi)$.

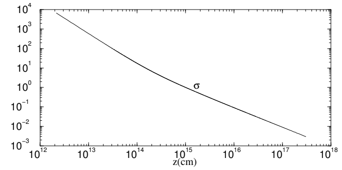

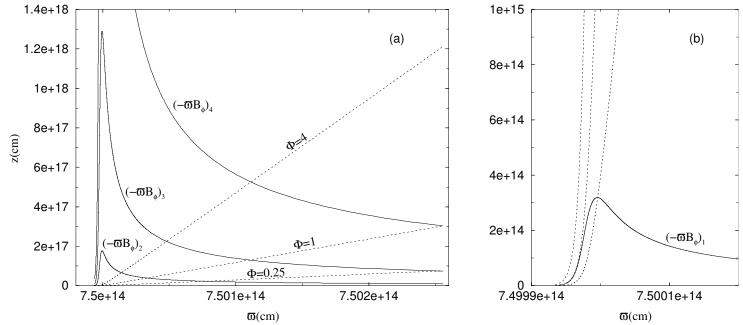

$J_\| < 0 \rightarrow J_\| > 0$

Summary of the previous results

- The shape is determined close to the source ($J_\parallel < 0$)
- Collimation is possible
- The acceleration continues at larger distances ($J_\parallel > 0$)
- The magnetic acceleration is eficient

- r self-similar: does not cover both ($J_\parallel \lessgtr 0$) cases ($F > 1$ is preferable)
- Alternatives:
  - z self similar (captuers both cases)
  - θ self-similar: applies to thermally driven flows near the axis (inside the light cylinder)
  - Fully numerical studies

Meet the observations

boundary conditions on the disk $\mathbf{B}$, T, $\xi(e^{\pm}$ or $e^{-}p^{+}$?), $V \sim C_s$, $V_\phi = \varpi\Omega$, size ($M_{\rm BH}$), $\dot{M}$	$\longrightarrow$	line shape $z = z(\varpi)$, $\mathbf{V}$, $\mathbf{B}$, ρ_0, P as function of distance along each fieldline

- bulk flow
- synchrotron emission (knowing $\mathbf{B}$ in space)
- positions of the shocks $\sim \gamma^2 c\Delta t$ (knowing γ) (Source variability Δt?)
- final value of σ (asymptotic $\mathbf{B} \to \mathbf{B}$ in shocks)
- polarizarion
- asymptotic width – opening angle

6.2 A. Mastichiadis: Particle acceleration and radiation in Blazar Jets

PARTICLE ACCELERATION
AND
RADIATION IN BLAZAR JETS

APOSTOLOS MASTICHIADIS

Physics Department
University of Athens

HIGH-ENERGY AGN OBSERVATIONS

- *GeV gamma-rays*
  3rd EGRET/CGRO Catalogue:
  66 high confidence + 27 low confidence sources

Population characteristics:
All blazars (BL Lac objects + flat spectrum radio quasars)
Power-law photon spectra
Some variable

- *TeV gamma-rays*
  Ground-based Cherenkov detectors (WHIPPLE, HEGRA, KANGAROO)
  2 high confidence sources (Mkn 421 and Mkn 501)
  + 4 strong candidates

Source characteristics:
Nearby (z~0.1) BL Lac objects
Power-law photon spectra + exponential cutoffs
Fast variability/flaring activity (~hours; mins!)
Multiwavelength monitoring campaigns:
strong correlation between X-ray and TeV gamma-ray fluxes

WHAT WE HAVE LEARNED SO FAR

- Gamma rays are produced in jets (radio-quiet AGN are also gamma-ray quiet)
- Radiation is highly amplified by Doppler boosting (otherwise TeV gamma rays would have been attenuated by photon-photon pair production in the source)

KEY QUESTIONS

- What are the mechanisms for gamma-ray production?
- Are the radiating particles electrons or protons?
- How are these particles accelerated?
- Why TeV gamma rays and X-rays are correlated?

OBJECTIVE

- Use particle radiation theories to obtain fits to both spectral and temporal behaviour of a specific source
  → information on parameters of radiating plasma (B-field, particle energies, Doppler factor, etc): source diagnostics
- Fast variability makes time-dependent calculations neccesssary

One-zone models

- **Uniform injection of relativistic electrons in a sphere of radius R –random B**
  → $Q(t,\gamma)=Q_0(t)\gamma^{-s}, \gamma \le \gamma_{max}$
- **Electron evolution → Solution of the kinetic equation for the electron distribution function in**
  i) steady state or
  ii) time-dependent fashion
- **Relevant processes**
  i) Synchrotron
  ii) Inverse Compton on
    a) external photons (EC models)
    b) synchrotron photons (SSC)
  iii) Photon-photon absorption
- **Electron distribution → radiated photon spectrum**
- **Fits to low state MW AGN spectra → tight constraints on parameters**
- **One free parameter** $t_{var} = R/\delta c$,
  δ is the Doppler factor of the blob
- **MK97: Flare fitting → change in one parameter + time-dependent evolution**
- **Usual suspects** Q_0, γ_{max}, **B, δ**

NUMERICAL SCHEME

AH + J.Kirk 1995

- Electrons

$$\frac{\partial n_e}{\partial t}(\gamma,t) + Q^e(\gamma,t) + \mathcal{L}^e(\gamma,t) = 0$$

injection terms
- external injection
- $\gamma+\gamma \to e^+e^-$ injection

loss terms
- synchrotron
- inverse Compton (Th & KN)
- adiabatic

- Photons

$$\frac{\partial n_\gamma}{\partial t}(x,t) + Q^\gamma(x,t) + \mathcal{L}^\gamma(x,t) = 0$$

source terms
- synchrotron
- inverse Compton

sink terms
- $\gamma+\gamma \to e^+e^-$ absorption
- synchrotron self abs^n

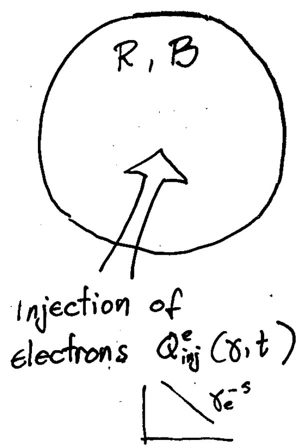

⟹ Time-dependent electron and photon spectra

Calculations in the blob frame → observer's frame

If no external photons → homogeneous SSC

ELECTRON EVOLUTION

Example 1

Electron injection

$Q(\gamma,t) = Q_0 \gamma^{-2}$

$\gamma < \gamma_{max}$

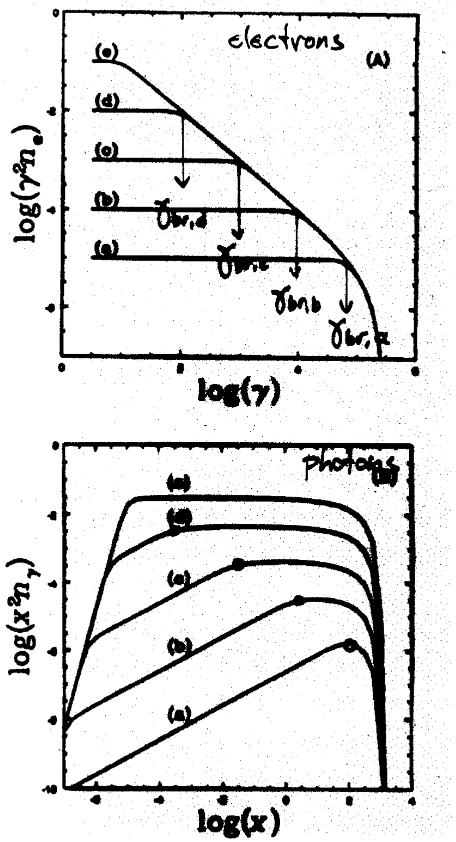

time increases

(a) → (e)

(e) steady state

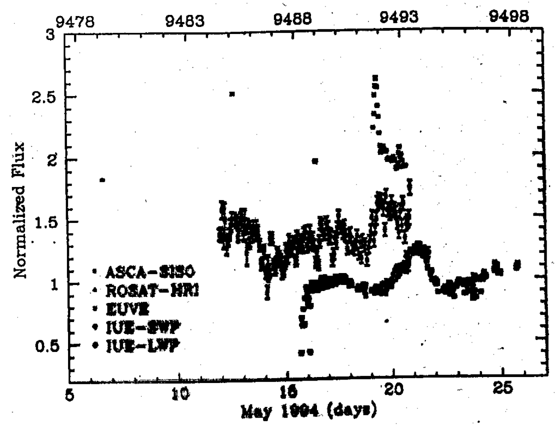

PKS 2155-304

Megan Urry et al (1997)

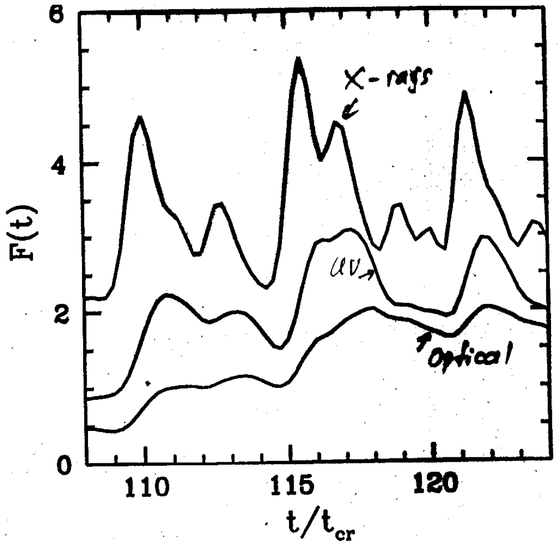

Stochastic fluctuations in the injection rate of relativistic electrons

(Kirk & Mastichiadis 1997)

AH + J Kirk 1997
spherical homogeneous
synchro self-Compton

Mkn 421

$B = 70$ mG
$R_b = 5.10^{16}$ cm
$\delta = 15$
$\rightarrow t_{var}^{abs} \simeq 1.2$ days

$Q_e = Q_0 \gamma^{-s}$ $\gamma < \gamma_{mx}$ electron injection $s = 1.7$, $\gamma_{mx} = 2.10^5$

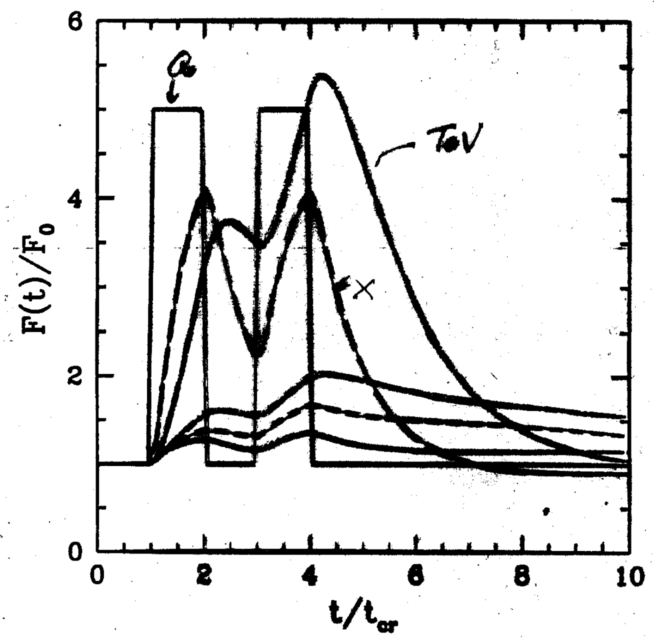

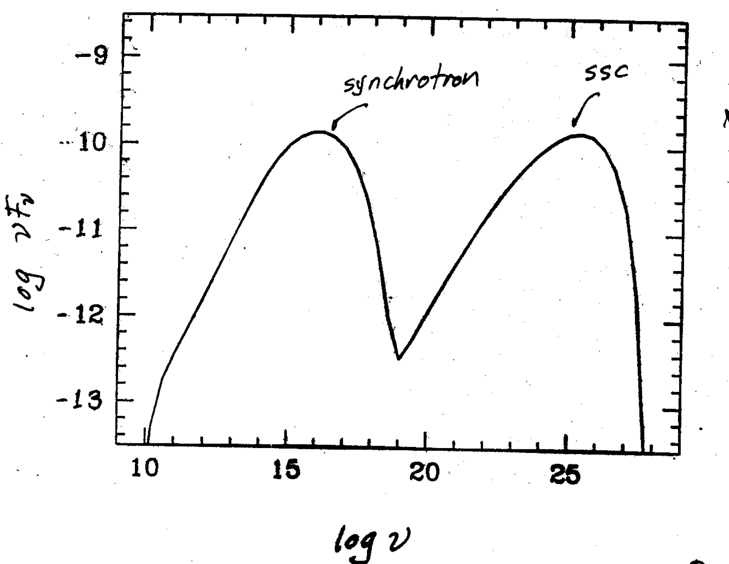

No external photons

Scaling: one ~~free~~ parameter $t_{var} = \frac{R}{\delta c}$

Satisfactory spectral fits for

$B = 70\, t_5^{-1/4}$ mG $\quad \gamma_{mx} = 2.10^5 t_5^{1/4}$

$R = 5.10^{16} t_5^{3/4}$ cm $\quad \delta = 15\, t_5^{-1/4}$

$t_5 = t_{var} / 10^5$ sec

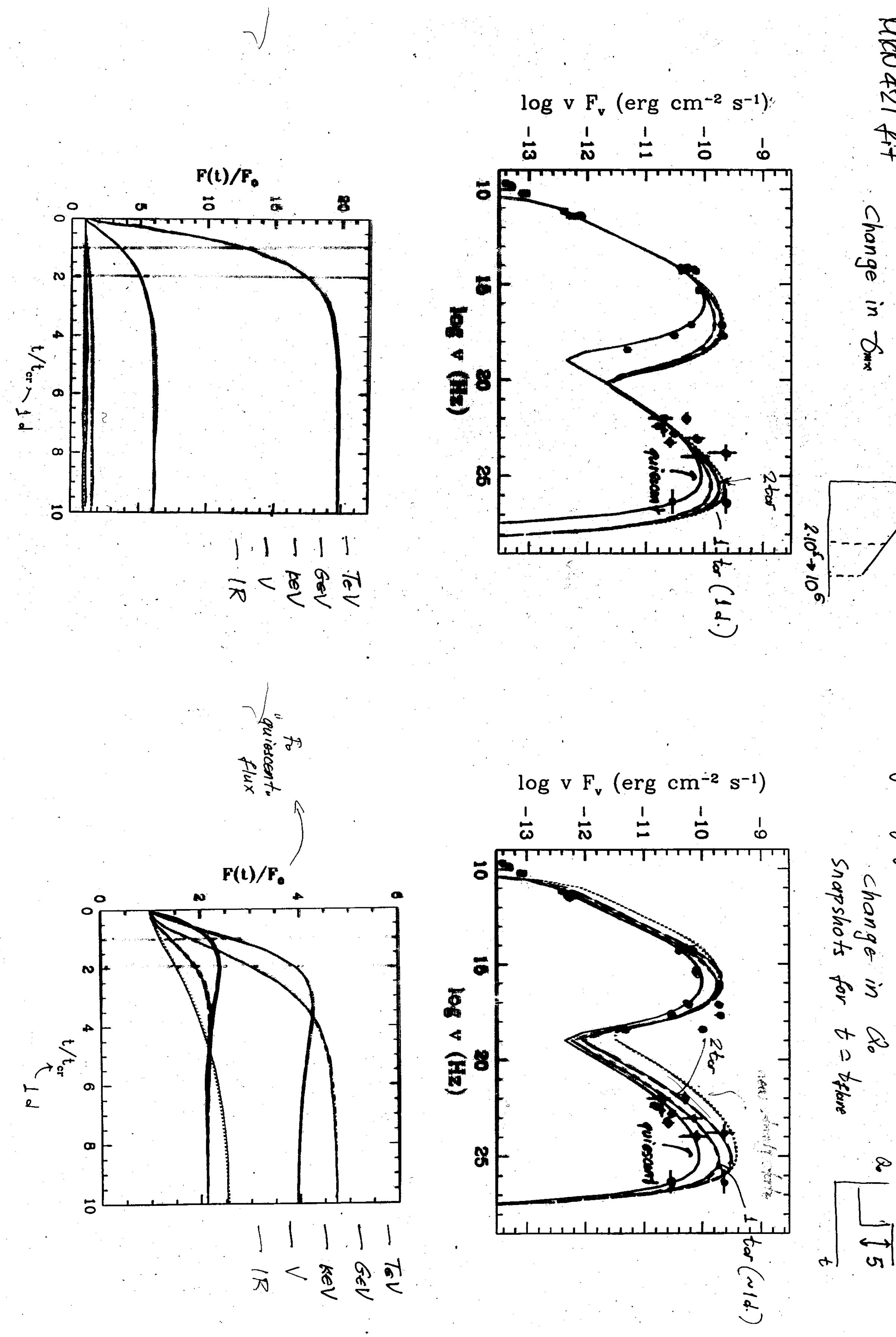

log ν F_ν (erg cm^-2 s^-1)
log ν (Hz)
F(t)/F_0
t/t_cr
quiescent
Change in γ_max
Change in Q_0
Snapshots for t = t_flare
TeV
GeV
keV
V
IR
quiescent flux

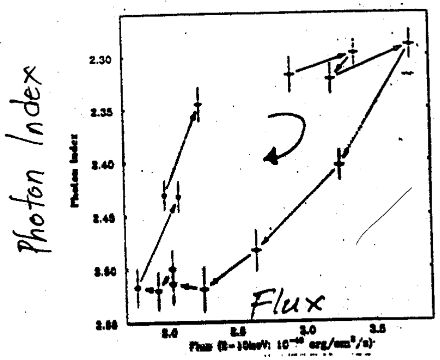

Mkn 421
Evolution of an X-ray flare
Takahashi et al.
1996

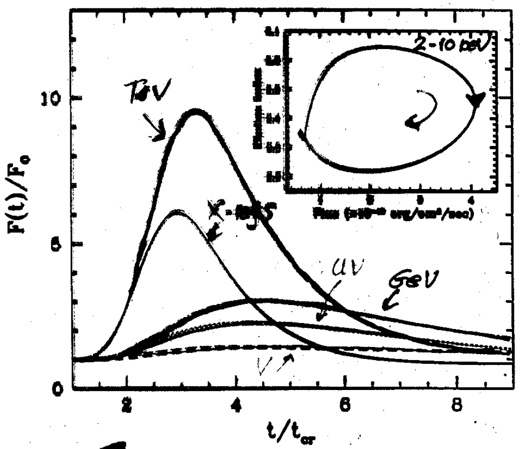

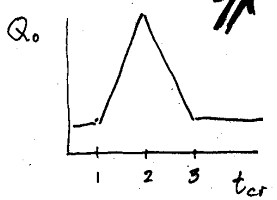

Source function
$Q(t) = Q_0(t)\,\gamma^{-s}$ $\gamma<\gamma_{max}$

One-zone models: A critique

1. Fast variability can be explained only with high Doppler factors:
   Mkn 421: **Flare timescales**
   ~few hours (RXTE)
   ~few minutes (Whipple, HEGRA)
   →consistent with δ~50
   (MK97: $\delta=15\left(\dfrac{t_{var}}{10^5\,\mathrm{sec}}\right)^{-1/4}$,
   Krawczynski et al. 2001)
2. **Derived loops in spectral** index *vs*. intensity plots **are always clockwise →** **Synchrotron/IC cooling faster** for higher **energies → Inherent property** of particle **injection at high energies**
   - BUT **sometimes** counter-clockwise loops **observed (e.g.** Fossati et al 2000)

- One **step back (and a way out):** replace the ``**ready**'' **injection** of high energy **electrons with** electron injection at *low* **energies and consequent** *acceleration* to *high* **energies** (c.f. shock acceleration in SNR) **→ advancing thin shock +** particle **escape and radiation into** cooling region → **two-zone models**

THE PHYSICAL PICTURE

- Picture as in Kirk, Rieger and Mastichiadis (1998—KRM):
Advancing shock with velocity υ_s (υ_s<<c in the jet frame)
Particles accelerate there and escape downstream where they cool and radiate.

- Acceleration zone

$$\frac{\partial N_e}{\partial t}+\frac{\partial}{\partial\gamma}\left[\left(\underbrace{\frac{\gamma}{t_{acc}}}_{\text{acceleration term}}-\underbrace{(\beta_S+\beta_C)\gamma^2}_{\text{loss term (syncr+ICS)}}\right)N_e\right]+\underbrace{\frac{N_e}{t_{esc}}}_{\text{escape term}}=\underbrace{Q\delta(\gamma-\gamma_0)}_{\text{injection term}}$$

- Cooling zone

$$\frac{\partial n_e}{\partial t}-\frac{\partial}{\partial\gamma}\left[\underbrace{(\beta_S+\beta_C)\gamma^2 n_e}_{\text{loss term (as above)}}\right]=\underbrace{\frac{N_e(\gamma,t)}{t_{esc}}\delta(x-x_s(t))}_{\text{injection term: electrons that escape from the acceleration zone}}$$

- Synchrotron +Inverse Compton emission:

$$I(\nu,\bar{t})=\int d\gamma.\underbrace{P(\nu,\gamma)}_{\text{synchr./ICS emissivity}}\int dx.n_e(x,\gamma,\bar{t}+\frac{x}{c})$$

Two changes over KRM:
- External photon inverse Compton: losses and spectrum
- `Bohm' acceleration timescale $t_{acc}^{-1}=\eta\frac{ceB}{E_e}$

- Does the introduction of a new acceleration scheme produce any different results?
- Relevance to observations?

BETWEEN STEADY STATES

- Rapid acceleration ($t_{acc}^{-1}\propto\gamma^{-1}$) of fresh particles up to γ_{max}
  → cooling of the highest energy particles first
  → initial flattening of the spectrum

blue line: t_{acc} after the onset of the flare
green line: $3t_{acc}$ >>
orange line: $5t_{acc}$ >>
black dashed line: new steady state

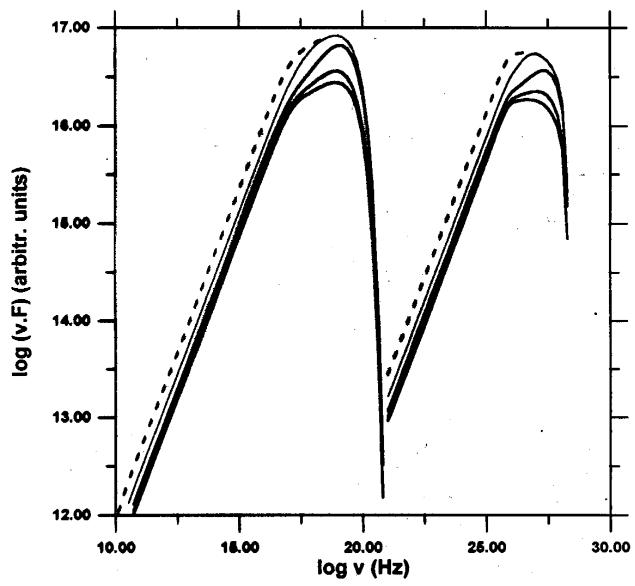

A MODEL FOR A FLARE

- To model a possible flare:
  $Q = Q_0$ for $t < t_1$
  $Q = Q_{fl}$ for $t_1 < t < t_2$
  $Q = Q_0$ for $t_2 < t$

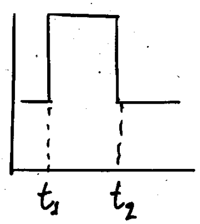

- Then the flare is characterised by two parameters:
  1. The change in Q.
  2. The duration of the above change ($t_{fl} = t_2 - t_1$).
- **If t_{fl}~ few t_{acc}, then there is no time for steady-state to be achieved → only time-dependent calculations are relevant.**
- **Example: $Q_{fl} = 3Q_0$ for $t_{fl} = 5t_{acc}$.**

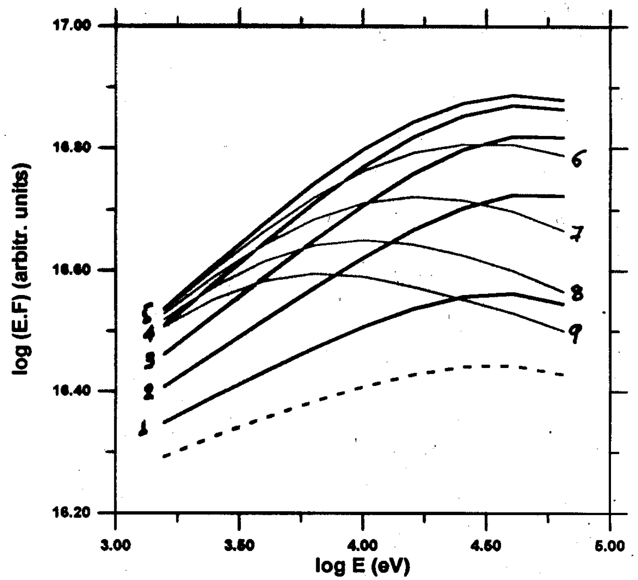

Solution

$$N(\gamma,t) = a\frac{1}{\gamma^2}\left(\frac{1}{\gamma} - \frac{1}{\gamma_{mx}}\right)^{\frac{t_{acc}-t_{esc}}{t_{esc}}} \Theta(\gamma-\gamma_0)\,\Theta(\gamma_1(t)-\gamma)$$

for $\gamma_0 < \gamma < \gamma_1(t)$

$$\gamma_1(t) = \left(\frac{1}{\gamma_{mx}} + \left[\frac{1}{\gamma_0} - \frac{1}{\gamma_{mx}}\right] e^{-t/t_{acc}}\right)^{-1}$$

$$a = Q_0\, t_{acc}\, \gamma_0^{\,t_{acc}/t_{esc}} \left(1 - \frac{\gamma_0}{\gamma_{mx}}\right)^{t_{acc}/t_{esc}}$$

$$\gamma_{mx} = (b_s\, t_{acc})^{-1}$$

Evolution of electron distribution function ($t_1 < t_2 < t_3$)

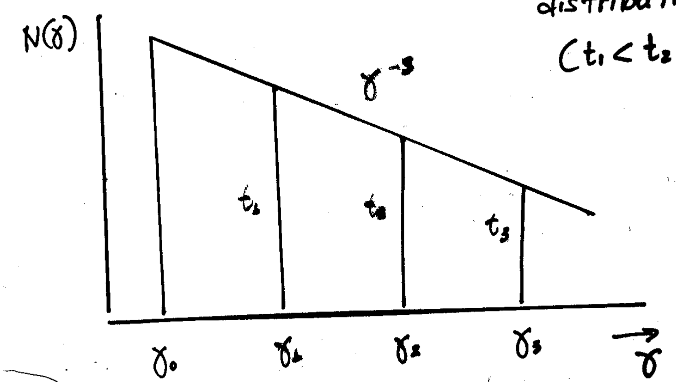

For $\gamma_1(t) \ll \gamma_{mx} \rightarrow \gamma_1(t) = \gamma_0\, e^{t/t_{acc}}$

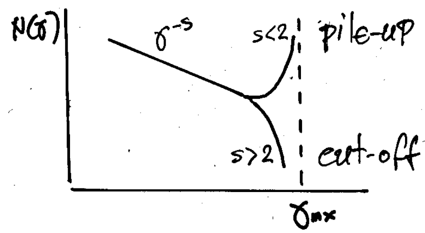

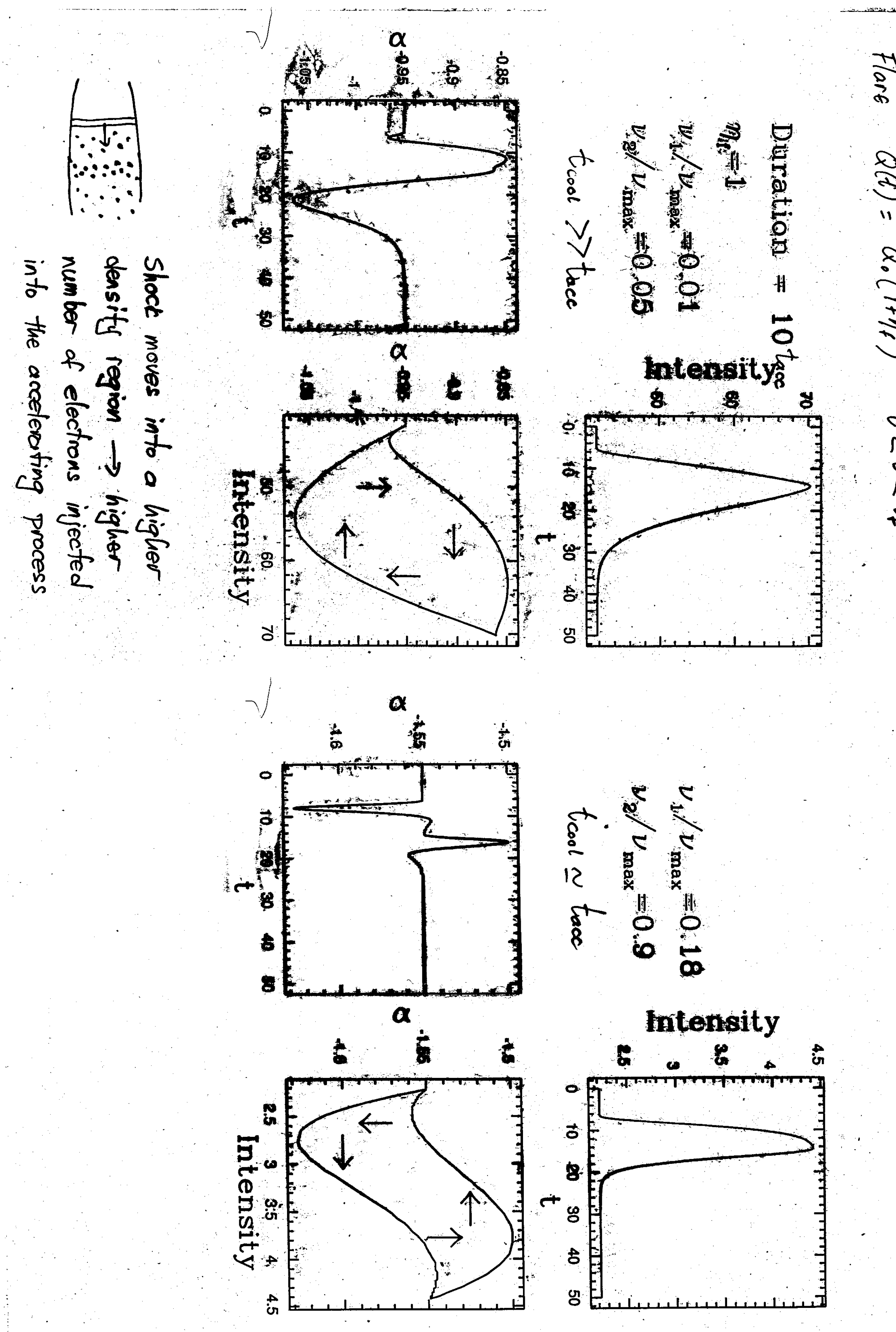
Duration = 10 t_{acc}
$t_{cool} >> t_{acc}$
$t_{cool} \simeq t_{acc}$
Intensity
Shock moves into a higher density region → higher number of electrons injected into the accelerating process

Conclusions

One zone models:
High energy particle injection, cooling and radiation.

- Steady state: Fits to AGN MW data (various epochs).
- Time dependent: Necessary for flares / continuous monitoring.
  - Problems:
    High δ's needed (~50)
    No anticlockwise loops (observed!)

Two zone models:
Application of diffusive shock acceleration in blazar jets

- MW steady state fits
- Flares: Changes in number of low energy particles injected or B-field
- 'Normal' δ-values
- Both CW +ACW loops (depending on the window of observation with respect to the high energy cutoff)

ENIGMA INTERFACE

1) Data modeling : MW snapshots (steady state) or continuous monitoring (time-dep) → source diagnostics (B, R, γ_{mx}, ...) (Trivial)

2) Particle acceleration (2-zone model) + SSC losses : interesting flaring behaviour [$Q_0 \uparrow$, $u_{sy} \uparrow \rightarrow \gamma_{mx} \downarrow$] (Complicated but ok)

3) Particle acceleration in MHD outflows : shock formation with well specified jump conditions → box model for shock acceleration → particle distr → → radiative signatures → observations (Hmm... Cyclopian ENIGMA II ?)

Chapter 7

Session VI: The power of jets (G. Ghisellini)

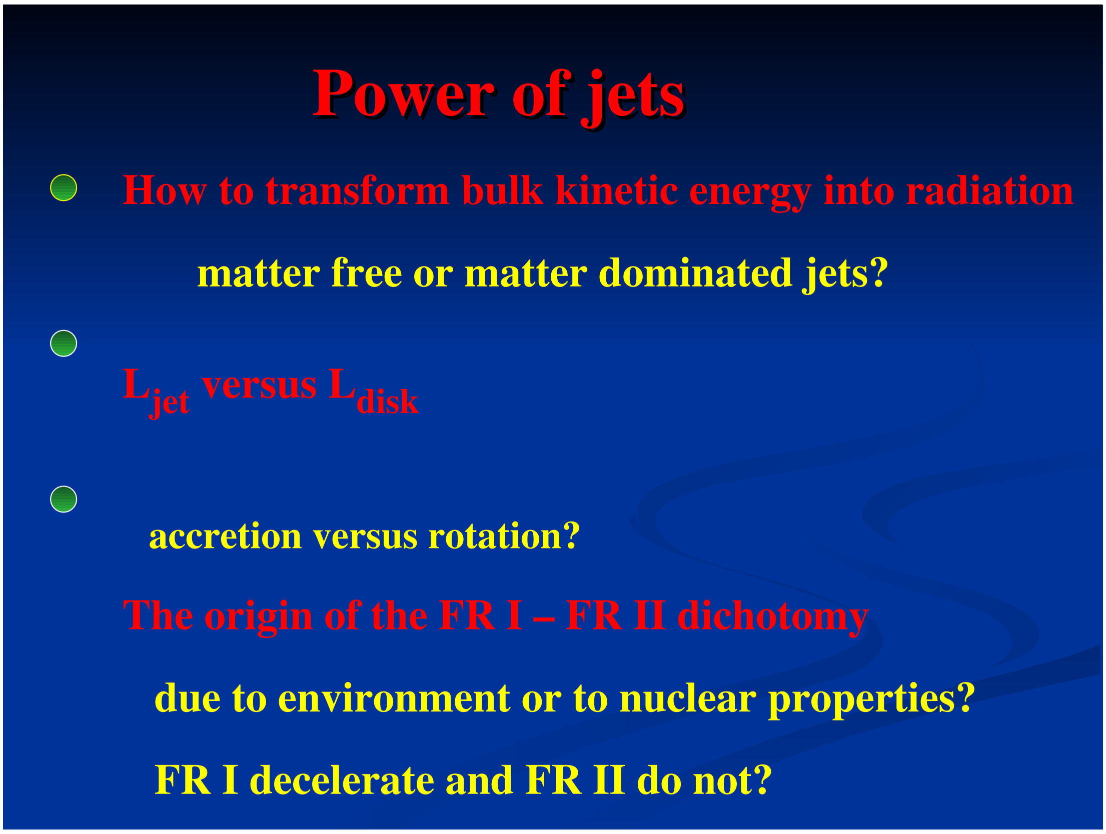

Matter free or matter dominated?

- Pairs or protons?
- Leptonic or hadronic?
- Matter or magnetic field?
- Acceleration up to what radius?
- Deceleration?

Jet versus Disk

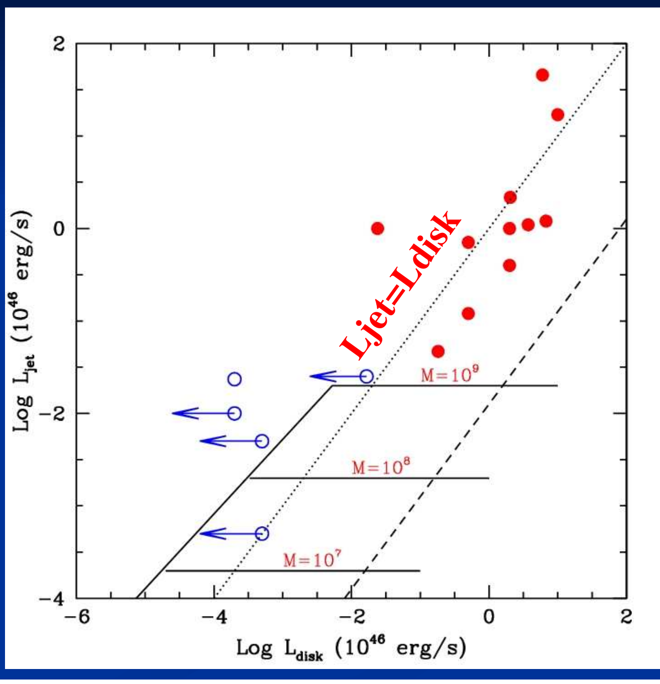

Tavecchio & Maraschi 2000

FR I versus FR II

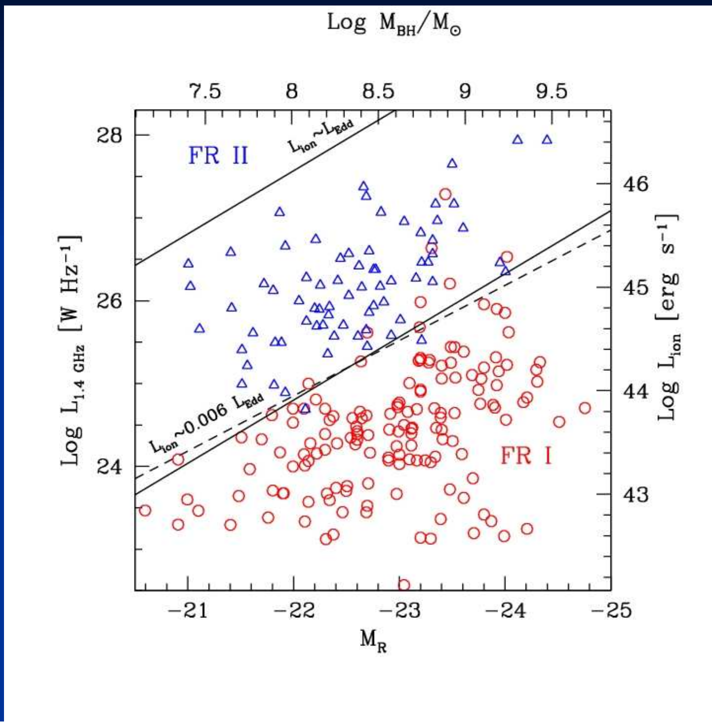

Ghisellini & Celotti 2001

7.1 S. Britzen: The kinematics of Jets

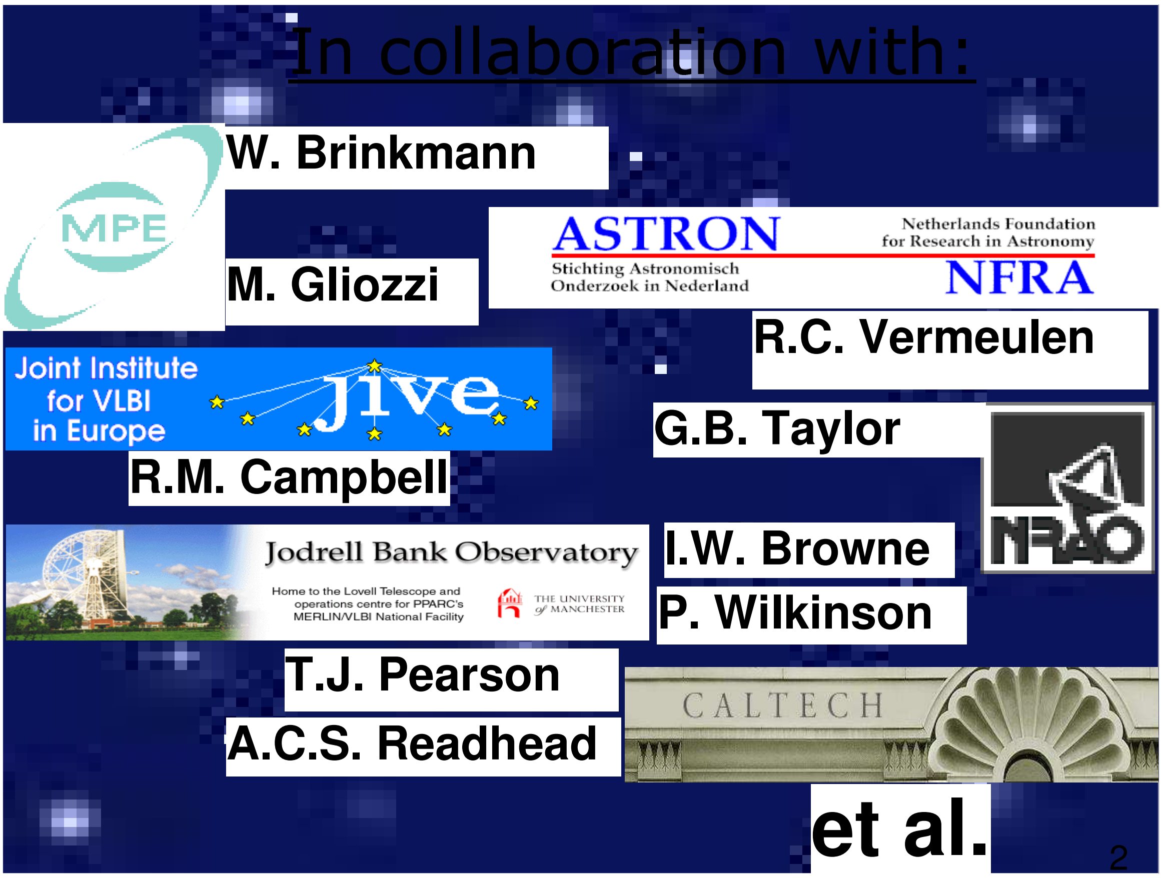
In collaboration with:
W. Brinkmann
MPE
M. Gliozzi
ASTRON
Stichting Astronomisch Onderzoek in Nederland
Netherlands Foundation for Research in Astronomy
NFRA
R.C. Vermeulen
Joint Institute for VLBI in Europe
JIVE
G.B. Taylor
NRAO
R.M. Campbell
Jodrell Bank Observatory
Home to the Lovell Telescope and operations centre for PPARC's MERLIN/VLBI National Facility
THE UNIVERSITY of MANCHESTER
I.W. Browne
P. Wilkinson
T.J. Pearson
CALTECH
A.C.S. Readhead
et al.
2

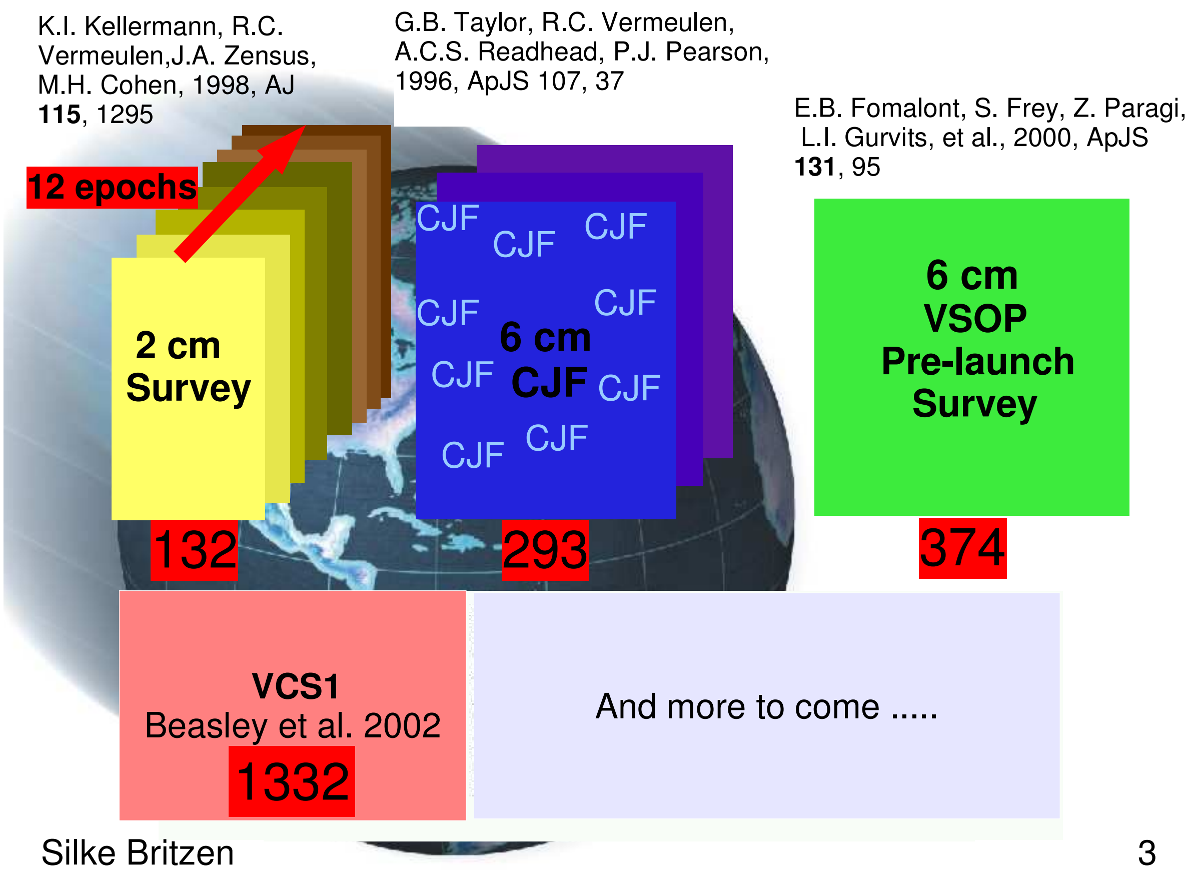
K.I. Kellermann, R.C. Vermeulen,J.A. Zensus, M.H. Cohen, 1998, AJ 115, 1295
G.B. Taylor, R.C. Vermeulen, A.C.S. Readhead, P.J. Pearson, 1996, ApJS 107, 37
E.B. Fomalont, S. Frey, Z. Paragi, L.I. Gurvits, et al., 2000, ApJS 131, 95
12 epochs
2 cm Survey
132
CJF CJF CJF CJF CJF
6 cm CJF
CJF CJF CJF CJF
293
6 cm VSOP Pre-launch Survey
374
VCS1
Beasley et al. 2002
1332
And more to come .....
Silke Britzen
3

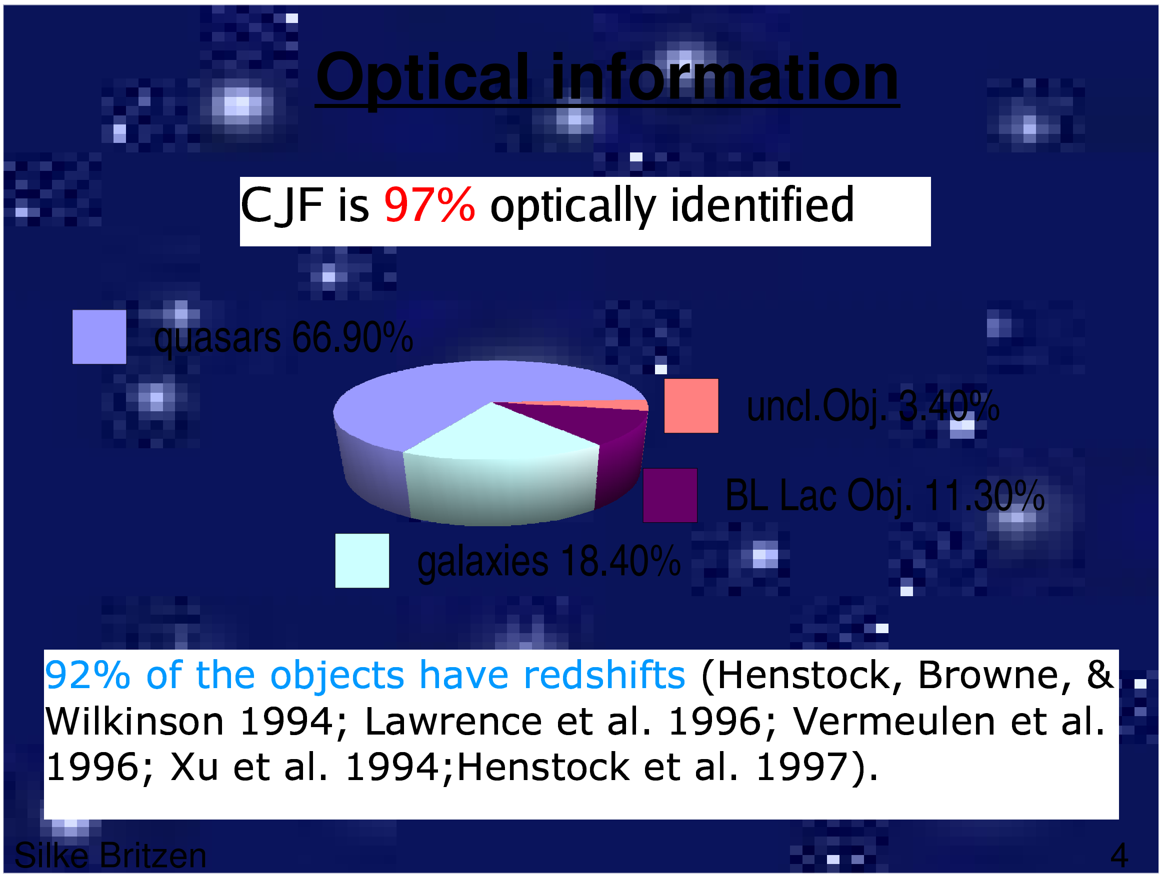
Optical information
CJF is 97% optically identified
quasars 66.90%
uncl.Obj. 3.40%
BL Lac Obj. 11.30%
galaxies 18.40%
92% of the objects have redshifts (Henstock, Browne, & Wilkinson 1994; Lawrence et al. 1996; Vermeulen et al. 1996; Xu et al. 1994;Henstock et al. 1997).
Silke Britzen
4

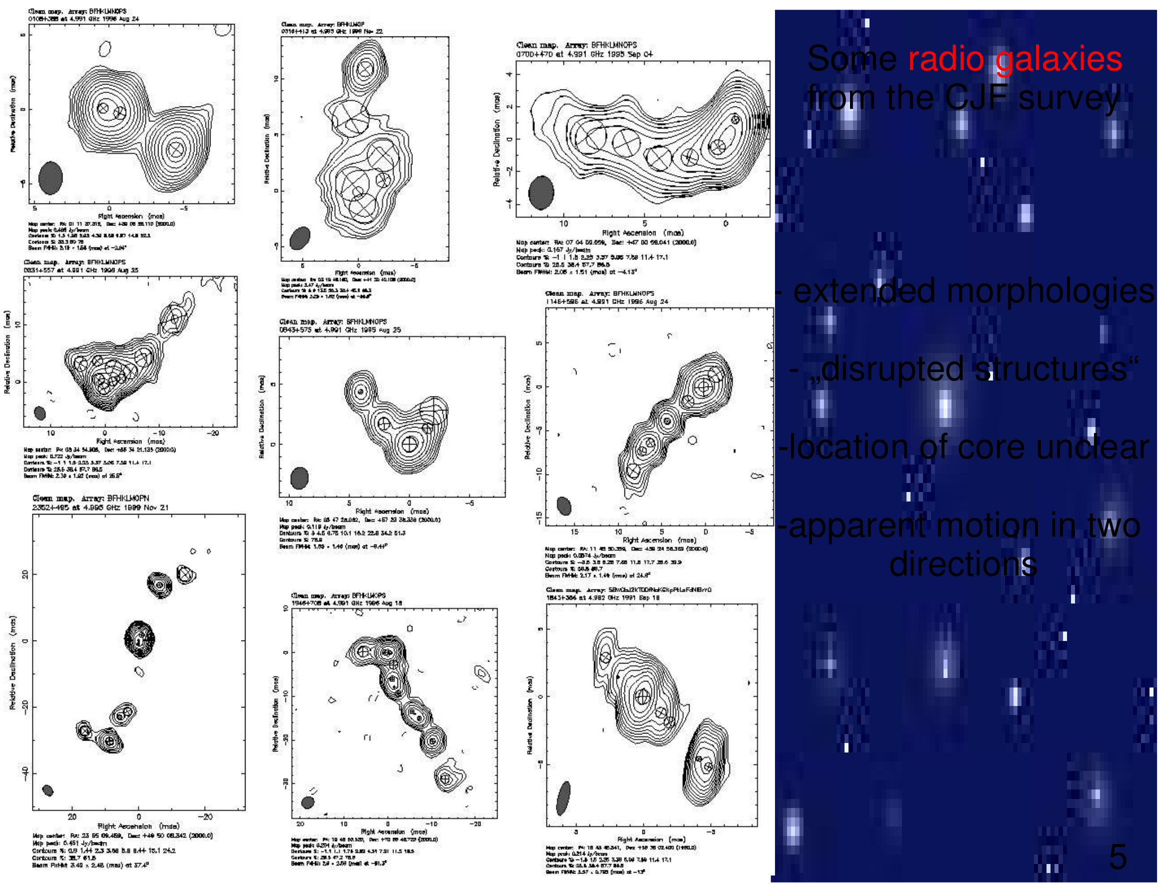
Some radio galaxies from the CJF survey
- extended morphologies
- „disrupted structures"
-location of core unclear
-apparent motion in two directions
5

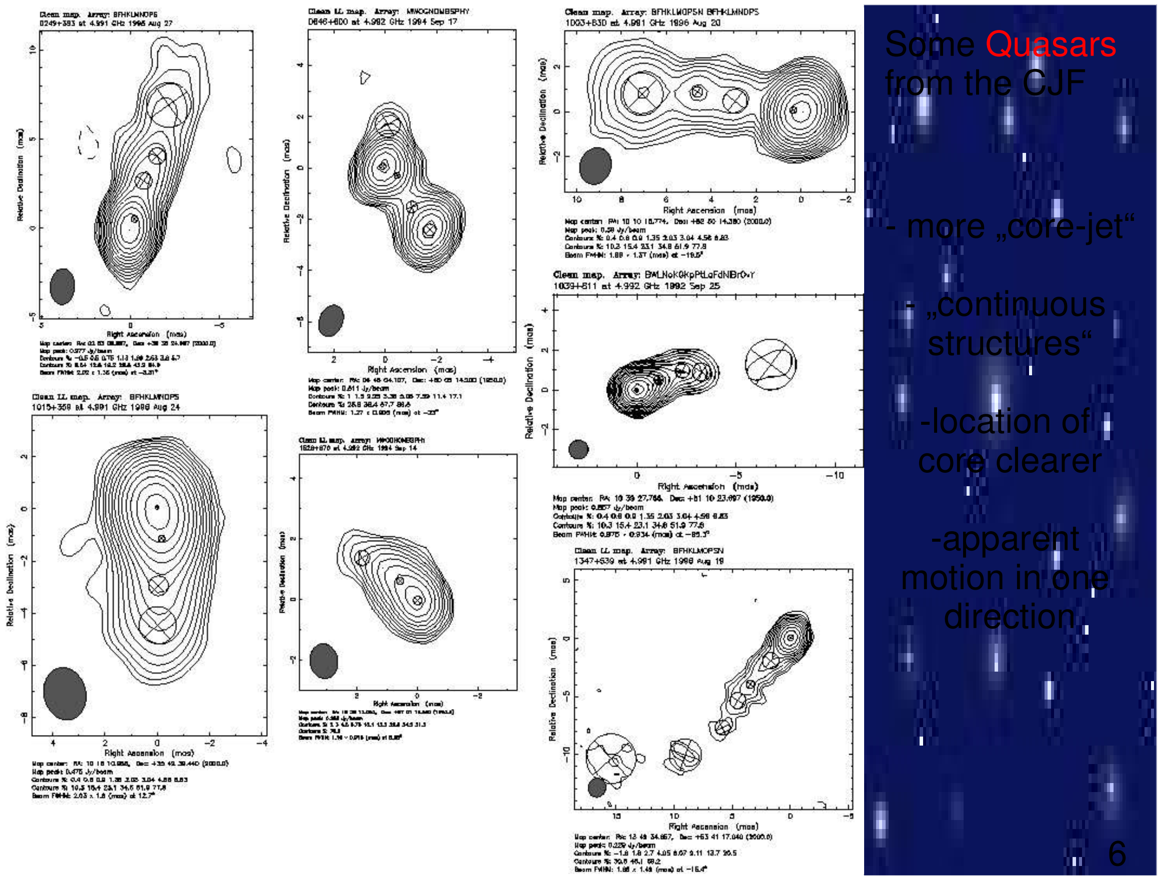
Some Quasars from the CJF
- more „core-jet“
- „continuous structures“
-location of core clearer
-apparent motion in one direction
6

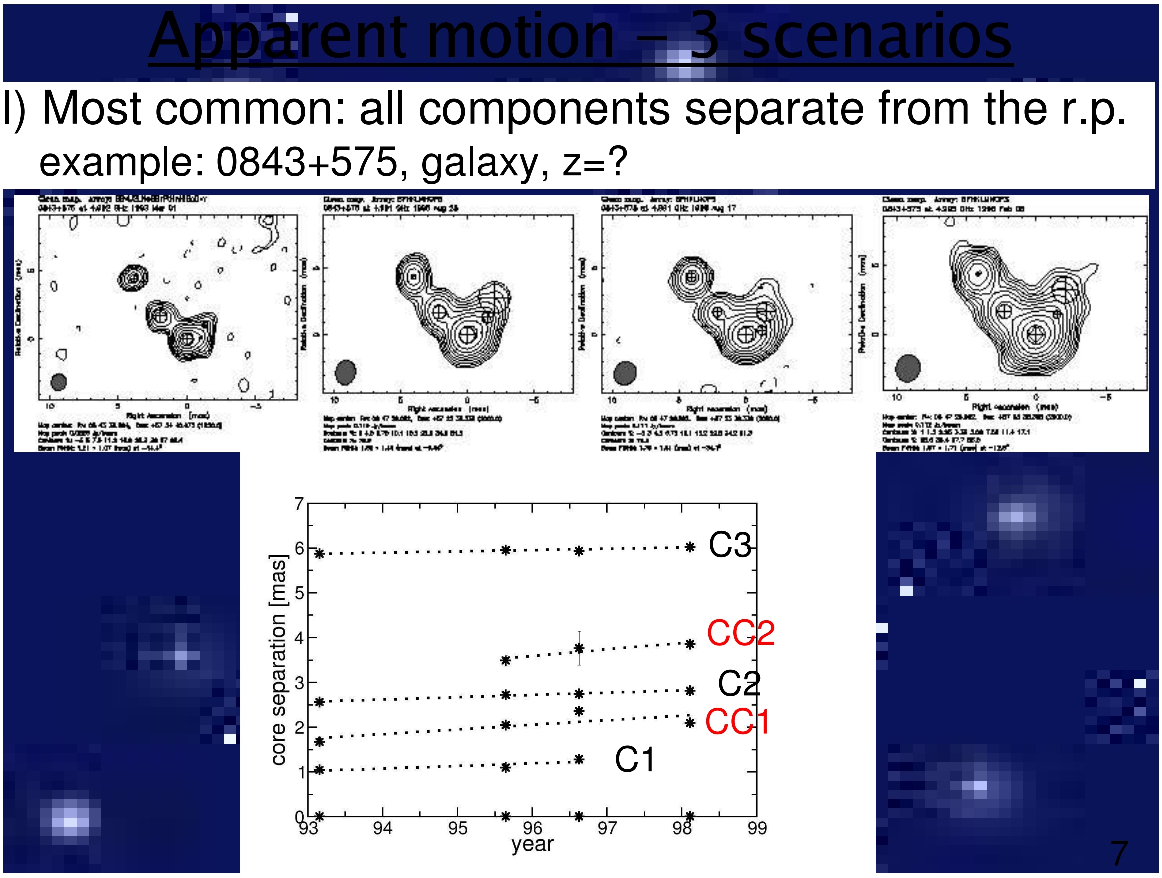
Apparent motion – 3 scenarios
I) Most common: all components separate from the r.p.
example: 0843+575, galaxy, z=?
core separation [mas]
year
C3
CC2
C2
CC1
C1
7

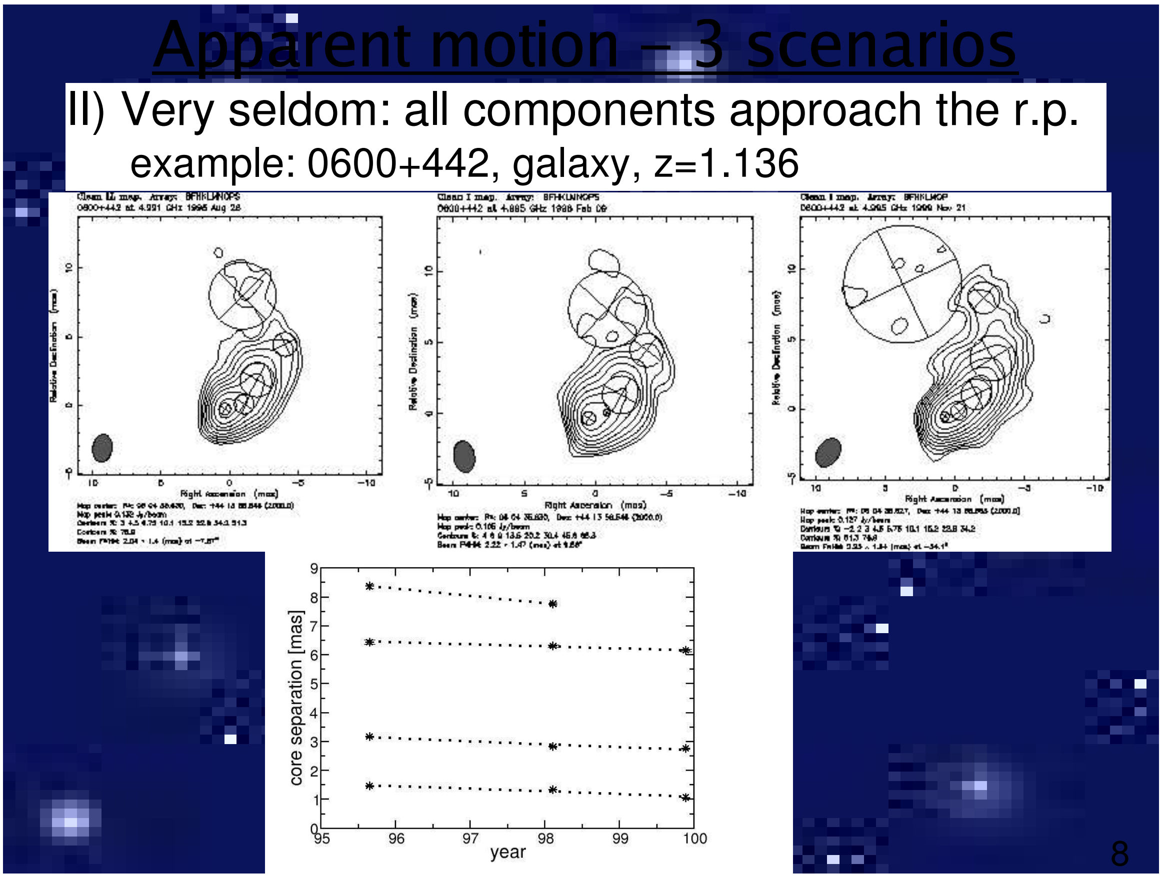
Apparent motion – 3 scenarios
II) Very seldom: all components approach the r.p.
example: 0600+442, galaxy, z=1.136
core separation [mas]
year
8

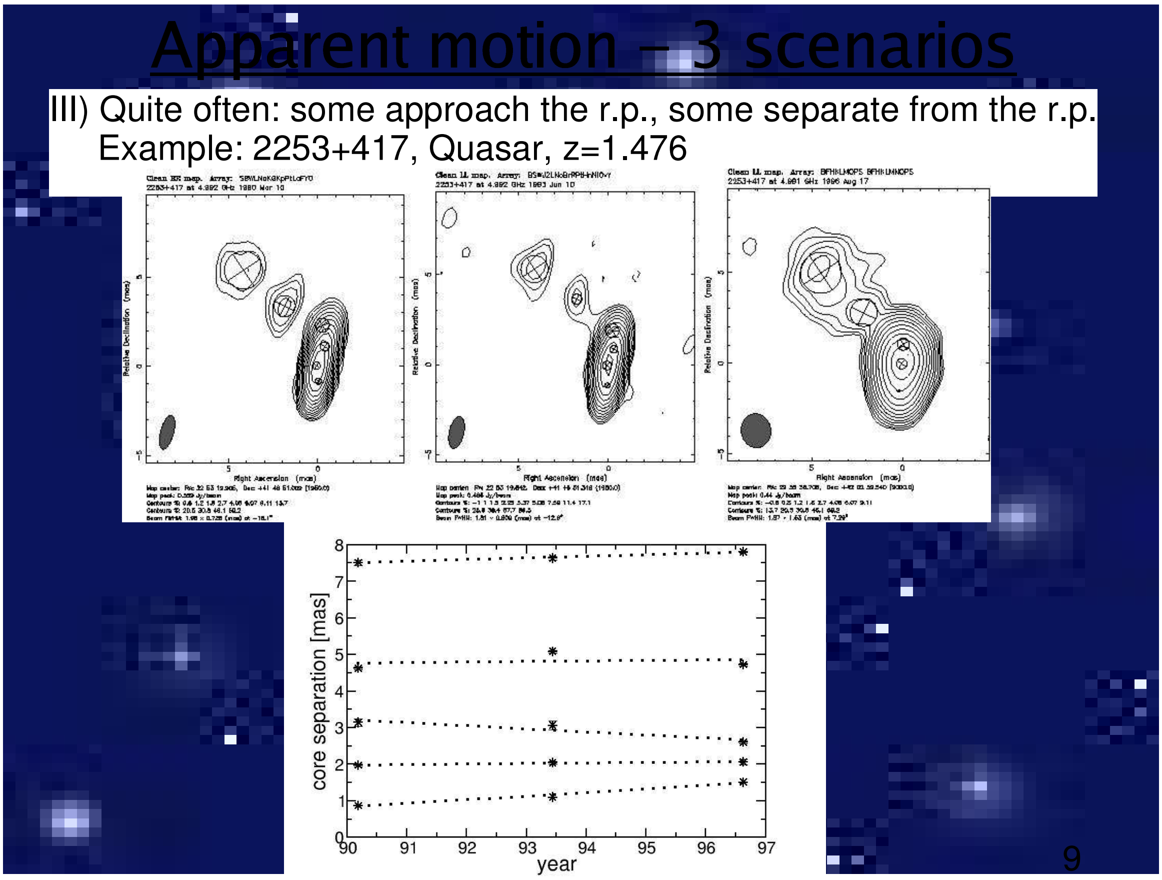
Apparent motion – 3 scenarios
III) Quite often: some approach the r.p., some separate from the r.p.
Example: 2253+417, Quasar, z=1.476
core separation [mas]
year
9

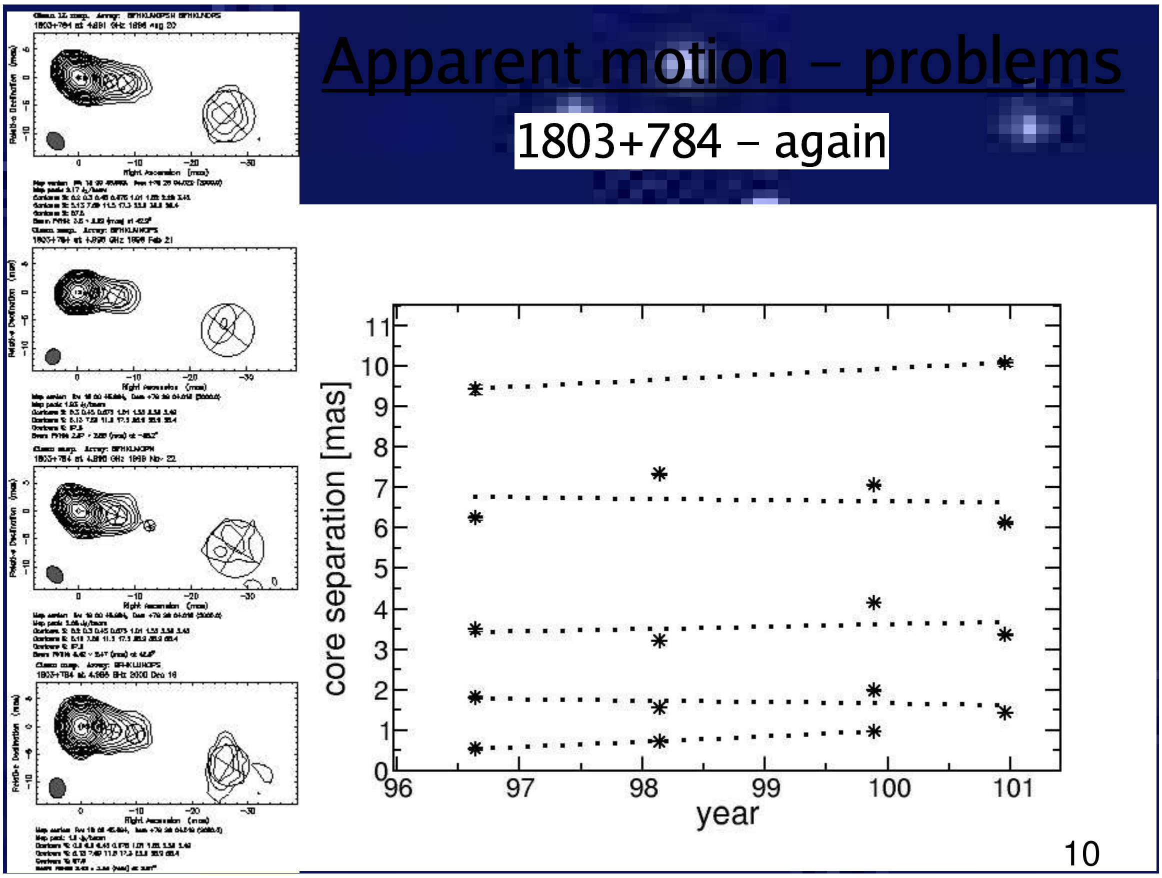
Apparent motion – problems
1803+784 – again
core separation [mas]
year
10

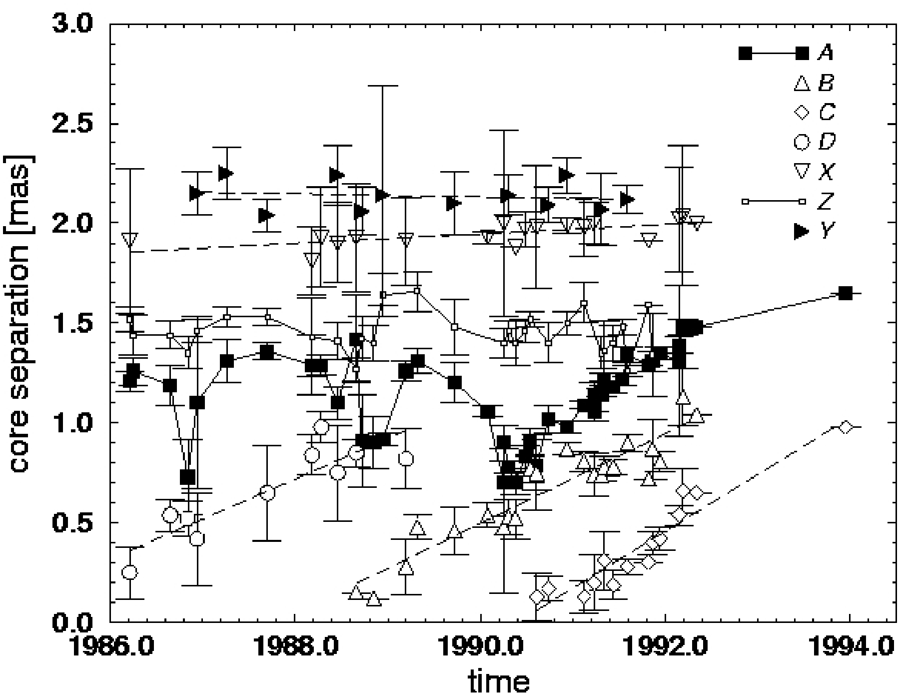
core separation [mas]
time
A
B
C
D
X
Z
Y

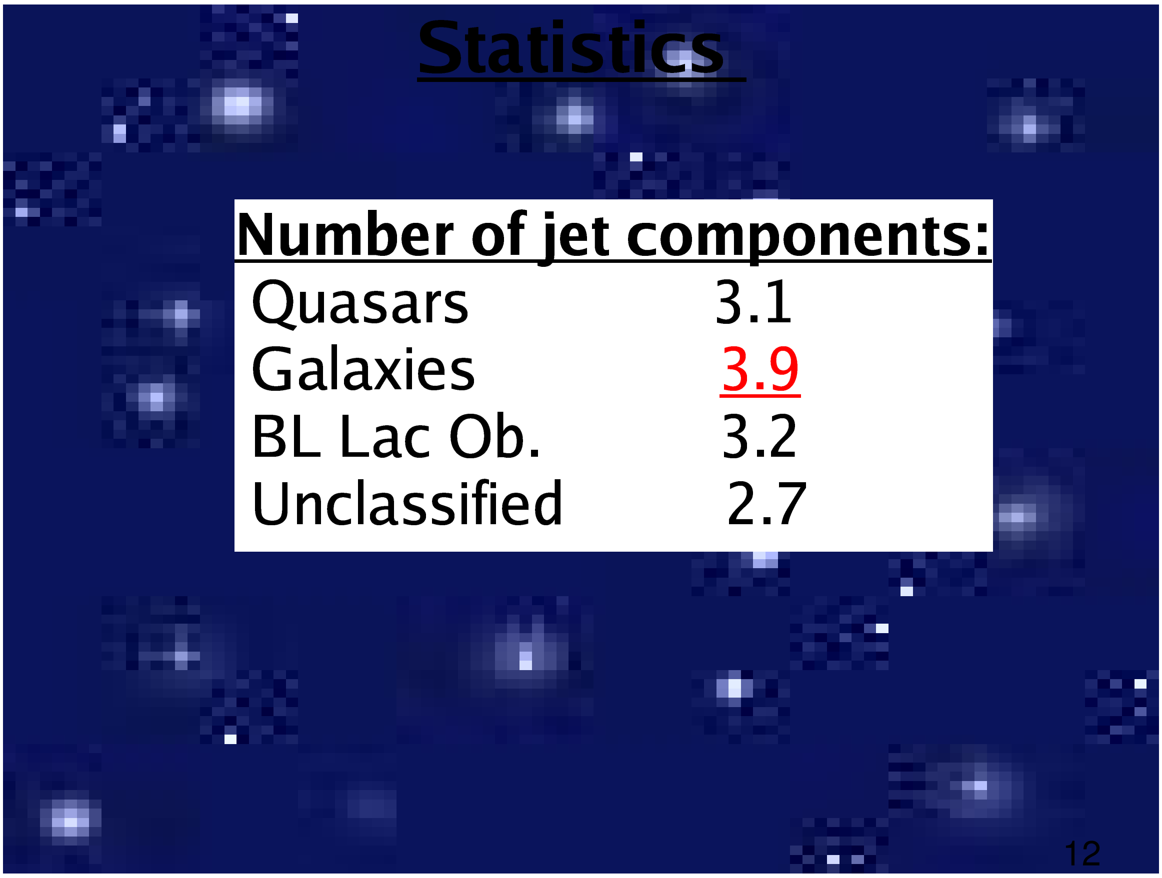
Statistics
Number of jet components:
Quasars 3.1
Galaxies 3.9
BL Lac Ob. 3.2
Unclassified 2.7
12

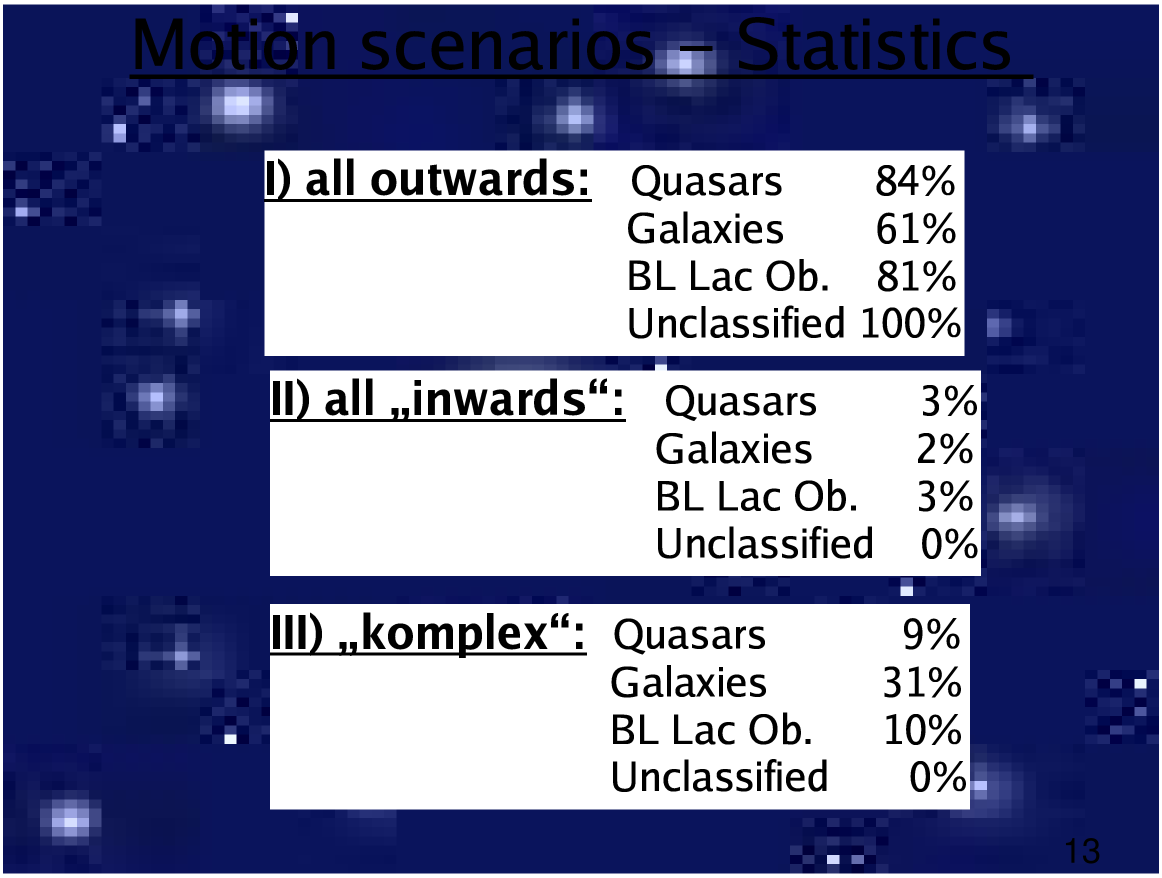
Motion scenarios – Statistics
I) all outwards: Quasars 84%
Galaxies 61%
BL Lac Ob. 81%
Unclassified 100%
II) all „inwards“: Quasars 3%
Galaxies 2%
BL Lac Ob. 3%
Unclassified 0%
III) „komplex“: Quasars 9%
Galaxies 31%
BL Lac Ob. 10%
Unclassified 0%
13

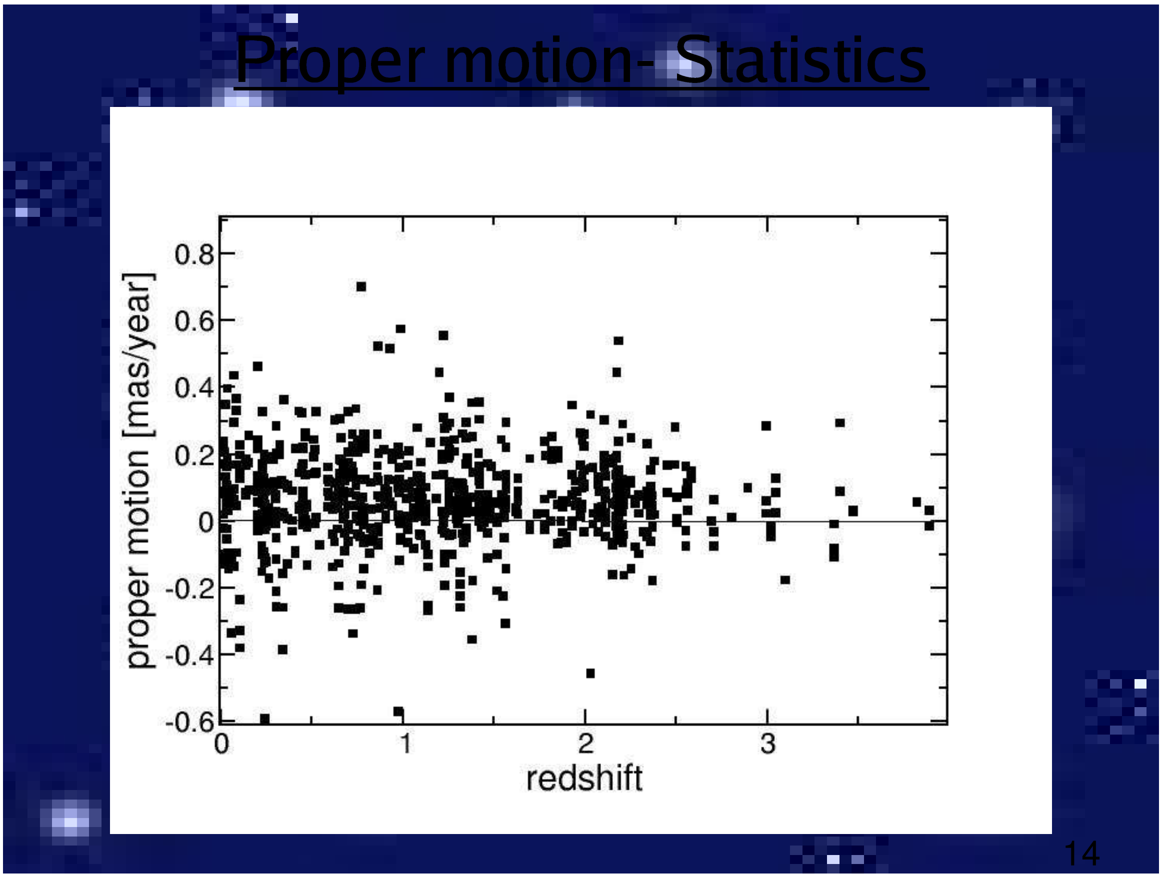
Proper motion- Statistics
proper motion [mas/year]
redshift
14

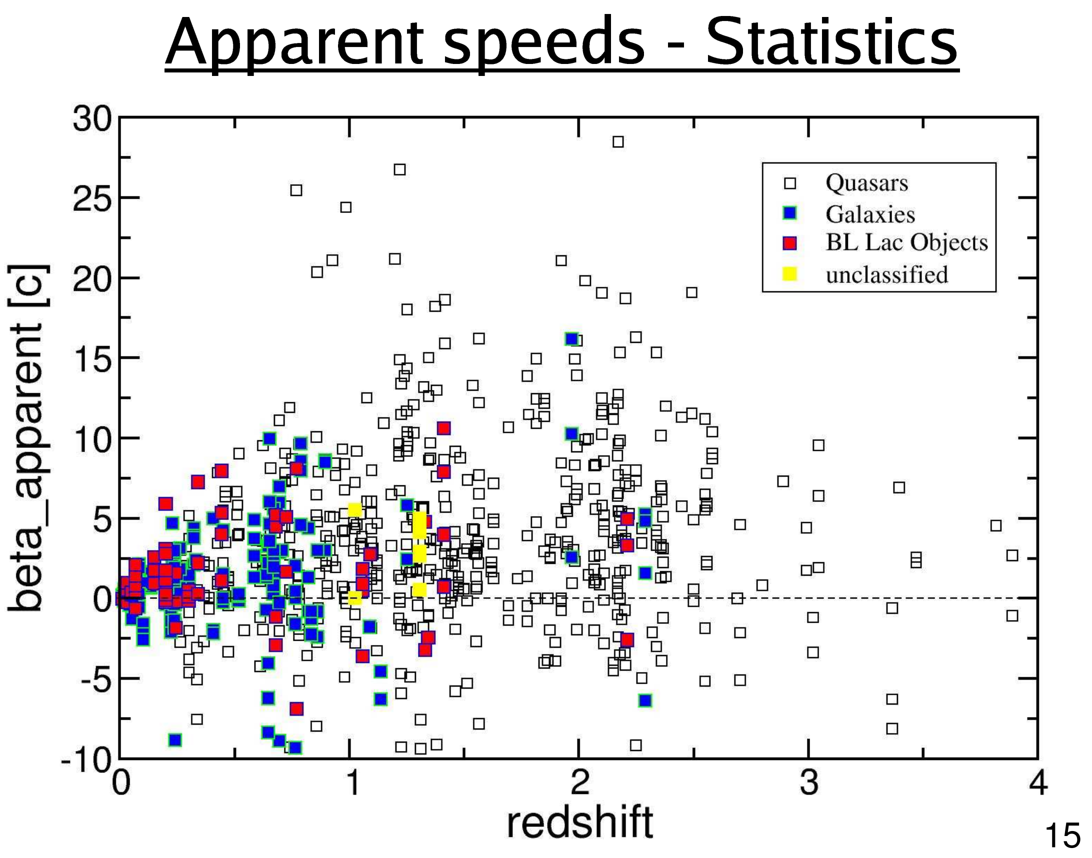
Apparent speeds - Statistics
beta_apparent [c]
redshift
Quasars
Galaxies
BL Lac Objects
unclassified
15


Quasars: 3.9 (5.7)c
BL Lac Ob.: 1.5 (3.0)c
Galaxies:1.1 (3.4)c
Unclassified: 3.0 (2.1)c

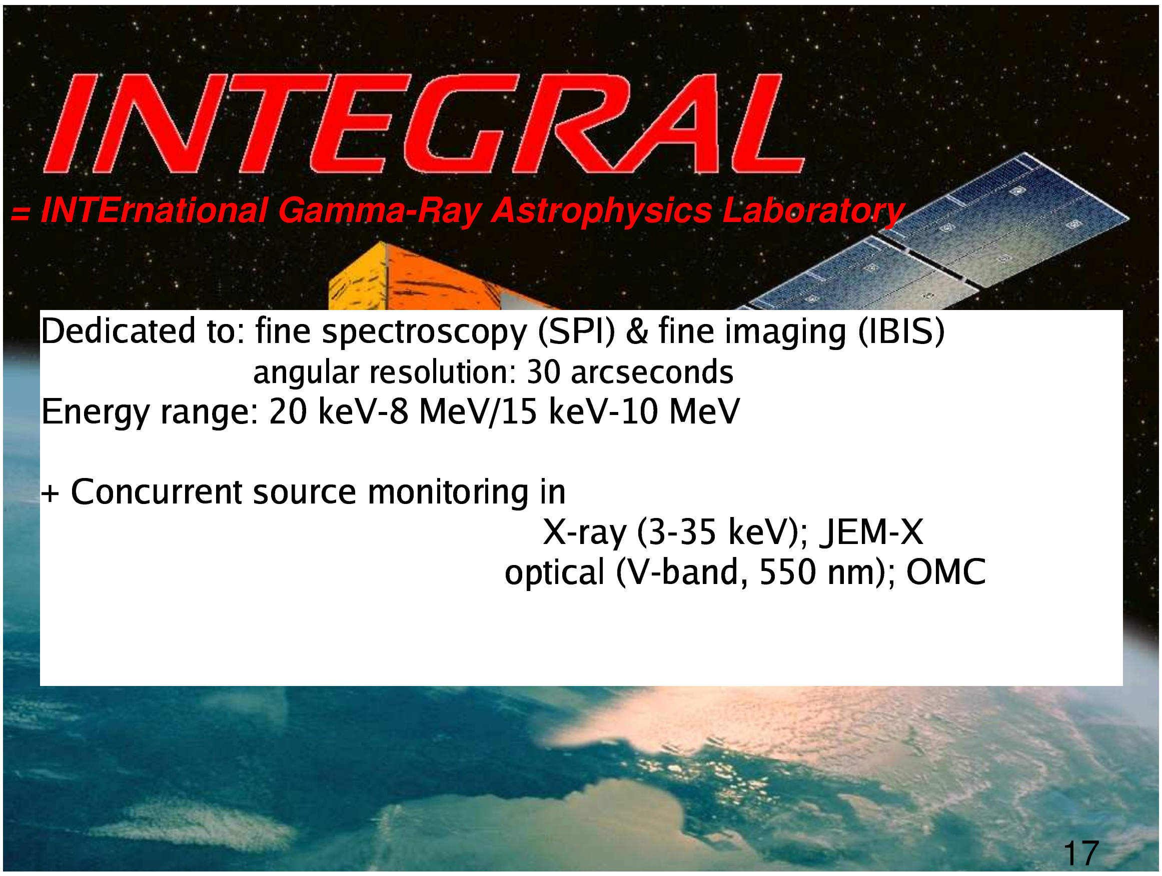
INTEGRAL
= INTErnational Gamma-Ray Astrophysics Laboratory
Dedicated to: fine spectroscopy (SPI) & fine imaging (IBIS)
angular resolution: 30 arcseconds
Energy range: 20 keV-8 MeV/15 keV-10 MeV
+ Concurrent source monitoring in
X-ray (3-35 keV); JEM-X
optical (V-band, 550 nm); OMC
17

Conclusions:

- tendency for class-dependant source-structures:
- galaxy-jets: more jet components
- BL Lac Obj.: curvature stronger

- 3 different motion scenarios
- galaxies reveal tendency for more complex scenarios

- quasars faster than BL Lac Ob., galaxies slowest sources

=> need for higher time sampling for sources with complex motion scenarios

=> INTEGRAL + multifrequency campaign

19

7.2 T. P. Krichbaum: High Resolution Studies of AGNs

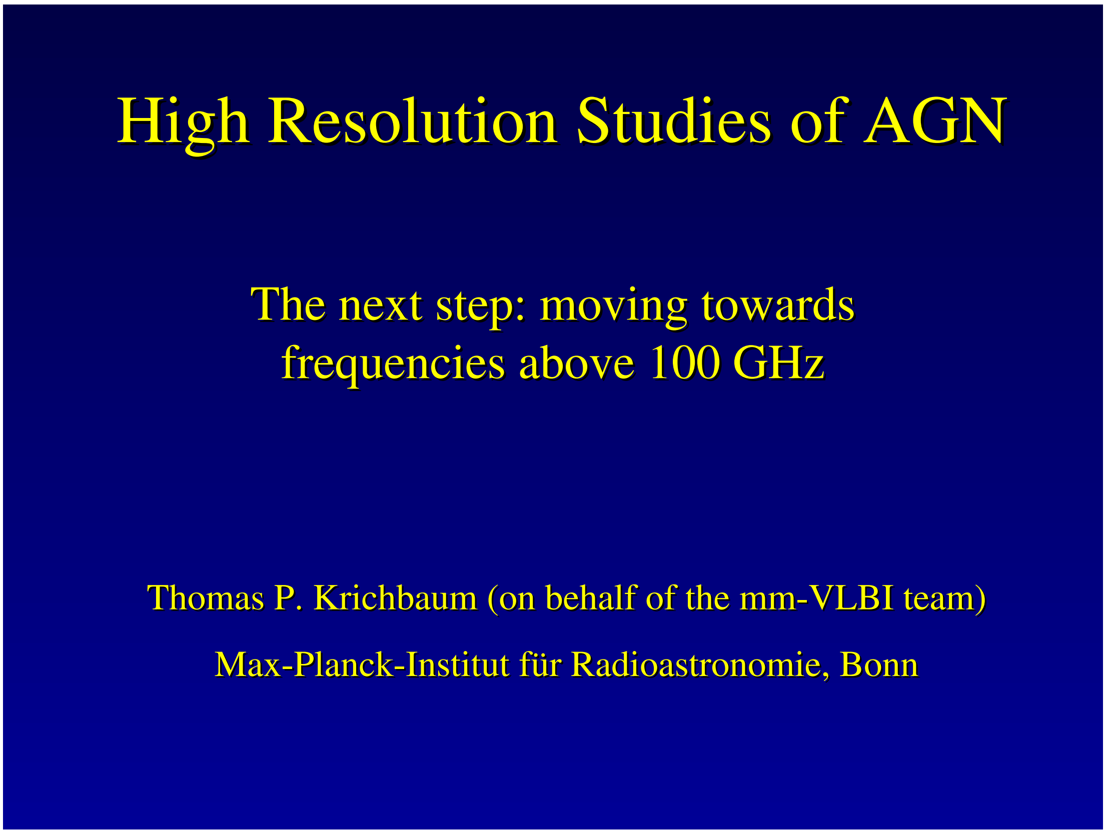

The MM-VLBI teams (3, 2, 1 mm)

Bonn: D. Graham, T. Krichbaum, A. Witzel, A. Zensus, et al.
(U. Bach, J. Klare, A. Pagels, W. Sohn)
IRAM: M. Bremer, A. Greve, M. Grewing, et al.
Onsala: J. Conway, R. Booth, et al.
Haystack: S. Doeleman, P. Phillips, et al.
NRAO: V. Dhawan, J. Ulvestad, et al.
Metsahovi: P. Könnönen, K. Wiik, E. Valtaoja, S. Urpo, et al.
ARO: H. Fagg, P.Strittmatter, L. Ziurys, et al.

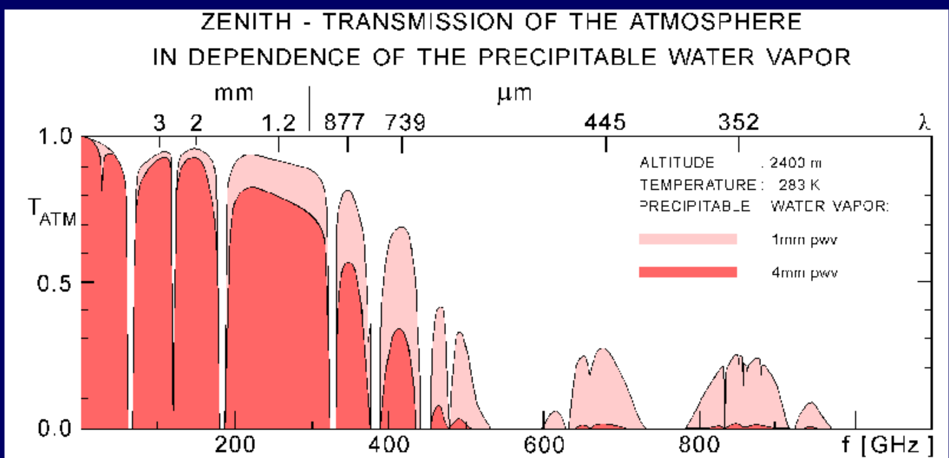

Atmospheric windows near 3, 2, 1.3 and 0.8 mm wavelength allow to observe astronomical sources from ground. With large telescopes partly at high altitudes, enhanced observing bandwidth (Gbit/s) and the future possibility to correct for variable water vapor quasi-instantanously, the sensitivity and the quality of the maps can be further improved.

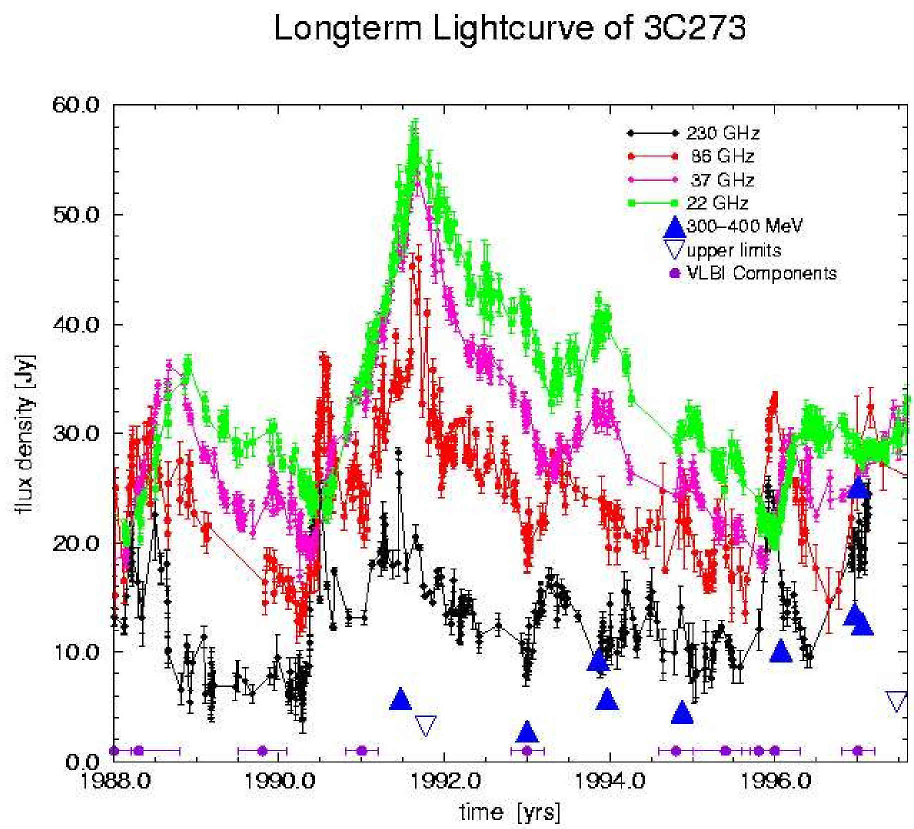
Longterm Lightcurve of 3C273
230 GHz
86 GHz
37 GHz
22 GHz
300–400 MeV
upper limits
VLBI Components
flux density [Jy]
time [yrs]

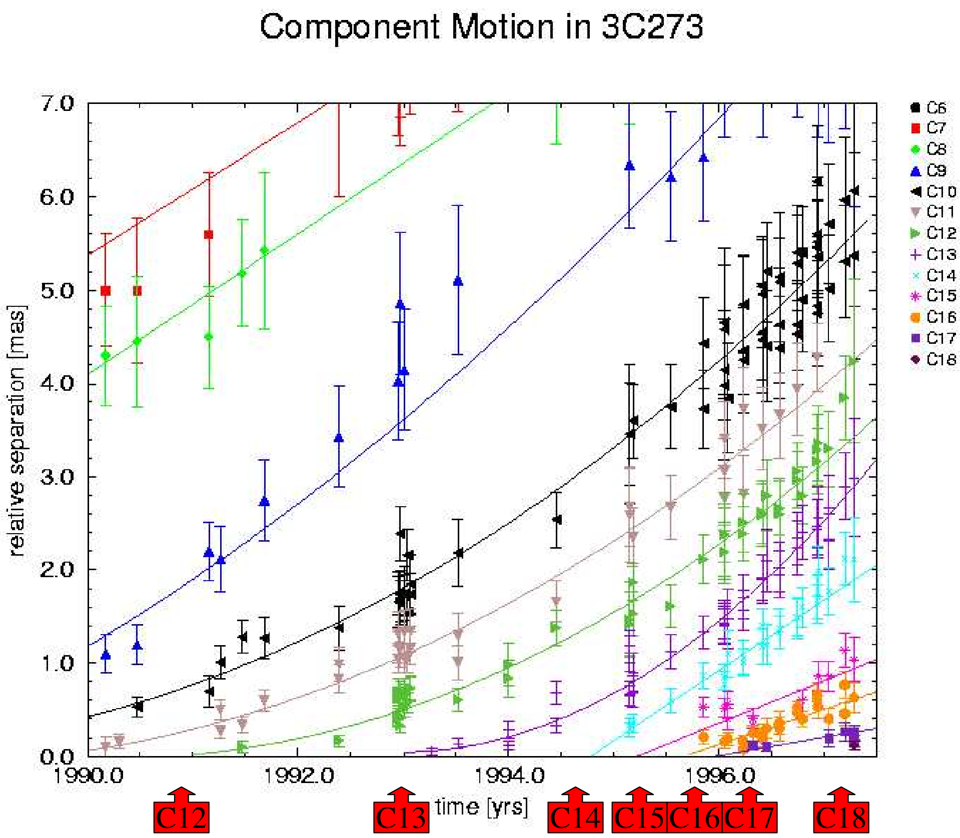
Component Motion in 3C273
C6
C7
C8
C9
C10
C11
C12
C13
C14
C15
C16
C17
C18
relative separation [mas]
time [yrs]
C12
C13
C14
C15
C16
C17
C18

Component Ejection Times and Outbursts

Id.	Ejection Time [yrs]	Gamma Flare Time of Max.	Onset of Flare (mm-radio)
C6	1980.0± 0.3		1980.6
C7	1982.4± 0.4		1982.3
C8	1984.6± 0.2		1984.2
C9	1988.0± 0.2		1987.8
C10	1988.3± 0.5		1988.0
C11	1989.8± 0.3		1990.3
C12	1991.0± 0.2	1991.47	1990.9
C13	1993.0± 0.2	1993.00	1993.1
		1993.86	
C14	1994.8± 0.2	1994.88	1994.3
C15	1995.4± 0.4		
C16	1995.8± 0.2	1996.08	1995.8
C17	1996.0± 0.3		
C18	1997.0± 0.2	1997.02	1996.8

In 3C273 Gamma rays escape from the VLBI jet at about 1000-2000 Schwarzschild radii !

$$t_0^{\rm VLBI} - t_0^{\rm mm} = 0.1 \pm 0.2$$
$$t_0^{\gamma} \quad - t_0^{\rm mm} = 0.3 \pm 0.3$$

This suggests:

$$t_0^{\rm mm} < t_0^{\rm VLBI} \le t_0^{\gamma}$$

with $_{app} \approx 4$ *near core* $\Rightarrow$

and" r being the radius at $= 1$

$r \le 0.1\ mas = 6 \cdot 10^{17}\ cm = 2000\ R_s$

Ejection Velocity and Optical Flux

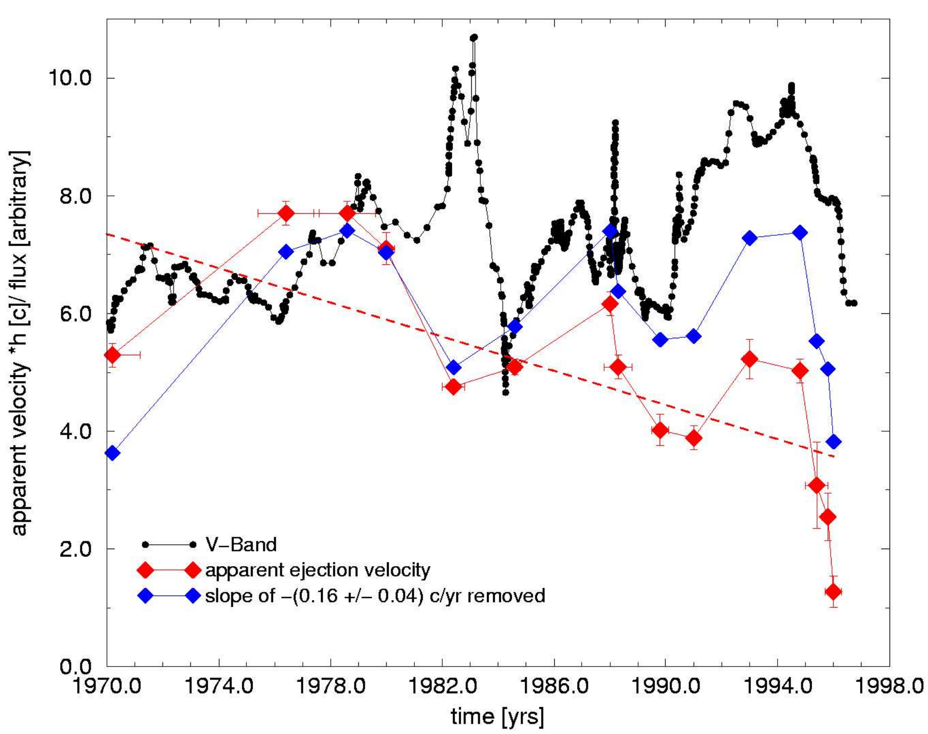

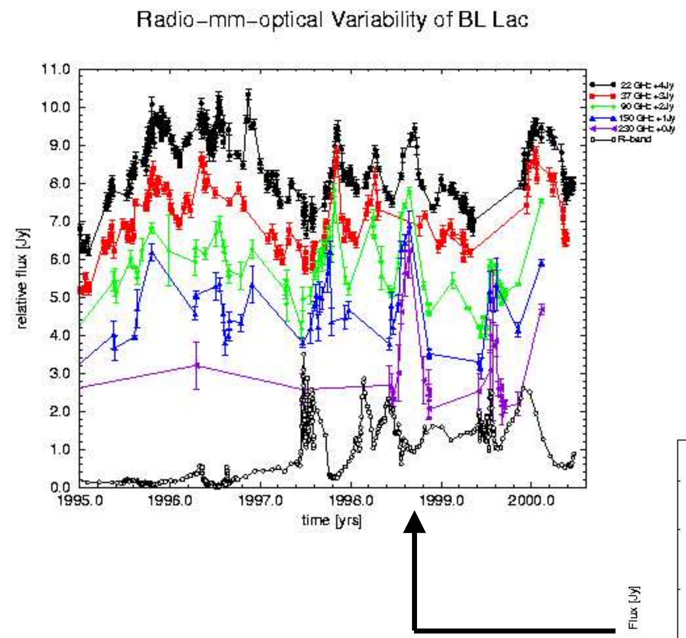

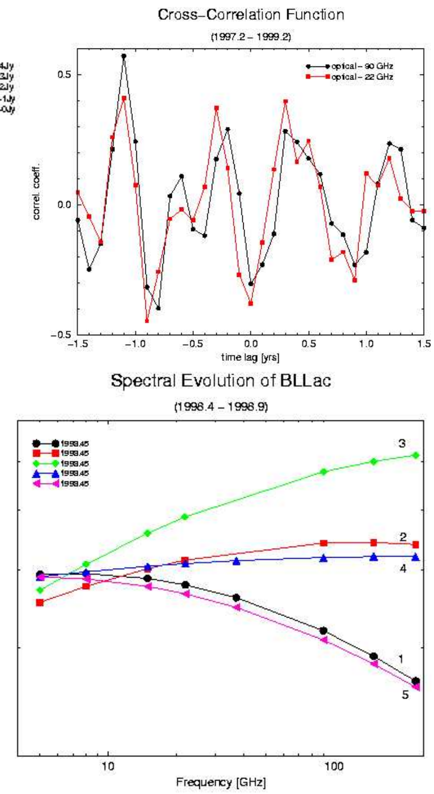

A geometrical origin of the quasi-periodic intensity variations ?

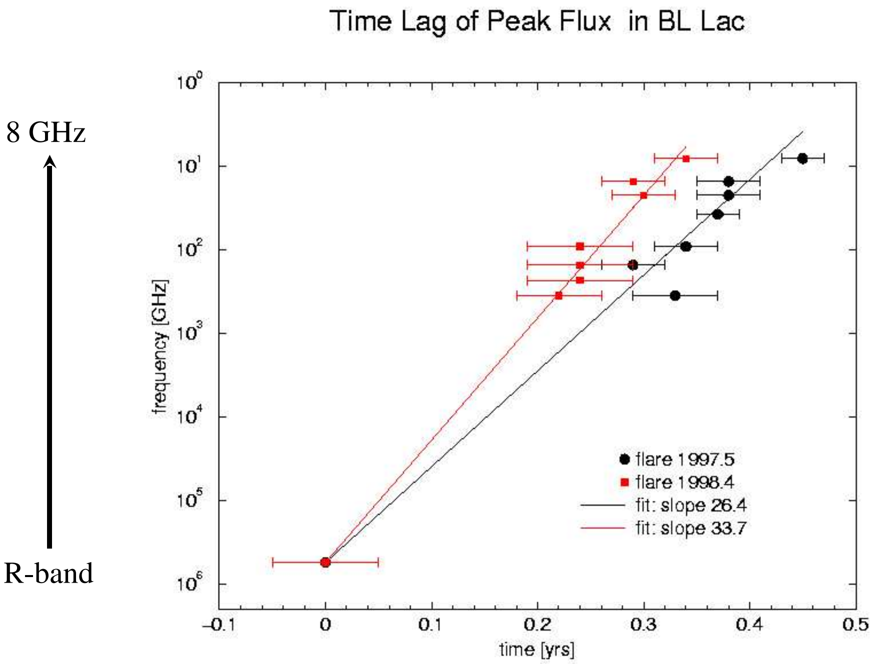

Global Millimeter-VLBI

High angular resolution studies with global VLBI at the shortest (mm-) wavelength allow to image with the finest angular resolution regions in AGN and other compact sources, which are self-absorbed (opaque) at the longer wavelengths.

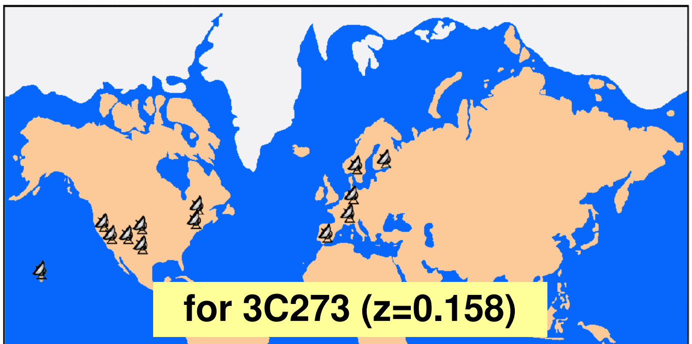

for 3C273 (z=0.158)

λ	ν	θ	A	R_s
[mm]	[GHz]	[μas]	[mpc]	$[10^9 M_s]$
3	86	55	97	1000
2	147	32	57	590
1.3	230	20	36	370

In the next years: go from 3mm (86 GHz) to 1mm (230 GHz)

How is the brightness temperature of jets changing towards the nucleus?

The widely accepted relativistic jet model predicts constant brightness temperature along the jet.

The jet formation, however, can invoke acceleration or deceleration at the jet base.

MM-VLBI imaging at 3mm and shorter wavelengths should reveal how the brightness temperature is changing.

Flux density per unit length of a relativistic jet

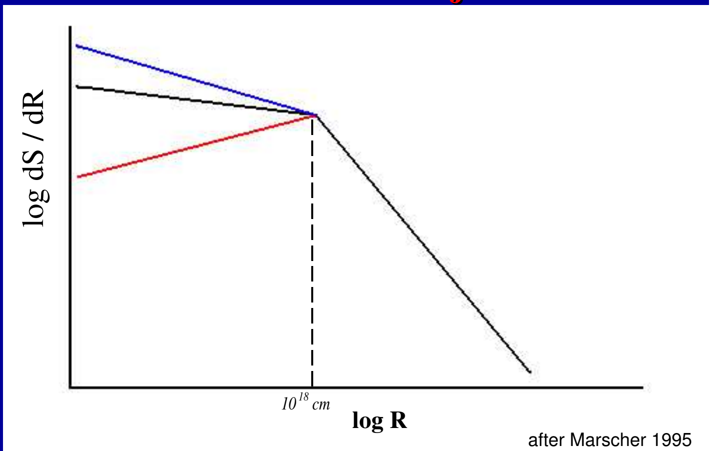

Brightness temperature distribution of VLBI cores

15 GHz (N=132)

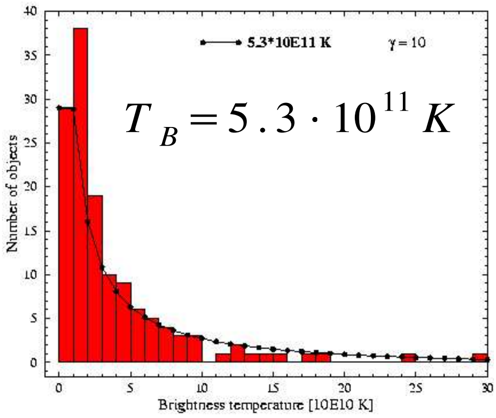

86 GHz (N=27)

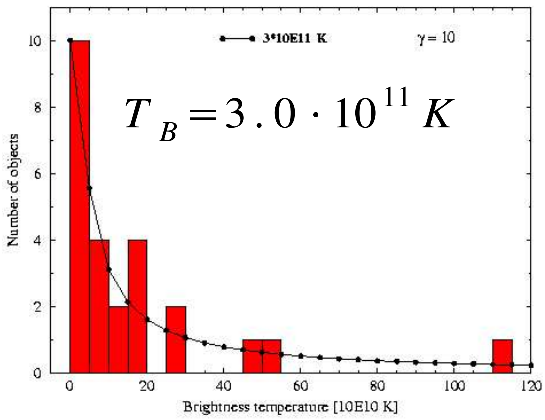

How does T_B change towards higher frequencies ?

$$_{[mas]} = \frac{1.1}{_{[GHz]}} \cdot \sqrt{\frac{S_{[Jy]}}{T_{B\,[10^{12}\,K]}}}$$

Lobanov et al. 2000

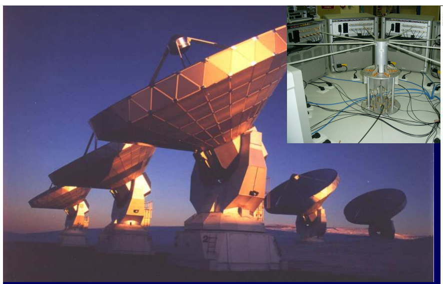

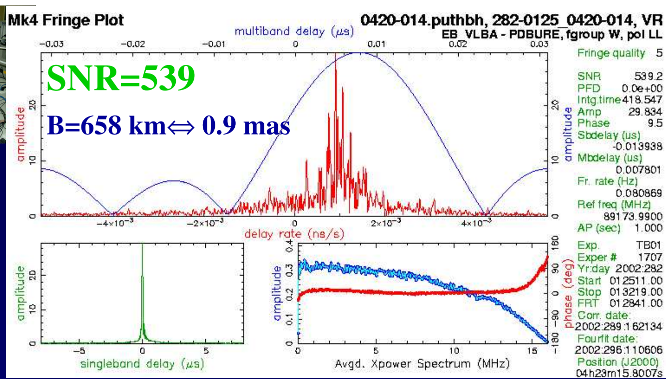

Source	S_tot	SNR(scan)
0420-014	8.9	77-539
NRAO150	7.6	122
NRAO530	5.9	26
SgrA*		18
1633+38	4.6	132-210
2145+067	6.7	158-236
3C454.3	6.1	39-119

Oct. 2002: all 6 antennas of the Plateau de Bure interferometer phased for 3mm-VLBI

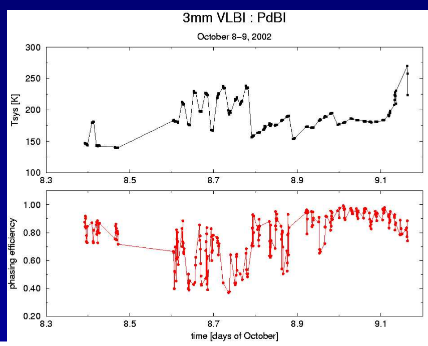

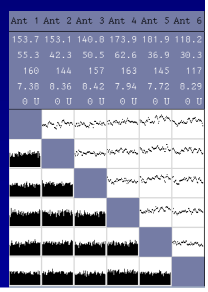

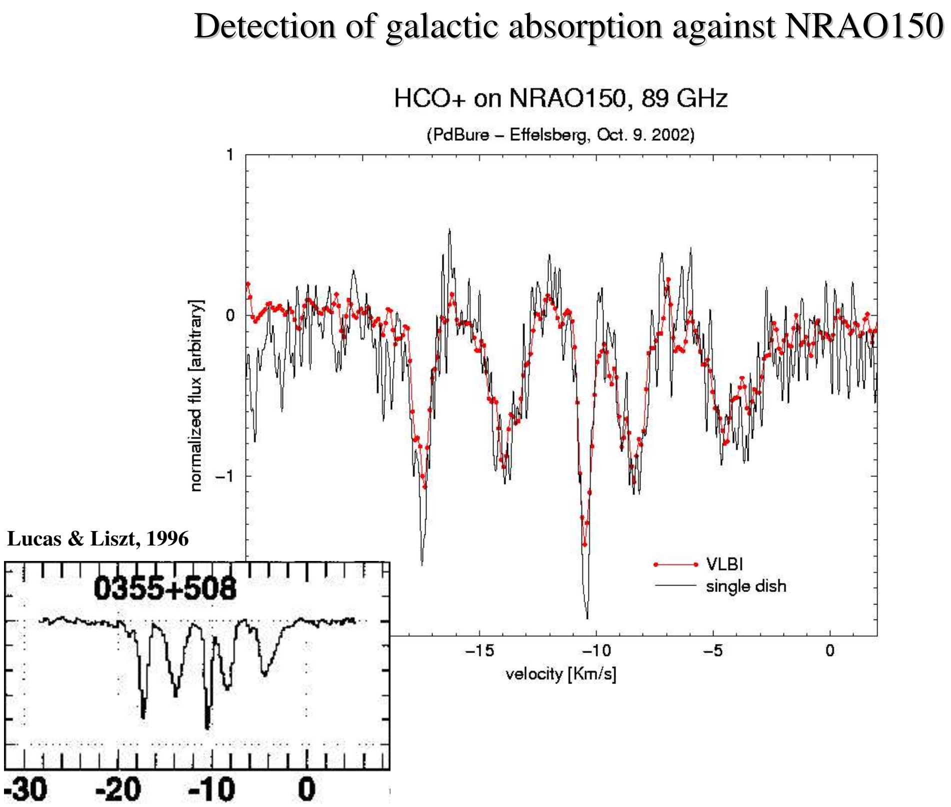
Detection of galactic absorption against NRAO150
HCO+ on NRAO150, 89 GHz
(PdBure – Effelsberg, Oct. 9. 2002)
normalized flux [arbitrary]
1
0
−1
−15
−10
−5
0
velocity [Km/s]
VLBI
single dish
Lucas & Liszt, 1996
0355+508
-30
-20
-10
0

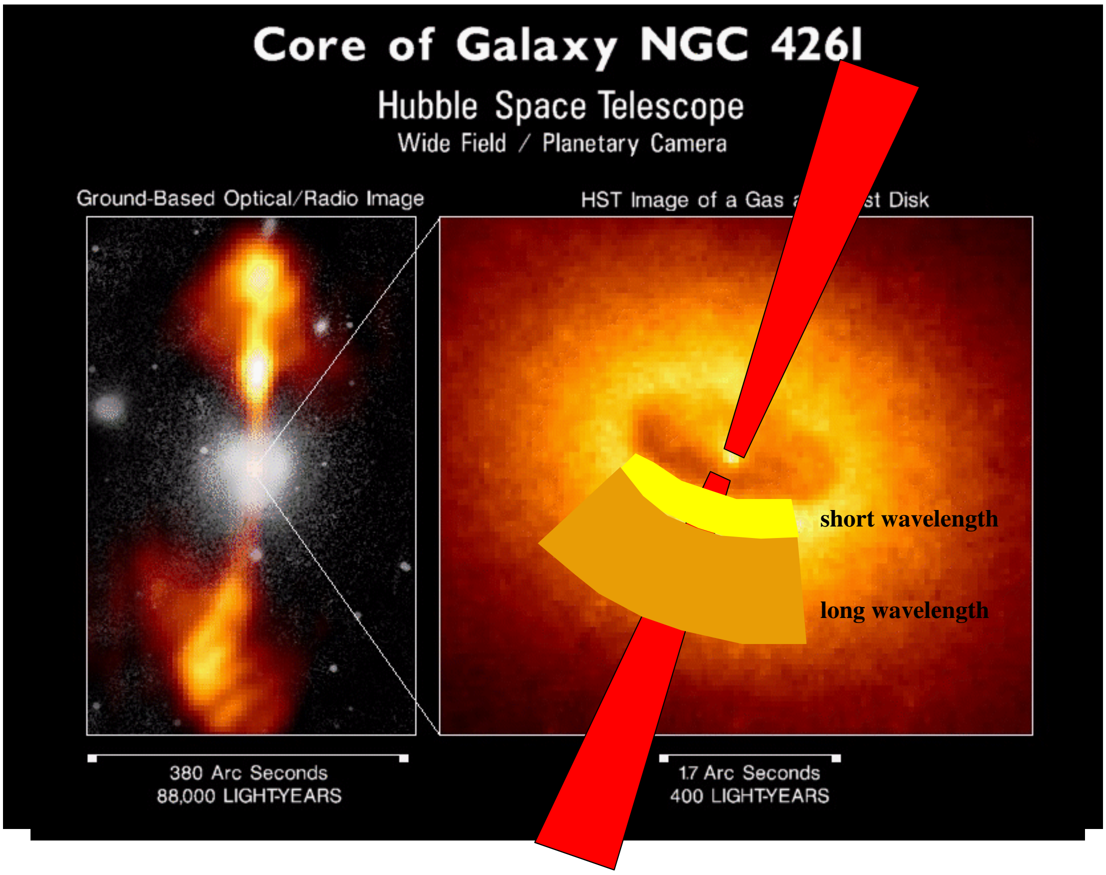
Core of Galaxy NGC 4261
Hubble Space Telescope
Wide Field / Planetary Camera
Ground-Based Optical/Radio Image
HST Image of a Gas a st Disk
short wavelength
long wavelength
380 Arc Seconds
88,000 LIGHT-YEARS
17 Arc Seconds
400 LIGHT-YEARS

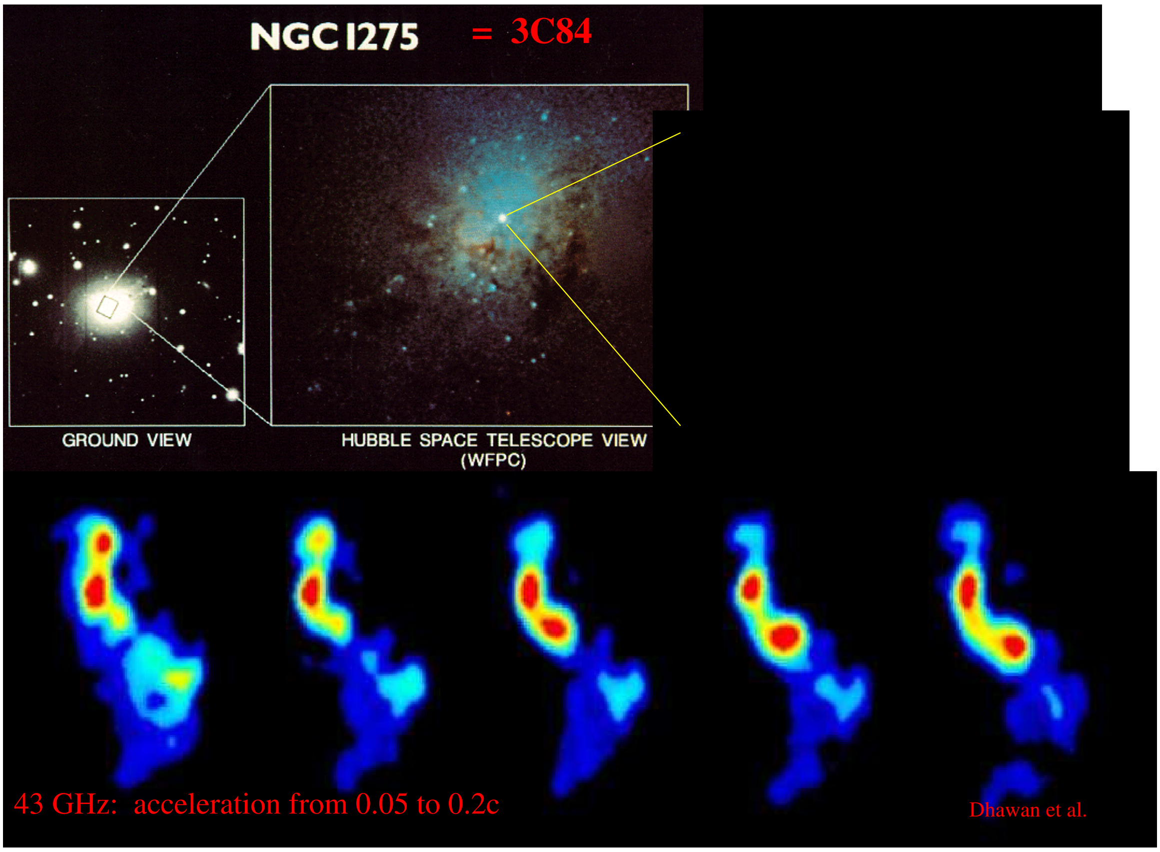
NGC 1275 = 3C84
GROUND VIEW
HUBBLE SPACE TELESCOPE VIEW (WFPC)
43 GHz: acceleration from 0.05 to 0.2c
Dhawan et al.

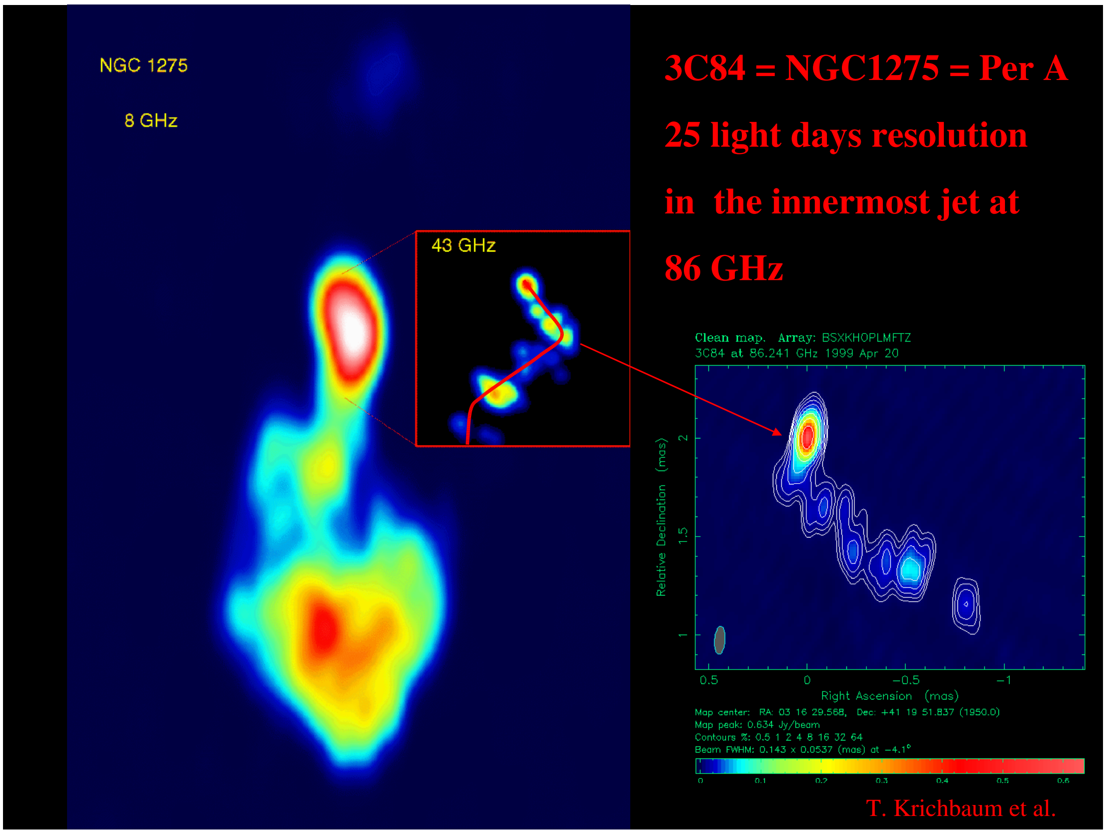
NGC 1275
8 GHz
43 GHz
3C84 = NGC1275 = Per A
25 light days resolution
in the innermost jet at
86 GHz
Clean map. Array: BSXKHOPLMFTZ
3C84 at 86.241 GHz 1999 Apr 20
Relative Declination (mas)
Right Ascension (mas)
Map center: RA: 03 16 29.568, Dec: +41 19 51.837 (1950.0)
Map peak: 0.634 Jy/beam
Contours %: 0.5 1 2 4 8 16 32 64
Beam FWHM: 0.143 x 0.0537 (mas) at −4.1°
T. Krichbaum et al.

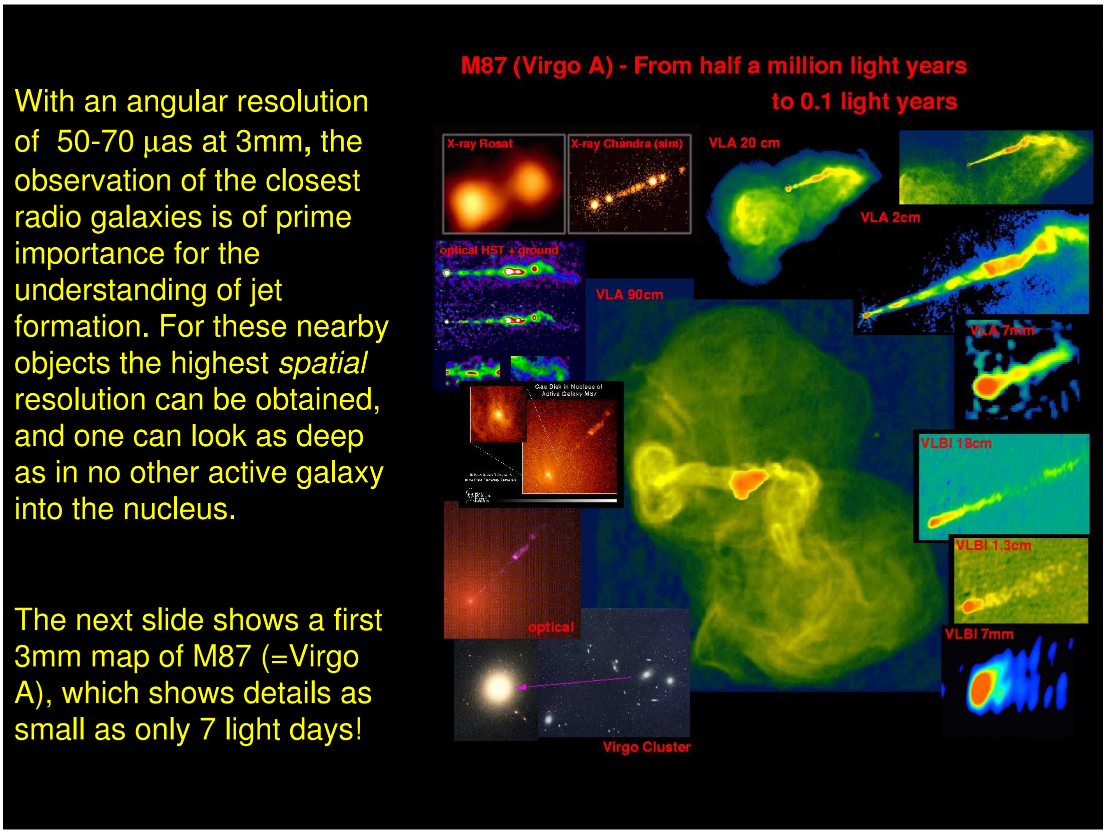
With an angular resolution of 50-70 µas at 3mm, the observation of the closest radio galaxies is of prime importance for the understanding of jet formation. For these nearby objects the highest *spatial* resolution can be obtained, and one can look as deep as in no other active galaxy into the nucleus.
The next slide shows a first 3mm map of M87 (=Virgo A), which shows details as small as only 7 light days!
M87 (Virgo A) - From half a million light years
to 0.1 light years
X-ray Rosat
X-ray Chandra (sim)
VLA 20 cm
VLA 2cm
optical HST + ground
VLA 90cm
VLA 7mm
VLBI 18cm
VLBI 1.3cm
optical
VLBI 7mm
Virgo Cluster

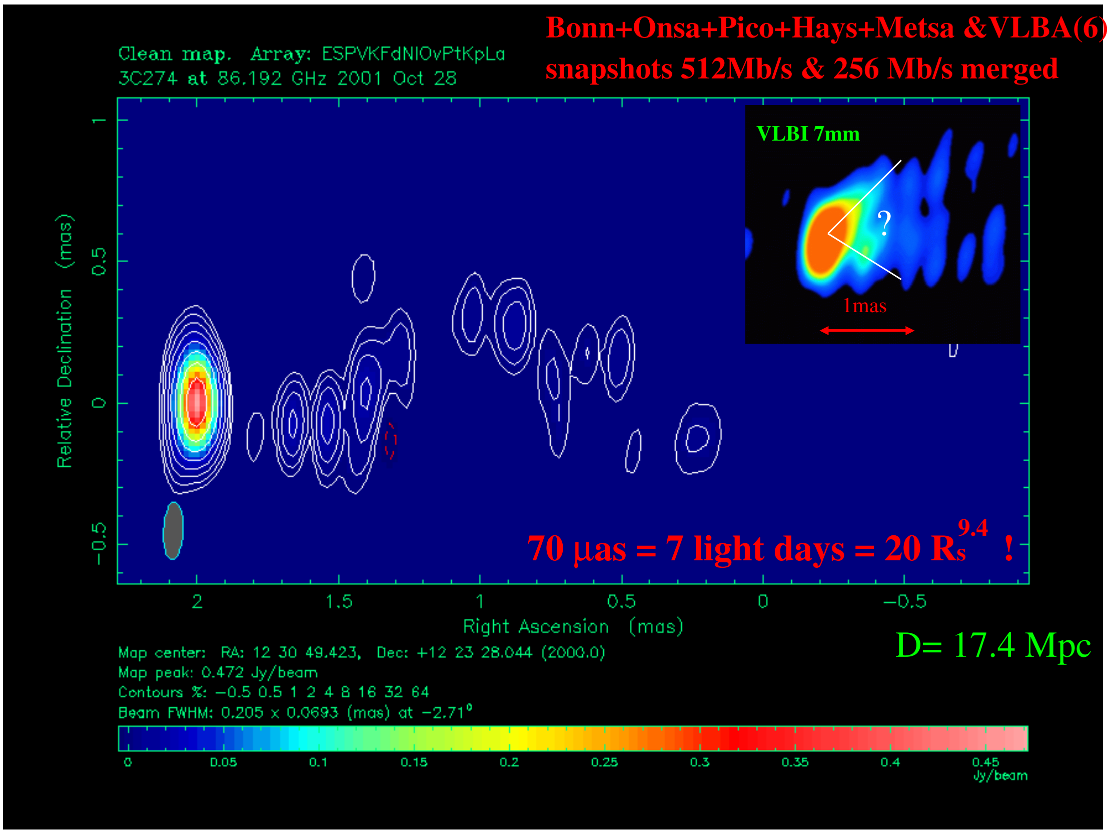
Bonn+Onsa+Pico+Hays+Metsa &VLBA(6)
snapshots 512Mb/s & 256 Mb/s merged
Clean map. Array: ESPVKFdNlOvPtKpLa
3C274 at 86.192 GHz 2001 Oct 28
VLBI 7mm
?
1mas
70 µas = 7 light days = 20 Rs 9.4 !
Relative Declination (mas)
Right Ascension (mas)
D= 17.4 Mpc
Map center: RA: 12 30 49.423, Dec: +12 23 28.044 (2000.0)
Map peak: 0.472 Jy/beam
Contours %: −0.5 0.5 1 2 4 8 16 32 64
Beam FWHM: 0.205 x 0.0693 (mas) at −2.71°
Jy/beam

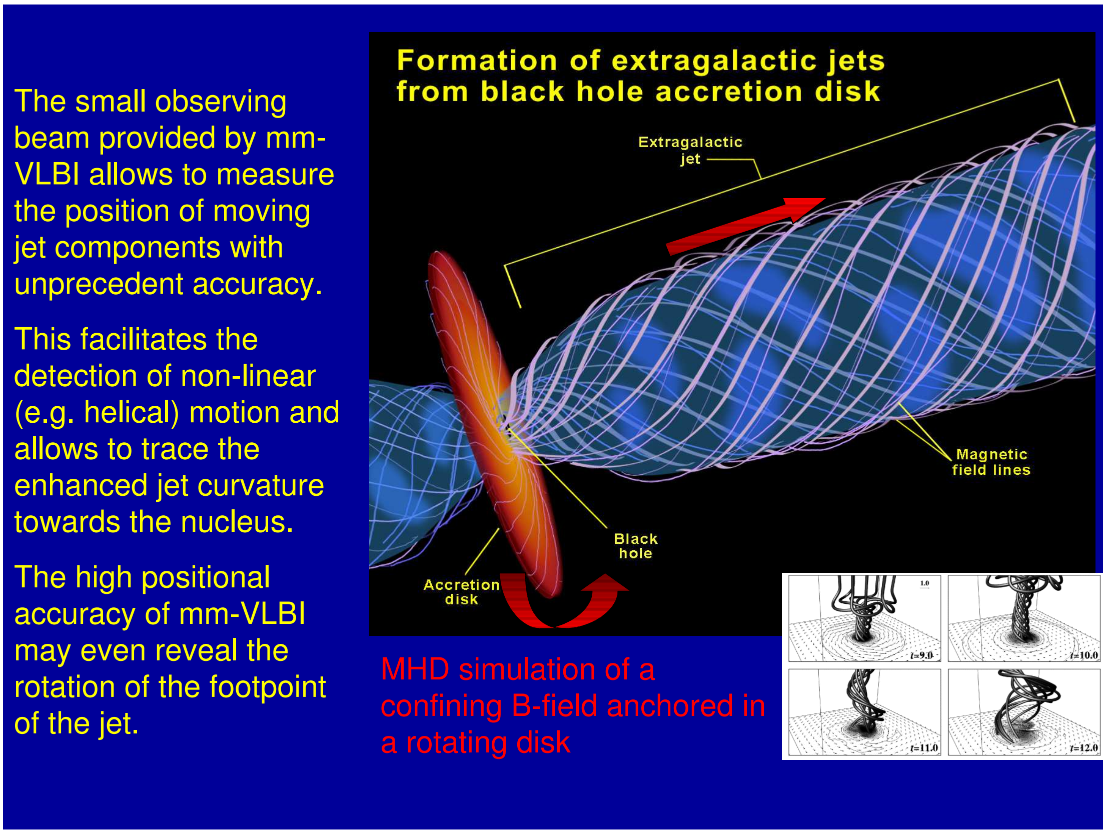
The small observing beam provided by mm-VLBI allows to measure the position of moving jet components with unprecedent accuracy.
This facilitates the detection of non-linear (e.g. helical) motion and allows to trace the enhanced jet curvature towards the nucleus.
The high positional accuracy of mm-VLBI may even reveal the rotation of the footpoint of the jet.
Formation of extragalactic jets from black hole accretion disk
Extragalactic jet
Magnetic field lines
Black hole
Accretion disk
MHD simulation of a confining B-field anchored in a rotating disk
t=9.0
t=10.0
t=11.0
t=12.0

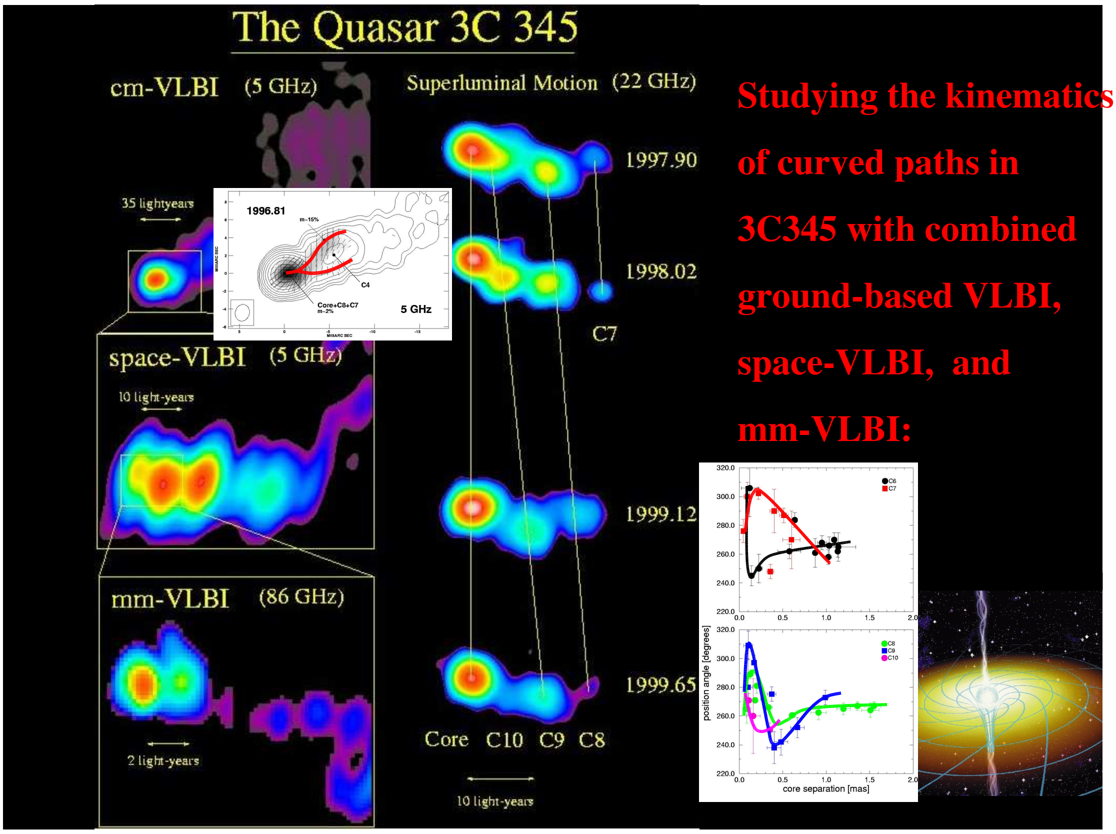
The Quasar 3C 345
cm-VLBI (5 GHz)
35 lightyears
1996.81
C4
Core+C6+C7
5 GHz
space-VLBI (5 GHz)
10 light-years
mm-VLBI (86 GHz)
2 light-years
Superluminal Motion (22 GHz)
1997.90
1998.02
C7
1999.12
1999.65
Core C10 C9 C8
10 light-years
Studying the kinematics of curved paths in 3C345 with combined ground-based VLBI, space-VLBI, and mm-VLBI:
position angle [degrees]
core separation [mas]

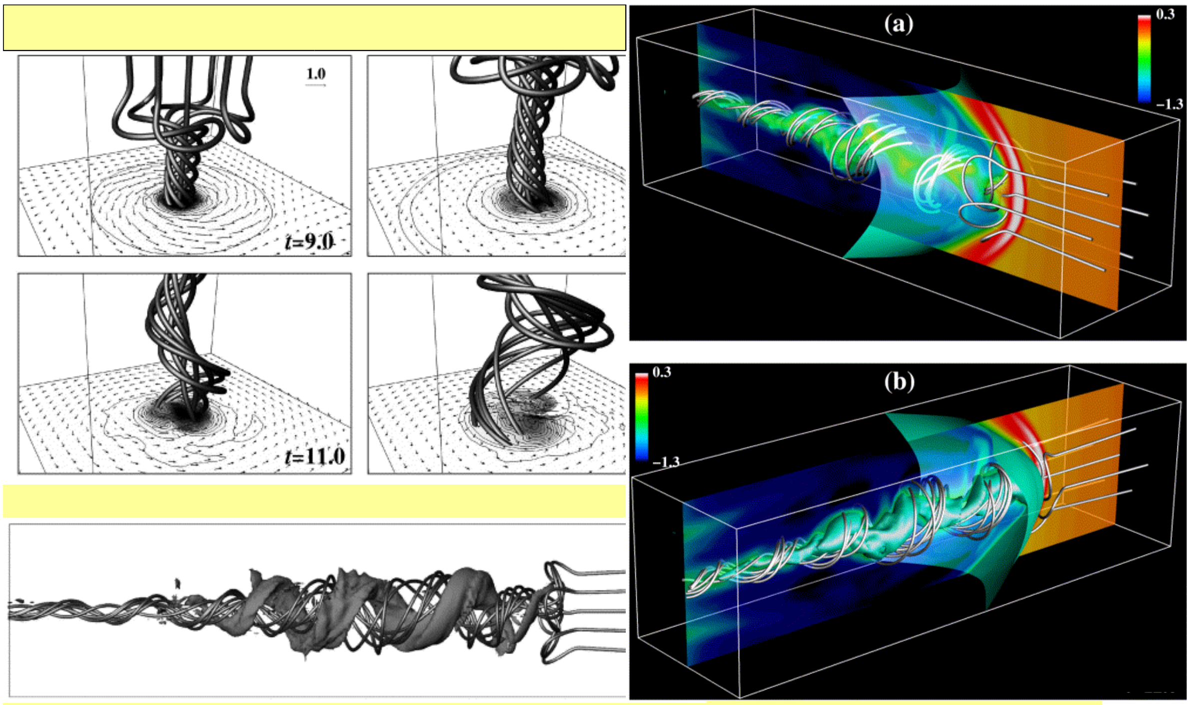

3-dimensional magnetohydrodynamic (MHD) jet simulations

Nakamura et al. 2001

The precessing jet gas burner

Fuel injection with a precessing flow reduces NO_x emission by up to 50 %:

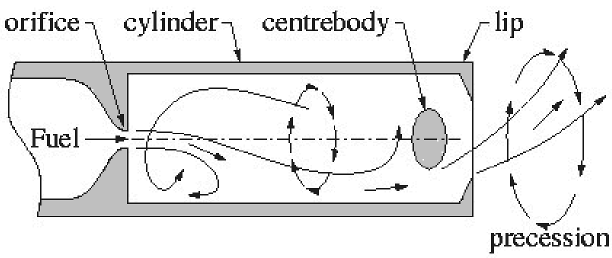

Luxton, Nathan & Luminis 1988

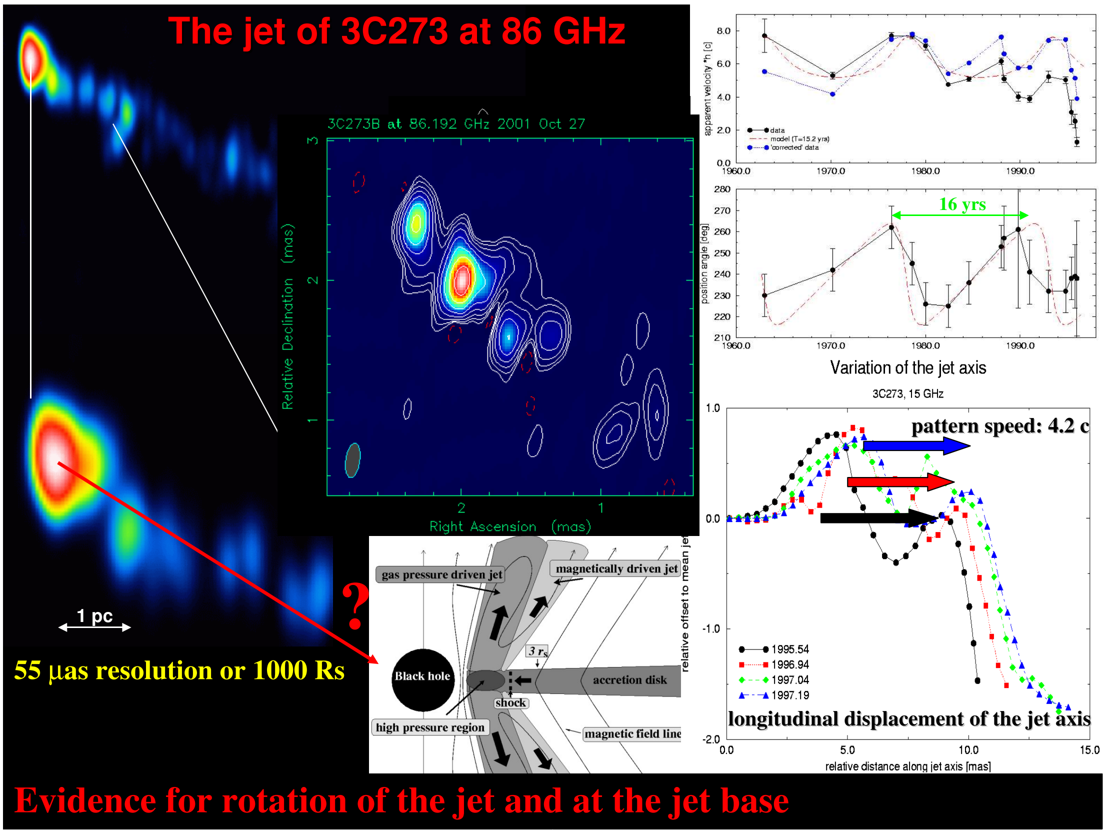

The jet of 3C273 at 86 GHz
3C273B at 86.192 GHz 2001 Oct 27
Relative Declination (mas)
Right Ascension (mas)
1 pc
55 µas resolution or 1000 Rs
gas pressure driven jet
magnetically driven jet
Black hole
accretion disk
shock
high pressure region
magnetic field line
Variation of the jet axis
16 yrs
3C273, 15 GHz
pattern speed: 4.2 c
1995.54
1996.94
1997.04
1997.19
longitudinal displacement of the jet axis
relative distance along jet axis [mas]
Evidence for rotation of the jet and at the jet base

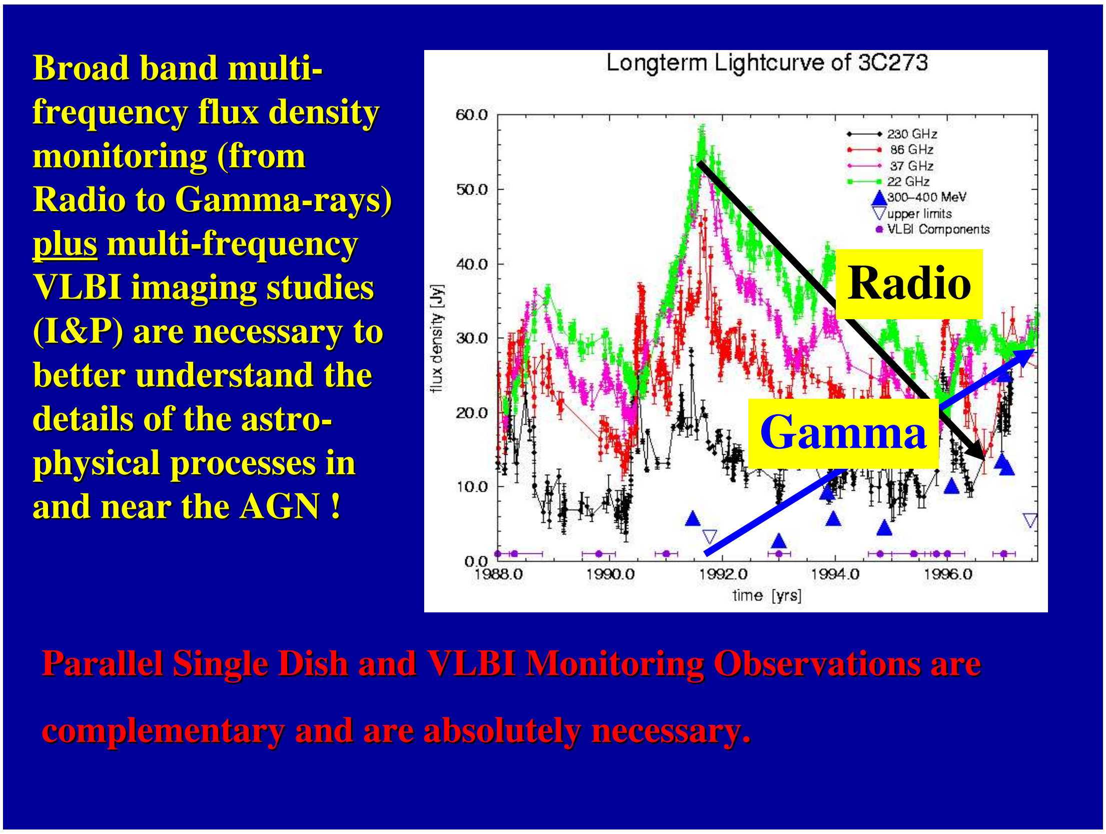

Broad band multi-frequency flux density monitoring (from Radio to Gamma-rays) plus multi-frequency VLBI imaging studies (I&P) are necessary to better understand the details of the astro-physical processes in and near the AGN !
Longterm Lightcurve of 3C273
230 GHz
86 GHz
37 GHz
22 GHz
300–400 MeV
upper limits
VLBI Components
Radio
Gamma
flux density [Jy]
time [yrs]
Parallel Single Dish and VLBI Monitoring Observations are complementary and are absolutely necessary.

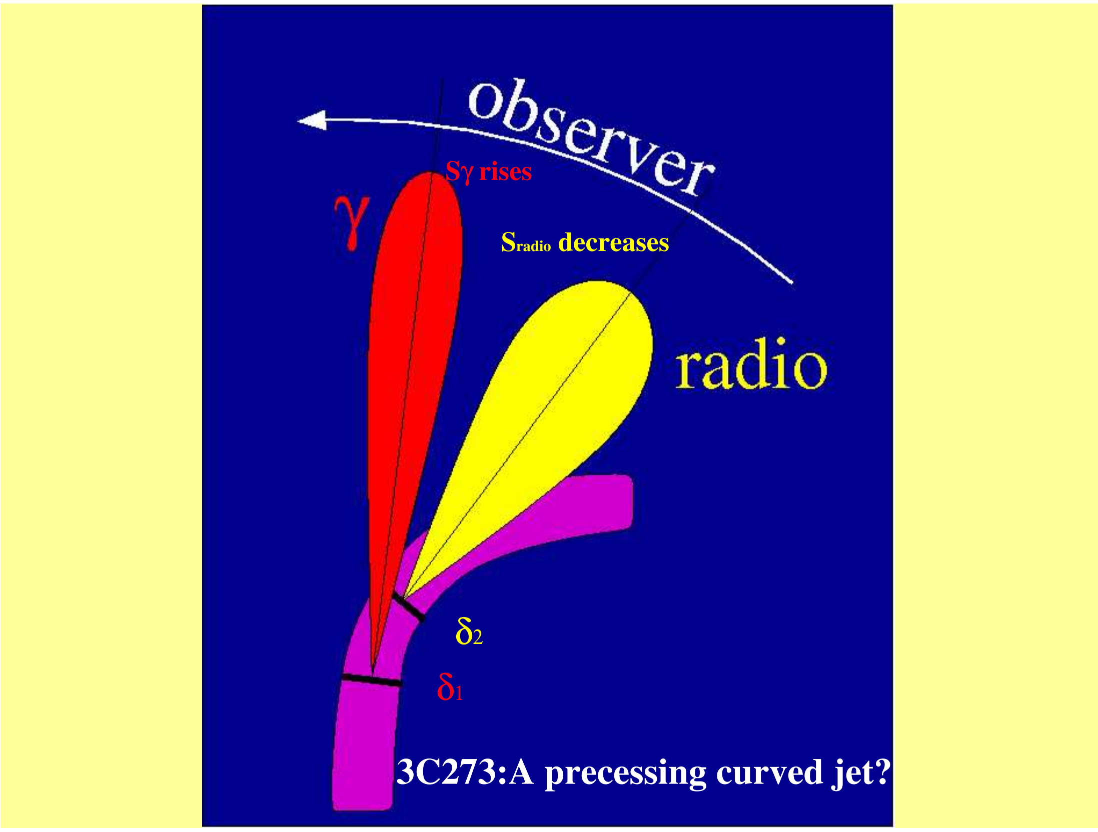
observer
Sγ rises
γ
Sradio decreases
radio
δ2
δ1
3C273:A precessing curved jet?

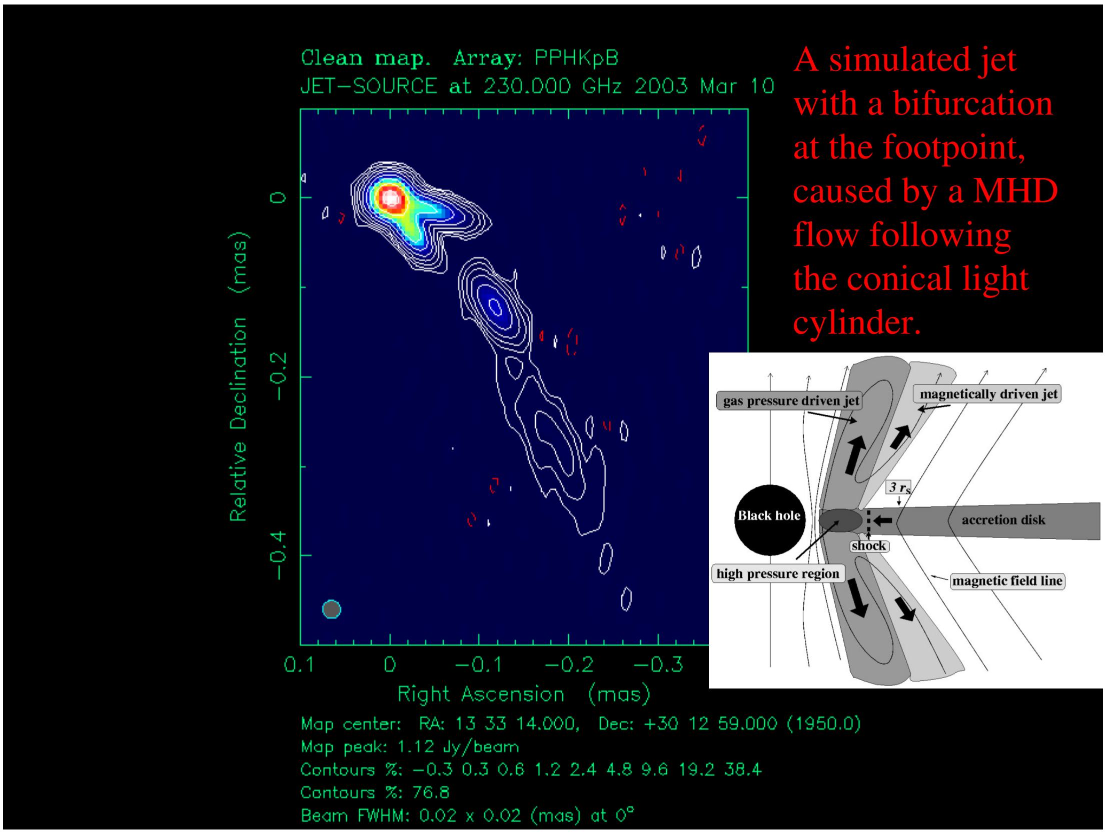
Clean map. Array: PPHKpB
JET-SOURCE at 230.000 GHz 2003 Mar 10
A simulated jet with a bifurcation at the footpoint, caused by a MHD flow following the conical light cylinder.
Relative Declination (mas)
Right Ascension (mas)
gas pressure driven jet
magnetically driven jet
Black hole
accretion disk
shock
high pressure region
magnetic field line
Map center: RA: 13 33 14.000, Dec: +30 12 59.000 (1950.0)
Map peak: 1.12 Jy/beam
Contours %: −0.3 0.3 0.6 1.2 2.4 4.8 9.6 19.2 38.4
Contours %: 76.8
Beam FWHM: 0.02 x 0.02 (mas) at 0°

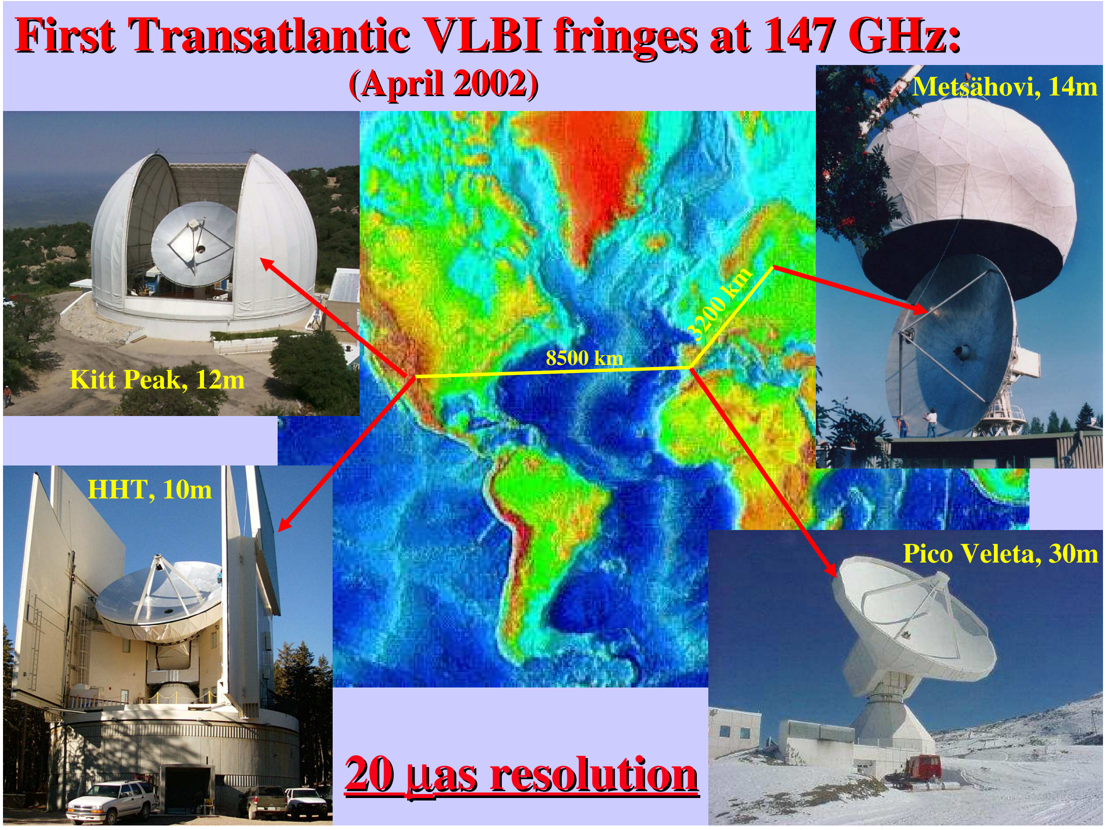

The SNR´s of the transatlantic VLBI detections at 147 GHz

(April 2002)

Source	Flux [Jy]	HHT-KP	HHT-PV	KP-PV	MET-PV
NRAO150	6.5	19	7	6	
0420-014	5.7	13	5?	5?	
3C279	21.1	49	75	20	10
1633+382	7.3	23	23	13	
3C345	4.7	7	6?	5?	
3C454.3	8.8	15	6?	5?	

Sources detected on the short baseline HHT-KP:
0133+476, 3C273, NRAO530, SgrA*, 1921-293, BL Lac, 2255-282

: detected   : marginally detected on long baselines

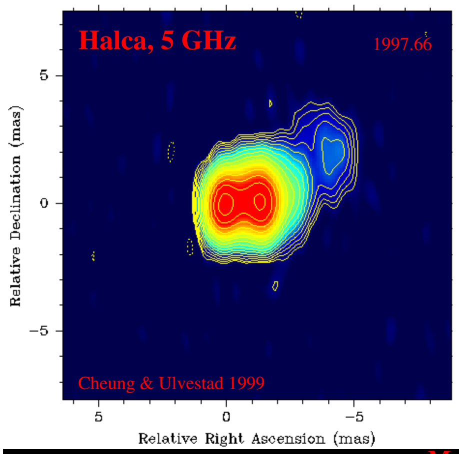

1633+382 = 4C38.41

OVV-QSO, z=1.814

historical maps:

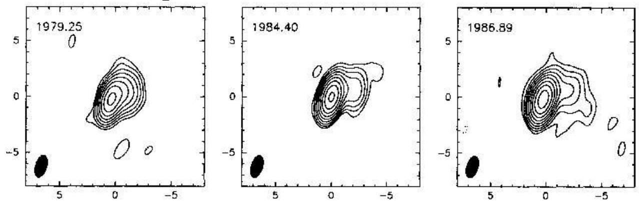

Barthel et al. 1995

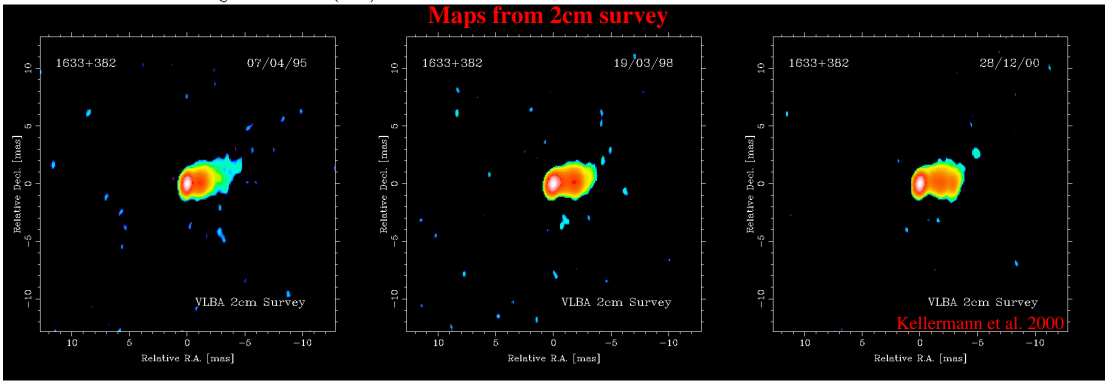

Preliminary results from an ongoing flux density monitoring of 1633+382.

This is the largest flare ever observed in this source and one of the strongest mm-flares.

Arrows indicate the times of VLBI observations. The monitoring still is going on.

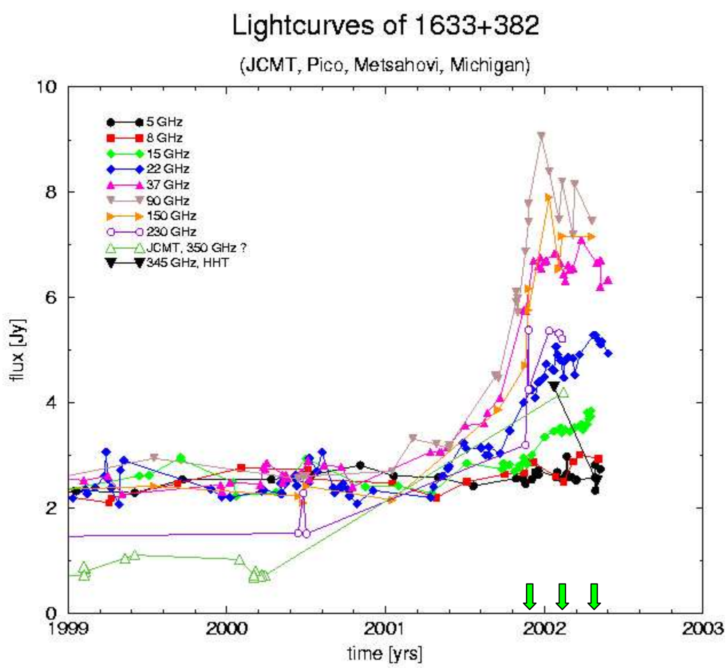

Krichbaum et al. 2002

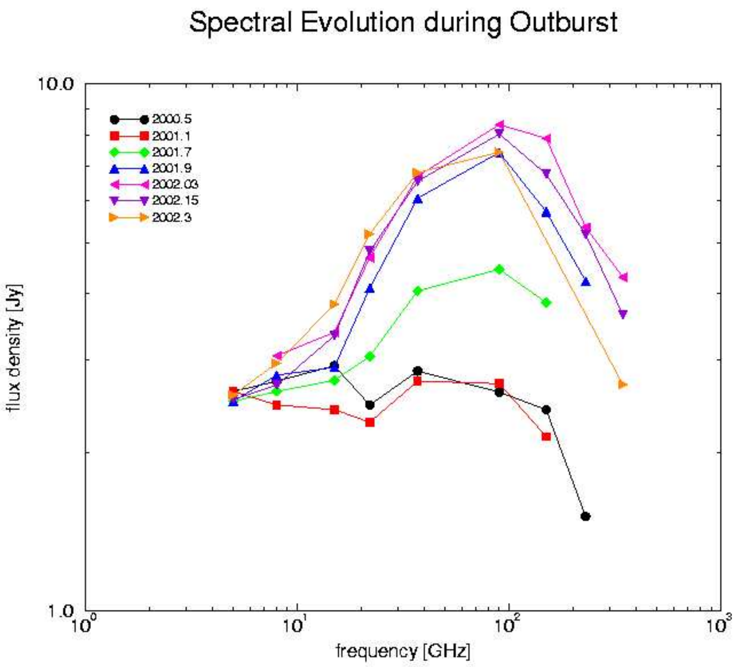
Spectral Evolution during Outburst
2000.5
2001.1
2001.7
2001.9
2002.03
2002.15
2002.3
flux density [Jy]
frequency [GHz]

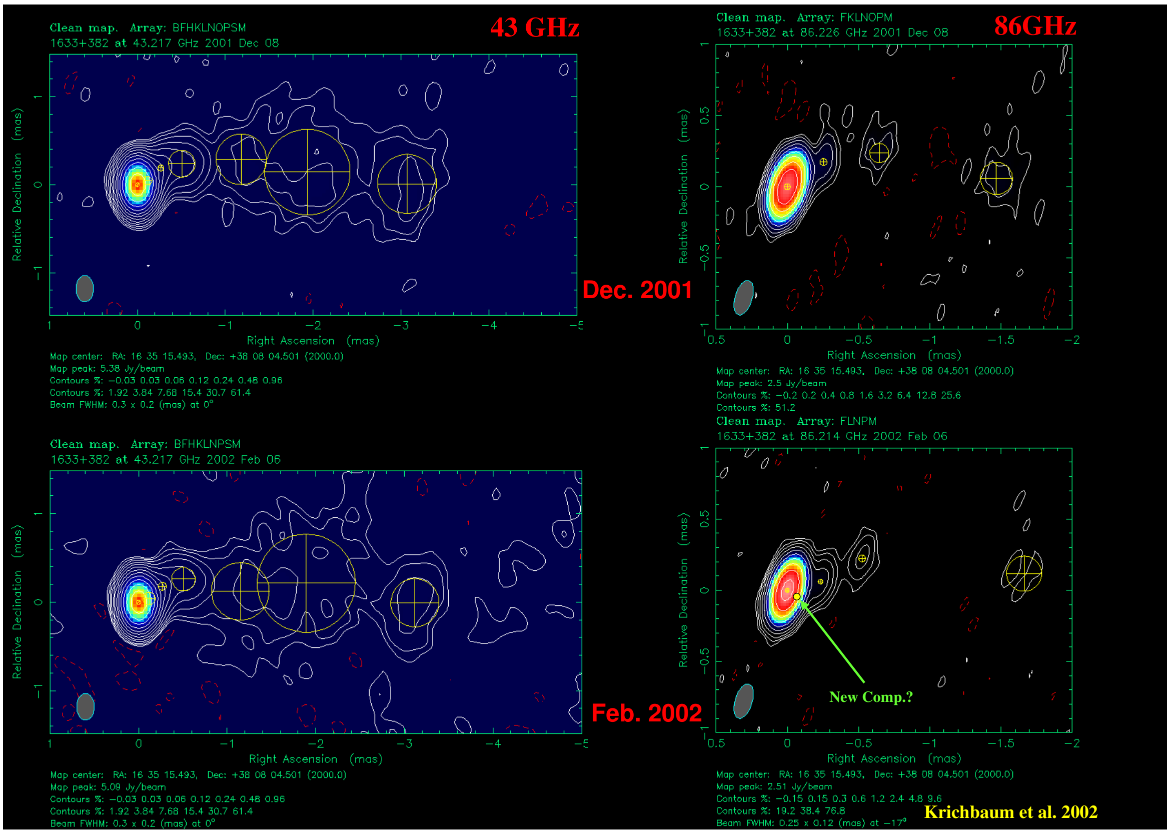
43 GHz
86GHz
Dec. 2001
Feb. 2002
New Comp.?
Krichbaum et al. 2002

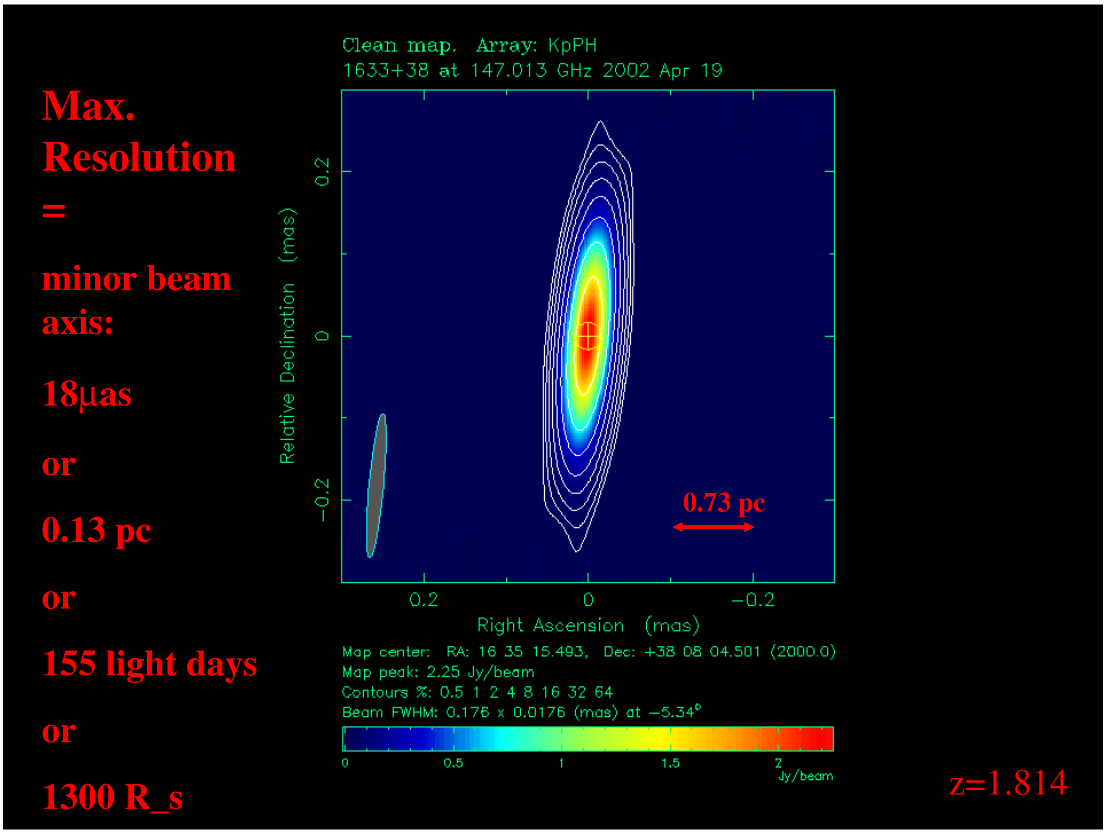
Max. Resolution =
minor beam axis:
18µas
or
0.13 pc
or
155 light days
or
1300 R_s
Clean map. Array: KpPH
1633+38 at 147.013 GHz 2002 Apr 19
Relative Declination (mas)
Right Ascension (mas)
0.73 pc
Map center: RA: 16 35 15.493, Dec: +38 08 04.501 (2000.0)
Map peak: 2.25 Jy/beam
Contours %: 0.5 1 2 4 8 16 32 64
Beam FWHM: 0.176 x 0.0176 (mas) at −5.34°
Jy/beam
z=1.814

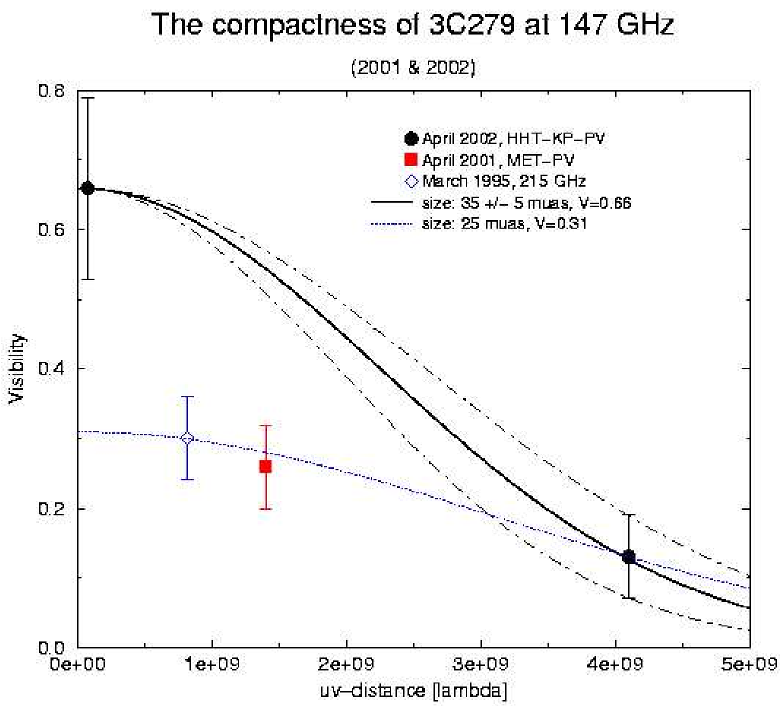
The compactness of 3C279 at 147 GHz
(2001 & 2002)
April 2002, HHT−KP−PV
April 2001, MET−PV
March 1995, 215 GHz
size: 35 +/− 5 muas, V=0.66
size: 25 muas, V=0.31
Visibility
uv−distance [lambda]

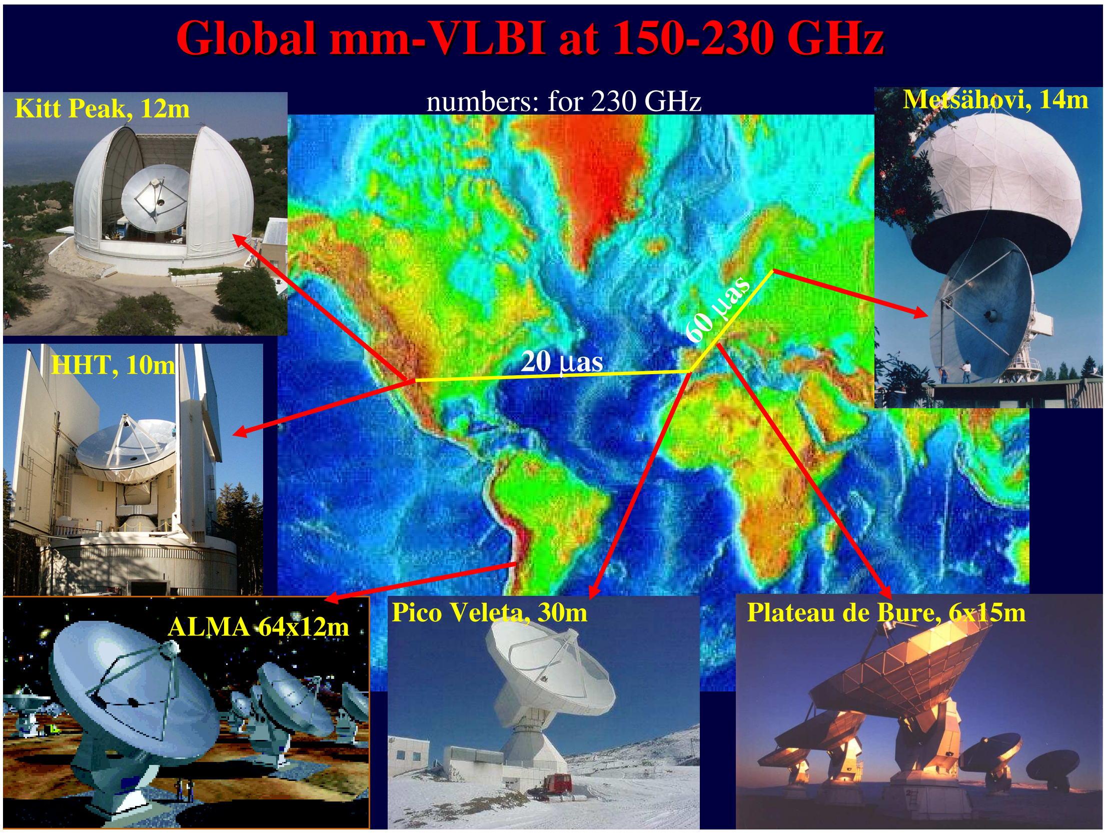

VLBI-detection limits at 1mm wavelengths

(7σ in [mJy])

	Pico	Bima	Sest/Apex	Kitt Peak	HHT	Carma
P. de Bure	144	213	317	388	400	144
Pico	—	259	386	473	486	176
Bima	—	—	564	690	711	257
Sest/Apex	—	—	—	921	947	343
Kitt Peak	—	—	—	—	1297	469
HHT	—	—	—	—	—	483

assume: 512 Mbit/s, 15 s coherence time, 2 bit sampling

expected detection limits:

Pico–HHT–KP–Bima: 260-1300 mJy

plus P.de Bure /Carma: $\geq$ 140 mJy

plus ALMA : $\geq$ 10 mJy

7.3 A. Brunthaler: III Zw 2: Evolution of a Radio Galaxy in a Nutshell

III Zw 2: Introduction

- III Zw 2, PG 0007+106, Mrk1501 (z=0.089)
- Discovered by Zwicky 1967
- Classified as Seyfert 1 galaxy (Arp 1968)
- also in PG-sample (Schmidt & Green 1983)
- probably interaction with nearby galaxies

- Core dominated flat spectrum
- Weak extended structure (Unger et al. 1987)

III Zw 2: variability

- extreme radio variability with 20-40 fold increase
- also optical (Lloyd 1984) and X-ray variability (Kaastra & de Korte 1983)
- (quasi-)periodic outbursts roughly every 5 years

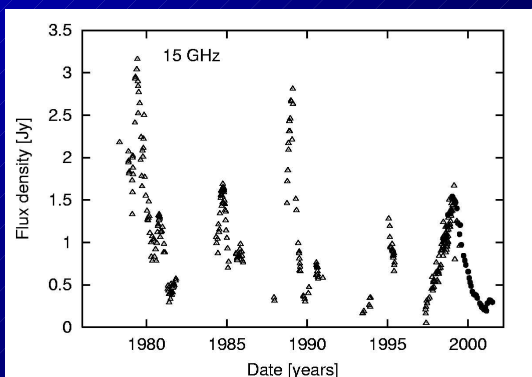

(Michigan + VLA monitoring)

III Zw 2: Radio-spectrum

- Outburst spectrum at start of new flare

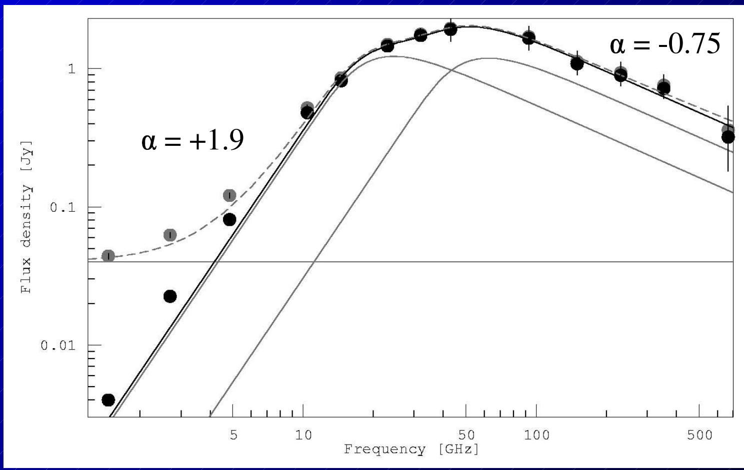

(Falcke et al., ApJ 1999)

- self-absorbed synchrotron spectrum
- turnover-frequency ~ 43 GHz (MPS – mm-peaked)

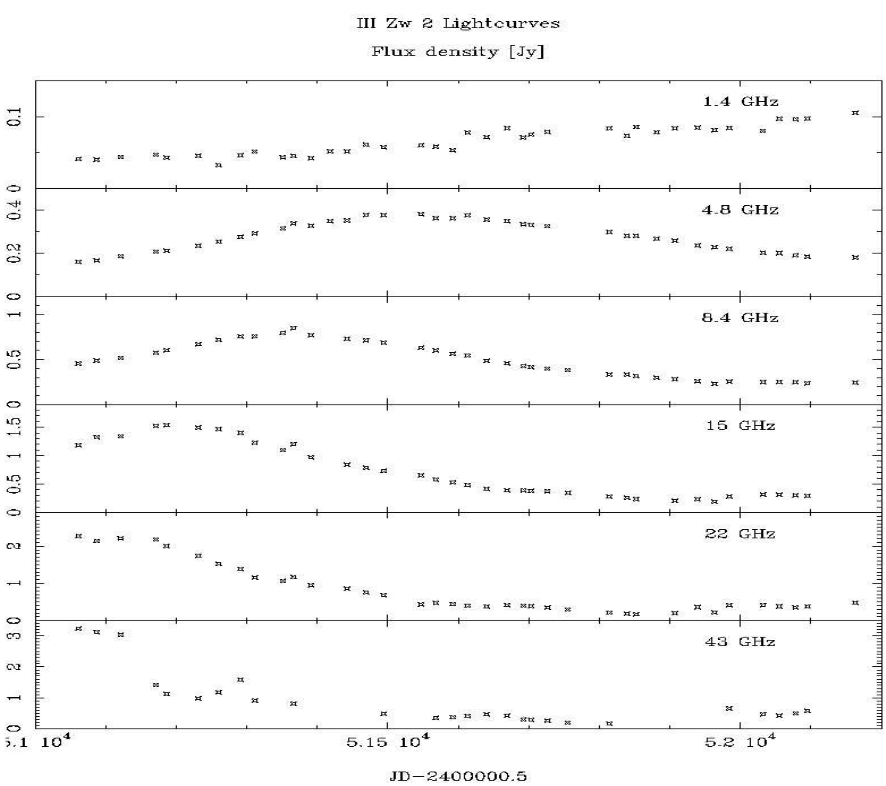

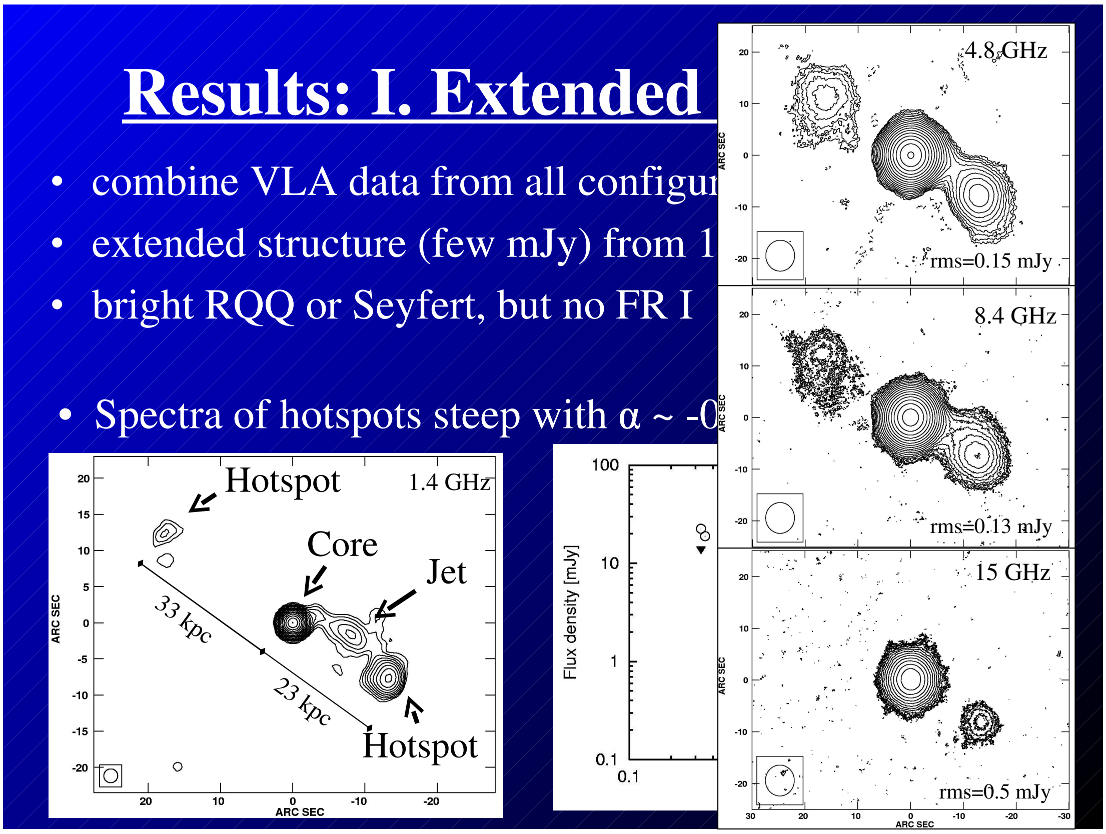
Results: I. Extended
combine VLA data from all configur
extended structure (few mJy) from 1
bright RQQ or Seyfert, but no FR I
Spectra of hotspots steep with α ~ -0
Hotspot
1.4 GHz
Core
Jet
33 kpc
23 kpc
Hotspot
ARC SEC
Flux density [mJy]
4.8 GHz
rms=0.15 mJy
8.4 GHz
rms=0.13 mJy
15 GHz
rms=0.5 mJy

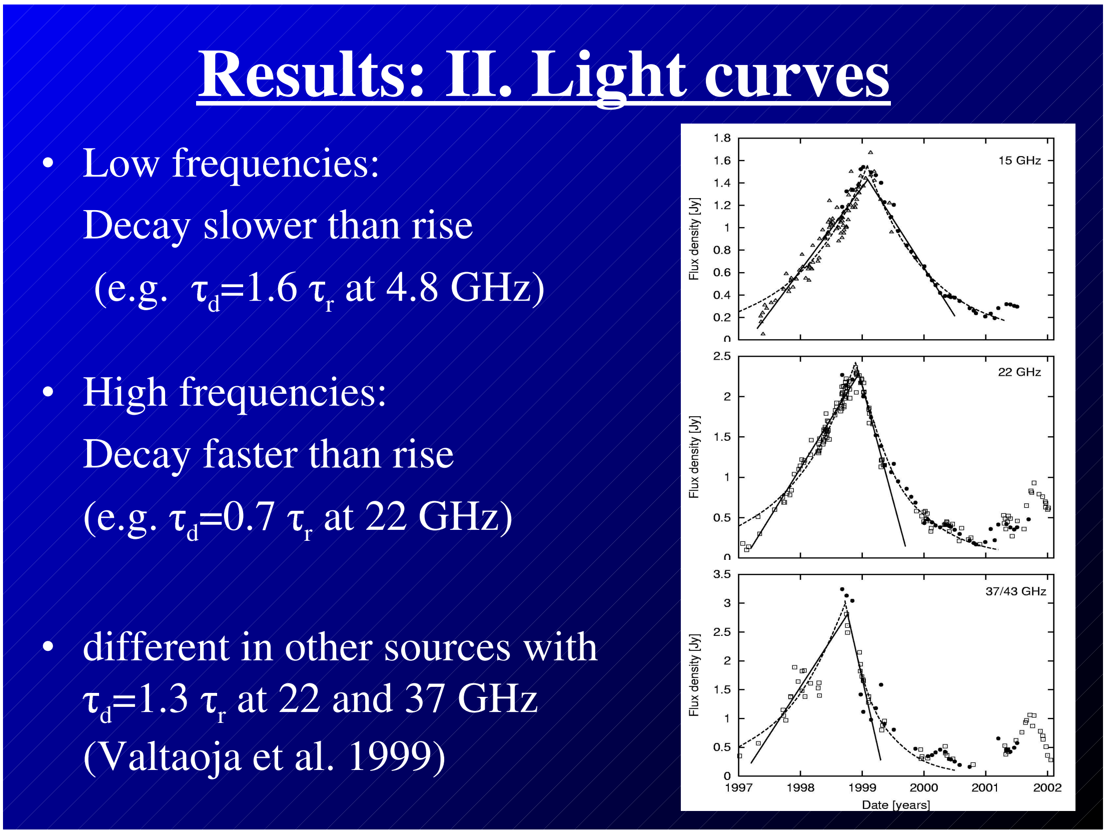
Results: II. Light curves
Low frequencies:
Decay slower than rise
(e.g. τd=1.6 τr at 4.8 GHz)
High frequencies:
Decay faster than rise
(e.g. τd=0.7 τr at 22 GHz)
different in other sources with
τd=1.3 τr at 22 and 37 GHz
(Valtaoja et al. 1999)
15 GHz
22 GHz
37/43 GHz
Flux density [Jy]
Date [years]

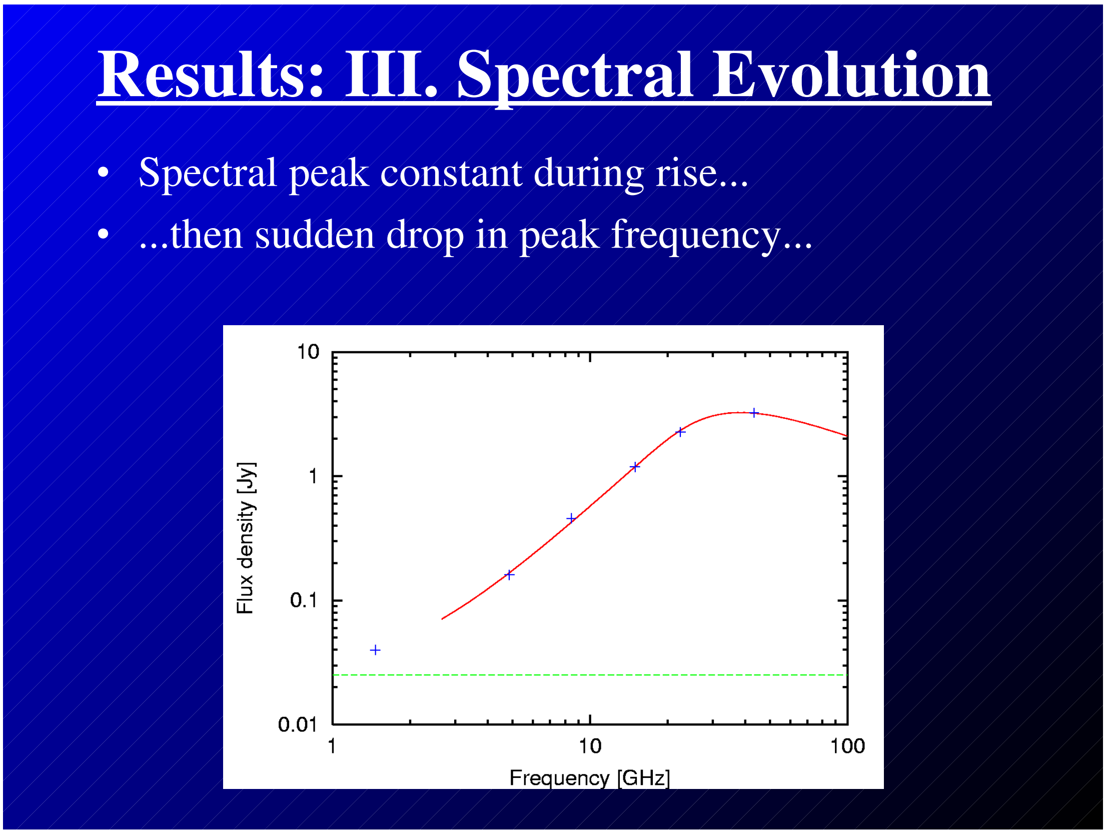
Results: III. Spectral Evolution
• Spectral peak constant during rise...
• ...then sudden drop in peak frequency...
Flux density [Jy]
10
1
0.1
0.01
1
10
100
Frequency [GHz]

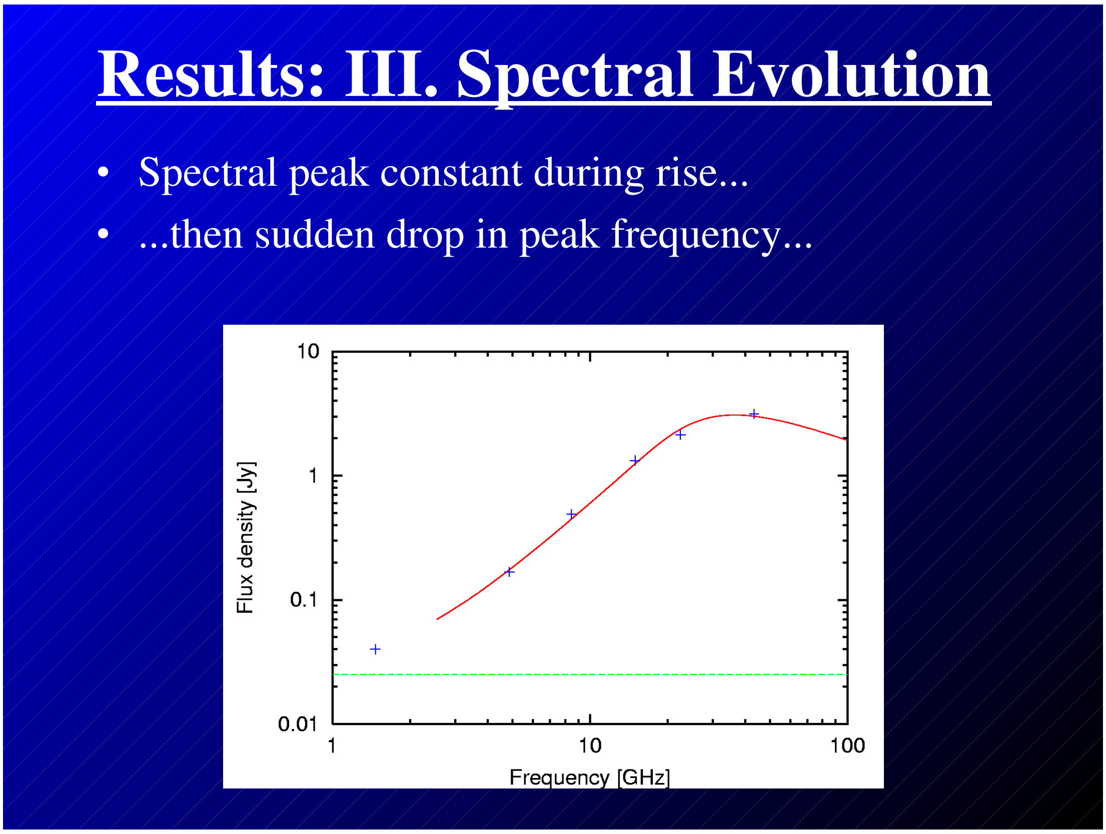
Results: III. Spectral Evolution
• Spectral peak constant during rise...
• ...then sudden drop in peak frequency...
Flux density [Jy]
10
1
0.1
0.01
1
10
100
Frequency [GHz]

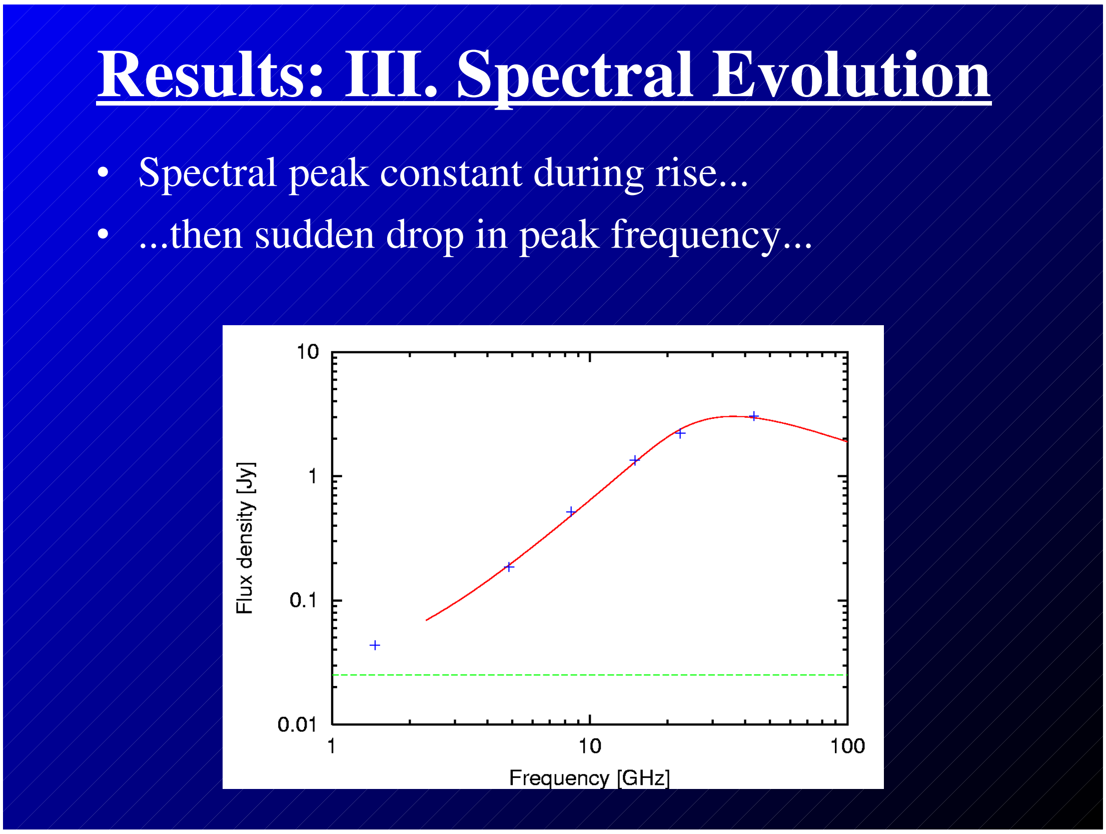
Results: III. Spectral Evolution
• Spectral peak constant during rise...
• ...then sudden drop in peak frequency...
Flux density [Jy]
Frequency [GHz]
10
1
0.1
0.01
1
10
100

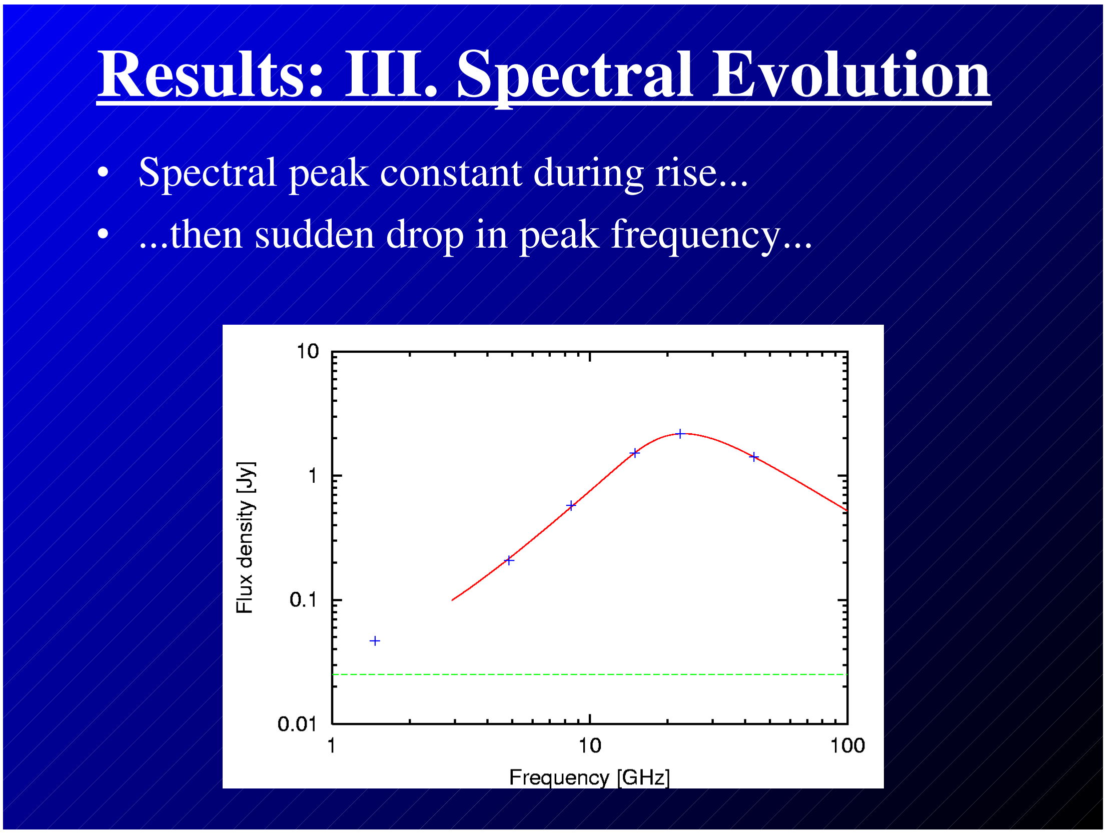
Results: III. Spectral Evolution
• Spectral peak constant during rise...
• ...then sudden drop in peak frequency...
Flux density [Jy]
Frequency [GHz]
10
1
0.1
0.01
1
10
100

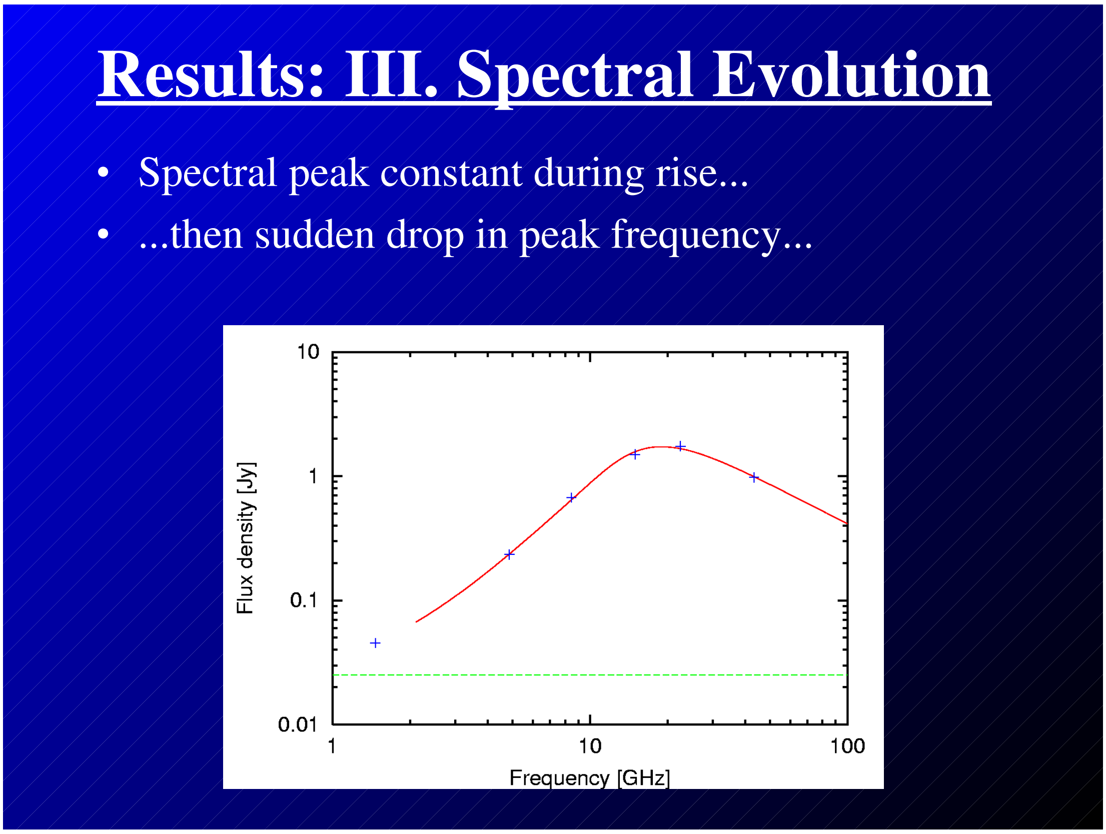
Results: III. Spectral Evolution
• Spectral peak constant during rise...
• ...then sudden drop in peak frequency...
10
1
0.1
0.01
Flux density [Jy]
1
10
100
Frequency [GHz]

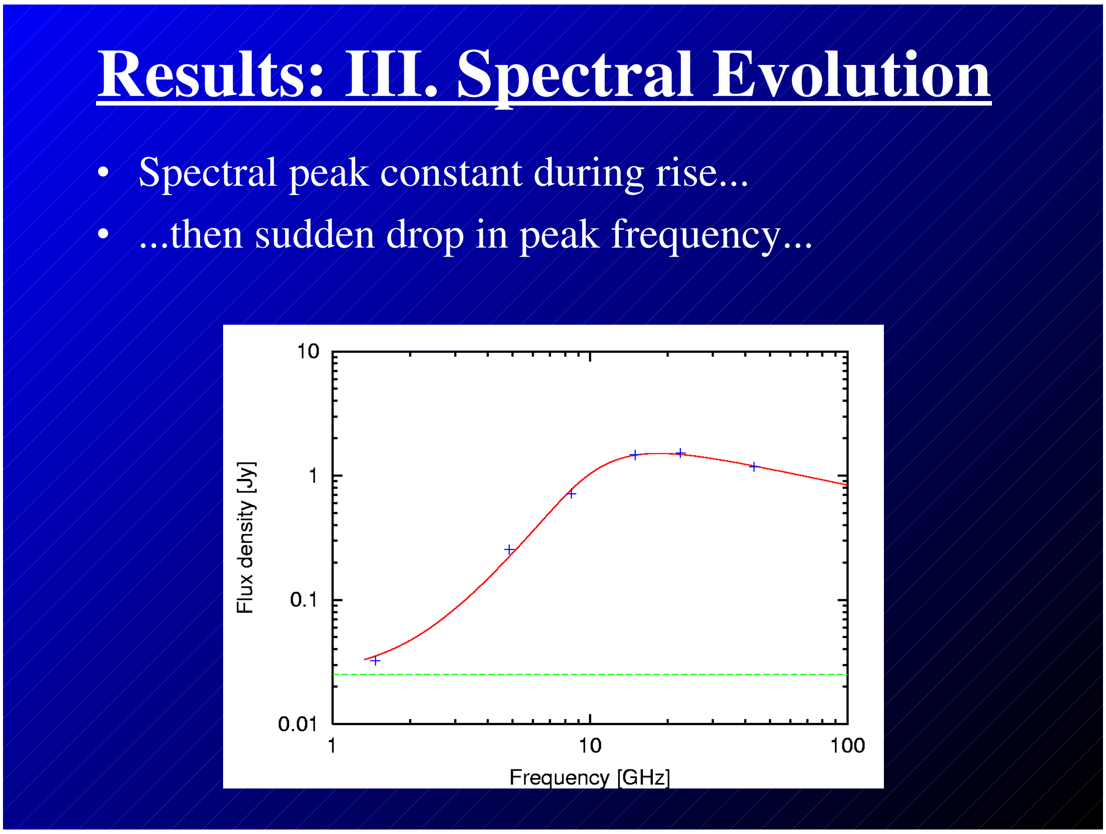
Results: III. Spectral Evolution
• Spectral peak constant during rise...
• ...then sudden drop in peak frequency...
10
1
0.1
0.01
Flux density [Jy]
1
10
100
Frequency [GHz]

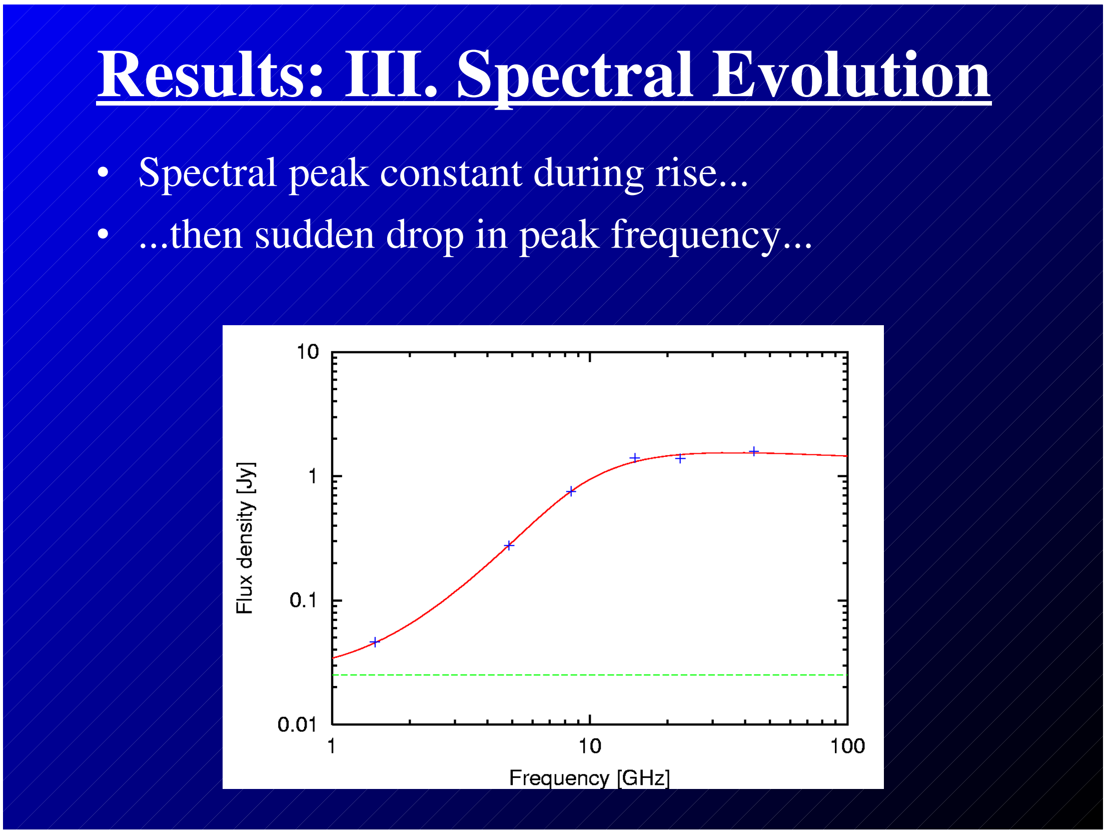
Results: III. Spectral Evolution
• Spectral peak constant during rise...
• ...then sudden drop in peak frequency...
Flux density [Jy]
Frequency [GHz]
10
1
0.1
0.01
1
10
100

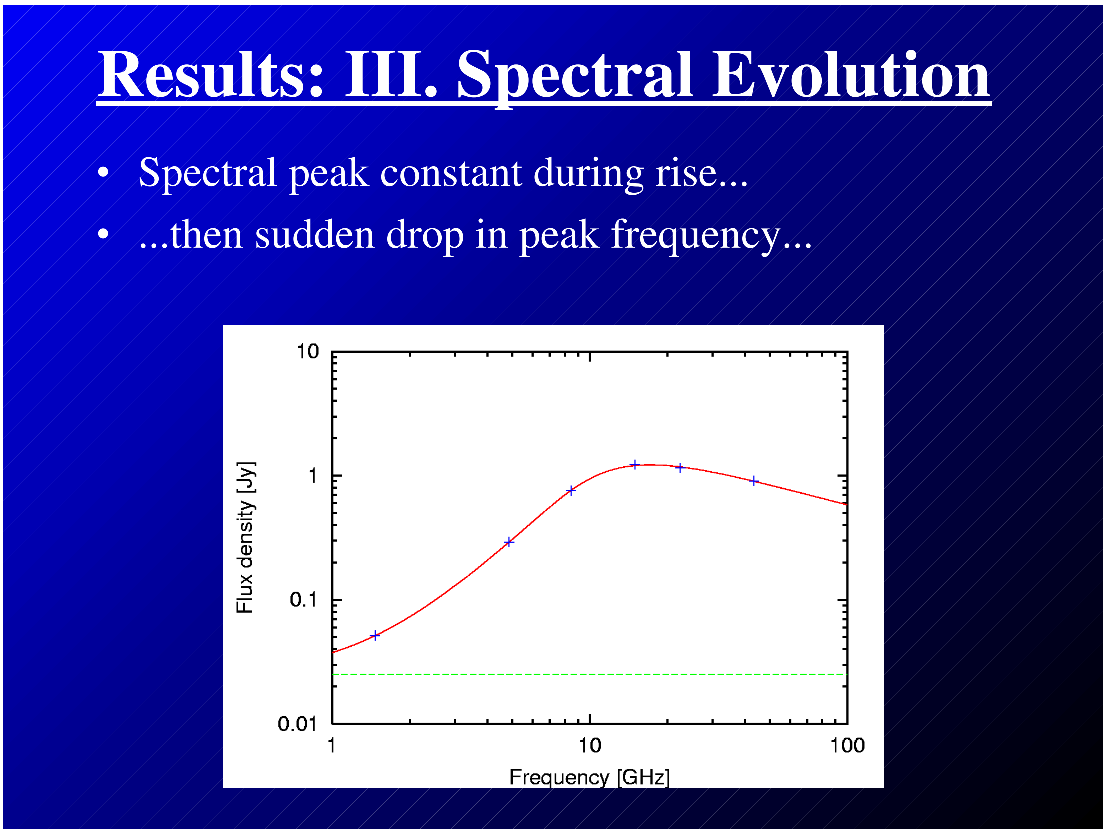
Results: III. Spectral Evolution
• Spectral peak constant during rise...
• ...then sudden drop in peak frequency...
Flux density [Jy]
Frequency [GHz]
10
1
0.1
0.01
1
10
100

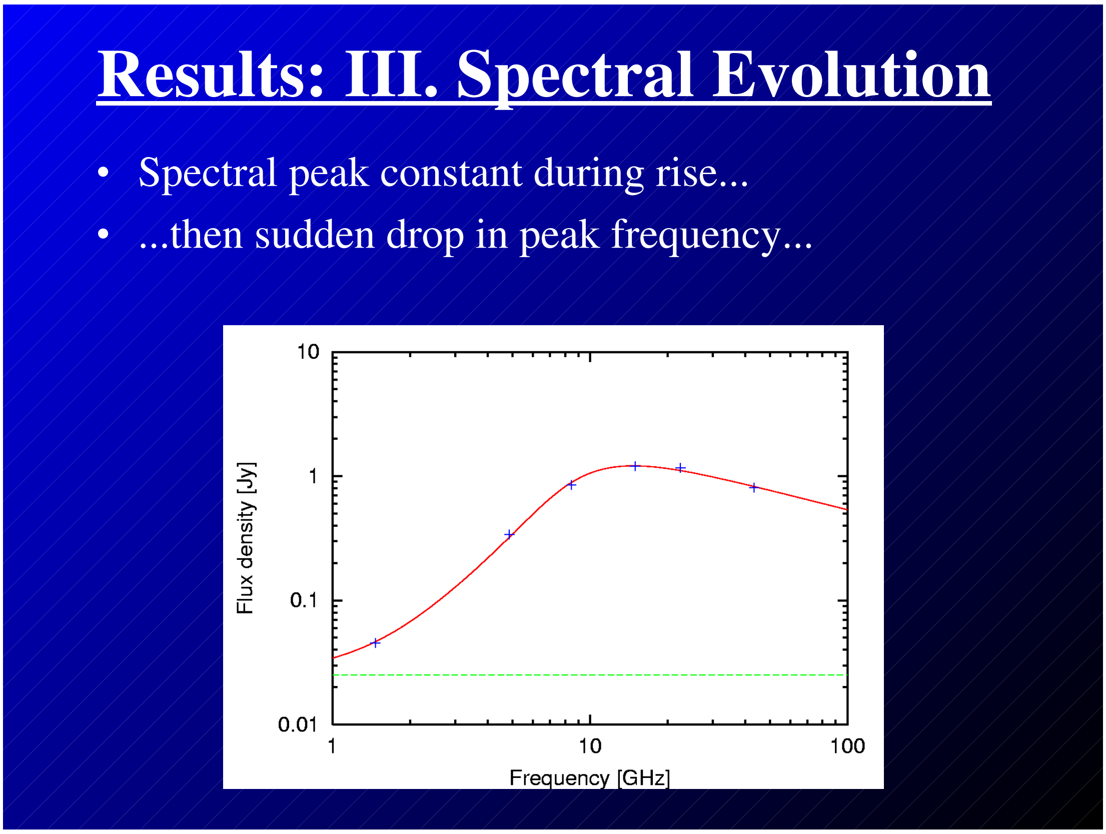
Results: III. Spectral Evolution
• Spectral peak constant during rise...
• ...then sudden drop in peak frequency...
10
1
0.1
0.01
Flux density [Jy]
1
10
100
Frequency [GHz]

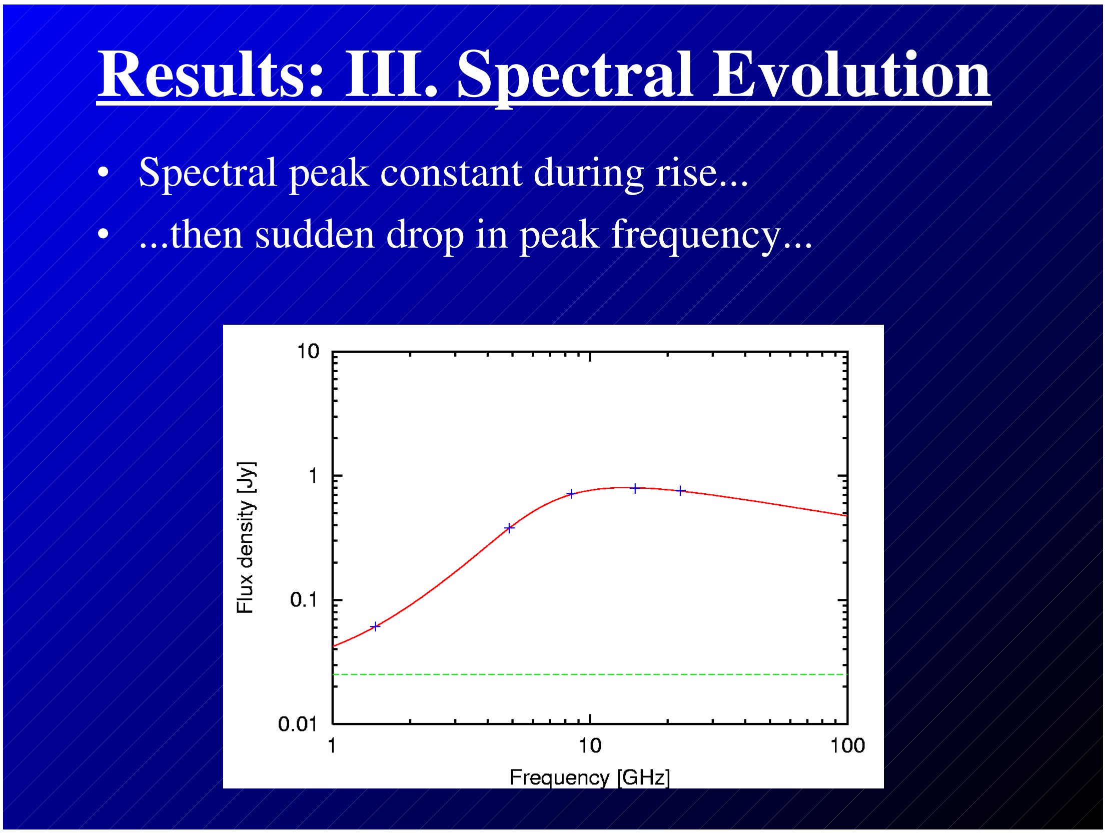
Results: III. Spectral Evolution
• Spectral peak constant during rise...
• ...then sudden drop in peak frequency...
10
1
0.1
0.01
Flux density [Jy]
1
10
100
Frequency [GHz]

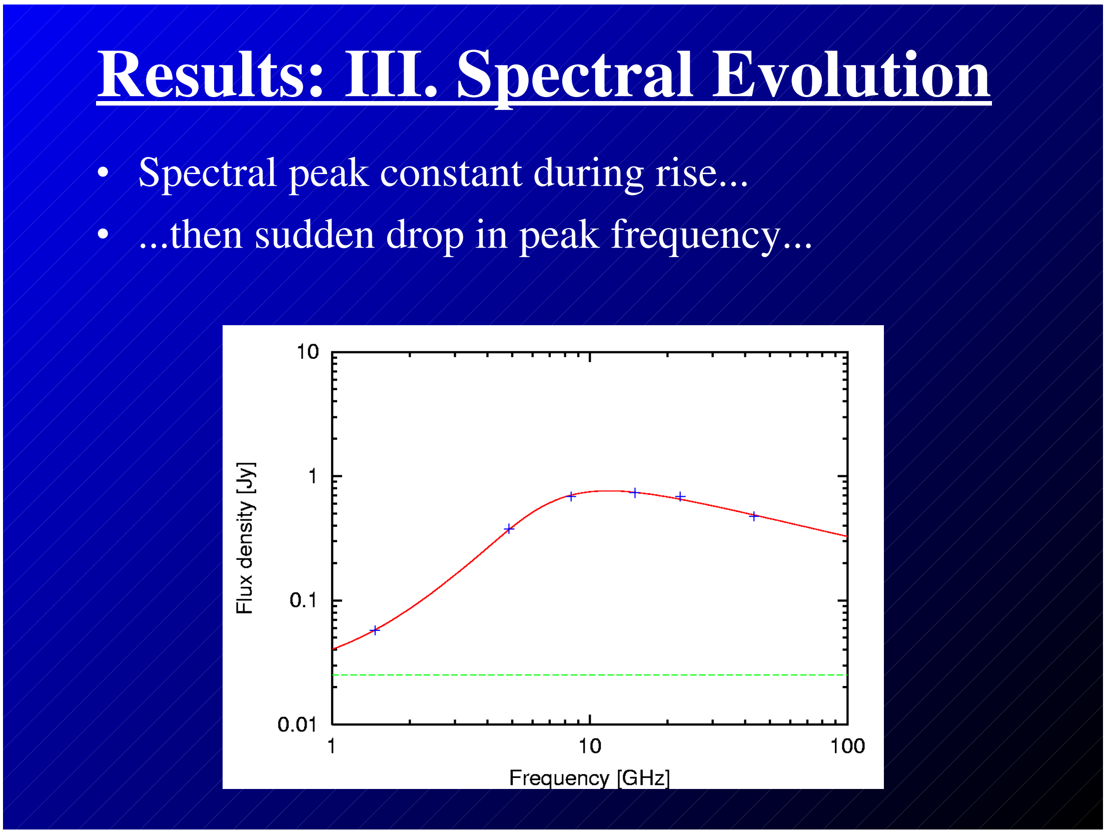
Results: III. Spectral Evolution
• Spectral peak constant during rise...
• ...then sudden drop in peak frequency...
Flux density [Jy]
Frequency [GHz]
10
1
0.1
0.01
1
10
100

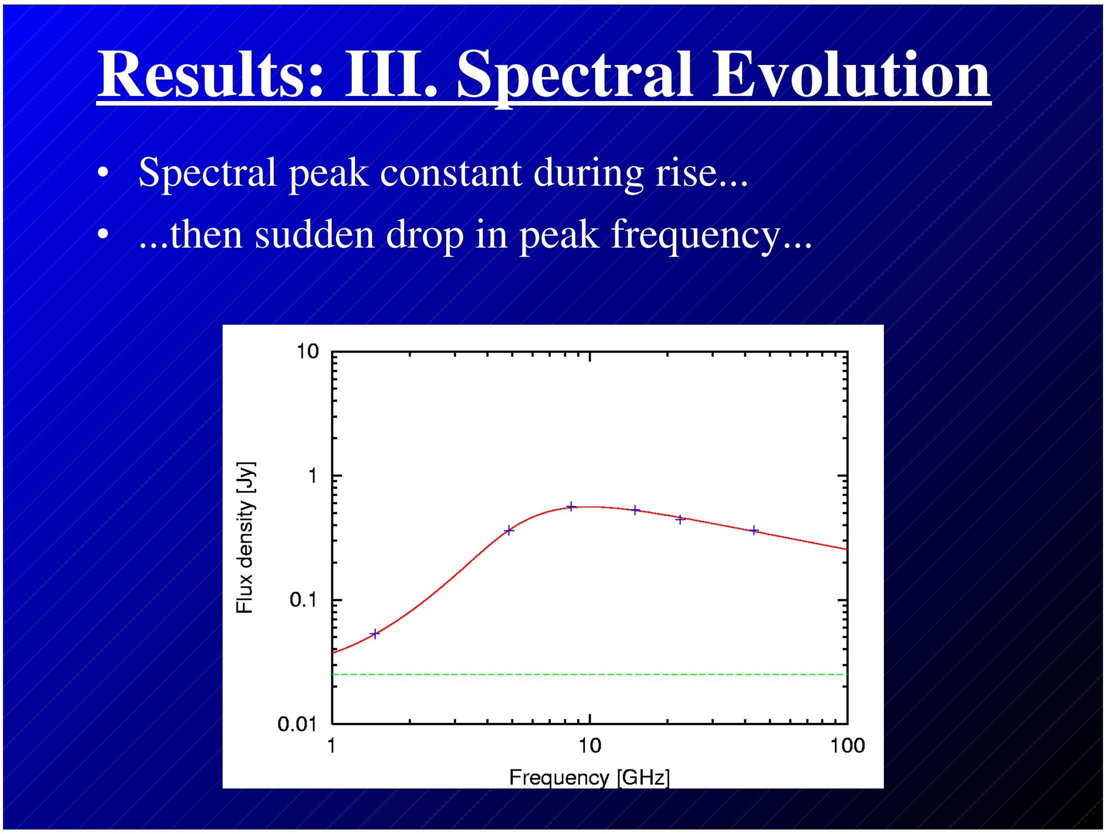
Results: III. Spectral Evolution
• Spectral peak constant during rise...
• ...then sudden drop in peak frequency...
Flux density [Jy]
Frequency [GHz]
10
1
0.1
0.01
1
10
100

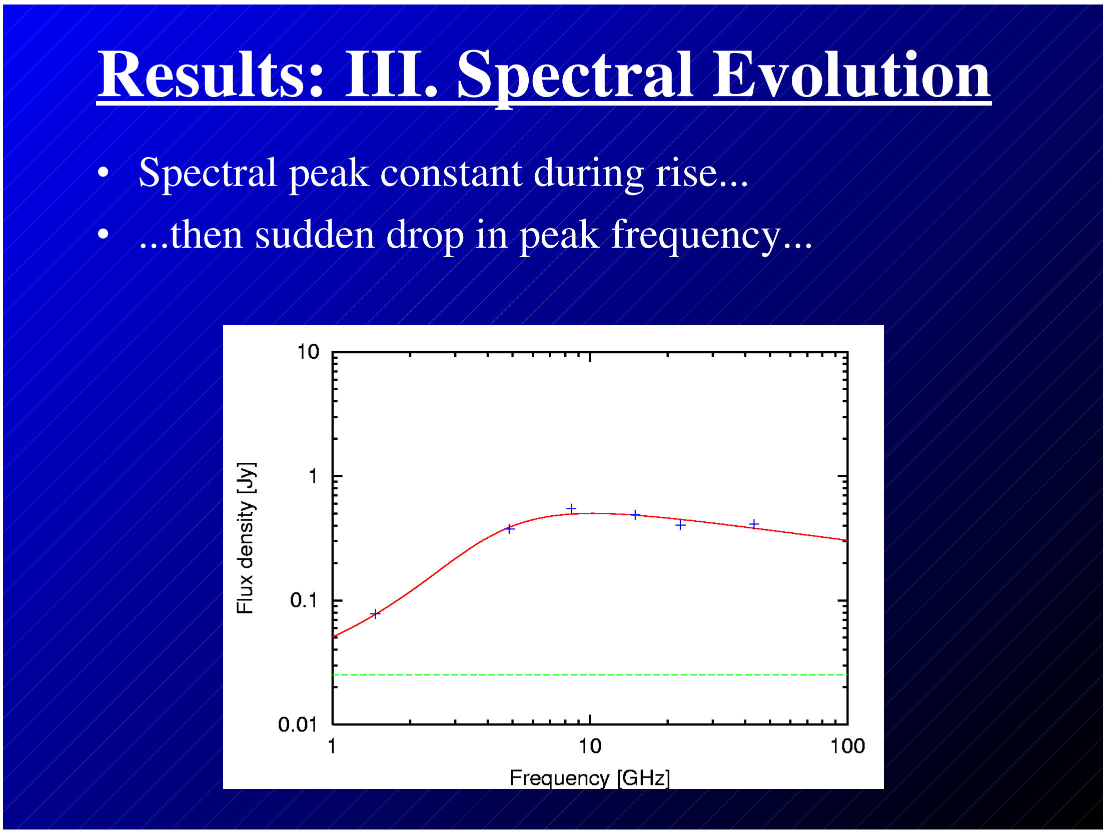
Results: III. Spectral Evolution
• Spectral peak constant during rise...
• ...then sudden drop in peak frequency...
10
1
0.1
0.01
Flux density [Jy]
1
10
100
Frequency [GHz]

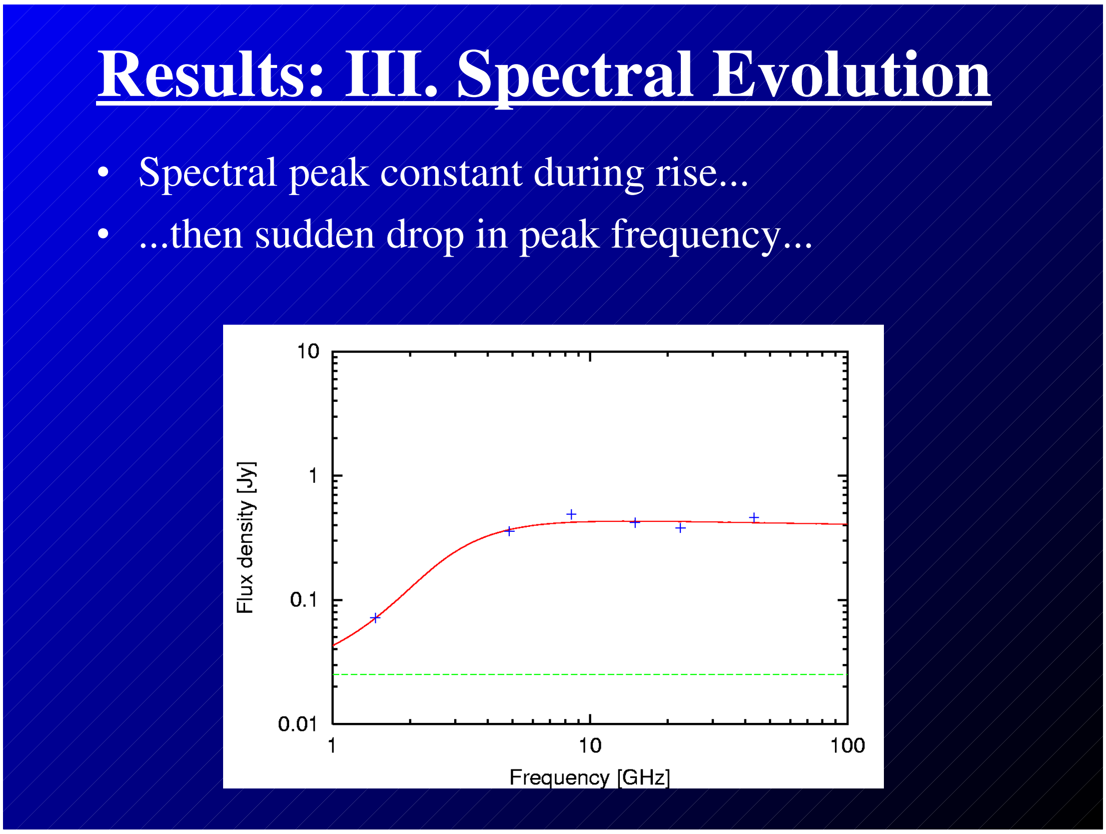
Results: III. Spectral Evolution
• Spectral peak constant during rise...
• ...then sudden drop in peak frequency...
10
1
0.1
0.01
Flux density [Jy]
1
10
100
Frequency [GHz]

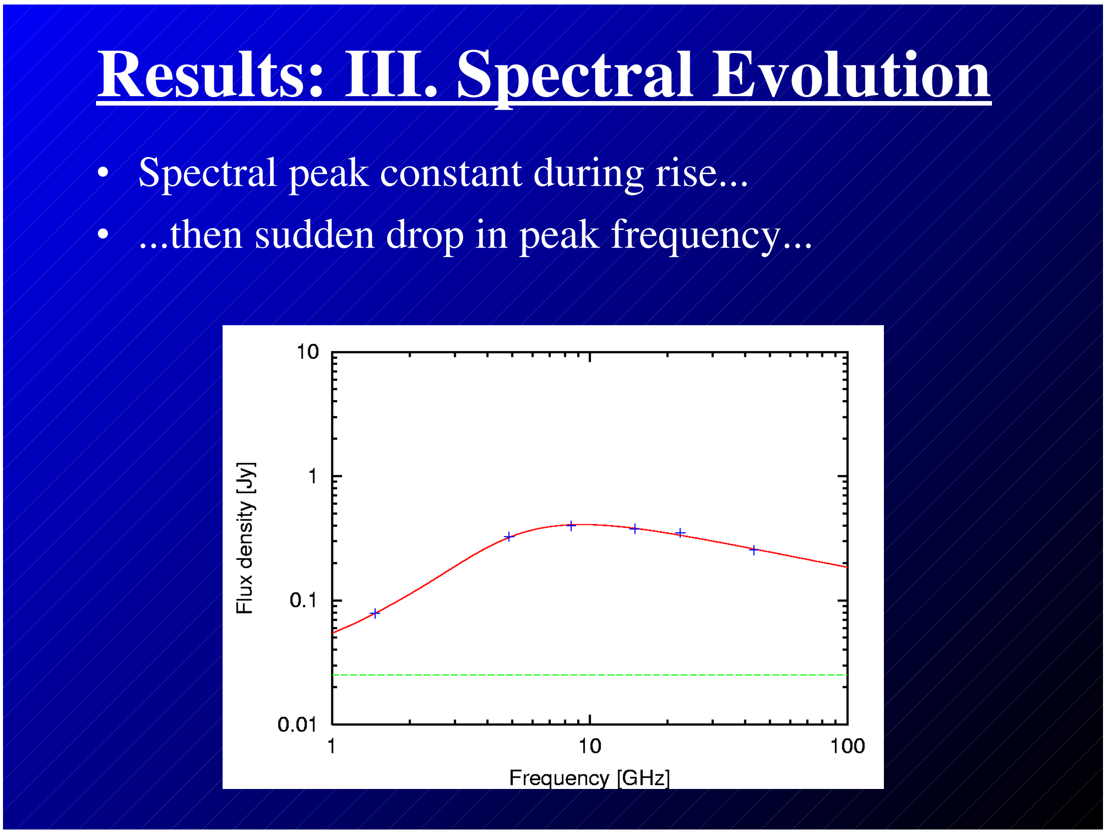
Results: III. Spectral Evolution
• Spectral peak constant during rise...
• ...then sudden drop in peak frequency...
Flux density [Jy]
10
1
0.1
0.01
1
10
100
Frequency [GHz]

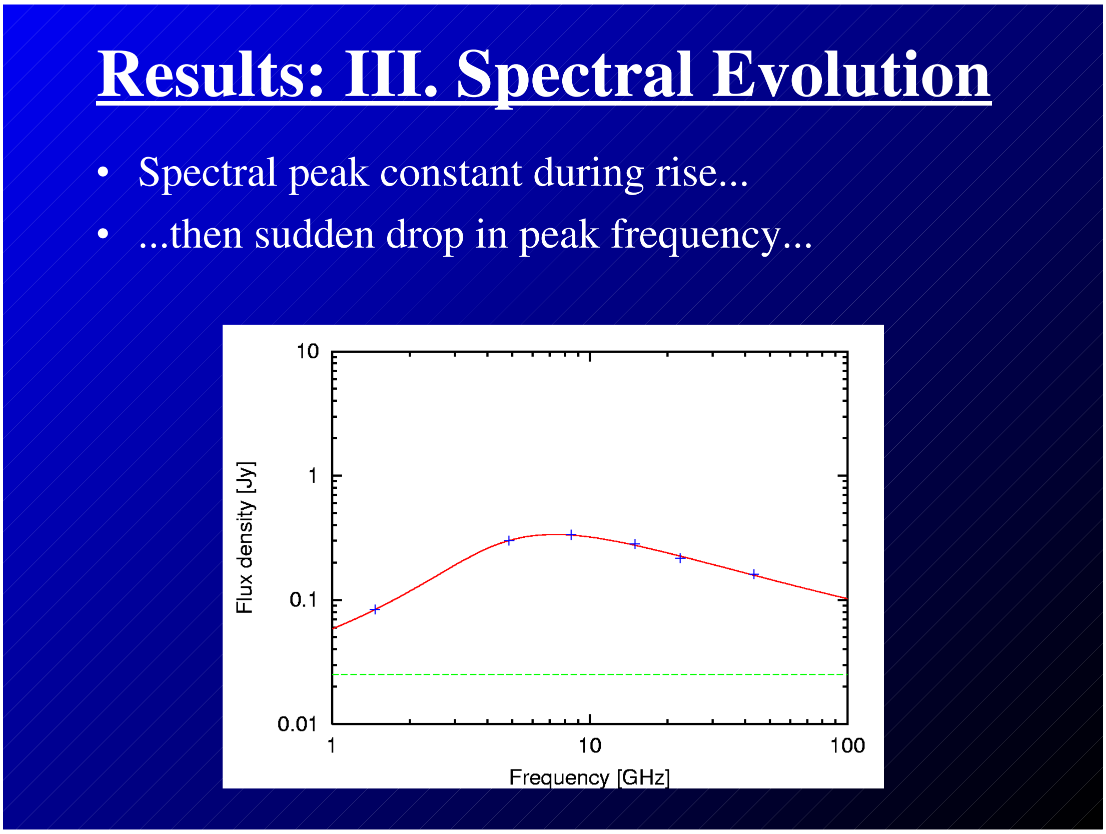
Results: III. Spectral Evolution
• Spectral peak constant during rise...
• ...then sudden drop in peak frequency...
Flux density [Jy]
10
1
0.1
0.01
1
10
100
Frequency [GHz]

Results: III. Spectral Evolution

- Spectral peak constant during rise...
- ...then sudden drop in peak frequency...

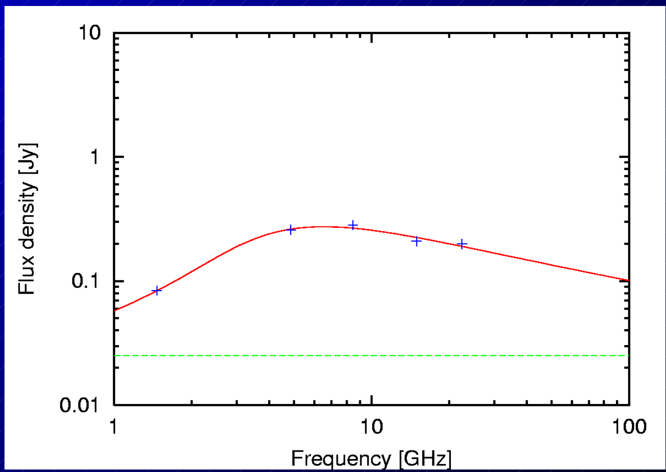

Results: III. Spectral Evolution

- Spectral peak constant during rise...
- ...then sudden drop in peak frequency...

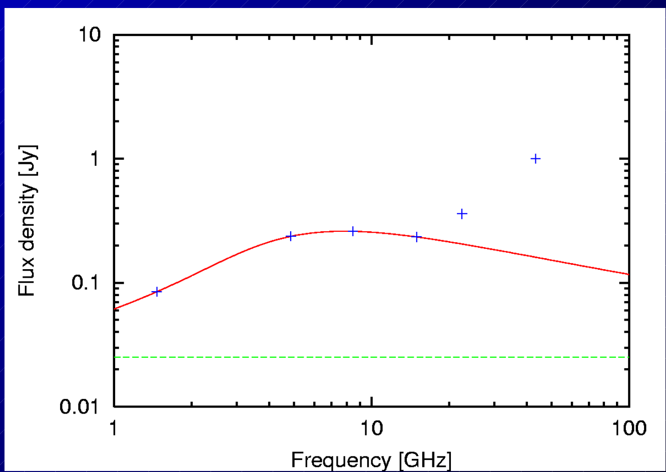

Results: IV. Structural evolution

- compact but resolved structure at 43 GHz
- fit point sources
- expansion speed: 1.25 c
- relativistic jet

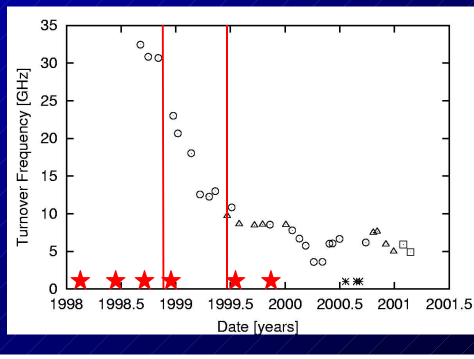

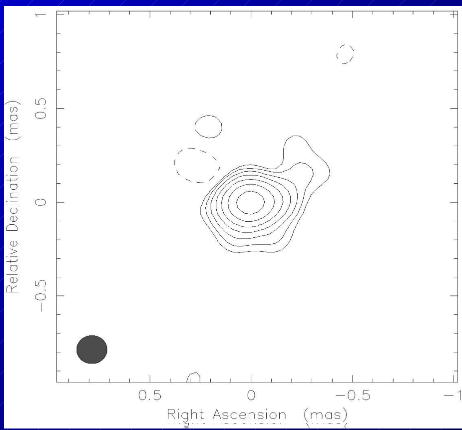

(Brunthaler et al., A&A 2000)

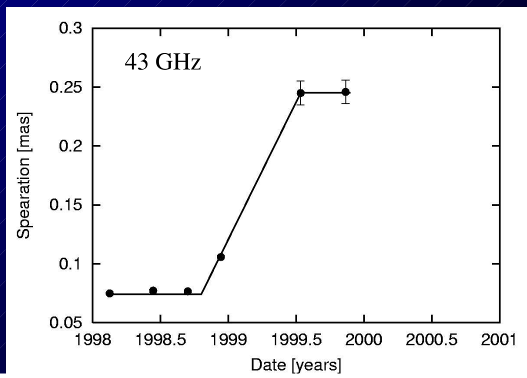

Results: IV. Structural evolution

- compact structure at 15 GHz
- fit two point sources
- expansion speed: 0.6 c
- contradiction to 43 GHz?

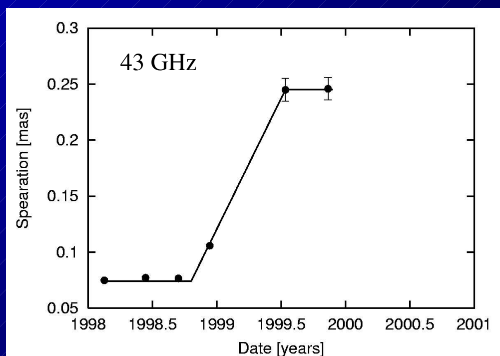

- III Zw 2 is optically thick at 15 GHz
  - One looks at the envelope
- Optically thin at 43 GHz
  - One looks into the source

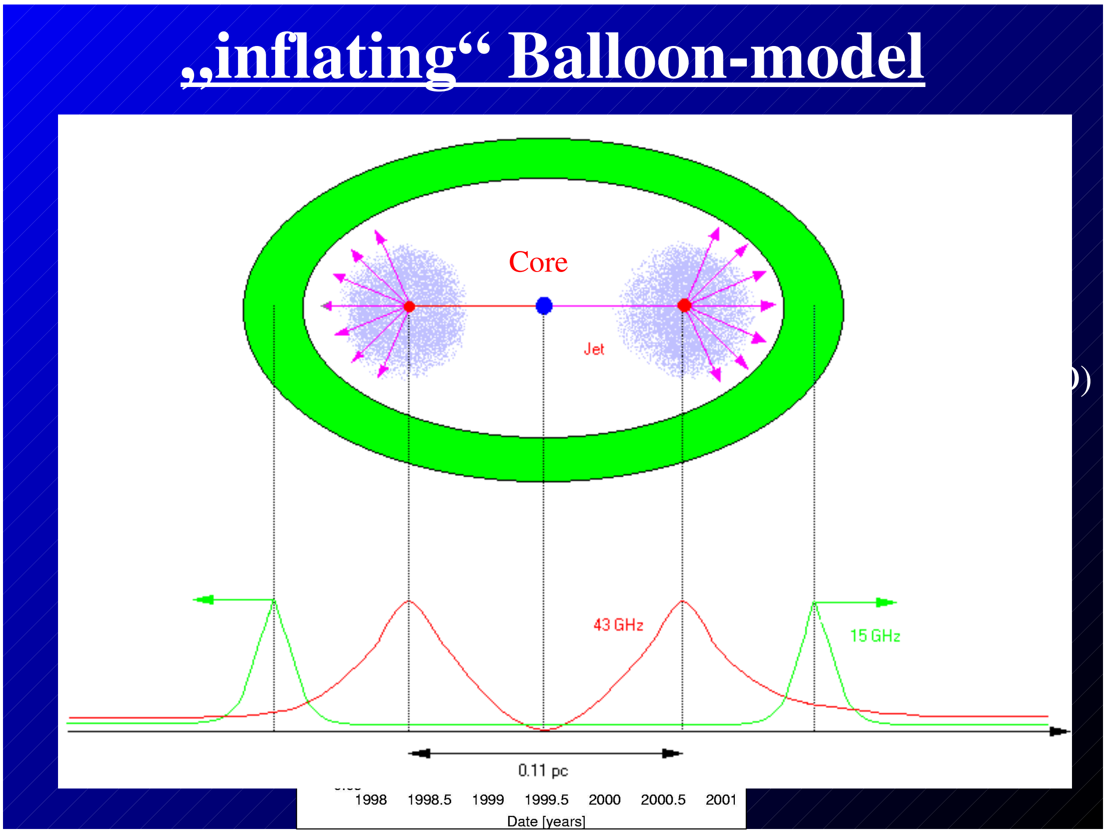

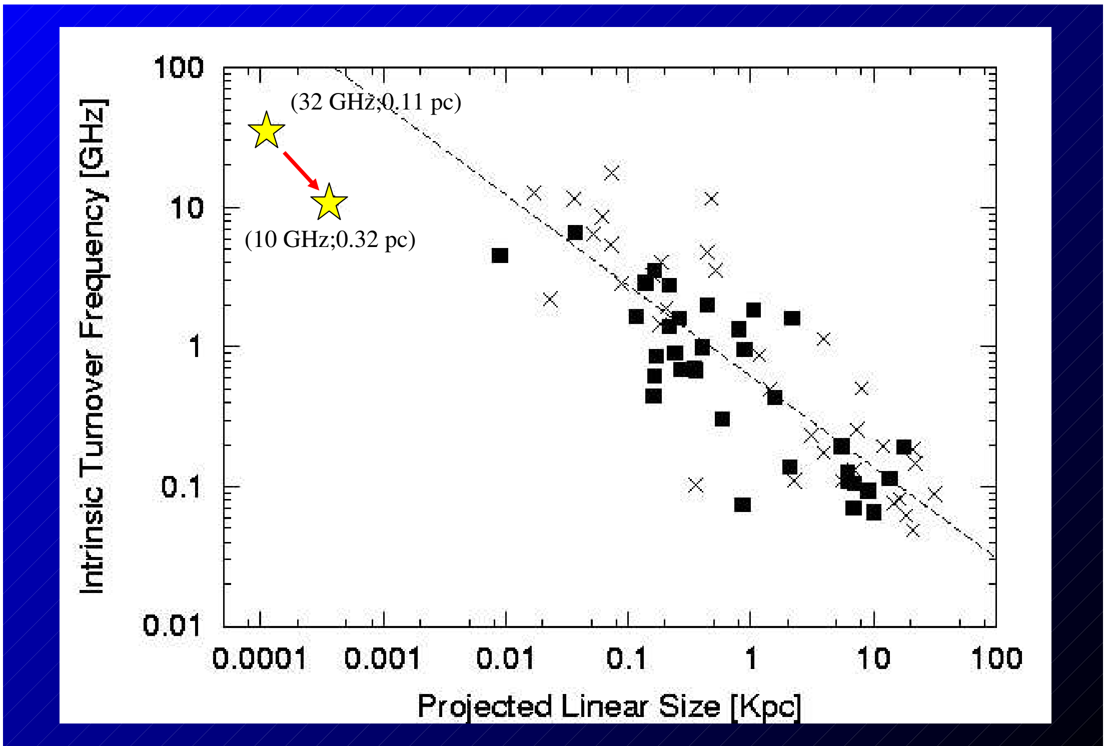

(adapted from O‘Dea & Baum 1997)

7.4 I. Agudo: VLBI Observations and Numerical Modelling of the Inner Jets in AGNs

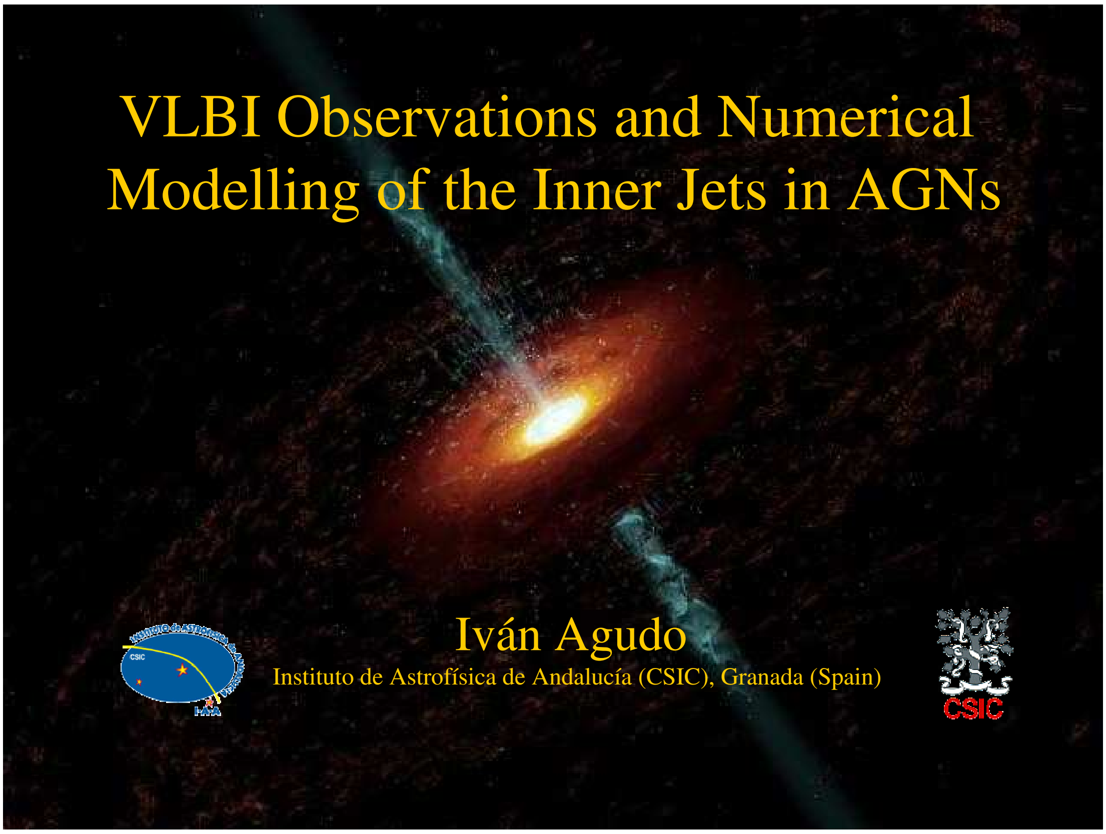

Overview of the Talk:

- Numerical modelling of the inner jet:
  - Relativistic hydrodynamic (RHD) and synchrotron emission simulations
  - A mechanism for the generation and evolution of stationary and superluminal components
- Polarimetric multi-frequency VLBI monitoring of radio jets
  - Monthly 43GHz monitoring of the radio galaxy 3C120. Application for the numerical model
  - The BL Lac 0735+178. Interaction with the external medium?
- A scheme for the spectral evolution of non-thermal electrons in relativistic simulations

Relativistic Hydrodynamical Simulations

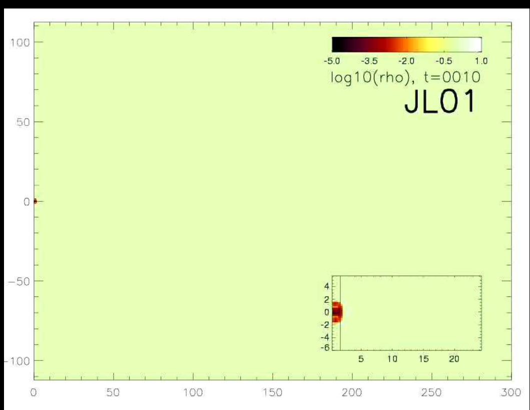

Martí et al.

We are interested in the study of the evolution and variability of actual relativistic jets

We make use of the *relativistic* hydrodynamical (HD) codes developed by Martí and Aloy (University of Valencia)

The RHD code (based on Martí et al. 1994) solves the time dependent conservation equations of mass, momentum and energy. An equation of state close the system of equations.

Radio Synchrotron Emission Computation

Simulated radio maps are obtained by computing the synchrotron emission from the HD results.

To do this it is needed:

- Distribute the energy among the electrons, usually assuming a power law →

$$N(E)\,\mathrm{d}E = N_o\,E^{-\gamma}\,\mathrm{d}E \quad , \quad E_{min} \leq E \leq E_{max}$$

- Magnetic field in equipartition
- We can compute the emission and absorption coefficients from

$$\varepsilon^{(i)} = \frac{\sqrt{3}}{8\pi}\frac{e^3}{mc^2}\,B\,\sin\vartheta \int_{E_{min}}^{E_{max}} N(E)\,[F(x) \pm G(x)]\,\mathrm{d}E$$

$$\kappa^{(i)} = -\frac{\sqrt{3}e^3}{8\pi m\nu^2}\,B\,\sin\vartheta \int_{E_{min}}^{E_{max}} E^2\,\frac{\mathrm{d}}{\mathrm{d}E}\left(\frac{N(E)}{E^2}\right)[F(x) \pm G(x)]\,\mathrm{d}E$$

Take into account the relativistic light aberration and time delays between different jet regions. This strongly determines the final jet structure seen by the observer.

Radio Synchrotron Emission Simulations

The emission code (based on Gómez et al. 1995) computes the synchrotron radiation from the RHD model by solving the radiation transfer equation, accounting for all the relativistic effects

↓

Generation of time dependent synthetic radio maps directly comparable with observations

Sequence of simulated radio maps

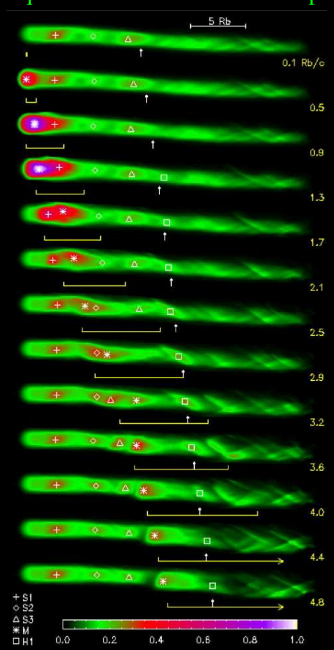

Aloy et al. (2003)

Generation of Stationary and Superluminal Components

- Study of the inner jet variability observed with VLBI
- The model explains how stationary and superluminal components of emission are generated (and evolves) as the result of the passage of a strong perturbation through the jet (Agudo et al. 2001)

The simulation:

Agudo et al. (2001)

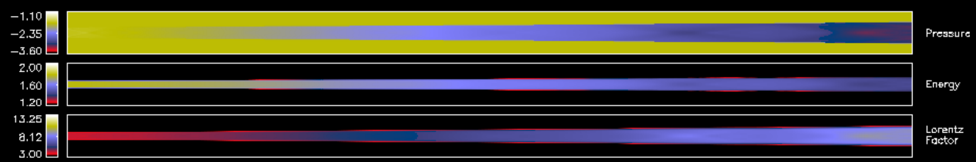

- We start from a fast (Γ_b=4), ultrarelativistic (γ=4/3), light (ρ_b/ρ_a=0.001), supersonic (M_b=1.69) jet in pressure equilibrium with the ambient medium
- Perturbing the model by:
  - Increasing the injection velocity: Γ_b=4 to Γ_t=10
  - With increase in pressure by a factor of 2
  - During a time interval of 0.75 R_b/c

Generation of Stationary and Superluminal Components

- Passage of the main perturbation (M) triggers local pinch instabilities in the surface of the jet
- Multiple "trailing shocks" appear after the main perturbation, not in the core
- Trailing shocks are conical recollimation shocks, in contrast to the plane perpendicular shock of the main perturbation (M).

Relative variation with respect to the undisturbed steady jet of the Lorentz Factor (logarithmic scale) at t=350 R_b/c.

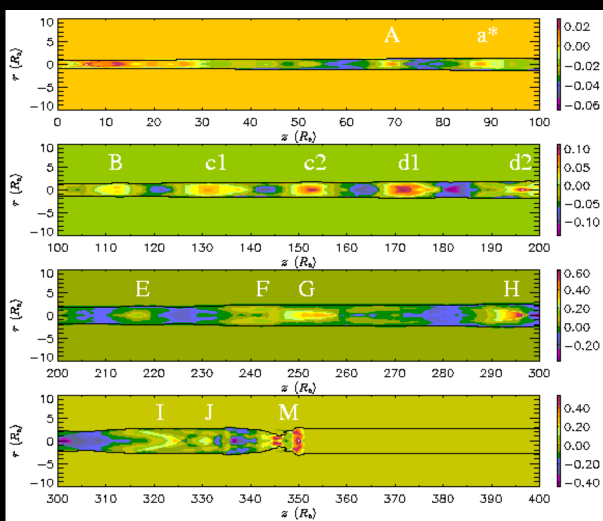

Different scale ranges in each panel.

Agudo et al. (2001)

Generation of Stationary and Superluminal Components

We compute the radio emission for a viewing angle of 10º for an optically thin frequency and using a convolving beam of 2 times the initial jet beam radius

Simulated Radio Maps of Relativistic Jets

Ivan Agudo	IAA (Spain)
Jose-Luis Gomez	IAA (Spain
Jose-Maria Marti	UV (Spain)
Jose-Maria Ibañez	UV (Spain)
Alan P. Marscher	BU (USA)
Antonio Alberdi	IAA (Spain)
Miguel-Angel Aloy	MPIfA (Germany)
Philip E. Hardee	UA (USA)

- Main (fast) component (M), ⇔ shock of the main perturbation
- M moves with an apparent speed of ~7c
- “Trailing components” are produced in the wake of M and move always at lower velocities

Generation of Stationary and Superluminal Components

- Components appearing farther downstream show larger apparent motions (episodically superluminal) and weaker flux densities (more difficult detection) ⇒ *Moving components.*

- Components appearing close to the core show subluminal motions and flux densities decreasing slowly with time ⇒ *Stationary components.*

Space -time diagram for the logarithm of the mean flux density in the observer’s frame.

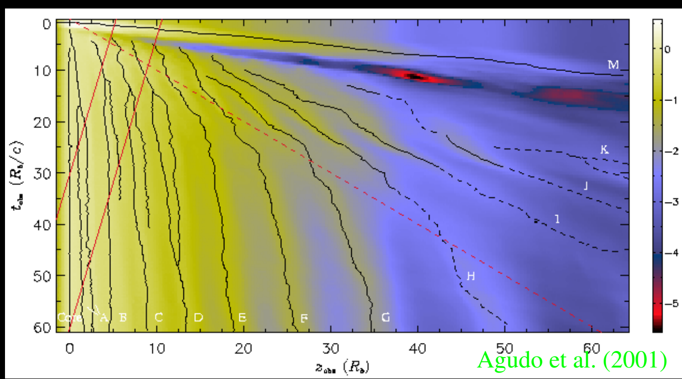

Agudo et al. (2001)

Mean intensity across slices normal to the jet axis and normalized to the mean core intensity. Black lines are trajectories of emission components with more than 0.5% the mean core intensity and dashed lines below this value. Red dashed line represents a speed equal to c.

This behavior has been observed in several sources (Tingay et al. 2001; Jorstad et al. 2001) and also in our VLBI monitoring of the radio galaxy 3C120

Monthly 43 GHz VLBI Monitoring of 3C120

- Very active and "close" (z=0.033, 150 Mpc)
- Allows the maximum linear resolution (up to 0.7 pc)
- We can study the emission evolution in scales of years

Observing program consisting of 16 monthly observing epochs from Nov. 1997 to Mar. 1999 at 43 GHz

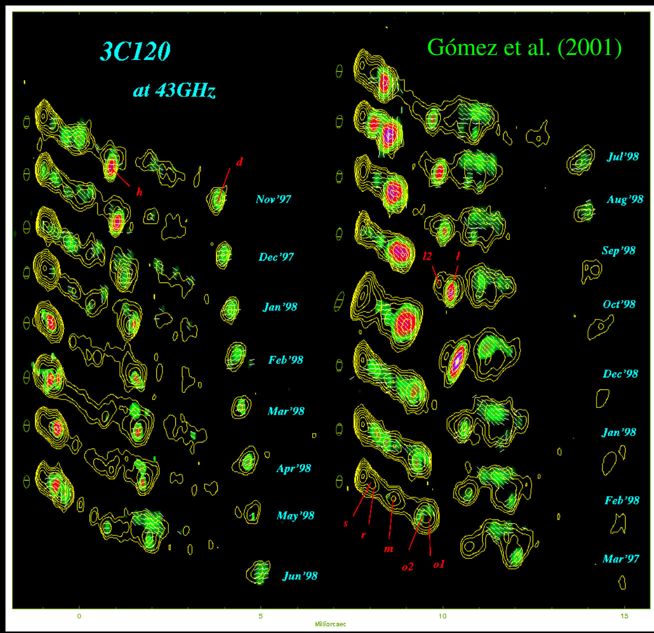

Contours represent *I*, color scale represents *P* and sticks show χ

Monthly 43 GHz VLBI Monitoring of 3C120

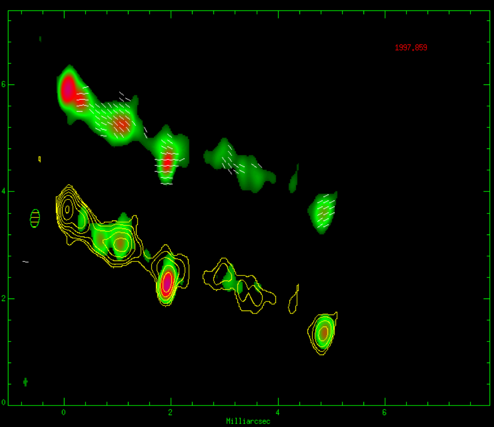

Components position vs. time

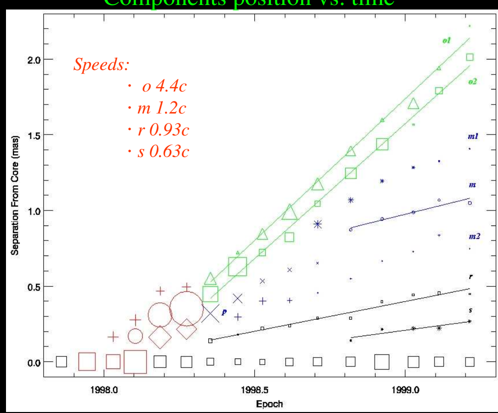

Gómez et al. (2001)

The head of the component *(o1&o2)* moves at a constant speed of 4.4c

New components:

- Appear in the weak of the main component
- With smaller velocities
- Increasing with distance to the core
- With lower emission

Monthly 43 GHz VLBI Monitoring of 3C120

Observations — Simulations

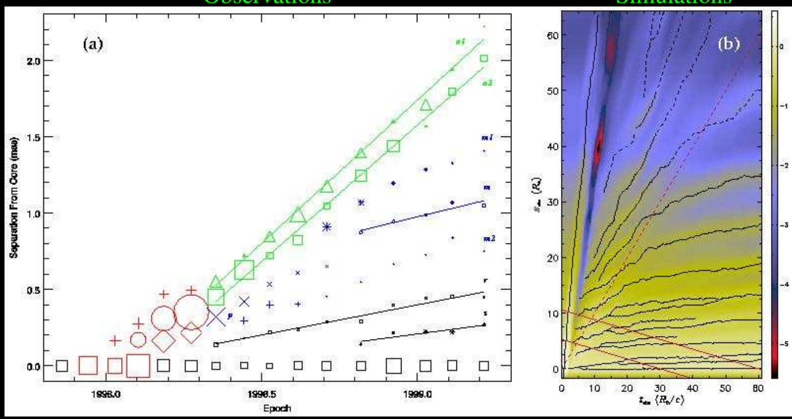

Comparison of the observations with the numerical simulations suggests that the internal structure in 3C120 is plausibly produced by the presence of the trailing phenomenon

Numerical simulations can provide a valid representation of the actual sources

Monthly 43 GHz VLBI Monitoring of 3C120

Gomez et al. (2000) found jet-external medium (EM) interaction in the region at ~3 mas from the core.

22 to 43 GHz spectral index map

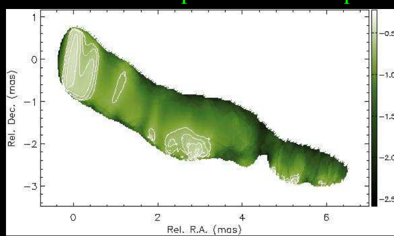

Gómez et al. (2000)

RM map of 3C120 between 15 and 43 GHz for Dec. 2000

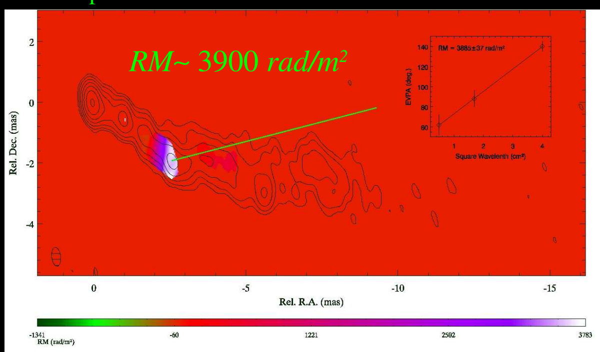

Gómez et al. (in prep.)

The interaction model is supported by the occurrence of:
-A bend in the jet
-Free-Free absorption
-Faraday rotation

BL Lac 0735+178. Interaction with the external medium?

VLBA at 15 GHz Feb. 1999

VSOP at 5 GHz Jan. 1999

Gabuzda, Gómez & Agudo (2001)

15 GHz VLBA observations show a sharply bent inner jet

VSOP observations at 5 GHz provide similar angular resolutions and reveal a fairly straight inner jet

BL Lac 0735+178. Interaction with the external medium?

5 to 15 GHz spectral index map

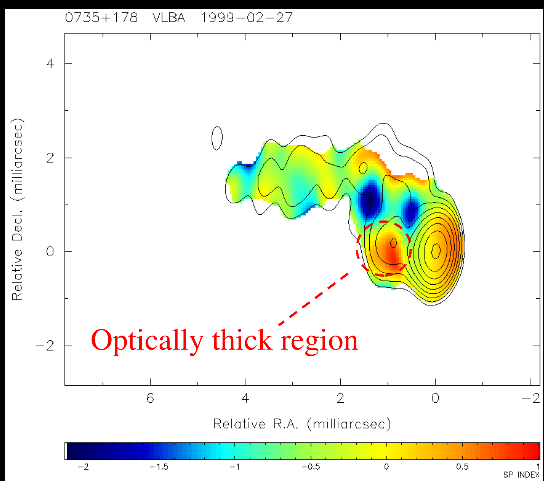

Gabuzda, Gómez & Agudo (2001)

Absorption

The "*missing*" bent in the VSOP (5 GHz) map is optically thick.

Compatible with free-free absorption

BL Lac 0735+178. Interaction with the external medium?

Faraday rotation

Faraday rotation found for the first sharp bend:

- Good fit for 4 frequencies

No clear RM for other regions

Jet-external medium model consistent with the occurrence of:

- A sharp bend
- Free-free absorption
- Faraday rotation

5-8.4 GHz RM map for April 1997

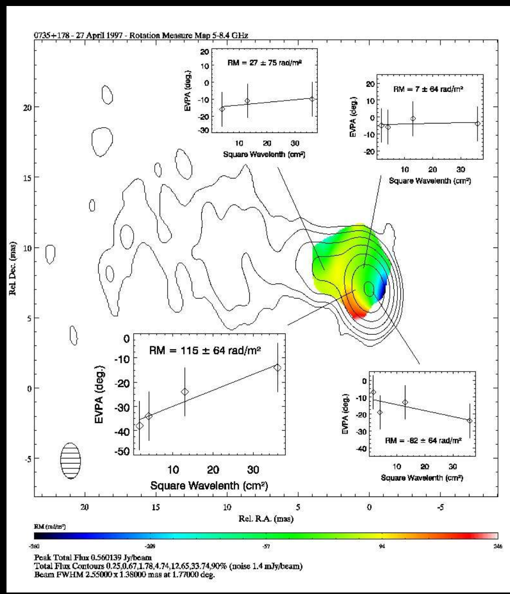

Agudo et al. (in prep.)
in collaboration with Denise Gabuzda

Electron Spectral Evolution Computation

- Radio emission produced by synchrotron
- X-ray emission models unclear yet:
  - Synchrotron?
  - Inverse Compton?
  - Both?
  - Particle acceleration?
- *To deep in this clues, A non thermal electron energy transport code will be of special interest.*

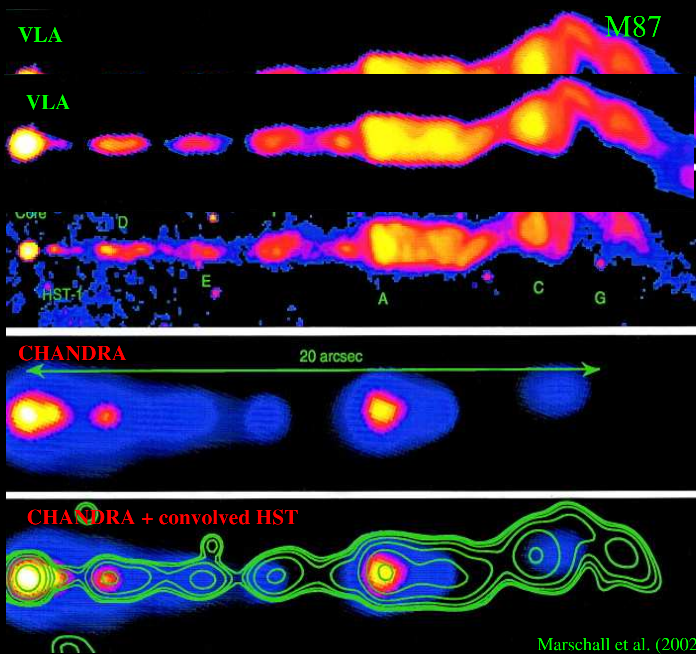

Marschall et al. (2002)

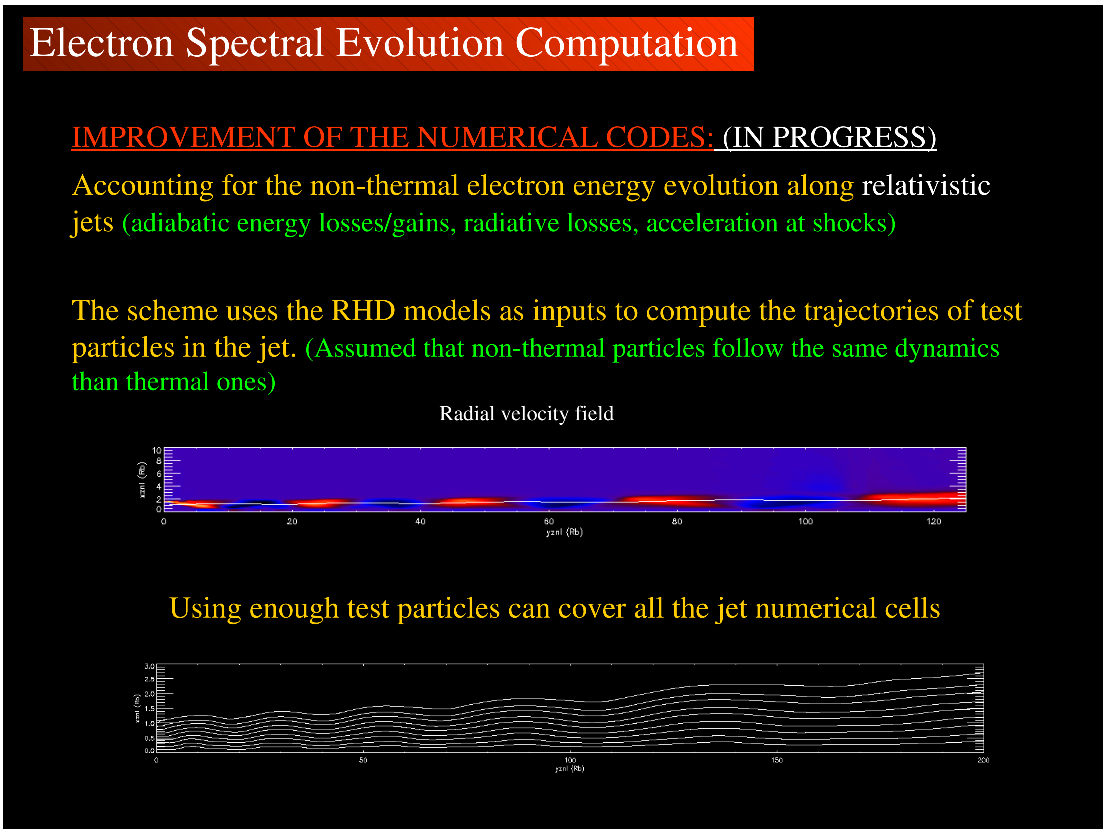
Electron Spectral Evolution Computation
IMPROVEMENT OF THE NUMERICAL CODES: (IN PROGRESS)
Accounting for the non-thermal electron energy evolution along relativistic jets (adiabatic energy losses/gains, radiative losses, acceleration at shocks)
The scheme uses the RHD models as inputs to compute the trajectories of test particles in the jet. (Assumed that non-thermal particles follow the same dynamics than thermal ones)
Radial velocity field
Using enough test particles can cover all the jet numerical cells

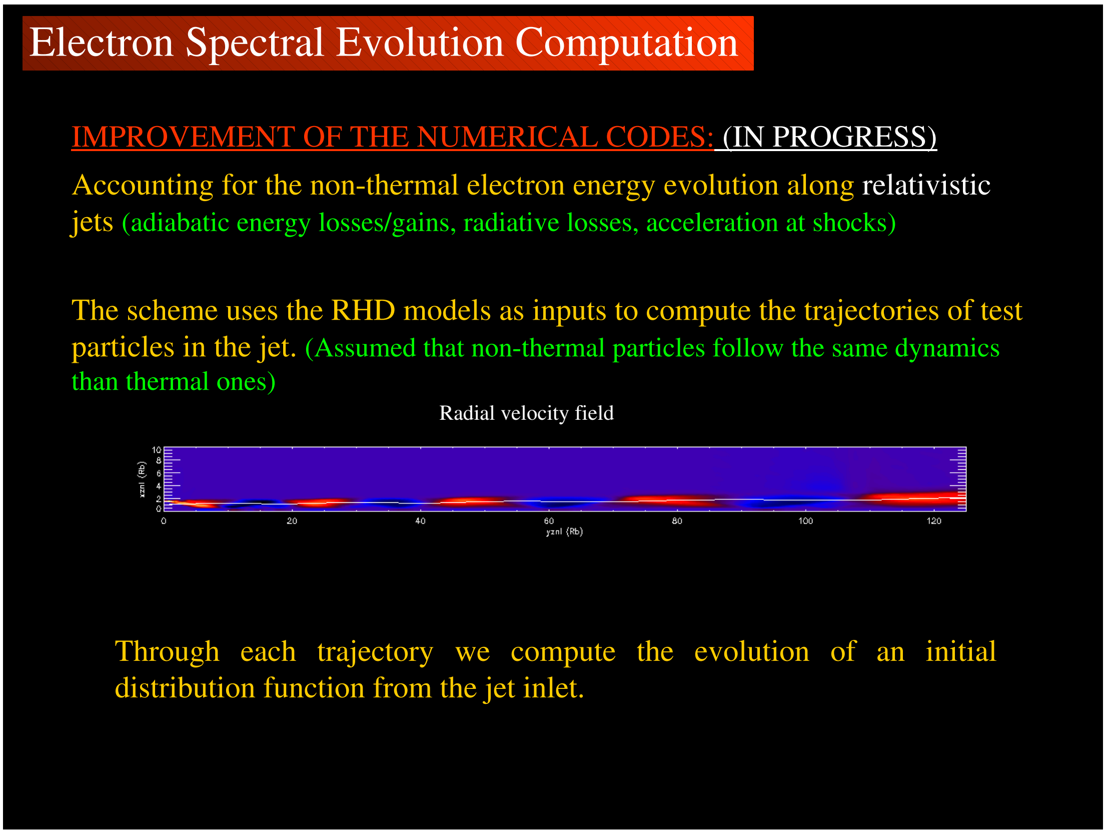
Electron Spectral Evolution Computation
IMPROVEMENT OF THE NUMERICAL CODES: (IN PROGRESS)
Accounting for the non-thermal electron energy evolution along relativistic jets (adiabatic energy losses/gains, radiative losses, acceleration at shocks)
The scheme uses the RHD models as inputs to compute the trajectories of test particles in the jet. (Assumed that non-thermal particles follow the same dynamics than thermal ones)
Radial velocity field
Through each trajectory we compute the evolution of an initial distribution function from the jet inlet.

Electron Spectral Evolution Computation

Distribution function evolution: $f(p,t) = f(p_0,t_0)\dfrac{V_p(p_0,t_0)\,V_x(t_0)}{V_p(p,t)\,V_x(t)}$ if mass conservation

Momentum evolution:

$$b(p) = \left(\frac{dp}{dt}\right)_{tot} = -\frac{1}{3}\left(\nabla \cdot v + \frac{d \ln}{dt}\right) p - b_l(p)$$

with

$$b_l(p,t) = b_{sync}(p,t) = \frac{4}{3}\frac{{}_T\, p^2}{m_e^2 c^2}(U_B)$$

Volume in momentum space evolution : $\dfrac{d \ln V_p}{dt} = 2\dfrac{b}{p} + \dfrac{db}{dp}$ with $V_p = 4\; p^2 \Delta p$

Volume in physical space evolution: $\dfrac{d \ln V_x}{dt} = -\dfrac{d \ln}{dt} \Rightarrow V_x(t) = V_x(t_0)\dfrac{(t_0)}{(t)}$

it is given by the plasma density evolution

Shock acceleration: addition of a new distribution function in the range [p_{inj}, p_{Np}]

$$f_{inj}(p(t_s+\;), t_s+\;) = 0 \;\forall\; p \in [p_0, p_{inj}]$$

$$f_{inj}(p(t_s+\;), t_s+\;) = f_{inj}\left(\frac{p(t_s+\;)}{p_{inj}}\right)^{-q_s} \;\forall\; p \in [p_{inj}, p_{N_p}]$$

Electron Spectral Evolution Computation

Applying this scheme for a set of test particles, covering all the numerical domain, we are able to compute the energy evolution along the jet

Using the result in the emission code will allow to obtain wide range energy emission simulations (radio to X-rays) of relativistic jets. This simulations will be directly comparable with observations.

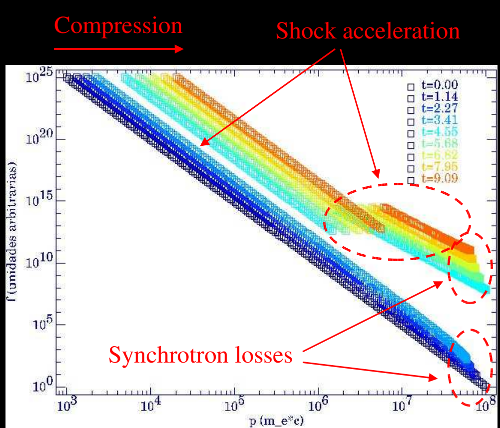

Agudo et al. (in preparation)

They will be of special interest to improve our knowledge of :

-High energy radiation mechanisms

-Acceleration processes

IN RELATIVISTIC JETS

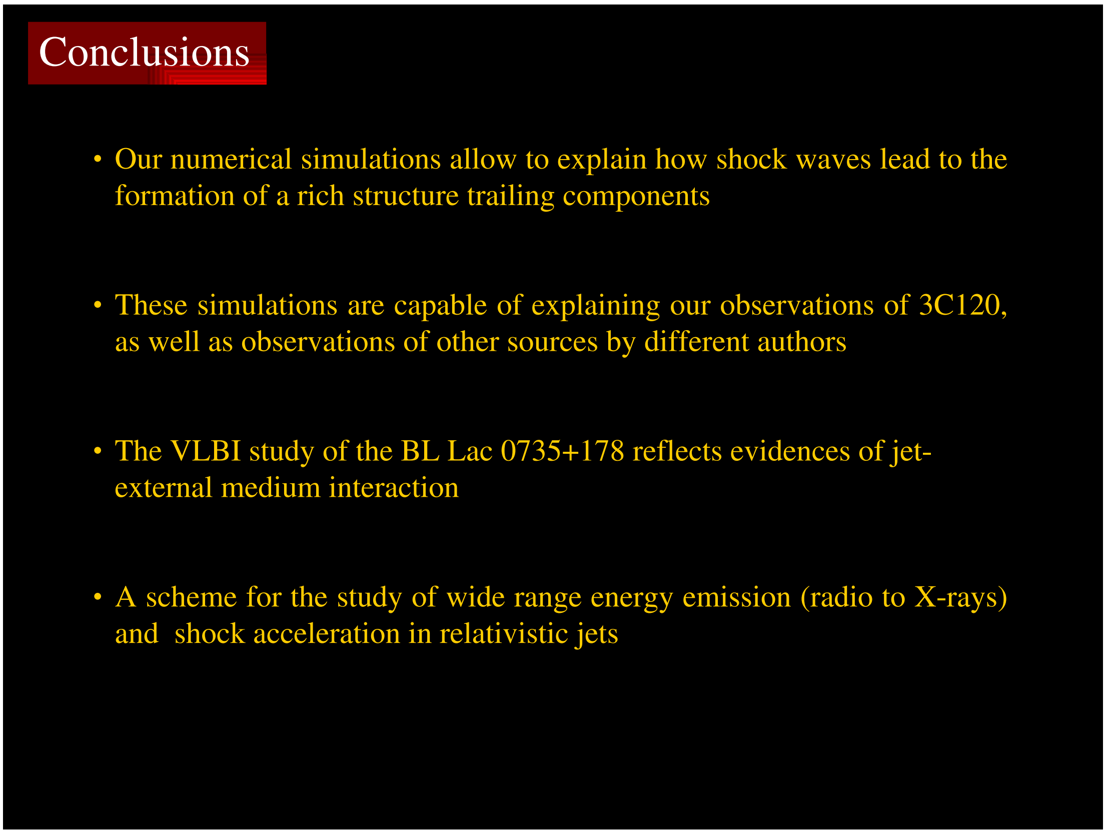
Conclusions
• Our numerical simulations allow to explain how shock waves lead to the formation of a rich structure trailing components
• These simulations are capable of explaining our observations of 3C120, as well as observations of other sources by different authors
• The VLBI study of the BL Lac 0735+178 reflects evidences of jet-external medium interaction
• A scheme for the study of wide range energy emission (radio to X-rays) and shock acceleration in relativistic jets

7.5 T. Arshakian: Statistical Analysis of bright radio sources at 15GHz

Statistical analysis of bright radio sources at 15GHz

T. G. Arshakian *

Max-Planck-Institut für Radioastronomie, Germany

May 8, 2003

Abstract

A revised sample of the high-frequency 2cm Very Large Base Array (VLBA) survey is studied to test the isotropic distribution in the sky and its uniform distribution in the space. The sample is complete to a flux-density limits of 1.5Jy and 2Jy for positive and negative declinations respectively. At present the sample comprises of 100 members and 23 candidates, all are active galactic nuclei. The two-dimensional Kolmogorov-Smirnov test indicates that there is no significant deviation from the isotropic distribution in the sky, while the V/Vmax test shows that the space distribution of active nuclei is not uniform at high confidence level (99.9%). This is indicative of a strong space/density evolution implying that active nuclei were more populous at high redshifts, $z \sim 2$.

*E-mail: tigar@mpifr-bonn.mpg.de

Statistical analysis of bright radio sources at 15GHz

- Sample Description
- Sky Distribution
- Space Distribution

Sample Description

History:
6 cm (5 GHz) survey – 2 cm (15 GHz) survey – 2 cm complete sample (MOJAVE sample, (http://www.cv.nrao.edu/∼mlister/MOJAVE/index.html).

The complete sample of 123 radio sources comprises of 101 members and 22 candidates. The selection criteria are:

- Declination greater than -20 degrees
- Galactic latitude $|b| > 2.5$ degrees
- Total 2 cm VLBA flux exceeding 1.5 Jy at any epoch since 1995 ($>$ 2 Jy for sources below the celestial equator)

All sources are:

- **active galactic nuclei** (AGN),
- **radio-loud**,
- **core-dominated**.

Most of them have **superluminal radio jets on parsec-scales**.

Sky Distribution

Hypothesis: the AGN are *distributed uniformly* in the sky.

- $A(\alpha) = \text{const}$ - uniform between $0h$ and $24h$.
- $D(\delta) = \sin(\delta)$.

Method1: 2D Kolmogorov-Smirnov test, $P(\alpha, \delta)$.
Result: No significant deviation from the uniform distribution.

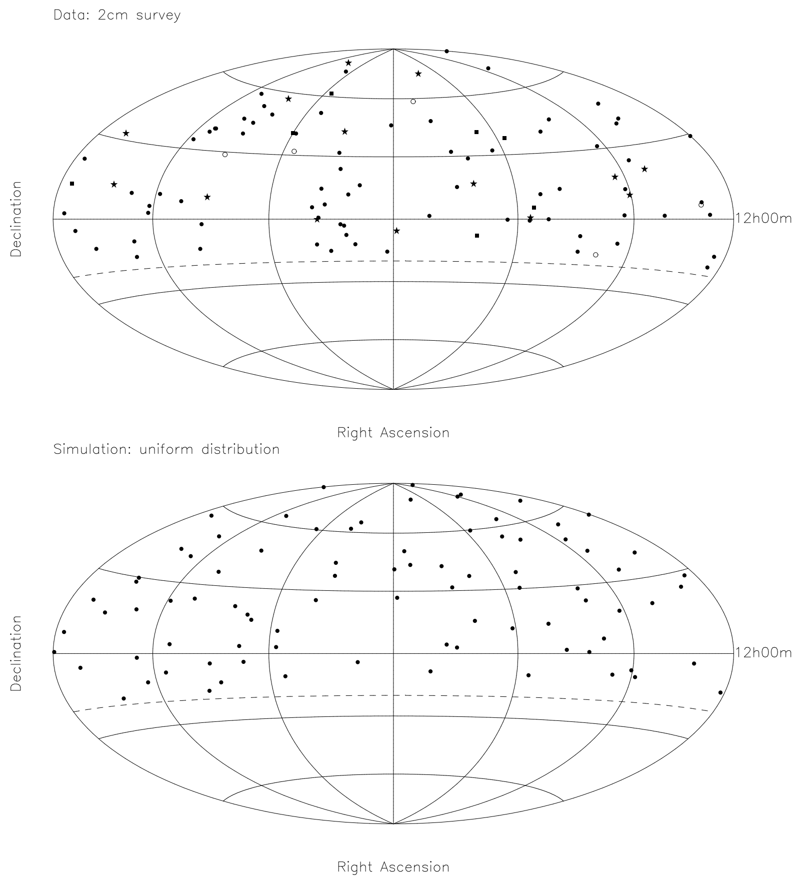

Figure 1: **Data:** the distribution of 99 AGN in the sky. **Simulation:** the uniform distribution.

Method2: 1D Kolmogorov-Smirnov test.

- Declinations - no significant deviation from the $\sin(\delta)$ distribution.
- Right Ascensions - uniform distribution can be rejected at 99.92% confidence level (Table 1)

Table 1: K-S test for Right Ascensions of AGN.

Redshift range	Number	Confidence level (%)
1.3–1.9	13	99.63
1.3–2	15	99.92
1.3–2.1	18	99.62
> 1.3	24	91.90

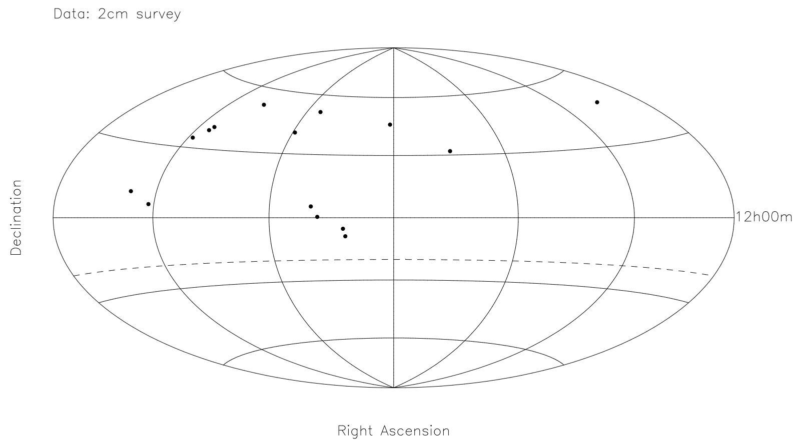

Figure 2: **Data:** the distribution of 15 AGN in in the redshift range between 1.3 and 2.

Space Distribution (V/V_{max})

Hypothesis: A *uniform distribution* of AGN in the space.
Method: $V/V_{\rm max}$ test – derived and valid for complete samples.

- V - is the volume of space enclosed by the redshift of the AGN having the certain flux density
- $V_{\rm max}$ - is the maximum volume of space within which this source could be observed and still be included in the complete sample.
- Theory: $\boxed{< V/V_{\rm max} >_{\rm t} = 0.5 \text{ and } \sigma = 1/\sqrt{12}}$.
- Significance of a difference between $< V/V_{\rm max} >_{\rm t}$ and $< V/V_{\rm max} >_{\rm obs}$.

Results:

Table 2: $V/V_{\rm max}$ test for 88 AGN ($H = 70$, $q_0 = 0.1$).

ID	Number	$< V/V_{\rm max} >$	Standard error	Confidence level (%)
Q	68	0.64	0.032	99.9
BL	13	0.64	0.07	75
G	7	0.57	0.12	16

Quasars (or jet activity phenomena) were more populous at large redshifts, $z = 2$.

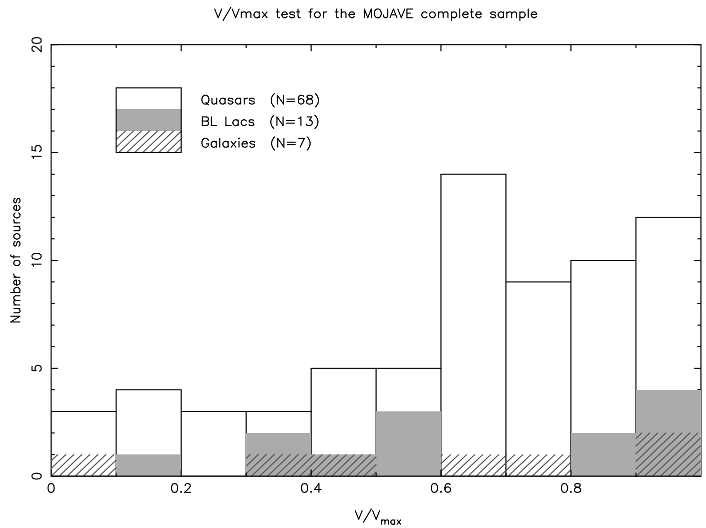

Figure 3: The distribution of $V/V_{\rm max}$ statistics for 88 AGN

Luminosity – $V/V_{\max}$ dependence:

- 35 low luminosity quasars, $P_{15\,\mathrm{GHz}} \leq 10^{27.84}$ W Hz^{-1}.
- 33 high luminosity quasars, $P_{15\,\mathrm{GHz}} \geq 10^{27.84}$ W Hz^{-1}.

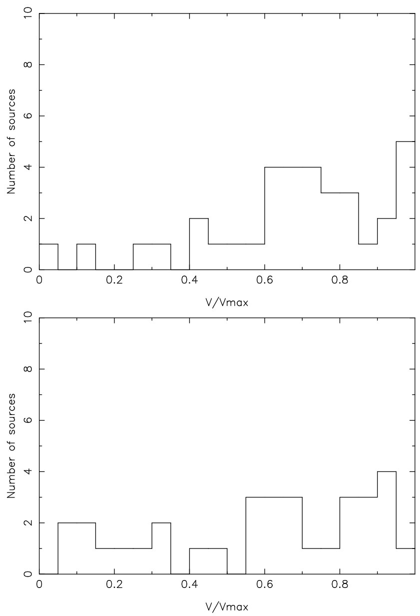

Figure 4: The distribution of $V/V_{\max}$ for **low** and **high** luminosity quasars.

Table 3: $V/V_{\max}$ test for **low** and **high** luminosity quasars.

$P_{15\,\mathrm{GHz}}$	Number	$< V/V_{\max} >$	Standard error	Confidence level (%)
Low	35	0.68	0.04	99.98
High	33	0.59	0.05	95

Student t test shows no significant difference (P = 84%) between the average values of $V/V_{\max}$ for low and high luminosity quasars.

More statistics needed to resolve this problem

ACKNOWLEDGMENTS

- Alexander von Humboldt Foundation
- 2 cm survey team:
  - Anton Zensus (my host)
  - Eduardo Ros
  - Marshal Cohen
  - Matt Lister

7.6 B. Sbarufatti: Spectroscopy of BL Lac objects

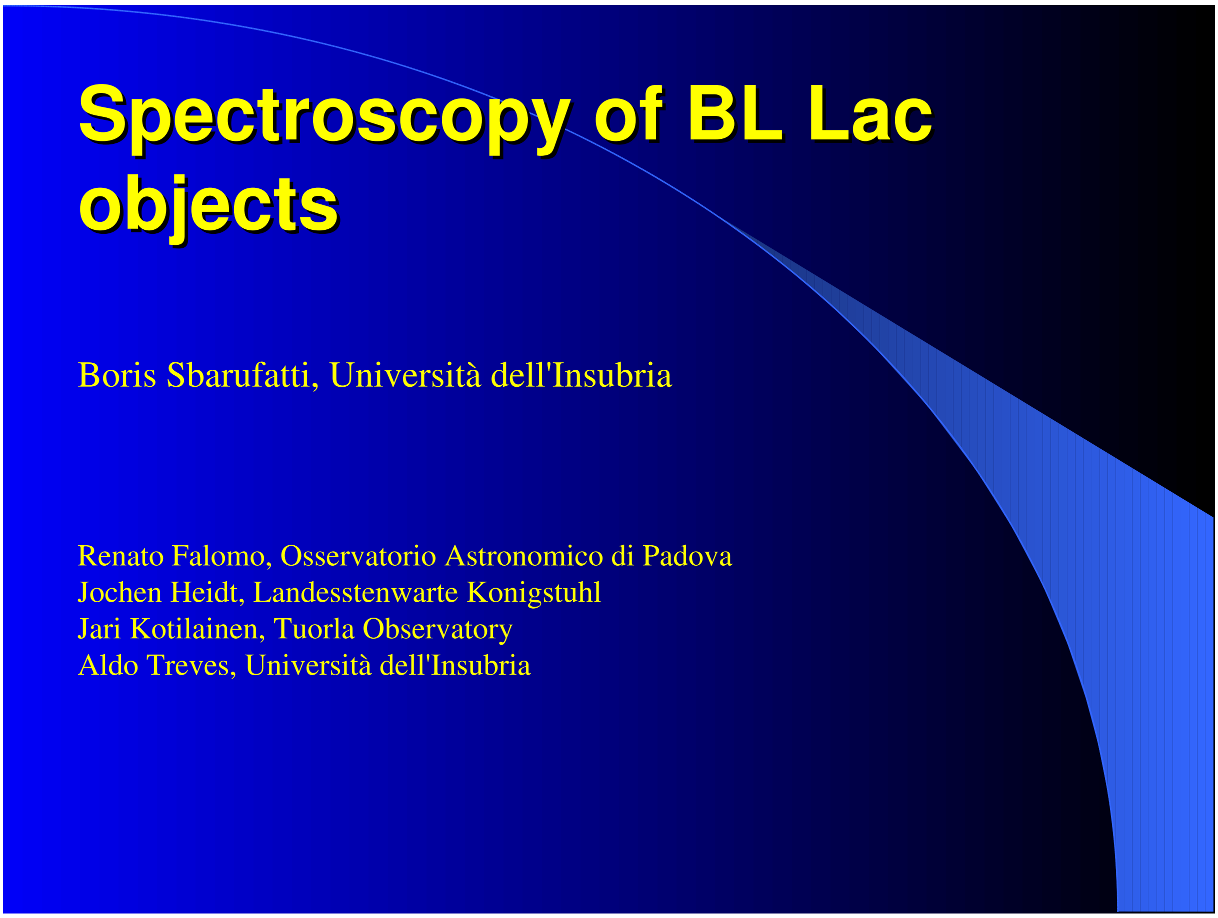

Spectroscopy of BL Lacs

- BL Lacs characterized by lack of spectral features
- Statistic of BLL redshift
- Results from recent observations at 4m telescopes
- Our program for VLT

Properties of BL Lacs

- Extragalactic radio sources (compact flat spectrum)
- Strong non-thermal emission (from radio to X and gamma)
- Featureless optical continuum (very weak emission lines)
- Flux variability (*large amplitude and short timescale*)
- High and variable polarization
- Superluminal motion
- Nuclei of massive elliptical galaxies

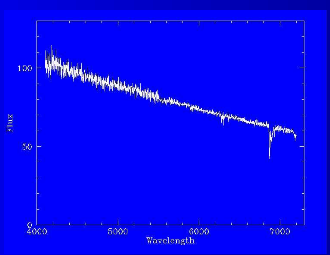

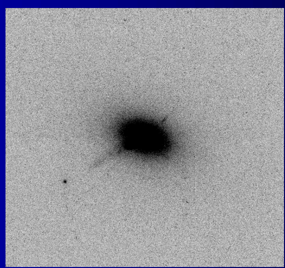

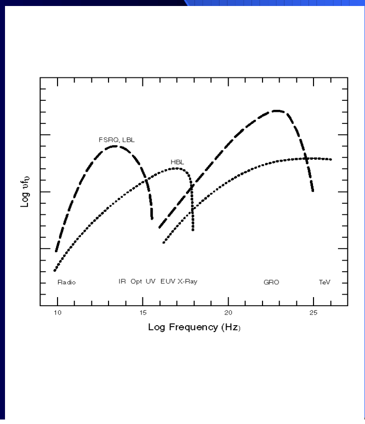

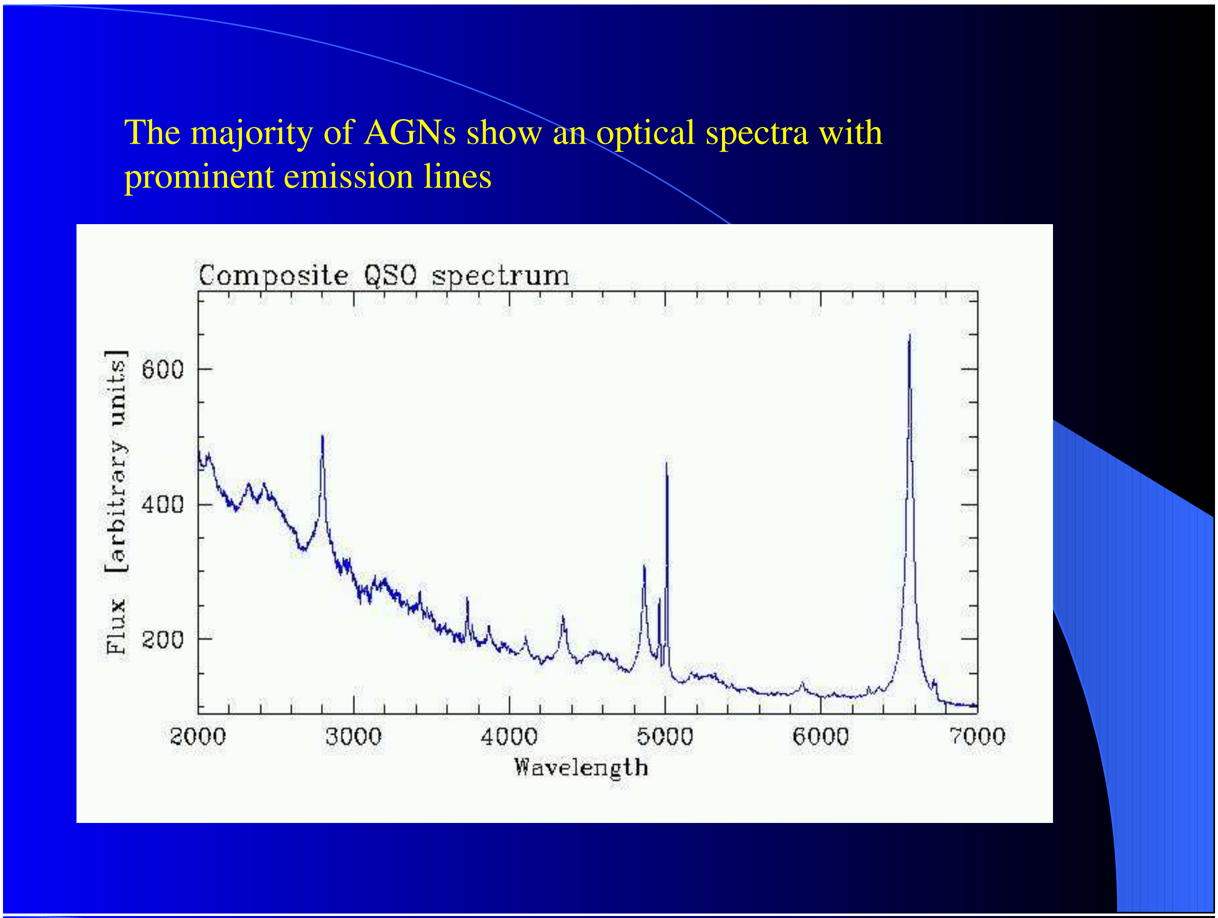
The majority of AGNs show an optical spectra with prominent emission lines
Composite QSO spectrum
Flux [arbitrary units]
600
400
200
2000
3000
4000
5000
6000
7000
Wavelength

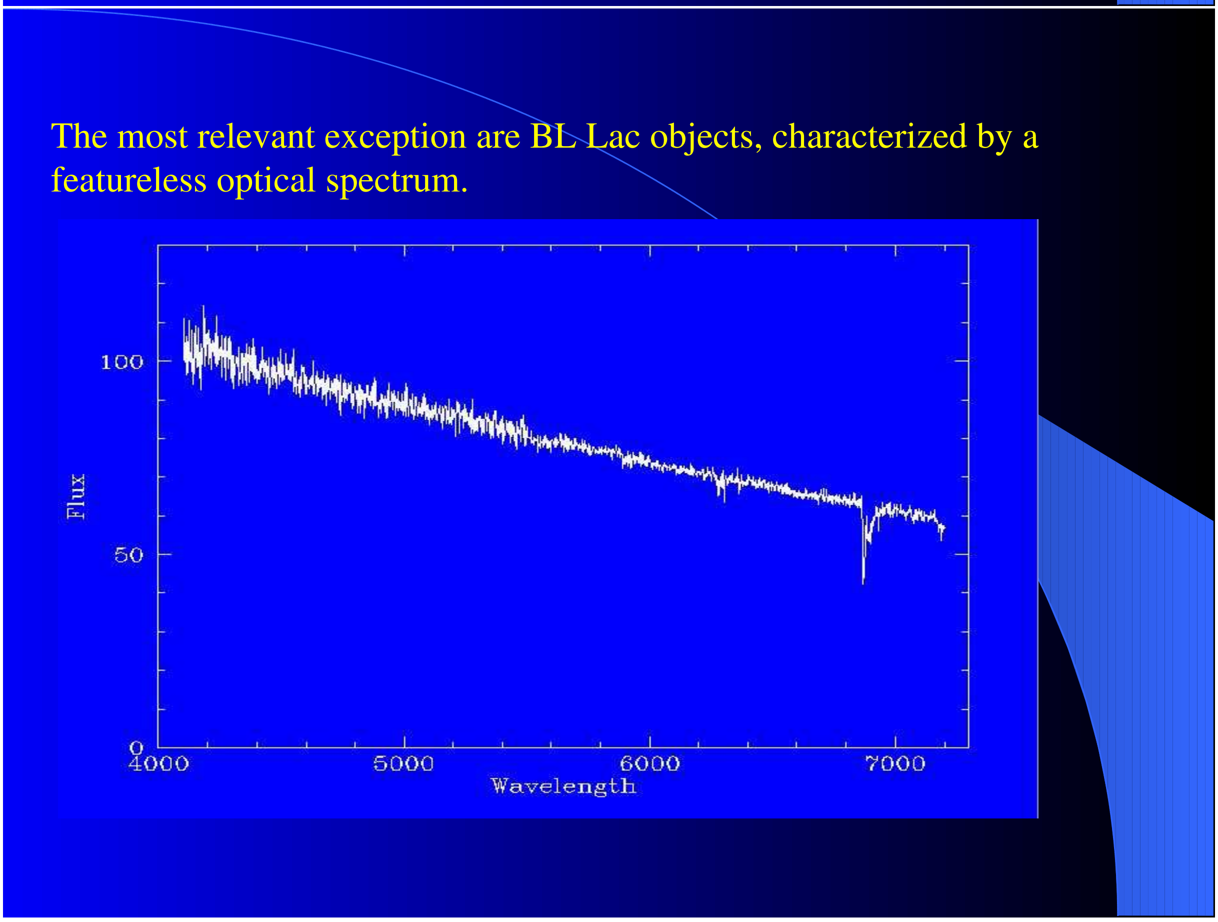
The most relevant exception are BL Lac objects, characterized by a featureless optical spectrum.
Flux
100
50
0
4000
5000
6000
7000
Wavelength

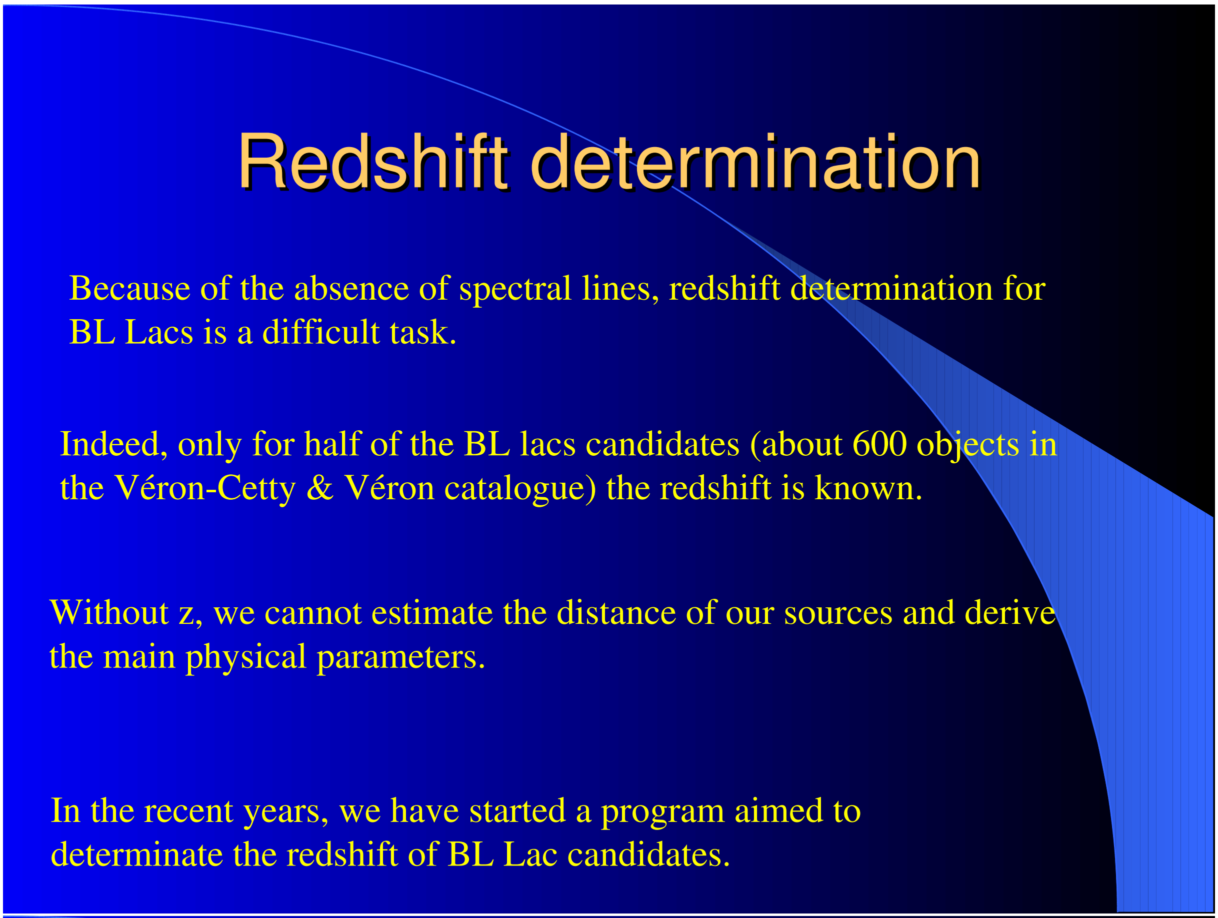
Redshift determination
Because of the absence of spectral lines, redshift determination for BL Lacs is a difficult task.
Indeed, only for half of the BL lacs candidates (about 600 objects in the Véron-Cetty & Véron catalogue) the redshift is known.
Without z, we cannot estimate the distance of our sources and derive the main physical parameters.
In the recent years, we have started a program aimed to determinate the redshift of BL Lac candidates.

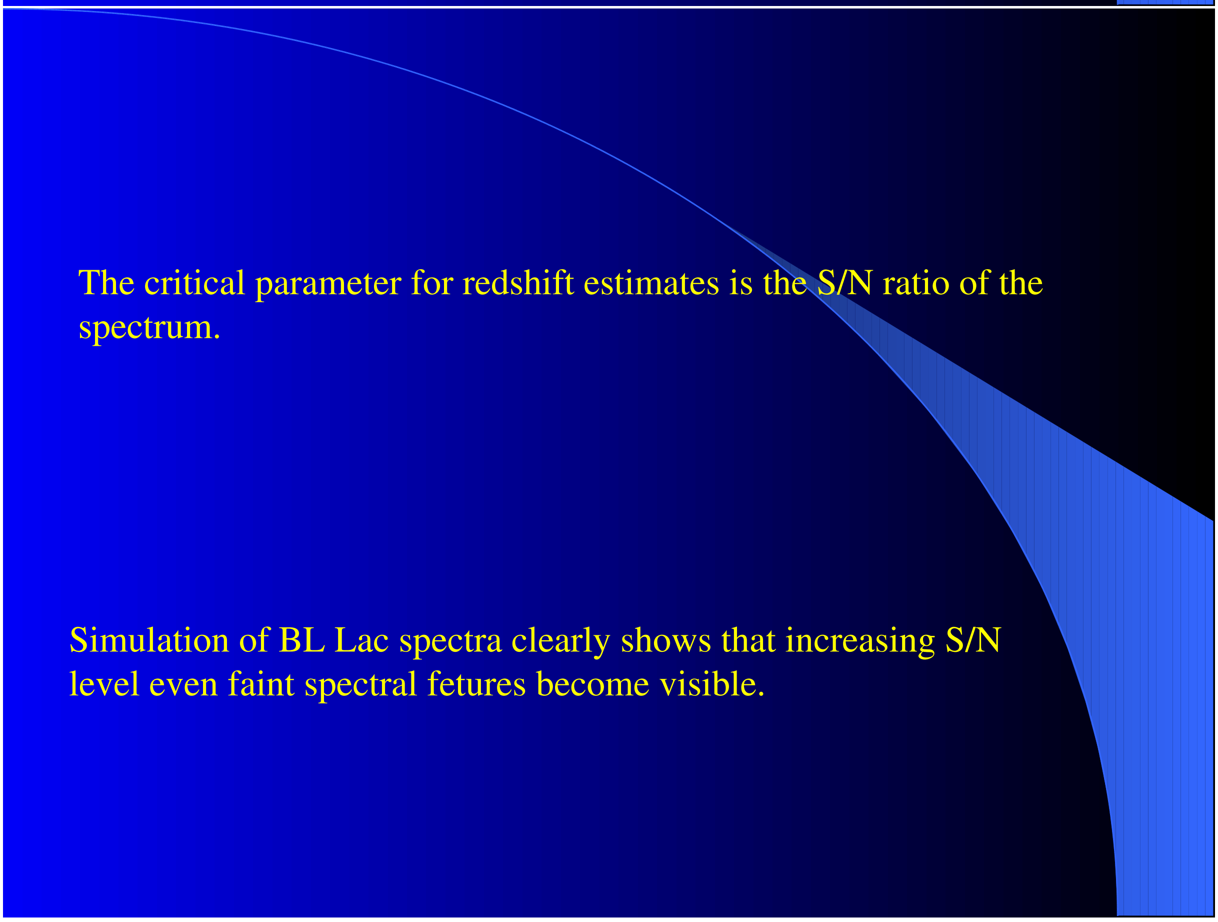
The critical parameter for redshift estimates is the S/N ratio of the spectrum.
Simulation of BL Lac spectra clearly shows that increasing S/N level even faint spectral fetures become visible.

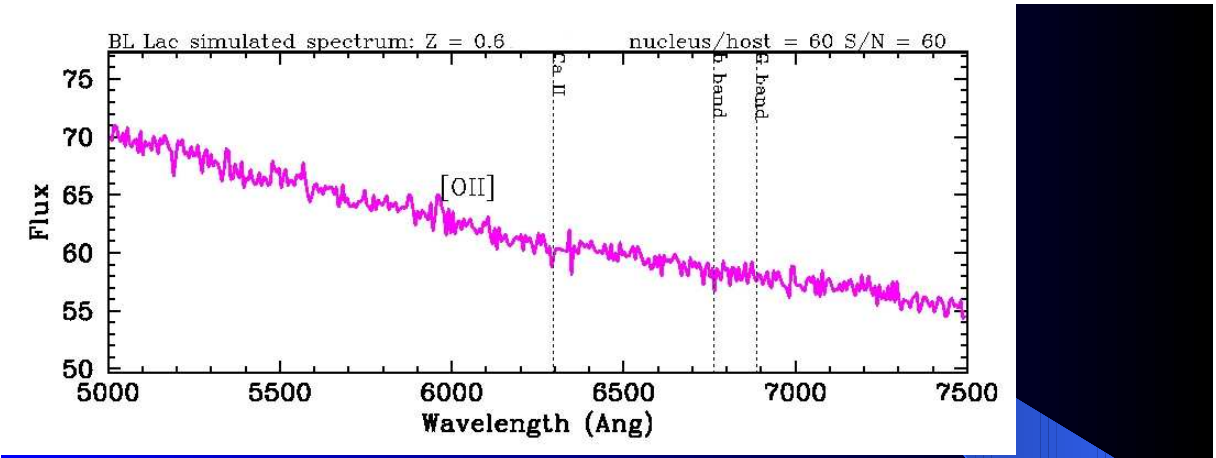
BL Lac simulated spectrum: Z = 0.6
nucleus/host = 60 S/N = 60
Ca II
h band
G band
[OII]
Flux
Wavelength (Ang)

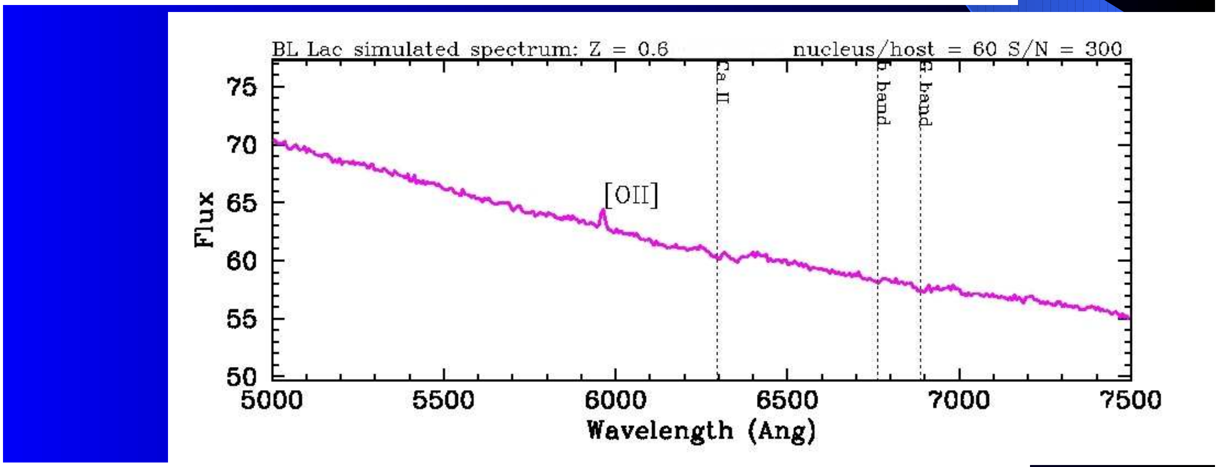
BL Lac simulated spectrum: Z = 0.6
nucleus/host = 60 S/N = 300
Ca II
h band
G band
[OII]
Flux
Wavelength (Ang)

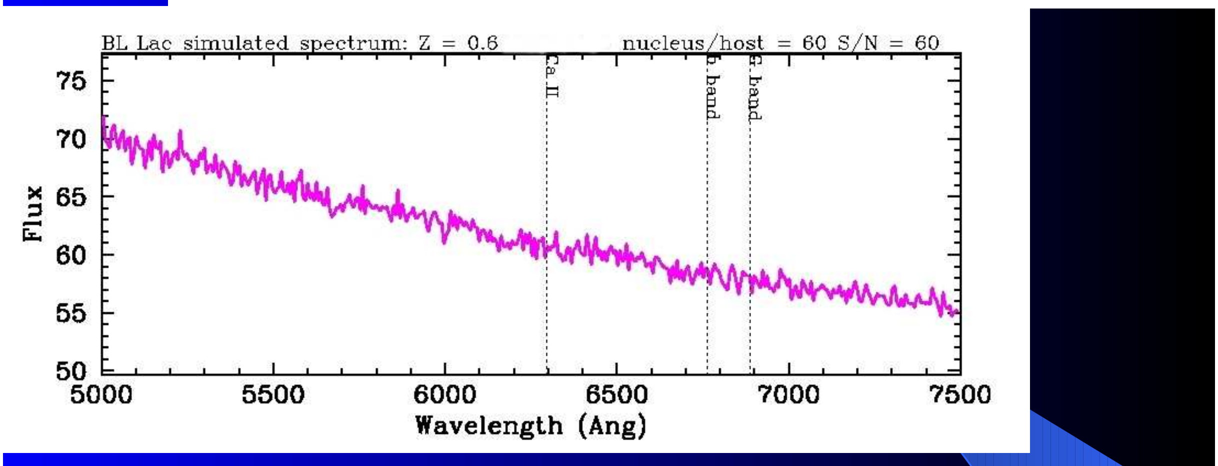
BL Lac simulated spectrum: Z = 0.6
nucleus/host = 60 S/N = 60
Ca II
h band
G band
Flux
Wavelength (Ang)

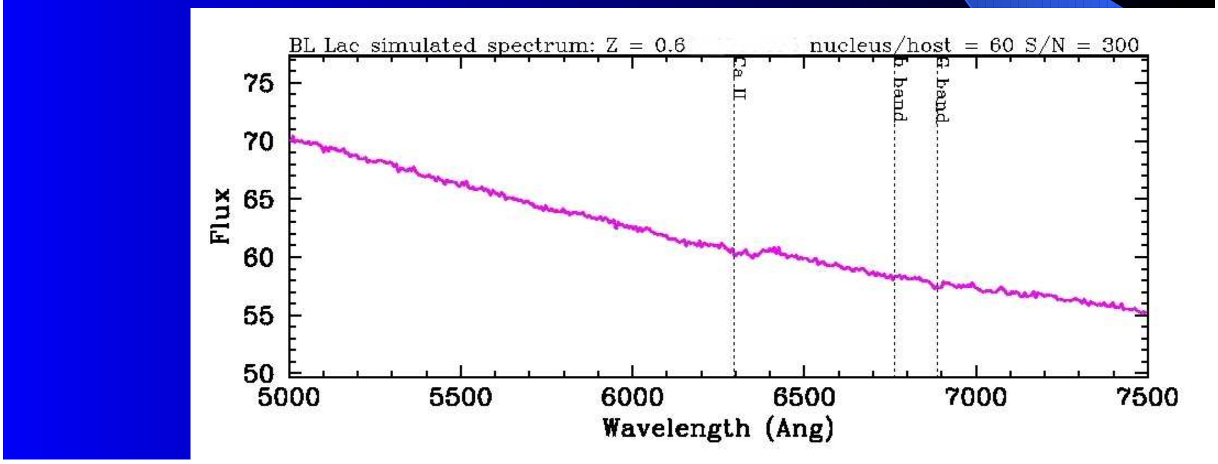
BL Lac simulated spectrum: Z = 0.6
nucleus/host = 60 S/N = 300
Ca II
h band
G band
Flux
Wavelength (Ang)

The 4 mt telescopes program

With 4 mt class telescopes (ESO 3.6m, NOT), we have carried spectroscopic observations of BL Lac candidates.

S/N level varies in the range 60-180, allowing us to estimate the redshift for sources brighter than m_v= 15 mag.

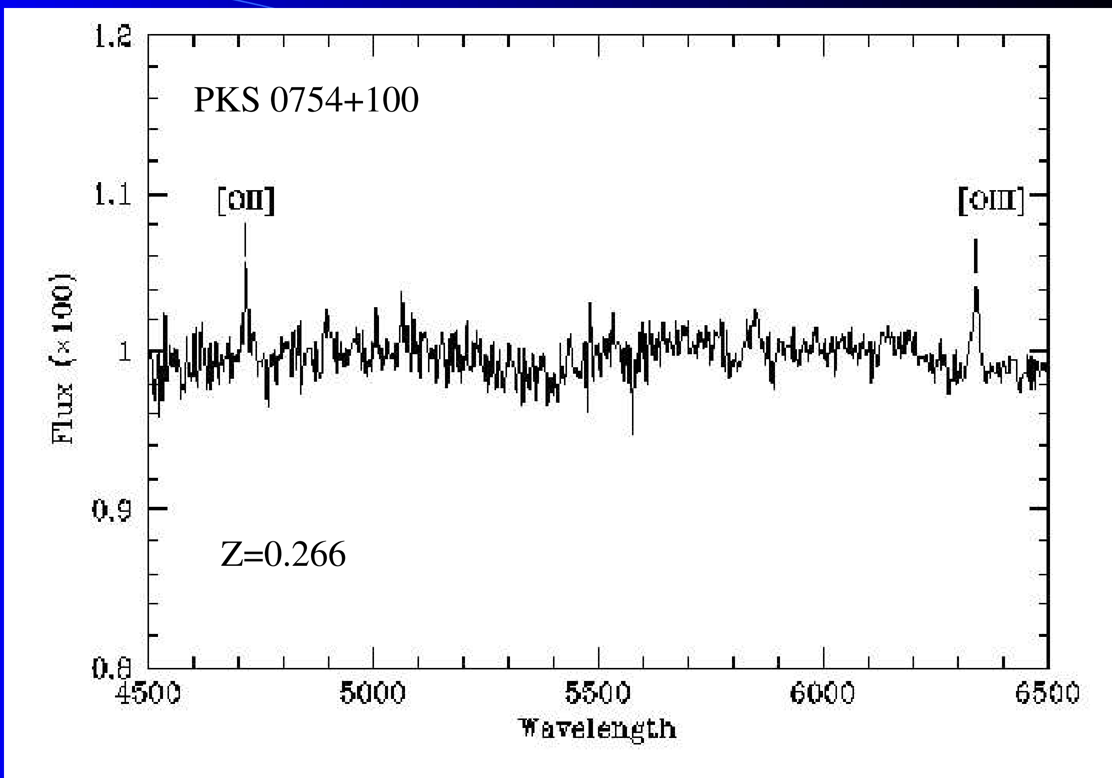

However, for fainter sources, we cannot estimate redshift even with 4 m class telescopes.

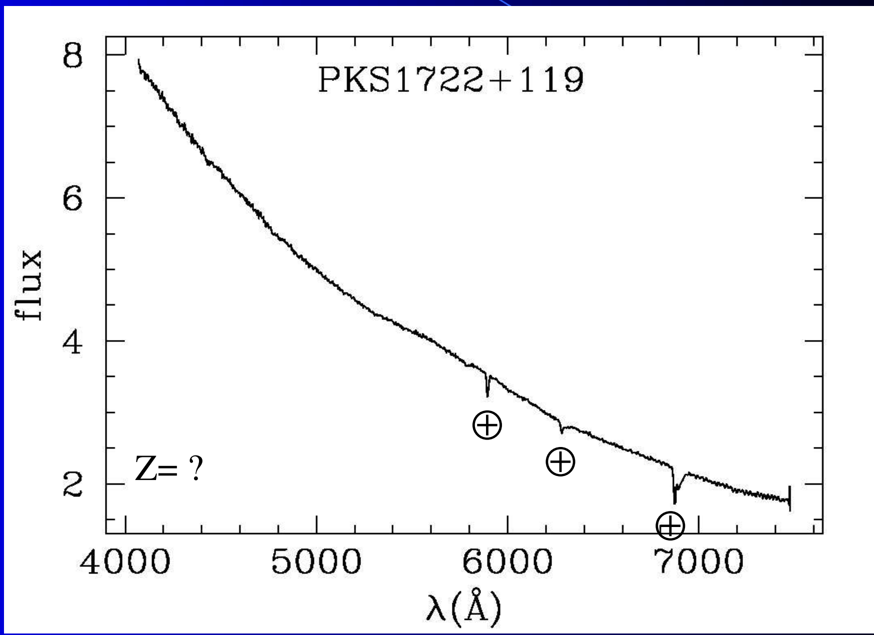

The VLT program

So, we need to reach higher S/N ratio

The solution is to use 8 m class telescopes, such VLT.

18 hours of allocated time in service mode for period 71 (April-September 2003).

07 April: First observations executed!!!

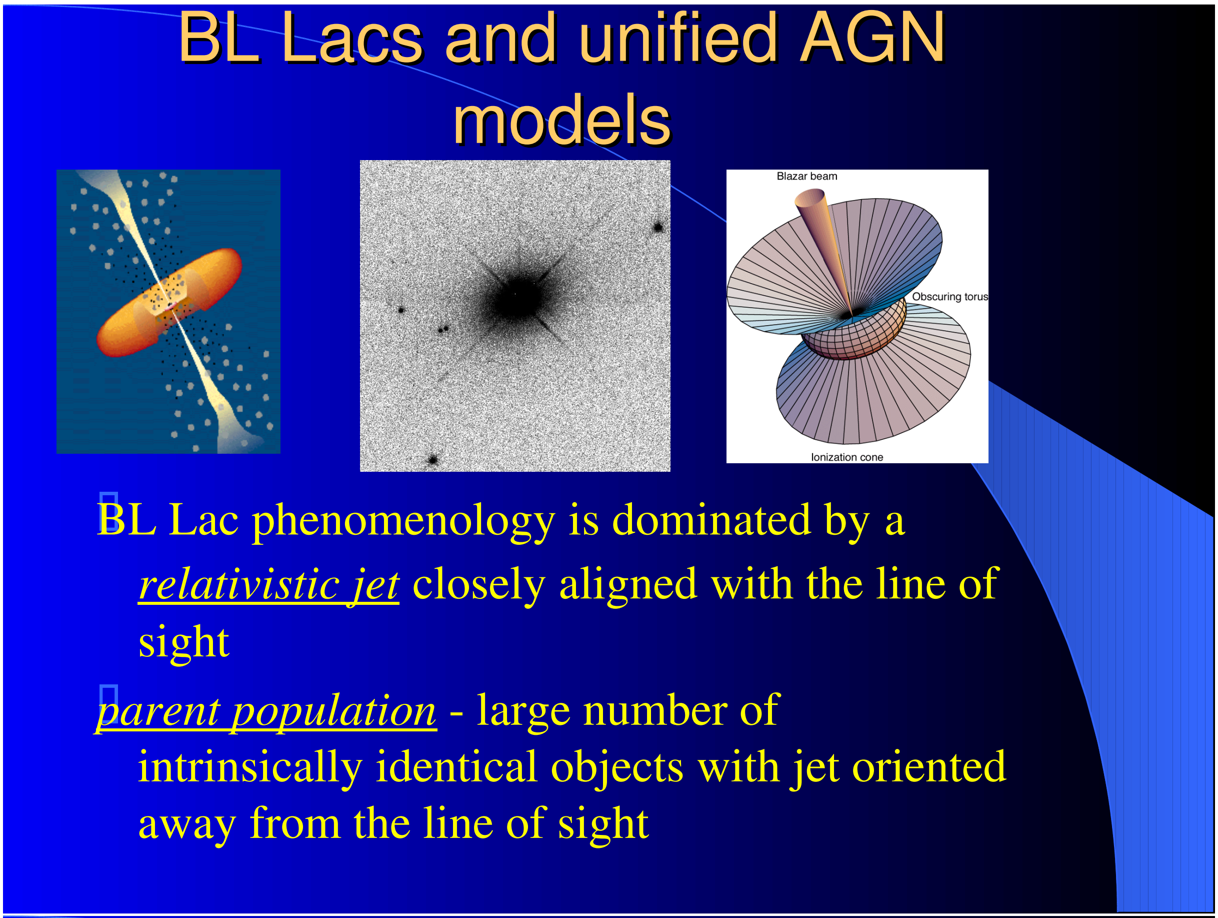
BL Lacs and unified AGN models
Blazar beam
Obscuring torus
Ionization cone
BL Lac phenomenology is dominated by a relativistic jet closely aligned with the line of sight
parent population - large number of intrinsically identical objects with jet oriented away from the line of sight

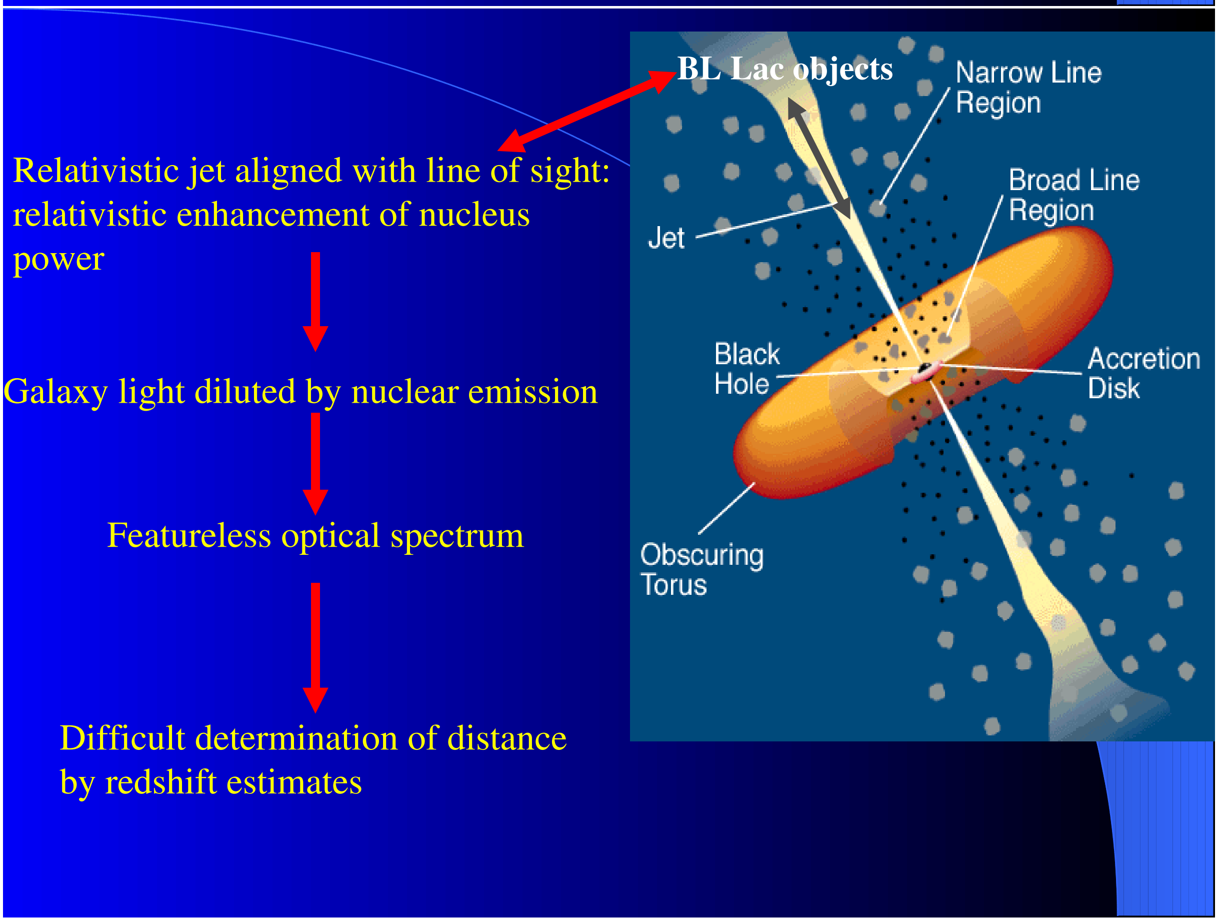
BL Lac objects
Narrow Line Region
Broad Line Region
Jet
Black Hole
Accretion Disk
Obscuring Torus
Relativistic jet aligned with line of sight: relativistic enhancement of nucleus power
Galaxy light diluted by nuclear emission
Featureless optical spectrum
Difficult determination of distance by redshift estimates

7.7 C. Raiteri: A helical jet model to explain the Mkn501 SED variations

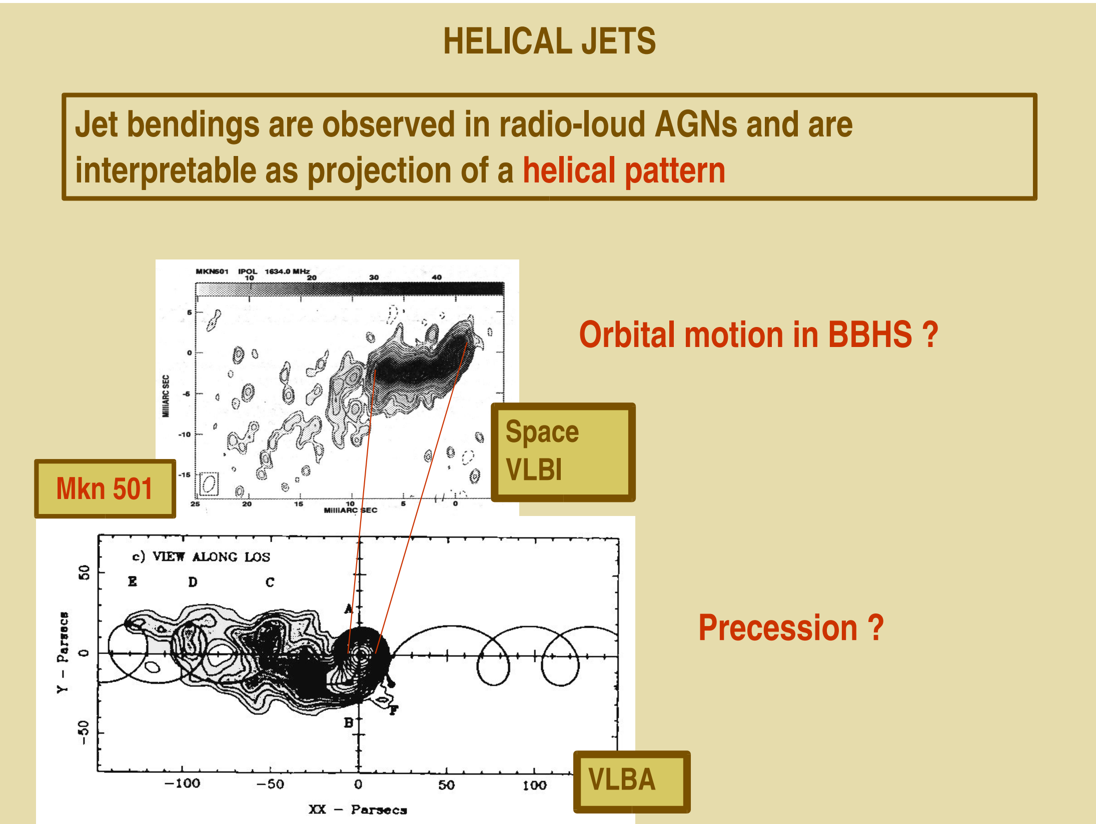

A HELICAL JET MODEL TO EXPLAIN BLAZAR VARIABILITY

Rotating helical jet (BBHS)

Inhomogeneous: emitted ν decreasing with increasing z (*delays of lower ν variations*)

Emissivity decreases with z (*lower radio flux at lower ν*)

SSC+Klein-Nishina

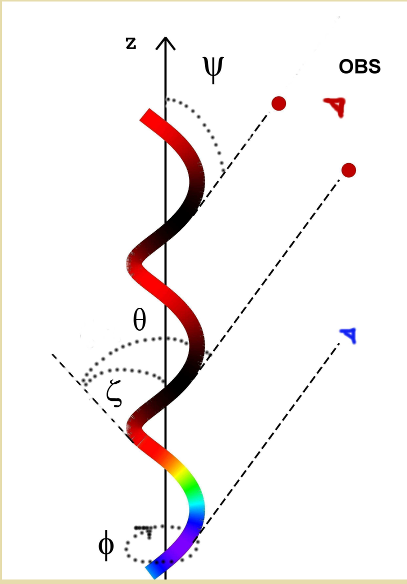

As the helix rotates, the flux at ν peaks when the part of the jet most contributing to it has minimum θ

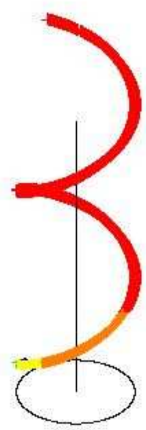

Long-term variations Observed in SEDs and light curves are obtained as a geometric effect, due to the helix rotation

Periodicity is easily explained

A critical test: Mkn 501

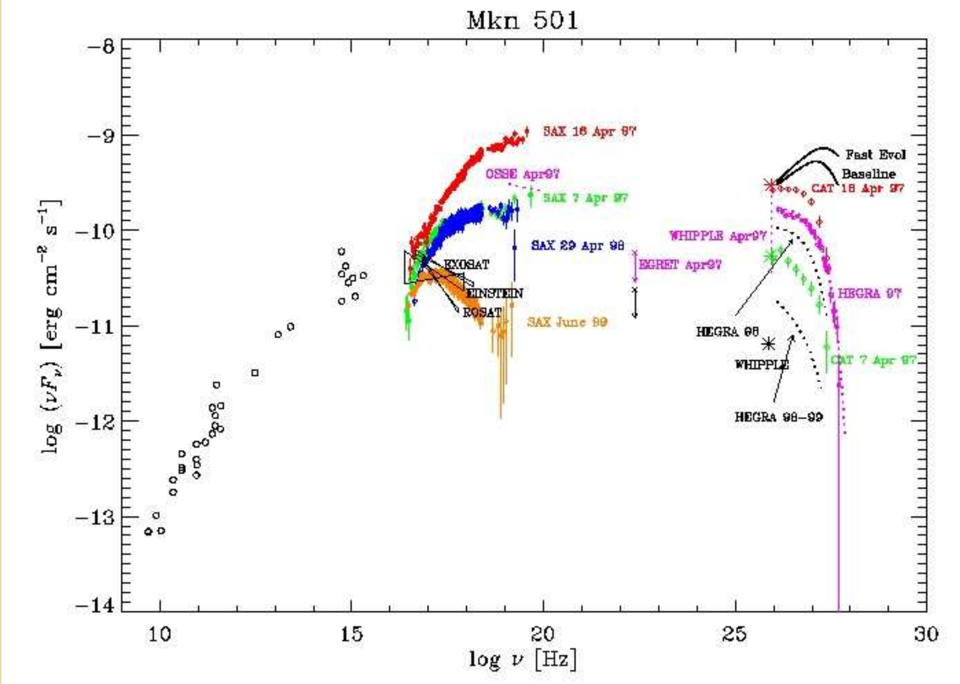

Trends of emitted frequencies along the jet

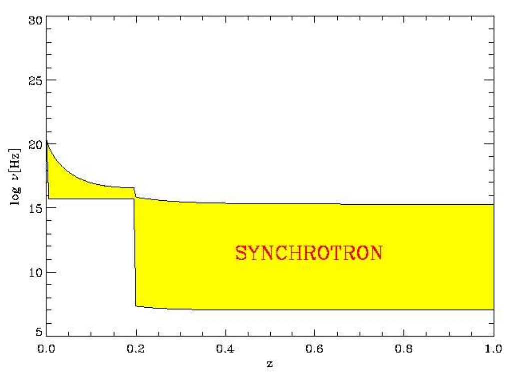

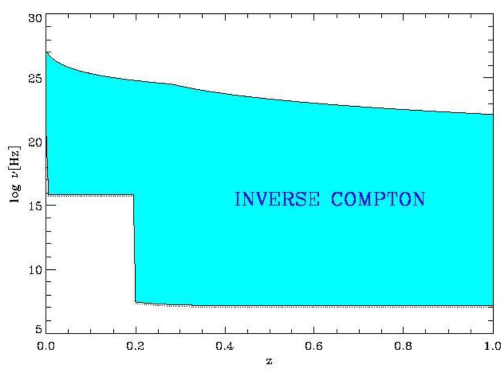

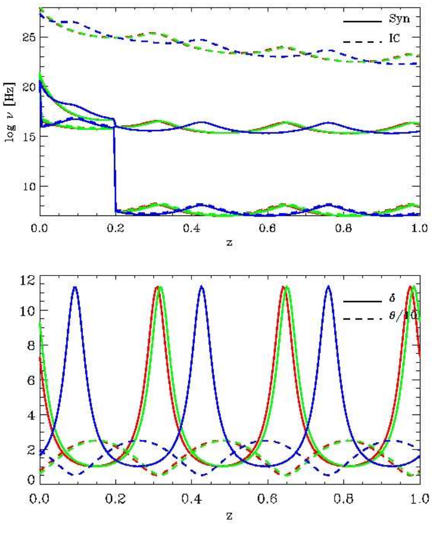
Syn
IC
log ν [Hz]
z
δ
θ/10
z

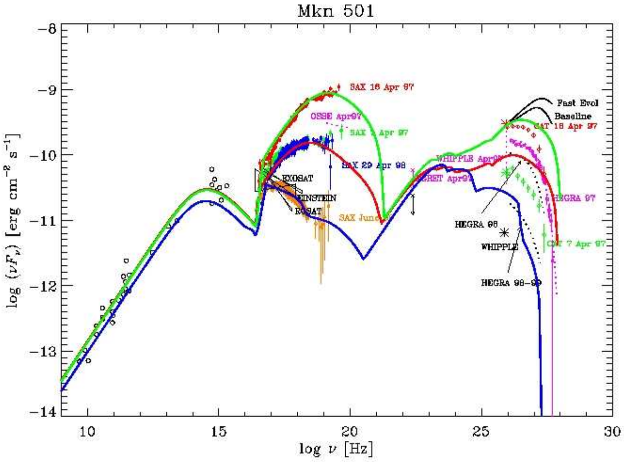
Mkn 501
log (νFν) [erg cm⁻² s⁻¹]
log ν [Hz]
SAX 16 Apr 97
OSSE Apr97
SAX 7 Apr 97
SAX 29 Apr 98
EXOSAT
EINSTEIN
SAX June
WHIPPLE Apr97
EGRET Apr97
Fast Evol
Baseline
CAT 16 Apr 97
HEGRA 97
HEGRA 98
WHIPPLE
HEGRA 98-99
CAT 7 Apr 97

7.8 M. Camenzind: Quo vadis Blazar Jets? Steps towars a Global Understanding

A Roadmap of Problems

- P1: The Host Galaxy and its Black Hole.
- P2: Are Jets launched by the Ergosphere ?
- What we learnt from FR II/Quasar Jets-Models:

  □Sedov phase □cigar phase □bubble phase
  □Beam Plasma is exotic ! (i-e, ee, or both)
  □Environment is essential, but now known ! □Nature of kpc-scale knots.
- P3: FR I/BL Lac – M87/Cen A as archetypes ?
- P4: Traversing the Bulge …what you observe in VLBI-mapping and monitoring !
- P5: Magnetic effects: Torsional Alfven Waves, Current Filamentation and Particle Acceleration
- □Palette of different codes is needed !

P1: The Host Galaxy, its Black Hole and its Environment

- Information required for individual sources:
- □Black Hole mass M_H ~ Bulge Mass and σ^4.
- □Black Hole spin a_H is completely unknown !
- □Bulge mass M_{Bulge} known for a few examples.
- □Gas mass in bulge (parsec-scale, question of dusty torus etc) largely unknown !
- □Relative accretion rate partially known !
- □Mass ejection rate ?
- □Inclination angle towards spin axis ?
- □Magnetisation of BH largely unknown !
- Except for some well observed examples: M87, M 84, Cyg A, Cen A

GALAXY SAMPLE. **Marconi & Hunter 2003**

Galaxy (1)	Type (2)	D (3)	σ_e (4)	M_{BH} (+,−) (5)	Ref (6)	R_{BH} (7)	N_{res} (8)	M_B (9)	M_J (10)	M_H (11)	M_K (12)	R_e (13)	M_{bul} (14)
Group 1													$M_{bulge} \sim R_e\ sigma^2$
NGC4258	Sbc	7.2	130	$3.9(0.1,0.1) \times 10^7$	m-1	0.28	71	-17.2	-20.9	-22.0	-22.4	0.92 ± 0.23	$1.1 \pm 0.3 \times 10^{10}$
M87	E0	16.1	375	$3.4(1.0,1.0) \times 10^9$	g-2	1.33	33	-21.5	-24.6	-25.2	-25.6	6.4 ± 1.6	$6.2 \pm 1.7 \times 10^{11}$
NGC3115	S0	9.7	230	$9.1(9.9,2.8) \times 10^8$	s-3	1.57	15	-20.2	-23.5	-24.2	-24.4	4.7 ± 1.2	$1.7 \pm 0.5 \times 10^{11}$
NGC4649	E1	16.8	385	$2.0(0.4,0.6) \times 10^9$	s-4	0.71	14	-21.3	-24.9	-25.5	-25.8	8.1 ± 2.0	$8.4 \pm 2.2 \times 10^{11}$
M81	Sb	3.9	165	$7.6(2.2,1.1) \times 10^7$	g-5	0.63	13	-18.2	-23.1	-23.9	-24.1	3.4 ± 0.9	$6.4 \pm 1.8 \times 10^{10}$
M84	E1	18.4	296	$1.0(2.0,0.6) \times 10^9$	g-6	0.55	11	-21.4	-24.7	-25.8	-25.7	8.2 ± 2.1	$5.0 \pm 1.4 \times 10^{11}$
M32	E2	0.8	75	$2.5(0.5,0.5) \times 10^6$	s-7	0.49	9.7	-15.8	-18.9	-19.7	-19.8	0.24 ± 0.06	$9.6 \pm 2.6 \times 10^8$
CenA	S0	4.2	150	$2.4(3.6,1.7) \times 10^8$	g-8	2.25	9.0	-20.8	-23.8	-24.3	-24.5	3.6 ± 0.9	$5.6 \pm 1.5 \times 10^{10}$
NGC4697	E4	11.7	177	$1.7(0.2,0.1) \times 10^8$	s-4	0.41	8.2	-20.2	-23.9	-24.5	-24.6	9.1 ± 2.3	$2.0 \pm 0.5 \times 10^{11}$
IC1459	E3	29.2	340	$1.5(1.0,1.0) \times 10^9$	s-9	0.39	7.8	-21.4	-24.8	-25.3	-25.9	8.2 ± 2.0	$6.6 \pm 1.8 \times 10^{11}$
NGC5252	S0	96.8	190	$1.0(0.2,0.4) \times 10^9$	g-10	0.25	5.1	-20.8	-24.4	-25.2	-25.6	9.7 ± 2.4	$2.4 \pm 0.9 \times 10^{11}$
NGC2787	SB0	7.5	140	$4.1(0.4,0.5) \times 10^7$	g-11	0.25	5.0	-17.3	-20.4	-21.1	-21.3	0.32 ± 0.08	$4.4 \pm 1.2 \times 10^9$
NGC4594	Sa	9.8	240	$1.0(1.0,0.7) \times 10^9$	s-12	1.57	5.0	-21.3	-24.2	-24.8	-25.4	5.1 ± 1.3	$2.0 \pm 0.5 \times 10^{11}$
NGC3608	E2	22.9	182	$1.9(1.0,0.6) \times 10^8$	s-4	0.22	4.4	-19.9	-23.4	-24.0	-24.1	4.3 ± 1.1	$9.9 \pm 2.7 \times 10^{10}$
NGC3245	S0	20.9	205	$2.1(0.5,0.5) \times 10^8$	g-13	0.21	4.2	-19.6	-22.4	-23.1	-23.3	1.3 ± 0.3	$3.9 \pm 1.0 \times 10^{10}$
NGC4291	E2	26.2	242	$3.1(0.8,2.3) \times 10^8$	s-4	0.18	3.6	-19.6	-23.1	-23.8	-23.9	2.3 ± 0.6	$9.5 \pm 2.5 \times 10^{10}$
NGC3377	E5	11.2	145	$1.0(0.9,0.1) \times 10^8$	s-4	0.38	3.6	-19.0	-22.7	-23.5	-23.6	5.4 ± 1.3	$7.8 \pm 2.1 \times 10^{10}$
NGC4473	E5	15.7	190	$1.1(0.4,0.8) \times 10^8$	s-4	0.17	3.4	-19.9	-23.1	-23.6	-23.8	2.8 ± 0.7	$6.9 \pm 1.9 \times 10^{10}$
CygnusA	E	240	270	$2.9(0.7,0.7) \times 10^9$	g-14	0.15	2.9	-21.9	-26.4	-26.9	-27.3	31 ± 8	$1.6 \pm 1.1 \times 10^{12}$
NGC4261	E2	31.6	315	$5.2(1.0,1.1) \times 10^8$	g-15	0.15	2.9	-21.1	-24.6	-25.4	-25.6	6.5 ± 1.6	$4.5 \pm 1.2 \times 10^{11}$
NGC4564	E3	15.0	162	$5.6(0.3,0.8) \times 10^7$	s-4	0.13	2.5	-18.9	-22.5	-23.3	-23.4	3.0 ± 0.7	$5.4 \pm 1.5 \times 10^{10}$
NGC4742	E4	15.5	90	$1.4(0.4,0.5) \times 10^7$	s-16	0.10	2.0	-18.9	-22.1	-22.8	-23.0	2.0 ± 0.5	$1.1 \pm 0.3 \times 10^{10}$
NGC3379	E1	10.6	206	$1.0(0.6,0.5) \times 10^8$	s-17	0.20	1.9	-19.9	-23.1	-23.7	-24.2	2.9 ± 0.7	$8.5 \pm 2.3 \times 10^{10}$
NGC1023	SB0	11.4	205	$4.4(0.5,0.5) \times 10^7$	s-18	0.08	1.6	-18.4	-22.6	-23.3	-23.5	1.2 ± 0.3	$3.4 \pm 0.9 \times 10^{10}$
NGC5845	E3	25.9	234	$2.4(0.4,1.4) \times 10^8$	s-4	0.15	1.4	-18.7	-22.0	-22.7	-23.0	0.50 ± 0.12	$1.9 \pm 0.5 \times 10^{10}$
NGC3384	S0	11.6	143	$1.6(0.1,0.2) \times 10^7$	s-4	0.06	1.2	-19.0	-21.7	-22.3	-22.6	0.49 ± 0.12	$7.0 \pm 1.9 \times 10^9$
NGC6251	E2	107.0	290	$6.1(2.0,2.1) \times 10^8$	g-19	0.06	1.2	-21.5	-25.4	-26.4	-26.6	11 ± 3	$6.7 \pm 1.8 \times 10^{11}$

RGs
&
BL Lacs
are
normal
ellipticals

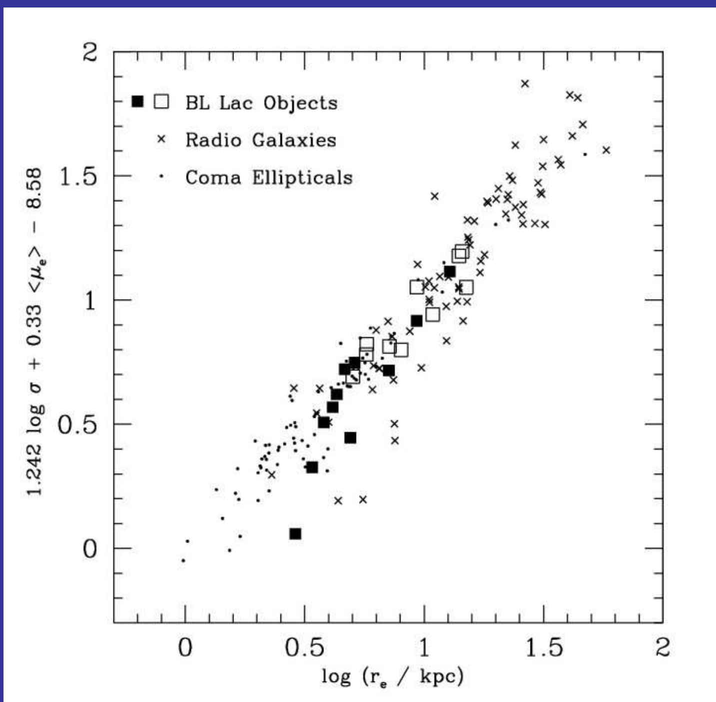

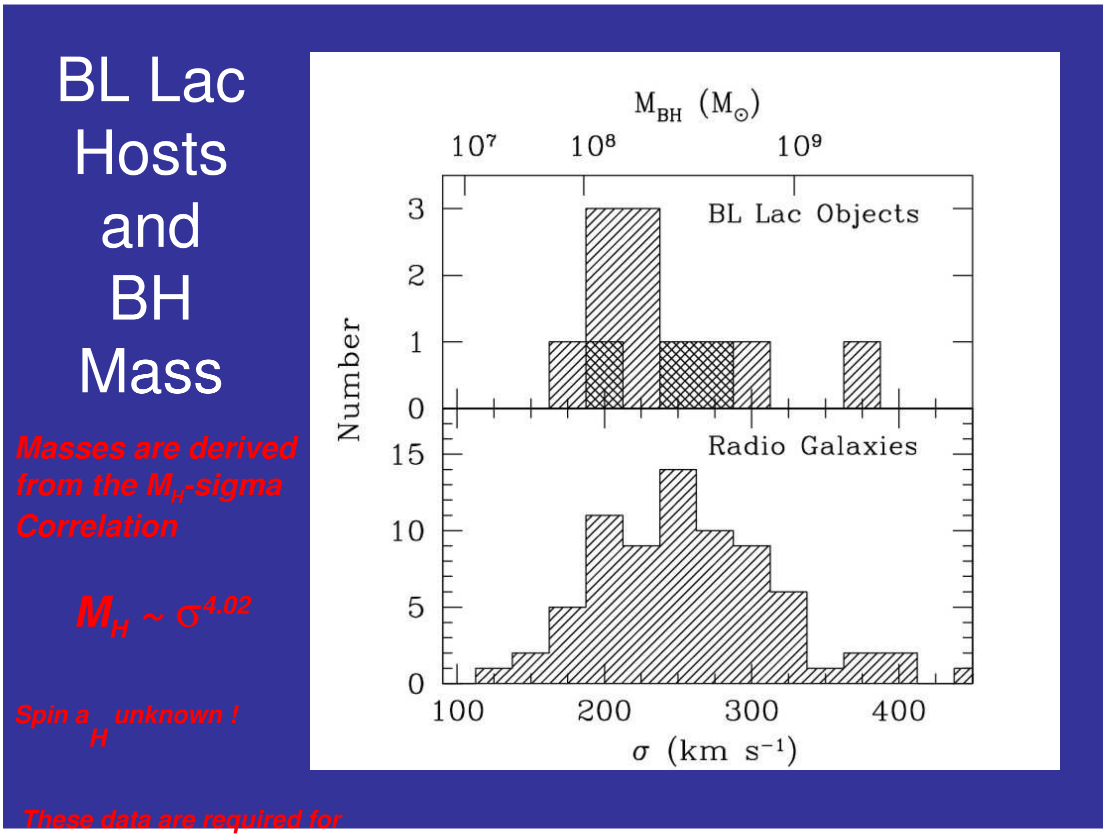
BL Lac Hosts and BH Mass
Masses are derived from the M_H-sigma Correlation
$M_H \sim \sigma^{4.02}$
Spin a_H unknown !
These data are required for
M_{BH} ($M_\odot$)
10^7 10^8 10^9
BL Lac Objects
Radio Galaxies
Number
3 2 1 0 15 10 5 0
100 200 300 400
σ (km s^{-1})

all sources !

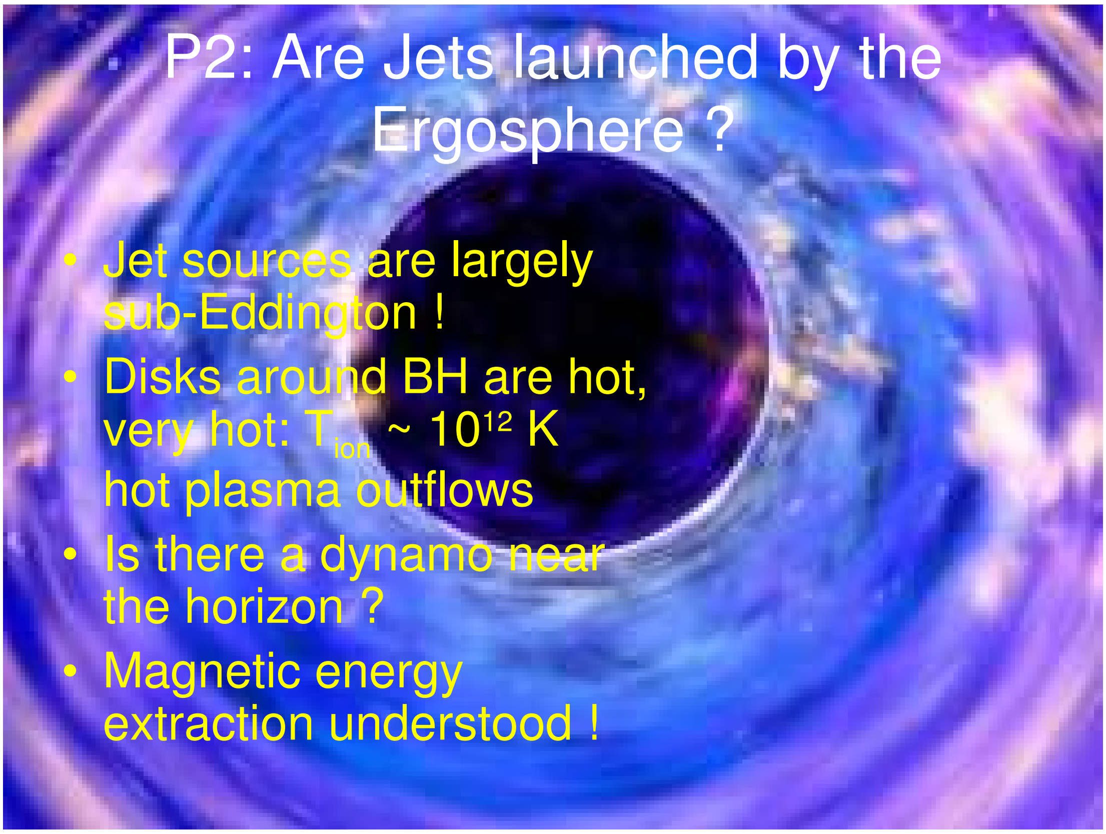
P2: Are Jets launched by the Ergosphere ?
• Jet sources are largely sub-Eddington !
• Disks around BH are hot, very hot: T_{ion} ~ 10^{12} K hot plasma outflows
• Is there a dynamo near the horizon ?
• Magnetic energy extraction understood !

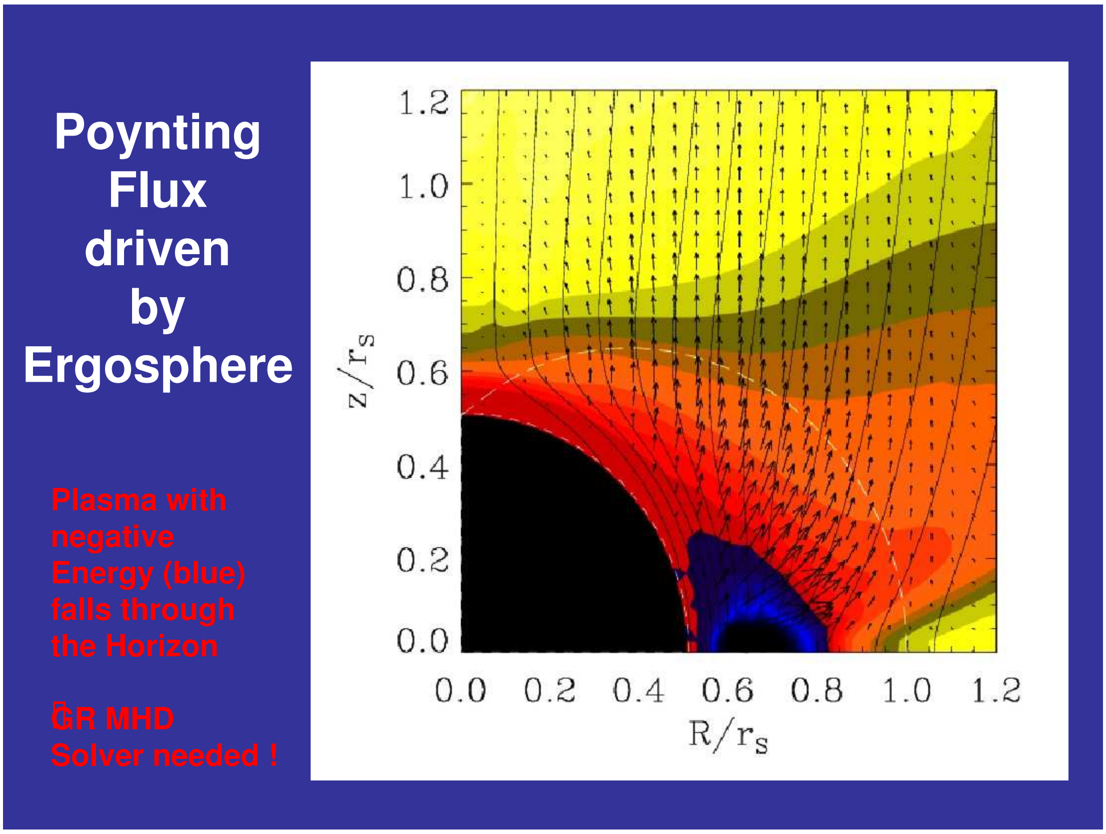
Poynting Flux driven by Ergosphere
Plasma with negative Energy (blue) falls through the Horizon
GR MHD Solver needed !
1.2
1.0
0.8
0.6
0.4
0.2
0.0
z/r_S
0.0 0.2 0.4 0.6 0.8 1.0 1.2
R/r_S

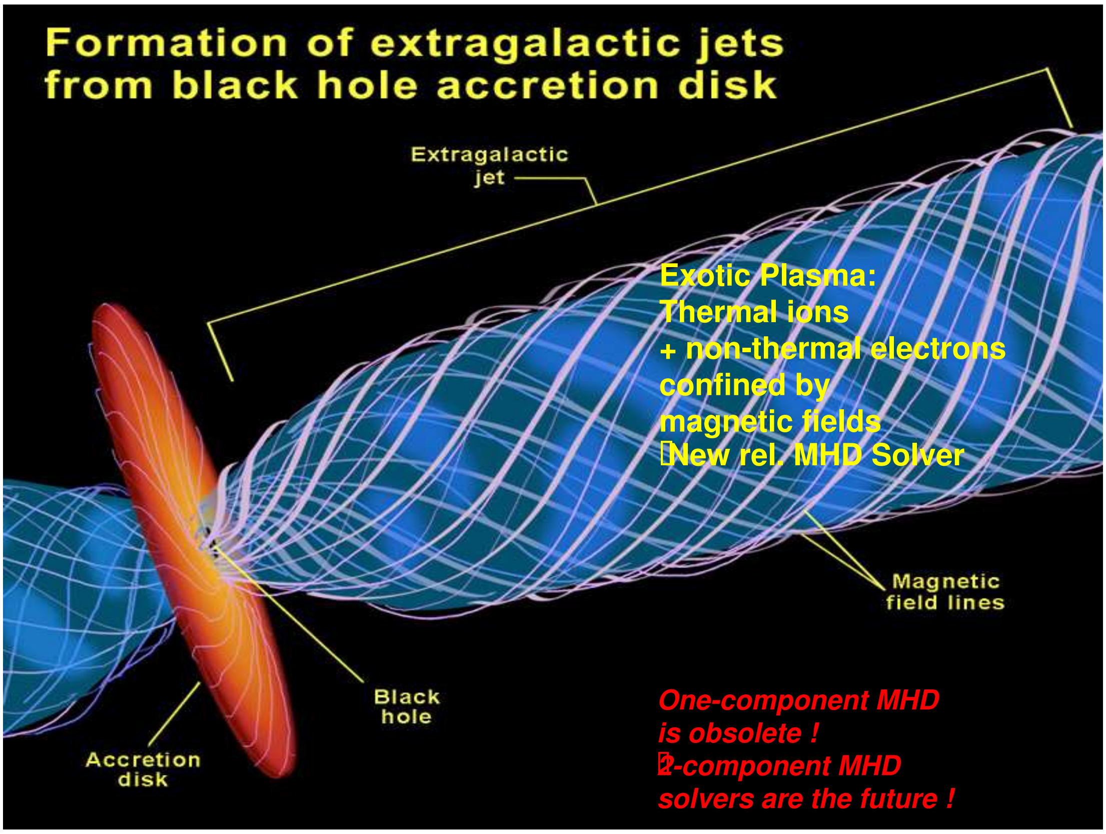
Formation of extragalactic jets from black hole accretion disk
Extragalactic jet
Exotic Plasma:
Thermal ions
+ non-thermal electrons
confined by
magnetic fields
New rel. MHD Solver
Magnetic field lines
Black hole
Accretion disk
One-component MHD
is obsolete !
2-component MHD
solvers are the future !

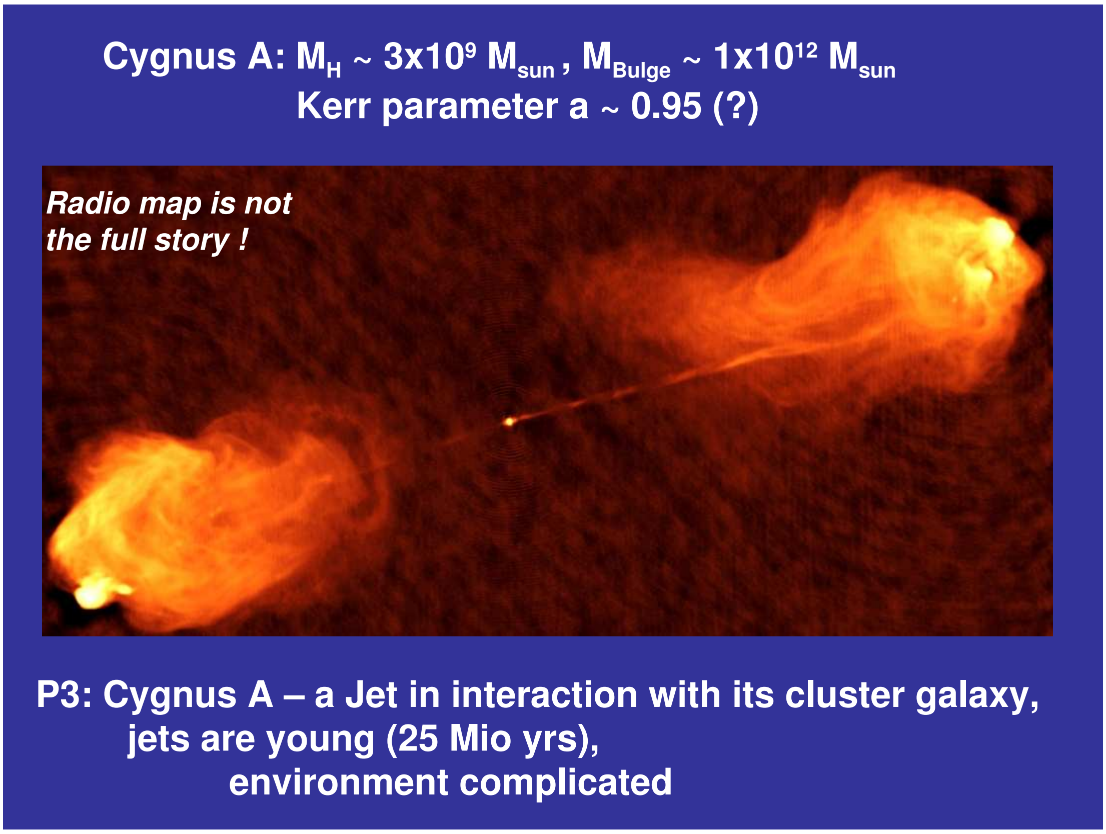
Cygnus A: $M_H \sim 3x10^9\ M_{sun}$, $M_{Bulge} \sim 1x10^{12}\ M_{sun}$
Kerr parameter a ~ 0.95 (?)
Radio map is not
the full story !
P3: Cygnus A – a Jet in interaction with its cluster galaxy,
jets are young (25 Mio yrs),
environment complicated

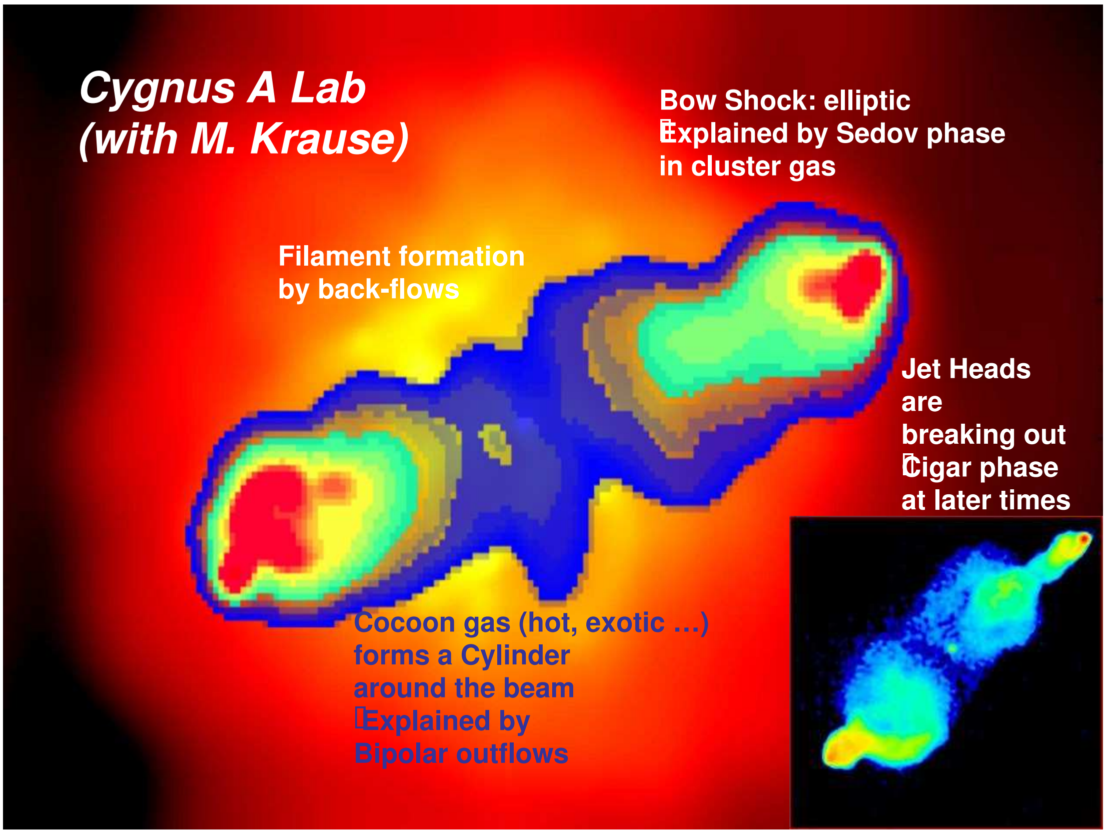
Cygnus A Lab
(with M. Krause)
Bow Shock: elliptic
Explained by Sedov phase
in cluster gas
Filament formation
by back-flows
Jet Heads
are
breaking out
Cigar phase
at later times
Cocoon gas (hot, exotic …)
forms a Cylinder
around the beam
Explained by
Bipolar outflows

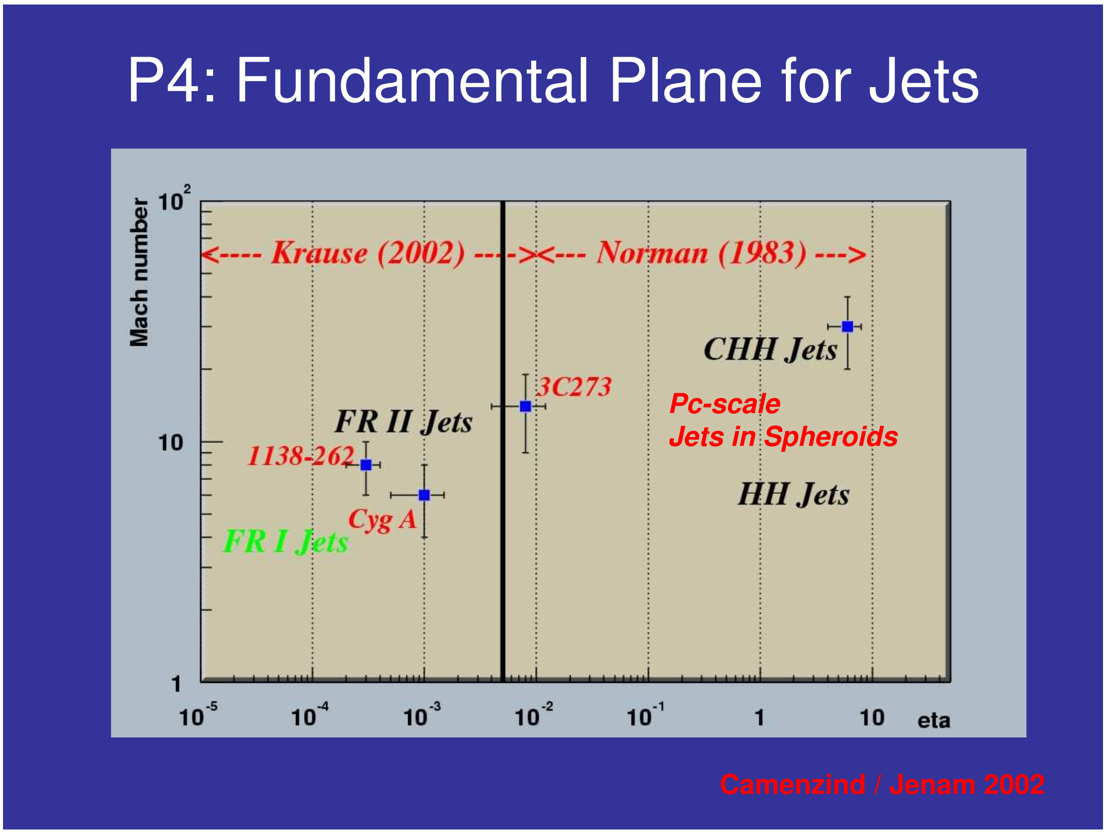
P4: Fundamental Plane for Jets
Mach number
eta
<---- Krause (2002) ---><--- Norman (1983) --->
CHH Jets
3C273
Pc-scale
Jets in Spheroids
FR II Jets
1138-262
HH Jets
Cyg A
FR I Jets
Camenzind / Jenam 2002

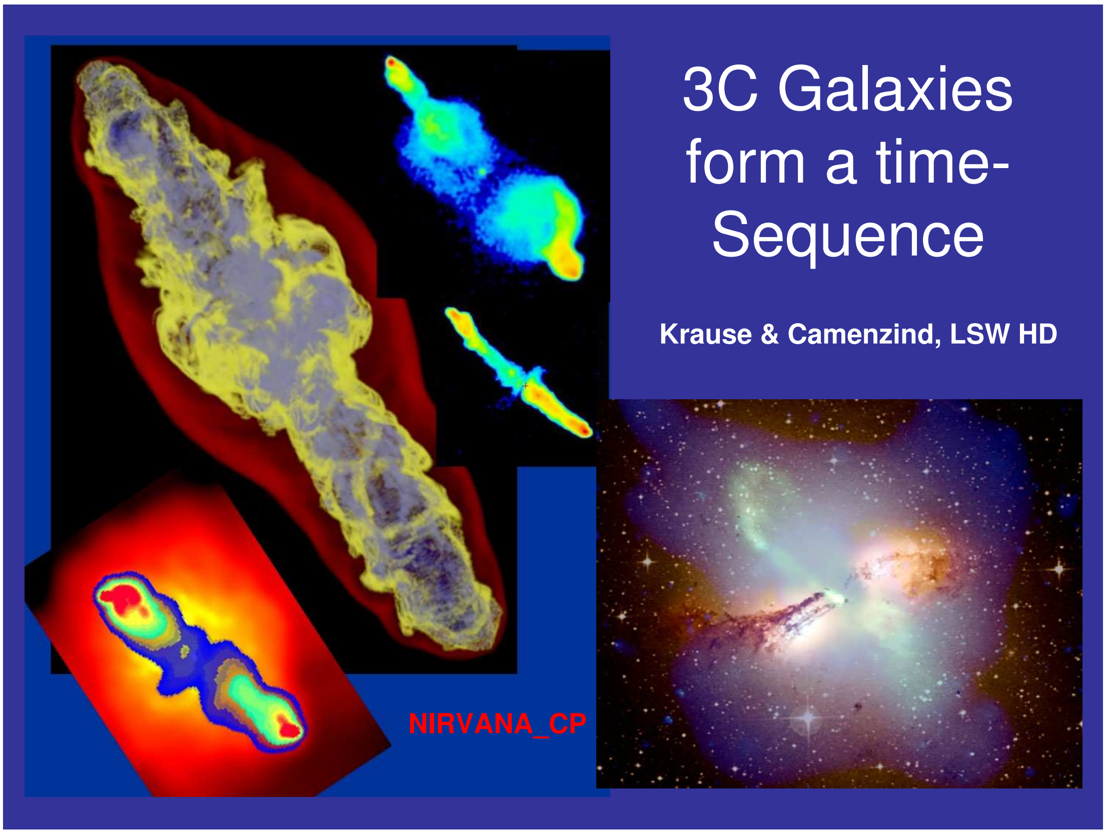
3C Galaxies
form a time-
Sequence
Krause & Camenzind, LSW HD
NIRVANA_CP

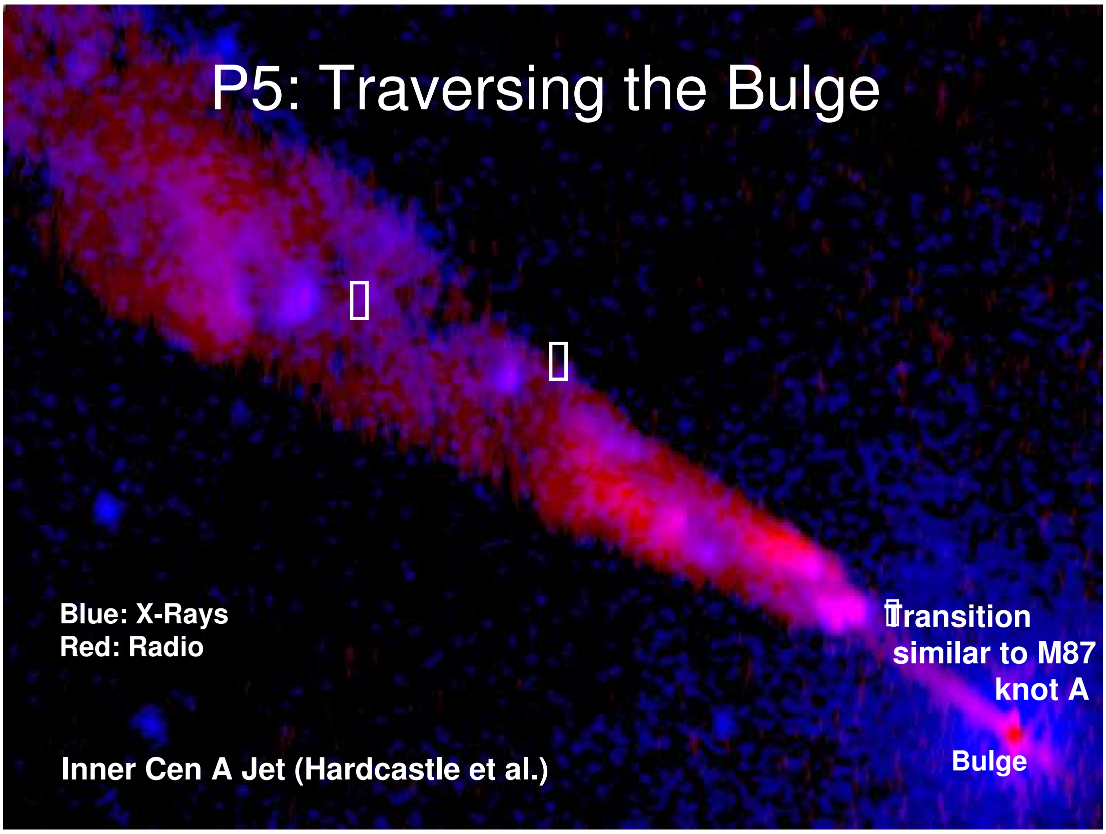
P5: Traversing the Bulge
Blue: X-Rays
Red: Radio
Transition
similar to M87
knot A
Bulge
Inner Cen A Jet (Hardcastle et al.)

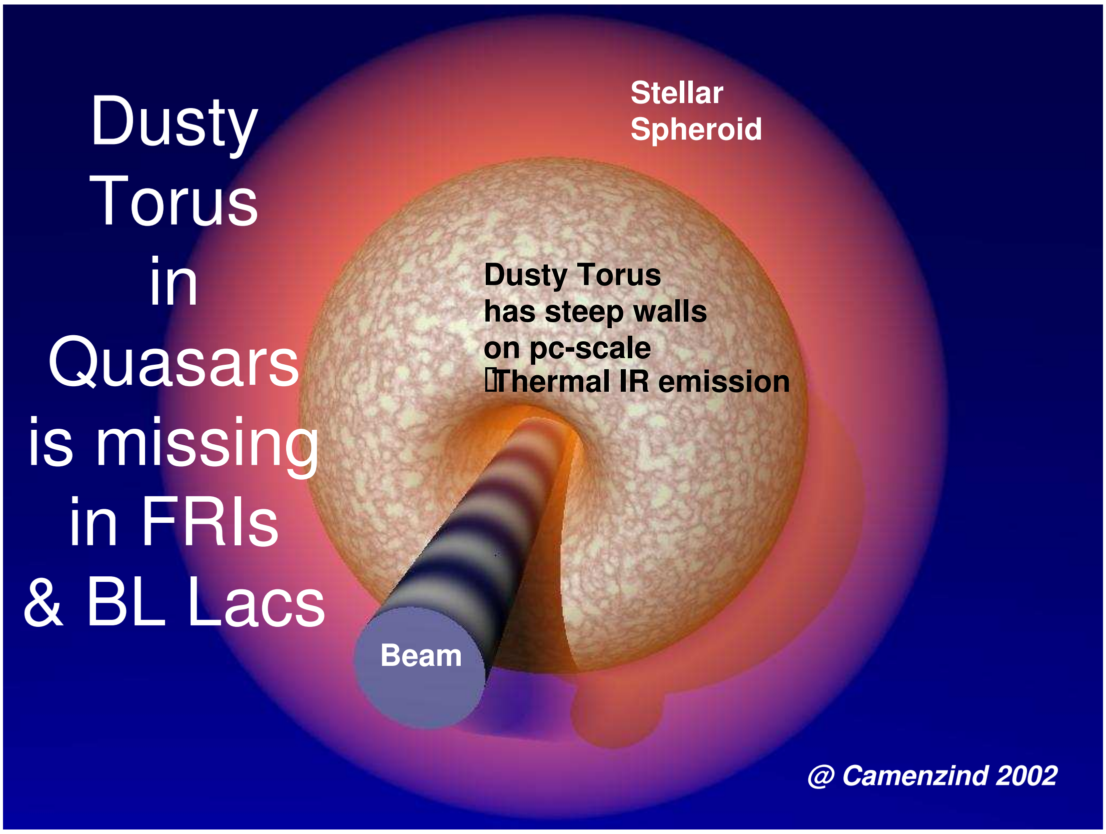
Dusty Torus in Quasars is missing in FRIs & BL Lacs
Stellar Spheroid
Dusty Torus
has steep walls
on pc-scale
Thermal IR emission
Beam
@ Camenzind 2002

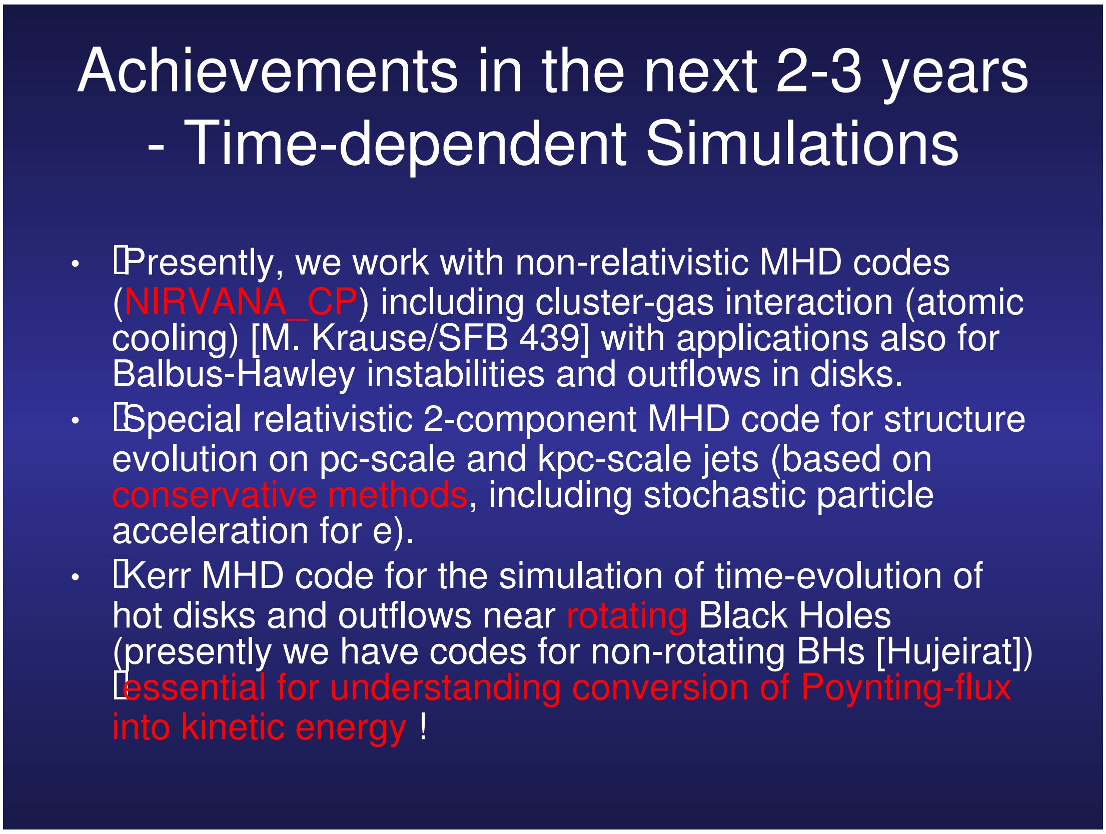
Achievements in the next 2-3 years - Time-dependent Simulations
• Presently, we work with non-relativistic MHD codes (NIRVANA_CP) including cluster-gas interaction (atomic cooling) [M. Krause/SFB 439] with applications also for Balbus-Hawley instabilities and outflows in disks.
• Special relativistic 2-component MHD code for structure evolution on pc-scale and kpc-scale jets (based on conservative methods, including stochastic particle acceleration for e).
• Kerr MHD code for the simulation of time-evolution of hot disks and outflows near rotating Black Holes (presently we have codes for non-rotating BHs [Hujeirat]) essential for understanding conversion of Poynting-flux into kinetic energy !

7.9 G. Krishna: Comments on S5 0716+714

DUTY CYCLES OF INOV

$$\text{Amplitude } \psi = \left[(D_{max} - D_{min})^2 - 2\sigma^2 \right]^{1/2}$$

	N	Nights	$\psi < 3\%$	$\psi > 3\%$
RQQ	7	29	~15%	—
LDQ	7	32	~15%	—
CDQ–LP	4	17	~15%	—
CDQ–HP	2	8	~10%	~50%
BL Lacs	6	26	~15%	~50%

MAIN INFERENCES

1 Relativistic jets may also be present in RQQs (on optically emitting, i.e., psec scales)

→ Motivation for more sensitive monitoring of RQQs

2 Radio loudness (not even a flat spectrum) has practically NO correlation with INOV

3 Primary link of INOV is with optical polarization

* INTRA-NIGHT OPTICAL VARIABILITY

LDQ: LOBE-DOMINATED QUASAR, CDQ: CORE-DOMINATED QUASAR

LP: OPT. POL. < 3% HP: OPT. POL. > 3%

7.10 G. Ghisellini: Power of jets

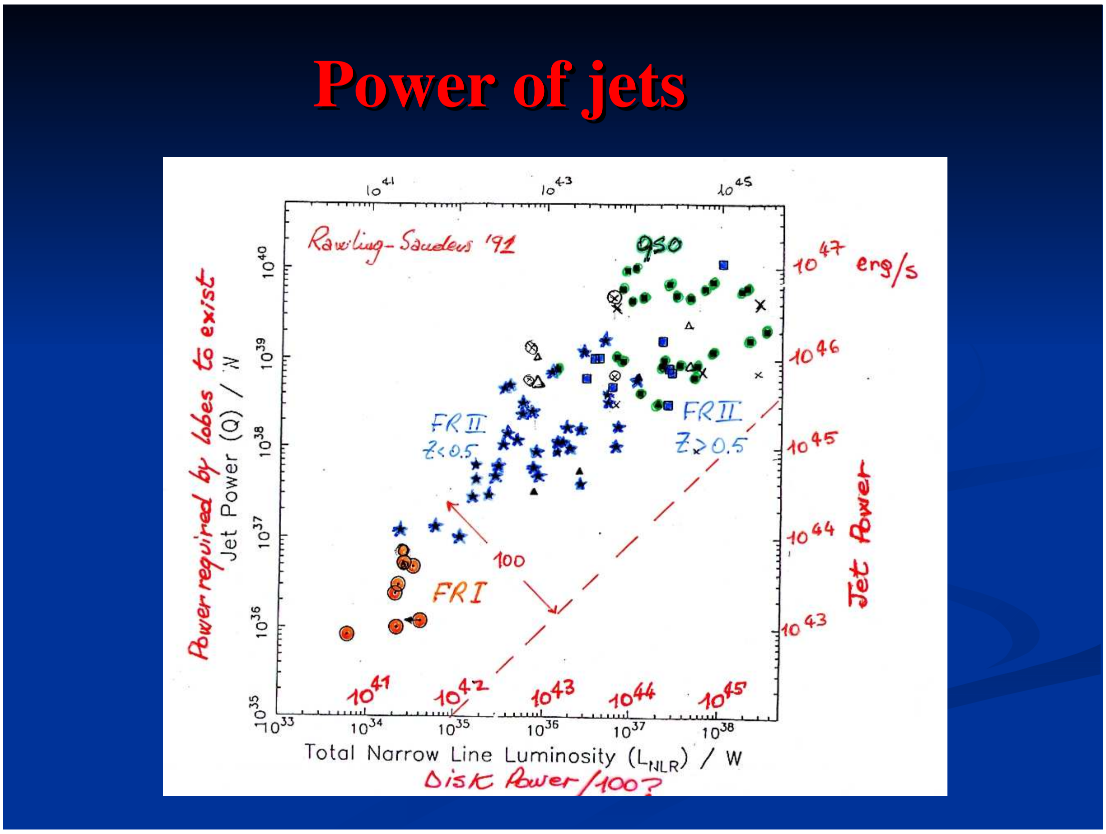

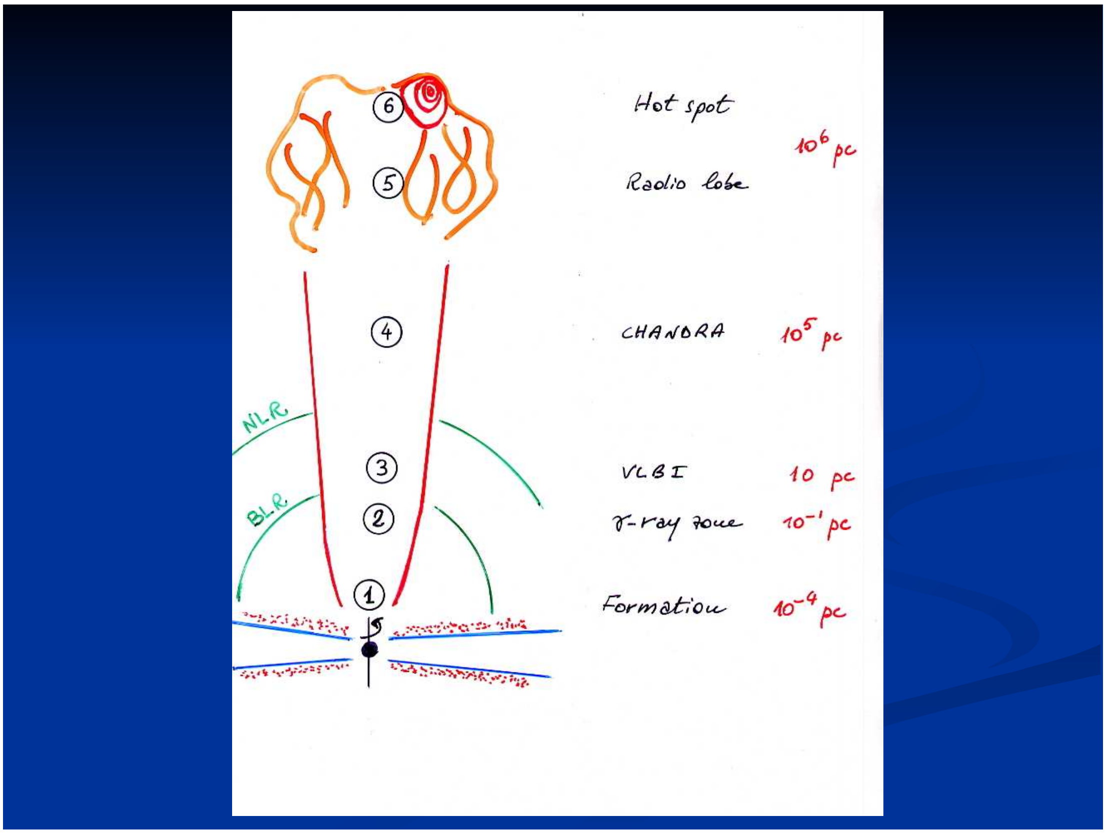
Hot spot
10^6 pc
Radio lobe
CHANDRA
10^5 pc
NLR
BLR
VLBI
10 pc
γ-ray zone
10^{-1} pc
Formation
10^{-4} pc

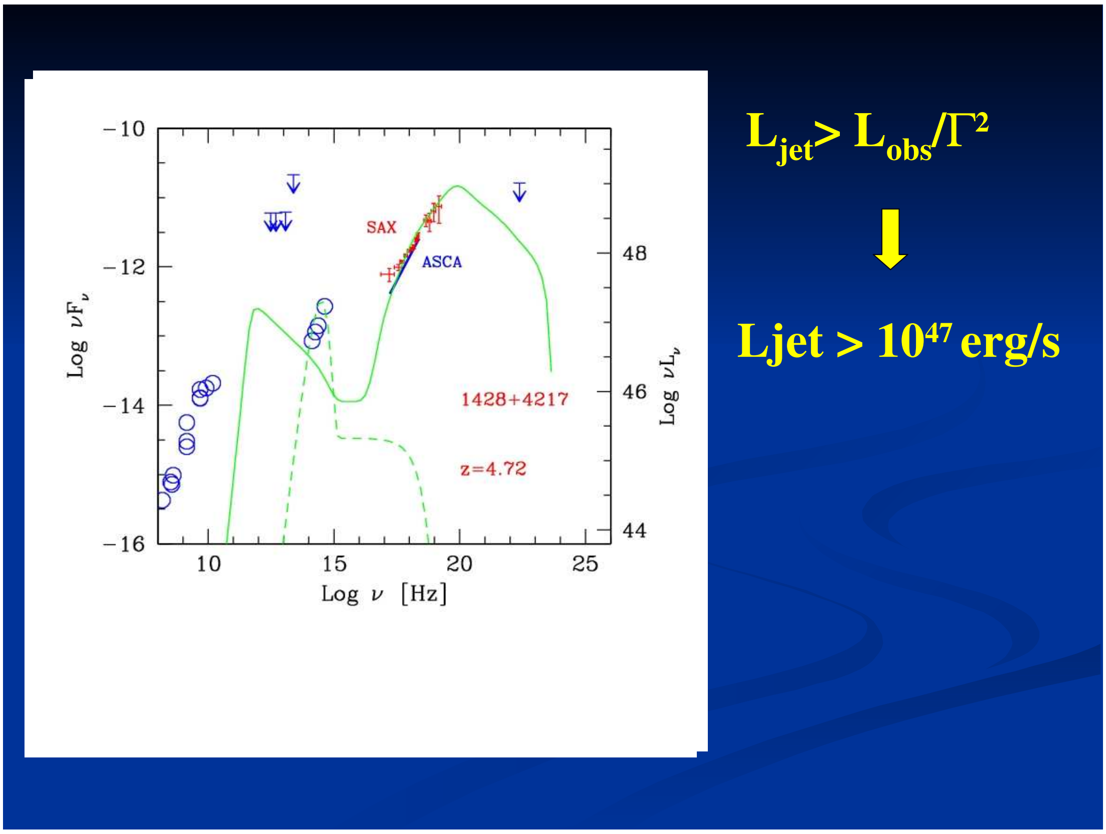
SAX
ASCA
1428+4217
z=4.72
Log νF_ν
Log νL_ν
Log ν [Hz]
$L_{jet} > L_{obs}/\Gamma^2$
Ljet > 10^{47} erg/s

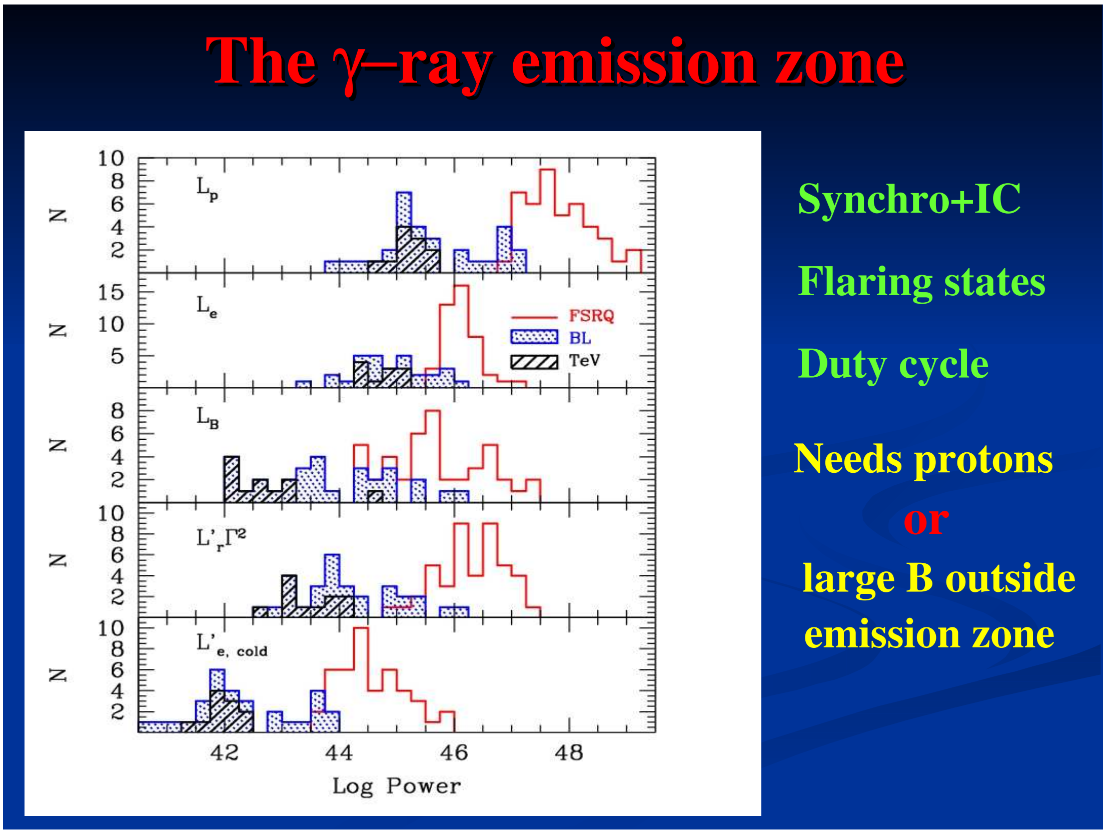
The γ–ray emission zone
N
L_p
L_e
L_B
$L'_r\Gamma^2$
$L'_{e,\,cold}$
FSRQ
BL
TeV
42
44
46
48
Log Power
Synchro+IC
Flaring states
Duty cycle
Needs protons
or
large B outside
emission zone

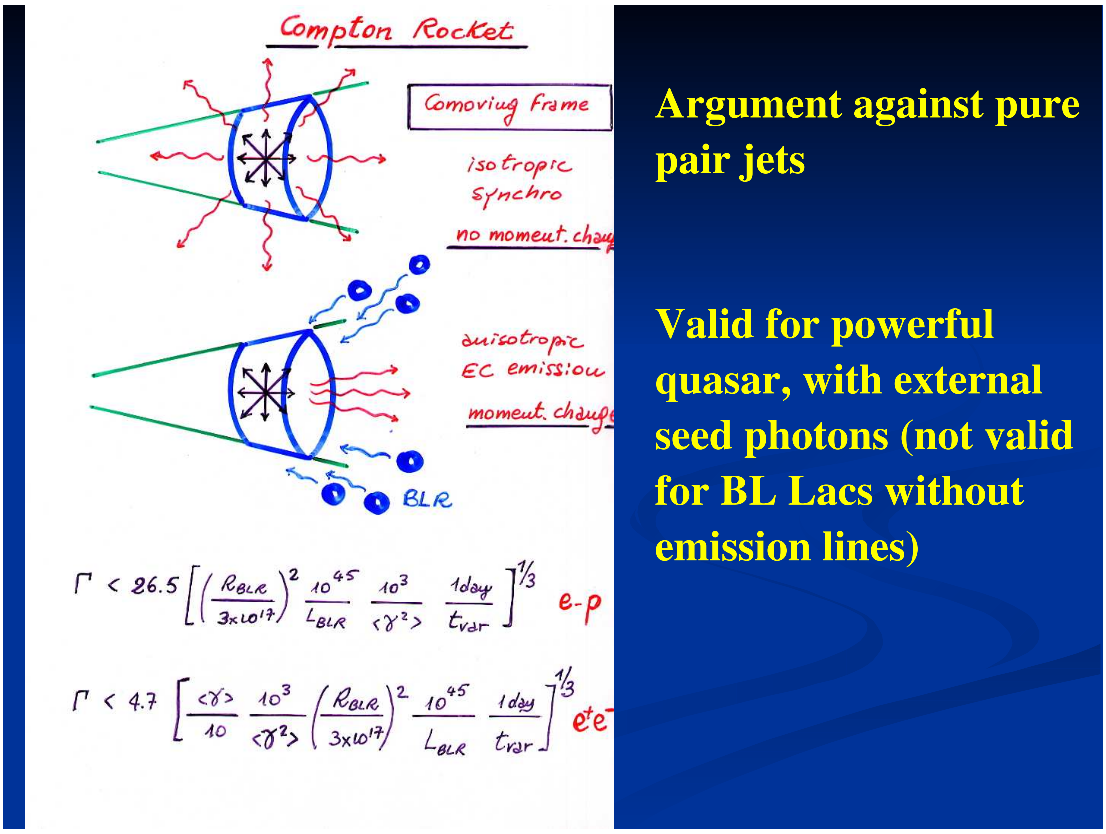
Compton Rocket
Comoving frame
isotropic
synchro
no moment. change
anisotropic
EC emission
moment. change
BLR
$\Gamma < 26.5 \left[\left(\frac{R_{BLR}}{3\times 10^{17}} \right)^2 \frac{10^{45}}{L_{BLR}} \frac{10^3}{\langle\gamma^2\rangle} \frac{1\,\mathrm{day}}{t_{var}} \right]^{1/3}$ e-p
$\Gamma < 4.7 \left[\frac{\langle\gamma\rangle}{10} \frac{10^3}{\langle\gamma^2\rangle} \left(\frac{R_{BLR}}{3\times 10^{17}} \right)^2 \frac{10^{45}}{L_{BLR}} \frac{1\,\mathrm{day}}{t_{var}} \right]^{1/3}$ e^+e^-
Argument against pure pair jets
Valid for powerful quasar, with external seed photons (not valid for BL Lacs without emission lines)

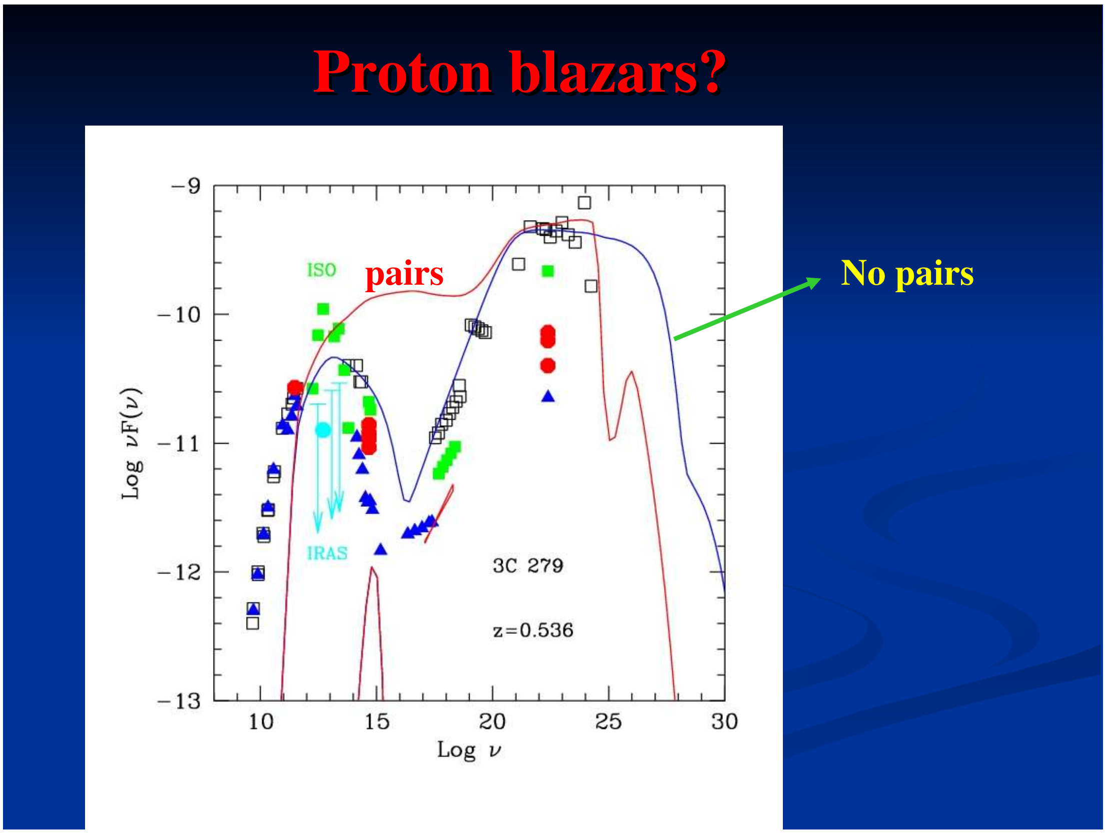
Proton blazars?
pairs
No pairs
ISO
IRAS
3C 279
z=0.536
Log νF(ν)
Log ν

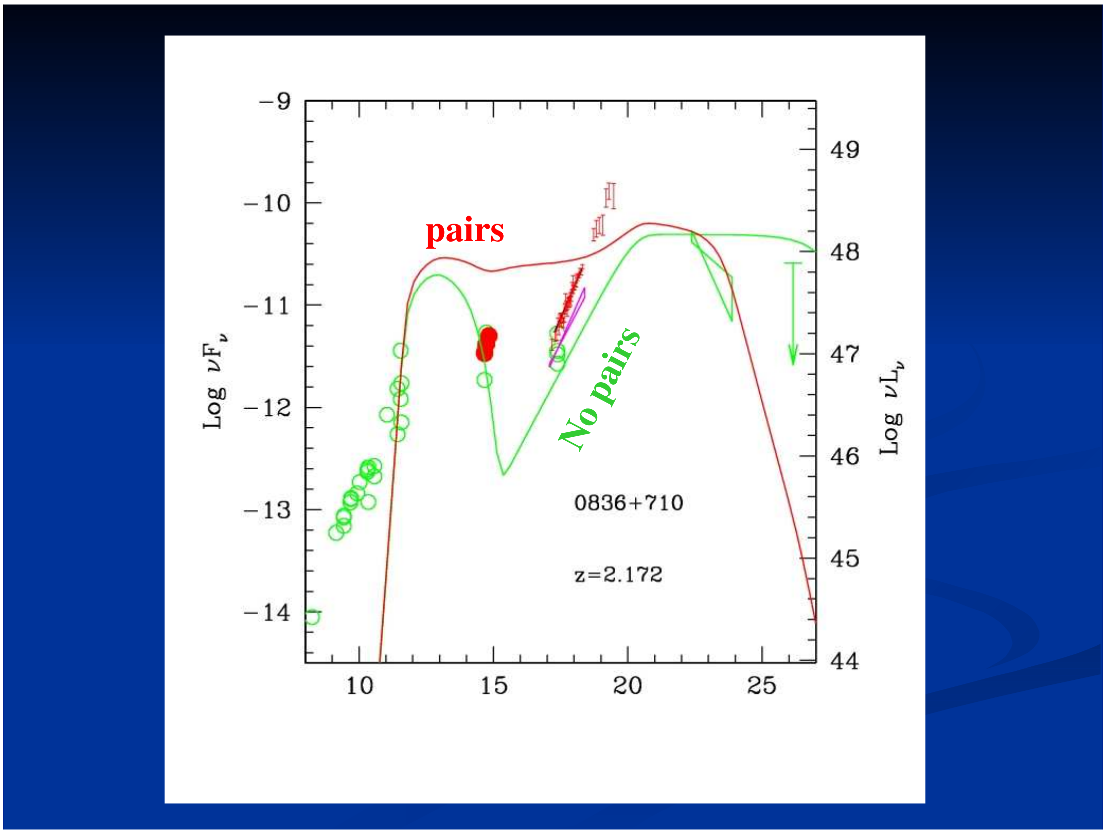
pairs
No pairs
0836+710
z=2.172
Log νFν
Log νLν

Large scale jets

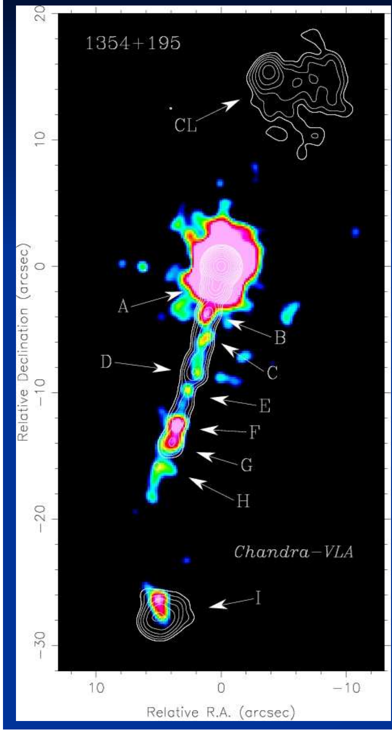

Preferred model: IC off CMB photons

Requires Γ~10 up to 100 kpcs

Most economic model

Energetics in agreement with γ-ray zone

Core vs large scale jet

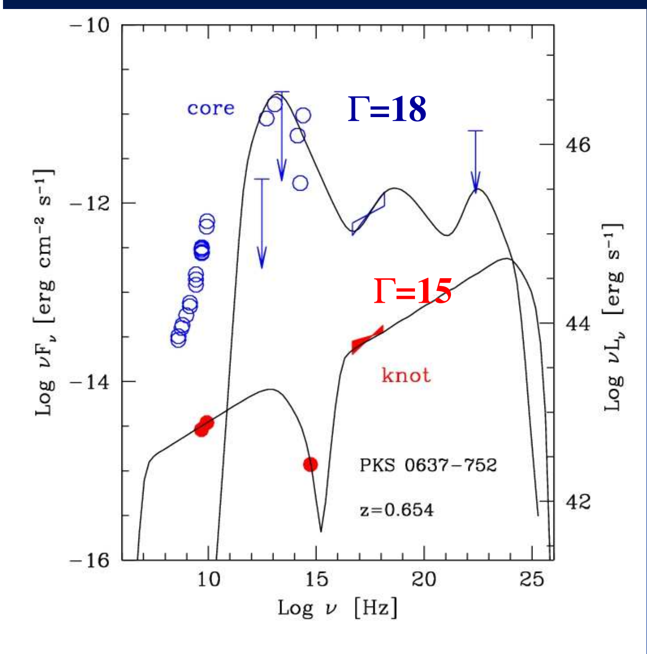

	core	knot
L_p	2×10^{47}	2×10^{47}
L_e	10^{45}	3×10^{45}
L_B	4×10^{45}	5×10^{46}

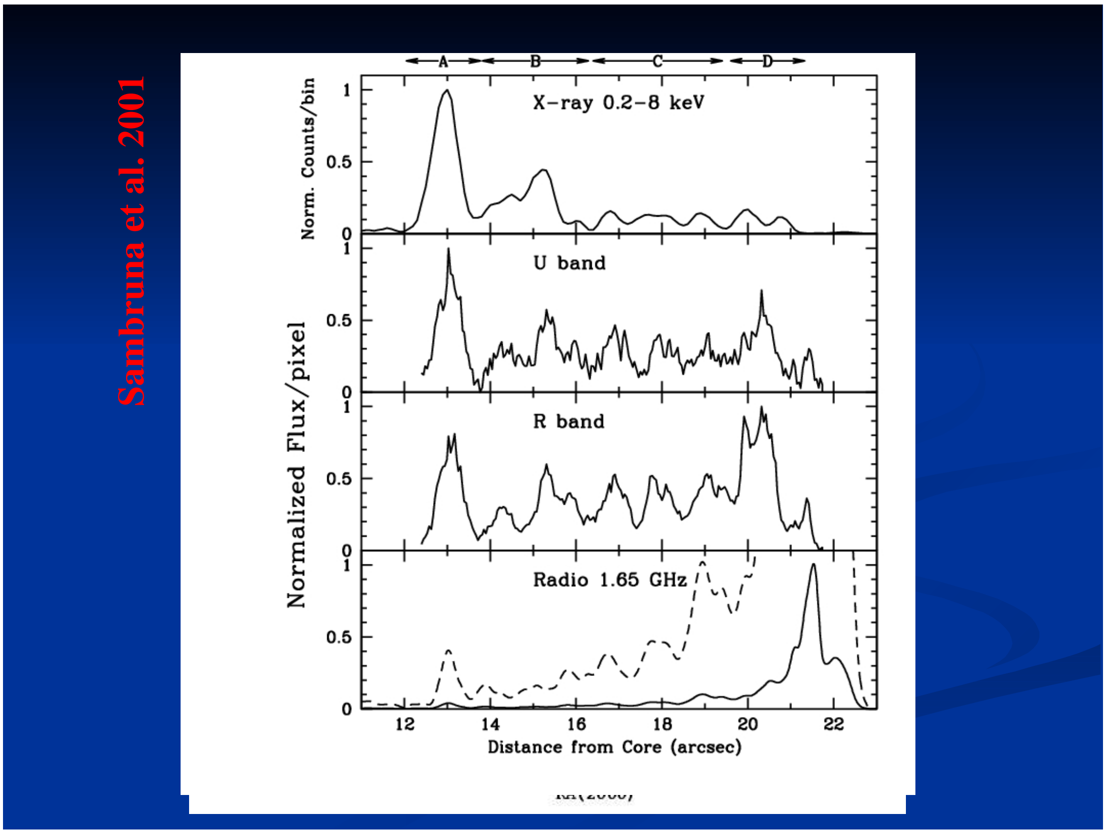
Sambruna et al. 2001
A
B
C
D
X-ray 0.2–8 keV
Norm. Counts/bin
U band
R band
Radio 1.65 GHz
Normalized Flux/pixel
Distance from Core (arcsec)

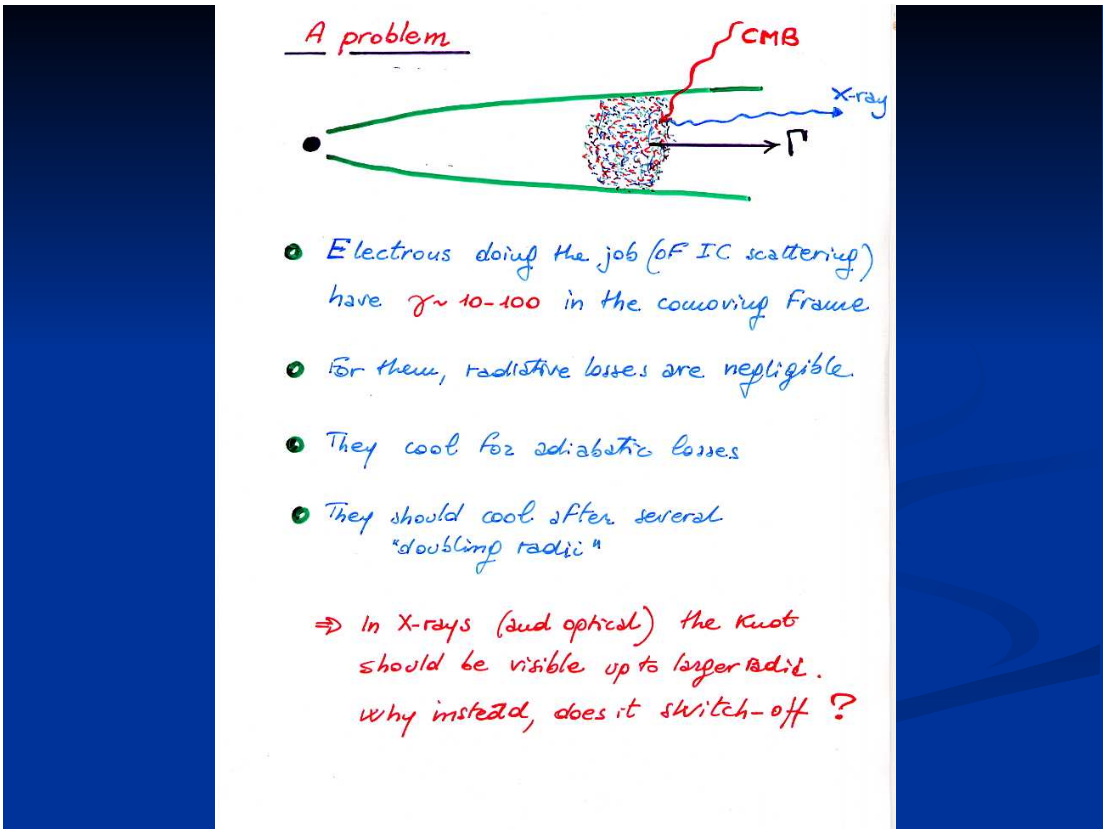
A problem
CMB
X-ray
Γ
Electrons doing the job (of IC scattering) have γ ~ 10–100 in the comoving frame
For them, radiative losses are negligible
They cool for adiabatic losses
They should cool after several "doubling radii"
⇒ In X-rays (and optical) the knot should be visible up to larger radii. Why instead, does it switch-off ?

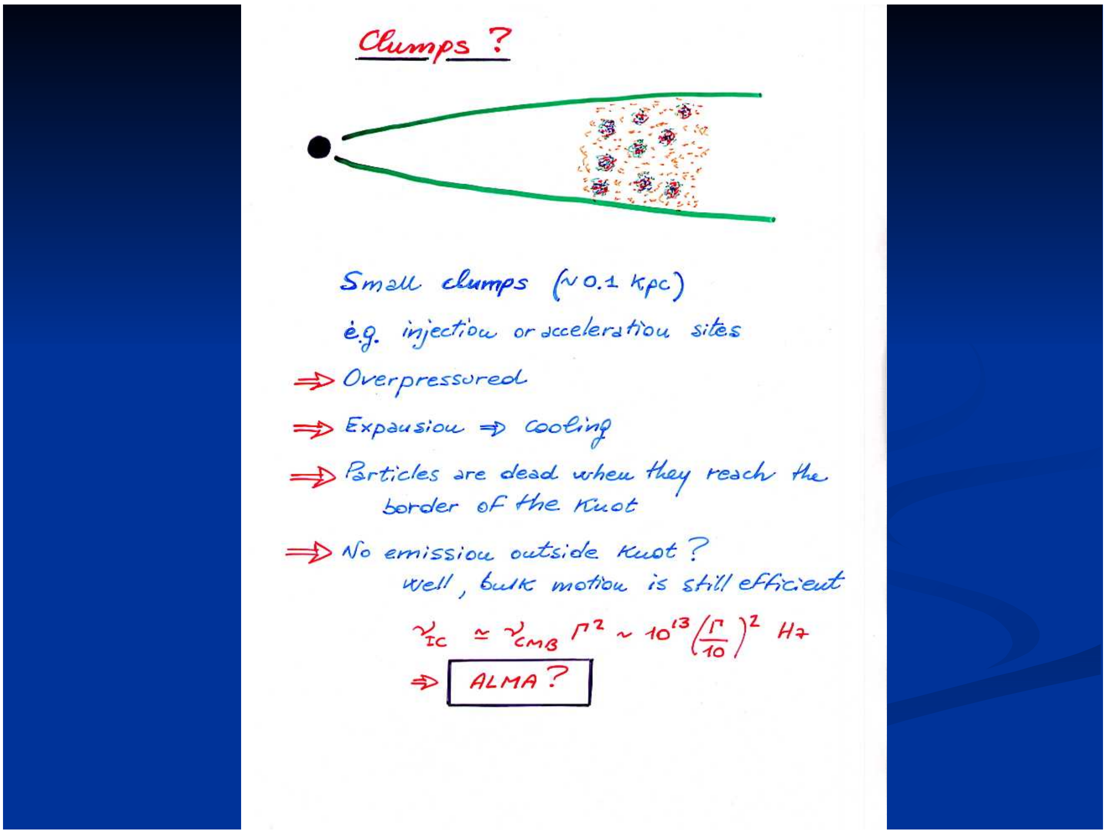
Clumps ?
Small clumps (~0.1 kpc)
e.g. injection or acceleration sites
⇒ Overpressured
⇒ Expansion ⇒ cooling
⇒ Particles are dead when they reach the border of the knot
⇒ No emission outside knot?
well, bulk motion is still efficient
$\nu_{IC} \simeq \nu_{CMB} \Gamma^2 \sim 10^{13} \left(\frac{\Gamma}{10}\right)^2$ Hz
⇒ ALMA ?

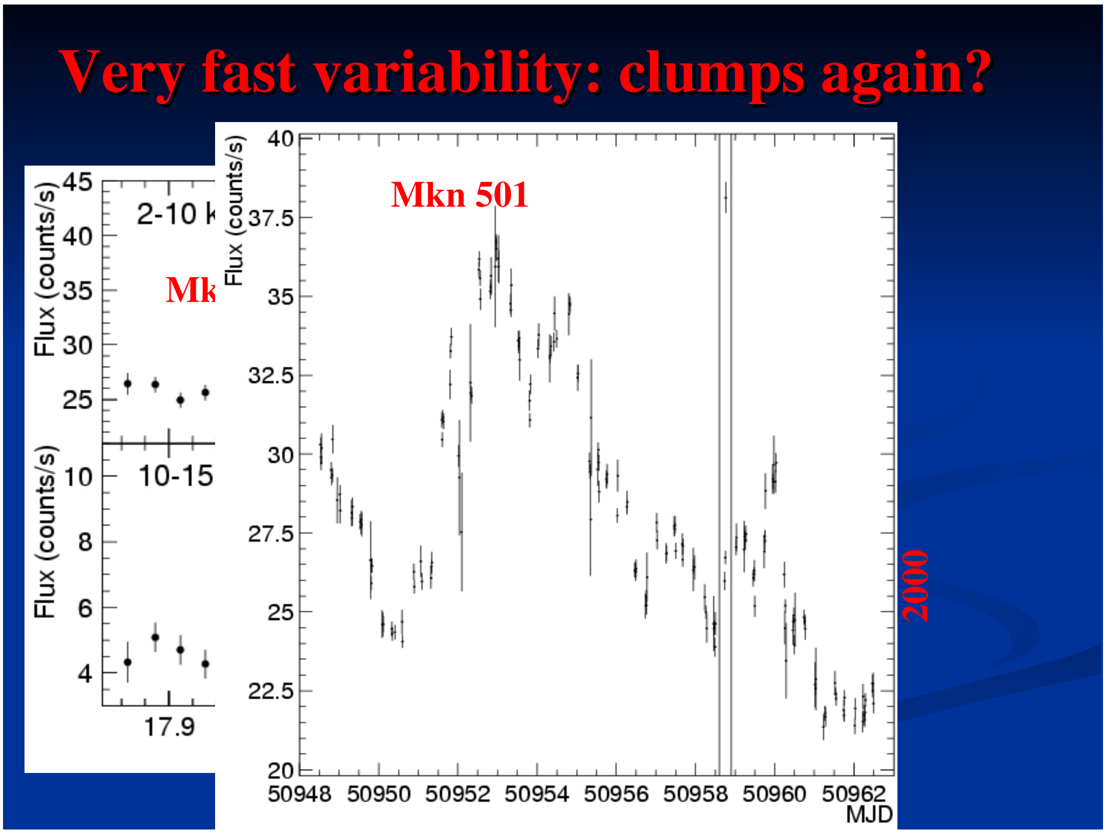
Very fast variability: clumps again?
Mkn 501
Flux (counts/s)
MJD
2-10 k
10-15
Mk
2000

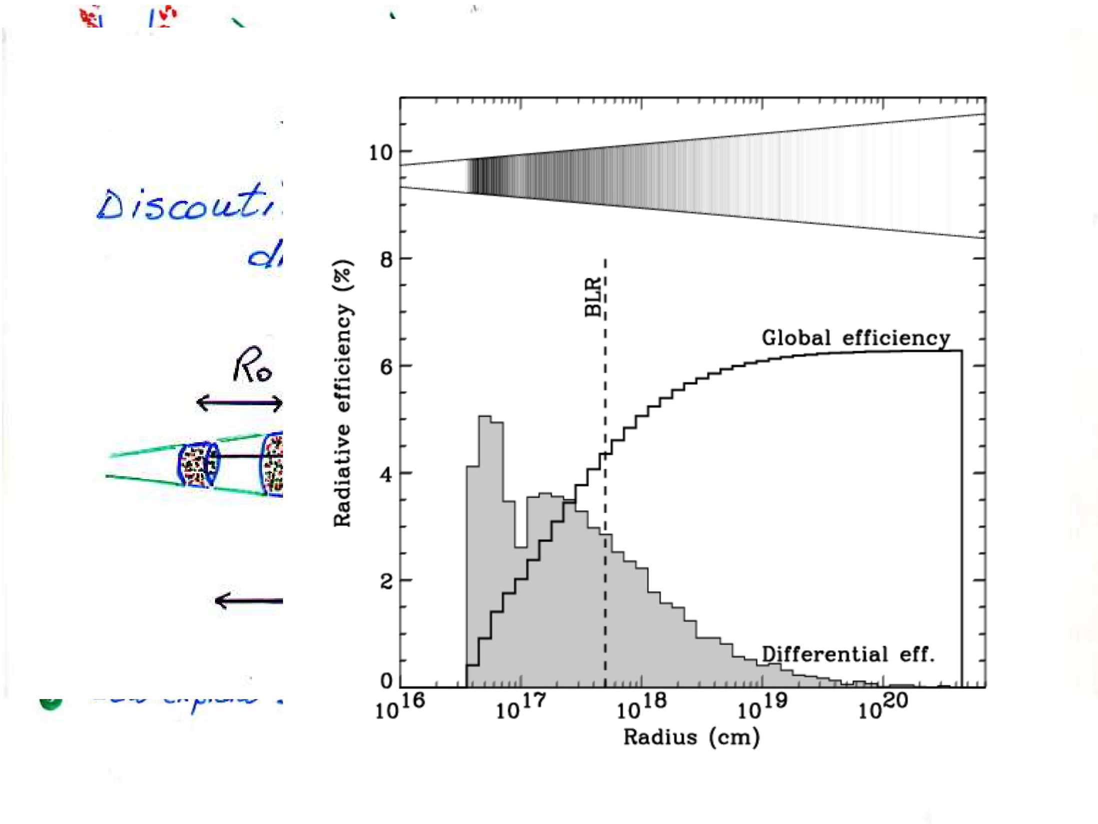
Discouti
Ro
BLR
Global efficiency
Differential eff.
Radiative efficiency (%)
Radius (cm)

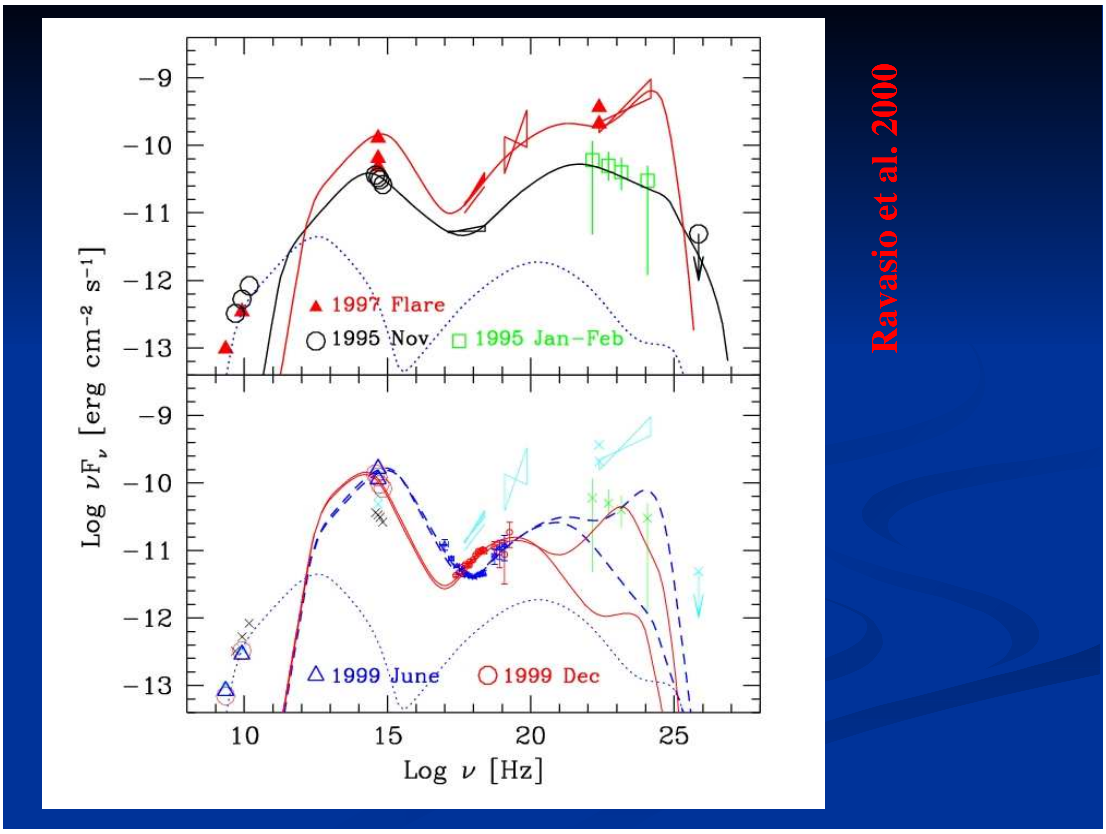
1997 Flare
1995 Nov
1995 Jan-Feb
1999 June
1999 Dec
Log νF_ν [erg cm^-2 s^-1]
Log ν [Hz]
Ravasio et al. 2000

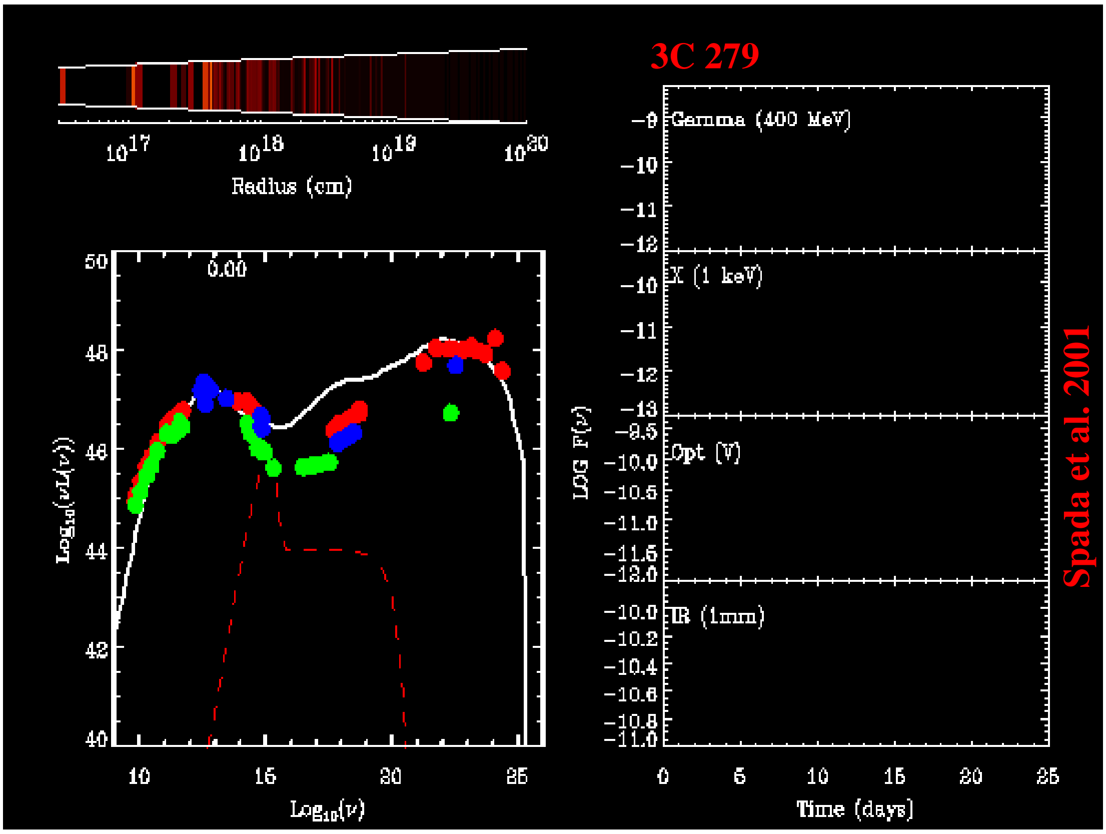
3C 279
Spada et al. 2001
Radius (cm)
0.00
Log10(ν)
Log10(νL(ν))
LOG F(ν)
Gamma (400 MeV)
X (1 keV)
Opt (V)
IR (1mm)
Time (days)

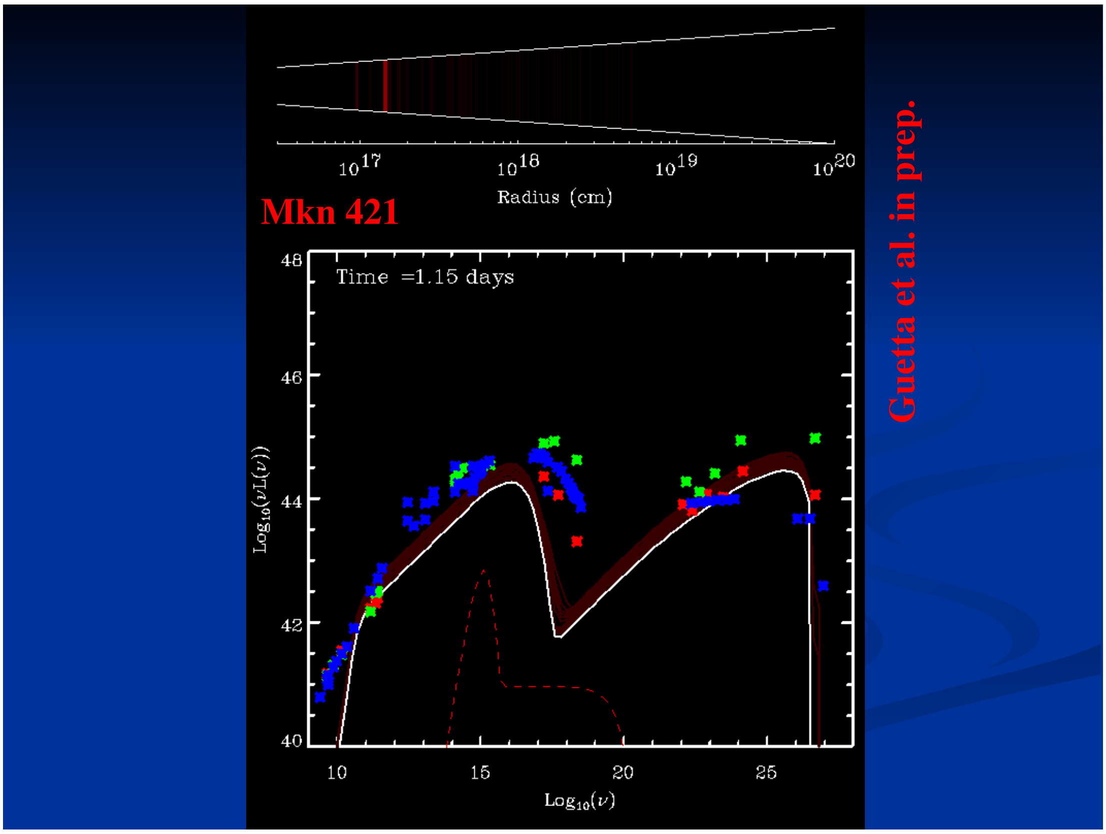
Mkn 421
Guetta et al. in prep.
Radius (cm)
Time =1.15 days
Log10(ν)
Log10(νL(ν))

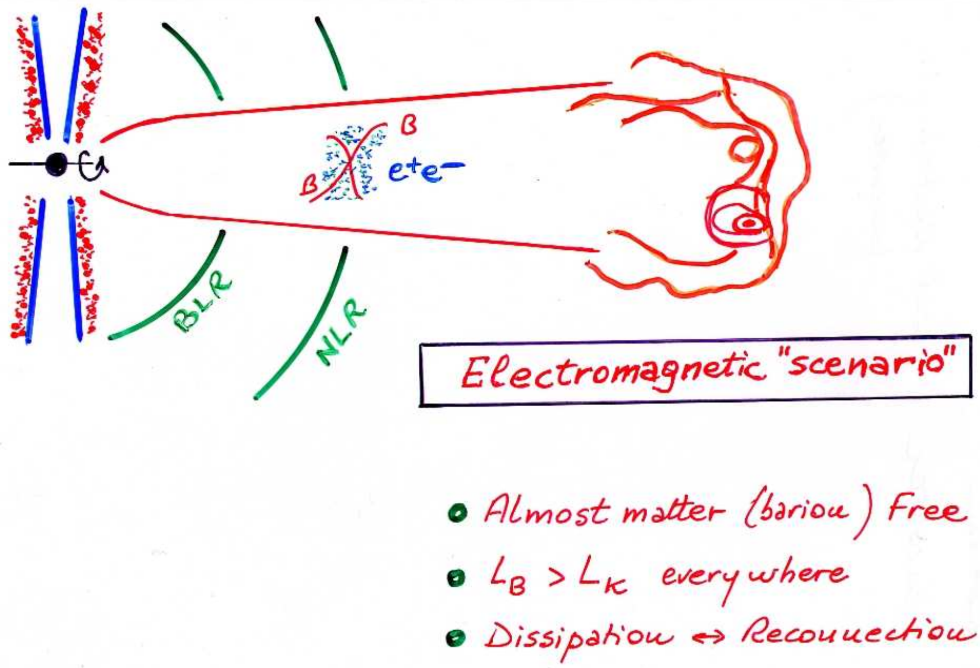

"Roger Blandford's scenario"

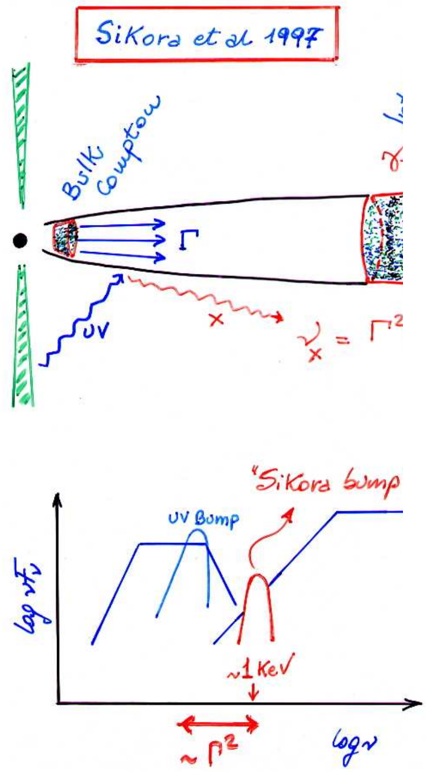

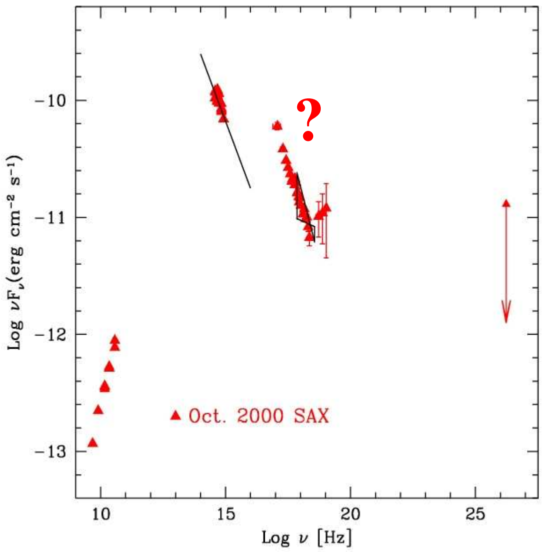

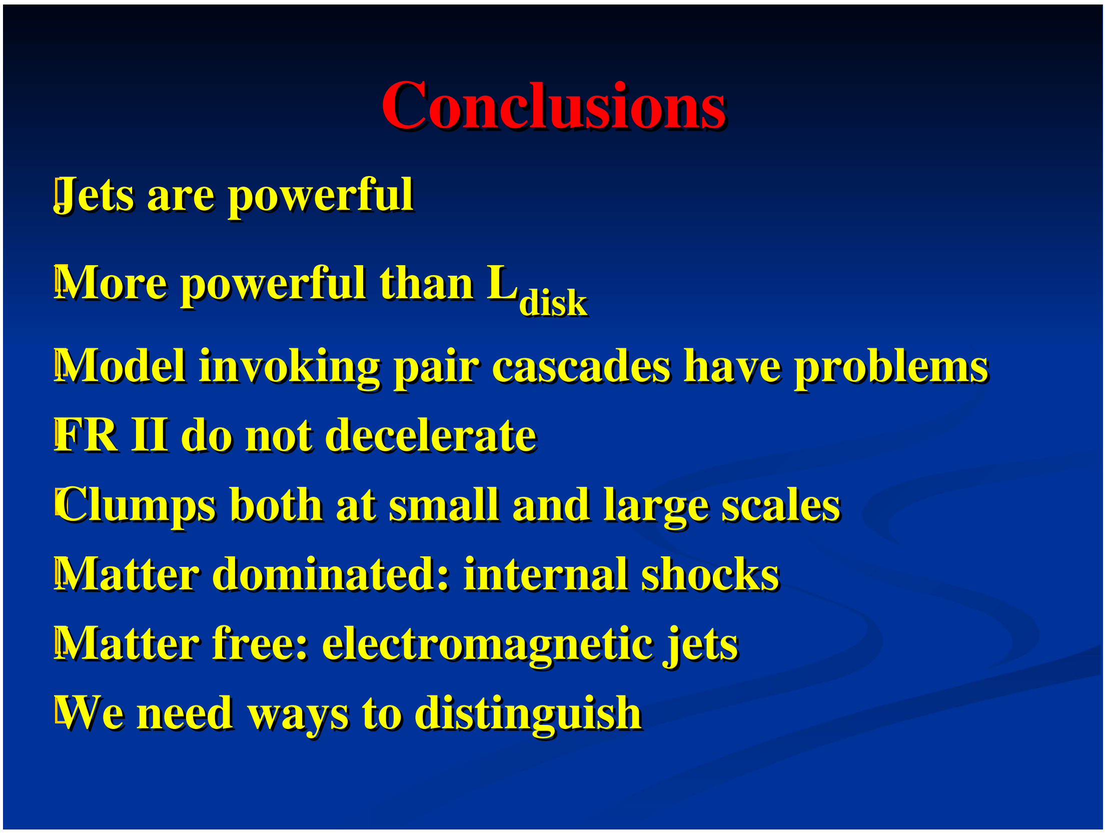
Conclusions
Jets are powerful
More powerful than L_{disk}
Model invoking pair cascades have problems
FR II do not decelerate
Clumps both at small and large scales
Matter dominated: internal shocks
Matter free: electromagnetic jets
We need ways to distinguish

7.11 M. Xilouris: The 2.3m telescope ARISTARCHOS

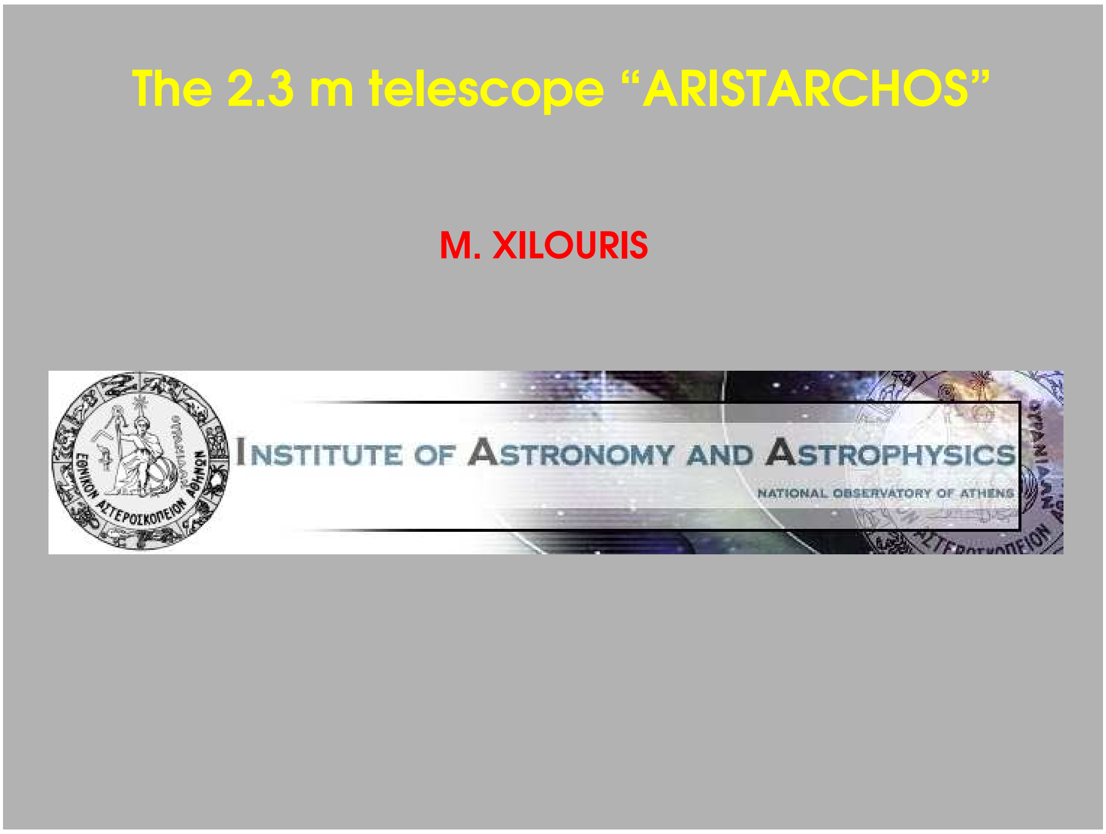

General presentation

- Diameter: 2.3 m , Focal ratio: f/8, Type: Ritchey-Chretien
- Site: mountain Chelmos (2340 m) Northern Peloponnese

Long. 22° 13' E, Lat. 37° 59' N

- Final acceptance on site (fall-2003)
- Operated by - INSTITUTE OF ASTRONOMY AND ASTROPHYSICS NATIONAL OBSERVATORY OF ATHENS
- Constructed by - ZEISS Carl Zeiss Jena GmbH Astronomical Instruments

The Site

Mountain Chelmos (Northern Peloponnese)

Elevation above sea level 2340 m

Distance to Athens 220 km

The telescope site

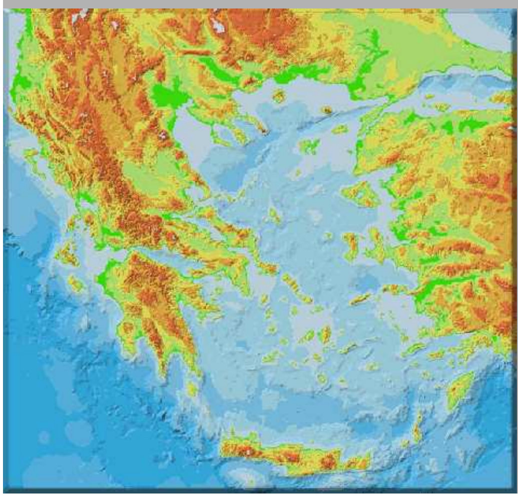

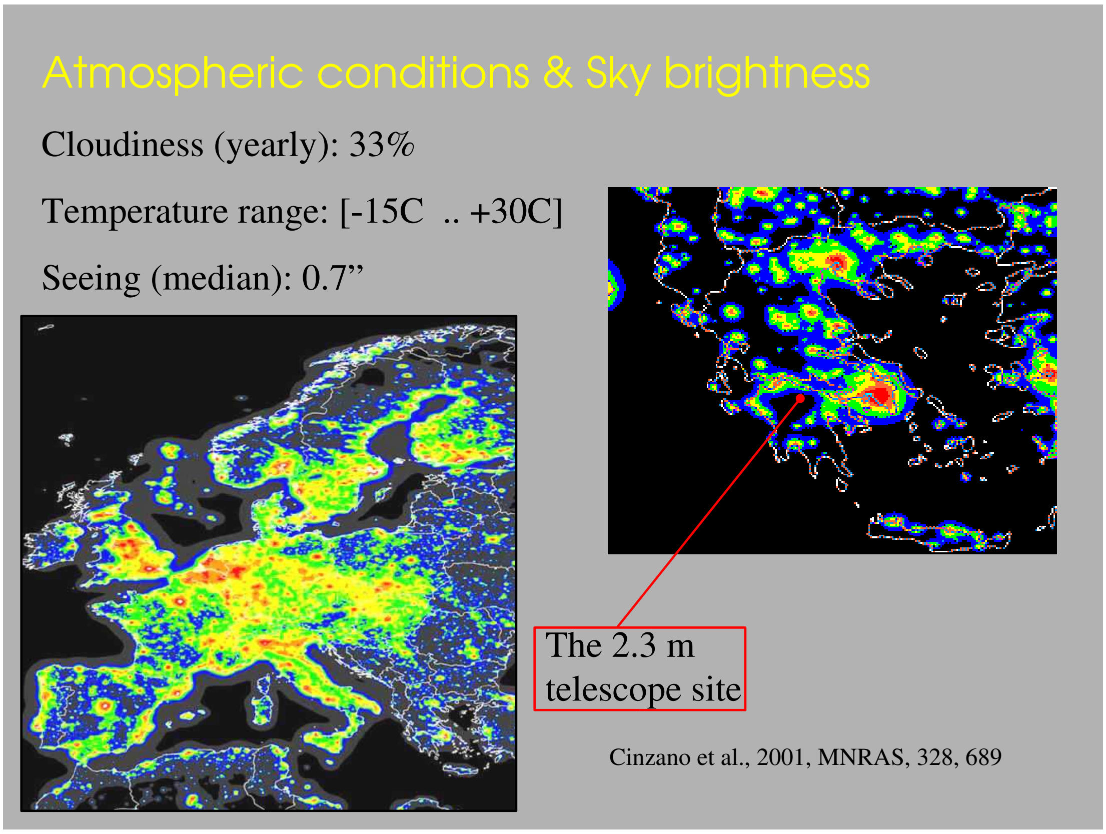
Atmospheric conditions & Sky brightness
Cloudiness (yearly): 33%
Temperature range: [-15C .. +30C]
Seeing (median): 0.7”
The 2.3 m telescope site
Cinzano et al., 2001, MNRAS, 328, 689

The telescope

Telescope and mirror.

JEISS – JENA

(March 2003)

OPTICS

Optical system:	**Ritchey-Chretien**
Primary mirror diameter:	**2280 mm**
Focal ratio:	**f/8**
Field of view RC-corrected:	**1.04 degrees (321.6 mm diameter)**
Field of view uncorrected:	**10.01 arcmin (52.8 mm diameter)**
Image scale:	**1" = 85 microns**
Image quality on axis:	**<0.35" (80% encircled energy, 350nm - 1000nm)**

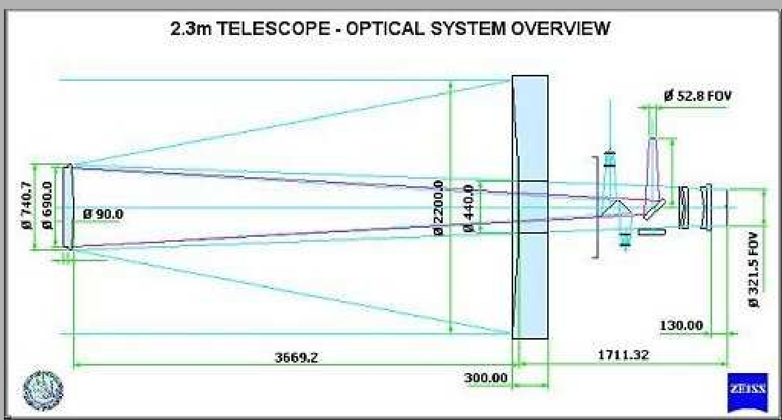

FEATURES OF THE TELESCOPE

Mounting system:	Altazimuth with 6 drives per axis
Encoding system:	2 tape encoders per axis with a resolution of 0.02 arcsec
Autoguiders:	2 off-axis autoguiders
Ports:	4 side-ports and 1 main-port (RC corrected wide-field)

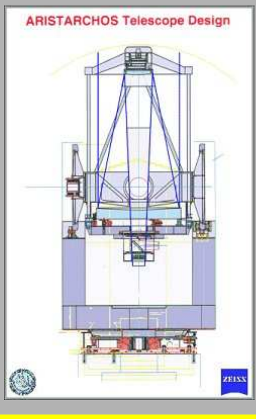

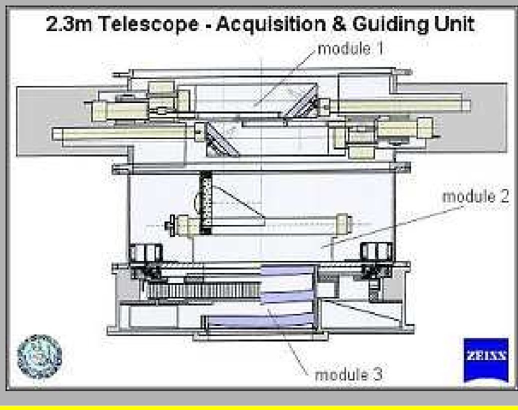

PERFORMANCE OF THE TELESCOPE

Maximum rate of movement:	2 degrees/sec on each axis
Accuracy of pointing:	< 4" up to z=70 degrees
Accuracy of tracking:	< 0.25" in 10 min, < 0.50" in 1 hour
Weight capacity at Cassegrain:	up to 300 kgr of instrumentation

Scientific Instruments

First light instruments

1024x

Model:
CCD Sensor:
CCD Format:
Coating:
Coolinng:
Filters:
Filter Configuration:

A 2048x2048 LN/CCD camera will soon be ordered

ICS

Ritchey-Chretien
2280 mm
f/8
1.04 degrees (321.6 diameter)
10.01 arcmin (52.8 diameter)

Low/Med

CCD Sensor:
CCD Format:
Gratings:
Resolutions:
Wavelength Range:

The prototype low dispersion spectrograph developed for the Liverpool Telescope

Scientific Instruments

Phase I instruments

Manchester Echelle Spectrograph

CCD Sensor:	**SITeAB, back-illuminated, Grade 1**
CCD Format:	**1024x1024, 24micron (0.28")**
Grating:	**echelle 31.6 grooves/mm**
Resolution:	**6 km/s (70 micron slit)**
Wavelebgth range:	**3900 Angstrom - 7500 Angstrom**
Performance:	**High resolution spectra, Low resolution spectra, Imaging**

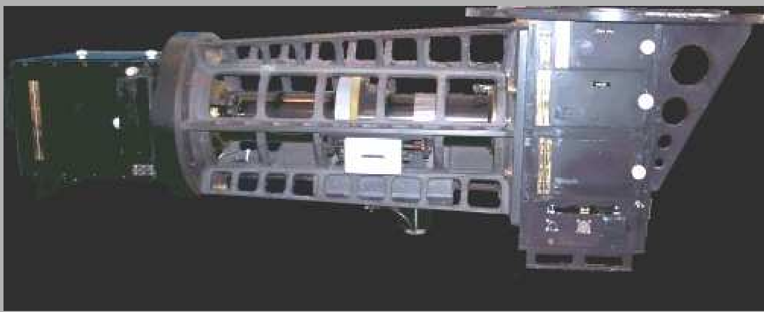

The MES *currently installed at the San Pedro Martin telescope in Mexico*

Scientific Instruments

Phase I instruments

ester Echelle Spectrometer

SITeAB, back-illuminated, Grade 1
1024x1024, 24 micron (0.28")
echelle 31.6 grooves/mm
6 km/s (70 micron slit)
3900 Angstrom - 7500 Angstrom
High resolution spectra, Low resolution spectra, Imaging

Model:
CCD Sensor:
CCD Format:
Coating:
Cooling:
Filters:

ULTRACAM – *currently at the 4.2 m W. Herschel telescope at the Canary Islands.*

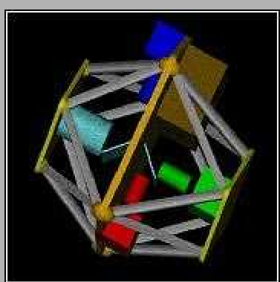

Mechanical Design

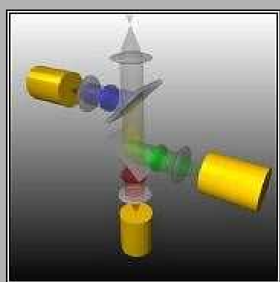

Optical Design

Chapter 8

A. Marscher: Multiwaveband Correlations

Multiwaveband Correlations

Alan Marscher* (Boston U., USA)

*ENIGMA ~~spy~~ advisor

ENIGMA Collaborators

Torino Obs. (Villata, Raiteri)
Perugia Obs. (Tosti)
Georgia (Kurtanidze) (quasi-ENIGMA)
Metsähovi gang (Valtaoja et al.)
Cork (Gabuzda)

Boston U. Co-conspirators

Jorstad, Sokolov

Others guilty by association

M. Aller, I. McHardy, P. Smith,
M. Lister, J. Stevens, T. Cawthorne,
W. Gear, I. Robson, Á. Stirling,
J.L. Gómez, T. Balonek, M. Gaskell,
J. Noble, H.R. Miller, V. Larionov,
...

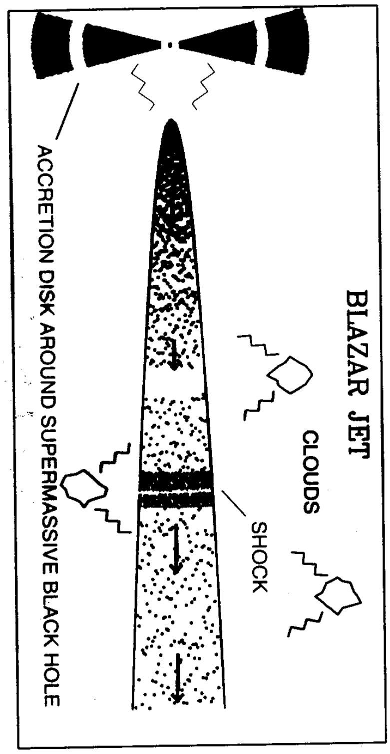

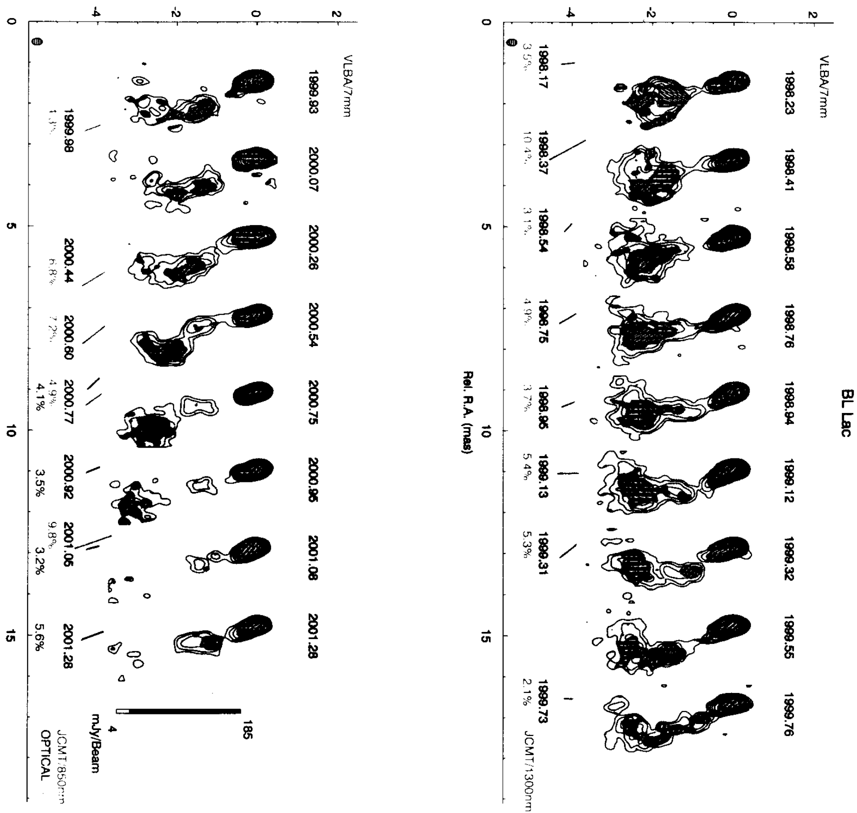

Stirling et al. (2003, MNRAS)
Jorstad et al. (2003) in prep

• X-ray activity (but not exact correspondence)
• superluminal ejection

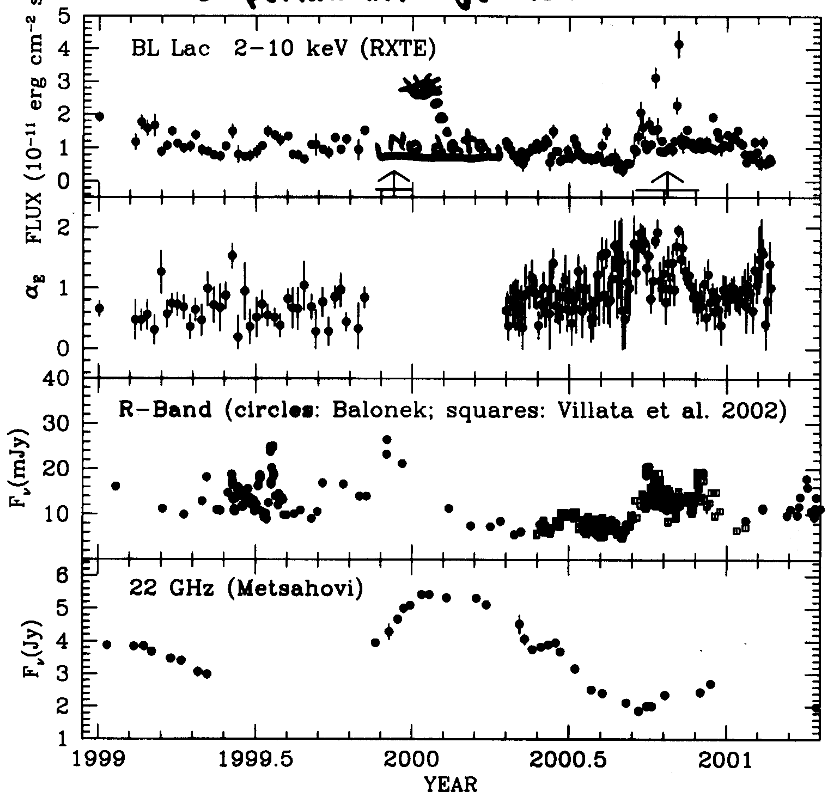

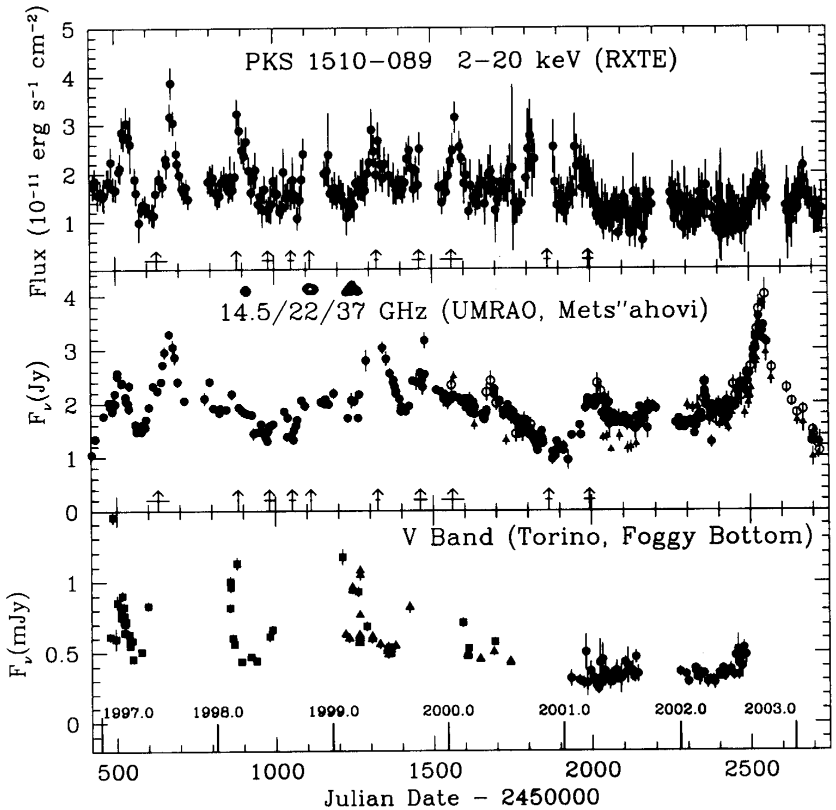

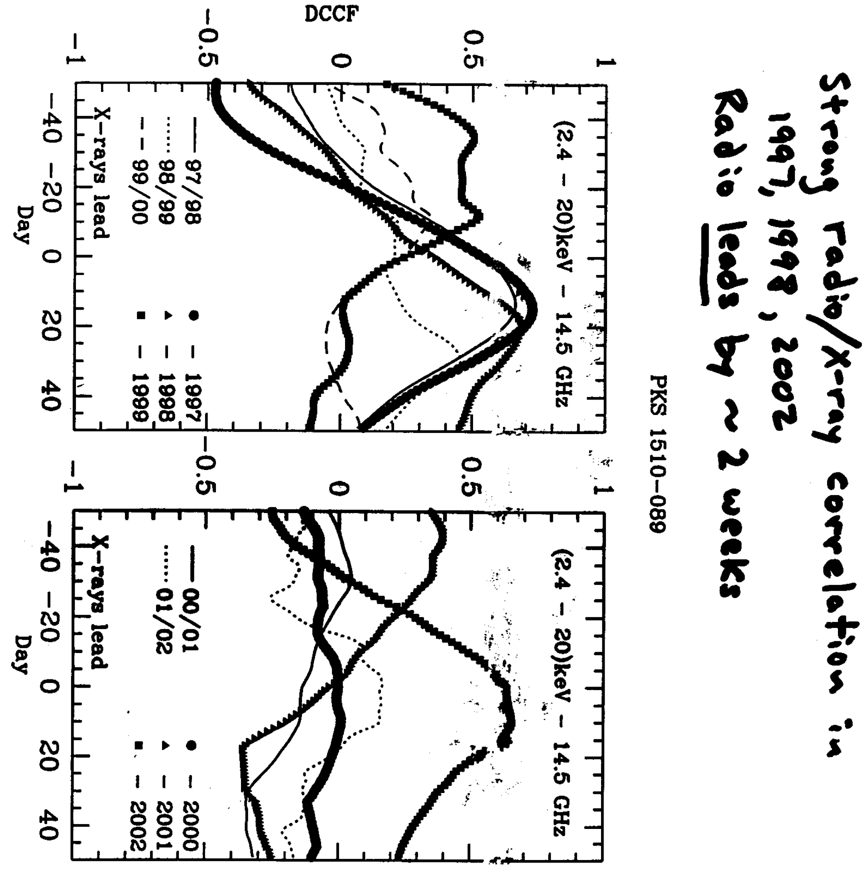
Strong radio/X-ray correlation in 1997, 1998, 2002
Radio leads by ~2 weeks
PKS 1510-089
DCCF
(2.4 - 20)keV - 14.5 GHz
97/98
98/99
99/00
X-rays lead
Day
1997
1998
1999
00/01
01/02
2000
2001
2002

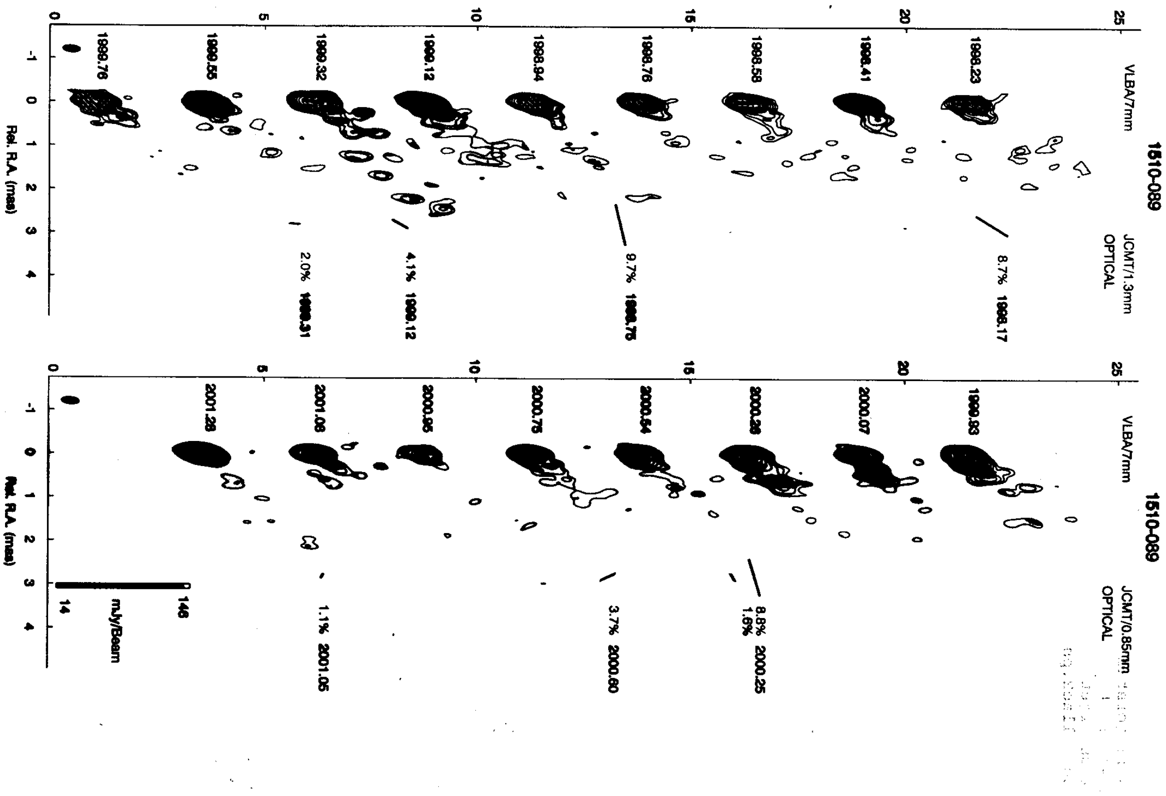
1510-089
VLBA/7mm
JCMT/1.3mm
OPTICAL
JCMT/0.85mm
Rel. R.A. (mas)
mJy/Beam

- 2 timescales : 0-3 days
  15-20 day optical leads
- Not one-to-one correspondence

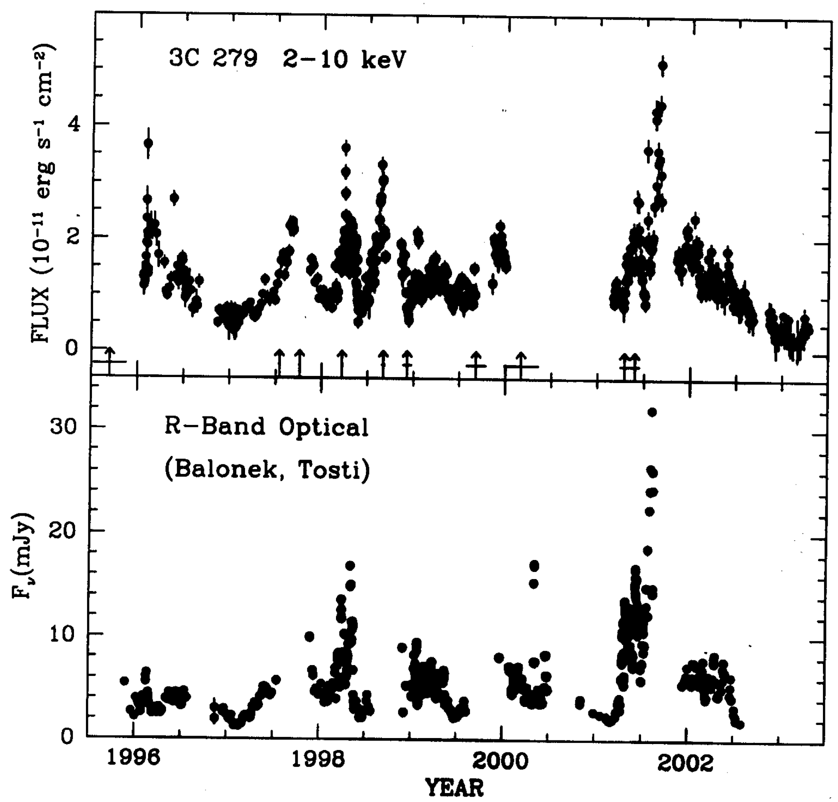

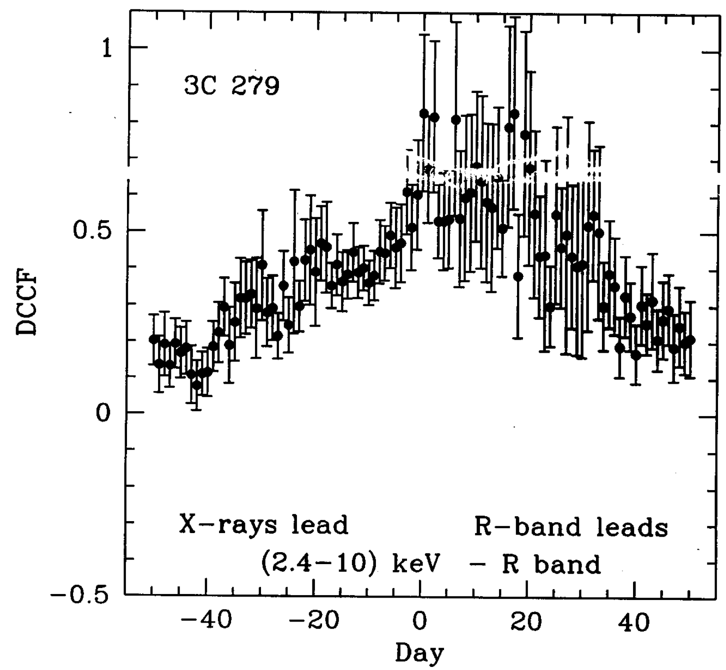

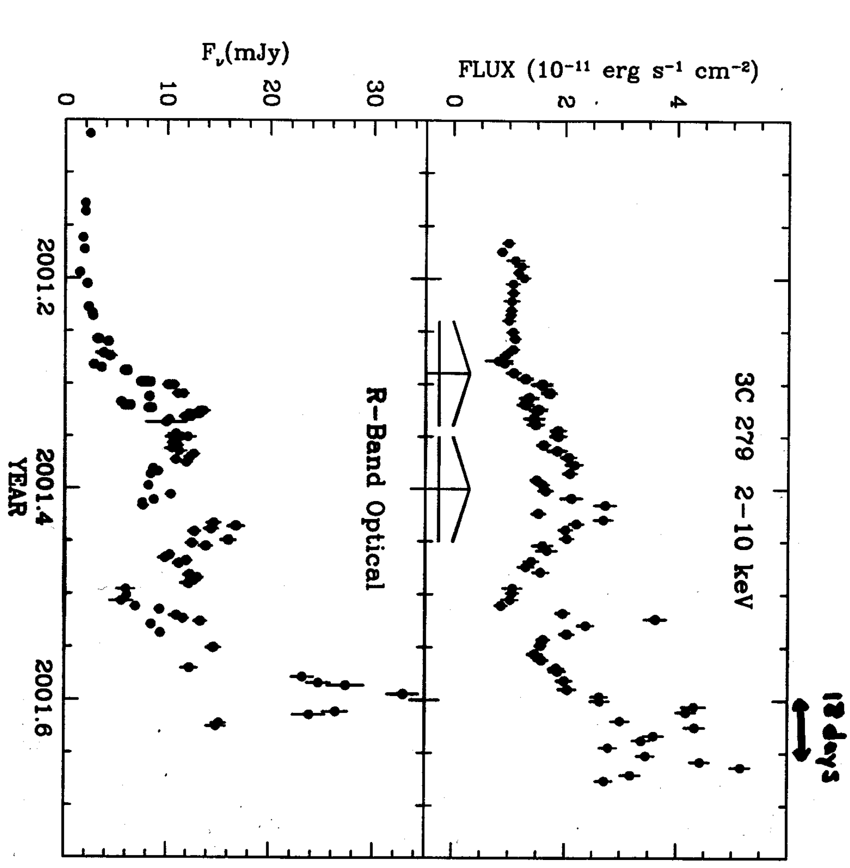
13 days
3C 279 2–10 keV
FLUX (10^-11 erg s^-1 cm^-2)
R-Band Optical
F_ν(mJy)
2001.2
2001.4
2001.6
YEAR

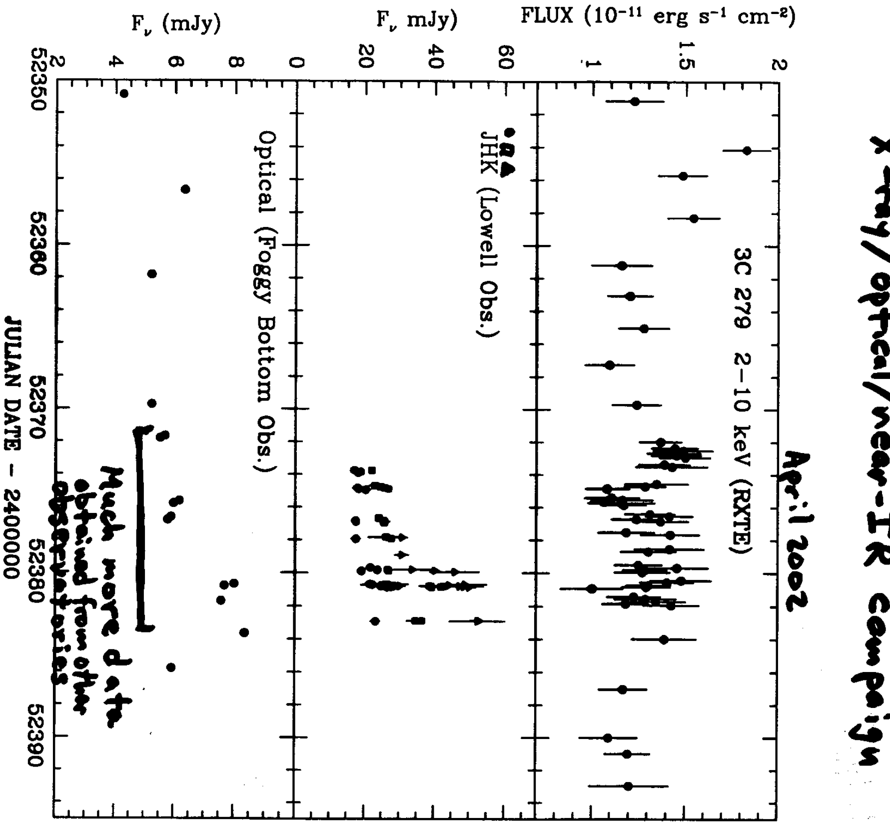
X-ray/optical/near-IR campaign
April 2002
3C 279 2–10 keV (RXTE)
FLUX (10^-11 erg s^-1 cm^-2)
JHK (Lowell Obs.)
F_ν mJy)
Optical (Foggy Bottom Obs.)
F_ν (mJy)
Much more data obtained from other observatories
52350
52360
52370
52380
52390
JULIAN DATE - 2400000

Quasar

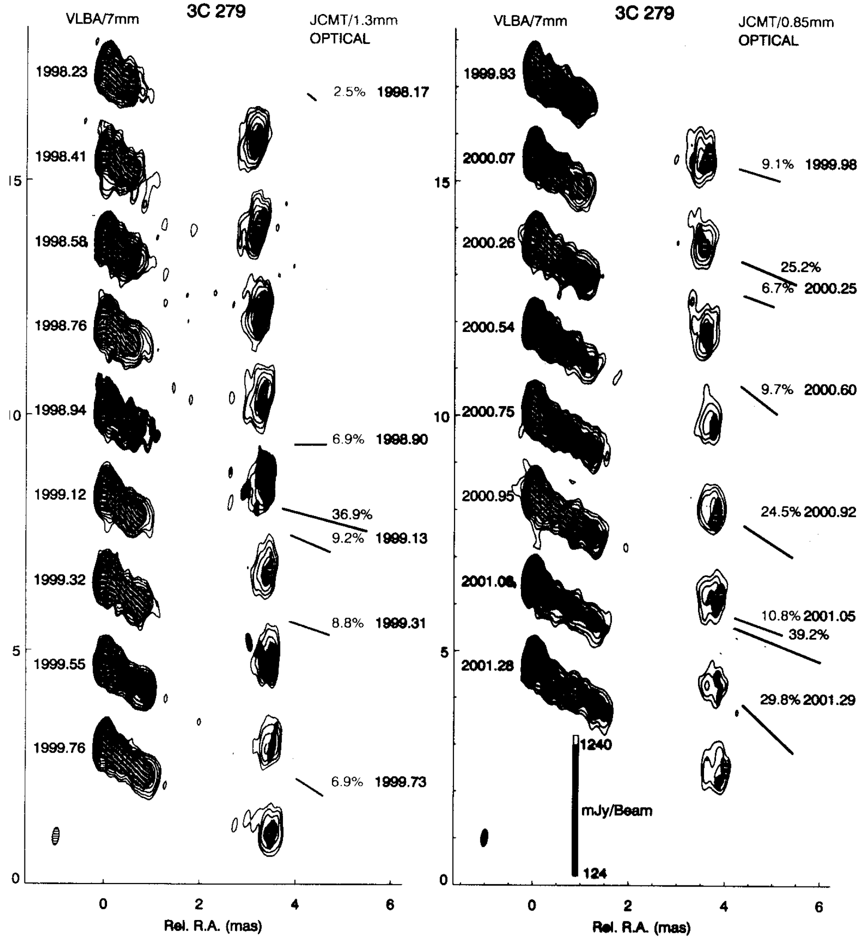
VLBA/7mm
3C 279
JCMT/1.3mm
OPTICAL
1998.23
1998.41
1998.58
1998.76
1998.94
1999.12
1999.32
1999.55
1999.76
2.5% 1998.17
6.9% 1998.90
36.9%
9.2% 1999.13
8.8% 1999.31
6.9% 1999.73
Rel. R.A. (mas)
VLBA/7mm
3C 279
JCMT/0.85mm
OPTICAL
1999.93
2000.07
2000.26
2000.54
2000.75
2000.95
2001.28
9.1% 1999.98
25.2%
6.7% 2000.25
9.7% 2000.60
24.5% 2000.92
10.8% 2001.05
39.2%
29.8% 2001.29
1240
mJy/Beam
124
Rel. R.A. (mas)

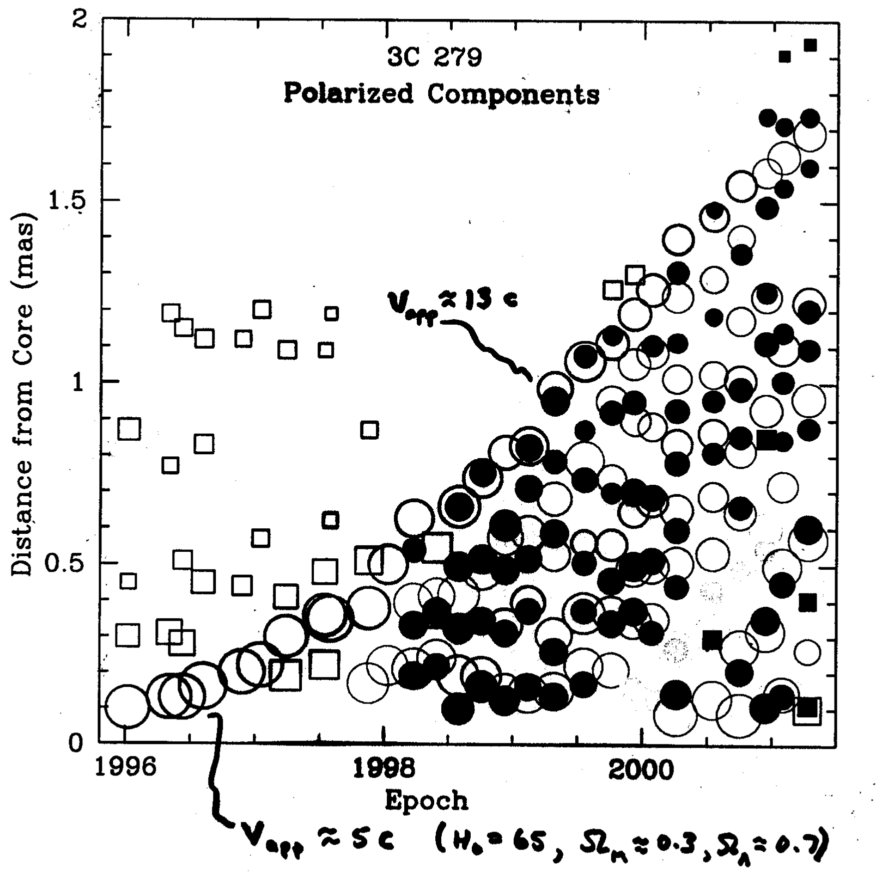
3C 279
Polarized Components
Distance from Core (mas)
Epoch
$V_{app} \approx 13\,c$
$V_{app} \approx 5\,c$ ($H_0 = 65$, $\Omega_m \approx 0.3$, $\Omega_\Lambda \approx 0.7$)

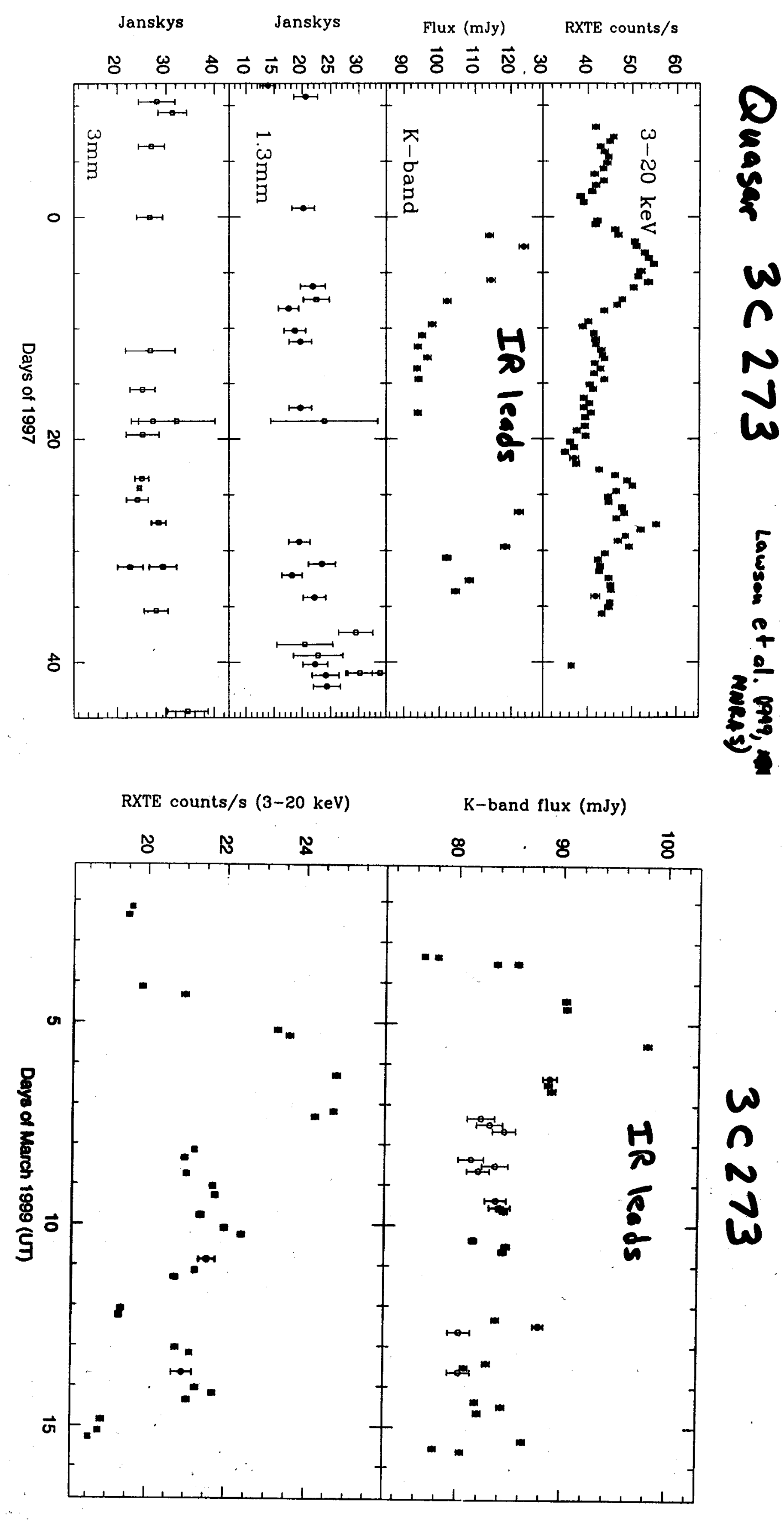
Quasar 3C 273
Lawson et al. (1999, MNRAS)
RXTE counts/s
3-20 keV
Flux (mJy)
K-band
IR leads
Janskys
1.3mm
Janskys
3mm
Days of 1997
3C 273
K-band flux (mJy)
IR leads
RXTE counts/s (3-20 keV)
Days of March 1999 (UT)

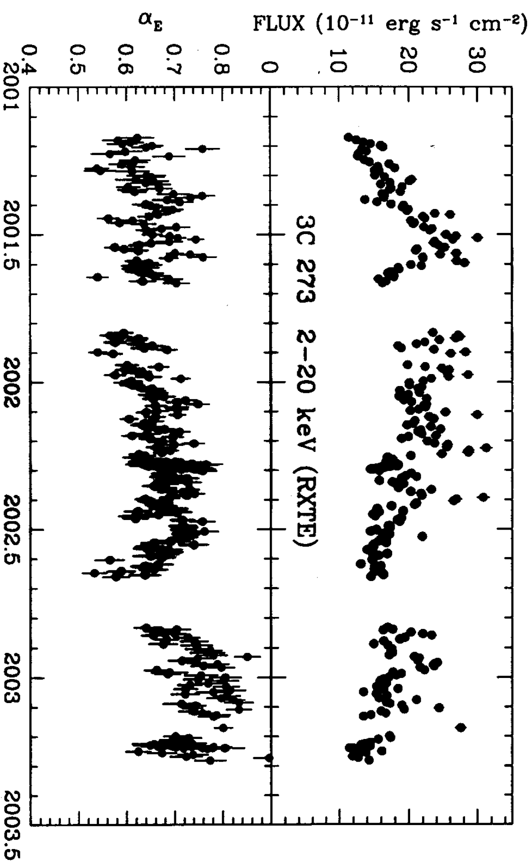
FLUX (10^{-11} erg s^{-1} cm^{-2})
α_E
3C 273 2–20 keV (RXTE)
YEAR

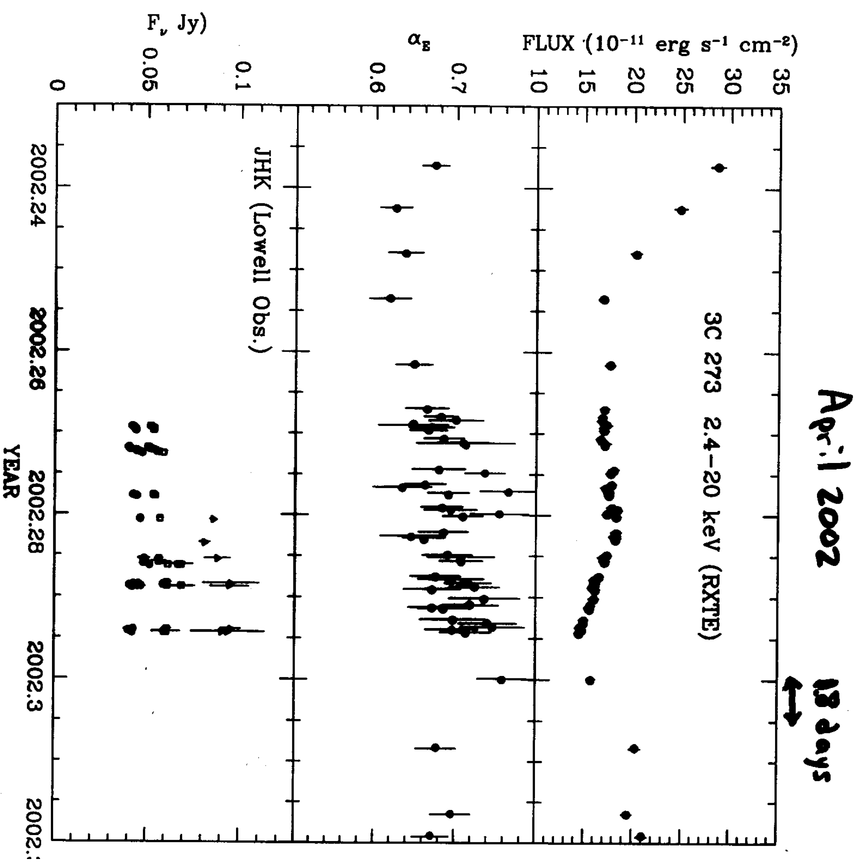
FLUX (10^{-11} erg s^{-1} cm^{-2})
α_E
F_ν Jy)
3C 273 2.4–20 keV (RXTE)
JHK (Lowell Obs.)
YEAR
April 2002
13 days

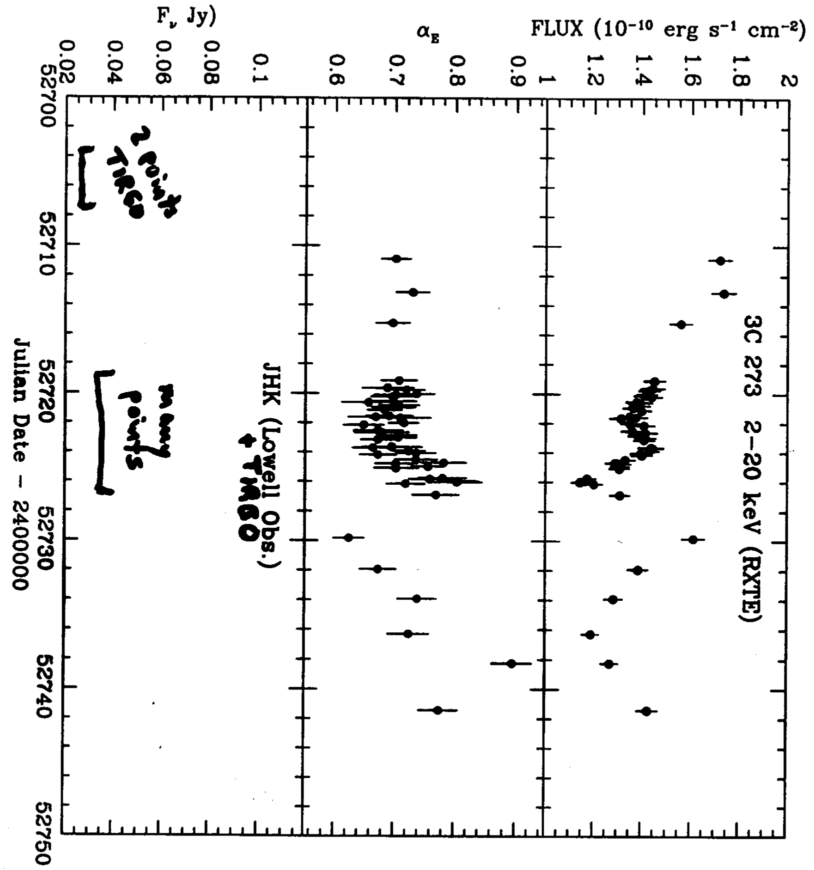
3C 273 2-20 keV (RXTE)
FLUX (10^{-10} erg s^{-1} cm^{-2})
α_E
F_ν Jy)
JHK (Lowell Obs.) + TIRGO
2 points TIRGO
many points
Julian Date - 2400000

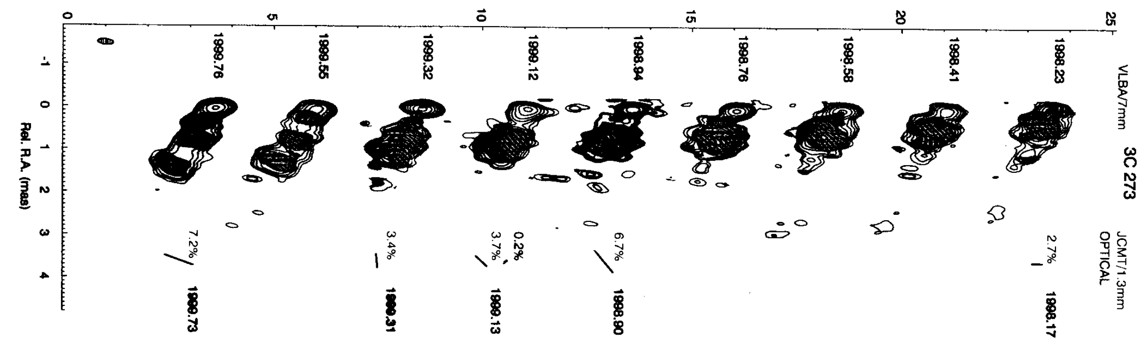
VLBA/7mm
3C 273
JCMT/1.3mm OPTICAL
Rel. R.A. (mas)

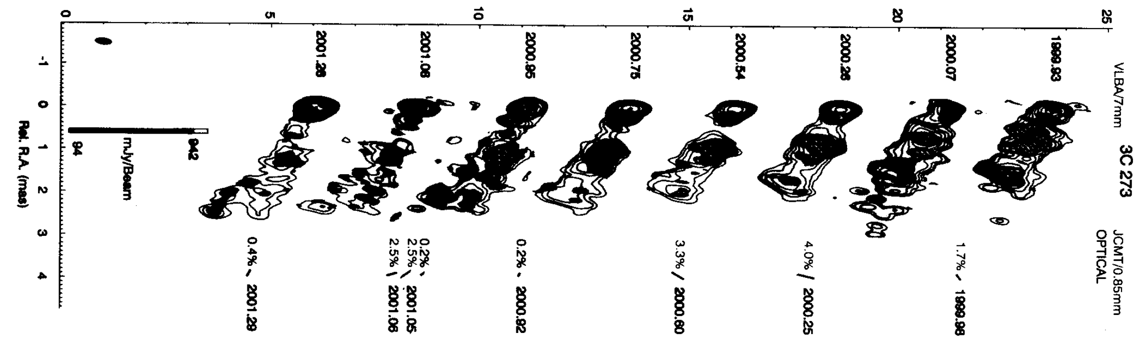
VLBA/7mm
3C 273
JCMT/0.85mm OPTICAL
mJy/Beam
Rel. R.A. (mas)

Why are there strong correlations but not one-to-one correspondence between X-ray + lower-ν variations?

- SSC is broad-band
  - seed photons from several decades of frequency

- Synchrotron knots are frequency-stratified (particles are accelerated at fronts, then advect away from fronts)

How can lower-ν variations lead X-ray?

- Light-travel effects in SSC
  - Seed photons need time to travel to each scattering electron
- X-ray "zone" can be different from synchrotron "zone" at a given ν_s [A. Sokolov is working on models]

of Synchroton "Seed" Photons to Inverse Compton X- + γ-rays

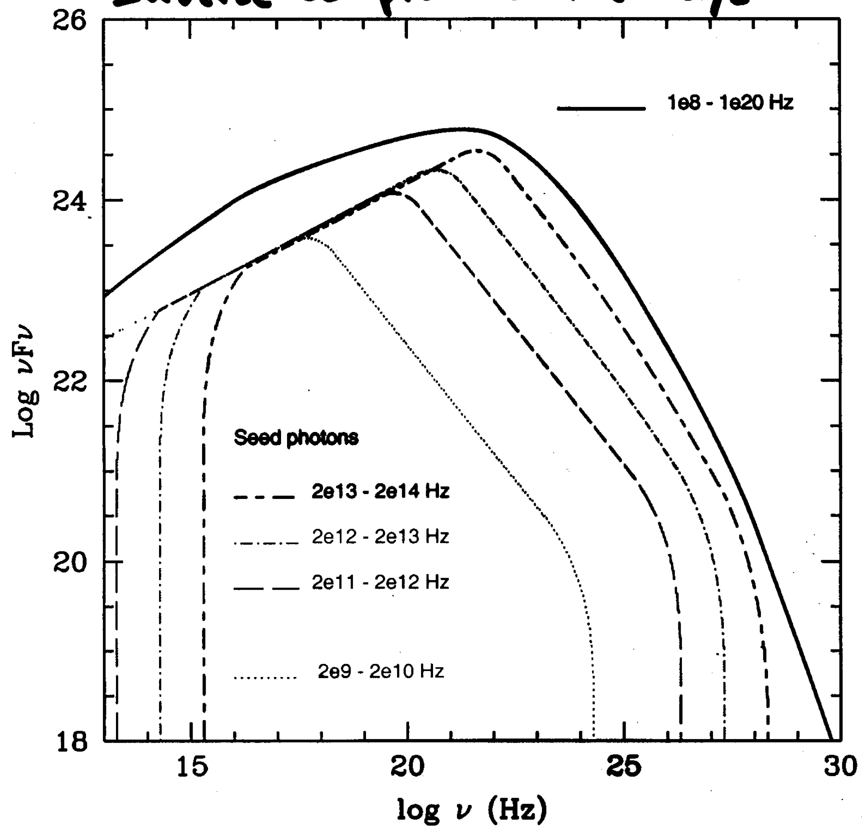

McHardy et al. (1999 MNRAS)

Frequency Stratification in Shocks
(Marscher + Gear 1985 Ap J)

Electrons accelerated at shock front

High-Energy electrons suffer radiative energy losses (highest energy first)

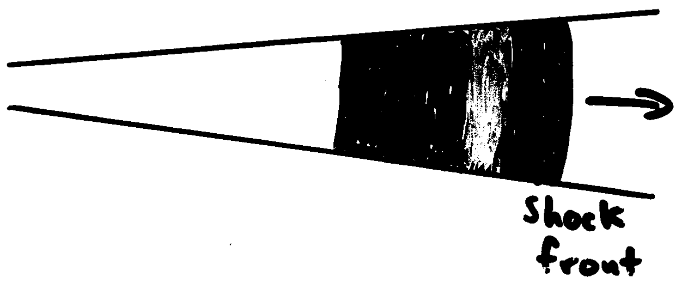

Higher frequencies vary earlier + with faster timescales

(Inverse) Compton losses: spectrum rises as turnover decreases
→ X-ray emission declines

Synchrotron losses: turnover frequency decreases while peak flux density remains ~ constant (X-ray emission declines)

Adiabatic: peak flux density + turnover decline

Chapter 9

Participants

Landessternwarte Heidelberg

S. Wagner, S. Britzen, M. Camenzind, M. Hauser, J. Heidt, G. Pülhofer, O. Kurtanidze, P. Strub

MPI für Radioastronomie

A. Witzel, I. Agudo, T. Arshakian, U. Bach, A. Brunthaler, G. Cimo, S. Friedrichs, L. Fuhrmann, V. Impellizzeri, M. Kadler, A. Kraus, T.P. Krichbaum, E. Körding, E. Middelberg, R. Mittal, A. Pagels, A. Polatidis, E. Ros, Bong Won Sohn, J.A. Zensus

Tuorla Observatory

L. Takalo,E. Lindfors, K. Nilsson, A. Sillanpää, E. Valtaoja

Metsähovi Radio Observatory

M. Tornikoski, A. Lähteenmäki

Osservatorio Astronomico di Torino

C. Raiteri, M. Villata

Osservatorio Astronomico di Brera

G. Ghisellini, B. Sbarufatti

University of Athens; IASA

I. Papadakis, N. Vlahakis, K. Tsinganos, A. Mastichiadis, M. Xilouris

Cork Institute of Technology

N. Smith, D. Gabuzda, A. Giltinan, L. Hanlon, J. Howard, P. Reynolds

International advisor

A. Marscher (Boston University)

9.1 Meeting photo

Figure 9.1: Photo by E. Middelberg